BRACE EFFECTIVENESS OF CROSS-FRAME LAYOUT AND CONNECTION DESIGN ON SKEWED STEEL BRIDGES DURING CONSTRUCTION

By

Chenqi Zhou

Submitted to the graduate degree program in Civil Engineering
and the Graduate Faculty of the University of Kansas
in partial fulfillment of the requirements for the degree of
Doctor of Philosophy.

Committee Chairman _____
Dr. Caroline Bennett

Committee Members _____
Dr. Adolfo Matamoros

_____
Dr. Jian Li

_____
Dr. William Collins

_____
Dr. Huazhen Fang

Date Defended: _____04/26/2019_____

The Dissertation Committee for Chenqi Zhou certifies
that this is the approved version of the following dissertation:

BRACE EFFECTIVENESS OF CROSS-FRAME LAYOUT AND CONNECTION DESIGN ON SKEWED STEEL BRIDGES DURING CONSTRUCTION

Committee Chairman

Dr. Caroline Bennett

Committee Members

Dr. Adolfo Matamoros

Dr. Jian Li

Dr. William Collins

Dr. Huazhen Fang

Date Approved:

EXECUTIVE SUMMARY

The Kansas Department of Transportation (KDOT)'s current design practice is to align cross-frames parallel to the skew angle to avoid problems associated with fit-up during erection. The American Association of State Highway and Transportation Officials (AASHTO) provisions for bridges with skew angle greater than 20 degrees are based on the assumption that cross-frames are oriented perpendicular to the girder line. There is a potentially significant discrepancy between assumptions implicit in the AASHTO Specifications and bridges that are designed with cross-frames placed parallel to the skew for skew angles between 20 and 40 degrees. An analytical approach was chosen to study the effects of cross-frame orientation, spacing, skew angle, and connection design upon flange stresses, bridge stability, and cross-frame stresses.

This dissertation is divided into three parts and appendices. The first part is the introduction for the dissertation. Parts 2 is the numerical findings of cross-frame layout, orientation, and spacing on lateral flange bending stresses of skewed steel bridges during construction. Part 3 is the analytical investigations of skew angle, cross-frame layout, cross-frame orientation, and cross-frame spacing on bridge stability and brace effectiveness.

Part 1: Introduction

Part 2: Skewed Steel Bridges - Effects of Cross-frame Layout on Lateral Flange Bending Stresses During Construction

Part 3: Skewed Steel Bridges - Cross-frame and Connection Design to Ensure Brace Effectiveness

Appendix A: Deformed Shapes of All Finite Element Models Included in the Parametric Study

Appendix B: AASHTO-Predicted Capacity Calculations

Appendix C: Girder Shell Elements Modeling and Dynamic Anaysis

Appendix D: Abutment Framing and Bearing Conditions

Appendix E: Single Girder Analysis

Part 2 was published in the Report No. K-TRAN: KU-13-3 in February 2016. Part 3 was published in the Report No. K-TRAN: KU-13-7 in March 2017.

ACKNOWLEDGEMENTS

I am deeply grateful for the guidance and support of Drs. Caroline Bennett, Adolfo Matamoros, Jian Li, William Collins, and Huazhen Fang. Their knowledge and experience has been invaluable in the creation of this thesis. The assistance and instruction of Hao Liu, Say Bun, Gary Simmons, Heidi Hassel, and Amanda Hartman has been greatly appreciated. I would like to also acknowledge support of the Kansas Department of Transportation (KDOT), University of Kansas Transportation Research Institute (KU TRI), and Transportation Pooled Fund Study TPF-5 (189). Lastly, I would like to thank my family for their continuous support and encouragement throughout all of my education.

TABLE OF CONTENTS

List of Figures

PART 1: INTRODUCTION

N/A

PART 2: SKEWED STEEL BRIDGES – EFFECTS OF CROSS-FRAME LAYOUT ON LATERAL FLANGE BENDING STRESSES DURING CONSTRUCTION

PART 3: SKEWED STEEL BRIDGES - CROSS-FRAME AND CONNECTION DESIGN TO ENSURE BRACE EFFECTIVENESS

APPENDIX B: AASHTO-PREDICTED

APPENDIX C: GIRDER SHELL ELEMENTS MODELING AND DYNAMIC ANALYSIS

APPENDIX D: ABUTMENT FRAMING AND BEARING CONDITIONS

APPENDIX E: SINGLE GIRDER MODEL ANALYSIS

APPENDIX F: CROSS-FRAME ANGLE WORK POINT FRAMING

List of Tables

PART 1: INTRODUCTION

N/A

PART 2: SKEWED STEEL BRIDGES – EFFECTS OF CROSS-FRAME LAYOUT ON LATERAL FLANGE BENDING STRESSES DURING CONSTRUCTION

PART 3: SKEWED STEEL BRIDGES - CROSS-FRAME AND CONNECTION DESIGN TO ENSURE BRACE EFFECTIVENESS

Part 1

INTRODUCTION

This dissertation is divided into three parts and appendices. The first part is the introduction for the dissertation. The Part 2 investigates the effects of cross-frame orientation and spacing on lateral flange bending stresses during the construction phase and evaluates AASHTO's interaction requirements for strong-axis and weak-axis bending demands. Parts 3 focuses on the effects of cross-frame orientation, skew angle, and connection design upon bridge system behavior and cross-frame stresses.

Part 2 of this dissertation quantified the effects of cross-frame orientation and cross-frame spacing on lateral flange bending stresses during the bridge construction phase and evaluated AASHTO's interaction requirement of weak-axis bending demands with strong-axis demands on the flanges. The American Association of State Highway and Transportation Officials (AASHTO) provisions for lateral flange bending stresses are based on the assumption that cross-frames are oriented perpendicular to the girder line whenever the skew angle is greater than 20 degrees. Current Kansas Department of Transportation (KDOT) design practice is to align cross-frames parallel to the skew angle to avoid problems associated with fit-up during erection. There is a potentially significant discrepancy between assumptions implicit in the AASHTO Specifications and bridges that are designed to be skewed between 20 and 40 degrees that include cross-frames placed parallel to the skew. In lieu of a refined analysis, the AASHTO-LRFD Bridge Design Specifications currently permit engineers examining bridges skewed more than 20 degrees to use a minimum value of f_l = 10 ksi for an interior girder and f_l = 7.5 ksi for an exterior girder. The estimates for f_l provided within the AASHTO-LRFD Bridge Design

Specifications are based on a limited data set for skewed bridges. Additionally, since the AASHTO-LRFD Design Specifications state that cross-frames or diaphragms should be placed in a staggered configuration when a bridge is skewed more than 20 degrees, the approximate values provided for f_l should not be expected to be indicative of the lateral flange bending stresses experienced when cross-frames are instead carried parallel to the skew in bridges skewed beyond 20 degrees.

Part 3 of this dissertation investigated the effects of cross-frame orientation, skew angle, and cross-frame connection upon bridge system behavior and cross-frame stresses. Skewed bridges in Kansas are often designed such that the cross-frames are carried parallel to the skew angle up to 40 degrees, while many other states place cross-frames perpendicular to the girder for skew angles greater than 20 degrees. Skewed-parallel cross-frames are longer and require different connections than cross-frames oriented perpendicular to the girder. As cross-frames lengthen, they become less stiff and less effective at distributing forces between girders if the same connecting elements are used. For the cross-frame / diaphragm elements to be able to brace the bridge girders, the brace elements must possess both sufficient strength and stiffness to restrain the girder from instability. While strength can be addressed by increasing the cross-sectional properties of the brace elements, providing sufficient stiffness is a more significant challenge. Stiffness of the brace system is dependent on both the brace elements and the type of connection made. Therefore it is important to determine whether the cross-frames and their corresponding connecting elements placed in a parallel-to-skew configuration are sufficiently designed to resist lateral torsional buckling demands using current KDOT practices.

Part 2

SKEWED STEEL BRIDGES - EFFECTS OF CROSS-FRAME LAYOUT ON LATERAL FLANGE BENDING STRESSES DURING CONSTRUCTION

C. Zhou[1], C.R. Bennett[2], A.B. Matamoros[3], J. Li[4]

ABSTRACT

The American Association of State Highway and Transportation Officials (AASHTO) provisions for lateral flange bending stresses are based on the assumption that cross-frames are oriented perpendicular to the girder line whenever the skew angle is greater than 20 degrees. Current Kansas Department of Transportation (KDOT) design practice is to align cross-frames parallel to the skew angle to avoid problems associated with fit-up and distortion-induced fatigue. There is a potentially significant discrepancy between assumptions implicit in the AASHTO Specifications and bridges that are designed to be skewed between 20 and 40 degrees that include cross-frames placed parallel to the skew.

Lateral flange bending stresses can arise from a number of sources, such as wind loading or eccentric concrete placement, but of particular interest are lateral flange bending stresses, f_l, that occur due to skew. Lateral flange bending stresses that occur in skewed bridge systems tend to develop due to lateral forces transferred through cross-frames which may connect adjacent girders at different span points. In lieu of a refined analysis, the AASHTO-LRFD Bridge Design Specifications currently permit engineers examining bridges skewed more than 20° to use a

Department of Civil, Environmental, and Architectural Engineering
University of Kansas, 1530 W. 15th St, Lawrence, KS 66045
Tel. (785) 864-3235, Fax. (785) 864-5631

[1] Chenqi Zhou, Bridge Engineer, Jacobs Engineering Group, James.Zhou@jacobs.com
[2] Caroline R. Bennett, PhD, PE, Associate Professor, University of Kansas, crb@ku.edu
[3] Adolfo B. Matamoros, PhD, PE, Professor, University of Texas at San Antonio, adolfo.matamoros@utsa.edu
[4] Jian Li, PhD, PE, Assistant Professor, University of Kansas, jianli@ku.edu

minimum value of f_l = 10 ksi for an interior girder and f_l = 7.5 ksi for an exterior girder. The estimates for f_l provided within the AASHTO-LRFD Bridge Design Specifications are based on a limited data set for skewed bridges. Additionally, since the AASHTO-LRFD Design Specifications state that cross-frames or diaphragms should be placed in a staggered configuration when a bridge is skewed more than 20°, the approximate values provided for f_l should not be expected to be indicative of the lateral flange bending stresses experienced when cross-frames are instead carried parallel to the skew in bridges skewed beyond 20°. Carrying cross-frames and diaphragms parallel to the skew angle in bridges skewed more than 20° is a practice implemented by some state DOTs, and is primarily done to minimize problems with cross-frame fit-up during erection.

The objectives of this study were to quantify the effects of cross-frame orientation and cross-frame spacing on lateral flange bending stresses during the bridge construction phase and to evaluate AASHTO's interaction requirement of weak-axis bending demands with strong-axis demands on the flanges. Stability is especially of concern during construction stages, before a composite concrete deck has hardened; in this stage, steel girders rely on intermediate cross-frames for stability. Detailed three-dimensional solid finite element models were used to investigate these parameters (skew angle, cross-frame spacing, and cross-frame orientation) on the lateral flange bending stresses during construction.

The authors have performed a study to investigate the effects of cross-frame orientation and skew angle upon lateral flange bending stresses, by examining lateral flange bending stresses in a suite of detailed 3D, solid finite element analyses of skewed bridge systems, in which cross-frame layout, spacing, and skew angle were varied. Skewed bridge systems with cross-frames placed parallel to the skew, systems with cross-frames arranged in a staggered configuration, and

bridges with cross-frames parallel to skew and unstaggered were considered. Cross-frame spacing of 4.57 m [15 ft] and 9.14 [30 ft] were examined. The models include geometric nonlinearities to assess the lateral deflection and lateral flange bending stresses in different bridge systems. Material nonlinearities were found to produce insignificant differences in the results and were not included in the full parametric analysis.

The findings of this study showed that cross-frame skew angle and cross-frame configuration had little effect on both vertical and lateral bending stresses. Cross-frame spacing had little effect on stress in the interior girder, but decreasing the cross-frame spacing significantly reduced lateral flange bending stresses in the exterior girder, as the overhang bracket loads produced significantly larger stresses with longer unbraced lengths. All exterior girders in the bridge with 9.1 m [30 ft] cross-frame spacing had stresses more than twice the minimum value for f_l recommended by AASHTO for exterior girders.

INTRODUCTION AND BACKGROUND

The American Association of State Highway and Transportation Officials (AASHTO) provisions for lateral flange bending stresses are based on the assumption that cross-frames are oriented perpendicular to the girder line whenever the skew angle is greater than 20°. Current Kansas Department of Transportation (KDOT) design practice is to align cross-frames parallel to the skew angle for bridges with skew angles up to 40°. This approach avoids problems associated with fit-up during erection and deck placement, and limits the potential for distortion-induced fatigue. However, there is a potentially significant discrepancy between assumptions implicit in

the AASHTO-LRFD Bridge Design Specifications (AASHTO 2010) and bridges that are designed to be skewed between 20 and 40° when cross-frames are placed parallel to the skew.

AASHTO (2010) defines a cross-frame as a transverse truss framework connecting adjacent longitudinal flexural components. In non-skewed (right) bridges under dead loads, only tensile forces develop in the intermediate cross-frame chords and only compressive forces develop in the cross-frame diagonals. However, in skewed bridges, most members of the intermediate cross-frames develop both compressive and tensile forces, depending on the loading condition. Skewed bearing lines subject the bridge to torsion by developing transverse load paths between the girders through the cross-frames. Furthermore, girder vertical displacements, major-axis bending stresses, and lateral flange bending stresses can be significantly influenced by large skew effects if the transverse load transfer is large (Ozgur 2011). On the other hand, it has been suggested that the effects of skew on forces induced in the cross-frame members may be neglected for skew angles 20° or less (Bishara and Elmir 1990).

Intermediate cross-frames in multi-beam steel bridges are used predominantly for lateral-load resistance, live load distribution, and reducing the unbraced length of the girder's compression flange, providing support against lateral-torsional buckling. Cross-frames also provide support against lateral bending and torsional buckling, particularly in skewed and curved bridges. In traditional designs for skewed and curved girders, gravity loads are assumed to be resisted by the girders and transverse loads are presumed to be resisted by the intermediate cross-frames. In actuality, the whole bridge acts as a system, with gravity loads producing stresses in the cross-frames as well as the girders, and girders also resisting lateral bending loads transmitted through the cross-frames.

Stability of the overall bridge system depends on cross-frames and diaphragms placed at discrete locations along the bridge to resist buckling loads. When the cross-frame or diaphragm elements are placed at any angle other than 90° against the girder line, their efficiency in transferring lateral loads is reduced due to a smaller lateral force component that is developed in the brace. Wang and Helwig (2008) note that although cross-frames placed parallel to skew can be effective at skew angles greater than 20°, the effects of connection flexibility and lowered brace stiffness due to longer braces becomes an issue that must be considered. This can be easily addressed from a strength perspective by increasing the cross-sectional properties of the brace elements such that the cross-frame/diaphragm has sufficient strength in the skewed position to transfer lateral forces from one girder to another. However, increasing the cross-frame member section properties results in an increase in their internal forces and vice versa (Bishara and Elmir 1990). The greater the skew angle, the larger the maximum forces induced in the cross-frame members (Bishara and Elmir 1990). While greater cross-frame forces would suggest greater bridge transverse stiffness and smaller girder lateral deflection, researchers have found that moments, rotations, and deflections increased with an increase in skew angle (Gupta and Kumar 1983).

Previous research has also shown that the larger the bridge skew, the larger the lateral load transfer becomes, influencing bottom flange lateral bending stress (Ozgur 2011). In skewed bridges, torsional moments created in the girders by the lateral deflection of their bottom flanges, while low in magnitude, were larger than in right bridges (Bishara and Elmir 1990). McConnell et al. (2014) found that bridge skew and cross-frame placement significantly influenced bottom flange lateral bending stress and indicated that placing cross-frames in the staggered configuration reduced a bridge's transverse stiffness. In the staggered configuration, cross-frame

forces cannot be directly balanced by a cross-frame on the opposite side of the girder section. This leads to a decrease in cross-frame forces, but an increase in flange lateral bending stresses and girder lateral deflection (McConnell et al. 2014).

Ensuring that cross-frame and brace elements have sufficient stiffness can be a more difficult task than ensuring sufficient strength. If the stiffness of the cross-frames approaches or exceeds that necessitated to restrain the girders, they can provide "nuisance stiffness" that increase stresses in the bottom flange that are not typically accounted for in design (Ozgur 2011). Increases in undesirable stiffness of the girders due to the location and stiffness of cross-frames/diaphragms often occur near skewed supports as well (Krupicka and Poellot 1993). Simply increasing the cross-sectional properties of the cross-frame members can increase both the unwanted stiffness of the cross-frames and induce greater internal forces in its members. These forces can be significantly greater than girder stresses in highly-skewed bridges (McConnell et al. 2013).

As a result, cross-frames are required by AASHTO to be oriented perpendicular to the girder line for skew angles greater than 20°, due to smaller cross-frame forces and smaller demand-to-capacity ratios for cross-frame stresses compared to cross-frames oriented parallel to the girder line. While this decreased stiffness would lead to greater lateral bending stresses in girders with cross-frames in the staggered configuration, studies showed that these lateral bending stresses were of low magnitudes (McConnell and Radovic 2014). Therefore, small increases in girder lateral stresses is seen as an efficient tradeoff for reduced cross-frame stresses afforded by placing cross-frames perpendicular to the girder. This is especially significant since cross-frames stresses are generally closer in magnitude to their limiting stresses than the girder stresses are to their yielding stresses (McConnell and Radovic 2014).

By orienting cross-frames perpendicular to the girder line, cross-frame forces are reduced at the expense of increased lateral bending stresses in flanges. However, the vertical displacements at the opposite ends of a given brace can differ substantially in a skewed-staggered bracing layout. This can result in large live load induced forces and fatigue stresses, with stiffer braces attracting larger forces (Hassel et al. 2012). While the influence of skew had little effect on the strength and stiffness requirements of the bracing oriented perpendicular to the girder lines, when bracing is oriented parallel to the skew angle, skew angle has a significant impact on the stiffness and strength requirements of the bracing (Wang and Helwig 2008). Brace elements should be designed for the basic stability requirements, considering the effects of cross-frame layout, stiffness, and strength requirements.

The objective of this study was to quantify the effects of cross-frame orientation and cross-frame spacing on lateral flange bending stresses during the construction phase and to evaluate AASHTO's interaction requirement of weak-axis and strong-axis bending demands on the flanges. Stability of the bridge girders is especially of concern during the construction stages of composite bridges, before the concrete deck is acting compositely with the steel girders, and in non-composite bridges. Additionally, stability of bridge girders must be accounted for in design of girders in negative bending regions, even after composite action has been achieved between the girder and deck. If cross-frames/diaphragms are carried parallel to the skew angle for skews up to 40° in a non-composite bridge or in a negative bending moment region of a composite bridge, those brace elements must be carefully designed such that they have sufficient strength and stiffness to brace the girders against lateral torsional buckling. Detailed three-dimensional solid finite element models were used to investigate these parameters. The suite of models included the following parameter variations:

- skew angle (0°, 20°, and 40°);
- cross-frame spacing (4.57 m [15 ft] and 9.1 m [30 ft]);
- and cross-frame orientation (skewed-staggered, skewed-parallel, and skewed-unstaggered)

BRIDGE GEOMETRY

The bridge geometry used within this study was adapted from American Iron and Steel Institute (AISI) Design Example 2 (AISI 1997). This geometry can be considered reasonably typical for a multi-girder highway overpass and its design is well-understood and widely available. The bridge consists two 27.4 m [90 ft] spans, composed of four continuous girders spaced at 3.1 m [10 ft] as presented in Figure 2.1. The girders were studied here in the non-composite condition, representative of bridge characteristics during construction. The girders were topped with a 203 mm [8.0 in] thick wet concrete deck with a 1.1 m [3.5 ft] roadway overhang and a 0.7 m [2.3 ft] construction walkway. The total deck width was 12.7 m [41.7 ft]. Both the roadway overhang and construction walkway were considered to be supported by 1.8 m [70 in] C-49-D overhang brackets, shown in Figure 2.2, spaced 1.0 m [40 in] on center. Separate built-up cross-sections were used in regions of positive and negative bending, as shown in (a) and 1(b). Each girder was supported by a pin at the central pier and roller supports at both ends.

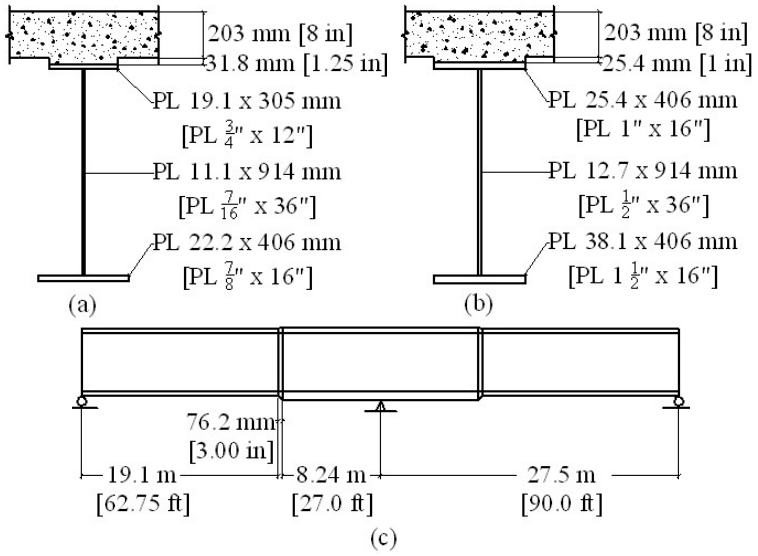

Figure 2.1 (a) Positive girder cross-section; (b) Negative girder cross-section; (c) Location of positive and negative cross-sections.

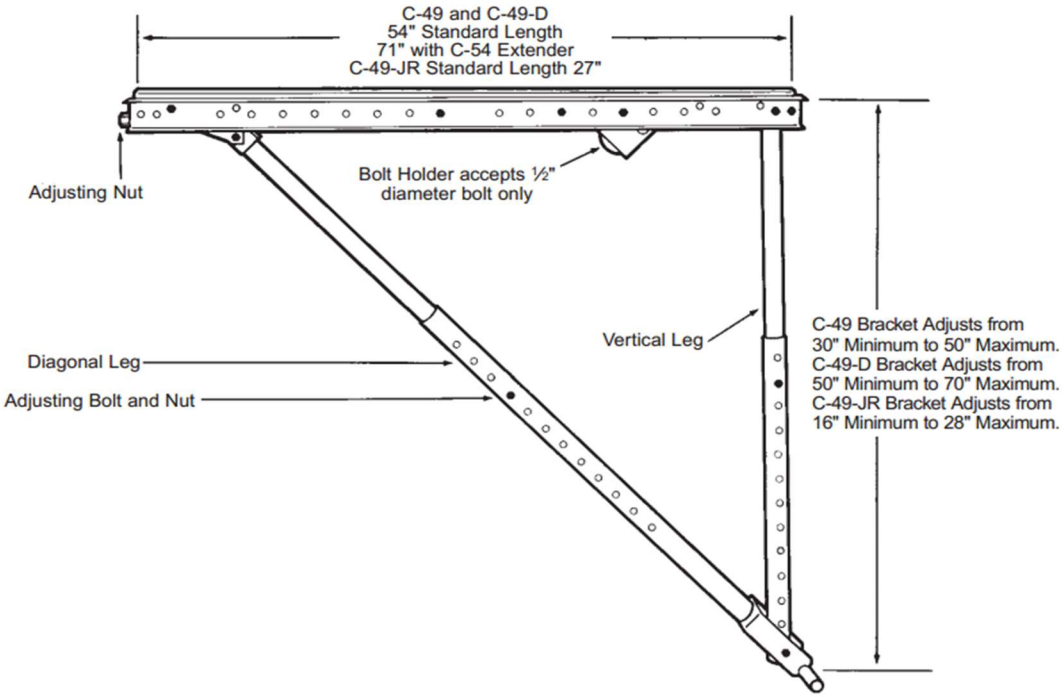

Figure 2.2 C-49 Overhang Bracket

Bridges with skewed supports are designed as such to accommodate highway alignment. Bracing may be placed parallel to the skew angle, or perpendicular to the girder line, in a staggered or unstaggered configuration. These configurations, shown in Figure 2.3 will be referred to as skewed-parallel, skewed-staggered, and skewed-unstaggered, respectively.

For all cases studied, the bridge system was modeled as in construction with girders and cross-frames in place but the concrete deck still wet. Therefore, the load induced by the weight of the concrete was considered, but the deck stiffness was considered not present.

AASHTO requires that bracing be placed perpendicular to the girder line whenever the skew angle is greater than 20°. However, KDOT design provisions allow the use of skewed-parallel configuration for angles up to 40° to reduce potential differential deflection and associated distortion-induced fatigue (KDOT 2010). For the analyses performed in this study, results for the skewed-parallel, skewed-staggered, and skewed-unstaggered configurations with 0°, 20°, and 40° skews were considered. Cross-frame spacing of 4.57 m [15 ft] and 9.1 m [30 ft] were modeled to study effects on lateral flange bending and system stability, although usually brace spacing is kept to less than 7.62 m [25 ft].

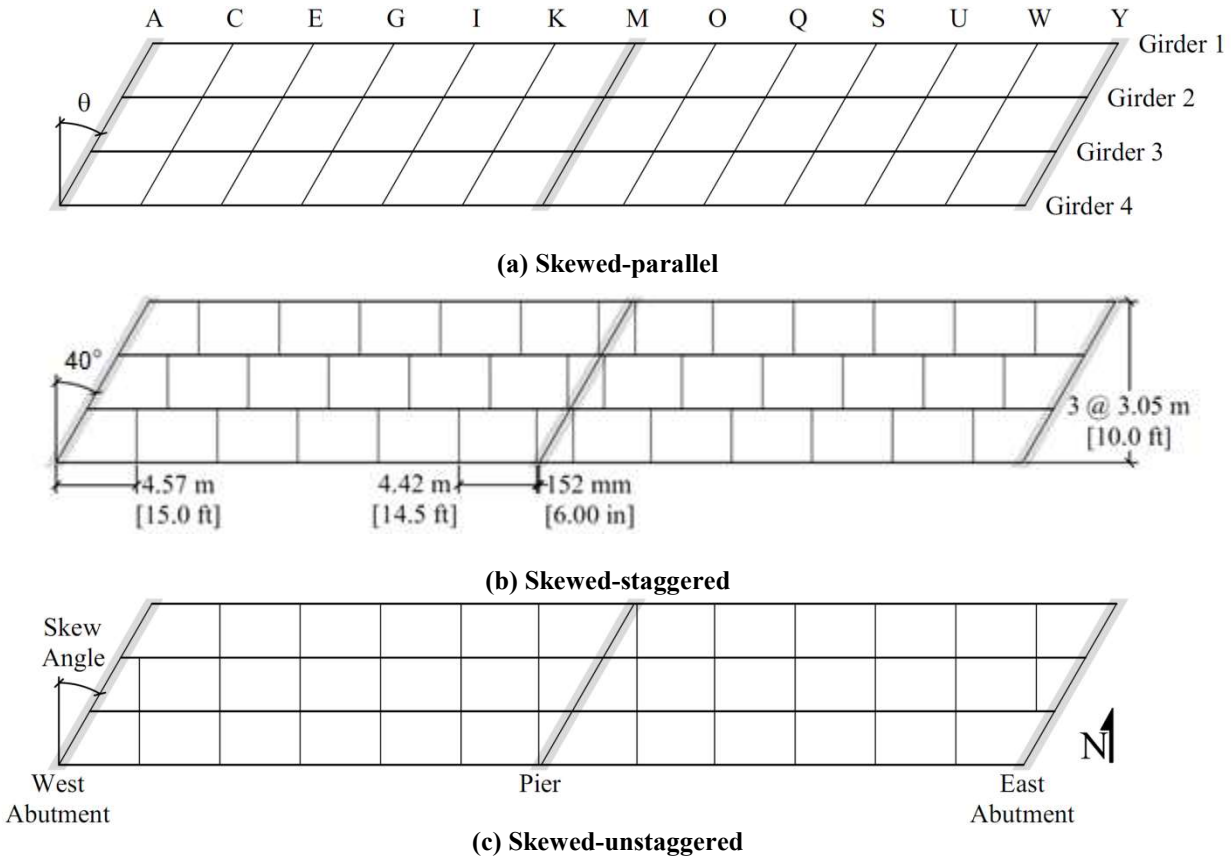

Figure 2.3 Bridge configurations (40° degree skew with 4.57 m [15.0 ft] cross-frame spacing)

Cross-frames, referring to truss-type lateral braces placed at discrete locations along a bridge layout, were used in all bridge configurations studied and consisted of three equal-leg angles spanning between connection stiffeners. A square plate was used to connect the diagonal legs at mid-length, as shown in Figure 2.4. Both connection stiffeners were modeled as being tied directly to the web and top and bottom flanges; attaching the connection stiffeners to the adjacent flanges is representative of current practice (post-1980s detailing). In bridges with skewed-parallel configurations, cross-frame length increased with skew angle and bent plate stiffeners were used to capture realistic construction considerations. The slenderness ratio for the

single angles was computed using provisions in American Institute of Steel Construction's Steel Construction Manual (AISC Manual, 2010) Section E5, and cross-frame stiffness was compared based on the approximate relative stiffness, $A\cos^3\theta$,where A is the cross-sectional area of one angle and θ is the skew angle (Yura 2001; Wang & Helwig 2008). This was done to ensure that cross-frames selected in the different models had similar stiffnesses. A slenderness ratio of approximately 140 was used for all angles, which is a commonly-used slenderness limit in design. An L108 x 108 x 12.7 mm [4-1/4 x 4-1/4 x 1/2 in] angle was selected for the skewed-staggered bridge. An L114 x 114 x 15.9 mm [4-1/2 x 4-1/2 x 5/8 in] angle was selected for the 20° skewed-parallel bridge. An L140 x 140 x 15.9 mm [5-1/2 x 5-1/2 x 5/8 in] angle was selected for the 40° skewed-parallel bridge. More details regarding the brace sizing and rationale are provided in Hassel (2011). Appendix F describes how framing of the angle members and work point may affect the behavior of the brace.

The design of the cross-frames in this study was designed solely based on an approximate relative stiffness and appropriate slenderness ratio. While the slenderness ratio is a typical value used in design, it is not based on a specific code requirement or optimized for this particular bridge geometry. In the design of the cross-frames, several other considerations will come into play such as fit-up of the cross-frames to the girders as well as fit-up of the angle members that make up the cross-frames. The type of brace pattern used will need to be determined, where different patterns may be selected for different parts of the bridge. Serviceability and fatigue requirements for the cross-frame members and connections will also need to be addressed. These requirements will change with different skew angles and orientations. The cross-frames selected for the models used were not meant to address these design considerations but only to provide

insight into the behavior of a lateral load transferring system for a theoretical, pre-designed bridge adapted from American Iron and Steel Institute (AISI) Design Example 2 (AISI 1997).

Connection stiffener dimensions are shown in Figure 2.4. A thickness of 9.5 mm [3/8 in] was selected for all connection stiffeners in skewed bridges with 4.57 m [15 ft] and 9.1 m [30 ft] cross-frame spacing.

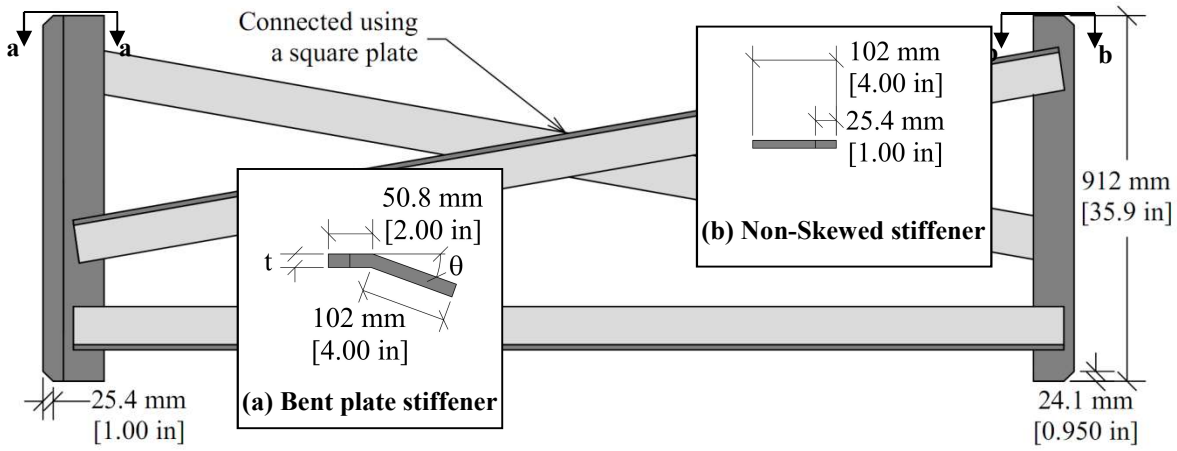

Figure 2.4 Connection stiffener geometry

Abutment diaphragms were modeled as having three equal-leg angle cross-sections spanning between connections plates in a K-brace, shown in Figure 2.5. A gusset plate was used to connect the diagonal legs to the bottom horizontal angle. The diagonal legs were tied directly to a MC12x50, which spans between connection stiffeners. An L108 x 108 x 12.7 mm [L4-1/4 x 4-1/4 x 1/2 in] angle was selected for the skewed-staggered bridge. An L114 x 114 x 15.9 mm [4-1/2 x 4-1/2 x 5/8 in] angle was selected for the 20° skewed-parallel bridge. An L140 x 140 x 15.9 mm [5-1/2 x 5-1/2 x 5/8 in] angle was selected for the 40° skewed-parallel bridge. The abutment connection stiffeners were tied to the web and top and bottom flanges. Abutment connection

stiffener dimensions are shown in Figure 2.5. An abutment connection stiffener thickness of 25.4 mm [1.0 in] was selected for all bridges.

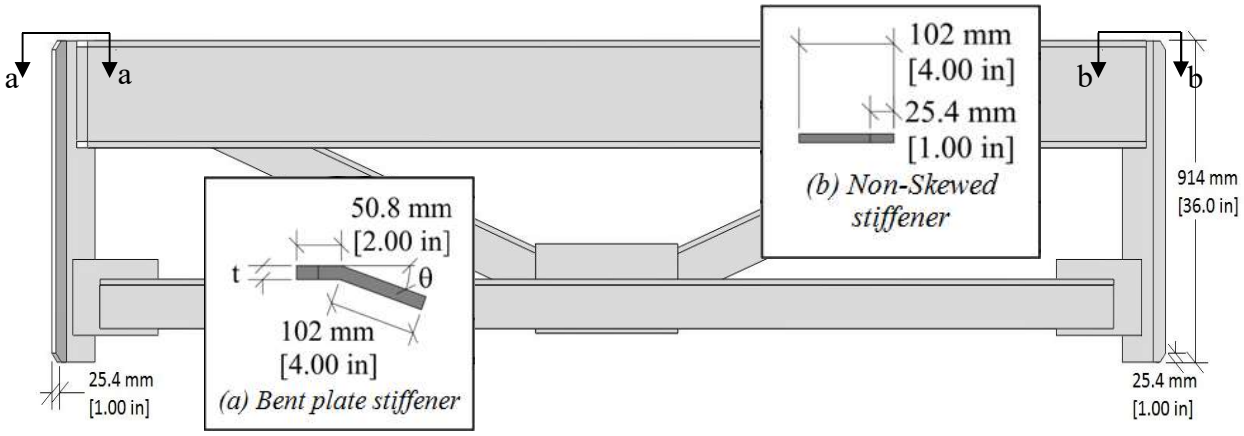

Figure 2.5 Abutment diaphragm and connection stiffener geometry

Intermediate transverse stiffeners with a thickness of 9.5 mm [1/2 in] were modeled every 4.57 m [15 ft] in bridges with 9.14 m [30 ft] cross-frame spacing. Figure 2.6 shows the transverse stiffener placement in a finite element model of the bridge with 9.14m [30 ft] cross-frame spacing. No intermediate transverse stiffeners were modeled in bridges with 4.57 m [15 ft] cross-frame spacing. 12.7 mm [1/2 in] thick transverse stiffeners were also used to stiffen the girder web at the abutments and pier supports. Two stiffeners spaced at 406 cm [16 in] were placed at each abutment girder support on each side of the web, except for the exterior girders where two additional stiffeners were placed 203 mm [8 in] apart on the exterior side of the web. Three 12.7 mm [1/2 in] thick transverse stiffeners spaced 203 mm [8 in] apart were placed on the exterior side of the web of the exterior girders at the center piers. Transverse stiffeners were tied directly to the web and to the top and bottom flanges.

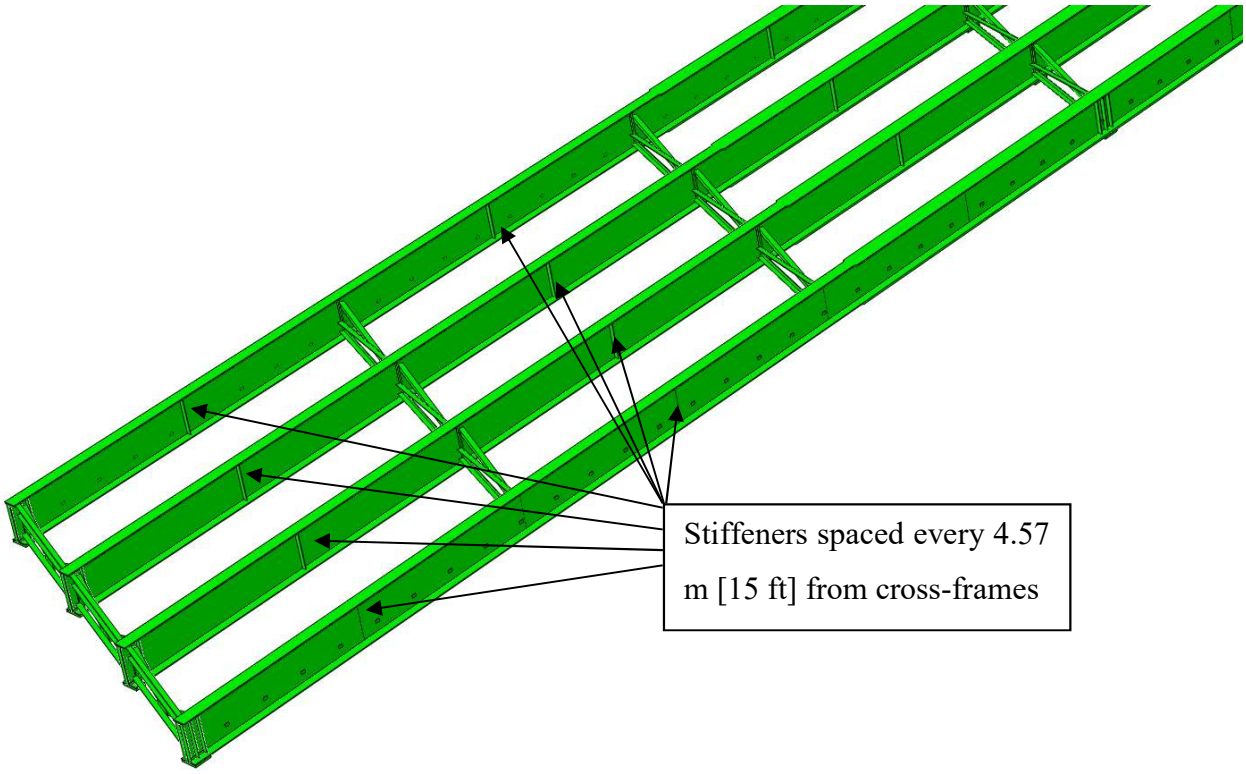

Figure 2.6 Stiffener placement in bridges with 9.14 m [30 ft] cross-frame spacing

MODELING METHODOLOGY

Three-dimensional, solid-element finite element (FE) models of the entire bridge were constructed using Abaqus v.6.10-2 for parametric analysis (Simulia, 2010). An example of one the bridge models is represented in Figure 2.7. C3D8R brick elements were used in the majority of the model, but C3D4 tetrahedral and C3D6 wedge elements were used to transition between mesh sizes where needed. Geometric nonlinearity was considered within the analyses.

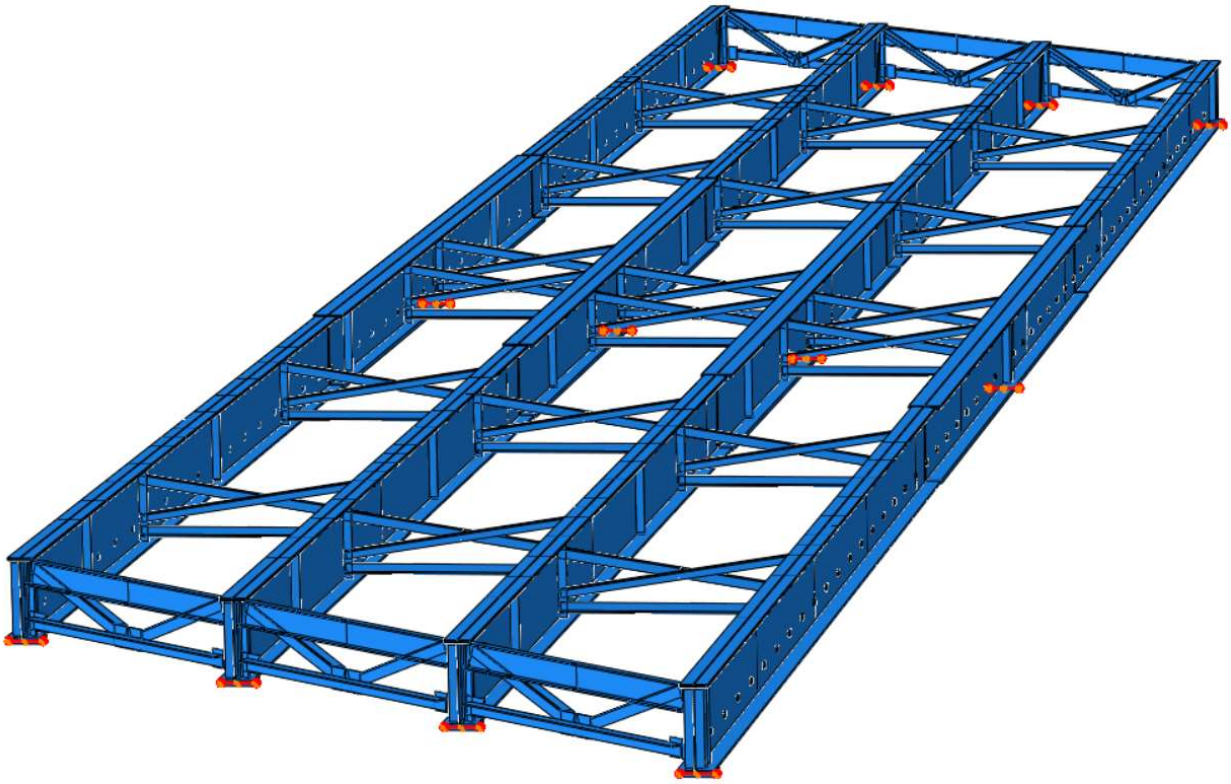

Figure 2.7 3D FEM model geometry of skewed-staggered bridge configuration (9.14 m [30 ft] cross-frame spacing)

Girder flanges and webs were modeled to have a modulus of elasticity of 200,000 MPa [29,000 ksi] and Poisson's ratio of 0.3. A mesh size of 25.4 mm [1 in] was used for web and

flange elements. The cross-frame angles were partitioned such that each leg was divided into two equal lengths and each angle into four equal parts, as shown in Figure 2.8. The cross-frame angles and stiffeners were then merged in Abaqus retaining intersecting boundaries. This procedure allowed the mesh to have a consistent size throughout each of the cross-frame members. A mesh size of 127 mm [5 in] was used for abutment diaphragm and cross-frames. A finer mesh size for the cross-frames resulted in convergence errors in some models. A mesh size of 965 mm [38 in] was used for the top flange covers, the purpose of which is described later. For all other parts, including transverse stiffeners, plates, and bearing pads, the mesh size was equal to the thickness of the part.

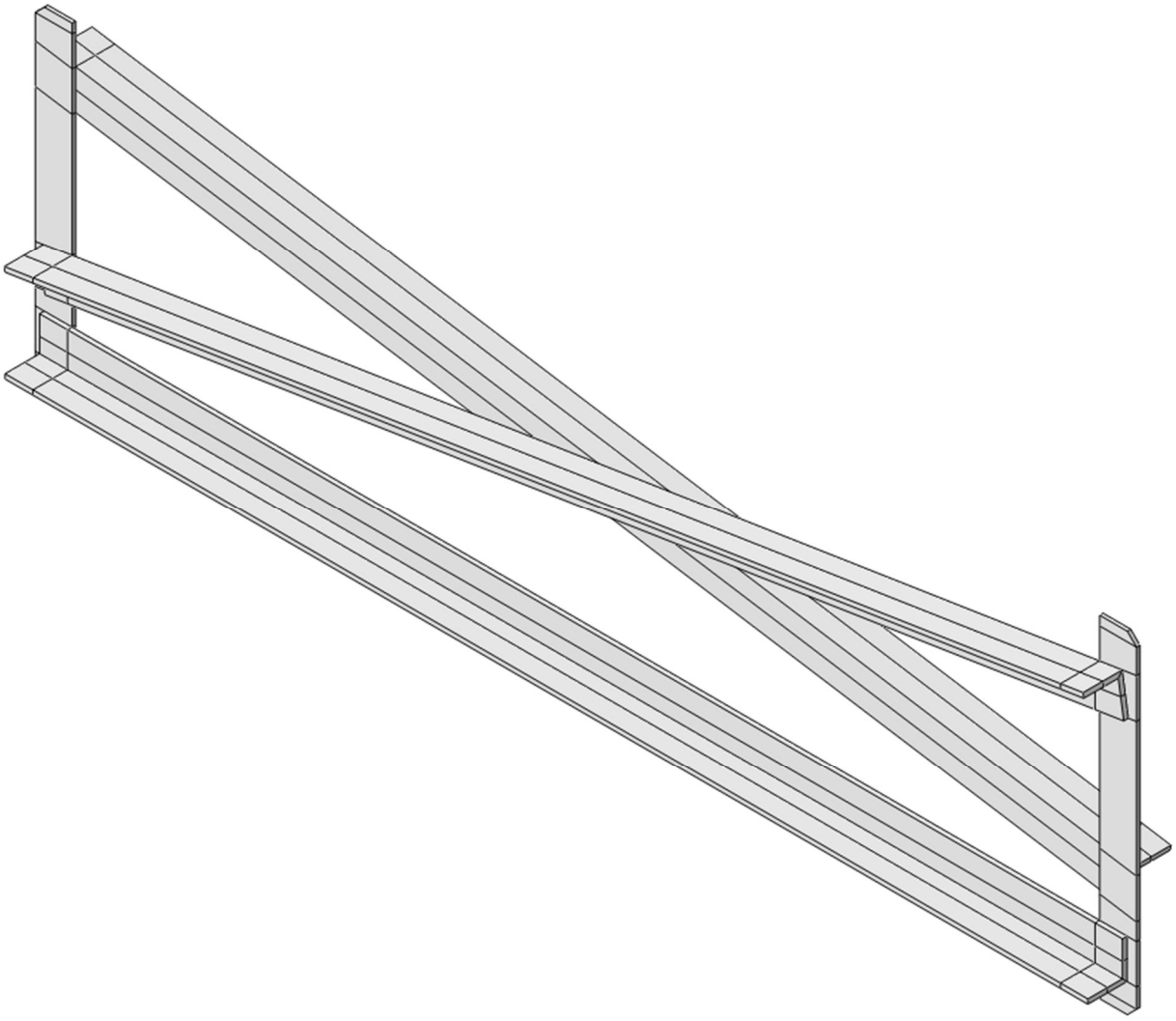

Figure 2.8 Cross-frame Angle Partitions

Steel overhang brackets typically support the construction walkway and screed rail during the construction phase of a bridge structure. The overhang brackets were not modeled directly within the parametric analysis, but the loads that they induced on the exterior girders were included in the parametric analysis. Reaction forces from the brackets on the web were calculated using a preliminary structural analysis model created in Mastan2 (Ziemian and McGuire 2000), shown in Figure 2.9, and applied to 63.5x102 mm [2-1/2 x 4 in] bracket plates

that were connected to the web using tie constraints. A total of 53 brackets spaced at 1 m [40 in] on center were used and each overhang bracket was modeled to be 1.8 m [70 in] long. Overhang brackets modeled in the preliminary Mastan2 analysis were considered to hold three 51x51 mm [2x2 in] wall stud joists (timber) supporting the 711 mm [28 in] wide construction walkway and a 102x102 mm [4x4 in] stud (timber) supporting the screed rail on each side of the bridge. Walkway loads were distributed over timber studs spaced 305 mm [12 in] on center.

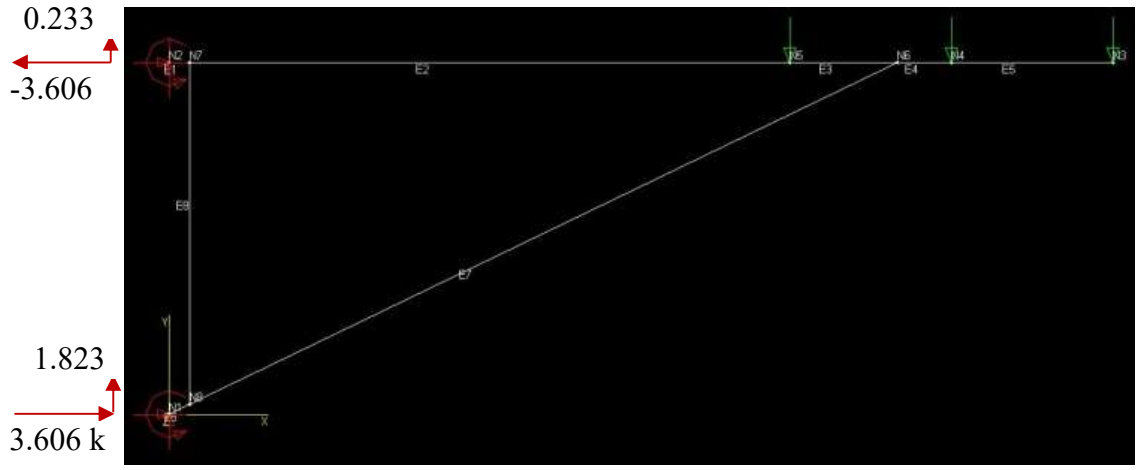

Figure 2.9 Bracket forces calculated from preliminary beam analysis performed in Mastan2

Plywood formwork supporting the wet concrete deck, typically used during construction, was not included in the parametric models because the slight stiffness contribution from the attached plywood was found to unrealistically affect lateral bending stresses within the models. Since real connections between plywood formwork and steel girders are generally not considered to develop sufficient lateral support, designers rightfully neglect the contributions of such formwork. Therefore, it was determined that the models would better reflect design practices by neglecting the plywood formwork.

Given the severe geometric nonlinear characteristics of the models, it was not surprising that significant challenges with convergence were initially encountered and high-order buckling modes occurred as modeling artifacts. To eliminate the high-order buckling modes that tended to occur in girder flanges in trial model executions, a very thin and flexible top flange "cover", with the same width as the top flange, was used to damp localized responses in the top flange. This compliant layer was assigned a thickness of 25 mm [1.0 in] in the positive moment region and 13 mm [1/2 in] in the negative moment region to accommodate the difference in thickness of the top flange in these two regions. The compliant layer was assigned a modulus of elasticity of 6895 MPa [1000 ksi]. Due to its low stiffness, use of this model control technique did not significantly affect the bending moment results, and this was verified through a comparison of models that included / did not include the compliant layer on the flange. To help mitigate localized instabilities, a dissipated energy fraction of 0.0002 with a maximum ratio of stabilization to strain energy of 0.05 was specified for automatic stabilization.

Surface-to-surface tie constraints were used to attach parts within models. Welds were not explicitly modeled, but rather, webs were tied directly to the flanges and all stiffeners were tied directly to the web and flanges. A 25.4 mm [1.0 in] triangular "weld" 406 mm [16 in] long was tied to the web and flanges at the girder ends to reduce high, localized stresses at abutment ends; this was necessary to achieve convergence in the models. Girder boundary conditions were modeled by applying a translational constraint over a narrow, 12.7 mm [1/2 in] strip of the bearing plate at support locations, shown in Figure 2.10. The square 406 mm [16 in] bearing plate was 51 mm [2.0 in] thick and was tied to the bottom flange at the mid-span and ends of the girders. Pinned support conditions were used to represent the center pier while roller support conditions were used to represent abutment piers.

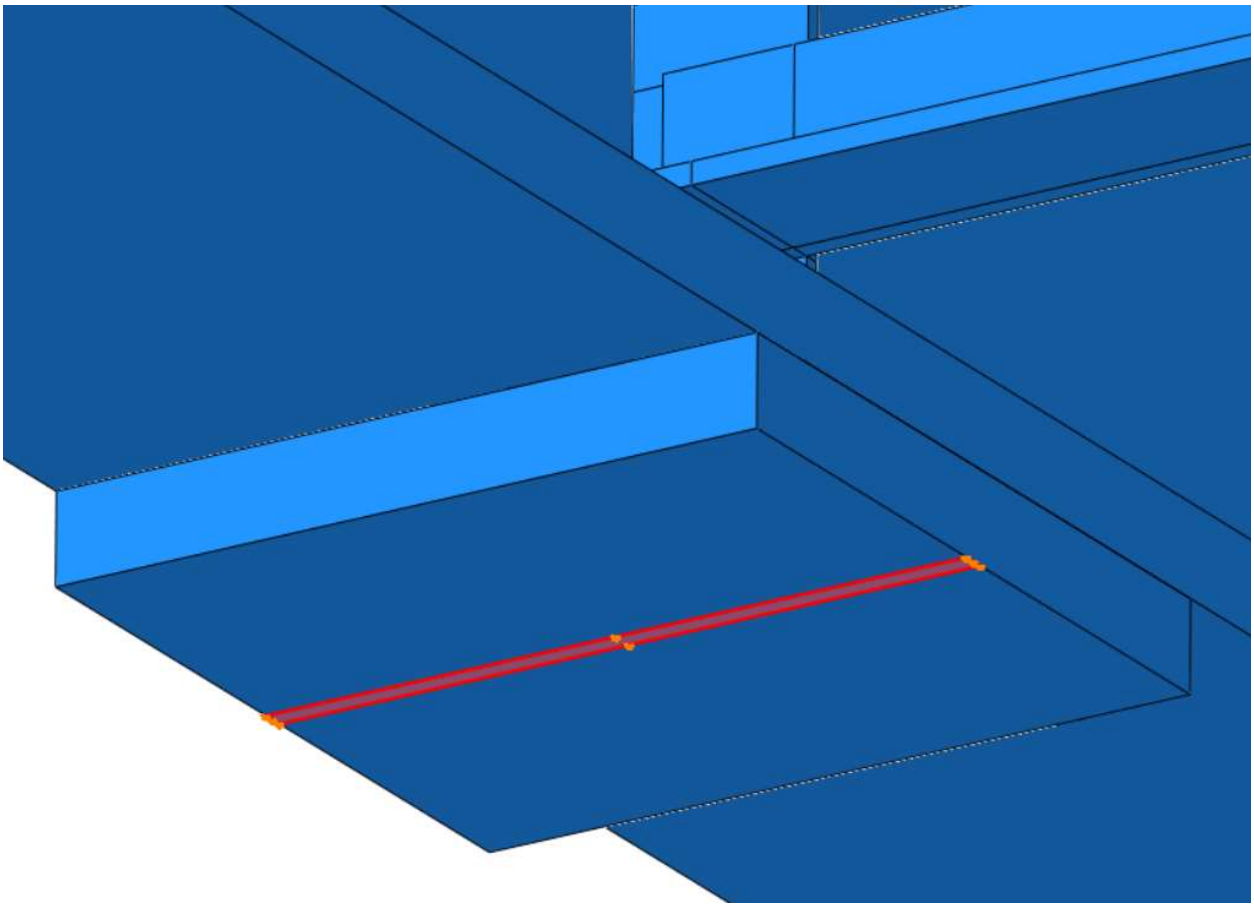

Figure 2.10 Bearing plate and boundary condition at support locations

APPLIED LOADS

The following dead and live loads applied in the models during the construction stage were based on The Kansas Department of Transportation Design Manual: Volume III Section 5.3 (KDOT 2010).

- A 203 mm [8.0 in] thick wet concrete deck with a density of 2563 kg/m^3 [160 lb/ft^3] was applied as a uniform pressure over the vertical projection of the web on the top flange cover and roadway overhang. The density included the weight of reinforcing steel and forms.
- A 27.2 mm [1.1 in] effective height of the concrete deck haunches was applied as a uniform pressure using a 2563 kg/m^3 [160 lb/ft^3] density over the vertical projection of the web on the top flange cover. This density included the weight of reinforcing steel and forms.
- Steel weight was applied to all steel parts (i.e. girders, stiffeners, and cross-frames) as a gravity load using a density of 7849 kg/m^3 [490 lb/ft^3].
- A 366 kg/m^2 [75 lb/ft^2] construction live load was applied as a uniform pressure over the vertical projection of the web on the top flange cover.
- A 744 kg/m [500 lb/ft] screed load was applied as a uniform pressure over a width of 102 mm [4.0 in] on the plywood screed rail. The reaction force from the bracket overhang was applied to the bracket plate on the girder web.
- A 801 kg/m^3 [50.0 lb/ft^3] walkway load was applied as a uniform pressure over the construction 711 mm [28 in] walkway surface. The reaction force from the bracket overhang was applied to the bracket plate on the girder web.

Dead and live loads from the tributary area on the deck were applied as a 13 mm [1/2 in] wide uniform pressure over the vertical projection of the web on the top flange cover, as shown in Figure 2.11. These loads were applied over the vertical web projection on the top flange cover rather than over the entire flange cover to prevent further artifacts of high-order buckling from occurring in the top flange. Screed and walkway loads were carried by overhang brackets. Reaction forces from the screed and walkway loads on the brackets were calculated using finite element analysis, as discussed. The horizontal component of the reaction force was applied over a 64 mm [2.5 in] by 102 mm [4.0 in] bracket plate tied to the web, as described previously.

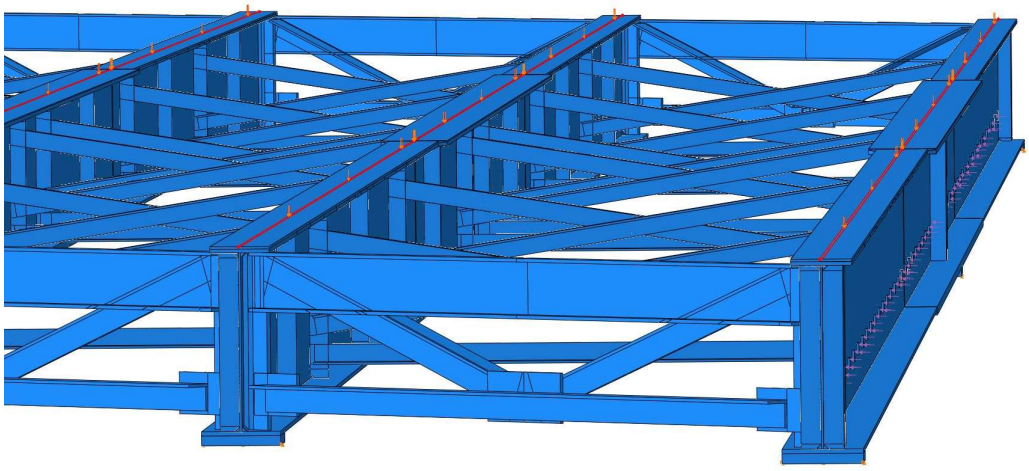

Figure 2.11 Deck dead load and construction live load applied to a bridge system model

Load combinations and load factors are presented in AASHTO Section 3.4 (AASHTO 2010). The Strength load combinations and load factors from AASHTO Table 3.4.1-1 were found to produce the controlling load combination during the construction stage (Zhou et al. 2015). Of

the Strength load combinations and load factors, Strength 1 was found to produce the largest stresses for all bridge configurations. Therefore, the Strength 1 load combination and load factor were used in the analyses.

Strength 1 (S1): 1.25 DC + 1.25 DW + 1.75 LL

Strength 3 (S2): 1.25 DC + 1.25 DW + 1.4 WS (including uplift)

Strength 4 (S4): 1.50 DC + 1.50 DW

Strength 5 (S5): 1.25 DC + 1.25 DW + 1.35 LL + 0.4 WS (no uplift)

where

DC = dead load of structural components

DW = dead load of wearing surface

LL = construction live load

WS = wind load on structure

STRESS CALCULATIONS

Flexural stresses, σ, were calculated from these moments using the bending stress equation:

$$\sigma = Mc/I$$

where:

M = flange or section bending moment

c = distance from the extreme fiber to the neutral axis

I = moment of inertia of the flange or section

Major and minor axis bending moments about the girder cross-section were obtained using section cuts along Girder 3 and Girder 4. Girder 3 is an interior girder, and Girder 4 is an

exterior girder; thus, different behavior was expected to occur between those girders. Due to symmetry within the models, Girder 3 produced similar results compared to Girder 2 (the other interior girder) and Girder 4 produced similar results compared to Girder 1 (the other exterior girder). Therefore, only Girder 3 and Girder 4 stresses are presented.

A free body cross-section in Abaqus is an area across which resultant forces and moments can be computed. Once such a cross-section is defined within the model, output vectors can include the magnitude and direction of the resultant moments across the specified area. Figure 2.12 shows the resultant moments occurring over the entire girder section (Figure 2.12a) and over just a flange (Figure 2.12b).

In all cases, moment values were extracted from locations where cross-frames connected to the web (where lateral flange bending stresses were expected to be at a maximum) and at the mid-point between two cross-frame locations along the girder (where localized effects were expected to be least influential).

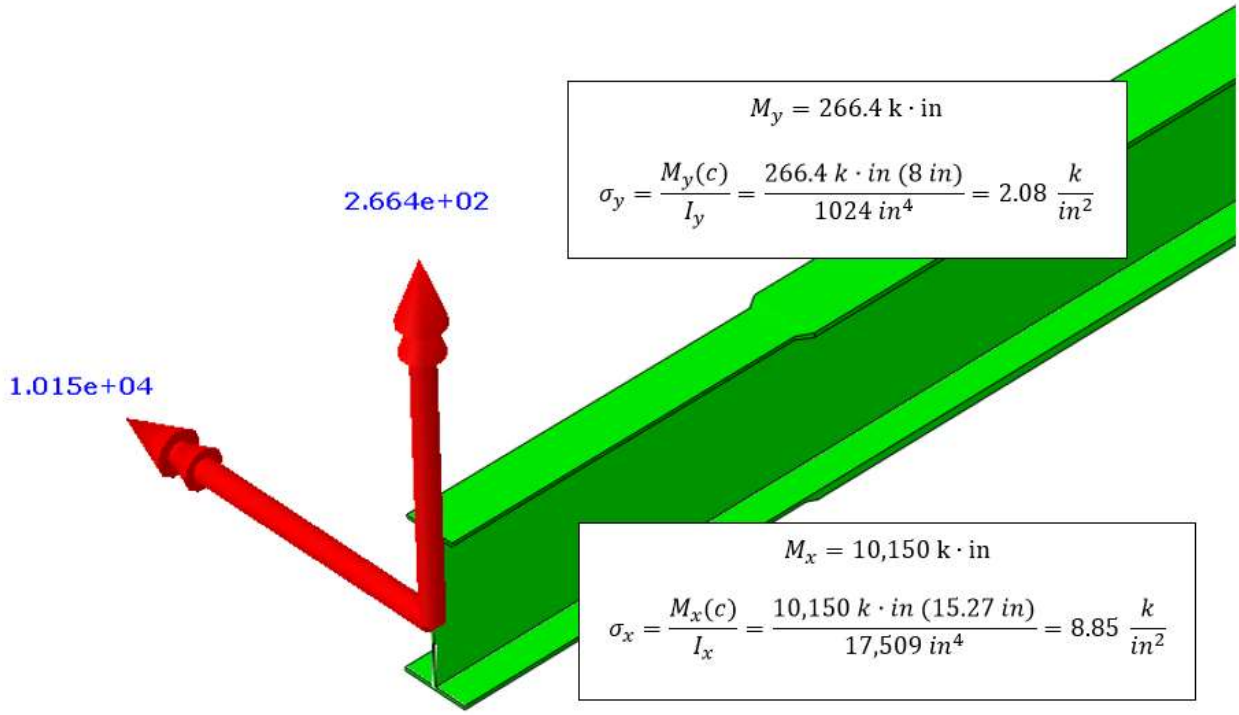

(a) Girder Section

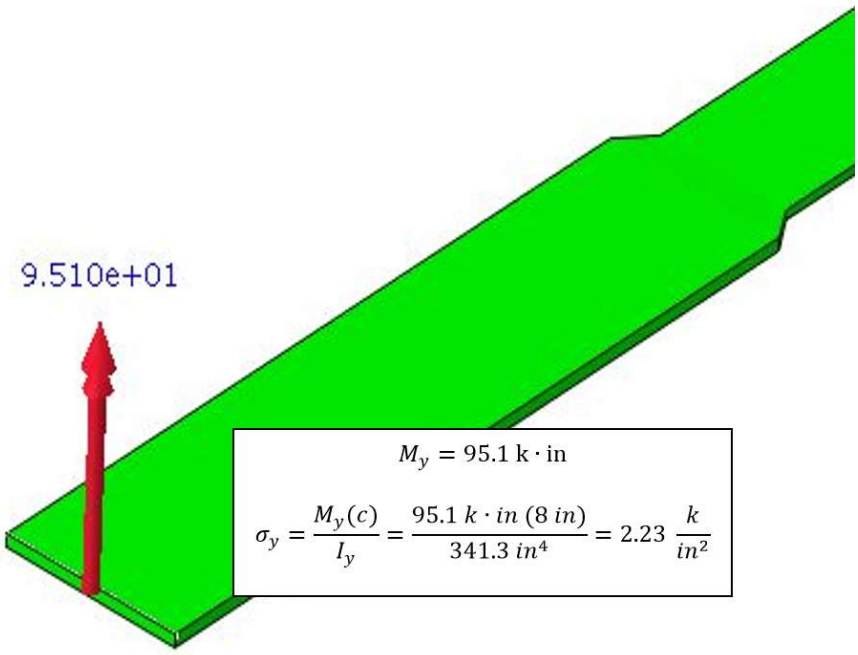

(b) Top Flange Section

Figure 2.12 Resultant moments displayed on the free body section and sample stress computation for (a) Girder Section and (b) Top Flange Section

STRONG-AXIS BENDING STRESS COMPUTATIONS

For the girder section in strong-axis bending in the positive flexure region, c was -538 mm [-21.2 in] from the top (compression) flange to the neutral axis. The girder section had an I_x value of 3.86×10^{-4} m^4 [9278 in^4] in strong-axis bending for the positive flexure region. For the girder section in strong-axis bending in the negative flexure region, the c value was 389 mm [15.3 in] taken from the bottom (compression) flange to the neutral axis. The girder section had an I_x value of 7.28×10^{-4} m^4 [17500 in^4] in strong-axis bending for the negative flexure region. Appendix B shows the interior and exterior girder design computations in both the positive and negative flexure regions.

Figure 2.12**Error! Reference source not found.** shows an illustration of the strong-axis bending stress distributions computed for the compression flange in a 40° skewed-parallel bridge with 13.7 m [45 ft] cross-frame spacing.

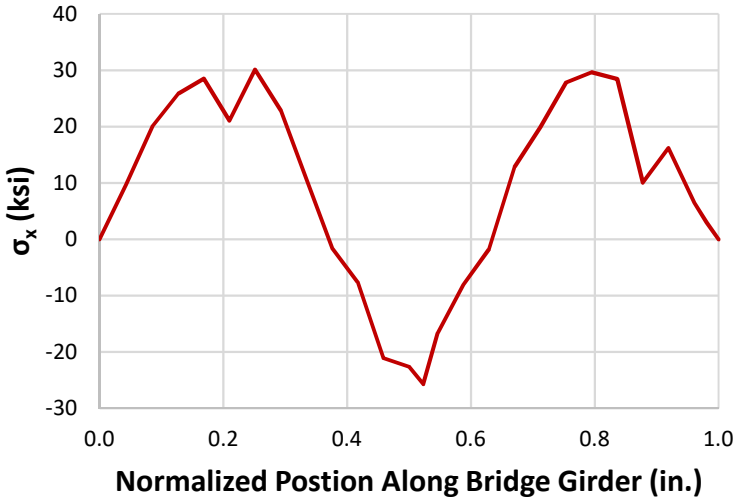

Figure 2.13 Girder 4 strong-axis sectional stresses (computed from M_x) in the 40° skewed-parallel bridge with 13.7 m [45 ft] cross-frame spacing.

WEAK-AXIS BENDING STRESS COMPUTATIONS

Two methods for computing lateral flange bending stresses were used:

(1) Weak-axis stresses in the flanges were computed using the weak-axis moment, M_y, extracted over the full-depth of the cross-section. Figure 2.14 shows an illustration of the weak-axis bending stress distributions computed for the compression flange in a 40° skewed-parallel bridge with 13.7 m [45 ft] cross-frame spacing. This moment was used in conjunction with the weak-axis bending moment of inertia for the entire cross-section. In this case, the *c* value was taken as 203 mm [8 in] for both the positive and negative regions. The girder section had an I_y value of 1.69×10^{-4} m^4 [407 in^4] in weak-axis bending for the positive flexure region and an I_y value of 4.26×10^{-4} m^4 [1024 in^4] in weak-axis bending for the negative flexure region.

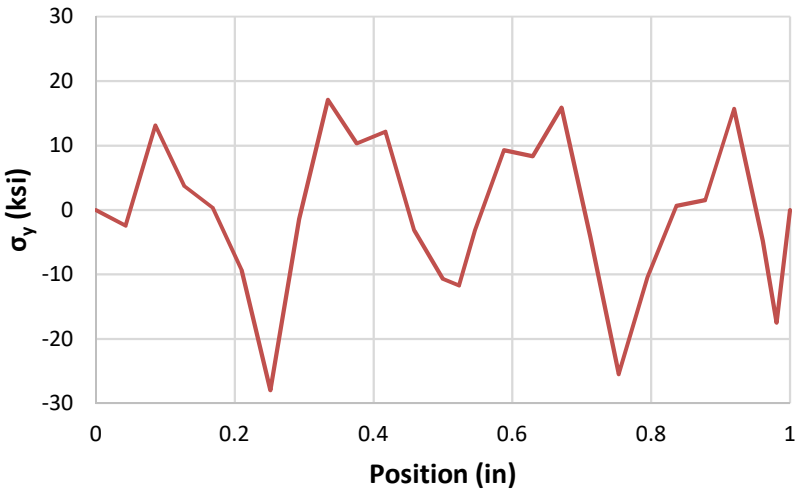

Figure 2.14 Girder 4 weak-axis sectional stress (computed from M_y) in the 40° skewed-parallel bridge with 13.7 m [45 ft] cross-frame spacing.

(2) Weak-axis stresses in the flanges were also computed using moments that were extracted from the top and bottom flanges, individually. When using this method, the moments were used in conjunction with the weak-axis bending moment of inertia for just the appropriate

flange section. The top flange section cut is shown in Figure 2.12(b) along with the resultant lateral flange bending moment. While AASHTO does not offer any guidance on which section to use when computing weak-axis bending stresses, other researchers (Jung and White 2006) have used elastic lateral bending stress, f_l, calculated from the flanges.

The top flange had a c value of 152 mm [6.0 in] in out-of-plane bending and an $I_{y,fl}$ value of 4.50×10^{-5} m^4 [108 in^4] in the positive flexure region and a c value of 203 mm [8.0 in] and an $I_{y,fl}$ value of 1.42×10^{-4} m^4 [341 in^4] in the negative flexure region. The bottom flange had a c value of 203 mm [8.0 in] in out-of-plane bending and an $I_{y,fl}$ value of 1.24×10^{-4} m^4 [298 in^4] in the positive flexure region and a c value of 203 mm [8.0 in] and an $I_{y,fl}$ value of 2.13×10^{-4} m^4 [683 in^4] in the negative flexure region.

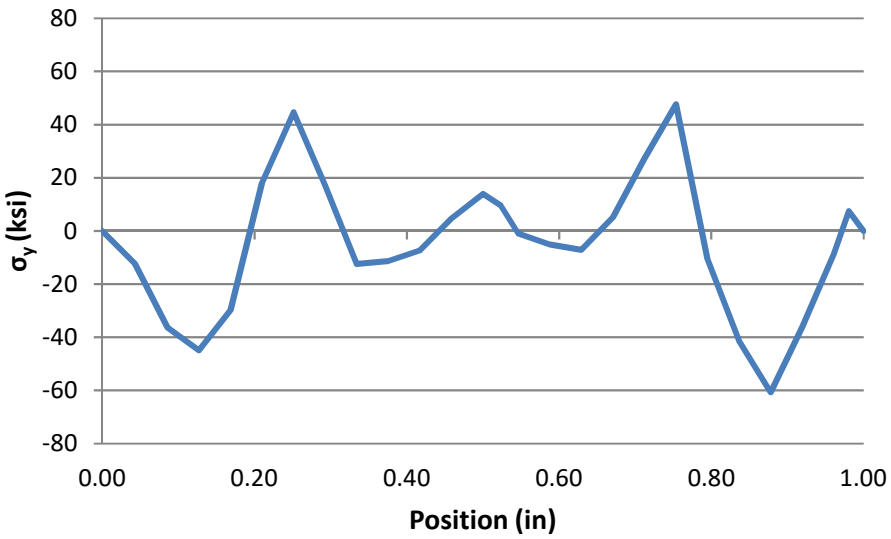

Figure 2.15 Girder 4 top flange out-of-plane stress (computed from $M_{y,fl}$) in the 40° skewed-parallel bridge with 13.7 m [45 ft] cross-frame spacing.

Comparison of Stresses Computed from Moments and Model-Extracted Stresses

Stresses were extracted directly from the top flange of Girder 4 in the FE models to compare against flexural stresses calculated from the bending moment. This comparison was performed because the stresses extracted directly from the models can be expected to include contributions from all directions of loading, and the comparison allowed for an assessment of the reasonableness of the assumption of pure strong-axis and pure weak-axis bending stress computations described in the previous two sections. The results between stresses directly extracted from the model and calculating stresses from bending moments were found to be congruent. Stresses were extracted from paths along the extreme edges and centerline of the exterior girder's top flange, as shown in Figure 2.16. Since stresses were obtained at every nodal point along the path, localized effects along the flange created a lot of noise in the data, resulting in the "choppiness" of the graphs. Stresses computed from moments were averaged across the section and therefore removed much of this noise. *S11* is indicative of stresses in the out-of-plane direction relative to the bridge girder line. *S22* are stresses in the vertical direction, and *S33* are stresses in the longitudinal direction. *S33* captures bending stresses about both strong and weak axes. Stresses – both computed and directly extracted – for the 40° skewed-parallel bridge with 13.7 m [45 ft] cross-frame spacing are shown in Figure 2.17 through Figure 2.20. While it is readily acknowledged that a 13.7 m [45 ft] cross-frame spacing is atypical of bridges constructed, the method for measuring and extracting element stresses would remain valid for any model type. *S33* stresses along the center Path B, shown in Figure 2.17, were comparable to strong-axis sectional stresses calculated from bending moments. Strong-axis bending stress was

found to dominate stresses at the center of the flange. The average of the two edge stresses in Figure 2.17 also produced values similar to the strong-axis bending stress. The average of the difference between S33 Path A and S33 Path C produced similar results compared to the top flange out-of-plane bending stress, shown in Figure 2.18 and Figure 2.19; the values are inverted for Path A stresses compared to Path C stresses due to sign convention. Given the general agreement, especially in trend, between extracted and computed stresses, the results for stresses are presented in terms of computed stresses.

Axial stress values, shown in Figure 2.20, were also examined. They were found to be small compared to strong and weak-axis sectional stresses at non-cross-frame locations and are not presented for the other bridge models.

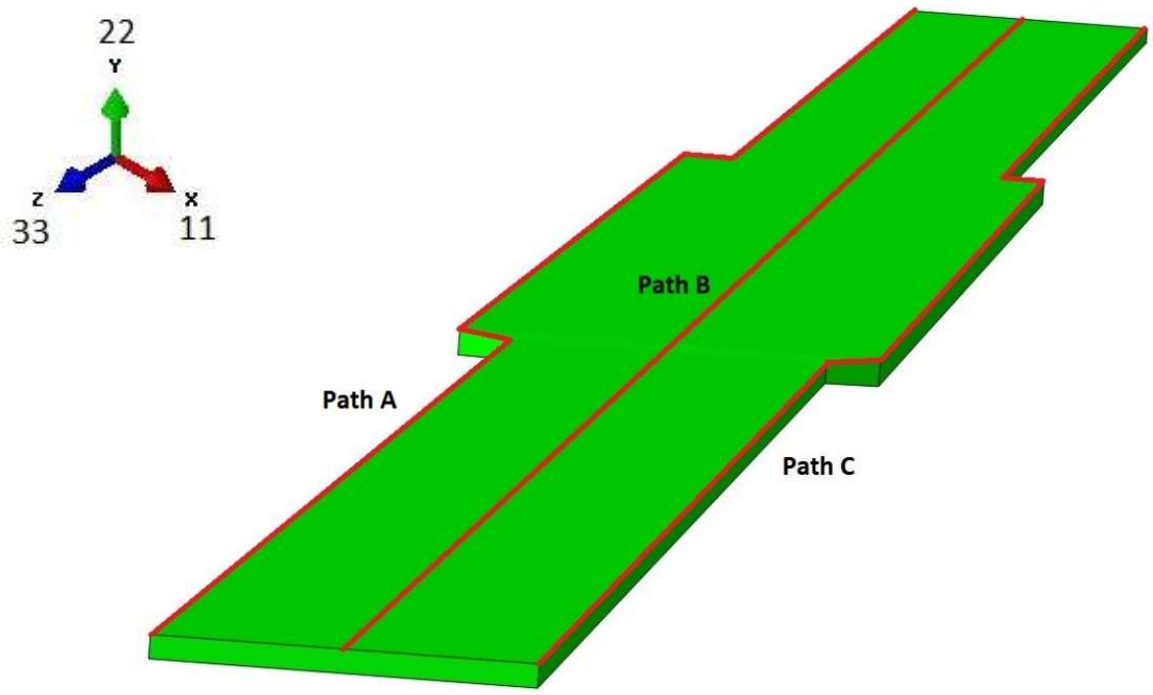

Figure 2.16 Stress paths along top flange used for direct extraction of stresses from the models

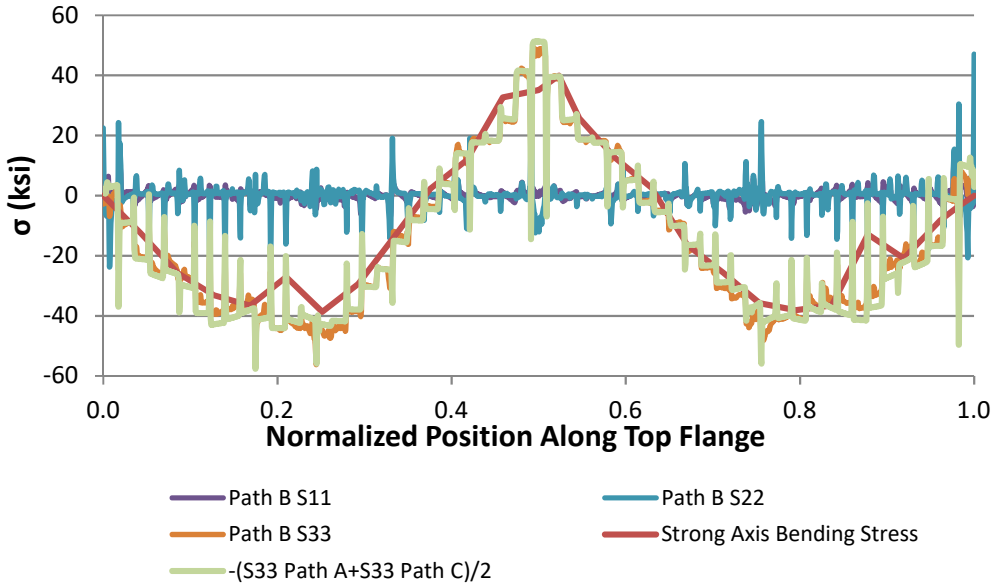

Figure 2.17 Stresses extracted directly from Path B in Girder 4, compared against strong-axis bending stresses computed using *Mc/I*

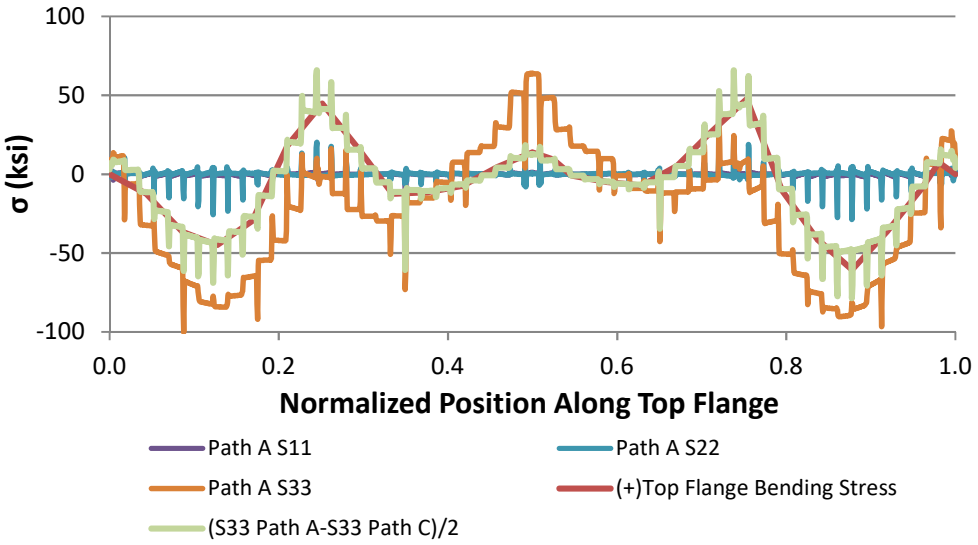

Figure 2.18 Stresses along Path A in Girder 4, compared against weak-axis tensile bending stresses in top flange computed using *Mc/I*

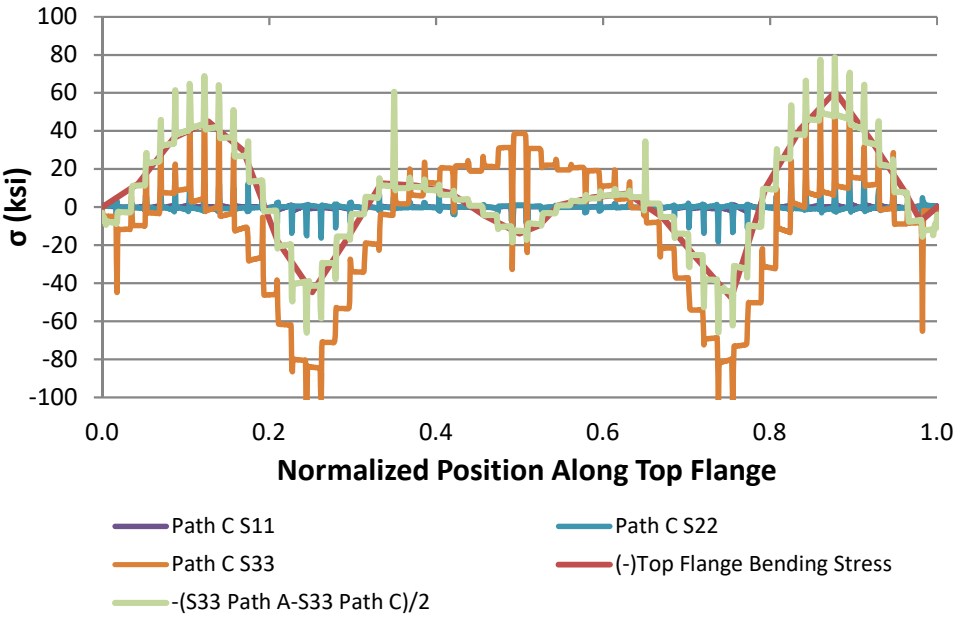

Figure 2.19 Stresses along Path C in Girder 4, compared against compressive weak-axis bending stresses in the top flange computed using *Mc/I*

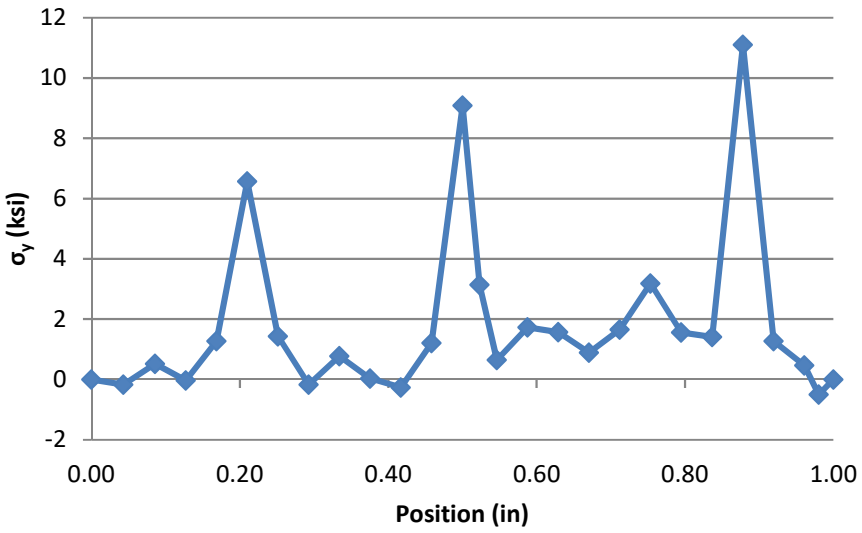

Figure 2.20 Girder 4 axial sectional stress

AASHTO INTERACTION EQUATION REQUIREMENTS

AASHTO (2010) presents interaction requirements combining minor-axis bending demands with major-axis demands based on factored loads:

$$f_{bu} + \frac{1}{3} f_l \leq \phi_f F_{nc} \quad \text{(AASHTO 6.10.8.1.1-1)}$$

where

f_{bu} = major-axis demand (ksi)

f_l = minor-axis demand (ksi)

ϕ_f = resistance factor for flexure, 1.0

F_{nc} = nominal resistance factor, 50 ksi

In lieu of refined analysis, AASHTO permits engineers to use a minimum of f_l = 69 MPa [10 ksi] for interior girders and f_l = 52 MPa [7.5 ksi] for exterior girders. These values are based on a

limited data set for skewed bridges. Therefore, it is important to further examine lateral flange bending stresses through refined analysis.

RESULTS

The results of this study are described in the following sections. First, a case is made for how geometric and material nonlinearity was considered in the modeling efforts, and why material nonlinearity was not included in the full parametric analysis. Then, the influence of the bracket overhangs is examined through a comparison of models that included and did not include the bracket overturning forces. Finally, the full parametric study is discussed in terms of girder stresses and AAHSTO's interaction equation resultants.

EFFECT OF GEOMETRIC NONLINEARITY

The 40° skewed-staggered and 40° skewed-parallel bridge models with 9.14 m [30 ft] cross-frame spacing was examined both with and without geometric nonlinearity to determine the influence of large displacement theory in the analyses. Both models with first order and nonlinear geometry definitions were assigned linear-elastic material properties.

The plots that follow are labeled by skew angle, configuration, and cross-frame spacing, and present a comparison of girder behavior between models that include linear-elastic and nonlinear geometric properties. Configurations are designated by *SS* for skewed-staggered, *SP* for skewed-parallel, and *SU* for skewed-unstaggered.

Figure 2.21 shows lateral deflection in Girder 4 along Path B in the top flange, labeled in Figure 2.16. Figure 2.22 shows the load multiplier versus peak lateral deflection in the top flange of Girder 4 along Path B, where the load multiplier is the percentage of applied load. The 40° skewed-staggered bridge with nonlinear geometry had a peak deflection difference of 22.1 mm [0.87 in] greater than the same model with linear geometry definitions. Given that the peak deflection was 23.1 mm [0.91 in] for the linear model, the nonlinear model had deflections almost twice that of the linear model. The same was true for the skewed-parallel model, where the magnitude difference was 21.3 mm [0.84 in].

Figure 2.23 through Figure 2.34 shows girder and flange bending stresses for Girder 3 and Girder 4. Strong-axis bending stresses in the exterior Girder 4 increased only 34 MPa [5.0 ksi] with the addition of nonlinear geometry effects. There was almost no difference in interior strong-axis sectional stresses for models with linear versus nonlinear definitions. The difference between interior out-of-plane bending stresses for the linear versus nonlinear models, including weak axis sectional stress, top flange bending stresses, and bottom flange bending stress, were greater than for the exterior out-of-plane bending stresses, where the stress difference between geometrically linear and nonlinear models were smaller. It was found that including geometric nonlinearity in the models produced significant higher order effects captured in both lateral deflection and bending stresses. These effects are expected to increase as brace distance is enlarged. Therefore, geometric nonlinearity was included in subsequent analyses.

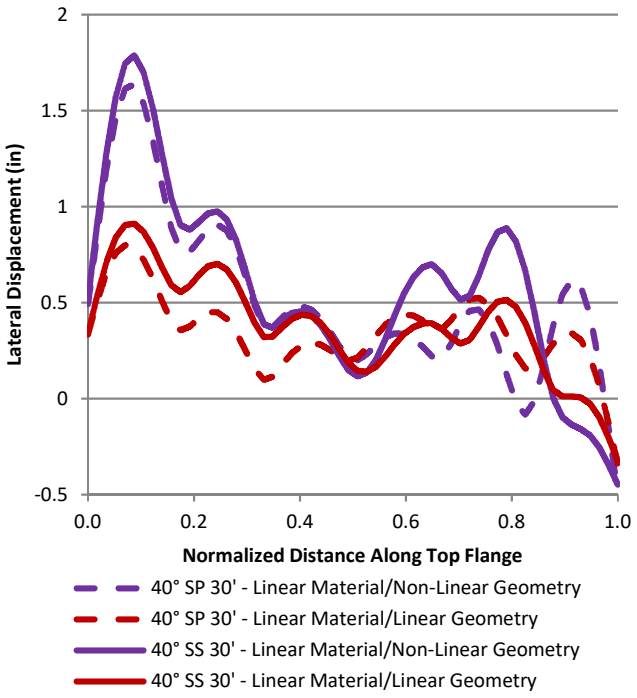

Figure 2.21 Lateral displacement along the top flange for model with linear-elastic vs. nonlinear geometry – exterior girder (G4)

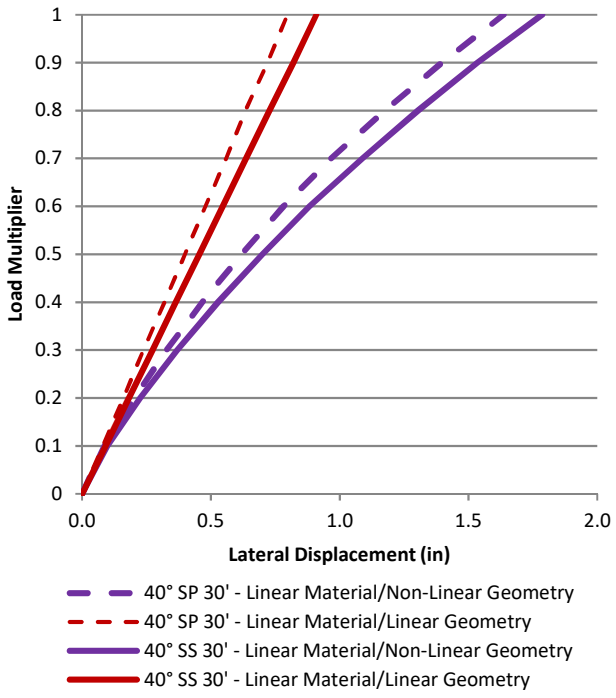

Figure 2.22 Load vs. peak lateral displacement for model with linear-elastic vs. nonlinear geometry – exterior girder (G4)

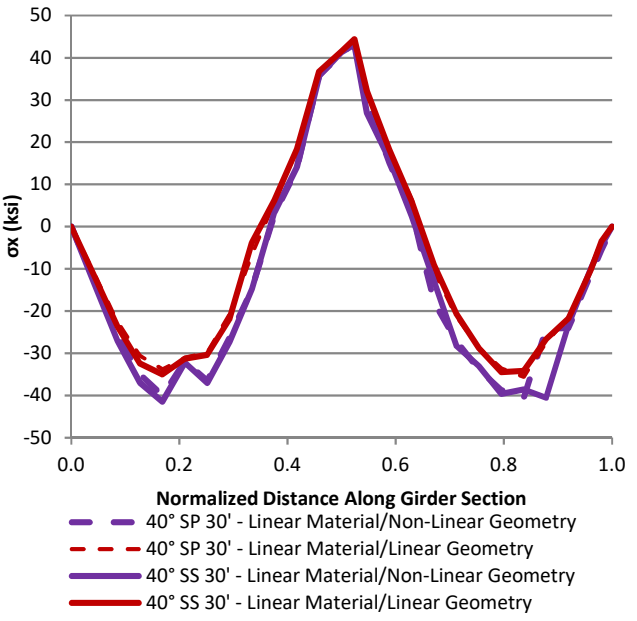

Figure 2.23 Strong-axis sectional stress from top flange for model with linear-elastic vs. nonlinear geometry – exterior girder (G4)

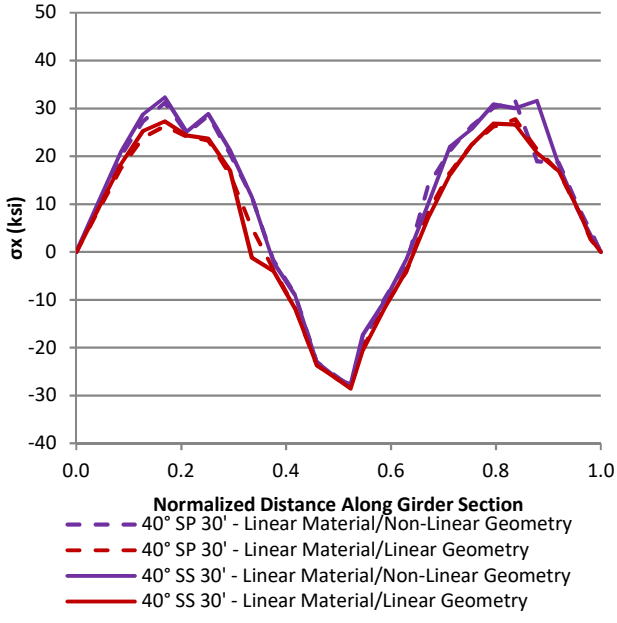

Figure 2.24 Strong-axis sectional stress from bottom flange for model with linear-elastic vs. nonlinear geometry – exterior girder (G4)

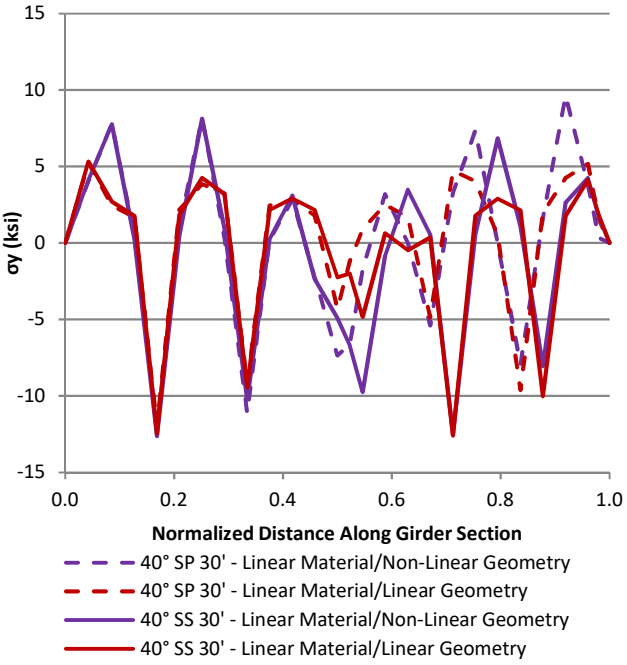

Figure 2.25 Weak-axis sectional stress from top flange for model with linear-elastic vs. nonlinear geometry – exterior girder (G4)

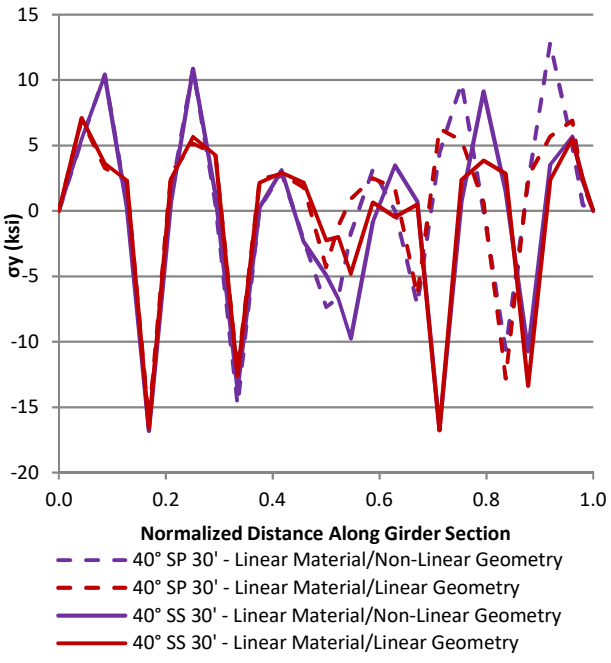

Figure 2.26 Weak-axis sectional stress from bottom flange for model with linear-elastic vs. nonlinear geometry – exterior girder (G4)

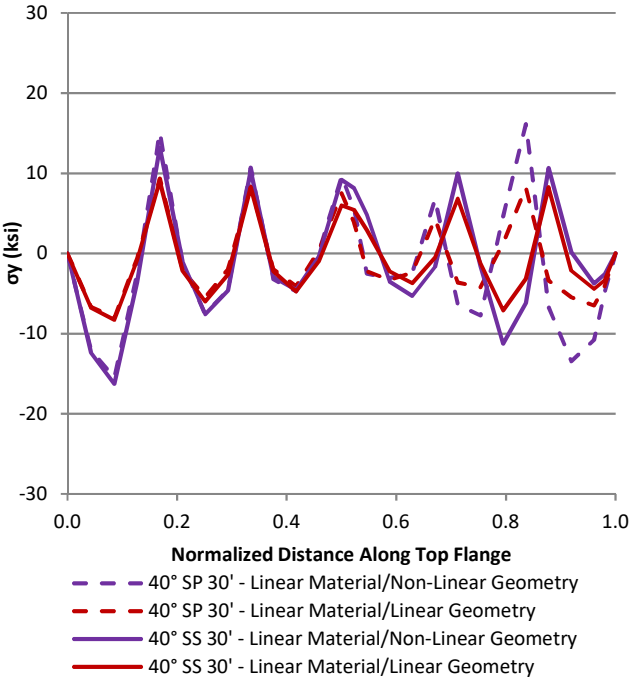

Figure 2.27 Top flange out-of-plane stress for model with linear-elastic vs. nonlinear geometry – exterior girder (G4)

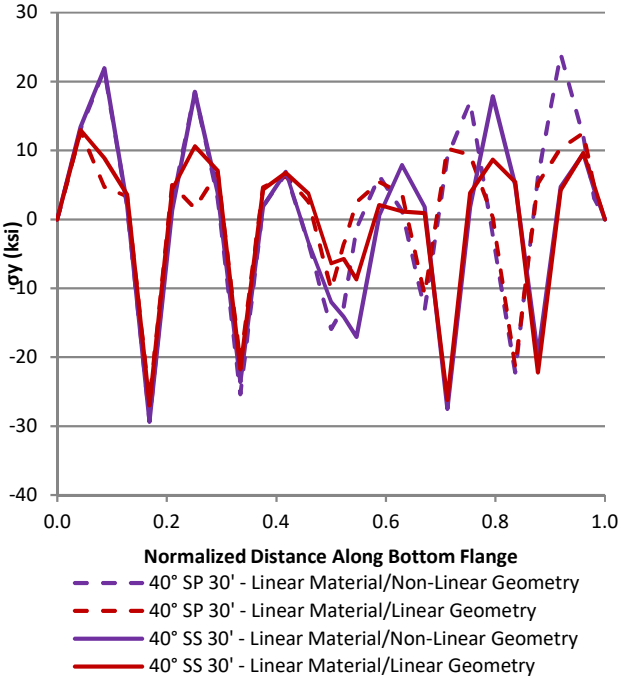

Figure 2.28 Bottom flange out-of-plane stress for model with linear-elastic vs. nonlinear geometry – exterior girder (G4)

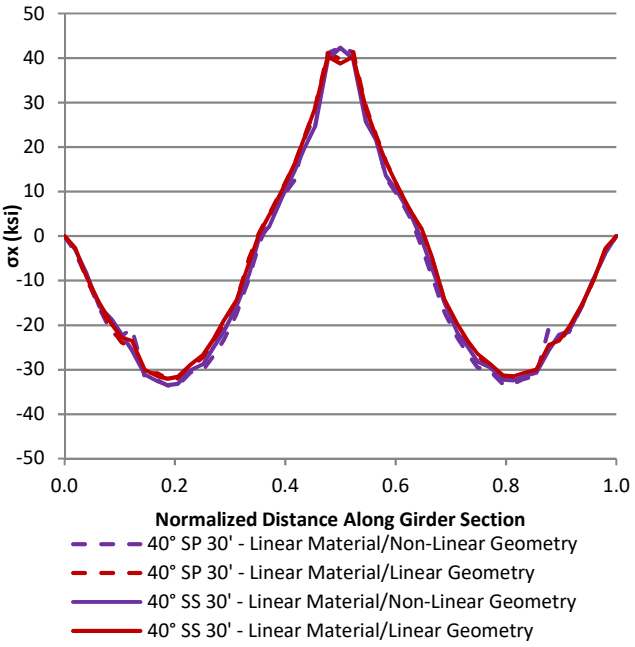

Figure 2.29 Strong-axis sectional stress from top flange for model with linear-elastic vs. nonlinear geometry – interior girder (G3)

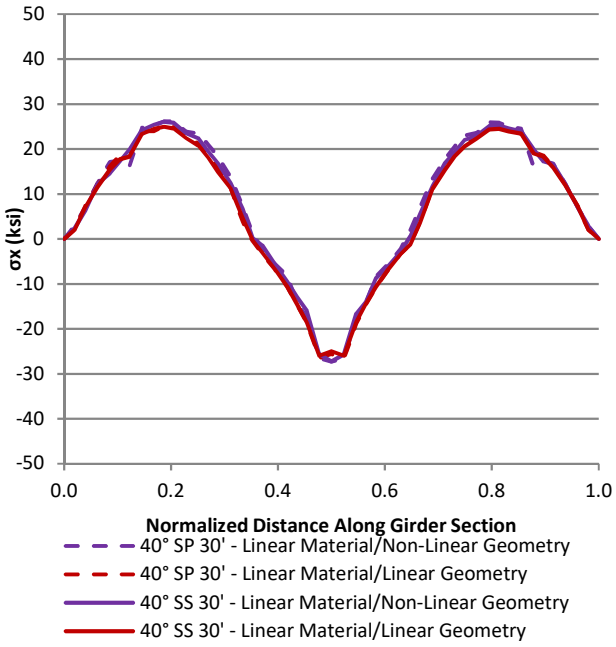

Figure 2.30 Strong-axis sectional stress from bottom flange for model with linear-elastic vs. nonlinear geometry – interior girder (G3)

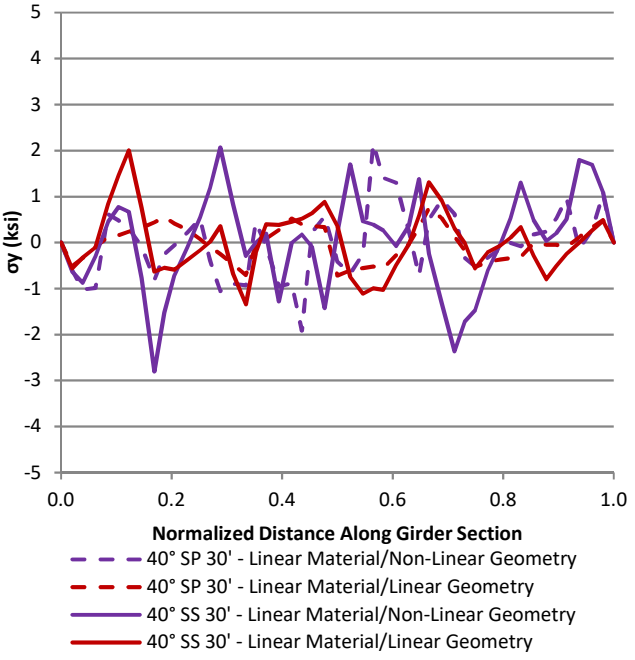

Figure 2.31 Weak-axis sectional stress from the top flange for model with linear-elastic vs. nonlinear geometry – interior girder (G3)

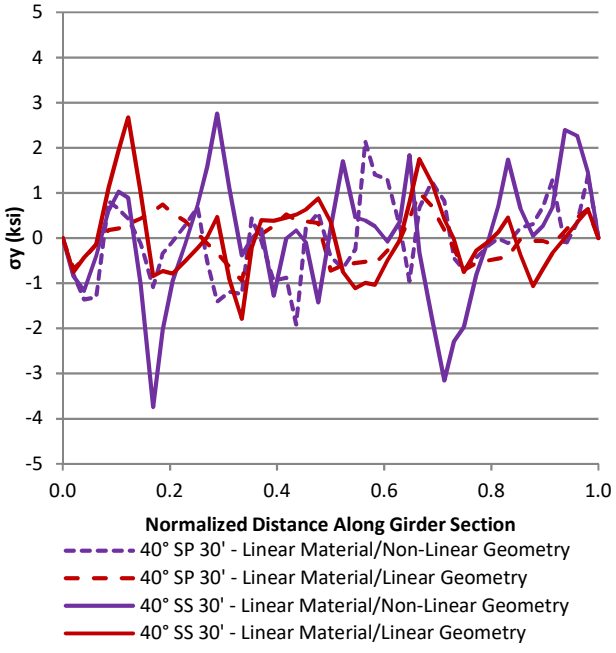

Figure 2.32 Weak-axis sectional stress from the bottom flange for model with linear-elastic vs. nonlinear geometry – interior girder (G3)

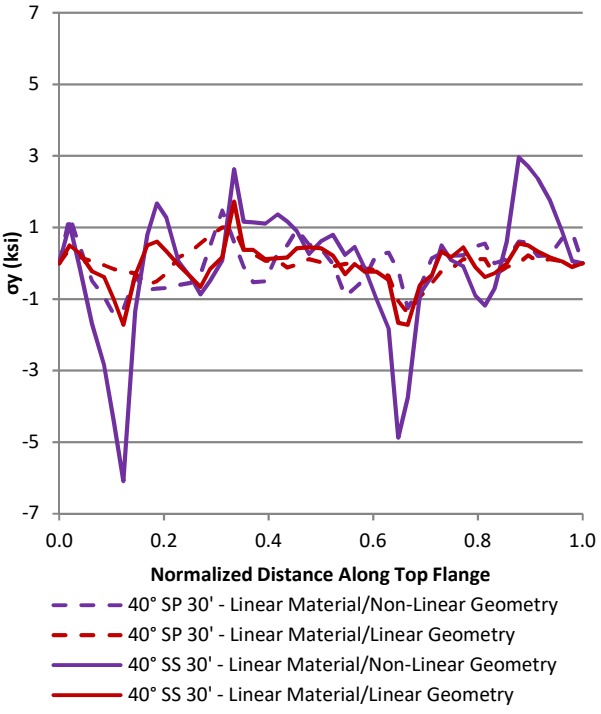

Figure 2.33 Top flange out-of-plane stress for model with linear-elastic vs. nonlinear geometry – interior girder (G3)

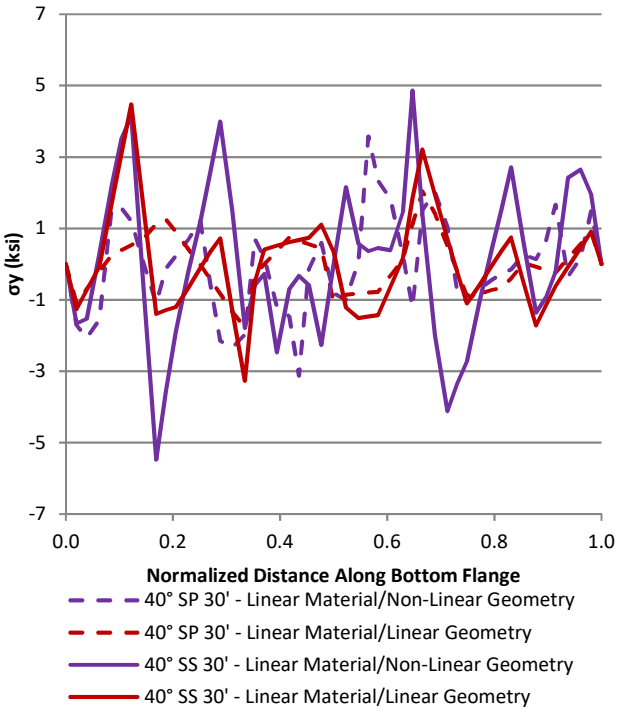

Figure 2.34 Bottom flange out-of-plane stress for model with linear-elastic vs. nonlinear geometry – interior girder (G3)

EFFECT OF MATERIAL NONLINEARITY

The 40° skewed-staggered bridge model with 4.57 m [15.0 ft] cross-frame spacing was examined both with and without material nonlinearity to determine the influence of material nonlinearity in the analysis. Both models with linear-elastic material definition and nonlinear material definition include geometric nonlinearity (i.e., captured second-order effects due to deformed geometry). The adopted nonlinear material properties are presented in Table 2.1 and Figure 2.35.

Table 2.1 Isotropic plastic hardening definition

Yield Stress (ksi)	Plastic Strain (in/in)
0	0
54.66	0
55.33	0.0367
58.20	0.0444
64.68	0.097
65.54	0.110
67.01	0.178
67.10	1.000

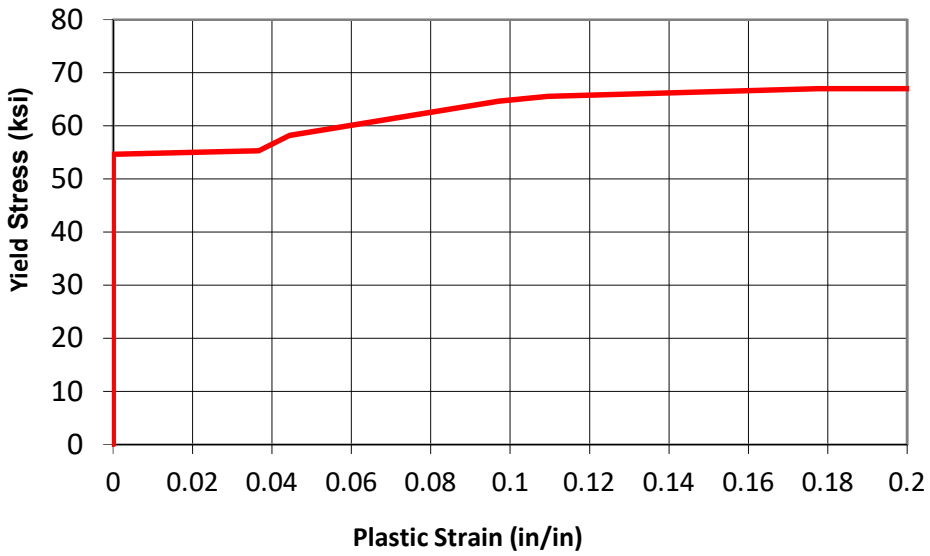

Figure 2.35 Steel material stress-strain curve used in the FE model with nonlinear material behavior

The plots that follow are labeled by skew angle, configuration, and cross-frame spacing, and present a comparison of girder behavior between models that include linear-elastic and nonlinear material properties. Configurations are designated by *SS* for skewed-staggered and *SP* for skewed-parallel. The lines in the graphs are right on top of each other, indicating that the material definition made little difference in the stresses produced.

Figure 2.36 shows lateral deflection in Girder 4 along Path B in the top flange. Figure 2.37 shows the applied load versus peak lateral deflection in Girder 4 along Path B in the top flange. Figure 2.38 through Figure 2.49 shows bending stresses for Girder 3 and Girder 4. It was found that including a nonlinear material model in the produced negligible differences in both lateral deflection and bending stresses. Therefore, material nonlinearity was not included in subsequent analyses, since it is a computationally expensive modeling technique.

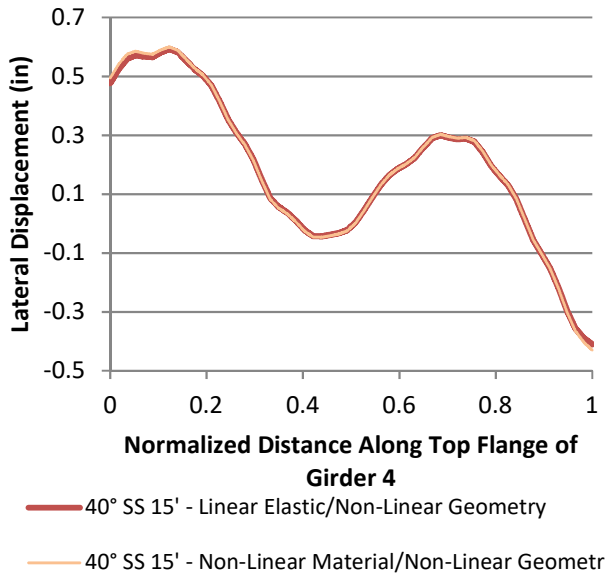

Figure 2.36 Lateral displacement along the top flange for model with linear-elastic vs. nonlinear material – exterior girder (G4)

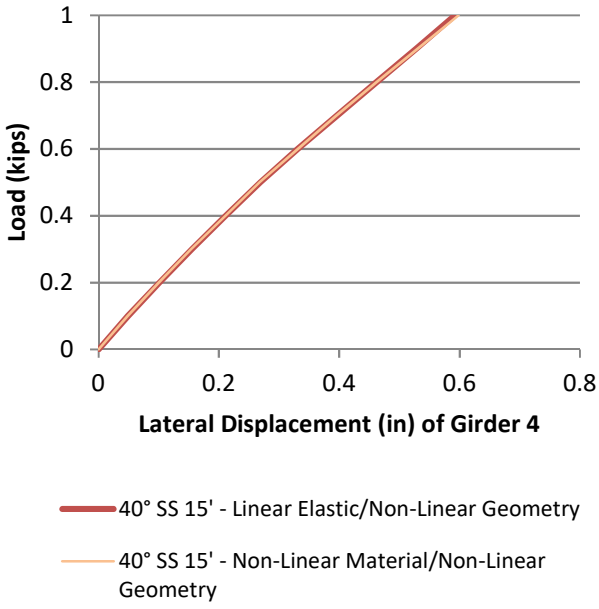

Figure 2.37 Load vs. peak lateral displacement for model with linear-elastic vs. nonlinear material – exterior girder (G4)

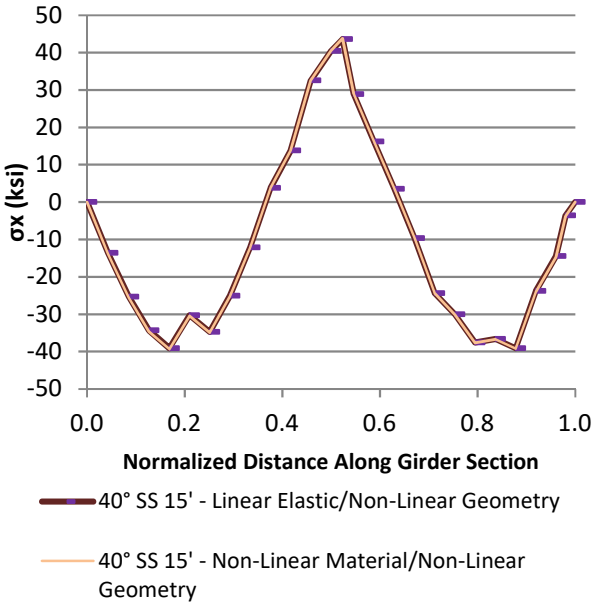

Figure 2.38 Strong-axis sectional stress from top flange for model with linear-elastic vs. nonlinear material – exterior girder (G4)

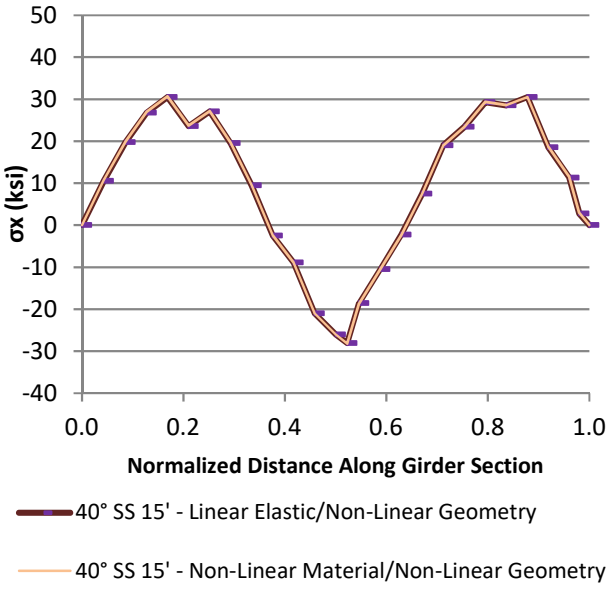

Figure 2.39 Strong-axis sectional stress from bottom flange for model with linear-elastic vs. nonlinear material – exterior girder (G4)

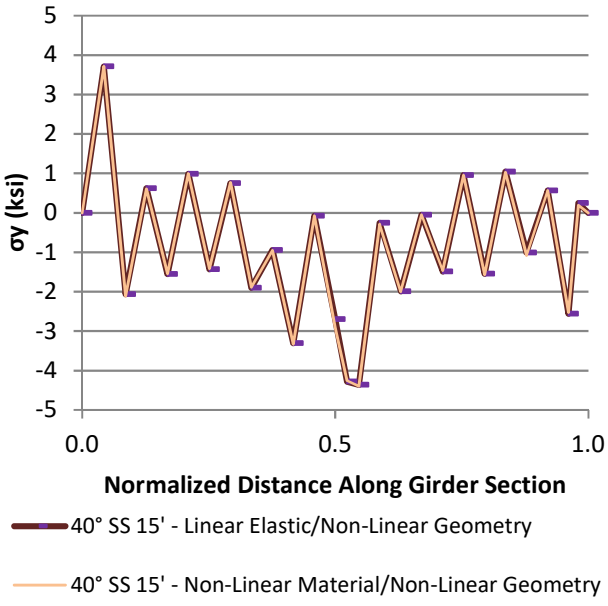

Figure 2.40 Weak-axis sectional stress from top flange for model with linear-elastic vs. nonlinear material – exterior girder (G4)

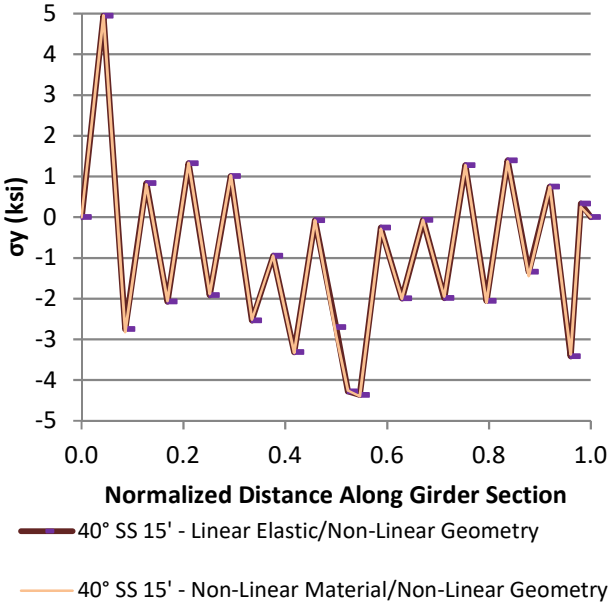

Figure 2.41 Weak-axis sectional stress from bottom flange for model with linear-elastic vs. nonlinear material – exterior girder (G4)

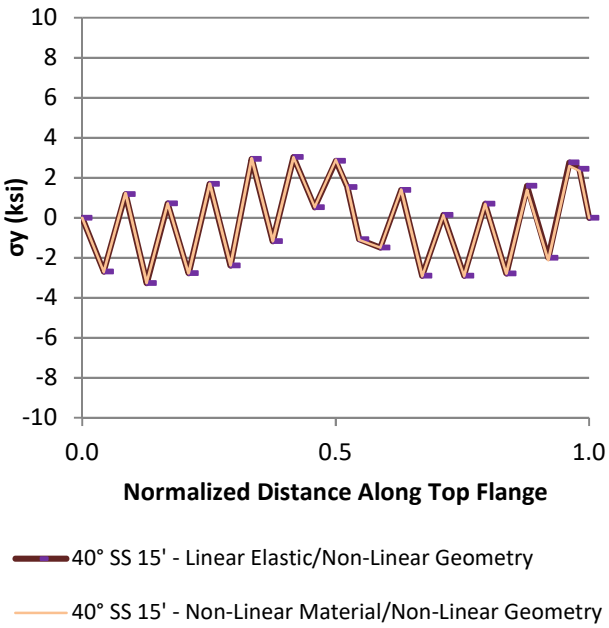

Figure 2.42 Top flange out-of-plane stress for model with linear-elastic vs. nonlinear material – exterior girder (G4)

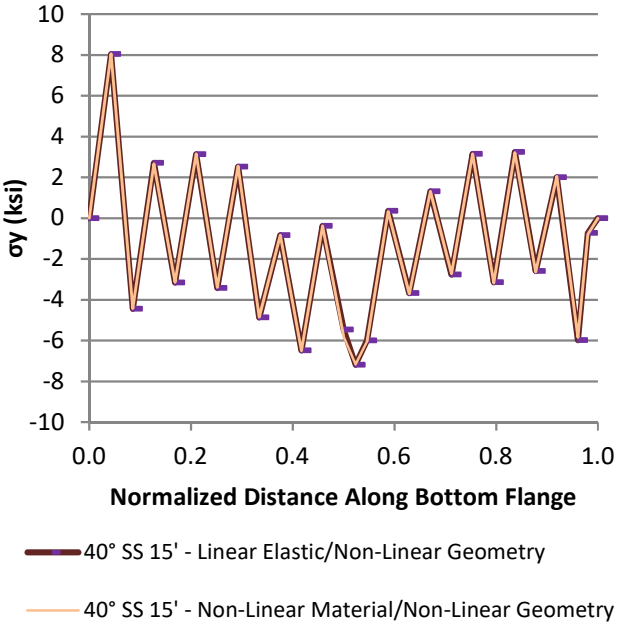

Figure 2.43 Bottom flange out-of-plane stress for model with linear-elastic vs. nonlinear material – exterior girder (G4)

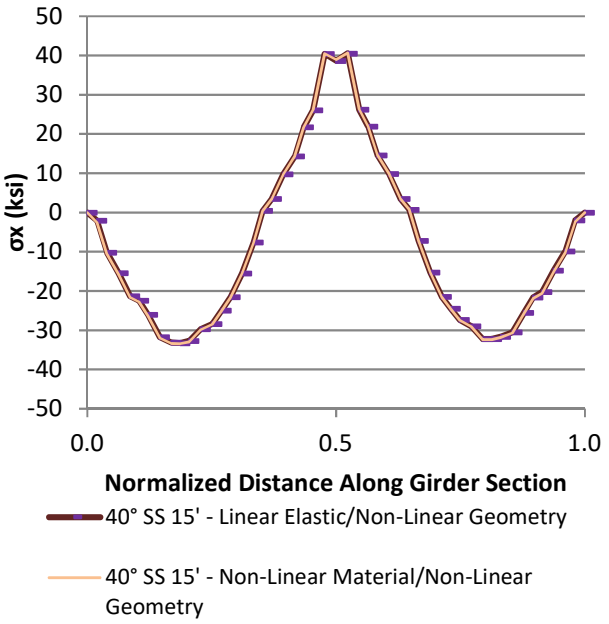

Figure 2.44 Strong-axis sectional stress from top flange for model with linear-elastic vs. nonlinear material – interior girder (G3)

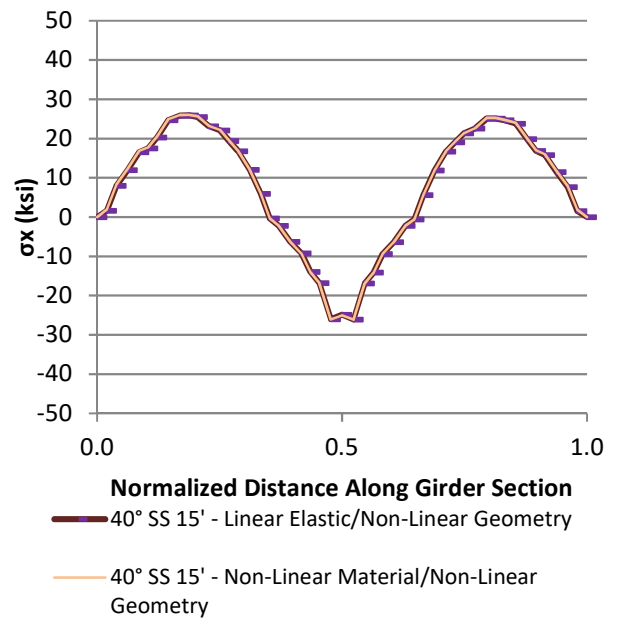

Figure 2.45 Strong-axis sectional stress from bottom flange for model with linear-elastic vs. nonlinear material – interior girder (G3)

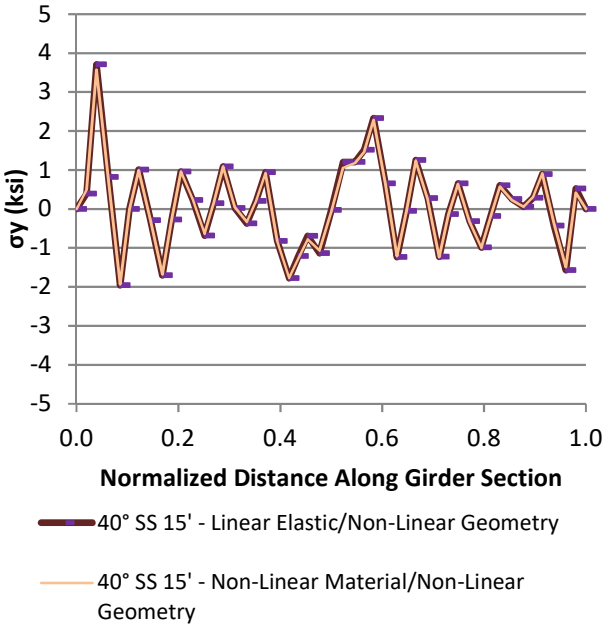

Figure 2.46 Weak-axis sectional stress from the top flange for model with linear-elastic vs. nonlinear material – interior girder (G3)

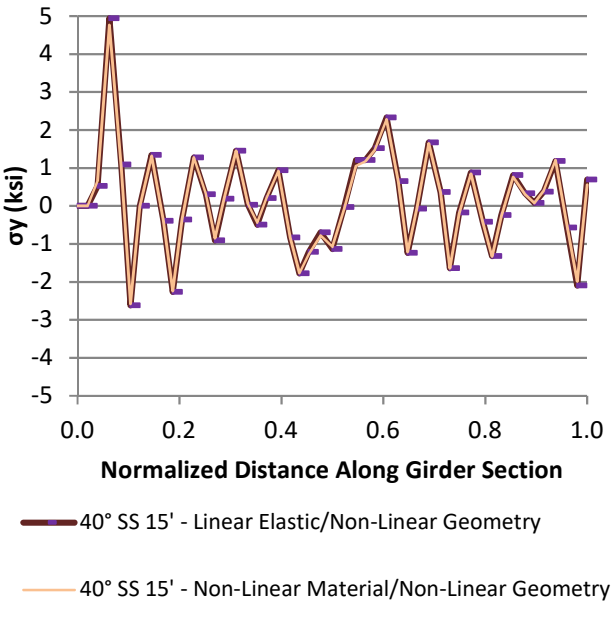

Figure 2.47 Weak-axis sectional stress from the bottom flange for model with linear-elastic vs. nonlinear material – interior girder (G3)

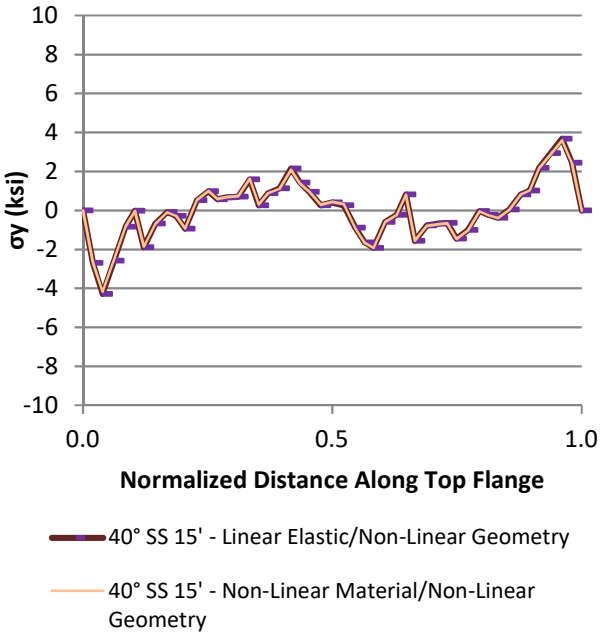

Figure 2.48 Top flange out-of-plane stress for model with linear-elastic vs. nonlinear material – interior girder (G3)

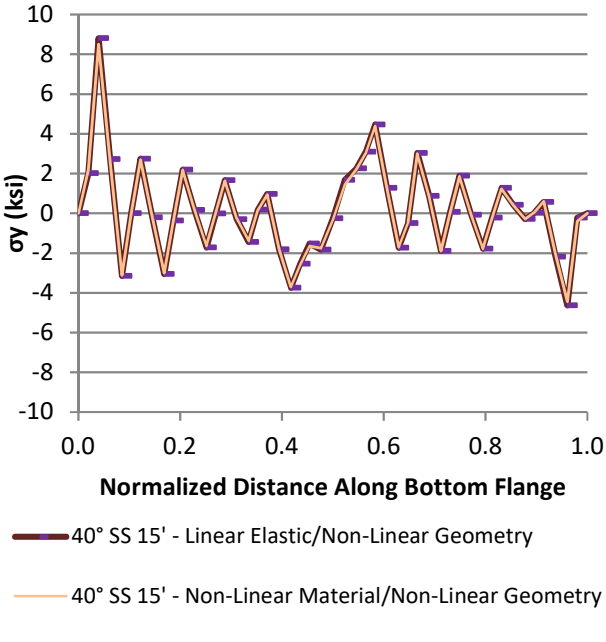

Figure 2.49 Bottom flange out-of-plane stress for model with linear-elastic vs. nonlinear material – interior girder (G3)

Effects of Overhang Bracket on System Behavior and Stability

Significant flange lateral bending may be caused by torsion from eccentric concrete deck and walkway overhang loads acting on cantilever forming brackets placed along the exterior girders, shown in Figure 2.50, in conjunction with skew angles exceeding 20° (AASHTO 2010). In these cases, AASHTO allows flange lateral bending to be considered at the discretion of the Engineer.

Data from a model of the 40° skewed-staggered bridge that included overhang bracket forces was compared with data from a model that accounted for the gravity load collected on the overhang but that was applied to the top flange of the exterior girders over the Girder 4 web, along the thick red line as shown in Figure 2.51.

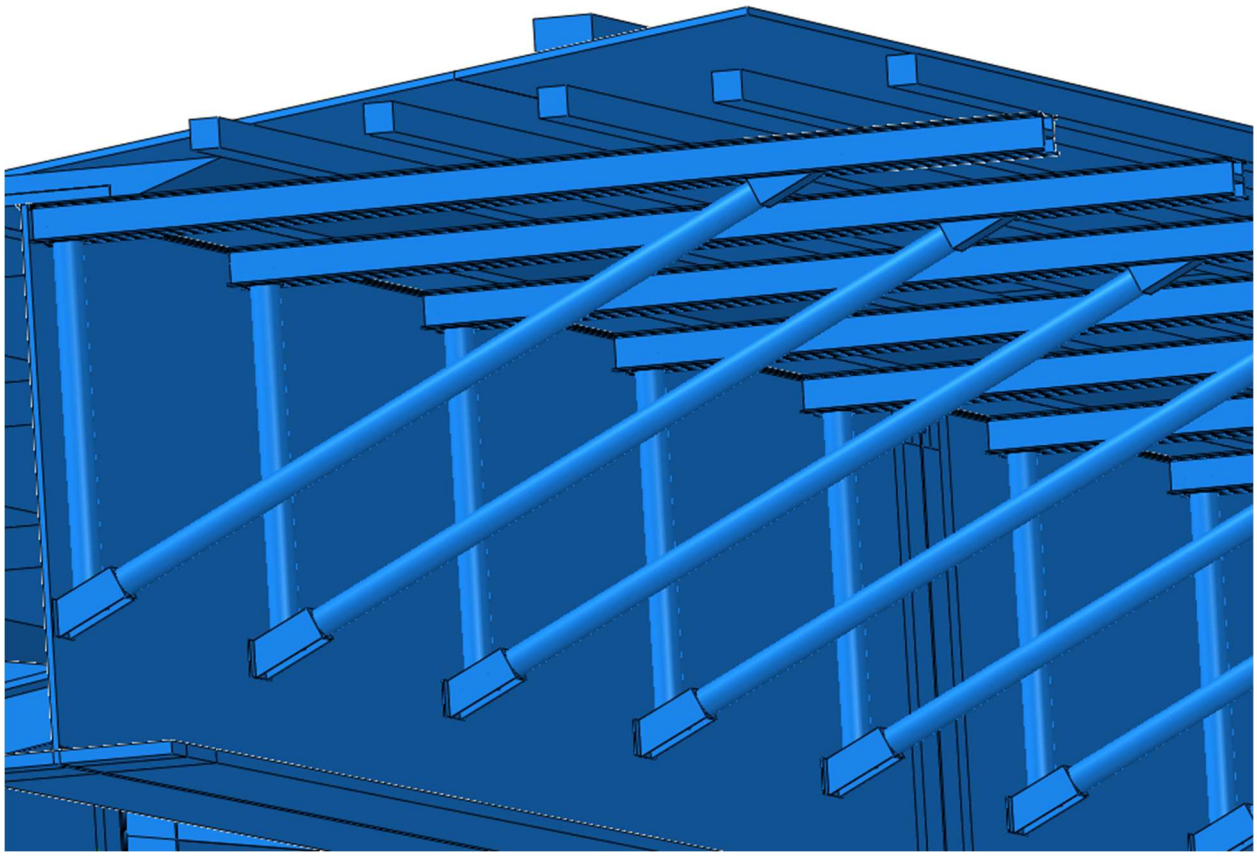

Figure 2.50 Overhang bracket geometry on exterior girder (not used in data collection)

The results show significant contribution of overhang loads to both lateral deflection in the exterior girder at all loading stages (Figure 2.52 and Figure 2.53) and out-of-plane flexural stresses in the exterior girder (Figure 2.56 through Figure 2.59). In-plane flexural stress for Girder 4, shown in Figure 2.54 and Figure 2.55, and stresses in Girder 3, shown in Figure 2.60 and Figure 2.61, remained consistent between the model with overhang loads and the model without overhang loads. Therefore, it can be concluded that overhang bracket loads contribute greatly to out-of-plane deflection and stresses in the exterior girders and had little effect on in-plane bending stresses. This comparison is an interesting one, because it highlights the difference in lateral flange bending stress that occurs in girders with and without the overturning effect of

the overhangs, and shows that the overhang brackets induce significant levels of lateral deformation and lateral stress in the exterior girders.

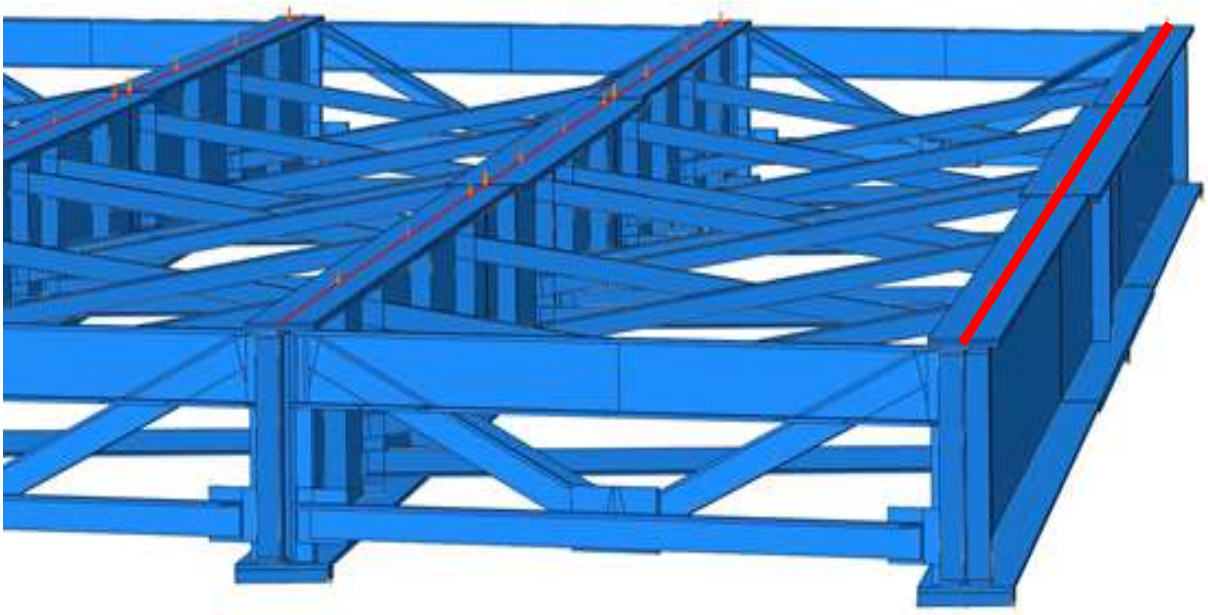

Figure 2.51 Model with no overhang bracket plates and overhang loads applied to the top of the exterior girder

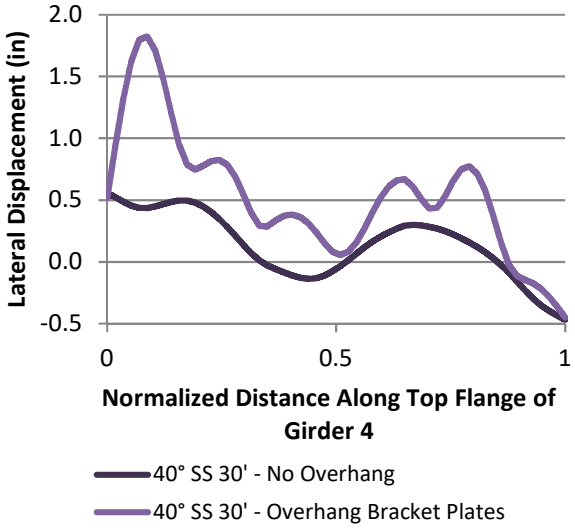

Figure 2.52 Lateral displacement along the top flange for model with overhang vs. no overhang – exterior girder (G4)

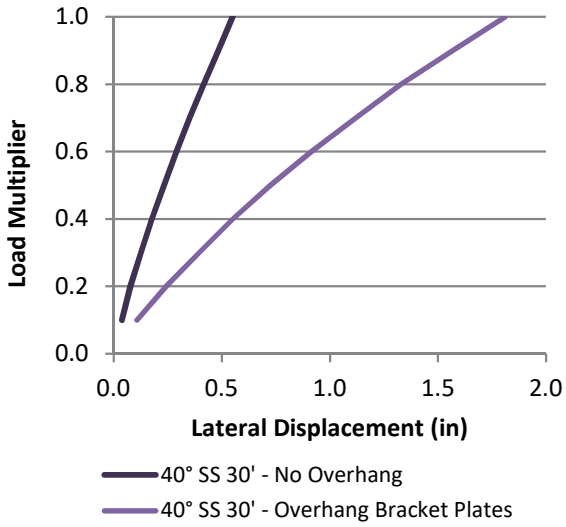

Figure 2.53 Load vs. peak lateral displacement for model with overhang vs. no overhang – exterior girder (G4)

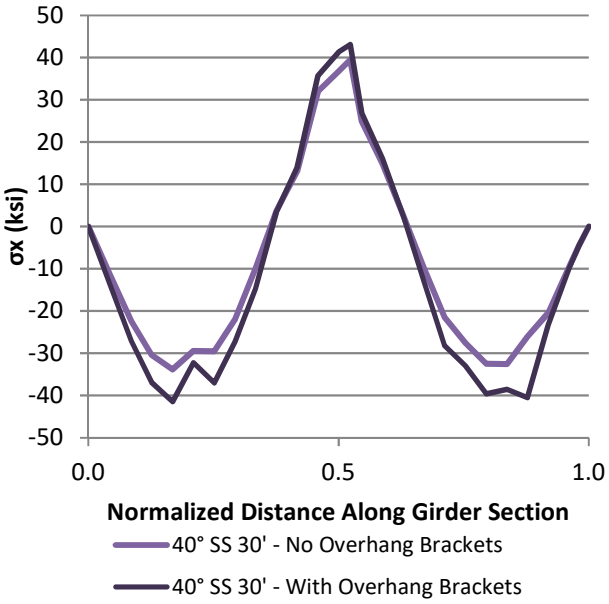

Figure 2.54 Strong-axis sectional stress from top flange for model with overhang vs. no overhang – exterior girder (G4)

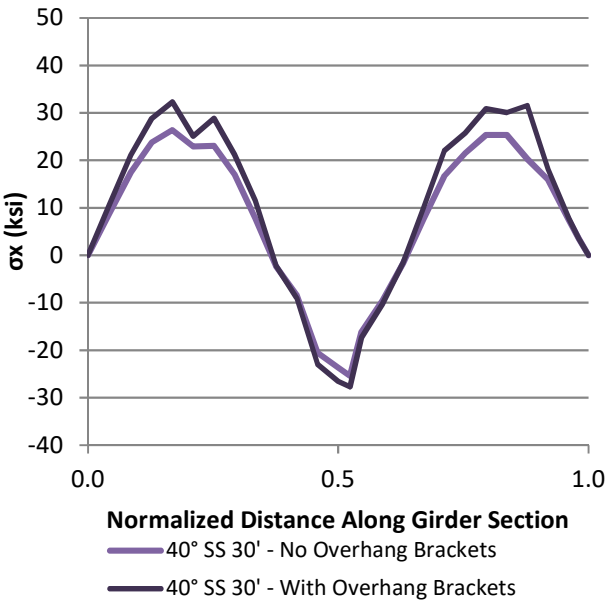

Figure 2.55 Strong-axis sectional stress from bottom flange for model with overhang vs. no overhang – exterior girder (G4)

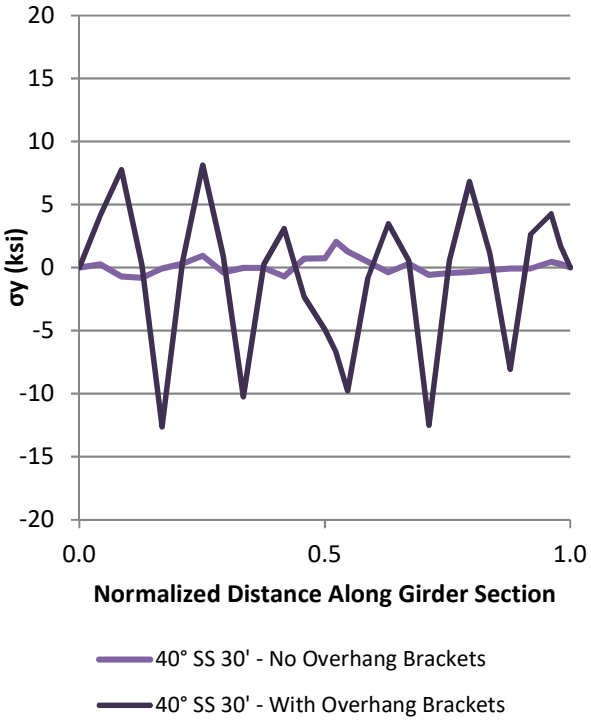

Figure 2.56 Weak-axis sectional stress from the top flange for model with overhang vs. no overhang – exterior girder (G4)

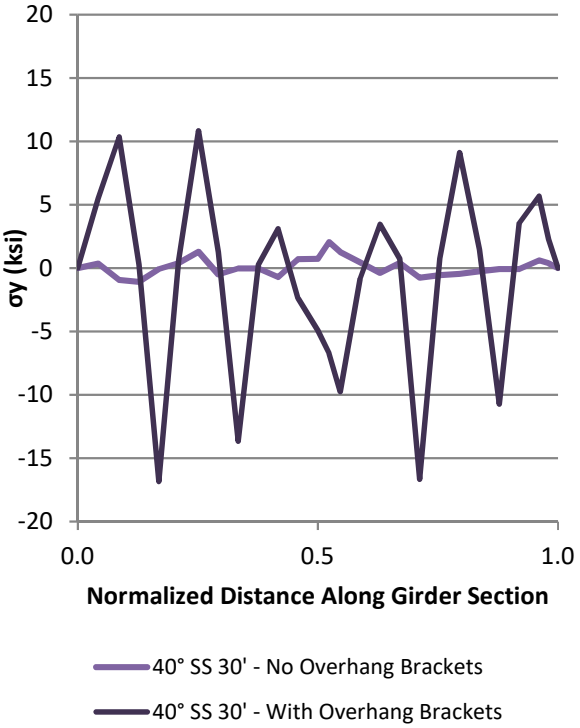

Figure 2.57 Weak-axis sectional stress from the bottom flange for model with overhang vs. no overhang – exterior girder (G4)

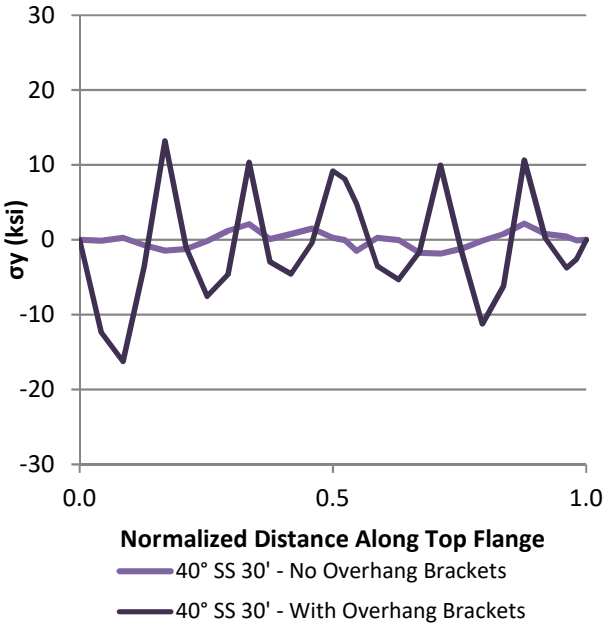

Figure 2.58 Top flange out-of-plane stress for model with overhang vs. no overhang – exterior girder (G4)

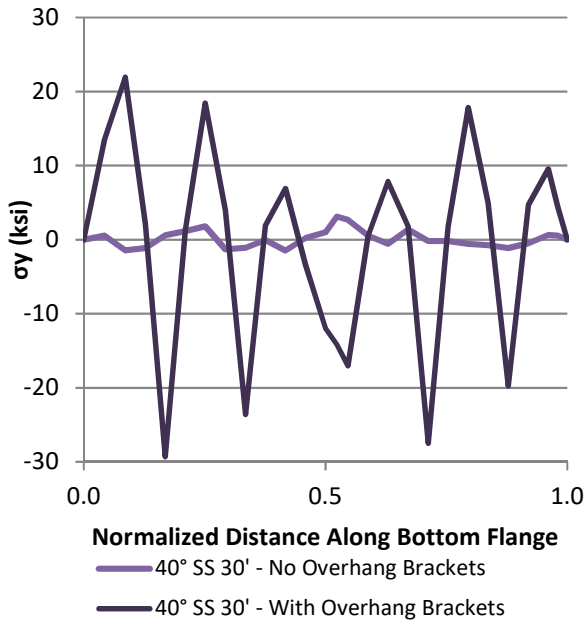

Figure 2.59 Bottom flange out-of-plane stress for model with overhang vs. no overhang – exterior girder (G4)

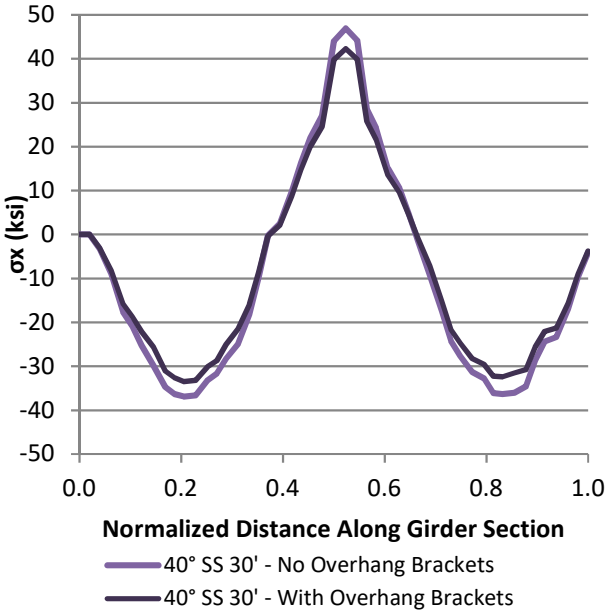

Figure 2.60 Strong-axis sectional stress from top flange for model with overhang vs. no overhang – interior girder (G3)

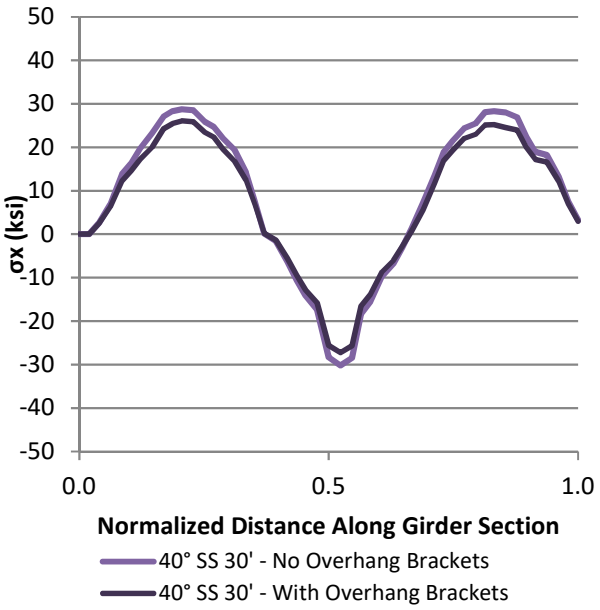

Figure 2.61 Strong-axis sectional stress from bottom flange for model with overhang vs. no overhang – interior girder (G3)

EXAMINATION OF SKEWED SYSTEM STABILITY THROUGH PARAMETRIC ANALYSIS

As described, the parametric study included variations of:

- Skew angle (0°, 20°, and 40°);
- Cross-frame spacing (4.57 m [15 ft] and 9.14 m [30 ft]); and
- Cross-frame orientation (skewed-staggered, skewed-parallel, and skewed-unstaggered)

Results from the parametric study were analyzed in terms of strong axis, weak axis, top flange, and bottom flange bending stress along with the AASHTO interaction equation resultant. It should be noted that results are based on a specific pre-designed bridge to provide insight into

the effect of each variation. Changes in the bridge geometry, boundary conditions, and connection designs will affect the stresses and deflection output.

Girder Bending Stress and AASHTO Interaction Equation Resultant

Figure 2.62 through Figure 2.75 shows strong axis bending stress and out-of-plane bending stress in the top flange, bottom flange, and girder section for Girder 3 (interior girder). The interaction equation resultant computed from the strong axis bending stress and compression flange is also presented. AASHTO's suggested value of 68.9 MPa [10 ksi] for the interior girder is marked by the horizontal black lines.

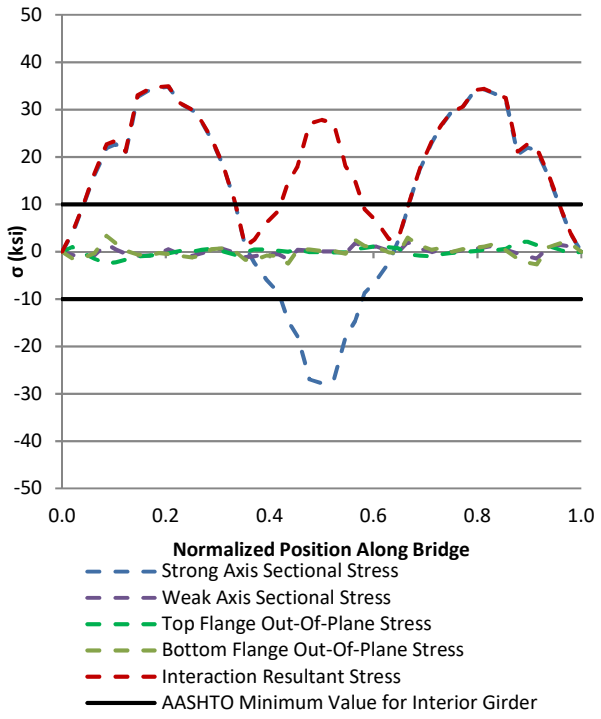

Figure 2.62 40 deg. skewed-parallel bridge with 15 ft cross-frame spacing – interior girder (G3)

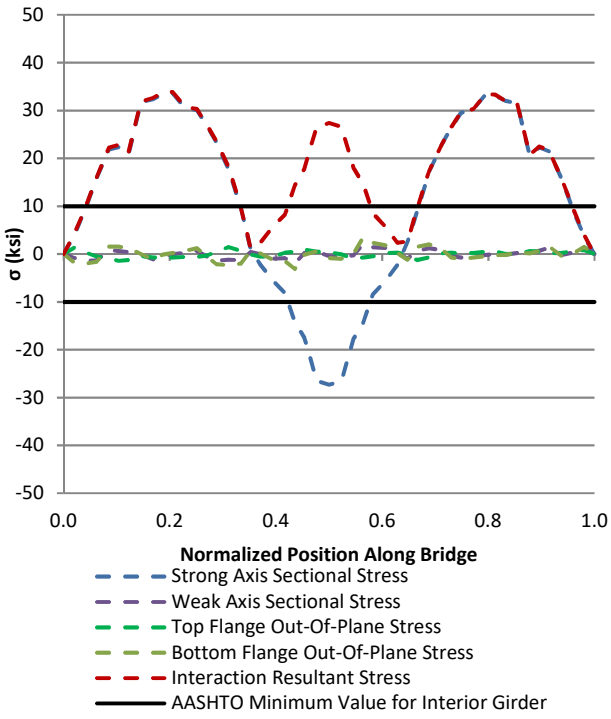

Figure 2.63 40 deg. skewed-parallel bridge with 30 ft cross-frame spacing - interior girder (G3)

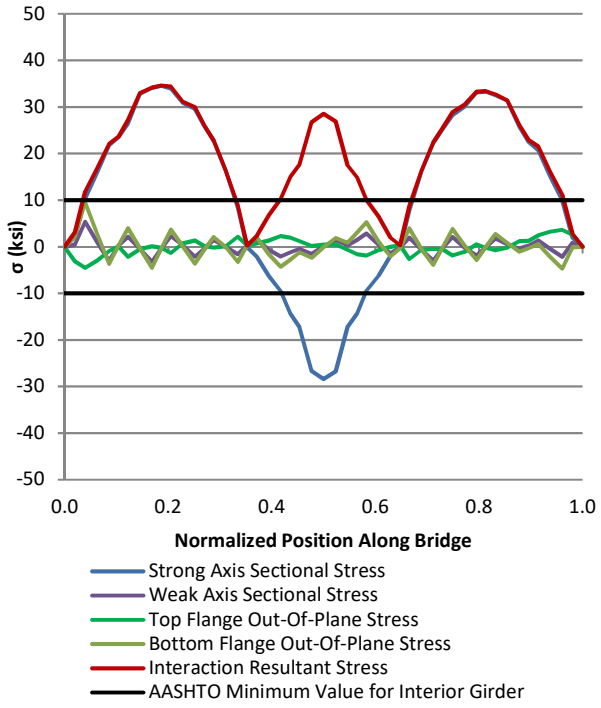

Figure 2.64 40 deg. skewed-staggered bridge with 15 ft cross-frame spacing – interior girder (G3)

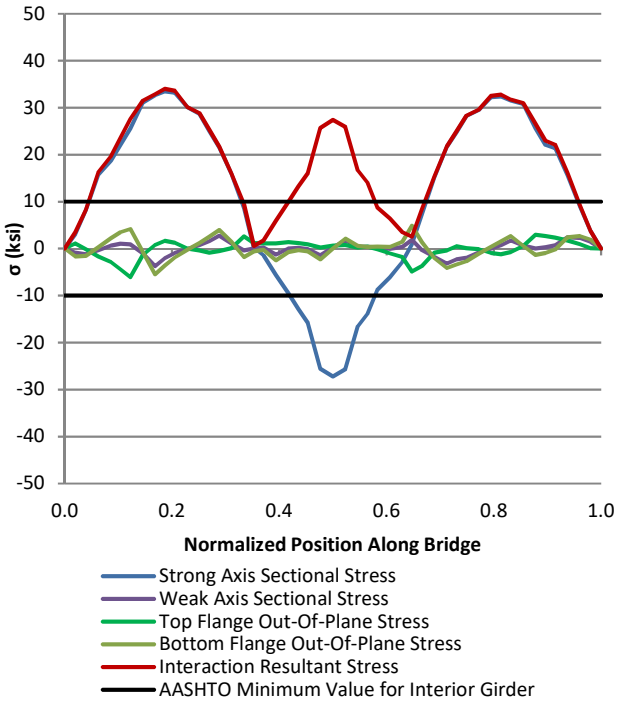

Figure 2.65 40 deg. skewed-staggered bridge with 30 ft cross-frame spacing – interior girder (G3)

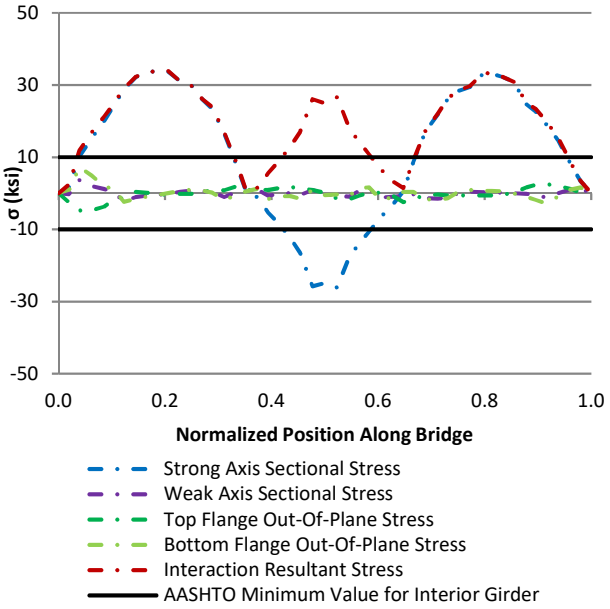

Figure 2.66 40 deg. skewed-unstaggered bridge with 15 ft cross-frame spacing – interior girder (G3)

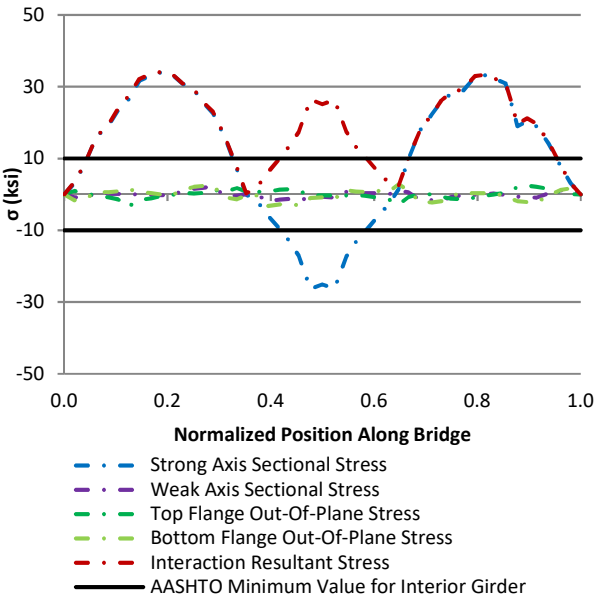

Figure 2.67 40 deg. skewed-unstaggered bridge with 30 ft cross-frame spacing – interior girder (G3)

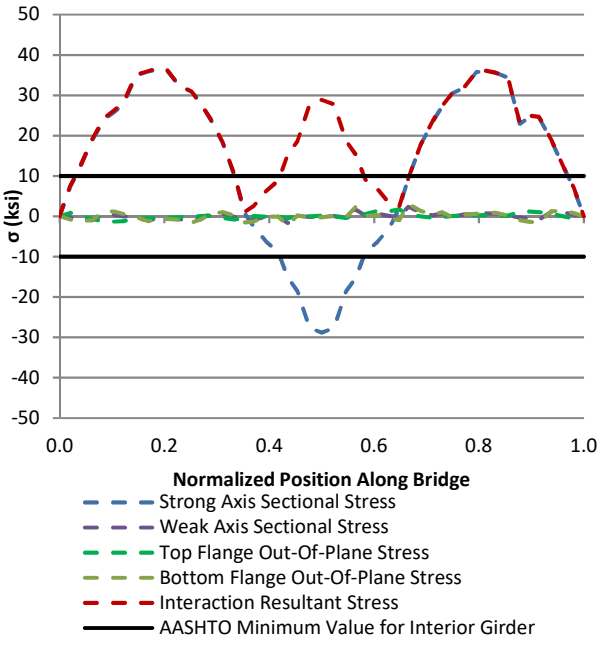

Figure 2.68 20 deg. skewed-parallel bridge with 15 ft cross-frame spacing – interior girder (G3)

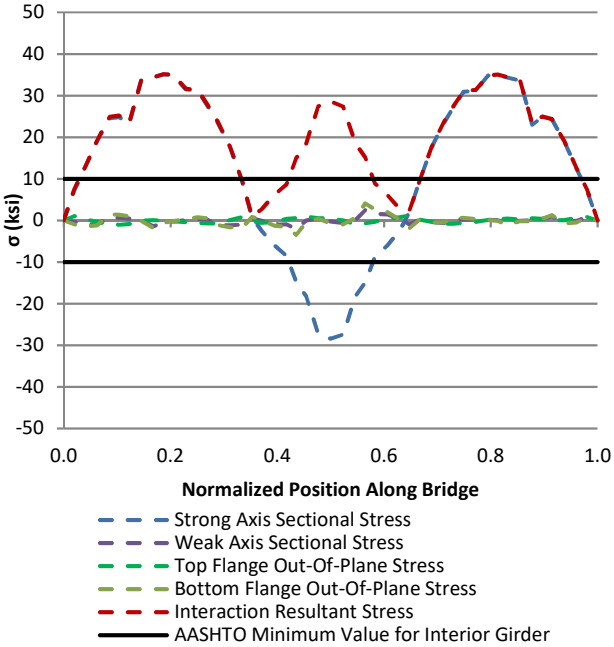

Figure 2.69 20 deg. skewed-parallel bridge with 30 ft cross-frame spacing – interior girder (G3)

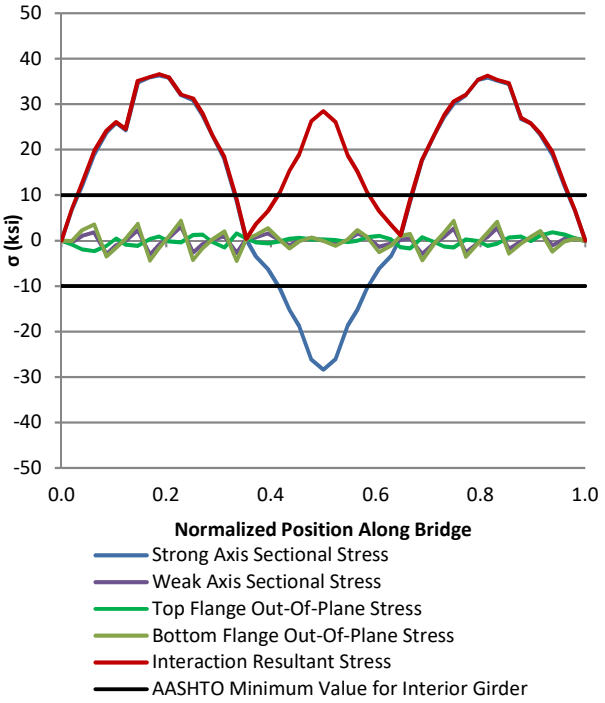

Figure 2.70 20 deg. skewed-staggered bridge with 15 ft cross-frame spacing – interior girder (G3)

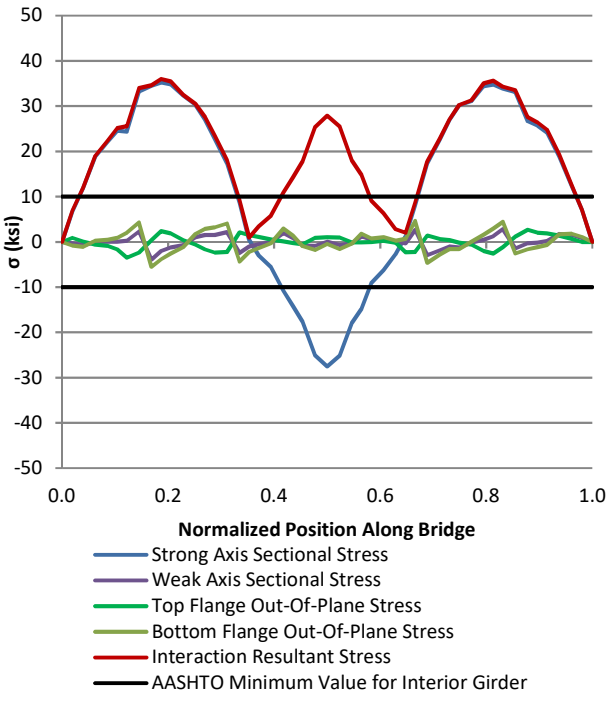

Figure 2.71 20 deg. skewed-staggered bridge with 30 ft cross-frame spacing – interior girder (G3)

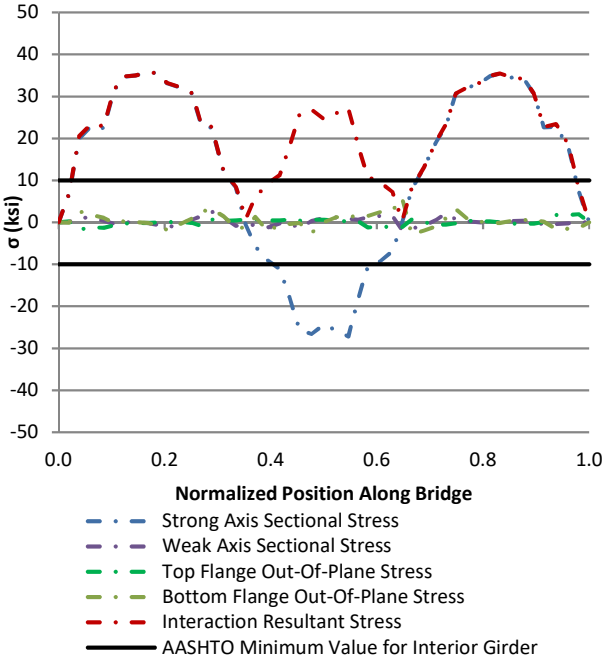

Figure 2.72 20 deg. skewed-unstaggered bridge with 15 ft cross-frame spacing – interior girder (G3)

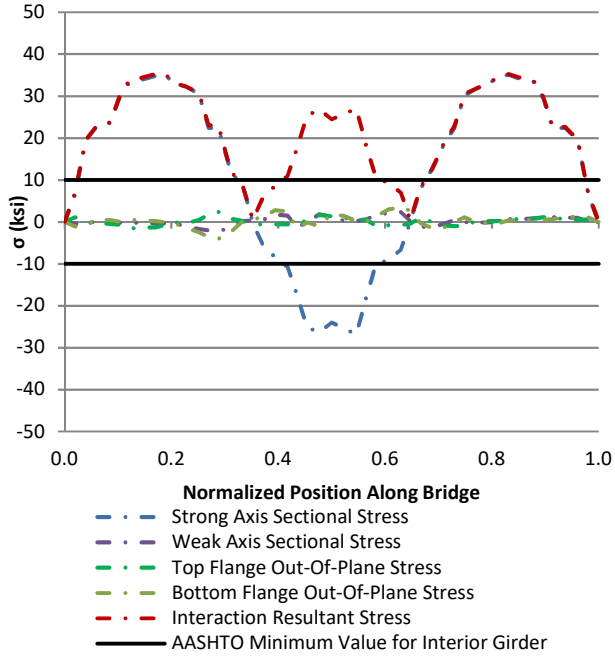

Figure 2.73 20 deg. skewed-unstaggered bridge with 30 ft cross-frame spacing – interior girder (G3)

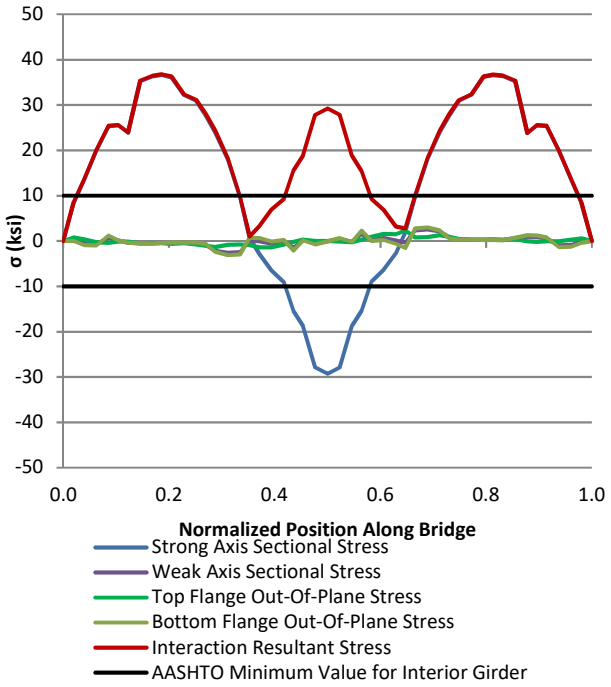

Figure 2.74 0 deg. non-skewed bridge with 15 ft cross-frame spacing – interior girder (G3)

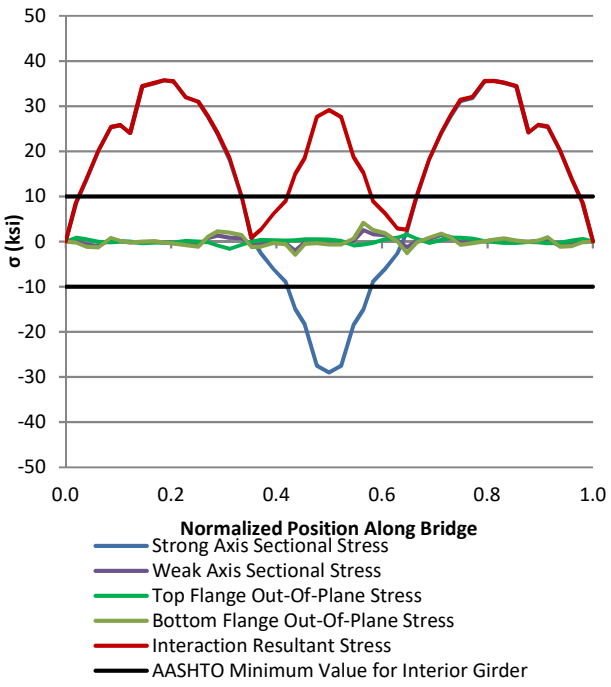

Figure 2.75 0 deg. non-skewed bridge with 30 ft cross-frame spacing – interior girder (G3)

Figure 2.76 through Figure 2.89 shows strong axis bending stress and out-of-plane bending stress in the top flange, bottom flange, and girder section for Girder 4 (exterior girder). The interaction equation resultant computed from the strong axis bending stress and compression flange is also shown. AASHTO's suggested value of 51.7 MPa [7.5 ksi] for the exterior girder is drawn by the horizontal black lines.

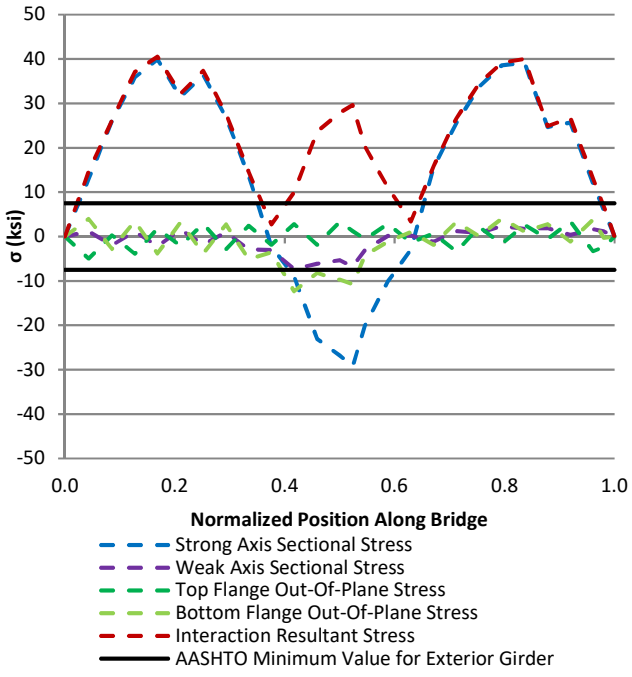

Figure 2.76 40 deg. skewed-parallel bridge with 15 ft cross-frame spacing – exterior girder (G4)

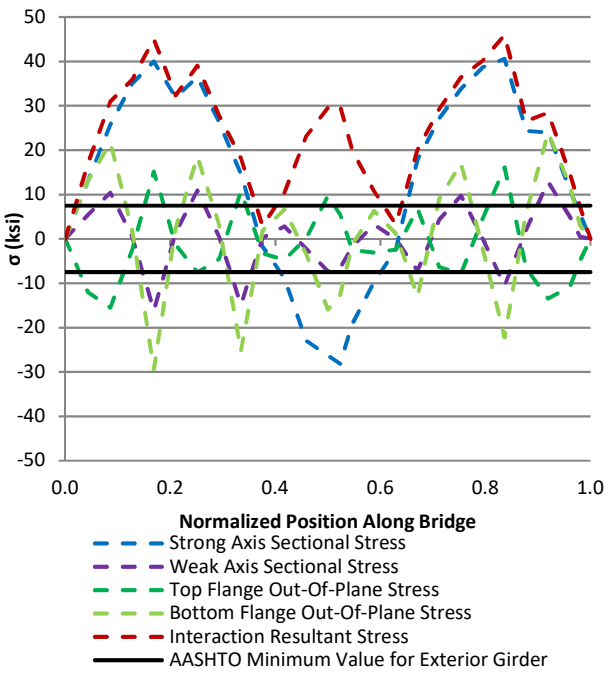

Figure 2.77 40 deg. skewed-parallel bridge with 30 ft cross-frame spacing – exterior girder (G4)

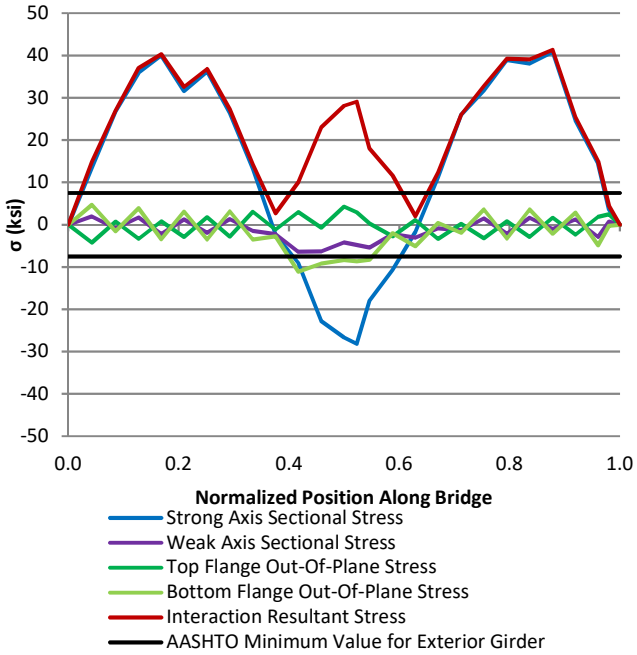

Figure 2.78 40 deg. skewed-staggered bridge with 15 ft cross-frame spacing – exterior girder (G4)

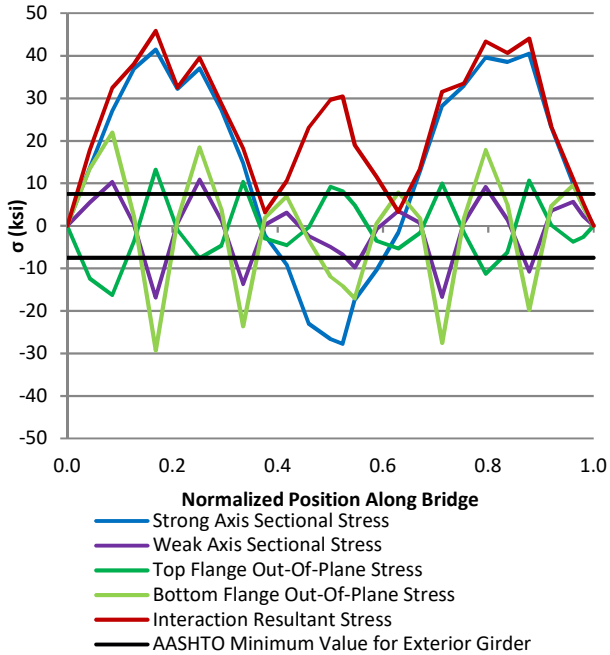

Figure 2.79 40 deg. skewed-staggered bridge with 30 ft cross-frame spacing – exterior girder (G4)

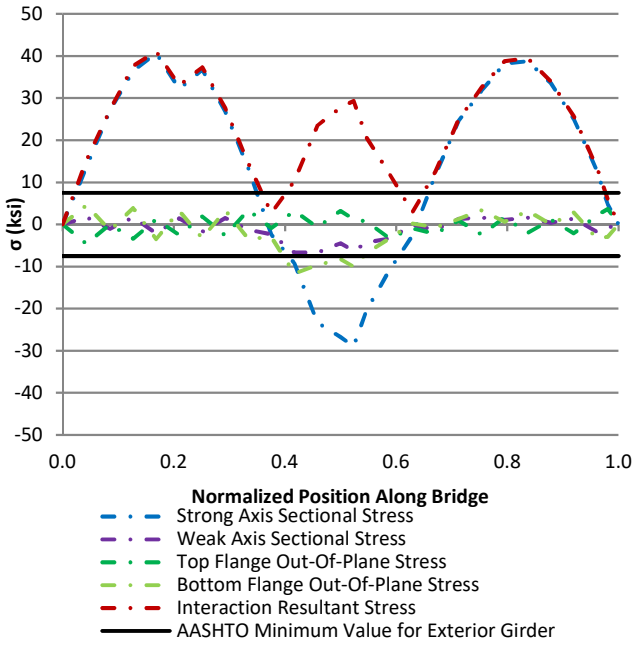

Figure 2.80 40 deg. skewed-unstaggered bridge with 15 ft cross-frame spacing – exterior girder (G4)

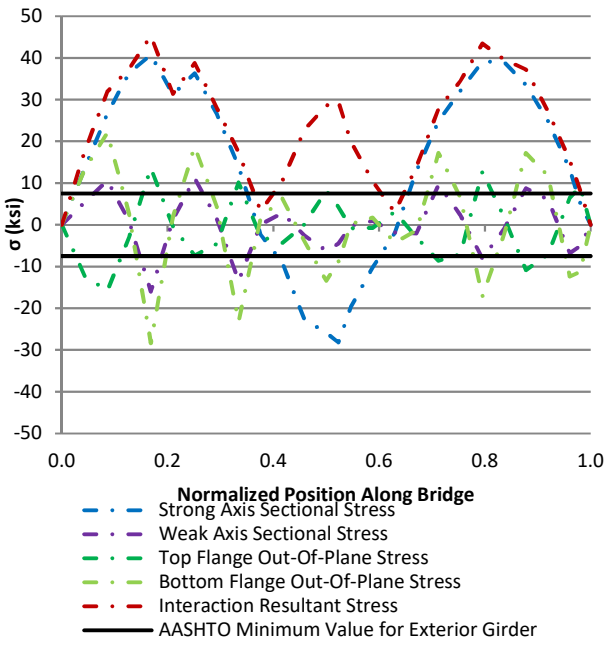

Figure 2.81 40 deg. skewed-unstaggered bridge with 30 ft cross-frame spacing – exterior girder (G4)

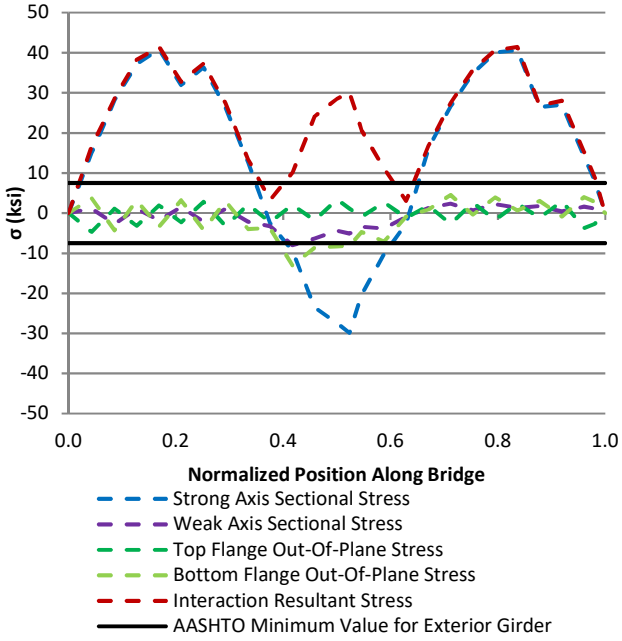

Figure 2.82 20 deg. skewed-parallel bridge with 15 ft cross-frame spacing – exterior girder (G4)

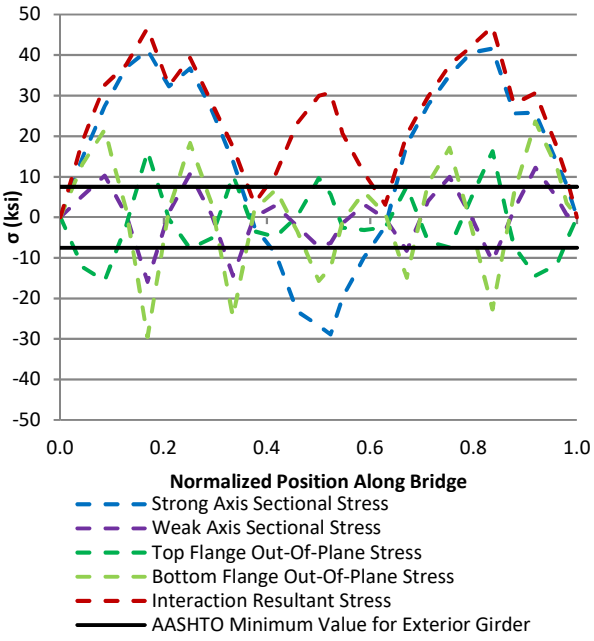

Figure 2.83 20 deg. skewed-parallel bridge with 30 ft cross-frame spacing – exterior girder (G4)

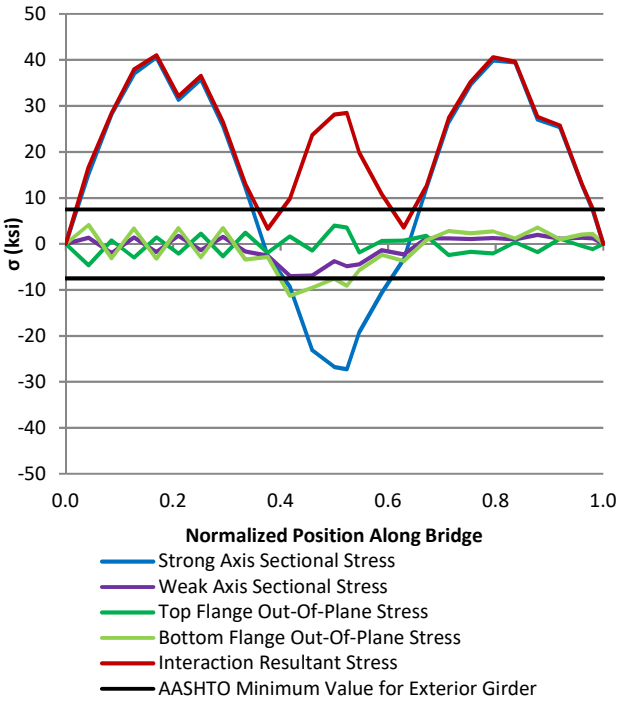

Figure 2.84 20 deg. skewed-staggered bridge with 15 ft cross-frame spacing – exterior girder (G4)

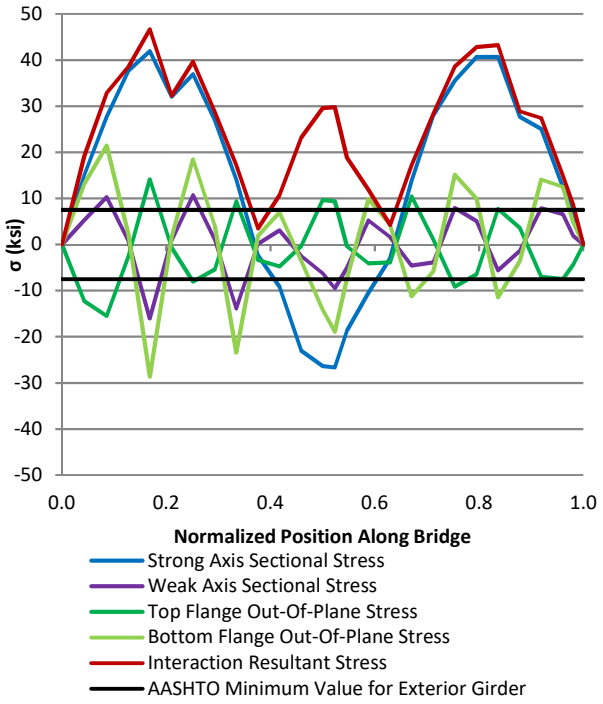

Figure 2.85 20 deg. skewed-staggered bridge with 30 ft cross-frame spacing – exterior girder (G4)

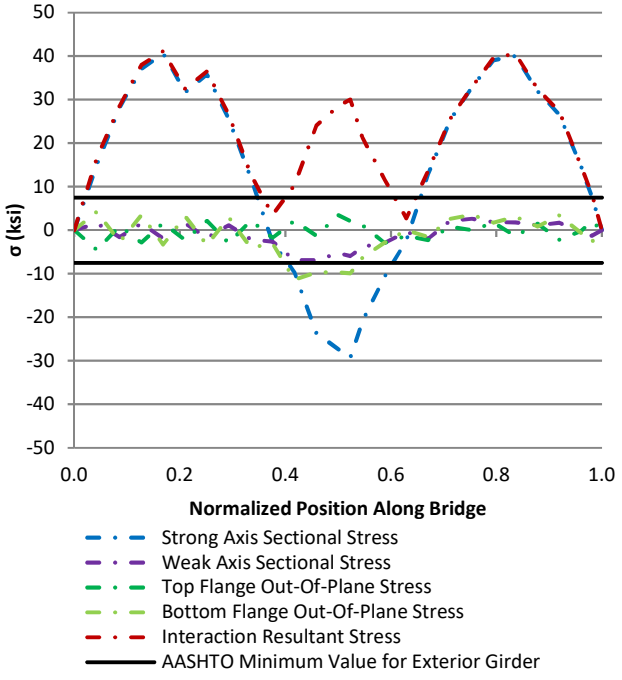

Figure 2.86 20 deg. skewed-unstaggered bridge with 15 ft cross-frame spacing – exterior girder (G4)

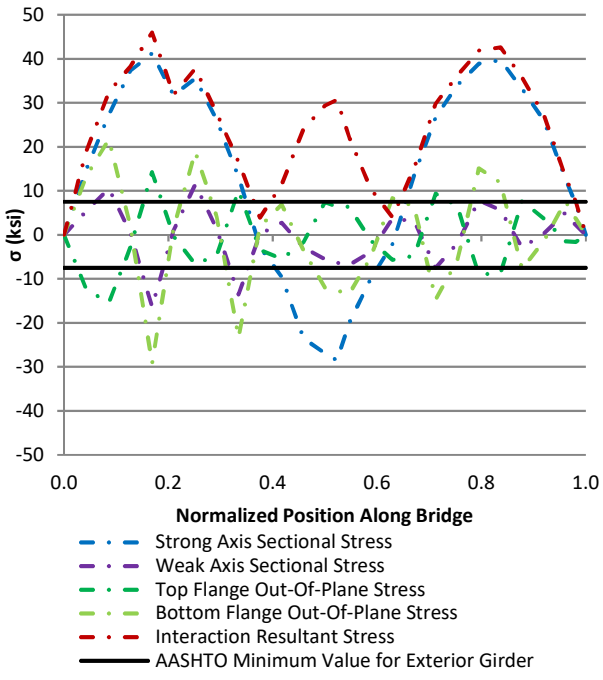

Figure 2.87 20 deg. skewed-unstaggered bridge with 30 ft cross-frame spacing – exterior girder (G4)

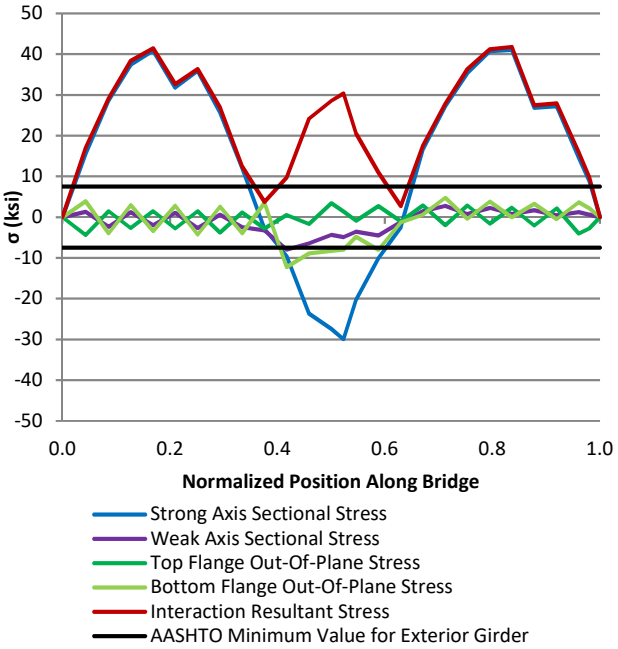

Figure 2.88 0 deg. non-skewed bridge with 15 ft cross-frame spacing – exterior girder (G4)

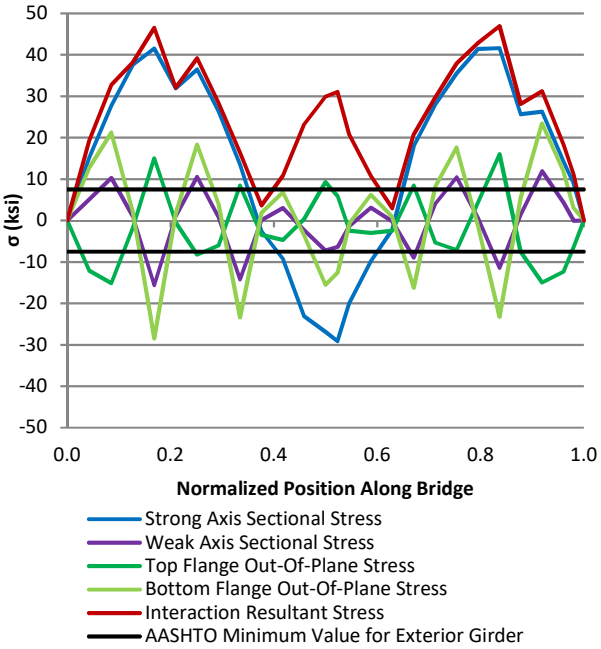

Figure 2.89 0 deg. non-skewed bridge with 30 ft cross-frame spacing – exterior girder (G4)

PEAK GIRDER BENDING STRESS AND PEAK AASHTO INTERACTION EQUATION RESULTANT

Table 2.2 through Table 2.15 show the maximum values for strong axis bending stress and lateral bending stress in the top flange, bottom flange, and weak axis girder section of interior girder, G3, for varying skew angles, cross-frame configurations, and cross-frame spacings. The AASHTO interaction equation resultant and yield factors, calculated as the ratio of the resultant divided by 344.7 MPa [50 ksi] steel yield stress, are also included. Both the positive and negative flexure regions are shown.

In the positive flexure region of Girder 3, the longest strong axis bending stress of 253 MPa [36.6 ksi] occurred in the 0-degree non-skewed bridge with 4.57 m [15 ft] cross-frame spacing. The smallest strong axis bending stress of 230 MPa [33.4 ksi] occurred in the positive flexure region of the 40-degree skewed-staggered bridge with 9.14 m [30 ft] cross-frame

spacing. The difference between the largest and smallest strong axis bending stress in Girder 3 was 23 MPa [3.2 ksi]. Therefore, skew angle, cross-frame configuration, and cross-frame spacing had a small effect on the vertical bending capacity of the interior girder in the positive bending region.

The largest magnitude of top flange lateral bending stress in the positive moment region occurred in the 40-degree skewed-staggered bridge with 9.14 m [30 ft]. It had a value of 42 MPa [6.1 ksi]. While the bottom flange typically produced larger lateral flange bending stress values compared to the top flange, the bottom flange is in tension in the positive moment region and does not impact the overall stability of the girder as much as the top compression flange. The magnitude of the largest bottom flange out-of-plane bending stress was 66 MPa [9.5 ksi] and it occurred in the 40-degree skewed-staggered bridge with 4.57 m [15 ft] cross-frame spacing. The smallest top flange lateral bending stress was 8 MPa [1.2 ksi], found in the 20-degree skewed-parallel bridge with 9.14 m [30 ft] cross-frame spacing. All lateral flange bending stresses in both the top and bottom flanges were within AASHTO's suggested value of 68.9 MPa [10 ksi] for the interior girder. Weak axis sectional bending stresses ranged from 37 MPa [5.4 ksi] in the 40-degree skewed-staggered bridge with 4.57 m [15 ft] cross-frame spacing to 10 MPa [1.4 ksi] in the 0, 20, and 40 degree skewed-parallel bridges with 9.14 m [30 ft] cross-frame spacing.

The largest interaction equation resultants in the positive flexure region, calculated using the top flange lateral bending stress, was 258 MPa [37.4 ksi] found in the 20-degree skewed-staggered with 4.57 m [15 ft] cross-frame spacing. The 20-degree skewed-parallel bridge with 4.57 m [15 ft] cross-frame spacing produced a close value of 256 [37.1 ksi], showing that cross-frame configuration had little effect on the overall interaction equation resultant in the interior girder. The smallest interaction equation resultant was 235 MPa [34.1 ksi] in the 40-degree

skewed-parallel bridge with 9.14 m [30 ft] cross-frame spacing. The equivalent yield ratios for largest and smallest resultants ranged from 1.34 to 1.46 relative to 345 MPa [50 ksi] steel.

In the negative flexure region, the largest strong axis bending stress of 202 MPa [29.3 ksi] occurred in the 0-degree non-skewed bridge with 4.57 m [15 ft] cross-frame spacing. The smallest strong axis bending stress of 180 MPa [26.1 ksi] occurred in the positive flexure region of the 40-degree skewed-unstaggered bridge with 4.57 m [15 ft] cross-frame spacing. The difference between the largest and smallest strong axis bending stress in the negative flexure region was only 22 MPa [3.2 ksi], same as in the positive flexure region.

The largest bottom flange lateral bending stress in the negative flexure region was 36 MPa [5.3 ksi] in the 40-degree skewed-staggered bridge with 4.57 m [15 ft] cross-frame spacing and the smallest stress was 12 MPa [1.8 ksi] in the 40 degree skewed-unstaggered bridge with 4.57 m [15 ft] cross-frame spacing. Lateral bending stresses in the bottom flange were larger than top flange and weak axis section out-of-plane bending stresses. These values were smaller than that found in the positive flexure region and most bridges produced magnitudes under half that of AASHTO's suggested value of 68.9 MPa [10 ksi]. Overall, the magnitude of stress variations between different configurations and between top flange, bottom flange, and weak axis sectional bending stresses were small in the interior girder.

The greatest interaction equation resultant computed using the bottom compression flange in the negative flexure region was 210 MPa [30.4 ksi], which occurred in the 0-degree non-skewed bridge with 9.14 m [30 ft] cross-frame spacing. The smallest interaction equation resultant in the same region was 184 MPa [26.7 ksi] in the 40-degree skewed-unstaggered bridge with 4.57 m [15 ft] cross-frame spacing. The difference between the largest and smallest

resultants was only 26 MPa [3.7 ksi]. These values produced relatively large yield ratios ranging from 1.64 to 1.87 in the negative moment region.

Strong axis and interaction equation resultant stresses in the interior girder typically decreased as cross-frame spacing increased for varying skew angles. As stated previously, lateral flange bending stresses had small magnitudes for both the 4.57 m [15 ft] and 9.14 m [30 ft] cross-frame spacings and varied without a clear pattern for the two cross-frame spacings. Overall, cross-frame spacing had little effect on strong axis bending stresses and almost no effect on lateral flange bending stresses in the interior girder.

Strong axis bending and interaction equation resultant stresses decreased with increasing skew angle in the Girder 3. Similar to varying cross-frame spacing, the low magnitudes in lateral bending stresses did not produce significant patterns for varying skew angles in the interior girder. Lateral bending stresses in both the positive and negative flexure regions decreased with increasing skew angle for some configurations and increased with others. Also, the 20 degree skewed bridges produced the largest lateral bending stresses in certain configurations while in other configurations it produced the smallest stresses.

With a few exceptions, the skewed-parallel configuration typically produced the largest strong axis bending stresses and usually had similar magnitude stresses as the skewed-staggered configuration in the interior girder. The skewed-unstaggered configuration generally produced the smallest values, although the relative stress differences between the three configurations were relatively small.

For out-of-plane bending stresses in Girder 3, the skewed-staggered configuration typically had the largest stress values and the skewed-parallel configuration had the smallest stresses in the positive flexure region for varying skew angle and cross-frame spacing. In the

negative flexure region, the opposite occurred in certain configurations for bottom flange or weak axis bending. However, exceptions include the skewed-unstaggered configuration, which produced the largest flange lateral bending stresses for certain configurations. Again, the lack of a clear pattern between varying cross-frame configurations may be due to overall low lateral bending stresses in the interior girder.

While the lateral bending stress magnitudes were small, the relative differences between strong axis bending stresses were very small as well. This may be the reason that there was no clear pattern for the interaction equation resultant for varying skew configurations. Generally, the skewed-parallel or skewed-staggered configuration produced the greatest resultant stresses and the skewed-parallel or skewed-unstaggered configuration produced the smallest resultant stresses depending on the skew angle, cross-frame spacing, and location in the positive or negative flexure region.

Table 2.2 AASHTO's interaction equation results for Girder 3 of the 40 degree skewed-parallel bridge with 4.57 m [15 ft] cross-frame spacing

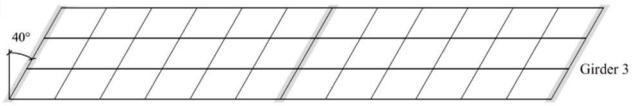

Load Combination	f_{bu}	f_l	$f_{bu} + 1/3\ f_l$	Yield Ratio
Strength 1 (ksi)	34.8	2.5	35.6	1.40
Strength 1 (MPa)	240	17	245.7	1.40

a) Top Flange – Positive Flexure Region

Load Combination	f_{bu}	f_l	$f_{bu} + 1/3\ f_l$	Yield Ratio
Strength 1 (ksi)	27.5	1.2	27.9	1.79
Strength 1 (MPa)	190	8	192.3	1.79

a) Top Flange – Negative Flexure Region

Load Combination	f_{bu}	f_l	$f_{bu} + 1/3\ f_l$	Yield Ratio
Strength 1 (ksi)	34.8	3.4	36.0	1.39
Strength 1 (MPa)	240	23	247.9	1.39

b) Bottom Flange – Positive Flexure Region

Load Combination	f_{bu}	f_l	$f_{bu} + 1/3\ f_l$	Yield Ratio
Strength 1 (ksi)	27.5	2.5	28.3	1.77
Strength 1 (MPa)	190	17	195.3	1.77

b) Bottom Flange – Negative Flexure Region

Load Combination	f_{bu}	f_l	$f_{bu} + 1/3\ f_l$	Yield Ratio
Strength 1 (ksi)	34.8	2.0	35.5	1.41
Strength 1 (MPa)	240	14	244.7	1.41

c) Weak Axis Girder Section – Positive Flexure Region

Load Combination	f_{bu}	f_l	$f_{bu} + 1/3\ f_l$	Yield Ratio
Strength 1 (ksi)	27.5	1.8	28.1	1.78
Strength 1 (MPa)	190	12	193.7	1.78

c) Strong Axis Girder Section – Negative Flexure Region

Table 2.3 AASHTO's interaction equation results for Girder 3 of the 40 degree skewed-parallel bridge with 9.14 m [30 ft] cross-frame spacing

Load Combination	f_{bu}	f_l	$f_{bu} + 1/3\ f_l$	Yield Ratio
Strength 1 (ksi)	33.7	1.5	34.1	1.46
Strength 1 (MPa)	232	10	235.4	1.46

a) Top Flange – Positive Flexure Region

Load Combination	f_{bu}	f_l	$f_{bu} + 1/3\ f_l$	Yield Ratio
Strength 1 (ksi)	27.3	0.9	27.6	1.81
Strength 1 (MPa)	188	6	190.2	1.81

a) Top Flange – Negative Flexure Region

Load Combination	f_{bu}	f_l	$f_{bu} + 1/3\ f_l$	Yield Ratio
Strength 1 (ksi)	33.7	2.3	34.4	1.45
Strength 1 (MPa)	232	16	237.4	1.45

b) Bottom Flange – Positive Flexure Region

Load Combination	f_{bu}	f_l	$f_{bu} + 1/3\ f_l$	Yield Ratio
Strength 1 (ksi)	27.3	3.6	28.5	1.76
Strength 1 (MPa)	188	25	196.3	1.76

b) Bottom Flange – Negative Flexure Region

Load Combination	f_{bu}	f_l	$f_{bu} + 1/3\ f_l$	Yield Ratio
Strength 1 (ksi)	33.7	1.4	34.1	1.47
Strength 1 (MPa)	232	10	235.2	1.47

c) Weak Axis Girder Section – Positive Flexure Region

Load Combination	f_{bu}	f_l	$f_{bu} + 1/3\ f_l$	Yield Ratio
Strength 1 (ksi)	27.3	2.2	28.0	1.79
Strength 1 (MPa)	188	15	193.0	1.79

c) Strong Axis Girder Section – Negative Flexure Region

Table 2.4 AASHTO's interaction equation results for Girder 3 of the 40 degree skewed-staggered bridge with 4.57 m [15 ft] cross-frame spacin

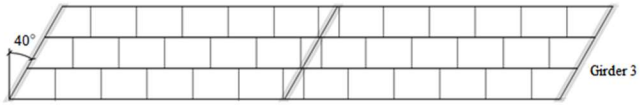

Load Combination	f_{bu}	f_l	$f_{bu} + 1/3\ f_l$	Yield Ratio
Strength 1 (ksi)	34.5	4.5	36.0	1.39
Strength 1 (MPa)	238	31	248.5	1.39

a) Top Flange – Positive Flexure Region

Load Combination	f_{bu}	f_l	$f_{bu} + 1/3\ f_l$	Yield Ratio
Strength 1 (ksi)	34.5	9.5	37.7	1.33
Strength 1 (MPa)	238	66	259.8	1.33

b) Bottom Flange – Positive Flexure Region

Load Combination	f_{bu}	f_l	$f_{bu} + 1/3\ f_l$	Yield Ratio
Strength 1 (ksi)	34.5	5.4	36.3	1.38
Strength 1 (MPa)	238	37	250.3	1.38

c) Weak Axis Girder Section – Positive Flexure Region

Load Combination	f_{bu}	f_l	$f_{bu} + 1/3\ f_l$	Yield Ratio
Strength 1 (ksi)	28.4	2.3	29.2	1.71
Strength 1 (MPa)	196	16	201.1	1.71

a) Top Flange – Negative Flexure Region

Load Combination	f_{bu}	f_l	$f_{bu} + 1/3\ f_l$	Yield Ratio
Strength 1 (ksi)	28.4	5.3	30.1	1.66
Strength 1 (MPa)	196	36	207.8	1.66

b) Bottom Flange – Negative Flexure Region

Load Combination	f_{bu}	f_l	$f_{bu} + 1/3\ f_l$	Yield Ratio
Strength 1 (ksi)	28.4	2.9	29.4	1.70
Strength 1 (MPa)	196	20	202.4	1.70

c) Strong Axis Girder Section – Negative Flexure Region

Table 2.5 AASHTO's interaction equation results for Girder 3 of the 40 degree skewed-staggered bridge with 9.14 m [30 ft] cross-frame spacin

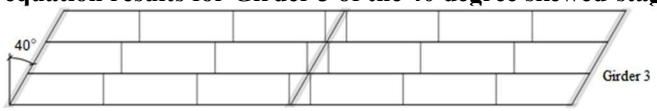

Load Combination	f_{bu}	f_l	$f_{bu} + 1/3\ f_l$	Yield Ratio
Strength 1 (ksi)	33.4	6.1	35.4	1.41
Strength 1 (MPa)	230	42	244.0	1.41

a) Top Flange – Positive Flexure Region

Load Combination	f_{bu}	f_l	$f_{bu} + 1/3\ f_l$	Yield Ratio
Strength 1 (ksi)	33.4	5.5	35.2	1.42
Strength 1 (MPa)	230	38	242.6	1.42

b) Bottom Flange – Positive Flexure Region

Load Combination	f_{bu}	f_l	$f_{bu} + 1/3\ f_l$	Yield Ratio
Strength 1 (ksi)	33.4	3.5	34.5	1.45
Strength 1 (MPa)	230	24	238.0	1.45

c) Weak Axis Girder Section – Positive Flexure Region

Load Combination	f_{bu}	f_l	$f_{bu} + 1/3\ f_l$	Yield Ratio
Strength 1 (ksi)	27.2	1.8	27.9	1.80
Strength 1 (MPa)	188	13	192.0	1.80

a) Top Flange – Negative Flexure Region

Load Combination	f_{bu}	f_l	$f_{bu} + 1/3\ f_l$	Yield Ratio
Strength 1 (ksi)	27.2	2.5	28.1	1.78
Strength 1 (MPa)	188	17	193.5	1.78

b) Bottom Flange – Negative Flexure Region

Load Combination	f_{bu}	f_l	$f_{bu} + 1/3\ f_l$	Yield Ratio
Strength 1 (ksi)	27.2	1.7	27.8	1.80
Strength 1 (MPa)	188	12	191.7	1.80

c) Strong Axis Girder Section – Negative Flexure Region

Table 2.6 AASHTO's interaction equation results for Girder 3 of the 40 degree skewed-unstaggered bridge with 4.57 m [15 ft] cross-frame spacing

Load Combination	f_{bu}	f_l	$f_{bu} + 1/3\, f_l$	Yield Ratio
Strength 1 (ksi)	33.8	4.8	35.4	1.41
Strength 1 (MPa)	233	33	244.3	1.41

a) Top Flange – Positive Flexure Region

Load Combination	f_{bu}	f_l	$f_{bu} + 1/3\, f_l$	Yield Ratio
Strength 1 (ksi)	26.1	1.8	26.7	1.87
Strength 1 (MPa)	180	12	184.1	1.87

a) Top Flange – Negative Flexure Region

Load Combination	f_{bu}	f_l	$f_{bu} + 1/3\, f_l$	Yield Ratio
Strength 1 (ksi)	33.8	7.3	36.3	1.38
Strength 1 (MPa)	233	50	250.1	1.38

b) Bottom Flange – Positive Flexure Region

Load Combination	f_{bu}	f_l	$f_{bu} + 1/3\, f_l$	Yield Ratio
Strength 1 (ksi)	26.1	1.8	26.7	1.87
Strength 1 (MPa)	180	12	184.2	1.87

b) Bottom Flange – Negative Flexure Region

Load Combination	f_{bu}	f_l	$f_{bu} + 1/3\, f_l$	Yield Ratio
Strength 1 (ksi)	33.8	3.7	35.1	1.43
Strength 1 (MPa)	233	25	241.7	1.43

c) Weak Axis Girder Section – Positive Flexure Region

Load Combination	f_{bu}	f_l	$f_{bu} + 1/3\, f_l$	Yield Ratio
Strength 1 (ksi)	26.1	1.2	26.5	1.89
Strength 1 (MPa)	180	8	182.8	1.89

c) Strong Axis Girder Section – Negative Flexure Region

Table 2.7 AASHTO's interaction equation results for Girder 3 of the 40 degree skewed-unstaggered bridge with 9.14 m [30 ft] cross-frame spacin

Load Combination	f_{bu}	f_l	$f_{bu} + 1/3\, f_l$	Yield Ratio
Strength 1 (ksi)	33.9	3.6	35.1	1.42
Strength 1 (MPa)	234	25	242.1	1.42

a) Top Flange – Positive Flexure Region

Load Combination	f_{bu}	f_l	$f_{bu} + 1/3\, f_l$	Yield Ratio
Strength 1 (ksi)	26.4	1.5	26.8	1.86
Strength 1 (MPa)	182	10	185.1	1.86

a) Top Flange – Negative Flexure Region

Load Combination	f_{bu}	f_l	$f_{bu} + 1/3\, f_l$	Yield Ratio
Strength 1 (ksi)	33.9	2.8	34.9	1.43
Strength 1 (MPa)	234	20	240.4	1.43

b) Bottom Flange – Positive Flexure Region

Load Combination	f_{bu}	f_l	$f_{bu} + 1/3\, f_l$	Yield Ratio
Strength 1 (ksi)	26.4	3.3	27.4	1.82
Strength 1 (MPa)	182	22	189.2	1.82

b) Bottom Flange – Negative Flexure Region

Load Combination	f_{bu}	f_l	$f_{bu} + 1/3\, f_l$	Yield Ratio
Strength 1 (ksi)	33.9	2.2	34.6	1.44
Strength 1 (MPa)	234	15	238.8	1.44

c) Weak Axis Girder Section – Positive Flexure Region

Load Combination	f_{bu}	f_l	$f_{bu} + 1/3\, f_l$	Yield Ratio
Strength 1 (ksi)	26.4	1.9	27.0	1.85
Strength 1 (MPa)	182	13	186.2	1.85

c) Strong Axis Girder Section – Negative Flexure Region

Table 2.8 AASHTO's interaction equation results for Girder 3 of the 20 degree skewed-parallel bridge with 4.57 m [15 ft] cross-frame spacing

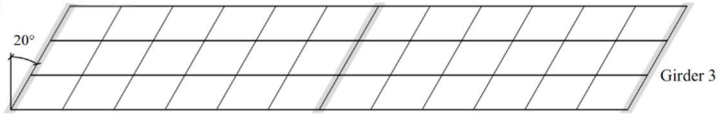

Load Combination	f_{bu}	f_l	$f_{bu} + 1/3\, f_l$	Yield Ratio
Strength 1 (ksi)	36.5	1.7	37.1	1.35
Strength 1 (MPa)	252	12	255.6	1.35

a) Top Flange – Positive Flexure Region

Load Combination	f_{bu}	f_l	$f_{bu} + 1/3\, f_l$	Yield Ratio
Strength 1 (ksi)	28.8	1.3	29.2	1.71
Strength 1 (MPa)	199	9	201.6	1.71

a) Top Flange – Negative Flexure Region

Load Combination	f_{bu}	f_l	$f_{bu} + 1/3\, f_l$	Yield Ratio
Strength 1 (ksi)	36.5	3.1	37.5	1.33
Strength 1 (MPa)	252	21	258.6	1.33

b) Bottom Flange – Positive Flexure Region

Load Combination	f_{bu}	f_l	$f_{bu} + 1/3\, f_l$	Yield Ratio
Strength 1 (ksi)	28.8	2.4	29.6	1.69
Strength 1 (MPa)	199	17	204.1	1.69

b) Bottom Flange – Negative Flexure Region

Load Combination	f_{bu}	f_l	$f_{bu} + 1/3\, f_l$	Yield Ratio
Strength 1 (ksi)	36.5	2.4	37.3	1.34
Strength 1 (MPa)	252	16	257.1	1.34

c) Weak Axis Girder Section – Positive Flexure Region

Load Combination	f_{bu}	f_l	$f_{bu} + 1/3\, f_l$	Yield Ratio
Strength 1 (ksi)	28.8	1.7	29.4	1.70
Strength 1 (MPa)	199	11	202.4	1.70

c) Strong Axis Girder Section – Negative Flexure Region

Table 2.9 AASHTO's interaction equation results for Girder 3 of the 20 degree skewed-parallel bridge with 9.14 m [30 ft] cross-frame spacing

Load Combination	f_{bu}	f_l	$f_{bu} + 1/3\, f_l$	Yield Ratio
Strength 1 (ksi)	35.1	1.2	35.5	1.41
Strength 1 (MPa)	242	8	245.0	1.41

a) Top Flange – Positive Flexure Region

Load Combination	f_{bu}	f_l	$f_{bu} + 1/3\, f_l$	Yield Ratio
Strength 1 (ksi)	28.4	1.0	28.8	1.74
Strength 1 (MPa)	196	7	198.2	1.74

a) Top Flange – Negative Flexure Region

Load Combination	f_{bu}	f_l	$f_{bu} + 1/3\, f_l$	Yield Ratio
Strength 1 (ksi)	35.1	1.9	35.8	1.40
Strength 1 (MPa)	242	13	246.5	1.40

b) Bottom Flange – Positive Flexure Region

Load Combination	f_{bu}	f_l	$f_{bu} + 1/3\, f_l$	Yield Ratio
Strength 1 (ksi)	28.4	4.1	29.8	1.68
Strength 1 (MPa)	196	28	205.3	1.68

b) Bottom Flange – Negative Flexure Region

Load Combination	f_{bu}	f_l	$f_{bu} + 1/3\, f_l$	Yield Ratio
Strength 1 (ksi)	35.1	1.4	35.6	1.41
Strength 1 (MPa)	242	9	245.3	1.41

c) Weak Axis Girder Section – Positive Flexure Region

Load Combination	f_{bu}	f_l	$f_{bu} + 1/3\, f_l$	Yield Ratio
Strength 1 (ksi)	28.4	2.5	29.2	1.71
Strength 1 (MPa)	196	17	201.6	1.71

c) Strong Axis Girder Section – Negative Flexure Region

Table 2.10 AASHTO's interaction equation results for Girder 3 of the 20 degree skewed-staggered bridge with 4.57 m [15 ft] cross-frame spacing

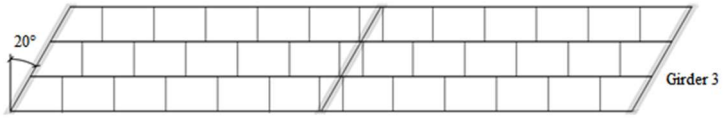

Load Combination	f_{bu}	f_l	$f_{bu} + 1/3\, f_l$	Yield Ratio
Strength 1 (ksi)	36.3	2.3	37.1	1.35
Strength 1 (MPa)	250	16	255.6	1.35

a) Top Flange – Positive Flexure Region

Load Combination	f_{bu}	f_l	$f_{bu} + 1/3\, f_l$	Yield Ratio
Strength 1 (ksi)	28.4	1.0	28.8	1.74
Strength 1 (MPa)	196	7	198.2	1.74

a) Top Flange – Negative Flexure Region

Load Combination	f_{bu}	f_l	$f_{bu} + 1/3\, f_l$	Yield Ratio
Strength 1 (ksi)	36.3	4.5	37.8	1.32
Strength 1 (MPa)	250	31	260.6	1.32

b) Bottom Flange – Positive Flexure Region

Load Combination	f_{bu}	f_l	$f_{bu} + 1/3\, f_l$	Yield Ratio
Strength 1 (ksi)	28.4	2.7	29.3	1.71
Strength 1 (MPa)	196	19	202.1	1.71

b) Bottom Flange – Negative Flexure Region

Load Combination	f_{bu}	f_l	$f_{bu} + 1/3\, f_l$	Yield Ratio
Strength 1 (ksi)	36.3	3.1	37.3	1.34
Strength 1 (MPa)	250	21	257.4	1.34

c) Weak Axis Girder Section – Positive Flexure Region

Load Combination	f_{bu}	f_l	$f_{bu} + 1/3\, f_l$	Yield Ratio
Strength 1 (ksi)	28.4	1.6	29.0	1.73
Strength 1 (MPa)	196	11	199.6	1.73

c) Strong Axis Girder Section – Negative Flexure Region

Table 2.11 AASHTO's interaction equation results for Girder 3 of the 20 degree skewed-staggered bridge with 9.14 m [30 ft] cross-frame spacing

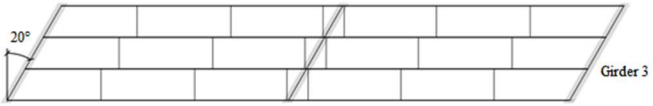

Load Combination	f_{bu}	f_l	$f_{bu} + 1/3\, f_l$	Yield Ratio
Strength 1 (ksi)	35.2	3.5	36.4	1.37
Strength 1 (MPa)	243	24	250.9	1.37

a) Top Flange – Positive Flexure Region

Load Combination	f_{bu}	f_l	$f_{bu} + 1/3\, f_l$	Yield Ratio
Strength 1 (ksi)	27.5	1.5	28.0	1.78
Strength 1 (MPa)	190	10	193.2	1.78

a) Top Flange – Negative Flexure Region

Load Combination	f_{bu}	f_l	$f_{bu} + 1/3\, f_l$	Yield Ratio
Strength 1 (ksi)	35.2	5.5	37.1	1.35
Strength 1 (MPa)	243	38	255.5	1.35

b) Bottom Flange – Positive Flexure Region

Load Combination	f_{bu}	f_l	$f_{bu} + 1/3\, f_l$	Yield Ratio
Strength 1 (ksi)	27.5	2.9	28.5	1.75
Strength 1 (MPa)	190	20	196.5	1.75

b) Bottom Flange – Negative Flexure Region

Load Combination	f_{bu}	f_l	$f_{bu} + 1/3\, f_l$	Yield Ratio
Strength 1 (ksi)	35.2	3.9	36.5	1.37
Strength 1 (MPa)	243	27	251.8	1.37

c) Weak Axis Girder Section – Positive Flexure Region

Load Combination	f_{bu}	f_l	$f_{bu} + 1/3\, f_l$	Yield Ratio
Strength 1 (ksi)	27.5	2.0	28.2	1.77
Strength 1 (MPa)	190	14	194.4	1.77

c) Strong Axis Girder Section – Negative Flexure Region

Table 2.12 AASHTO's interaction equation results for Girder 3 of the 20 degree skewed-unstaggered bridge with 4.57 m [15 ft] cross-frame spacin

Load Combination	f_{bu}	f_l	$f_{bu} + 1/3\, f_l$	Yield Ratio
Strength 1 (ksi)	35.7	1.9	36.4	1.38
Strength 1 (MPa)	246	13	250.7	1.38

a) Top Flange – Positive Flexure Region

Load Combination	f_{bu}	f_l	$f_{bu} + 1/3\, f_l$	Yield Ratio
Strength 1 (ksi)	27.2	1.2	27.6	1.81
Strength 1 (MPa)	187	8	190.2	1.81

a) Top Flange – Negative Flexure Region

Load Combination	f_{bu}	f_l	$f_{bu} + 1/3\, f_l$	Yield Ratio
Strength 1 (ksi)	35.7	5.8	37.7	1.33
Strength 1 (MPa)	246	40	259.6	1.33

b) Bottom Flange – Positive Flexure Region

Load Combination	f_{bu}	f_l	$f_{bu} + 1/3\, f_l$	Yield Ratio
Strength 1 (ksi)	27.2	2.8	28.1	1.78
Strength 1 (MPa)	187	19	193.9	1.78

b) Bottom Flange – Negative Flexure Region

Load Combination	f_{bu}	f_l	$f_{bu} + 1/3\, f_l$	Yield Ratio
Strength 1 (ksi)	35.7	2.6	36.6	1.37
Strength 1 (MPa)	246	18	252.2	1.37

c) Weak Axis Girder Section – Positive Flexure Region

Load Combination	f_{bu}	f_l	$f_{bu} + 1/3\, f_l$	Yield Ratio
Strength 1 (ksi)	27.2	1.6	27.7	1.81
Strength 1 (MPa)	187	11	191.0	1.81

c) Strong Axis Girder Section – Negative Flexure Region

Table 2.13 AASHTO's interaction equation results for Girder 3 of the 20 degree skewed-unstaggered bridge with 9.14 m [30 ft] cross-frame spacing

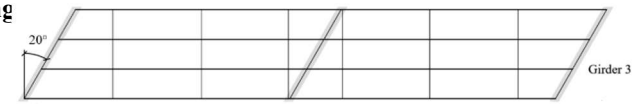

Load Combination	f_{bu}	f_l	$f_{bu} + 1/3\, f_l$	Yield Ratio
Strength 1 (ksi)	35.1	2.4	35.9	1.39
Strength 1 (MPa)	242	16	247.7	1.39

a) Top Flange – Positive Flexure Region

Load Combination	f_{bu}	f_l	$f_{bu} + 1/3\, f_l$	Yield Ratio
Strength 1 (ksi)	26.8	1.7	27.4	1.82
Strength 1 (MPa)	185	12	188.9	1.82

a) Top Flange – Negative Flexure Region

Load Combination	f_{bu}	f_l	$f_{bu} + 1/3\, f_l$	Yield Ratio
Strength 1 (ksi)	35.1	4.0	36.5	1.37
Strength 1 (MPa)	242	28	251.5	1.37

b) Bottom Flange – Positive Flexure Region

Load Combination	f_{bu}	f_l	$f_{bu} + 1/3\, f_l$	Yield Ratio
Strength 1 (ksi)	26.8	3.6	28.0	1.78
Strength 1 (MPa)	185	25	193.3	1.78

b) Bottom Flange – Negative Flexure Region

Load Combination	f_{bu}	f_l	$f_{bu} + 1/3\, f_l$	Yield Ratio
Strength 1 (ksi)	35.1	2.1	35.8	1.40
Strength 1 (MPa)	242	15	247.1	1.40

c) Weak Axis Girder Section – Positive Flexure Region

Load Combination	f_{bu}	f_l	$f_{bu} + 1/3\, f_l$	Yield Ratio
Strength 1 (ksi)	26.8	2.4	27.6	1.81
Strength 1 (MPa)	185	16	190.5	1.81

c) Strong Axis Girder Section – Negative Flexure Region

Table 2.14 AASHTO's interaction equation results for Girder 3 of the 0 degree non-skewed bridge with 4.57 m [15 ft] cross-frame spacing

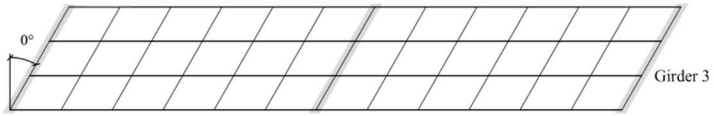

Load Combination	f_{bu}	f_l	$f_{bu} + 1/3\, f_l$	Yield Ratio
Strength 1 (ksi)	36.6	2.3	37.4	1.34
Strength 1 (MPa)	253	16	258.0	1.34

a) Top Flange – Positive Flexure Region

Load Combination	f_{bu}	f_l	$f_{bu} + 1/3\, f_l$	Yield Ratio
Strength 1 (ksi)	29.3	1.6	29.8	1.68
Strength 1 (MPa)	202	11	205.3	1.68

a) Top Flange – Negative Flexure Region

Load Combination	f_{bu}	f_l	$f_{bu} + 1/3\, f_l$	Yield Ratio
Strength 1 (ksi)	36.6	3.1	37.7	1.33
Strength 1 (MPa)	253	21	259.8	1.33

b) Bottom Flange – Positive Flexure Region

Load Combination	f_{bu}	f_l	$f_{bu} + 1/3\, f_l$	Yield Ratio
Strength 1 (ksi)	29.3	2.3	30.0	1.67
Strength 1 (MPa)	202	16	206.9	1.67

b) Bottom Flange – Negative Flexure Region

Load Combination	f_{bu}	f_l	$f_{bu} + 1/3\, f_l$	Yield Ratio
Strength 1 (ksi)	36.6	2.6	37.5	1.33
Strength 1 (MPa)	253	18	258.6	1.33

c) Weak Axis Girder Section – Positive Flexure Region

Load Combination	f_{bu}	f_l	$f_{bu} + 1/3\, f_l$	Yield Ratio
Strength 1 (ksi)	29.3	1.6	29.8	1.68
Strength 1 (MPa)	202	11	205.4	1.68

c) Strong Axis Girder Section – Negative Flexure Region

Table 2.15 AASHTO's interaction equation results for Girder 3 of the 0 degree non-skewed bridge with 9.14 m [30 ft] cross-frame spaci

Load Combination	f_{bu}	f_l	$f_{bu} + 1/3\, f_l$	Yield Ratio
Strength 1 (ksi)	35.7	1.6	36.2	1.38
Strength 1 (MPa)	246	11	249.8	1.38

a) Top Flange – Positive Flexure Region

Load Combination	f_{bu}	f_l	$f_{bu} + 1/3\, f_l$	Yield Ratio
Strength 1 (ksi)	29.0	0.9	29.3	1.71
Strength 1 (MPa)	200	6	201.9	1.71

a) Top Flange – Negative Flexure Region

Load Combination	f_{bu}	f_l	$f_{bu} + 1/3\, f_l$	Yield Ratio
Strength 1 (ksi)	35.7	2.5	36.5	1.37
Strength 1 (MPa)	246	17	251.9	1.37

b) Bottom Flange – Positive Flexure Region

Load Combination	f_{bu}	f_l	$f_{bu} + 1/3\, f_l$	Yield Ratio
Strength 1 (ksi)	29.0	4.2	30.4	1.65
Strength 1 (MPa)	200	29	209.5	1.65

b) Bottom Flange – Negative Flexure Region

Load Combination	f_{bu}	f_l	$f_{bu} + 1/3\, f_l$	Yield Ratio
Strength 1 (ksi)	35.7	1.4	36.2	1.38
Strength 1 (MPa)	246	10	249.3	1.38

c) Weak Axis Girder Section – Positive Flexure Region

Load Combination	f_{bu}	f_l	$f_{bu} + 1/3\, f_l$	Yield Ratio
Strength 1 (ksi)	29.0	2.6	29.9	1.68
Strength 1 (MPa)	200	18	205.8	1.67

c) Strong Axis Girder Section – Negative Flexure Region

Table 2.16 through Table 2.29 shows the maximum values of strong axis bending stress and lateral bending stress in the top flange, bottom flange, and weak axis girder section for Girder 4. AASHTO interaction equation results and yield factors, calculated as the ratio of the resultant divided by 344.7 MPa [50 ksi] steel yield stress, are also included. Results for both the positive and negative flexure regions are given.

In the positive moment region, the largest strong axis bending stress was 289 MPa [41.9 ksi], which occurred in the 20-degree skewed-staggered bridge with 9.14 m [30 ft] cross-frame spacing. The smallest strong axis bending moment in the positive moment region was 275 MPa [39.9 ksi], which occurred in the 40-degree skewed-parallel bridge with 4.57 m [15 ft] cross-frame spacing. Skew angle, configuration, and cross-frame spacing had little effect on the vertical bending moment in the exterior girder as the difference between the largest and smallest values was only 14 MPa [2.0 ksi].

In the positive moment region of Girder 4, the largest top flange lateral bending stress was 112 MPa [16.3 ksi], found in the 40-degree skewed-staggered bridge with 9.14 m [30 ft] cross-frame spacing. The smallest top flange lateral bending stress in the positive moment region was 29 MPa [4.2 ksi], found in the 40-degree skewed-staggered bridge with 4.57 m [15 ft] cross-frame spacing. Cross-frame spacing had the greatest effect on top flange lateral bending stress, with stresses in the 4.57 m [15 ft] cross-frame spacing models ranging from 29 MPa [4.2 ksi] to 34 MPa [5.0 ksi] and stresses in the 9.14 m [30 ft] cross-frame spacing models ranging from 106 MPa [15.4 ksi] to 112 MPa [16.3 ksi]. While the bridges with 4.57 m [15 ft] cross-frame spacings produced small magnitude lateral flange bending stresses, all bridges with 9.14 m [30 ft] cross-frame spacing had values more than twice the default value recommended by AASHTO

for the exterior girder, likely due to the large overhang loading. Values that exceed 51.7 MPa [7.5 ksi] in compression are highlighted in the tables.

The largest bottom flange lateral bending stress in the positive moment region was 207 MPa [30 ksi], which occurred in the 40-degree skewed-staggered bridge with 9.14 m [30 ft] cross-frame spacing. The smallest bottom flange lateral bending stress was 28 MPa [4.1 ksi], occurring in the positive moment region of the 20-degree skewed-staggered bridge with 4.57 m [15 ft] cross-frame spacing. While the magnitude of bottom flange lateral bending stresses is larger than top flange lateral bending stresses in the positive moment region, the tension flange will have less effect on the stability of the girder than the compression flange. As with the top flange, cross-frame spacing had a greater effect on magnitude of stresses in the flange than skew angle or configuration.

Lateral bending stress about the weak axis of the girder section was greatest in the 20-degree skewed-unstaggered bridge with 9.14 m [30 ft] cross-frame spacing, with a magnitude of 113 MPa [16.4 ksi] in the positive flexure region. The smallest weak axis girder sectional stress in the positive moment region was 14 MPa [2.0 ksi], found in the 20 degree skewed-staggered bridge with 4.57 m [15 ft] cross-frame spacing. Similar to the flanges, the skew angle and configuration did not have as much effect on the overall magnitude of stresses as cross-frame spacing.

In the positive moment region, the largest interaction equation resultant calculated using the top flange bending stress was 325 MPa [47.1 ksi]. This value was found in both the 20-degree skewed-staggered and 20 degree skewed-parallel bridge with 9.14 m [30 ft] cross-frame spacing. The equivalent yield ratio for this value was 1.06. The smallest resultant calculated using the top flange bending stress was 287 MPa [41.6 ksi], which occurred in the 40-degree

skewed-parallel bridge with 4.57 m [15 ft] cross-frame spacing. The equivalent yield ratio for the smallest resultant was 1.20 relative to steel with 345 MPa [50 ksi] yield strength.

In the negative moment region, the largest strong axis bending stress was 206 MPa [29.9 ksi], which occurred in both the 0-degree non-skewed bridge with 4.57 m [15 ft] cross-frame spacing and the 20-degree skewed-parallel bridge with 4.57 m [15 ft] cross-frame spacing. The smallest strong axis bending moment in the negative moment region was 184 MPa [26.7 ksi], which occurred in the 20-degree skewed-staggered bridge with 9.14 m [30 ft] cross-frame spacing. As in the positive flexure region, strong axis bending stresses were similar across varying skew angle, configuration, and cross-frame spacing. The difference between the largest and smallest values was only 22.1 MPa [3.2 ksi].

In the negative moment region, the largest top flange lateral bending stress was 68 MPa [9.9 ksi], found in the 40 degree skewed-parallel bridge with 9.14 m [30 ft] cross-frame spacing. The smallest top flange lateral bending stress in the negative moment region was 22 MPa [3.3 ksi], found in the 40 degree skewed-unstaggered bridge with 4.57 m [15 ft] cross-frame spacing. The top flange in the negative moment region is in tension and will not control stability of the girder given the low magnitudes.

The largest bottom flange lateral bending stress in the negative moment region was 130 MPa [18.9 ksi], which occurred in the 20-degree skewed-staggered bridge with 9.14 m [30 ft] cross-frame spacing. The smallest bottom flange lateral bending stress was 77 MPa [11.1 ksi], occurring in the negative moment region of the 40-degree skewed-staggered bridge with 4.57 m [15 ft] cross-frame spacing. As with the top flange, cross-frame spacing had a greater effect on magnitude of stresses in the flange than skew angle or configuration. Bottom flange lateral bending stresses with smaller values were found in the 4.57 m [15 ft] cross-frame spacing

models and with larger values produced by the 9.14 m [30 ft] cross-frame spacing models. Stresses in the 4.57 m [15 ft] cross-frame spacing models ranged from 77 MPa [11.1 ksi] to 90 MPa [13.1 ksi] and stresses in the 9.14 m [30 ft] cross-frame spacing models ranged from 92 MPa [13.4 ksi] to 130 MPa [18.9 ksi]. In the negative flexure region, all bridges had lateral bending stresses larger than the 51.7 MPa [7.5 ksi] value recommended by AASHTO for exterior girders.

Lateral bending stresses about the weak axis of the girder section was greatest in the 40 degree skewed-staggered bridge with 9.14 m [30 ft] cross-frame spacing, with a magnitude of 67 MPa [9.8 ksi] in the negative flexure region. The smallest weak axis girder section stress in the negative moment region was 43 MPa [6.2 ksi], found in the 20-degree skewed-staggered bridge with 4.57 m [15 ft] cross-frame spacing. Like the flanges, the skew angle and configuration did not have as much effect on the overall magnitude of stresses as cross-frame spacing.

In the negative moment region, the greatest interaction equation resultant calculated using the bottom flange bending stress was 236 MPa [34.3 ksi]. This value was found in the 0-degree non-skewed bridge with 9.14 m [30 ft] cross-frame spacing. The equivalent yield ratio for this value was 1.46, which is larger than the 1.02 value found in the positive flexure region. The smallest resultant calculated using bottom flange bending stresses was 214 MPa [31.0 ksi], which occurred in the 20-degree skewed-staggered bridge with 4.57 m [15 ft] cross-frame spacing. The equivalent yield ratio for the smallest resultant was 1.61 relative to 345 MPa [50 ksi] yield strength steel.

In Girder 4, for any given cross-frame spacing and configuration, strong axis bending stresses generally remained the same or slightly decreased with increasing skew angle. Lateral bending stresses were similar or slightly increased with increasing skew angle. As strong axis

bending stresses were of greater magnitude than lateral bending stresses, the interaction equation resultants were overall similar or slightly decreased with increasing skew angle in the exterior girder.

For any given skew angle and configuration in exterior girder, G4, strong axis bending stresses generally increased slightly in the positive moment region and decreased slightly in the negative moment region with increasing cross-frame spacing. Lateral flange and weak axis bending stresses increased significantly in the positive bending region when cross-frame spacing increased from 4.57 m [15 ft] to 9.14 m [30 ft]. Lateral bending stresses in the negative moment region typically increased for top and bottom flange stresses and slightly decreased for weak axis sectional stresses with increased cross-frame spacing. The interaction equation resultant increased with longer cross-frame spacings in the positive moment region from both an increase in strong axis and lateral bending stresses. Increasing the cross-frame spacing, the interaction equation resultant increased slightly with top flange bending stresses in the negative bending region and was similar or decreased slightly when calculated using bottom flange bending stresses or weak axis bending stresses.

Bending stress variations in Girder 4 between skewed-staggered, skewed-parallel, and skewed-unstaggered configurations were typically small and did not play a large role in defining girder stress patterns. For bridges with 20-degree skew angle and 4.57 m [15 ft] and 9.14 m [30 ft] cross-frame spacings, strong axis bending stresses were almost the same or decreased from the skewed-parallel to the skewed-staggered configuration. For 40-degree skewed bridges in the positive bending region, strong axis bending stresses were typically largest in the skewed-staggered configuration and smallest in the skewed-parallel configuration, although the difference in magnitudes were small. For 40-degree skewed bridges in the negative bending

region, the skewed-parallel and skewed-unstaggered configuration produced the largest strong axis bending stresses and the skewed-staggered configuration produced the smallest peak stresses in the exterior girder.

With exception of 40-degree skewed bridges with 9.14 m [30 ft] cross-frame spacing, out-of-plane bending stresses were typically greatest in the skewed-parallel configuration and smallest in the skewed-staggered configuration for the positive flexure region of Girder 4. In the negative flexure region, some configurations showed a similar pattern as the positive flexure region while others configurations produced larger lateral bending stresses in the skewed-staggered configuration and smaller stresses in the skewed-parallel and skewed-unstaggered configuration. For lateral bending stresses in the 40-degree skewed bridges with 9.14 m [30 ft] cross-frame spacing, peak stresses decreased from the skewed-staggered configuration to the skewed-parallel configuration, and the skewed-unstaggered configuration produced the smallest stresses. For all models, stress variations between the different skew configurations were relatively small or equal in the exterior girder. As mentioned previously, cross-frame spacing had a much greater effect on lateral bending stress than any other factor due to the large overhang load eccentricity.

As the differences in both the strong axis and lateral bending stresses were small for all skew configurations in the exterior girder, peak interaction resultant values did not show any discernible patterns between the three configurations for varying skew angle and cross-frame spacing. Similar to its component stresses, the resultant stress magnitudes between different configurations were small.

Table 2.16 AASHTO's interaction equation results for Girder 4 of the 40 degree skewed-parallel bridge with 4.57 m [15 ft] cross-frame spacing

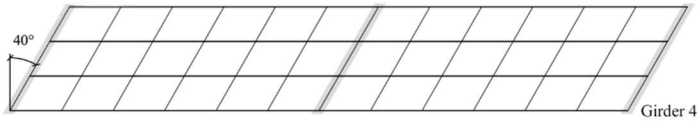

Load Combination	f_{bu}	f_l	$f_{bu} + 1/3\ f_l$	Yield Ratio
Strength 1 (ksi)	39.9	5.0	41.6	1.20
Strength 1 (MPa)	275	34	286.6	1.20

a) Top Flange – Positive Flexure Region

Load Combination	f_{bu}	f_l	$f_{bu} + 1/3\ f_l$	Yield Ratio
Strength 1 (ksi)	29.2	3.4	30.3	1.65
Strength 1 (MPa)	201	23	209.0	1.65

a) Top Flange – Negative Flexure Region

Load Combination	f_{bu}	f_l	$f_{bu} + 1/3\ f_l$	Yield Ratio
Strength 1 (ksi)	39.9	5.1	41.6	1.20
Strength 1 (MPa)	275	35	287.0	1.20

b) Bottom Flange – Positive Flexure Region

Load Combination	f_{bu}	f_l	$f_{bu} + 1/3\ f_l$	Yield Ratio
Strength 1 (ksi)	29.2	12.3	33.3	1.50
Strength 1 (MPa)	201	85	229.7	1.50

b) Bottom Flange – Negative Flexure Region

Load Combination	f_{bu}	f_l	$f_{bu} + 1/3\ f_l$	Yield Ratio
Strength 1 (ksi)	39.9	2.9	40.9	1.22
Strength 1 (MPa)	275	20	281.9	1.22

c) Weak Axis Girder Section – Positive Flexure Region

Load Combination	f_{bu}	f_l	$f_{bu} + 1/3\ f_l$	Yield Ratio
Strength 1 (ksi)	29.2	7.3	31.6	1.58
Strength 1 (MPa)	201	50	218.1	1.58

c) Strong Axis Girder Section – Negative Flexure Region

Table 2.17 AASHTO's interaction equation results for Girder 4 of the 40 degree skewed-parallel bridge with 9.14 m [30 ft] cross-frame spacing

Load Combination	f_{bu}	f_l	$f_{bu} + 1/3\ f_l$	Yield Ratio
Strength 1 (ksi)	40.6	16.1	46.0	1.09
Strength 1 (MPa)	280	111	316.9	1.09

a) Top Flange – Positive Flexure Region

Load Combination	f_{bu}	f_l	$f_{bu} + 1/3\ f_l$	Yield Ratio
Strength 1 (ksi)	28.2	9.9	31.4	1.59
Strength 1 (MPa)	194	68	216.7	1.59

a) Top Flange – Negative Flexure Region

Load Combination	f_{bu}	f_l	$f_{bu} + 1/3\ f_l$	Yield Ratio
Strength 1 (ksi)	40.6	29.4	50.4	0.99
Strength 1 (MPa)	280	202	347.3	0.99

b) Bottom Flange – Positive Flexure Region

Load Combination	f_{bu}	f_l	$f_{bu} + 1/3\ f_l$	Yield Ratio
Strength 1 (ksi)	28.2	15.9	33.4	1.49
Strength 1 (MPa)	194	110	230.6	1.49

b) Bottom Flange – Negative Flexure Region

Load Combination	f_{bu}	f_l	$f_{bu} + 1/3\ f_l$	Yield Ratio
Strength 1 (ksi)	40.6	16.2	46.0	1.09
Strength 1 (MPa)	280	112	317.1	1.09

c) Weak Axis Girder Section – Positive Flexure Region

Load Combination	f_{bu}	f_l	$f_{bu} + 1/3\ f_l$	Yield Ratio
Strength 1 (ksi)	28.2	7.4	30.6	1.63
Strength 1 (MPa)	194	51	211.0	1.63

c) Strong Axis Girder Section – Negative Flexure Region

Table 2.18 AASHTO's interaction equation results for Girder 4 of the 40 degree skewed-staggered bridge with 4.57 m [15 ft] cross-frame spacing

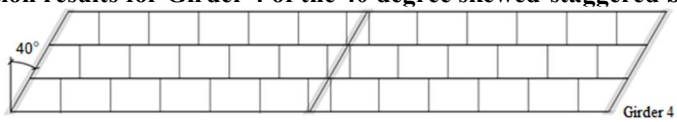

Load Combination	f_{bu}	f_l	$f_{bu} + 1/3\, f_l$	Yield Ratio
Strength 1 (ksi)	40.8	4.2	42.2	1.18
Strength 1 (MPa)	281	29	291.0	1.18

a) Top Flange – Positive Flexure Region

Load Combination	f_{bu}	f_l	$f_{bu} + 1/3\, f_l$	Yield Ratio
Strength 1 (ksi)	28.2	4.3	29.6	1.69
Strength 1 (MPa)	194	29	203.9	1.69

a) Top Flange – Negative Flexure Region

Load Combination	f_{bu}	f_l	$f_{bu} + 1/3\, f_l$	Yield Ratio
Strength 1 (ksi)	40.8	4.9	42.4	1.18
Strength 1 (MPa)	281	34	292.5	1.18

b) Bottom Flange – Positive Flexure Region

Load Combination	f_{bu}	f_l	$f_{bu} + 1/3\, f_l$	Yield Ratio
Strength 1 (ksi)	28.2	11.1	31.9	1.57
Strength 1 (MPa)	194	77	219.7	1.57

b) Bottom Flange – Negative Flexure Region

Load Combination	f_{bu}	f_l	$f_{bu} + 1/3\, f_l$	Yield Ratio
Strength 1 (ksi)	40.8	2.9	41.8	1.20
Strength 1 (MPa)	281	20	288.0	1.20

c) Weak Axis Girder Section – Positive Flexure Region

Load Combination	f_{bu}	f_l	$f_{bu} + 1/3\, f_l$	Yield Ratio
Strength 1 (ksi)	28.2	6.4	30.3	1.65
Strength 1 (MPa)	194	44	208.9	1.65

c) Strong Axis Girder Section – Negative Flexure Region

Table 2.19 AASHTO's interaction equation results for Girder 4 of the 40 degree skewed-staggered bridge with 9.14 m [30 ft] cross-frame spacing

Load Combination	f_{bu}	f_l	$f_{bu} + 1/3\, f_l$	Yield Ratio
Strength 1 (ksi)	41.5	16.3	46.9	1.07
Strength 1 (MPa)	286	112	323.2	1.07

a) Top Flange – Positive Flexure Region

Load Combination	f_{bu}	f_l	$f_{bu} + 1/3\, f_l$	Yield Ratio
Strength 1 (ksi)	27.7	9.2	30.8	1.62
Strength 1 (MPa)	191	63	212.4	1.62

a) Top Flange – Negative Flexure Region

Load Combination	f_{bu}	f_l	$f_{bu} + 1/3\, f_l$	Yield Ratio
Strength 1 (ksi)	41.5	30.0	51.4	0.97
Strength 1 (MPa)	286	207	354.7	0.97

b) Bottom Flange – Positive Flexure Region

Load Combination	f_{bu}	f_l	$f_{bu} + 1/3\, f_l$	Yield Ratio
Strength 1 (ksi)	27.7	17.1	33.4	1.50
Strength 1 (MPa)	191	118	230.4	1.50

b) Bottom Flange – Negative Flexure Region

Load Combination	f_{bu}	f_l	$f_{bu} + 1/3\, f_l$	Yield Ratio
Strength 1 (ksi)	41.5	16.8	47.1	1.06
Strength 1 (MPa)	286	116	324.6	1.06

c) Weak Axis Girder Section – Positive Flexure Region

Load Combination	f_{bu}	f_l	$f_{bu} + 1/3\, f_l$	Yield Ratio
Strength 1 (ksi)	27.7	9.8	31.0	1.61
Strength 1 (MPa)	191	67	213.7	1.61

c) Strong Axis Girder Section – Negative Flexure Region

Table 2.20 AASHTO's interaction equation results for Girder 4 of the 40 degree skewed-unstaggered bridge with 4.57 m [15 ft] cross-frame spacing

Load Combination	f_{bu}	f_l	$f_{bu} + 1/3\, f_l$	Yield Ratio
Strength 1 (ksi)	40.7	4.6	42.2	1.18
Strength 1 (MPa)	280	32	291.0	1.18

a) Top Flange – Positive Flexure Region

Load Combination	f_{bu}	f_l	$f_{bu} + 1/3\, f_l$	Yield Ratio
Strength 1 (ksi)	29.0	3.3	30.0	1.66
Strength 1 (MPa)	200	22	207.2	1.66

a) Top Flange – Negative Flexure Region

Load Combination	f_{bu}	f_l	$f_{bu} + 1/3\, f_l$	Yield Ratio
Strength 1 (ksi)	40.7	4.6	42.2	1.19
Strength 1 (MPa)	280	31	290.9	1.19

b) Bottom Flange – Positive Flexure Region

Load Combination	f_{bu}	f_l	$f_{bu} + 1/3\, f_l$	Yield Ratio
Strength 1 (ksi)	29.0	11.7	32.9	1.52
Strength 1 (MPa)	200	80	226.5	1.52

b) Bottom Flange – Negative Flexure Region

Load Combination	f_{bu}	f_l	$f_{bu} + 1/3\, f_l$	Yield Ratio
Strength 1 (ksi)	40.7	2.1	41.4	1.21
Strength 1 (MPa)	280	14	285.2	1.21

c) Weak Axis Girder Section – Positive Flexure Region

Load Combination	f_{bu}	f_l	$f_{bu} + 1/3\, f_l$	Yield Ratio
Strength 1 (ksi)	29.0	6.7	31.2	1.60
Strength 1 (MPa)	200	46	215.1	1.60

c) Strong Axis Girder Section – Negative Flexure Region

Table 2.21 AASHTO's interaction equation results for Girder 4 of the 40 degree skewed-unstaggered bridge with 9.14 m [30 ft] cross-frame spacing

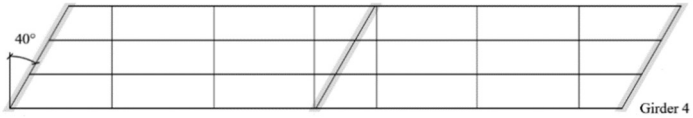

Load Combination	f_{bu}	f_l	$f_{bu} + 1/3\, f_l$	Yield Ratio
Strength 1 (ksi)	40.8	15.8	46.0	1.09
Strength 1 (MPa)	281	109	317.3	1.09

a) Top Flange – Positive Flexure Region

Load Combination	f_{bu}	f_l	$f_{bu} + 1/3\, f_l$	Yield Ratio
Strength 1 (ksi)	28.2	8.2	30.9	1.62
Strength 1 (MPa)	194	57	213.3	1.62

a) Top Flange – Negative Flexure Region

Load Combination	f_{bu}	f_l	$f_{bu} + 1/3\, f_l$	Yield Ratio
Strength 1 (ksi)	40.8	28.4	50.2	1.00
Strength 1 (MPa)	281	196	346.2	1.00

b) Bottom Flange – Positive Flexure Region

Load Combination	f_{bu}	f_l	$f_{bu} + 1/3\, f_l$	Yield Ratio
Strength 1 (ksi)	28.2	13.4	32.7	1.53
Strength 1 (MPa)	194	92	225.3	1.53

b) Bottom Flange – Negative Flexure Region

Load Combination	f_{bu}	f_l	$f_{bu} + 1/3\, f_l$	Yield Ratio
Strength 1 (ksi)	40.8	16.0	46.1	1.08
Strength 1 (MPa)	281	110	317.7	1.08

c) Weak Axis Girder Section – Positive Flexure Region

Load Combination	f_{bu}	f_l	$f_{bu} + 1/3\, f_l$	Yield Ratio
Strength 1 (ksi)	28.2	6.2	30.3	1.65
Strength 1 (MPa)	194	43	208.7	1.65

c) Strong Axis Girder Section – Negative Flexure Region

Table 2.22 AASHTO's interaction equation results for Girder 4 of the 20 degree skewed-parallel bridge with 4.57 m [15 ft] cross-frame spacing

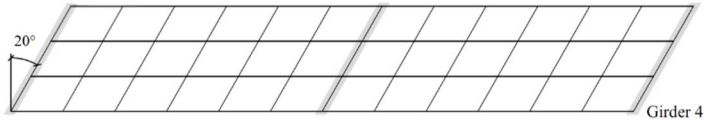

Load Combination	f_{bu}	f_l	$f_{bu} + 1/3\, f_l$	Yield Ratio
Strength 1 (ksi)	40.9	4.7	42.4	1.18
Strength 1 (MPa)	282	32	292.4	1.18

a) Top Flange – Positive Flexure Region

Load Combination	f_{bu}	f_l	$f_{bu} + 1/3\, f_l$	Yield Ratio
Strength 1 (ksi)	29.9	3.4	31.0	1.61
Strength 1 (MPa)	206	24	213.6	1.61

a) Top Flange – Negative Flexure Region

Load Combination	f_{bu}	f_l	$f_{bu} + 1/3\, f_l$	Yield Ratio
Strength 1 (ksi)	40.9	4.5	42.4	1.18
Strength 1 (MPa)	282	31	292.0	1.18

b) Bottom Flange – Positive Flexure Region

Load Combination	f_{bu}	f_l	$f_{bu} + 1/3\, f_l$	Yield Ratio
Strength 1 (ksi)	29.9	13.1	34.2	1.46
Strength 1 (MPa)	206	90	235.8	1.46

b) Bottom Flange – Negative Flexure Region

Load Combination	f_{bu}	f_l	$f_{bu} + 1/3\, f_l$	Yield Ratio
Strength 1 (ksi)	40.9	2.7	41.8	1.20
Strength 1 (MPa)	282	19	287.9	1.20

c) Weak Axis Girder Section – Positive Flexure Region

Load Combination	f_{bu}	f_l	$f_{bu} + 1/3\, f_l$	Yield Ratio
Strength 1 (ksi)	29.9	8.0	32.5	1.54
Strength 1 (MPa)	206	55	224.2	1.54

c) Strong Axis Girder Section – Negative Flexure Region

Table 2.23 AASHTO's interaction equation results for Girder 4 of the 20 degree skewed-parallel bridge with 9.14 m [30 ft] cross-frame spacing

Load Combination	f_{bu}	f_l	$f_{bu} + 1/3\, f_l$	Yield Ratio
Strength 1 (ksi)	41.6	16.3	47.1	1.06
Strength 1 (MPa)	287	112	324.5	1.06

a) Top Flange – Positive Flexure Region

Load Combination	f_{bu}	f_l	$f_{bu} + 1/3\, f_l$	Yield Ratio
Strength 1 (ksi)	28.9	9.7	32.1	1.56
Strength 1 (MPa)	199	67	221.3	1.56

a) Top Flange – Negative Flexure Region

Load Combination	f_{bu}	f_l	$f_{bu} + 1/3\, f_l$	Yield Ratio
Strength 1 (ksi)	41.6	29.5	51.5	0.97
Strength 1 (MPa)	287	204	354.9	0.97

b) Bottom Flange – Positive Flexure Region

Load Combination	f_{bu}	f_l	$f_{bu} + 1/3\, f_l$	Yield Ratio
Strength 1 (ksi)	28.9	15.7	34.1	1.47
Strength 1 (MPa)	199	108	235.2	1.47

b) Bottom Flange – Negative Flexure Region

Load Combination	f_{bu}	f_l	$f_{bu} + 1/3\, f_l$	Yield Ratio
Strength 1 (ksi)	41.6	15.9	46.9	1.07
Strength 1 (MPa)	287	110	323.6	1.07

c) Weak Axis Girder Section – Positive Flexure Region

Load Combination	f_{bu}	f_l	$f_{bu} + 1/3\, f_l$	Yield Ratio
Strength 1 (ksi)	28.9	7.3	31.3	1.60
Strength 1 (MPa)	199	50	215.8	1.60

c) Strong Axis Girder Section – Negative Flexure Region

Table 2.24 AASHTO's interaction equation results for Girder 4 of the 20 degree skewed-staggered bridge with 4.57 m [15 ft] cross-frame spacing

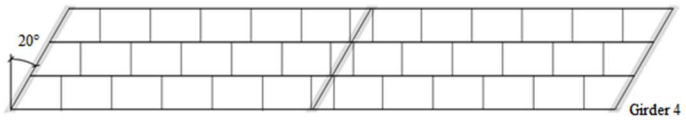

Load Combination	f_{bu}	f_l	$f_{bu} + 1/3\ f_l$	Yield Ratio
Strength 1 (ksi)	40.6	4.7	42.1	1.19
Strength 1 (MPa)	280	32	290.4	1.19

a) Top Flange – Positive Flexure Region

Load Combination	f_{bu}	f_l	$f_{bu} + 1/3\ f_l$	Yield Ratio
Strength 1 (ksi)	40.6	4.1	41.9	1.19
Strength 1 (MPa)	280	28	289.2	1.19

b) Bottom Flange – Positive Flexure Region

Load Combination	f_{bu}	f_l	$f_{bu} + 1/3\ f_l$	Yield Ratio
Strength 1 (ksi)	40.6	2.0	41.2	1.21
Strength 1 (MPa)	280	14	284.4	1.21

c) Weak Axis Girder Section – Positive Flexure Region

Load Combination	f_{bu}	f_l	$f_{bu} + 1/3\ f_l$	Yield Ratio
Strength 1 (ksi)	27.3	4.0	28.6	1.75
Strength 1 (MPa)	188	27	197.1	1.75

a) Top Flange – Negative Flexure Region

Load Combination	f_{bu}	f_l	$f_{bu} + 1/3\ f_l$	Yield Ratio
Strength 1 (ksi)	27.3	11.3	31.0	1.61
Strength 1 (MPa)	188	78	213.9	1.61

b) Bottom Flange – Negative Flexure Region

Load Combination	f_{bu}	f_l	$f_{bu} + 1/3\ f_l$	Yield Ratio
Strength 1 (ksi)	27.3	7.0	29.6	1.69
Strength 1 (MPa)	188	48	203.9	1.69

c) Strong Axis Girder Section – Negative Flexure Region

Table 2.25 AASHTO's interaction equation results for Girder 4 of the 20 degree skewed-staggered bridge with 9.14 m [30 ft] cross-frame spacing

Load Combination	f_{bu}	f_l	$f_{bu} + 1/3\ f_l$	Yield Ratio
Strength 1 (ksi)	41.9	15.5	47.1	1.06
Strength 1 (MPa)	289	107	324.7	1.06

a) Top Flange – Positive Flexure Region

Load Combination	f_{bu}	f_l	$f_{bu} + 1/3\ f_l$	Yield Ratio
Strength 1 (ksi)	41.9	28.7	51.5	0.97
Strength 1 (MPa)	289	198	355.1	0.97

b) Bottom Flange – Positive Flexure Region

Load Combination	f_{bu}	f_l	$f_{bu} + 1/3\ f_l$	Yield Ratio
Strength 1 (ksi)	41.9	16.0	47.3	1.06
Strength 1 (MPa)	289	111	326.0	1.06

c) Weak Axis Girder Section – Positive Flexure Region

Load Combination	f_{bu}	f_l	$f_{bu} + 1/3\ f_l$	Yield Ratio
Strength 1 (ksi)	26.7	9.7	29.9	1.67
Strength 1 (MPa)	184	67	205.9	1.67

a) Top Flange – Negative Flexure Region

Load Combination	f_{bu}	f_l	$f_{bu} + 1/3\ f_l$	Yield Ratio
Strength 1 (ksi)	26.7	18.9	33.0	1.52
Strength 1 (MPa)	184	130	227.2	1.52

b) Bottom Flange – Negative Flexure Region

Load Combination	f_{bu}	f_l	$f_{bu} + 1/3\ f_l$	Yield Ratio
Strength 1 (ksi)	26.7	9.5	29.8	1.68
Strength 1 (MPa)	184	65	205.5	1.68

c) Strong Axis Girder Section – Negative Flexure Region

Table 2.26 AASHTO's interaction equation results for Girder 4 of the 20 degree skewed-unstaggered bridge with 4.57 m [15 ft] cross-frame spacing

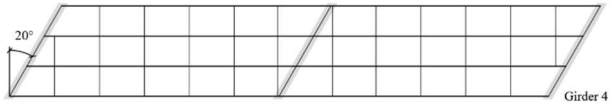

Load Combination	f_{bu}	f_l	$f_{bu} + 1/3\, f_l$	Yield Ratio
Strength 1 (ksi)	40.6	4.57	42.1	1.19
Strength 1 (MPa)	280	31	290.5	1.19

a) Top Flange – Positive Flexure Region

Load Combination	f_{bu}	f_l	$f_{bu} + 1/3\, f_l$	Yield Ratio
Strength 1 (ksi)	29.3	3.5	30.5	1.64
Strength 1 (MPa)	202	24	210.1	1.64

a) Top Flange – Negative Flexure Region

Load Combination	f_{bu}	f_l	$f_{bu} + 1/3\, f_l$	Yield Ratio
Strength 1 (ksi)	40.6	4.3	42.0	1.19
Strength 1 (MPa)	280	30	289.9	1.19

b) Bottom Flange – Positive Flexure Region

Load Combination	f_{bu}	f_l	$f_{bu} + 1/3\, f_l$	Yield Ratio
Strength 1 (ksi)	29.3	11.4	33.1	1.51
Strength 1 (MPa)	202	78	228.2	1.51

b) Bottom Flange – Negative Flexure Region

Load Combination	f_{bu}	f_l	$f_{bu} + 1/3\, f_l$	Yield Ratio
Strength 1 (ksi)	40.6	2.6	41.5	1.21
Strength 1 (MPa)	280	18	286.0	1.21

c) Weak Axis Girder Section – Positive Flexure Region

Load Combination	f_{bu}	f_l	$f_{bu} + 1/3\, f_l$	Yield Ratio
Strength 1 (ksi)	29.3	6.9	31.6	1.58
Strength 1 (MPa)	202	48	217.9	1.58

c) Strong Axis Girder Section – Negative Flexure Region

Table 2.27 AASHTO's interaction equation results for Girder 4 of the 20 degree skewed-unstaggered bridge with 9.14 m [30 ft] cross-frame spacing

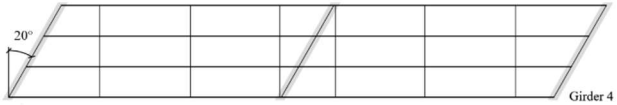

Load Combination	f_{bu}	f_l	$f_{bu} + 1/3\, f_l$	Yield Ratio
Strength 1 (ksi)	41.2	15.4	46.4	1.08
Strength 1 (MPa)	284	106	319.6	1.08

a) Top Flange – Positive Flexure Region

Load Combination	f_{bu}	f_l	$f_{bu} + 1/3\, f_l$	Yield Ratio
Strength 1 (ksi)	28.5	7.4	31.0	1.61
Strength 1 (MPa)	197	51	213.6	1.61

a) Top Flange – Negative Flexure Region

Load Combination	f_{bu}	f_l	$f_{bu} + 1/3\, f_l$	Yield Ratio
Strength 1 (ksi)	41.2	29.3	51.0	0.98
Strength 1 (MPa)	284	202	351.5	0.98

b) Bottom Flange – Positive Flexure Region

Load Combination	f_{bu}	f_l	$f_{bu} + 1/3\, f_l$	Yield Ratio
Strength 1 (ksi)	28.5	13.5	33.0	1.51
Strength 1 (MPa)	197	93	227.6	1.51

b) Bottom Flange – Negative Flexure Region

Load Combination	f_{bu}	f_l	$f_{bu} + 1/3\, f_l$	Yield Ratio
Strength 1 (ksi)	41.2	16.4	46.7	1.07
Strength 1 (MPa)	284	113	322.1	1.07

c) Weak Axis Girder Section – Positive Flexure Region

Load Combination	f_{bu}	f_l	$f_{bu} + 1/3\, f_l$	Yield Ratio
Strength 1 (ksi)	28.5	6.8	30.8	1.62
Strength 1 (MPa)	197	47	212.3	1.62

c) Strong Axis Girder Section – Negative Flexure Region

Table 2.28 AASHTO's interaction equation results for Girder 4 of the 0 degree non-skewed bridge with 4.57 m [15 ft] cross-frame spacing

Load Combination	f_{bu}	f_l	$f_{bu} + 1/3\, f_l$	Yield Ratio
Strength 1 (ksi)	41.0	4.4	42.5	1.18
Strength 1 (MPa)	283	30	292.9	1.18

a) Top Flange – Positive Flexure Region

Load Combination	f_{bu}	f_l	$f_{bu} + 1/3\, f_l$	Yield Ratio
Strength 1 (ksi)	29.9	3.4	31.1	1.61
Strength 1 (MPa)	206	24	214.2	1.61

a) Top Flange – Negative Flexure Region

Load Combination	f_{bu}	f_l	$f_{bu} + 1/3\, f_l$	Yield Ratio
Strength 1 (ksi)	41.0	4.8	42.6	1.17
Strength 1 (MPa)	283	33	293.8	1.17

b) Bottom Flange – Positive Flexure Region

Load Combination	f_{bu}	f_l	$f_{bu} + 1/3\, f_l$	Yield Ratio
Strength 1 (ksi)	29.9	12.3	34.0	1.47
Strength 1 (MPa)	206	84	234.5	1.47

b) Bottom Flange – Negative Flexure Region

Load Combination	f_{bu}	f_l	$f_{bu} + 1/3\, f_l$	Yield Ratio
Strength 1 (ksi)	41.0	2.8	42.0	1.19
Strength 1 (MPa)	283	19	289.2	1.19

c) Weak Axis Girder Section – Positive Flexure Region

Load Combination	f_{bu}	f_l	$f_{bu} + 1/3\, f_l$	Yield Ratio
Strength 1 (ksi)	29.9	8.0	32.6	1.53
Strength 1 (MPa)	206	55	224.7	1.53

c) Strong Axis Girder Section – Negative Flexure Region

Table 2.29 AASHTO's interaction equation results for Girder 4 of the 0 degree non-skewed bridge with 9.14 m [30 ft] cross-frame spacing

Load Combination	f_{bu}	f_l	$f_{bu} + 1/3\, f_l$	Yield Ratio
Strength 1 (ksi)	41.6	16.0	47.0	1.06
Strength 1 (MPa)	287	111	323.8	1.06

a) Top Flange – Positive Flexure Region

Load Combination	f_{bu}	f_l	$f_{bu} + 1/3\, f_l$	Yield Ratio
Strength 1 (ksi)	29.1	9.3	32.2	1.55
Strength 1 (MPa)	201	64	222.1	1.55

a) Top Flange – Negative Flexure Region

Load Combination	f_{bu}	f_l	$f_{bu} + 1/3\, f_l$	Yield Ratio
Strength 1 (ksi)	41.6	28.5	51.1	0.98
Strength 1 (MPa)	287	196	352.4	0.98

b) Bottom Flange – Positive Flexure Region

Load Combination	f_{bu}	f_l	$f_{bu} + 1/3\, f_l$	Yield Ratio
Strength 1 (ksi)	29.1	15.5	34.3	1.46
Strength 1 (MPa)	201	107	236.3	1.46

b) Bottom Flange – Negative Flexure Region

Load Combination	f_{bu}	f_l	$f_{bu} + 1/3\, f_l$	Yield Ratio
Strength 1 (ksi)	41.6	15.6	46.8	1.07
Strength 1 (MPa)	287	107	322.8	1.07

c) Weak Axis Girder Section – Positive Flexure Region

Load Combination	f_{bu}	f_l	$f_{bu} + 1/3\, f_l$	Yield Ratio
Strength 1 (ksi)	29.1	7.2	31.5	1.59
Strength 1 (MPa)	201	50	217.3	1.59

c) Strong Axis Girder Section – Negative Flexure Region

CONCLUSIONS

The results of a study aimed at investigating the effect of skew angle and cross-frame layout on lateral flange bending stresses in skewed steel bridges showed that for this particular bridge design:

- Overall, neither skew angle nor cross-frame configuration had a clearly discernable effect on lateral bending stresses.
- Skew angle, cross-frame configuration, and cross-frame spacing had little effect on vertical bending capacity as the range between strong axis bending stresses for the different parameters was only 23 MPa [3.2 ksi] in the interior girder and 14 MPa [2.0 ksi] in the exterior girder.
- The magnitude of lateral bending stress variations between different configurations were small in the interior girder, and all lateral flange stresses in the interior girder were within AASHTO's suggested value of 68.9 MPa [10 ksi].
- Cross-frame configuration had little effect on the overall magnitude and pattern of stress variation for bridges with cross-frames spaced less than 9.14 m [30 ft]. The largest range between the largest and smallest interaction equation resultant stress was only 26 MPa [3.7 ksi].
- Strong axis bending and interaction equation resultant stresses slightly decreased with increasing skew angle, but skew angle had little effect on resultant stresses in either girders.
- Cross-frame spacing had little effect on strong axis bending stress and almost no effect on lateral bending stress in the interior girder.

- However, in the exterior girder, cross-frame spacing had a significant effect on lateral bending stresses. While bridges with 4.57 m [15 ft] cross-frame spacing were associated with small lateral flange bending stresses, all bridges with 9.14 m [30 ft] cross-frame spacing had stresses more than twice that of 51.7 MPa [7.5 ksi] recommended by AASHTO for exterior girders, likely due to the large overhang loads.
- In the exterior girder, the largest interaction equation resultant for top flange bending stress in the positive moment region was 325 MPa [47.1 ksi], corresponding to an equivalent yield ratio of 1.06 for 345 MPa [50 ksi] steel.

Decreased cross-frame spacing provided more brace support and helped reduce lateral flange bending stresses. The cross-frame skew angle was found to have little effect on bending stresses in general. There was very little difference between the 0, 20, and 40 degree skewed bridges in terms of lateral flange bending stresses, f_l, for cross-frames spaced less than 9.14 m [30 ft]. Based on values of f_l alone in this study, the 20 degree limit for placing cross-frames perpendicular to the girder line may not be warranted. However, cross-frames placed parallel to skew for larger skew angles, while reducing problems with fit-up and distortion induced fatigue, increases connection flexibility and lowers brace stiffness, thus requiring larger members. These connections also become more complicated to fabricate and increases construction costs. Nevertheless, the skew angle is dependent on the roadway approach and is difficult for the engineer to adjust. Therefore it is up to the engineer to select the type of cross-frame and orientation which optimizes the design while considering construction and erection criterias.

Cross-frame configuration also had little effect on stresses in general. While the stress magnitudes were significant, stress ranges for strong axis and lateral bending stresses were small

for any given cross-frame spacing. In this study, cross-frames placed parallel to skew performed similarly to cross-frames placed perpendicular to the girder line. Based on the research performed in this paper, cross-frames placed parallel to skew effectively braced the girder members while reducing cross-frames forces, as a smaller portion of the lateral load is carried by the cross-frames with increasing skew.

As skew angles become larger, designers will have to consider the increased fabrication cost of using longer, heavier members for a skewed-parallel configuration combined with the benefit of reduced fit-up costs and better fatigue performance. Cross-frames are also typically connected to the girders when lifted into their final positions. Increasing the weight of these lifts may require the usage of heavier equipment, which increases the cost and design requirements. Therefore in the design of cross-frames, it is important to consider ease of fit-up, constructability, and serviceability along with strength and stiffness requirements. While Part 2 did not specifically focus on cross-frame behavior or stresses, Part 3 examines the behavior of cross-frames members and show that the brace effectiveness was not an issue for spacings less than 9.14 m [30 ft].

Although the results did not invalidate AASHTO's interaction equation requirements, the minimum yield ratio computed was only six percent in the exterior girder using top flange out-of-plane bending stresses for this particular bridge design. Lateral flange bending stresses found in the top flange of the positive moment region in the exterior girder was over twice that of AASHTO's recommended value of 51.7 MPa [7.5 ksi] for bridges with 9.14 m [30 ft] cross-frame spacing. However, the f_l values presented in AASHTO was not intended to include overhang brackets or other sources of large lateral loading. When these forces are identified, a

refined analysis is required. These loads will be specific to each bridge design and the f_l values presented in AASHTO does not account for them.

Without large lateral bending forces acting on the bridge, f_l will be small in magnitude. It was found from placing the overhang loads as a vertical load on the exterior girder of the 40 degree skewed-staggered bridge with 9.14 m [30 ft] cross-frame spacing that maximum top flange lateral deflection in the exterior girder was only 12.7 mm [0.5 in] and maximum stresses in the same girder reached 20.7 MPa [3.0 ksi]. With the overhang loads applied through the overhang brackets, top flange lateral deflection reach as high as 45.7 mm [1.8 in] and maximum out-of-plane stresses was as large as 207 MPa [30 ksi]. While cross-frame orientation had little effect on the magnitude of f_l, lateral flange bending stresses should be accounted for based on the specific conditions of the bridge. These may include wind loads, construction loads, large overhang loads, eccentric concrete placement, and other sources of lateral loading. Overall, lateral flange bending stresses in the exterior girder during construction were found to be significantly larger than the minimum values prescribed in the AASHTO-LRFD Bridge Design Specification. In the case of this design, the engineer may consider increasing the flange width, providing more transverse stiffeners, or adding lateral bracing to reduce lateral flange bending.

REFERENCES

AASHTO (2010). “LRFD Bridge Design Specifications.” *American Association of State Highway and Transportation Officials,* Washington, D.C.

AISC (2010). “Steel Construction Manual, 14th Ed.” *American Institute of Steel Construction*, Chicago, IL.

AISI Example 2: Two-Span Continuous Composite I Girder (1997). *American Iron and Steel Institute*.

Bishara, A. and Elmir, W. (1990). "*Interaction between Cross Frames and Girders*." J. Struct. Eng., 10.1061/(ASCE)0733-9445(1990)116:5(1319), 1319-1333.

Gupta, Y. P., Kumar, A. (1983). “Structural Behaviour of Interconnected Skew Slab-Girder Bridges,” Journal of the Institution of Engineers (India), Civil Engineering Division, 64, 119-124.

Hassel, H. (2011). “An Analytical Evaluation of Distortion-Induced Fatigue in Steel Bridges,” thesis, presented to University of Kansas, at Lawrence, KS in partial fulfillment of the requirements for the° of Master of Civil Engineering.

Hassel, H., Bennett, C., Matamoros, A., and Rolfe, S. (2012). “Parametric analysis of cross-frame layout on distortion-induced fatigue in skewed steel bridges.” J. Bridge Eng., 10.1061/(ASCE)BE.19435592.0000388, 601–611.

Jung, S.-K., and White, D.W. (2006). “Shear Strength of Horizontally Curved Steel I-Girders – Finite Element Analysis Studies,” *Journal of Constructional Steel Research*, 62(4), 329-342.

KDOT. (2010). “Design Manual: Volume III – Bridge Selection.” *Kansas Department of Transportation*.

Krupicka, G., and Poellot, B. (1993). “Nuisance Stiffness,” HDR Engineering, Inc., Bridgeline, 4(1), 3.

McConnell, J., Ambrose, K., and Radovic, M. (2013). “Cross-Frame Forces in Skewed Steel I-Girder Bridges: Field Testing and Applications to System-Capacity”, Presented at 2013 ASCE / SEI Structures Congress, Pittsburgh, PA, May 2-4, 2013.

McConnell, J., Radovic, M. (2014). “Evaluation of Cross-frame Designs for Highly Skewed Steel I-Girder Bridges.” Presented at 31st Annual International Bridge Conference, Engineers Society of Western Pennsylvania, Pittsburg, PA, IBC 14-47.

McConnell, J., Radovic, M., and Ambrose, K. (2014). “Cross-Frame Forces in Skewed Steel I-Girder Bridges: Field Measurements and Finite Element Analysis”, University of Delaware Center for Bridge Engineering, Final Report to Delaware Department of Transportation.

Ozgur, C. (2011). “Influence Of Cross-Frame Detailing On Curved And Skewed Steel I-Girder Bridges”, Doctoral Dissertation, Georgia Institute of Technology.

Quadrato, C., Battistini, A., Frank, K., Helwig, T., & Engelhardt, M. (2010). Improved cross-frame connection details for steel bridges with skewed supports. Transportation Research Record: Journal of the Transportation Research Board, (2200), 29-35.

Simulia. (2010). ABAQUS FEA Version 6.10-2. Providence, RI. http://www.simulia.com.

Wang, L. and Helwig, T.A. (2008). "Stability Bracing Requirements for Steel Bridge Girders with Skewed Supports." *Journal of Bridge Engineering*, 13(2), 149-157.

Yura, J. (2001). "Fundamentals of Beam Bracing." *Engineering Journal*, AISC, First Quarter, 11-26.

Zhou, C., Bennett, C., Matamoros, A., Li, J., and Rolfe, S. "Skewed Steel Bridges, Part I: Effect of Cross-Frame Layout on Lateral Flange Bending Stresses," Final Report to the Kansas Department of Transportation, Project KTRAN KU-13-3, September, 2015.

Ziemian, R. D. and McGuire, W. (2000). Mastan2 Version 3.5. http://www.mastan2.com

Part 3

SKEWED STEEL BRIDGES - CROSS-FRAME AND CONNECTION DESIGN TO ENSURE BRACE EFFECTIVENESS

J. Zhou[1], C.R. Bennett[2], A.B. Matamoros[3], J. Li[4]

ABSTRACT

Skewed bridges in Kansas are often designed such that the cross-frames are carried parallel to the skew angle up to 40°, while many other states place cross-frames perpendicular to the girder for skew angles greater than 20°. Skewed-parallel cross-frames are longer and require different connections than cross-frames oriented perpendicular to the girder. As cross-frames lengthen, they become less stiff and less effective at distributing forces between girders if the same connecting elements are used. For the cross-frame / diaphragm elements to be able to brace the bridge girders, the brace elements must possess both sufficient strength and stiffness to restrain the girder from instability. While strength can be addressed by increasing the cross-sectional properties of the brace elements, providing sufficient stiffness is a more significant challenge. Stiffness of the brace system is dependent on both the brace elements and the type of connection made (Yura et al. 1992; Yura 2001). Therefore it is important to determine whether the cross-frames and their corresponding connecting elements placed in a parallel-to-skew configuration are sufficiently designed to resist lateral torsional buckling demands using current KDOT practices.

Department of Civil, Environmental, and Architectural Engineering
University of Kansas, 1530 W. 15th St, Lawrence, KS 66045
Tel. (785) 864-3235, Fax. (785) 864-5631

[1] James Zhou, Bridge Engineer, Jacobs Engineering Group, James.Zhou@jacobs.com
[2] Caroline R. Bennett, PhD, PE, Associate Professor, University of Kansas, crb@ku.edu
[3] Adolfo B. Matamoros, PhD, PE, Professor, University of Texas at San Antonio, adolfo.matamoros@utsa.edu
[4] Jian Li, PhD, PE, Assistant Professor, University of Kansas, jianli@ku.edu

In a suite of detailed 3D, solid finite element analyses models of skewed bridge systems, cross-frame layout, connection thickness and type, and skew angle were varied. Skewed bridge systems with cross-frames placed parallel to the skew angle as well as systems with cross-frames arranged in a staggered configuration were considered. Varying bent plate connection thicknesses and a half-pipe connection were also analyzed. Cross-frame spacing of 4.57 m [15 ft] and 9.14 [30 ft] were examined; severe cross-frame spacing of 13.7 m [45 ft] was also considered to examine behavior at very long unbraced lengths. The models include geometric nonlinearities to assess the lateral deflection and lateral flange bending stresses in different bridge systems. Material nonlinearities were found to produce insignificant differences in the results previously discussed and were not included in the full parametric analysis.

The findings of this study showed that skew angle, skew configuration, and connection type all influenced the strength and stiffness of the bridge system. The skewed-staggered configuration produced larger lateral deflections in the girders compared to the skewed-parallel configuration. With a couple of exceptions, the skewed-staggered configuration also produced larger cross-frame stresses compared to the skewed-parallel configuration. Larger skew angles resulted in smaller lateral deflections. As the skew angles increased, cross-frame compression stresses generally remained the same or increased while maximum cross-frame tension stresses generally decreased. Thicker bent plates produced larger lateral displacements, with the 12.7 mm [1/2 in] and 25.4 mm [1.0 in] thick bent plates producing similar lateral displacement values. For skewed configurations, cross-frame stress generally increased with thicker bent plates, with 12.7 mm [1/2 in] and 25.4 mm [1.0 in] thick bent plates producing similar cross-frame tension stresses. For the non-skewed configuration, cross-frame stresses decreased with thicker bent

plates. The half-pipe connection was shown to correspond with smaller magnitudes of lateral deflections than bent plate connections.

Finally, the data showed that cross-frame placed parallel to skew up to an angle of 40° performed similar to or better than cross-frames oriented perpendicular to skew for every given skew angle and connection type.

INTRODUCTION AND BACKGROUND

The American Association of State Highway and Transportation Officials (AASHTO) provisions for lateral flange bending stresses are based on the assumption that cross-frames are oriented perpendicular to the girder line whenever the skew angle is greater than 20° (AASHTO 2010). Current Kansas Department of Transportation (KDOT) design practice is to align cross-frames parallel to the skew angle for bridges with skew angles up to 40°. This approach avoids problems associated with fit-up during erection and deck placement. However, there is a potentially significant discrepancy between assumptions implicit in the AASHTO-LRFD Bridge Design Specifications (AASHTO 2010) and bridges that are designed to be skewed between 20 and 40° when cross-frames are placed parallel to the skew.

AASHTO (2010) defines a cross-frame as a transverse truss framework connecting adjacent longitudinal flexural components. In non-skewed (right) bridges under dead loads, only tensile forces develop in the intermediate cross-frame chords and only compressive forces develop in the cross-frame diagonals. However, in skewed bridges, most members of the intermediate cross-frames develop both compressive and tensile forces, depending on the loading condition. Skewed bearing lines subject the bridge to torsion by developing transverse load paths

between the girders through the cross-frames. Furthermore, girder vertical displacements, major-axis bending stresses, and lateral flange bending stresses can be significantly influenced by large skew effects if the transverse load transfer is large (Ozgur 2011). On the other hand, it has been suggested that the effects of skew on forces induced in the cross-frame members may be neglected for skew angles 20° or less (Bishara and Elmir 1990).

Intermediate cross-frames in multi-beam steel bridges are used predominantly for lateral-load resistance, live load distribution, and reducing the unbraced length of the girder's compression flange, providing support against lateral-torsional buckling. Cross-frames also provide support against lateral bending and torsional buckling, particularly in skewed and curved bridges. In traditional designs for skewed and curved girders, gravity loads are assumed to be resisted by the girders and transverse loads are presumed to be resisted by the intermediate cross-frames. In actuality, the whole bridge acts as a system, with gravity loads producing stresses in the cross-frames as well as the girders, and girders also resisting lateral bending loads transmitted through the cross-frames.

Stability of the overall bridge system depends on cross-frames and diaphragms placed at discrete locations along the bridge to resist buckling loads. For these cross-frame and diaphragm elements to effectively brace the bridge girders, both sufficient strength and stiffness are required to restrain the girder from instability. These dual criteria for bracing systems were first presented for column-buckling behavior (Winter 1958). While the buckling behavior of beams is more complicated, dual bracing criteria (strength and stiffness) still apply to beam bracing systems.

When the cross-frame/diaphragm elements are placed at any angle other than 90° against the girder line, their efficiency in transferring lateral loads is reduced due to a smaller lateral force component that is developed in the brace. Wang and Helwig (2008) note that although

cross-frames placed parallel to skew can be effective at skew angles greater than 20°, the effects of connection flexibility and lowered brace stiffness due to longer braces becomes an issue that must be considered. This can be easily addressed from a strength perspective by increasing the cross-sectional properties of the brace elements such that the cross-frame/diaphragm has sufficient strength in the skewed position to transfer lateral forces from one girder to another. However, increasing the cross-frame member section properties results in an increase in their internal forces and vice versa (Bishara and Elmir 1990). Because of this, the greater the skew angle, the larger the maximum forces induced in the cross-frame members (Bishara and Elmir 1990). While greater cross-frame forces would suggest greater bridge transverse stiffness and smaller girder lateral deflection, research have found that moments, rotations, and deflections increased with an increase in skew angle (Gupta and Kumar 1983).

Previous research has also shown that the larger the bridge skew, the larger the lateral load transfer becomes, influencing bottom flange lateral bending stress (Ozgur 2011). In skewed bridges, torsional moments created in the girders by the lateral deflection of their bottom flanges, while small in magnitude, were larger than in right bridges (Bishara and Elmir 1990). McConnell et al. (2014) found that bridge skew and cross-frame placement significantly influenced bottom flange lateral bending stress and indicated that placing cross-frames in the staggered configuration reduced a bridge's transverse stiffness. In the staggered configuration, cross-frame forces cannot be directly balanced by a cross-frame on the opposite side of the girder section. This leads to a decrease in cross-frame forces, but an increase in flange lateral bending stresses and girder lateral deflection (McConnell et. al 2014).

Ensuring that cross-frame and brace elements have sufficient stiffness can be a more difficult task than ensuring sufficient strength. If the stiffness of the cross-frames approaches or

exceeds that necessitated to restrain the girders, they can provide “nuisance stiffness” that increase stresses in the bottom flange that are not typically accounted for in design (Ozgur 2011). Increases in undesirable stiffness of the girders due to the location and stiffness of cross-frames/diaphragms often occur near skewed supports as well (Krupicka and Poellot 1993). Simply increasing the cross-sectional properties of the cross-frame members can increase both the unwanted stiffness of the cross-frames and induce greater internal forces in its members. These forces can be significantly greater than girder stresses in highly-skewed bridges (McConnell et al. 2013).

As a result, cross-frames are required by AASHTO to be oriented perpendicular to the girder line for skew angles greater than 20°, due to smaller cross-frame forces and smaller demand-to-capacity ratios for cross-frame stresses compared to cross-frames oriented parallel to the girder line. While this decreased stiffness would lead to greater lateral bending stresses in girders with cross-frames in the staggered configuration, studies showed that these lateral bending stresses were of low magnitudes (McConnell and Radovic 2014). Therefore, small increases in girder lateral stresses is seen as an efficient tradeoff for reduced cross-frame stresses afforded by placing cross-frames perpendicular to the girder. This is especially significant since cross-frames stresses are generally closer in magnitude to their limiting stresses than the girder stresses are to their yielding stresses (McConnell and Radovic 2014).

By orienting cross-frames perpendicular to the girder line, cross-frame forces are reduced at the expense of increased lateral bending stresses in flanges. However, the vertical displacements at the opposite ends of a given brace can differ substantially in a skewed-staggered bracing layout. This can result in large live load induced forces and distortion induced fatigue, with stiffer braces attracting larger forces (Hassel et al. 2012). While the influence of

skew had little effect on the strength and stiffness requirements of the bracing oriented perpendicular to the girder lines, when bracing is oriented parallel to the skew angle, skew angle has a significant impact on the stiffness and strength requirements of the bracing (Wang and Helwig 2008). Brace elements should be designed for the basic stability requirements, considering the effects of cross-frame layout, stiffness, and strength requirements.

Stiffness of the brace system is dependent on both the brace elements and the type of connection made (Yura et al. 1992; Yura 2001). Moreover, effectiveness of the cross-frame/diaphragm is also dependent upon the stiffness of the girder web. Even if skewed brace elements have sufficient strength and stiffness to transfer lateral flange bending stresses, the connecting elements tying the brace elements to the girder may act as a "fuse" in the system if the connecting elements possess insufficient stiffness. Based on previous studies that the researchers have performed (Hassel et al. 2012), this can be the case when bent-plate connection types are utilized in a skewed bridge system.

The objective of this study was to provide guidance concerning the design of cross-frame/diaphragm elements oriented parallel to the skew angle as well as the connecting elements. Stability of the bridge girders is especially of concern during the construction stages, before the concrete deck is acting compositely with the steel girders, and in a non-composite bridge. Additionally, stability of bridge girders must be accounted for in design of girders in negative bending regions, even after composite action has been achieved between the girder and deck. If cross-frames/diaphragms are carried parallel to the skew angle for skews up to 40° in a non-composite bridge or in a negative bending moment region of a composite bridge, those brace elements must be carefully designed such that they have sufficient strength and stiffness to brace the girders against lateral torsional buckling. Detailed three-dimensional solid finite element

models were used to investigate these parameters. The suite of models included the following parameter variations:

- skew angle (0°, 20°, and 40°);
- cross-frame spacing (4.57 m [15 ft], 9.14 m [30 ft], and 13.7 m [45 ft]);
- cross-frame orientation (skewed-staggered, skewed-parallel, and skewed unstaggered); and
- cross-frame connection type (9.5 mm [3/8 in] thick bent plate connection, 12.7 mm [1/2 in] thick bent plate connection, 25.4 mm [1.0 in] thick bent plate connection, and a half-pipe connection detail)

BRIDGE GEOMETRY

The bridge geometry used within this study was adapted from American Iron and Steel Institute (AISI) Design Example 2 (AISI 1997). This geometry can be considered reasonably typical for a multi-girder highway overpass and its design is well-understood and widely available. The bridge consists two 27.4 m [90 ft] spans, composed of four continuous girders spaced at 3.1 m [10 ft] as presented in Figure 3.1. The girders were studied here in the non-composite condition, representative of bridge characteristics during construction. The girders were topped with a 203 mm [8.0 in] thick wet concrete deck with a 1.1 m [3.5 ft] roadway overhang and a 0.7 m [2.3 ft] construction walkway. The total deck width was 12.7 m [41.7 ft]. Both the roadway overhang and construction walkway were considered to be supported by 1.8 m [70 in] C-49-D overhang brackets, shown in Figure 3.2, spaced 1.0 m [40 in] on center. Separate built-up cross-sections

were used in regions of positive and negative bending, as shown in Figure 3.1(a) and Figure 3.1(b). Each girder was supported by a pin at the central pier and roller supports at both ends.

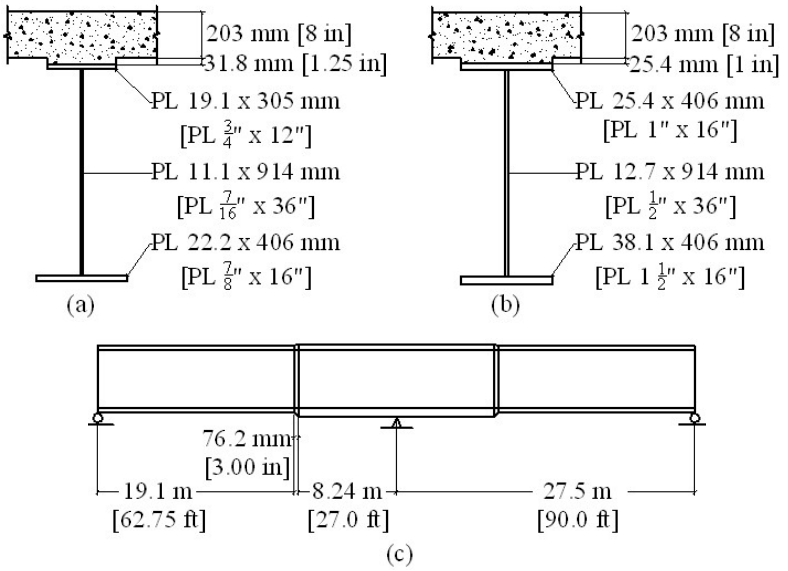

Figure 3.1 (a) Positive girder cross-section; (b) Negative girder cross-section; (c) Location of positive and negative cross-sections.

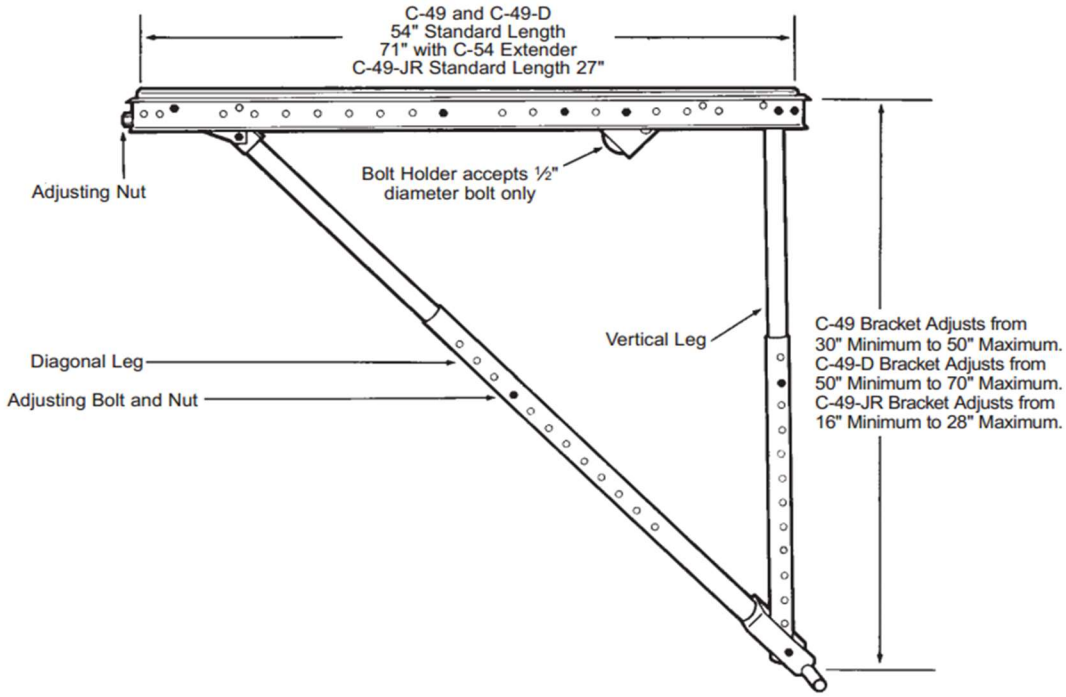

Figure 3.2 C-49 Overhang Bracket

Bridges with skewed supports are designed as such to accommodate highway alignment. Bracing may be placed parallel to the skew angle, or perpendicular to the girder line, usually in a staggered configuration. These configurations, shown in Figure 3.3 will be referred to as skewed-parallel and skewed-staggered, respectively.

AASHTO requires that bracing be placed perpendicular to the girder line whenever the skew angle is greater than 20°. However, KDOT design provisions allow the use of skewed-parallel configuration for angles up to 40° to reduce potential differential deflection in the cross-frame (KDOT 2010). For the analyses performed in this study, results for the skewed-parallel, skewed-staggered, and skewed-unstaggered configurations with 0°, 20°, and 40° skews were considered. Cross-frame spacing of 4.57 m [15 ft], 9.14 m [30 ft], and 13.7 m [45 ft] were modeled to study effects on lateral flange bending and system stability, although usually brace spacing is kept to less than 7.62 m [25 ft].

For all cases studied, the bridge system was modeled in construction, with the girders and cross-frames in place but the concrete deck still wet. Therefore, the load induced by the weight of the concrete was considered with the stiffness of the deck not present, structurally.

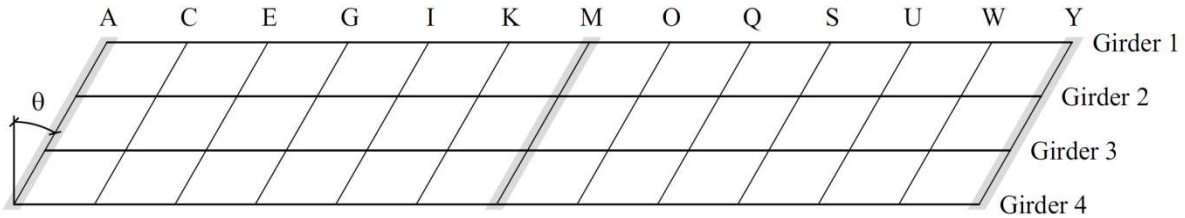

(a) Skewed-parallel

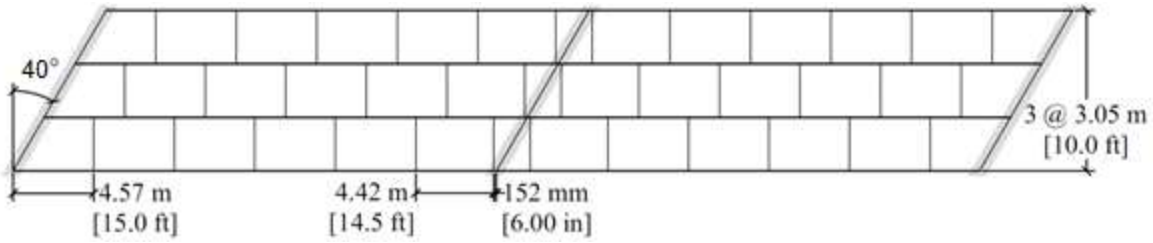

(c) Skewed-staggered

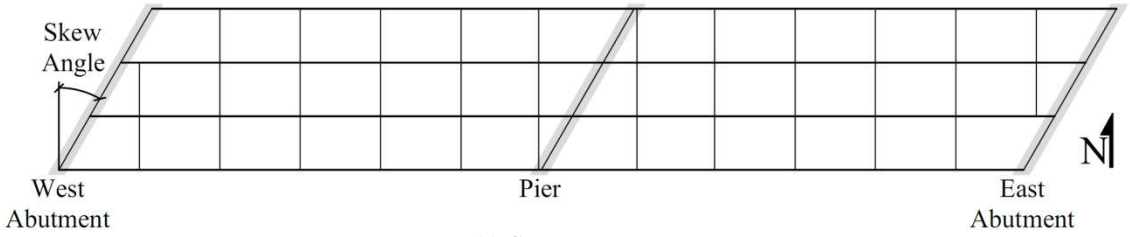

(c) Skewed-unstaggered

Figure 3.3 Bridge configurations (40° skew with 4.57 m [15.0 ft] cross-frame spacing)

Cross-frames, referring to truss-type lateral braces placed at discrete locations along a bridge layout, were used in all bridge configurations studied and consisted of three equal-leg angles spanning between connection stiffeners. A square plate was used to connect the diagonal legs at mid-length, as shown in Figure 3.4. Both connection stiffeners were modeled as being tied directly to the web and top and bottom flanges; attaching the connection stiffeners to the adjacent flanges is representative of current practice (post-1980s detailing). In bridges with skewed-parallel configurations, cross-frame length increased with skew angle and bent plate stiffeners were used to capture realistic construction considerations.

The slenderness ratio for the single angles was computed using provisions in American Institute of Steel Construction's Steel Construction Manual (AISC Manual, 2010) Section E5, and cross-frame stiffness was compared based on the approximate relative stiffness, $A\cos^3\theta$, where A is the cross-sectional area of one angle and θ is the skew angle (Yura 2001; Wang & Helwig 2008). This was done to ensure that cross-frames selected in the different models had

similar stiffnesses. A slenderness ratio of approximately 140 was used for all angles, which is a commonly-used slenderness limit in design. An L108 x 108 x 12.7 mm [L4-1/4 x 4-1/4 x 1/2 in] angle was selected for the skewed-staggered bridge. An L114 x 114 x 15.9 mm [4-1/2 x 4-1/2 x 5/8 in] angle was selected for the 20° skewed-parallel bridge. An L140 x 140 x 15.9 mm [5-1/2 x 5-1/2 x 5/8 in] angle was selected for the 40° skewed-parallel bridge. More details regarding the brace sizing and rationale are provided in Hassel (2011). A look at how framing of the angle members and work point affect the behavior of the brace is presented in Appendix F.

The design of the cross-frames in this study was designed solely based on an approximate relative stiffness and appropriate slenderness ratio. While the slenderness ratio is a typical value used in design, it is not based on a specific code requirement or optimized for this particular bridge geometry. In the design of the cross-frames, several other considerations will come into play such as fit-up of the cross-frames to the girders as well as fit-up of the angle members that make up the cross-frames. The type of brace pattern used will need to be determined, where different patterns may be selected for different parts of the bridge. Serviceability and fatigue requirements for the cross-frame members and connections will also need to be addressed. These requirements will change with different skew angles and orientations. The cross-frames selected for the models used were not meant to address these design considerations but only to provide insight into the behavior of a lateral load transferring system for a theoretical, pre-designed bridge adapted from American Iron and Steel Institute (AISI) Design Example 2 (AISI 1997).

Connection stiffener dimensions are shown in Figure 3.4. A thickness of 9.5 mm [3/8 in] was selected for all connection stiffeners in skewed bridges with 4.57 m [15 ft] and 9.14 m [30 ft] cross-frame spacing. Stiffener thicknesses of 9.5 mm [3/8 in], 12.7 mm [1/2 in], and 25.4 mm [1.0 in] were selected for a cross-frame spacing of 13.7 m [45 ft].

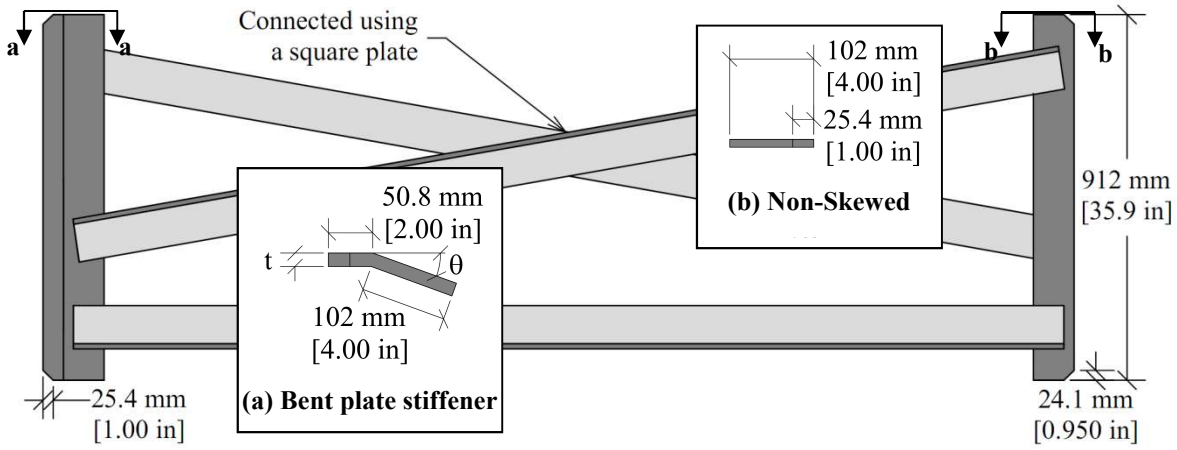

Figure 3.4 Connection stiffener geometry

Abutment diaphragms were modeled as having three equal-leg angle cross-sections spanning between connections plates in a K-brace, shown in Figure 3.5. A gusset plate was used to connect the diagonal legs to the bottom horizontal angle. The diagonal legs were tied directly to a MC12x50, which spans between connection stiffeners. An L108 x 108 x 12.7 mm [L4-1/4 x 4-1/4 x 1/2 in] angle was selected for the skewed-staggered bridge. An L114 x 114 x 15.9 mm [4-1/2 x 4-1/2 x 5/8 in] angle was selected for the 20° skewed-parallel bridge. An L140 x 140 x 15.9 mm [5-1/2 x 5-1/2 x 5/8 in] angle was selected for the 40° skewed-parallel bridge. The abutment connection stiffeners were tied to the web and top and bottom flanges. Abutment connection stiffener dimensions are shown in Figure 3.5. An abutment connection stiffener thickness of 25.4 mm [1.0 in] was selected for all bridges. A detailed discussion of the influence of abutment detailing is provided in Appendix D.

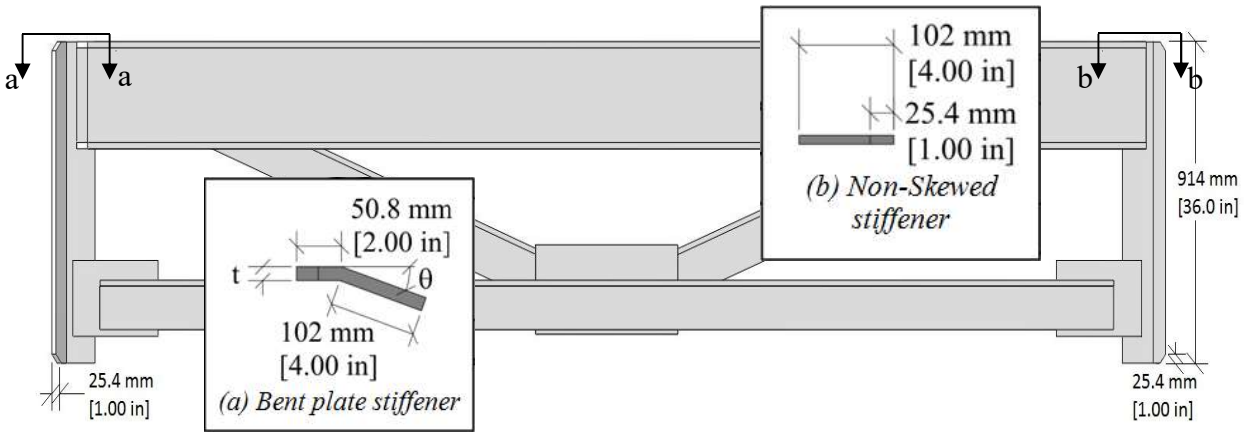

Figure 3.5 Abutment diaphragm and connection stiffener geometry

A round half-pipe connection stiffener developed at the University of Texas-Austin has been shown to increase buckling capacity by as much as 80% due to a significant increase in the warping stiffness of the cross section (Quadrato et al. 2010). An additional benefit of using a round stiffener is that perpendicular connections to the cross-frame tab can be made regardless of the skew angle. Cross-frames modeled with half-pipe connections were considered in this study; they consisted of three equal-leg angle cross-sections spanning between connection stiffeners. A square plate was used to connect the diagonal legs at mid-length, shown in Figure 3.6. The round half-pipe stiffener was connected to the web and top and bottom flanges. The same angles were used in the cross-frames with half-pipe connections as in the cross-frames with bent plate stiffeners.

Quadrato et al. (2010) found that girder buckling capacity increased with pipe diameter significantly more than pipe thickness, so long as the pipe is thick enough to resist local buckling. Therefore, the half-pipe adopted in the models in this study were that of an HSS10-3/4 x 1/2, which is the largest diameter pipe that can be accommodated by the flange widths in the girder geometry studied. The half-pipe studied had an outer diameter of 273 mm [10-3/4 in] and

a thickness of 12.7 mm [1/2 in], shown in Figure 3.6. The cross-frame tab connecting the angles to the half-pipe was 102 mm [4.0 in] wide and 9.5 mm [3/8 in] thick for all half-pipe connections.

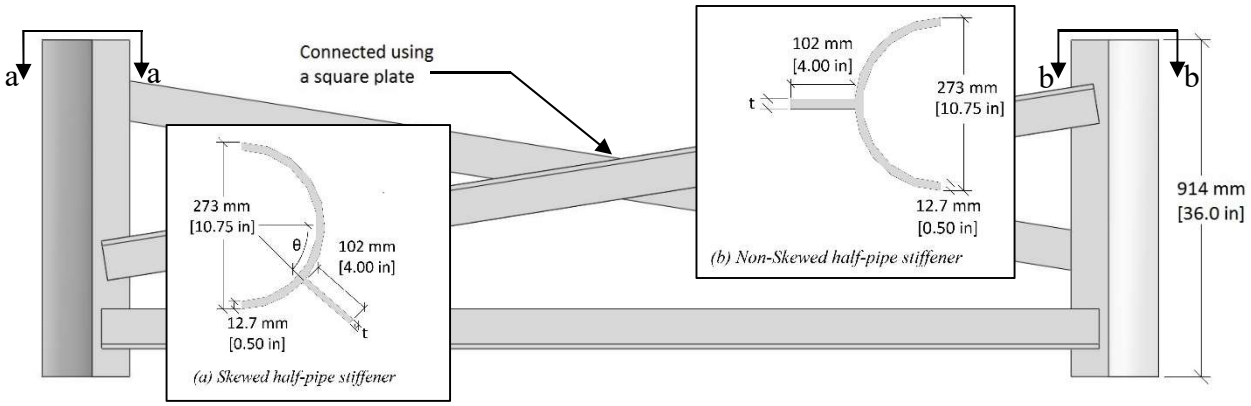

Figure 3.6 Cross-frame and half-pipe connection geometry

Abutment diaphragms with half-pipe connections were modeled with the same angle members as used with abutment diaphragms with the bent plate connection, in a K-brace configuration as shown in Figure 3.7. A gusset plate was used to connect the diagonal legs to the bottom horizontal angle as well, tied directly to a MC12x50 spanning between the connection stiffeners. An HSS10.75x1/2 was used for the half-pipe connection, with an outer diameter of 273 mm [10.75 in] and a thickness of 12.7 mm [1/2 in]. The half-pipe stiffeners were tied directly to the web and both top and bottom flanges. Abutment connection half-pipe and stiffener dimensions are shown in Figure 3.7. An abutment connection stiffener thickness of 25.4 mm [1.0 in] was used for all bridges modeled.

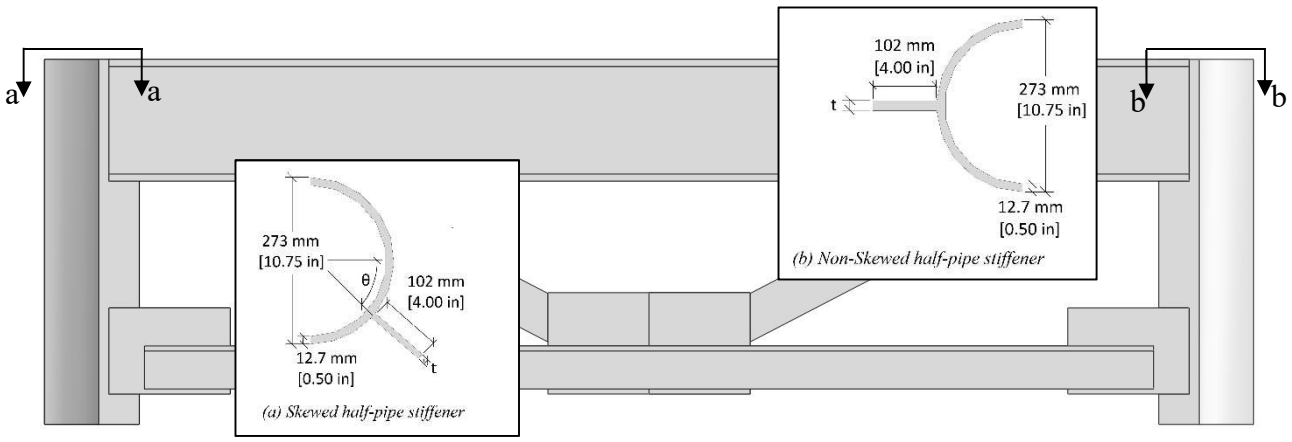

Figure 3.7 Abutment diaphragm with half-pipe connection geometry

Intermediate transverse stiffeners with a thickness of 9.5 mm [1/2 in] were modeled every 4.57 m [15 ft] in bridges with 9.14 m [30 ft] and 13.7 m [45 ft] cross-frame spacing. Figure 3.8 shows the transverse stiffener placement in a finite element model of the bridge with 9.14m [30 ft] cross-frame spacing. No intermediate transverse stiffeners were modeled in bridges with 4.57 m [15 ft] cross-frame spacing. 12.7 mm [1/2 in] thick transverse stiffeners were also used to stiffen the girder web at the abutments and pier supports. Two stiffeners spaced at 406 cm [16 in] were placed at each abutment girder support on each side of the web, except for the exterior girders where two additional stiffeners were placed 203 mm [8.0 in] apart on the exterior side of the web. Three 12.7 mm [1/2 in] thick transverse stiffeners spaced 203 mm [8.0 in] apart were placed on the exterior side of the web of the exterior girders at the center piers. Transverse stiffeners were tied directly to the web and to the top and bottom flanges.

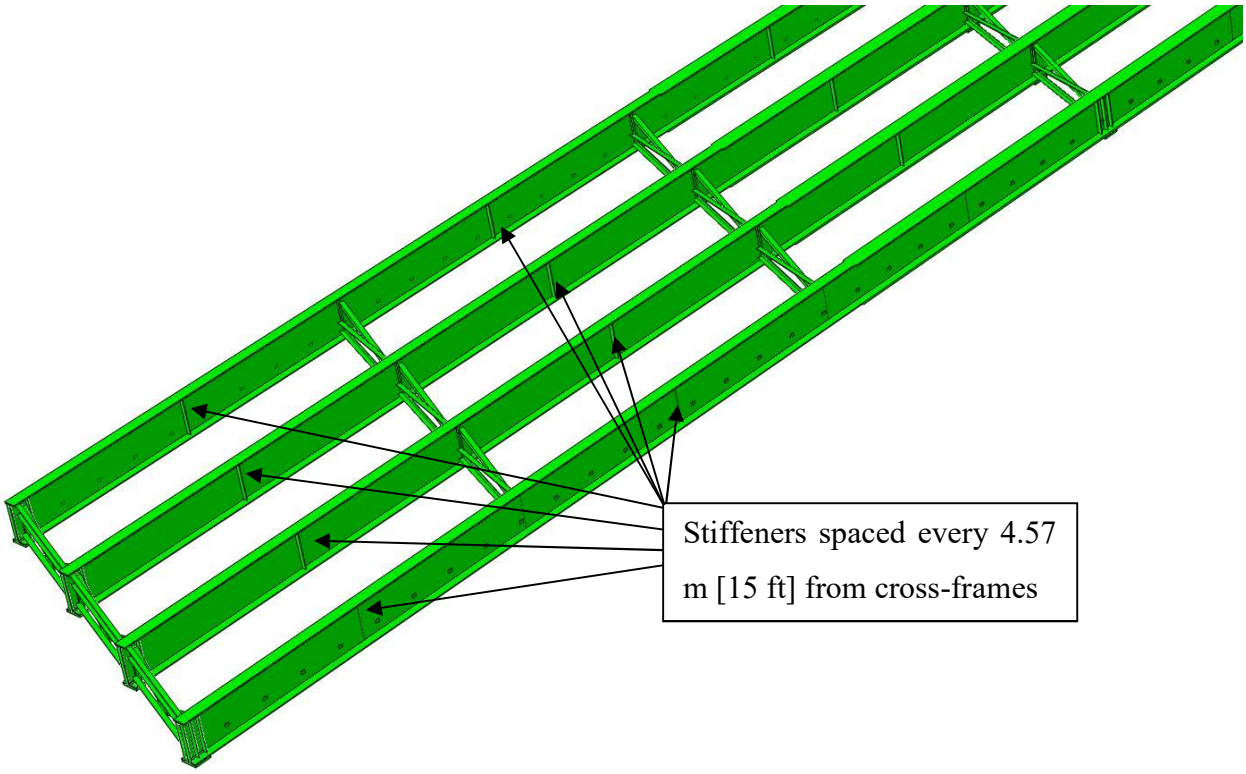

Figure 3.8 Stiffener placement in bridges with 9.14 m [30 ft] cross-frame spacing

MODELING METHODOLOGY

Three-dimensional, solid-element finite element (FE) models of the entire bridge were constructed using Abaqus v.6.10-2 for parametric analysis (Simulia, 2010). An example of one the bridge models is represented in Figure 3.9. C3D8R brick elements were used in the majority of the model, but C3D4 tetrahedral and C3D6 wedge elements were used to transition between mesh sizes where needed. Geometric nonlinearity was considered within each of the analyses.

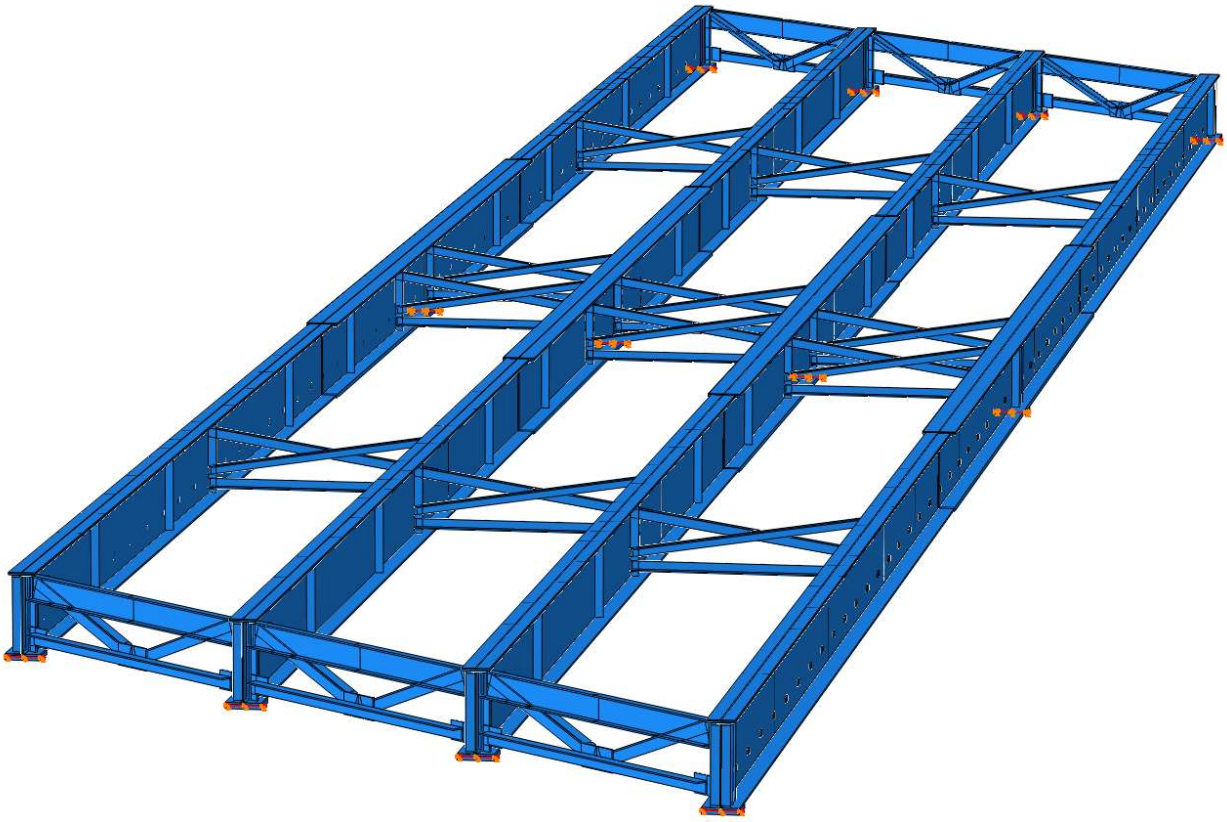

Figure 3.9 3D FEM model geometry of skewed-staggered bridge configuration (13.7 m [45 ft] cross-frame spacing)

Girder flanges and webs were modeled to have a modulus of elasticity of 200,000 MPa [29,000 ksi] and Poisson's ratio of 0.3. A mesh size of 25.4 mm [1.0 in] was used for web and flange elements. The cross-frame angles were partitioned such that each leg was divided into two equal lengths and each angle into four equal parts, as shown in Figure 3.10, to maintain consistent and uniform meshing. The cross-frame angles and stiffeners were then merged in Abaqus retaining intersecting boundaries. A mesh size of 127 mm [5.0 in] was used for abutment diaphragm and cross-frames. A finer mesh size for the cross-frames resulted in convergence errors in some models. A mesh size of 965 mm [38 in] was used for the top flange covers, the

purpose of which is described later. For all other parts, including transverse stiffeners, plates, and bearing pads, the mesh size was equal to the thickness of the part.

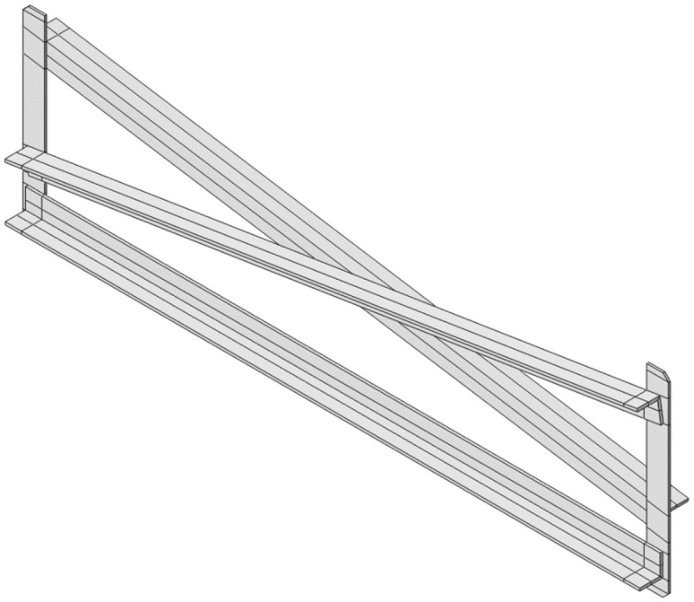

Figure 3.10 Cross-frame Angle Partitions

Steel overhang brackets typically support the construction walkway and screed rail during the construction phase of a bridge structure. As discussed in Part 2, the overhang brackets were not modeled directly within the parametric analysis, but the loads that they induced on the exterior girders were included in the parametric analysis. Refer to Part 2 of this dissertation on modeling of the overhang brackets, formwork, ties, welds, and boundary conditions.

APPLIED LOADS

Dead and live loads applied in the models during the construction stage were based on The Kansas Department of Transportation Design Manual: Volume III Section 5.3 (KDOT 2010). Load combinations and load factors are presented in AASHTO Section 3.4 (AASHTO 2010).

The Strength load combinations and load factors from AASHTO Table 3.4.1-1 were found to produce the controlling load combination during the construction stage (Zhou et al. 2015). Of the Strength load combinations and load factors, Strength 1 was found to produce the largest stresses for all bridge configurations. Therefore, the Strength 1 load combination and load factor were used in the analyses. Part 2 of this dissertation describes the applied loads, load combinations, and load factors used.

STRESS CALCULATIONS

Flexural stresses, σ, were calculated from these moments using the bending stress equation, as discussed in Part 2:

$$\sigma = Mc/I$$

where:

M = flange or section bending moment

c = distance from the extreme fiber to the neutral axis

I = moment of inertia of the flange or section

Major and minor axis bending moments about the girder cross-section were obtained using section cuts along Girder 3 and Girder 4. Part 2 describes the moment extraction process and validation.

Strong-Axis Bending Stress Computations

The section properties and techniques used to arrive at the strong-axis bending stress distributions are described in Part 2 of this dissertation. Appendix B shows the interior and exterior girder design computations in both the positive and negative flexure regions.

Weak-Axis Bending Stress Computations

Two methods for computing lateral flange bending stresses were used, discussed in Part 2:

(1) Weak-axis stresses in the flanges were computed using the weak-axis moment, M_y, extracted over the full-depth of the cross-section. This moment was used in conjunction with the weak-axis bending moment of inertia for the entire cross-section. Values for the neutral axis and weak axis moment of inertia are given in Part 2 and calculated in Appendix B.

(2) Weak-axis stresses in the flanges were also computed using moments that were extracted from the top and bottom flanges individually.

Comparison of Stresses Computed from Moments and Model-Extracted Stresses

The results between stresses directly extracted from the model and calculating stresses from bending moments were found to be congruent, as discussed in Part 2. Stresses were extracted from paths along the extreme edges and centerline of the exterior girder's top flange, as shown in

Figure 3.11. Given the general agreement, especially in trend, between extracted and computed stresses, the results for stresses are presented in terms of computed stresses.

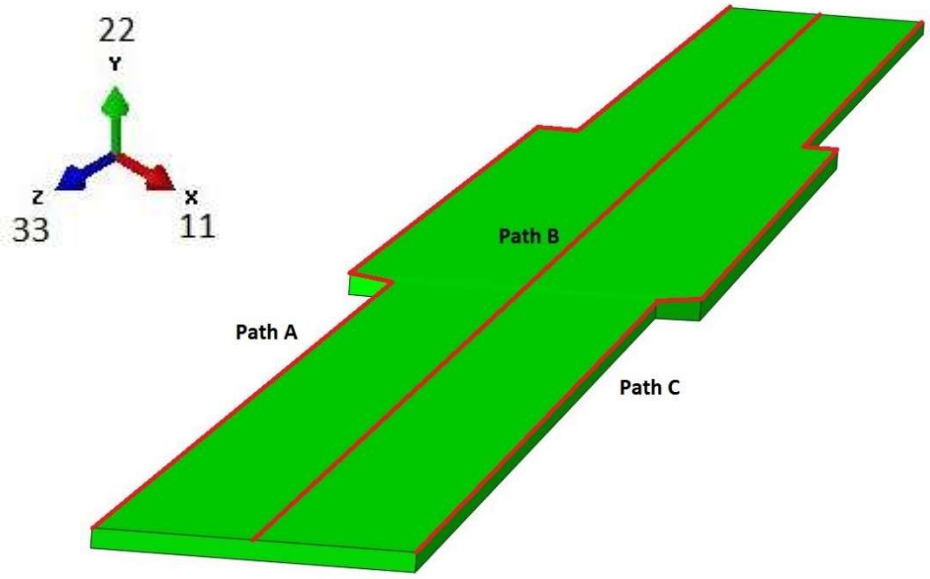

Figure 3.11 Stress paths along top flange used for direct extraction of stresses from the models

RESULTS

The results of this study are described in the following sections. First, a case is made for how material nonlinearity was considered in the modeling efforts, and why it was not included in the full parametric analysis. Then, the influence of the bracket overhangs is examined through a comparison of models that included and did not include the bracket overturning forces. Finally, the full parametric study is discussed in terms of load-deflection relationships, girder stresses, cross-frame stresses, and deformation modes. Throughout these discussions, reference will made to Span 1 or Span 2 of the bridge; the two bridge spans are labeled in Figure 3.12 for reference. As stated in Part 2, it should be noted that results are based on a specific pre-designed bridge to

provide insight into the effect of each variation. Changes in the bridge geometry, boundary conditions, and connection designs will affect the stresses and deflection.

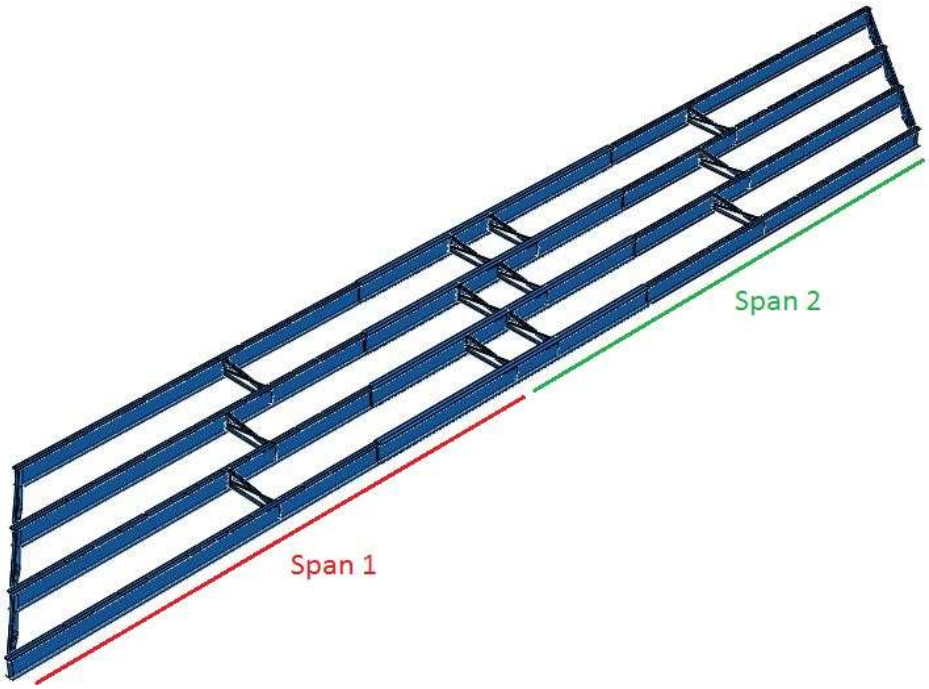

Figure 3.12 Spans labels

EFFECT OF GEOMETRIC NONLINEARITY

Part 2 displays a comparison of girder behavior between models that include linear-elastic and nonlinear geometric properties. It was found that including geometric nonlinearity in the models produced significant higher order effects captured in both lateral deflection and bending stresses. These effects are expected to increase as brace distance is enlarged. Therefore, geometric nonlinearity was included in subsequent analyses.

EFFECT OF MATERIAL NONLINEARITY

The adopted nonlinear material properties are presented in Part 2. It was found that including a nonlinear material model in the produced negligible differences in both lateral deflection and bending stresses. Therefore, material nonlinearity was not included in subsequent analyses, since it is a computationally expensive modeling technique.

EFFECTS OF OVERHANG BRACKET ON SYSTEM BEHAVIOR AND STABILITY

Significant flange lateral bending may be caused by torsion from eccentric concrete deck and walkway overhang loads acting on cantilever forming brackets placed along the exterior girders in conjunction with skew angles exceeding 20° (AASHTO 2010). In these cases, the flange lateral bending may be considered at the discretion of the Engineer.

Gravity load collected on the overhang was applied to the top flange of the exterior girders over the Girder 4 web, along the thick red line as shown in Figure 3.13. The results show significant contribution of overhang loads to both lateral deflection in the exterior girder at all loading stages and out-of-plane flexural stresses in the exterior girder, discussed in Part 2. It can be concluded that overhang brackets loads contribute greatly to out-of-plane deflection and stresses in the exterior girders and had little effect on in-plane bending stresses.

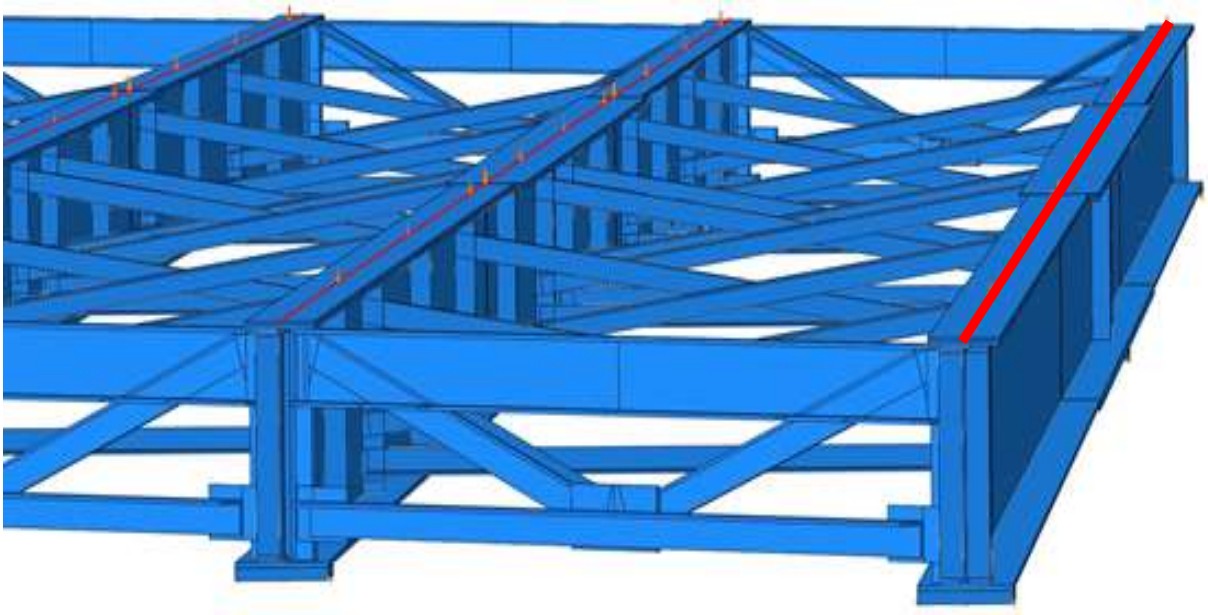

Figure 3.13 Model with no overhang bracket plates and overhang loads applied to the top of the exterior girder

EXAMINATION OF SKEWED SYSTEM STABILITY THROUGH PARAMETRIC ANALYSIS

As described, the parametric study included variations of:

- Skew angle (0°, 20°, and 40°);
- Cross-frame spacing (4.57 m [15 ft], 9.14 m [30 ft], and 13.7 m [45 ft]);
- Cross-frame orientation (skewed-staggered, skewed-parallel, and skewed-unstaggered); and
- Cross-frame connection type (9.5 mm [3/8 in] thick bent plate connection, 12.7 mm [1/2 in] thick bent plate connection, 25.4 mm [1.0 in] thick bent plate connection, and a half-pipe connection detail)

Results from the parametric study were analyzed in terms of load-deflection behavior, lateral flange stresses, cross-frame forces, and structural deformations. **Throughout the discussion that follows, results for the bridge system with 13.7 m [45 ft] cross-frame spacing is often**

focused on. This is not because such a system is necessarily believed to be practical or advisable, but because it highlights and amplifies the stability characteristics of the bridge systems as the parameters studied were varied, allowing differences in behavior to be examined.

LATERAL DEFLECTIONS

Lateral deflections along the length of the top flange of Girder 4 are presented in Figure 3.14 (a) through (g). The values were extracted at the top surface and along the center of the flange, shown as in Path B. Positive bending represents bending towards the exterior side of the bridge while negative bending represents bending towards the bridge interior. Span 1, labeled in Figure 3.12, produced larger lateral displacements than Span 2. Skewed-staggered bridges produced much larger lateral displacements in Span 1 compared to Span 2 due to placement of the cross-frames while top flange lateral displacements were similar between Span 1 and Span 2 for the skewed-parallel bridge configuration with 13.7 m [45 ft] cross-frame spacing. The top flanges of bridges with 4.57 m [15 ft] and 9.14 m [30 ft] cross-frame spacings tended to bend towards the bridge interior at the abutment of Span 2, due to the effect of increased stiffness from additional cross-frames compared to bridges with 13.7 m [45 ft] cross-frame spacing. Maximum deflections occurred in Span 1 near mid-brace between the abutment and first cross-frame, with the exception of the unskewed bridge with 4.57 m [15 ft] cross-frame spacing, where peak deflections occurred at mid-span.

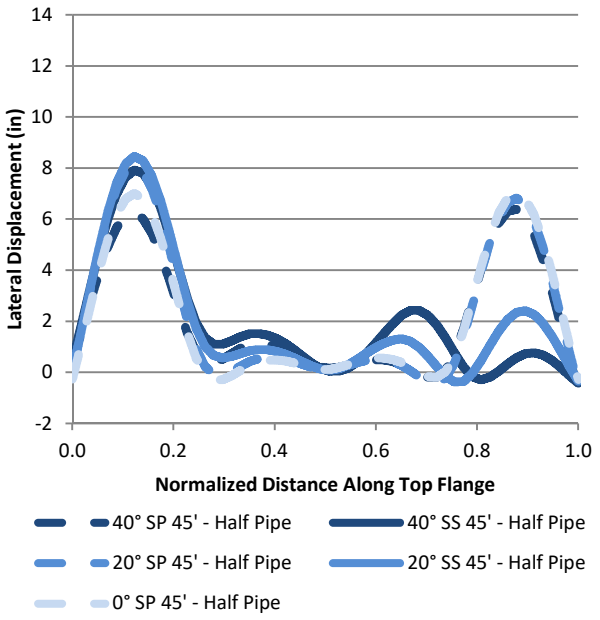

a) **Half-pipe connection, 13.7 m [45 ft] cross-frame spacing**

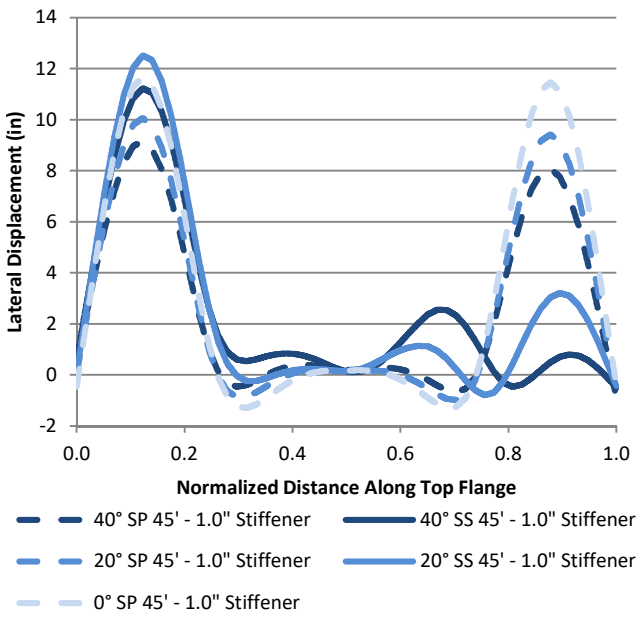

b) **25.4mm [1.0 in] stiffener connection, 13.7 m [45 ft] cross-frame spacing**

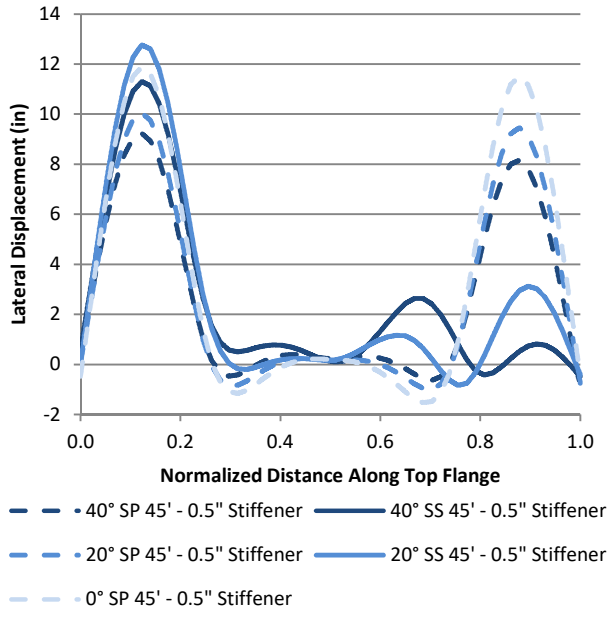

c) **12.7mm [1/2 in] stiffener connection, 13.7 m [45 ft] cross-frame spacing**

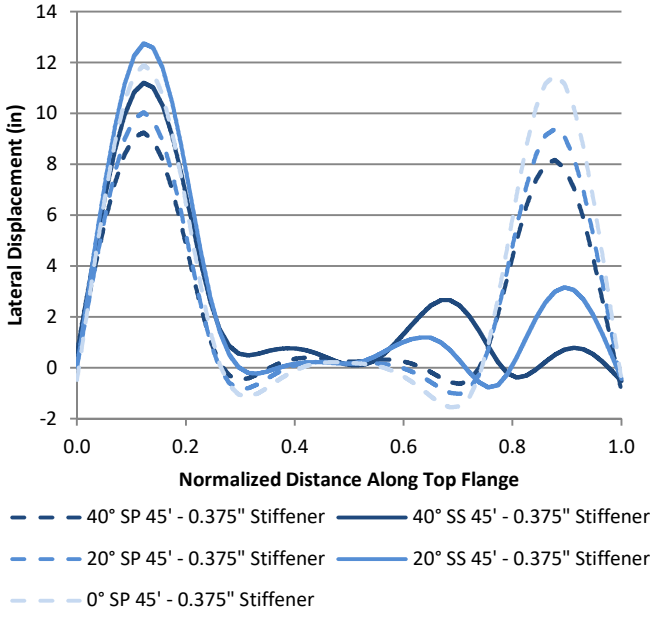

d) **9.53mm [3/8 in] stiffener connection, 13.7 m [45 ft] cross-frame spacing**

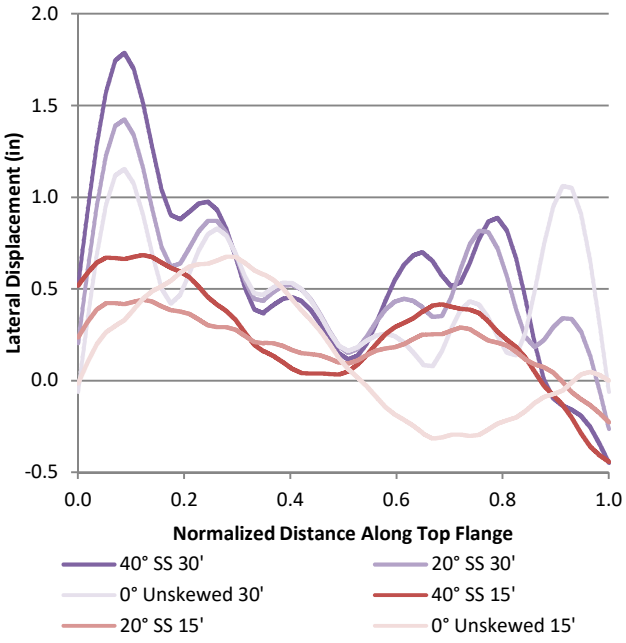

e) **Skewed-staggered, 9.14 m [30 ft] and 4.57 m [15 ft] cross-frame spacing**

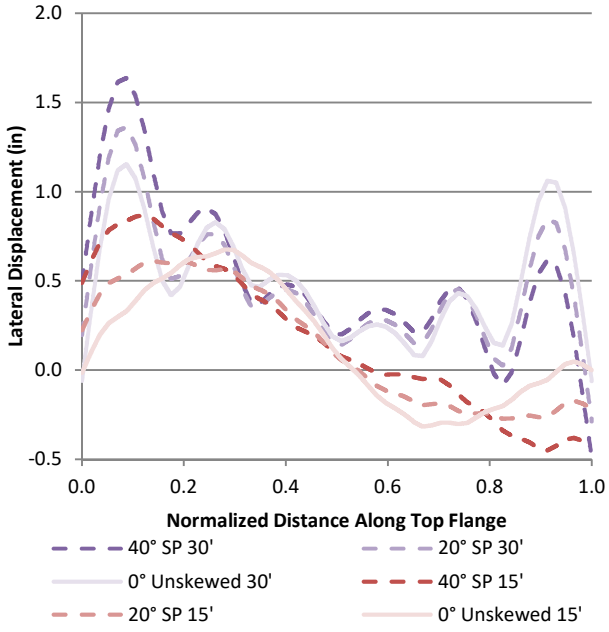

f) **Skewed-parallel, 9.14 m [30 ft] and 4.57 m [15 ft] cross-frame spacing**

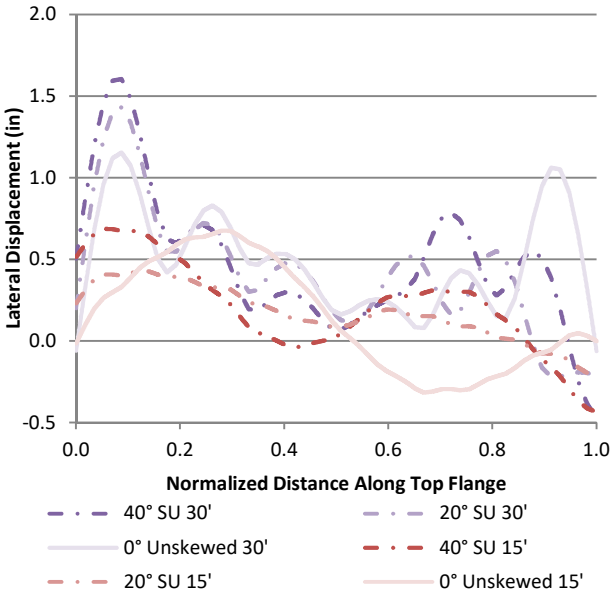

g) **Skewed-unstaggered, 9.14 m [30 ft] and 4.57 m [15 ft] cross-frame spacing**

Figure 3.14 Lateral displacement along Girder 4 top flange

Peak deflections were extracted from Span 1 because the unbraced length was consistent between skewed-staggered, skewed-unstaggered, and skewed-parallel configurations in that span. Figure 3.15 (a) through (h) shows the peak lateral deflection at varying load multipliers in Span 1 of the exterior Girder 4, grouped by connection type for the 13.7 m [45 ft] spacing models and by configuration for models with 4.57 m [15 ft] and 9.14 m [30 ft] cross-frame spacing. Almost all of the load-deflection curves were smooth and slowly flattened as load was increased, showing that rapid loss of load-carrying resistance in the girder did not occur for most models. Many of these exterior girders appeared to be exhibiting roll-over behavior, as a small increment of load resulted in a significant increase in deflection towards 100 percent of the load applied. This behavior is believed to be largely driven by the overturning force from the overhang brackets, which produces significant geometric nonlinearity (P-delta effects) in the exterior girders. The roll-over response became more exaggerated with increased cross-frame spacing, as might be expected.

The 0° non-skewed bridge with 4.57 m [15 ft] cross-frame spacing and the 20° skewed-parallel bridge with 4.57 m [15 ft] cross-frame spacing exhibited a sudden increase in lateral displacement near full loading, which may indicate a more conventional lateral-torsional buckling response. Shorter spans and cross-frames placed parallel to the skew angle may correspond more with traditional buckling behavior in the girder as load increases; these configurations are more effective at preventing buckling at smaller loads until a critical load is reached and large lateral deflections occur. Nevertheless, the exterior girder flange in bridges that had 9.14 m [30 ft] cross-frame spacing did not displace laterally more than 46 mm [1.8 in] and bridges with 4.57 m [15 ft] cross-frame spacing did not displace laterally more than 22 mm [0.87 in].

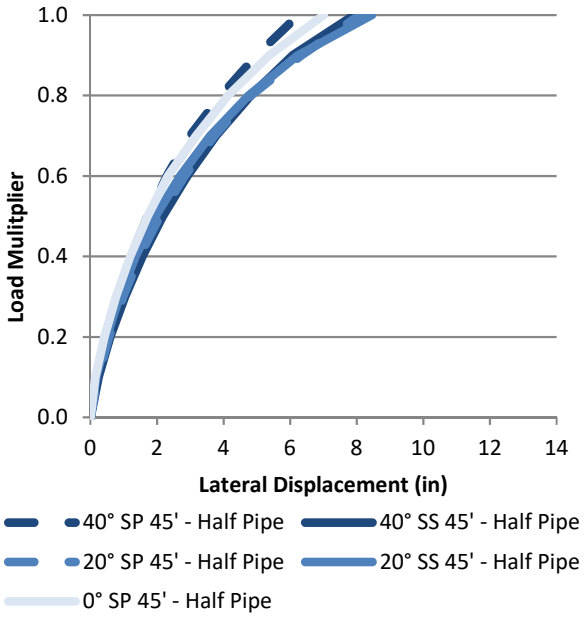

a) **Half-pipe connection, 13.7 m [45 ft] cross-frame spacing**

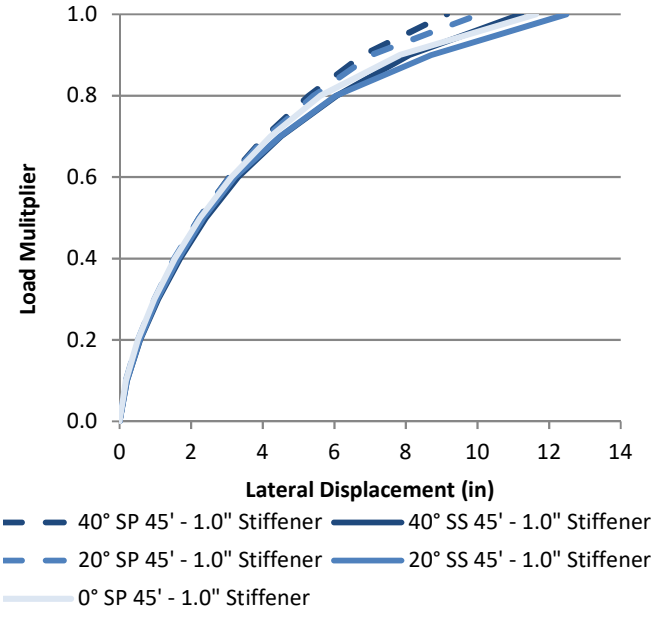

b) **25.4mm [1.0 in] stiffener connection, 13.7 m [45 ft] cross-frame spacing**

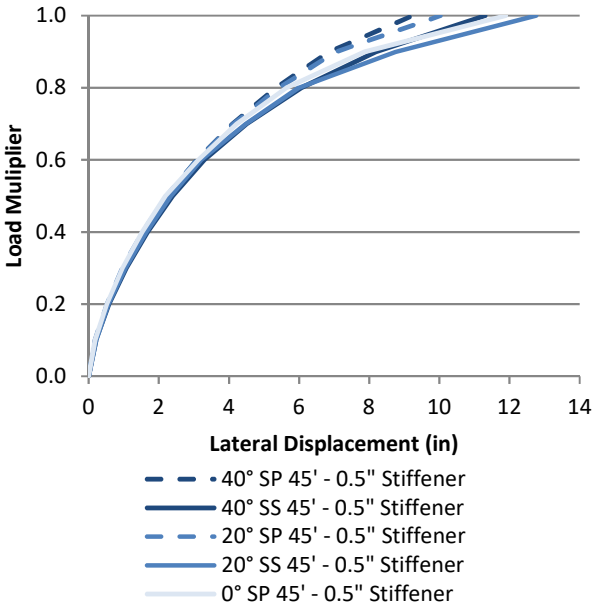

c) **12.7mm [1/2 in] stiffener connection, 13.7 m [45 ft] cross-frame spacing**

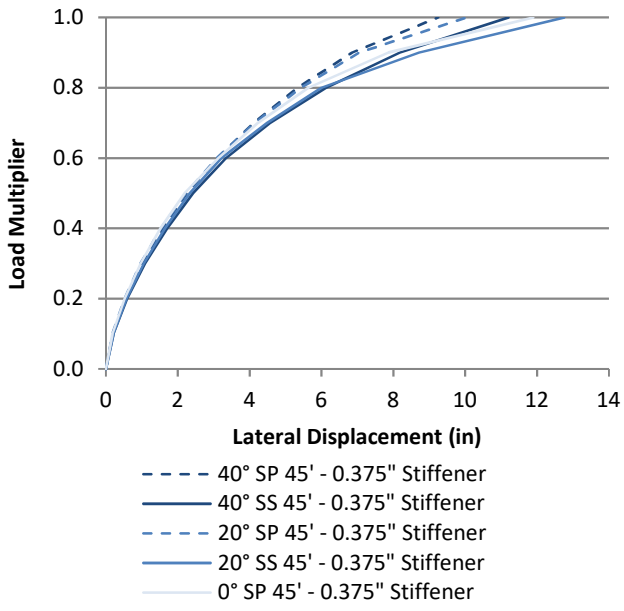

d) **9.53mm [3/8 in] stiffener connection, 13.7 m [45 ft] cross-frame spacing**

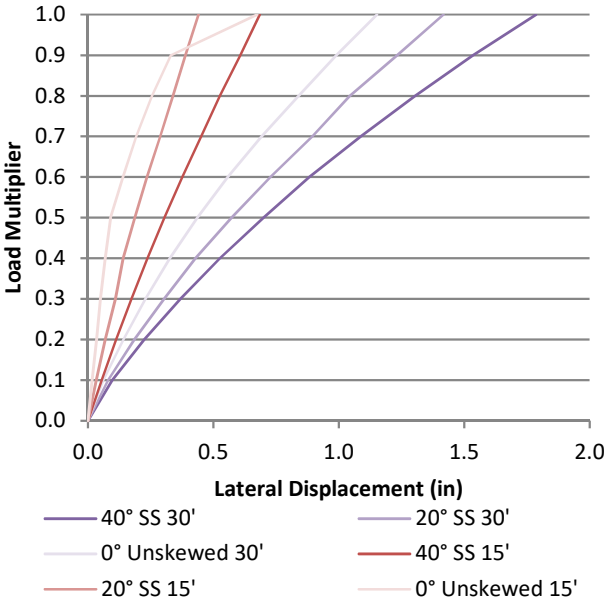

e) Skewed-staggered, 9.14 m [30 ft] and 4.57 m [15 ft] cross-frame spacing

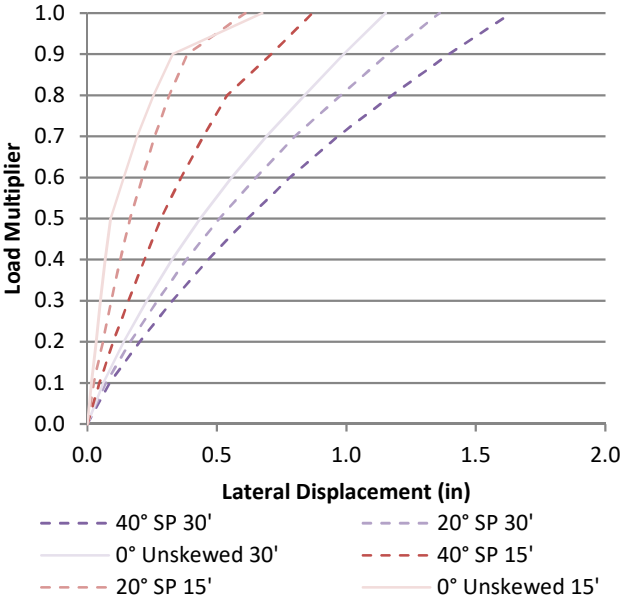

f) Skewed-parallel, 9.14 m [30 ft] and 4.57 m [15 ft] cross-frame spacing

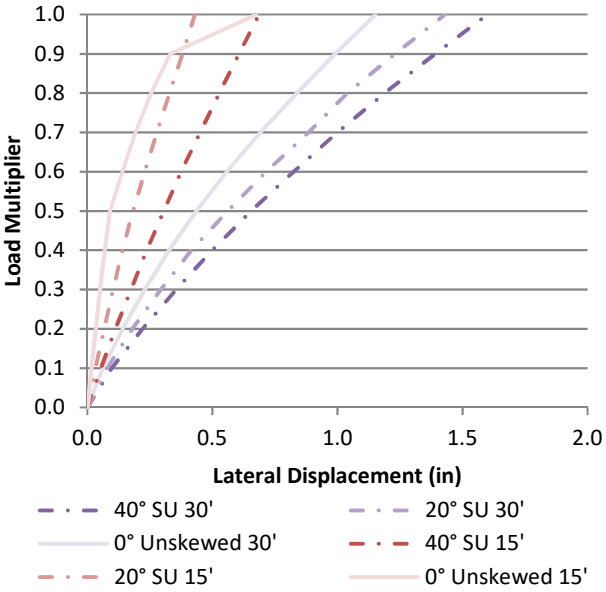

h) Skewed-unstaggered, 9.14 m [30 ft] and 4.57 m [15 ft] cross-frame spacing

Figure 3.15 Load vs. peak lateral displacement

Figure 3.16 (a) through (d) shows the peak lateral displacement in the top (compression) flange of Girder 4 in the positive bending region of the bridge, *grouped by connection type* for the 13.7 m [45 ft] cross-frame spacing models. The 40° skewed-parallel bridge was most resistant to lateral displacement while the 20° skewed-staggered bridge with stiffener connections was most susceptible to lateral deformations for any given connection type. The 20° skewed-staggered bridges with 9.5 mm [3/8 in] and 13 mm [1/2 in] thick stiffeners produced the maximum lateral displacements of 325 mm [12.8 in] while the 40° skewed-parallel bridge with half-pipe connection produced the smallest lateral displacement value of 158 mm [6.2 in]. For the same skew angle, the skewed-parallel configuration performed better than the skewed-staggered configuration in the 13.7 m [45 ft] spacing models (i.e., corresponded with smaller lateral displacements of the compression flange). Lateral displacements also increased with decreasing skew angle for all models except the 0° non-skewed bridge with half-pipe connection, where the lateral displacements were between that of the 40 and 20° skewed bridges.

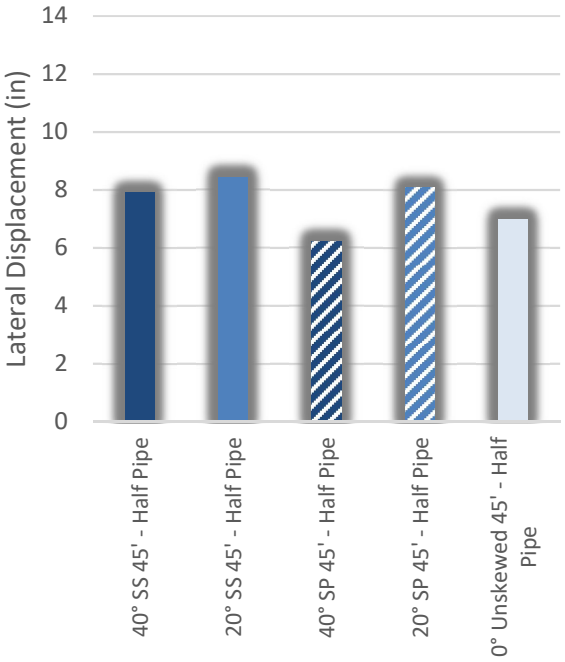

a) **Half-pipe connection, 13.7 m [45 ft] cross-frame spacing**

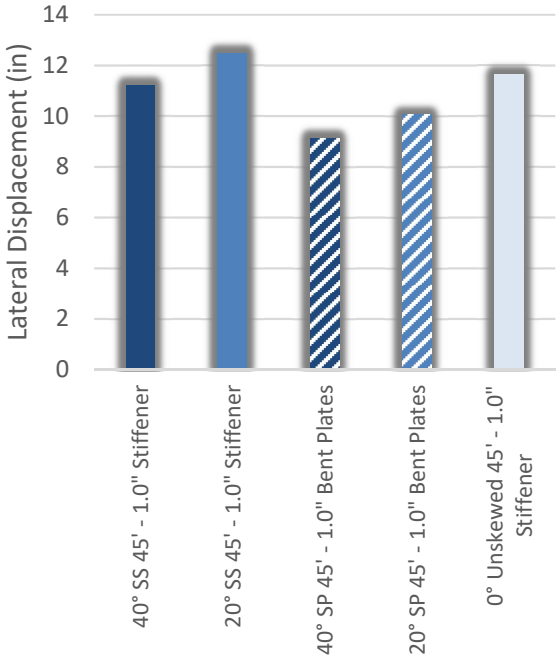

b) **25.4 mm [1.0 in] stiffener connection, 13.7 m [45 ft] cross-frame spacing**

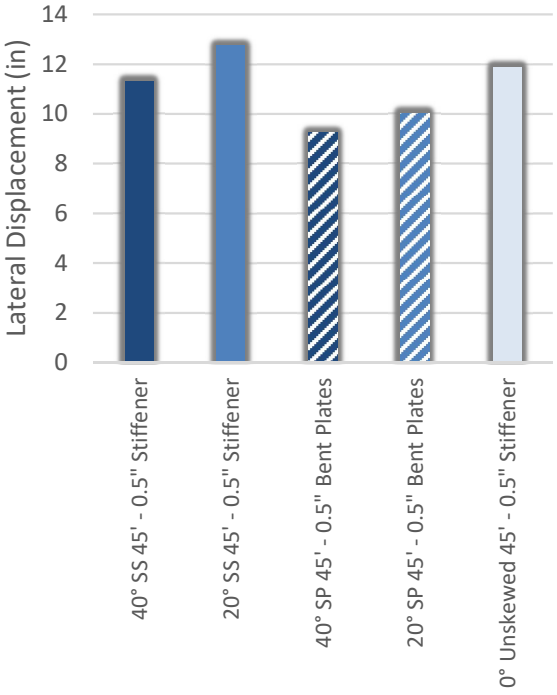

c) **12.7 mm [1/2 in] stiffener connection, 13.7 m [45 ft] cross-frame spacing**

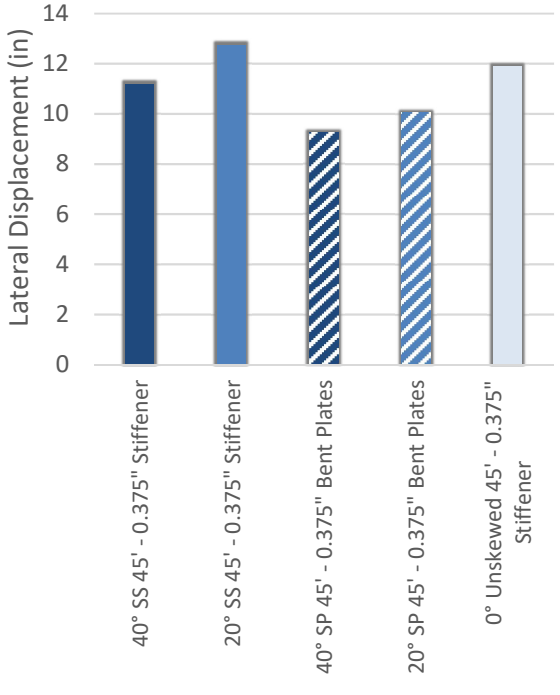

d) **9.5 mm [3/8 in] stiffener connection, 13.7 m [45 ft] cross-frame spacing**

Figure 3.16 Girder 4 peak lateral displacement at 100% load, grouped by connection type

Figure 3.17 (a) through (e) shows the peak lateral displacements in the top (compression) flange of Girder 4 in the positive bending region, *grouped by skew angle and configuration*. The results show that the half-pipe connection performed best for any given skew angle and configuration (i.e., this connection was found to best limit girder compression flange lateral displacements). Lateral displacements in the exterior girder were minimally affected by varying cross-frame stiffener thicknesses. The maximum displacement was found in the 20° degree skewed-staggered bridge with 13.7 m [45 ft] cross-frame spacing and 9.5 mm [3/8 in] stiffeners.

Figure 3.18 (f) and (h) show peak lateral displacements for the 4.57 m [15 ft] and 9.14 m [30 ft] cross-frame spacing models. Lateral displacements decreased with decreasing angle of skew, with the exception of the non-skewed bridge with 4.57 m [15 ft] cross-frame spacing. The non-skewed bridge with 4.57 m [15 ft] spacing produced lateral displacements between that of the 40 and 20° skewed bridges with the same cross-frame spacing. The overall magnitude of the displacements for the 4.57 m [15 ft] and 9.14 m [30 ft] cross-frame spacing models were relatively low. For 9.14 m [30 ft] cross-frame spacing models, the 40° skewed-staggered bridge with produced the largest deflection of 4.5 mm [1.8 in]. For bridges with 4.57 m [15 ft] cross-frame spacings, the 40° skewed-parallel model produced the largest deflection of 22 mm [0.87 in]. The differences in deflection values between the skewed-staggered, skewed-unstaggered, and skewed-parallel configurations for the same skew angle were small for these smaller cross-frame spacings.

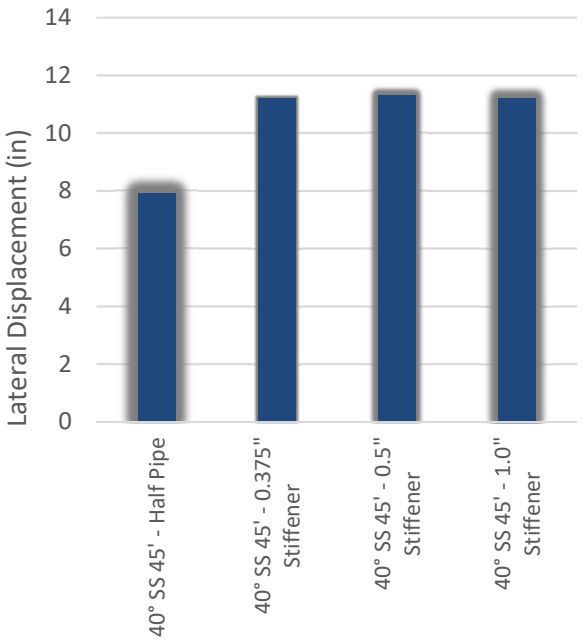

a) 40° skewed-staggered, 13.7 m [45 ft] cross-frame spacing

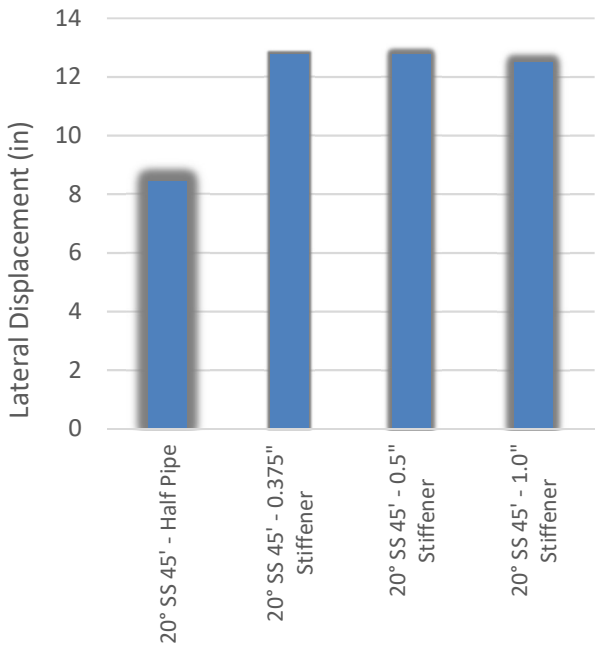

b) 20° skewed-staggered, 13.7 m [45 ft] cross-frame spacing

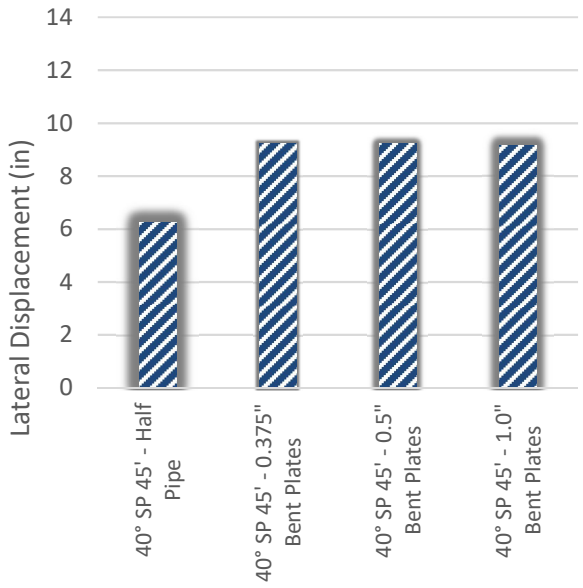

c) 40° skewed-parallel, 13.7 m [45 ft] cross-frame spacing

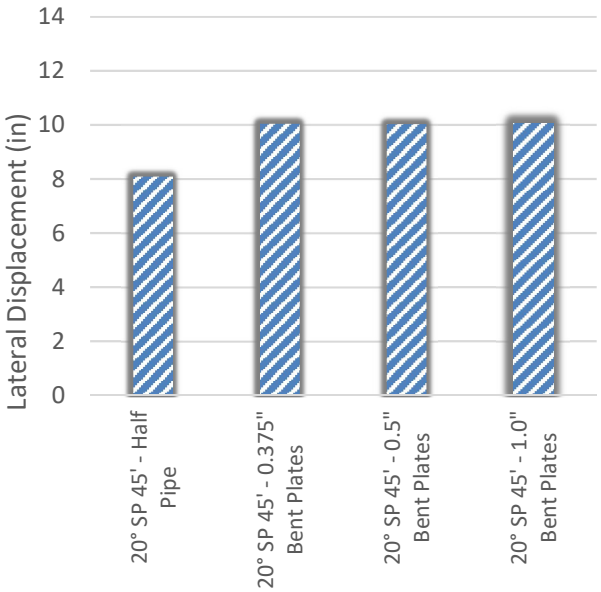

d) 20° skewed-parallel, 13.7 m [45 ft] cross-frame spacing

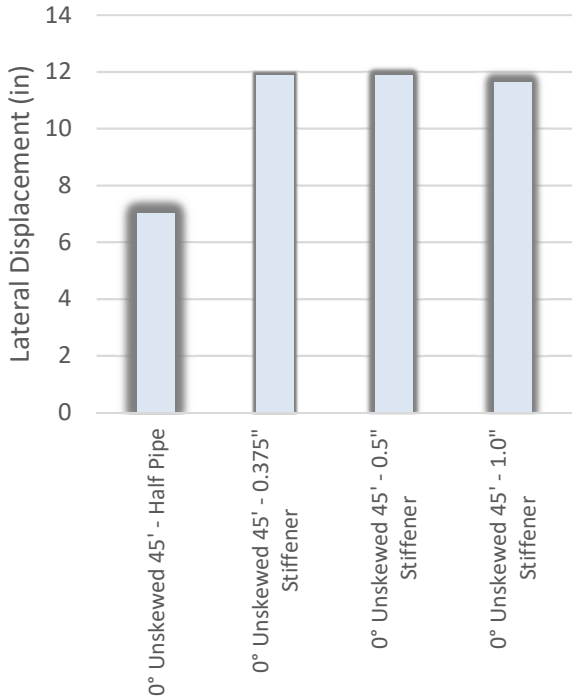

e) 0° unskewed, 13.7 m [45 ft] cross-frame spacing

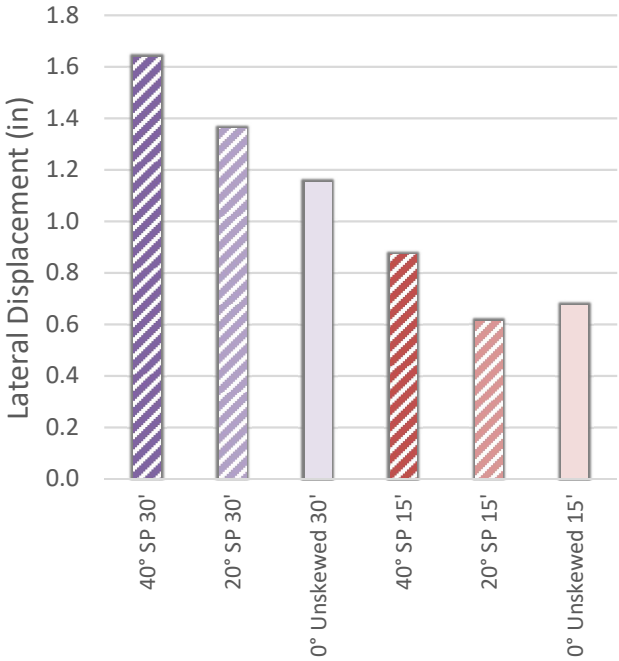

f) Skewed-staggered, 9.14 m [30 ft] and 4.57 m [15 ft] cross-frame spacing

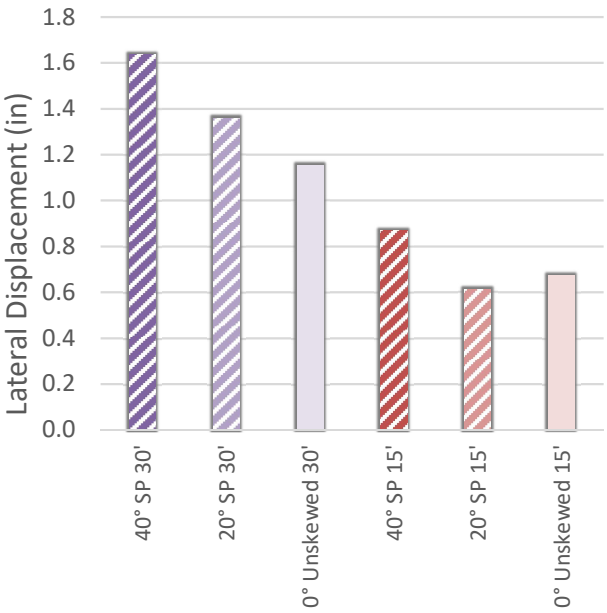

g) Skewed-parallel, 9.14 m [30 ft] and 4.57 m [15 ft] cross-frame spacing

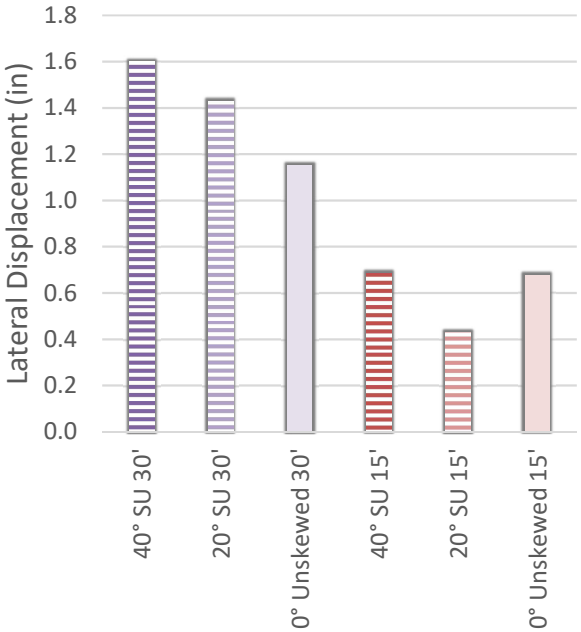

h) Skewed-unstaggered, 9.14 m [30 ft] and 4.57 m [15 ft] cross-frame spacing

Figure 3.17 Girder 4 peak lateral displacement at 100% load, grouped by skew angle and configuration

CROSS-FRAME STRESSES AND BEHAVIOR

The FE results were examined in terms of cross-frame stresses and behavior to gain a fuller picture of the bridge system behavior from the parametric analyses. A schematic of the cross-frame geometry included in the models is shown in Figure 3.18 with labeled cross-frame members.

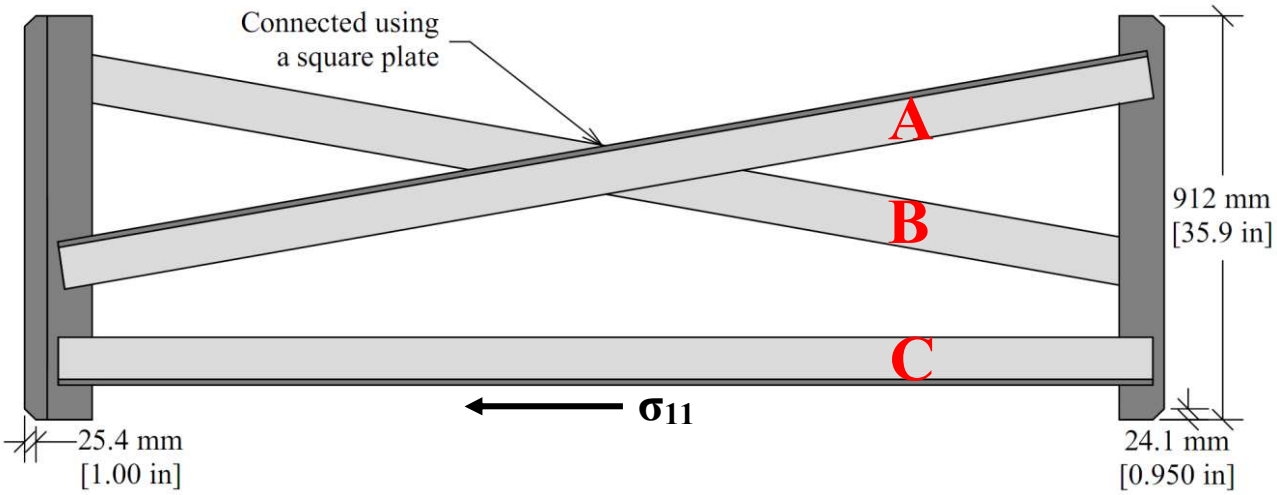

Figure 3.18 Cross-frame angle member labels and stress direction

Results for cross-frame Member C are presented because Member C is a compression member and has the longest unbraced length of Members A, B, and C, and therefore it controlled buckling capacity amongst the cross-frame angle members. (Members A and B were connected at the midpoint and thus have a shorter unbraced length.)

For the 13.7 m [45 ft] and 9.14 m [30 ft] cross-frame spacing models, the first interior cross-frame in Span 1, circled in Figure 3.19, was selected because the peak lateral deflection occurred near that location and maximum stresses were found in that cross-frame. For the 4.16 m

[15 ft] cross-frame spacing models, the cross-frame at mid-span of Span 1 was selected because it produced the maximum stresses and it matches the location of the cross-frame selected for the 13.7 m [45 ft] spacing models.

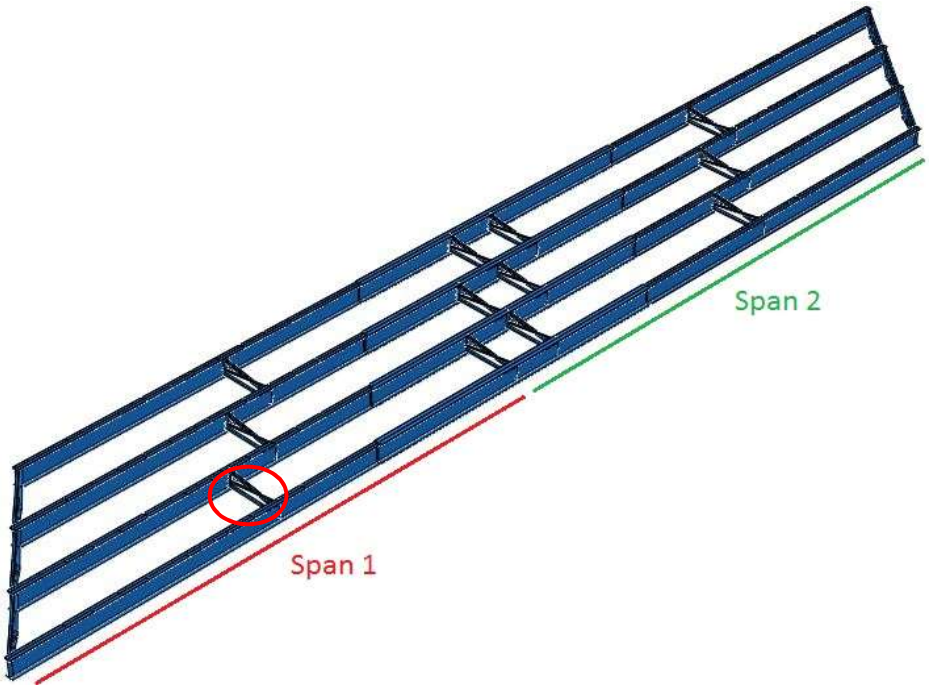

Figure 3.19 Cross-frame location corresponding to presented results for cross-frame stresses

Figure 3.20 and Figure 3.21 show the cross-frame member stresses in the local longitudinal direction of Member C, as labeled in Figure 3.18. The longitudinal stress direction of the cross-frame angle members, denoted as σ_{11}, captures all stresses in the *11*-direction, and includes both axial and bending stresses. Stresses were calculated as the average of the element stresses obtained by creating a cross-sectional cut through Member C.

Figure 3.20 presents the cross-frame angle member stresses, *grouped by connection type* for the 13.7 m [45 ft] cross-frame spacing models. The 40° skewed-parallel model consistently

produced the smallest stress magnitudes for varying skew angles and configurations, followed by the 20° skewed-parallel model. It should be noted that although the cross-frame member length increases with increasing skew angle for a skewed-parallel configuration, the component of the force perpendicular to the girder line, that is the direct path for transferring lateral forces between girders, decreases with increasing skew angle. It can be seen that the skewed-parallel configuration always produced smaller axial stresses than the skewed-staggered configuration for the same skew angle. Varying skew angles with the same skewed-staggered configuration also produced similar stress values, as the cross-frame member length and orientation are the same for the skewed-staggered configuration regardless of skew angle.

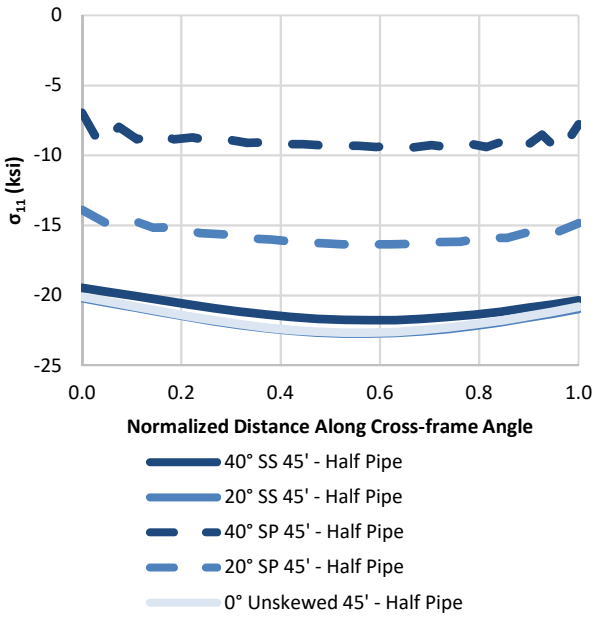

a) Half-pipe connection, 13.7 m [45 ft] cross-frame spacing

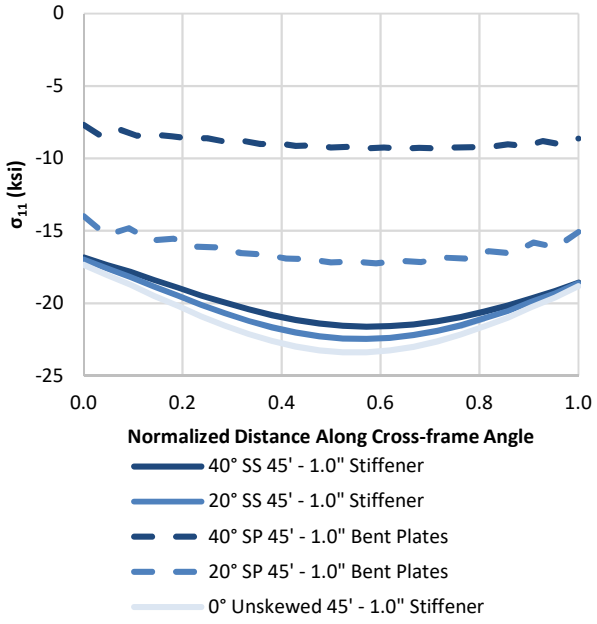

b) 25.4mm [1.0 in] stiffener connection, 13.7 m [45 ft] cross-frame spacing

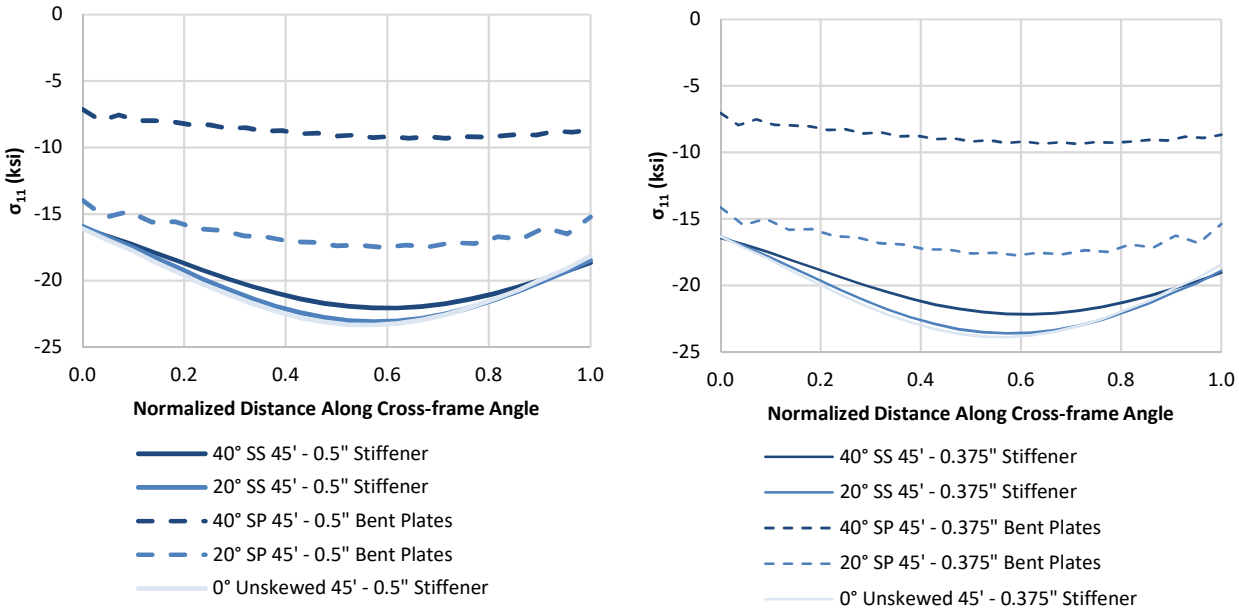

c) 12.7mm [1/2 in] stiffener connection, 13.7 m [45 ft] cross-frame spacing

d) 9.53mm [3/8 in] stiffener connection, 13.7 m [45 ft] cross-frame spacing

Figure 3.20 Cross-frame angle σ_{11} in member C, grouped by connection type

Figure 3.21 (a) through (e) shows the cross-frame angle member stresses in the local longitudinal direction of Member C, *grouped by skew angle and configuration* for all cross-frame spacings. For any given skew angle and configuration, the 4.57 m [15 ft] cross-frame spacing models always produced the smallest cross-frame stresses while the 13.7 m [45 ft] cross-frame spacing always produced the largest stresses. While the models that included the half-pipe connection sometimes produced larger stresses near the connection ends, the connection type did not produce significant differences in stress magnitudes at a location removed from the connection.

Figure 3.21 (f) through (h) groups cross-frame angle member stresses by configuration for the 4.57 m [15 ft] and 9.14 m [30 ft] cross-frame spacing models. The 4.57 m [15 ft] cross-frame spacing models produced smaller stresses than the 9.14 m [30 ft] cross-frame spacing

models, which can be expected as there are twice as many braces when the cross-frame spacing is halved. For any given skew angle and cross-frame spacing, the skewed-staggered configuration produced the largest stresses, with the skewed-unstaggered configuration following closely behind. The skewed-parallel configuration produced the smallest cross-frame member stresses among the three cross-frame configurations.

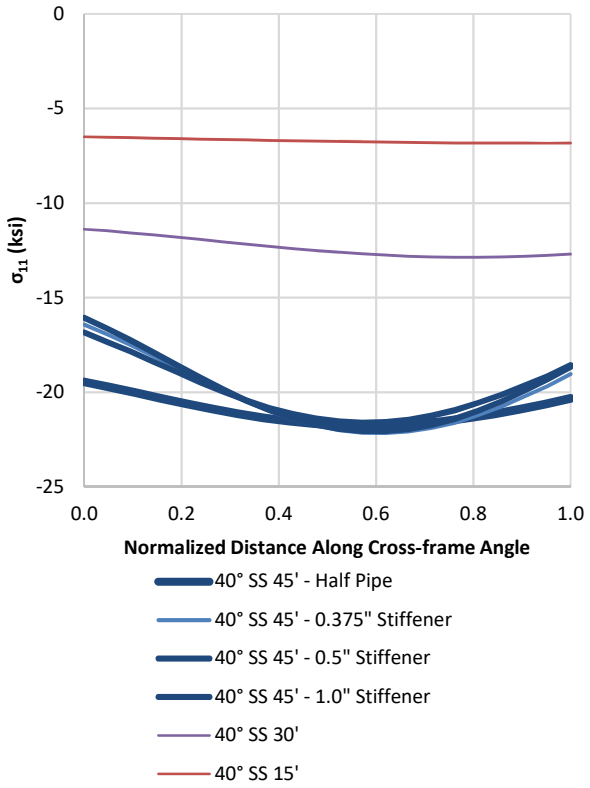

a) 40° skewed-staggered

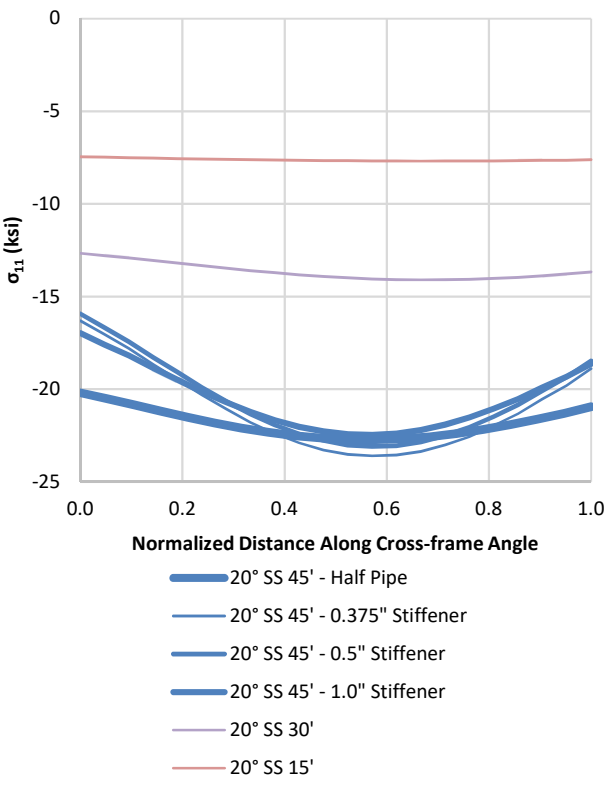

b) 20° skewed-staggered

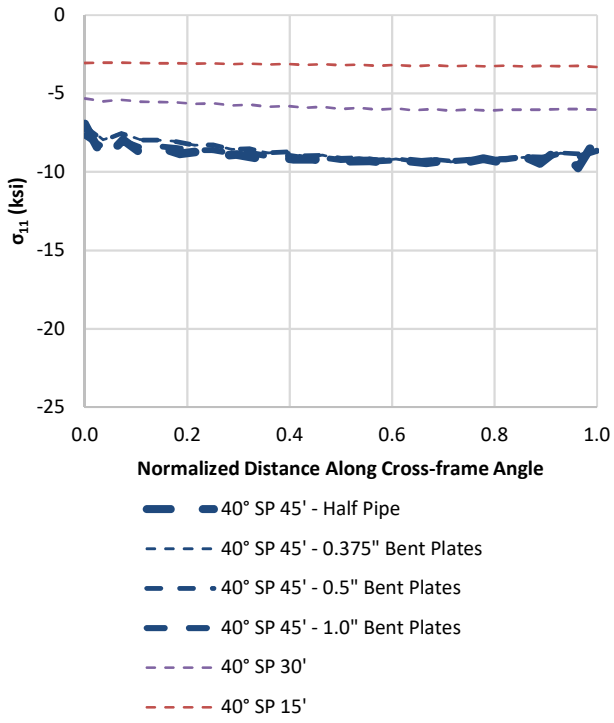

c) **40° skewed-parallel**

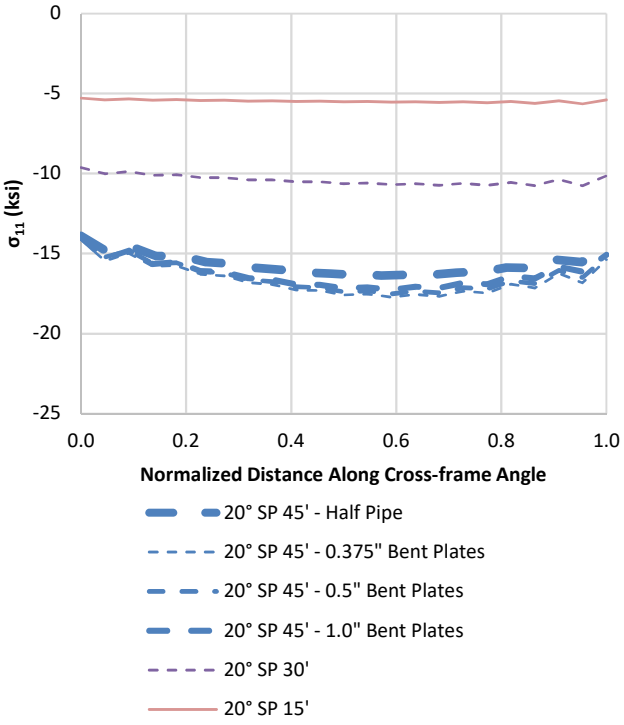

d) **20° skewed-parallel**

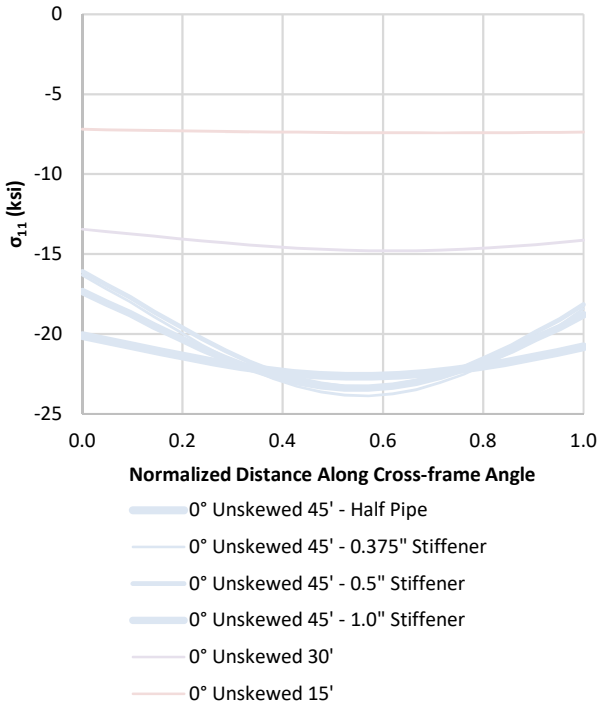

e) **Non-skewed bridge**

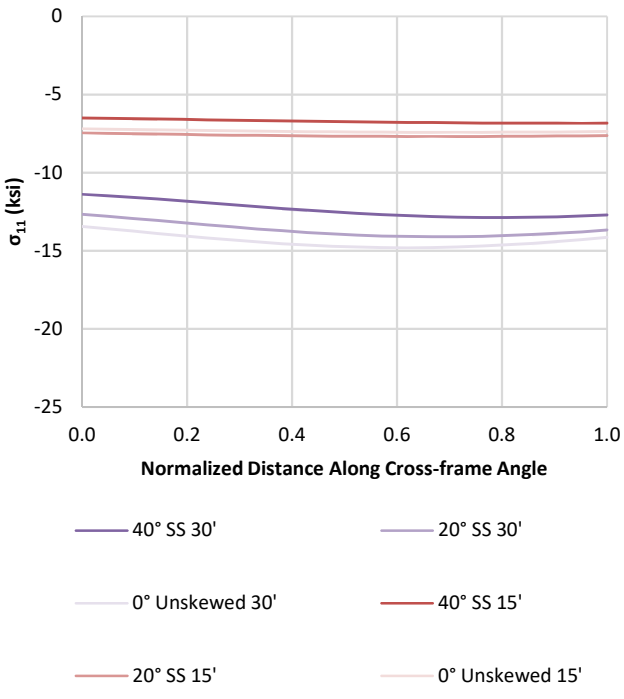

f) **Skewed-staggered, 9.14 m [30 ft] and 4.57 m [15 ft] spacing**

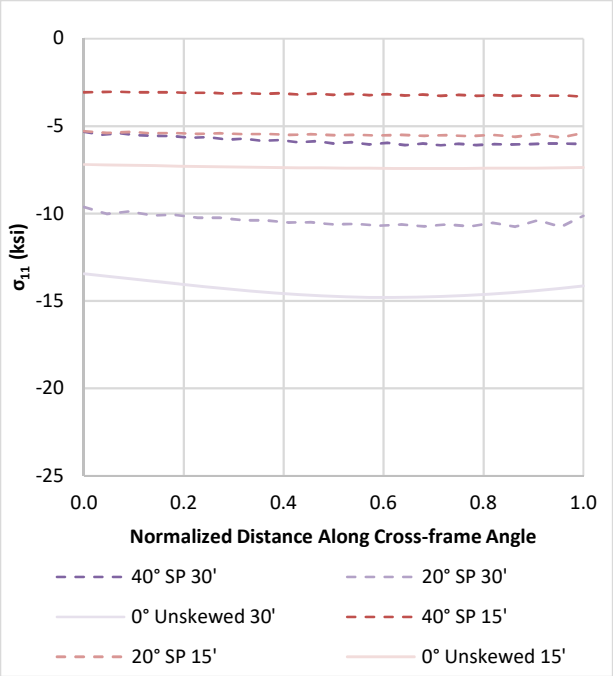

g) Skewed-parallel, 9.14 m [30 ft] and 4.57 m [15 ft] spacing

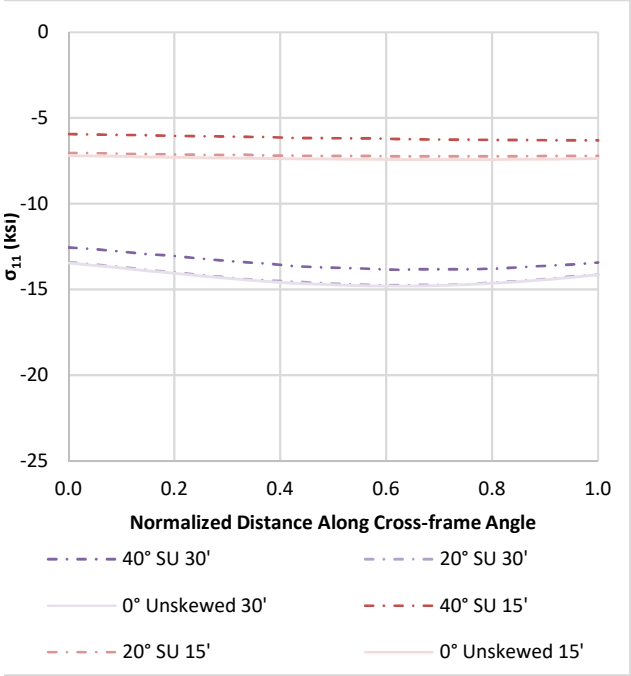

h) Skewed-unstaggered, 9.14 m [30 ft] and 4.57 m [15 ft] spacing

Figure 3.21 Cross-frame angle σ_{11} in member C, grouped by skew angle and configuration

In Figure 3.22 and Figure 3.23, the cross-frame angle member stresses, σ_{11}, in Member C are shown normalized by their critical buckling stress. In Figure 3.24 and Figure 3.25, the peak values of the same stresses are normalized by their critical buckling stress. Normalizing the angle member stresses by their respective critical buckling values allowed for a comparison between angle members of different lengths which varied with skew angle. Member C angle lengths, L, and critical buckling stresses, σ_{cr}, are shown in Table 3.1. The critical buckling stress, σ_{cr}, was equated as Euler's critical load, P_{cr}, applied per cross-sectional area, A, of the cross-frame angle member:

$$\sigma_{cr} = P_{cr}/A$$

where

P_{cr} = Euler's critical buckling load

A = cross-sectional area

Euler's critical load, P_{cr}, is given by the expression:

$$P_{cr} = \frac{\pi^2 E * I_Z}{(K*L)^2}$$

where

E = modulus of elasticity of the member material

I_z = moment of inertia about the weak principal axis

K = effective length factor, conservatively taken as 1.0 for pinned-pinned

L = unsupported length of the member

Table 3.1 Member C angle section properties and critical buckling values

Skew Angle	Configuration	Connection Type	I_z (mm^4) [in^4]	L (mm) [in]	P_{cr} (kN) [kips]	A (mm^2) [in^2]	σ_{cr} (MPa) [ksi]
0, 20, 40	Skewed-Staggered	Stiffener	1.153E+06 [2.769]	2985 [117.5]	255.6 [57.45]	2581 [4.000]	99.03 [14.36]
0, 20, 40	Skewed-Staggered	Half-pipe	1.153E+06 [2.769]	2713 [106.8]	309.3 [69.53]	2581 [4.000]	119.8 [17.38]
20	Skewed-Parallel	Stiffener	1.679E+06 [4.035]	3086 [121.5]	348.2 [78.27]	3377 [5.234]	103.1 [14.95]
20	Skewed-Parallel	Half-pipe	1.679E+06 [4.035]	2924 [115.1]	388.0 [87.22]	3377 [5.234]	114.9 [16.66]
40	Skewed-Parallel	Stiffener	3.136E+06 [7.535]	3840 [151.2]	419.6 [94.32]	4183 [6.484]	100.3 [14.55]
40	Skewed-Parallel	Half-pipe	3.136E+06 [7.535]	3706 [145.9]	450.6 [101.3]	4183 [6.484]	107.7 [15.62]
0, 20, 40	Skewed-Unstaggered	Stiffener	1.153E+06 [2.769]	2985 [117.5]	255.6 [57.45]	2581 [4.000]	99.03 [14.36]

Figure 3.22 (a) through (d) presents the cross-frame angle member stresses normalized by their critical buckling stress, *grouped by connection type* for the 13.7 m [45 ft] cross-frame spacing models. The 40° skewed-parallel model consistently produced the smallest stress

magnitudes for varying skew angles and configurations, followed by the 20° skewed-parallel model. It should be noted that although the cross-frame member length increases with increasing skew angle for a skewed-parallel configuration, the component of the force perpendicular to the girder line, that is the direct path for transferring lateral forces between girders, decreases with increasing skew angle. It can be seen that the skewed-parallel configuration always produced smaller axial stresses than the skewed-staggered configuration for the same skew angle. Varying skew angles with the same skewed-staggered configuration also produced similar stress values, as the cross-frame member length and orientation are the same for the skewed-staggered configuration regardless of skew angle.

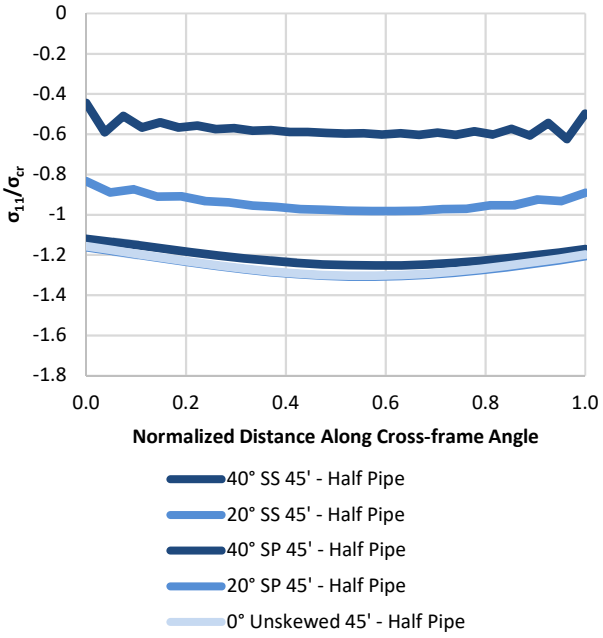

a) Half-pipe connection, 13.7 m [45 ft] cross-frame spacing

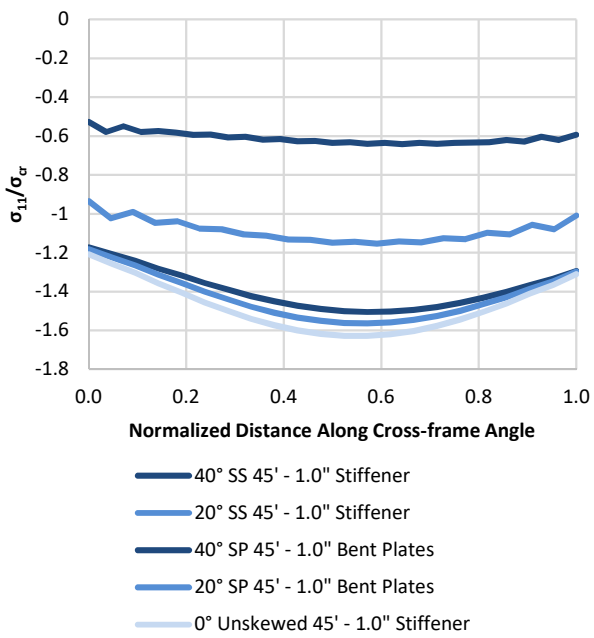

b) 25.4mm [1.0 in] stiffener connection, 13.7 m [45 ft] cross-frame spacing

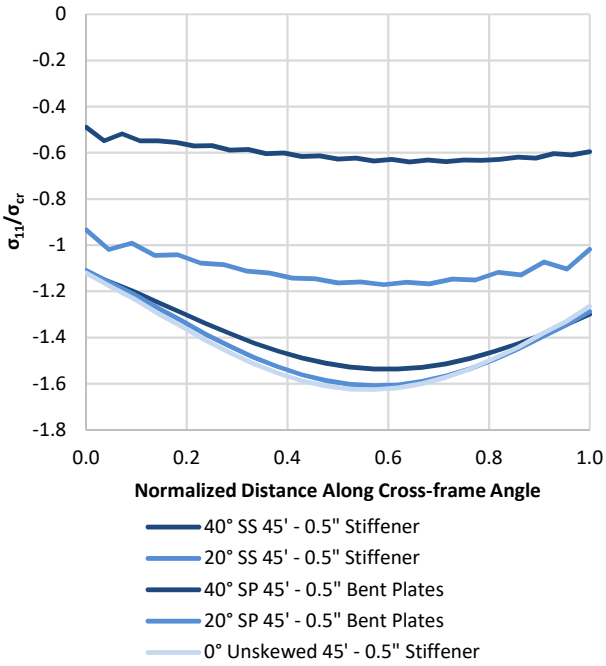

c) 12.7mm [1/2 in] stiffener connection, 13.7 m [45 ft] cross-frame spacing

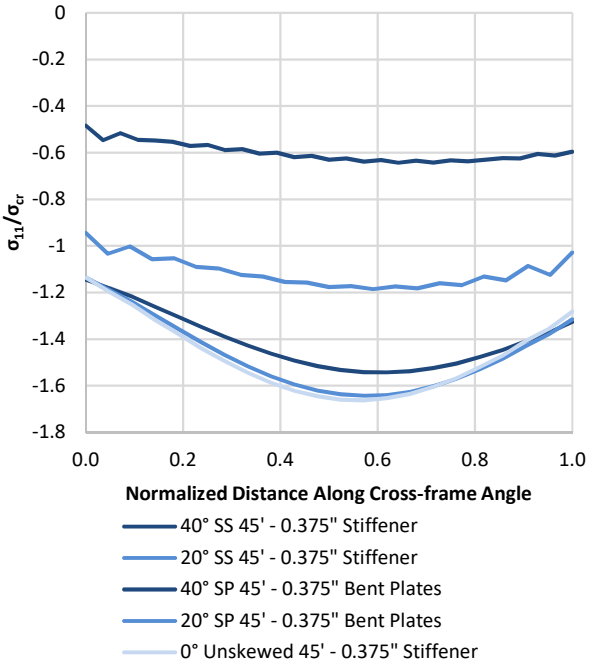

d) 9.53mm [3/8 in] stiffener connection, 13.7 m [45 ft] cross-frame spacing

Figure 3.22 Cross-frame angle σ_{11} normalized by critical buckling stress in member C, grouped by connection type

Figure 3.23 (a) through (e) shows the cross-frame angle member stresses normalized by their critical buckling stress, *grouped by skew angle and configuration* for all cross-frame spacings. For any given skew angle and configuration, the 4.57 m [15 ft] cross-frame spacing models always produced the smallest cross-frame stresses while the 13.7 m [45 ft] cross-frame spacing always produced the largest stresses. While the models that included the half-pipe connection sometimes produced larger stresses near the connection ends, the connection type did not produce significant differences in stress magnitudes at a location removed from the connection.

Figure 3.23 (f) through (h) groups cross-frame angle member stresses by configuration for the 4.57 m [15 ft] and 9.14 m [30 ft] cross-frame spacing models. The 4.57 m [15 ft] cross-

frame spacing models produced smaller stresses than the 9.14 m [30 ft] cross-frame spacing models, which can be expected as there are twice as many braces when the cross-frame spacing is halved. For any given skew angle and cross-frame spacing, the skewed-staggered configuration produced the largest stresses, with the skewed-unstaggered configuration following closely behind. The skewed-parallel configuration produced the smallest cross-frame member stresses among the three cross-frame configurations.

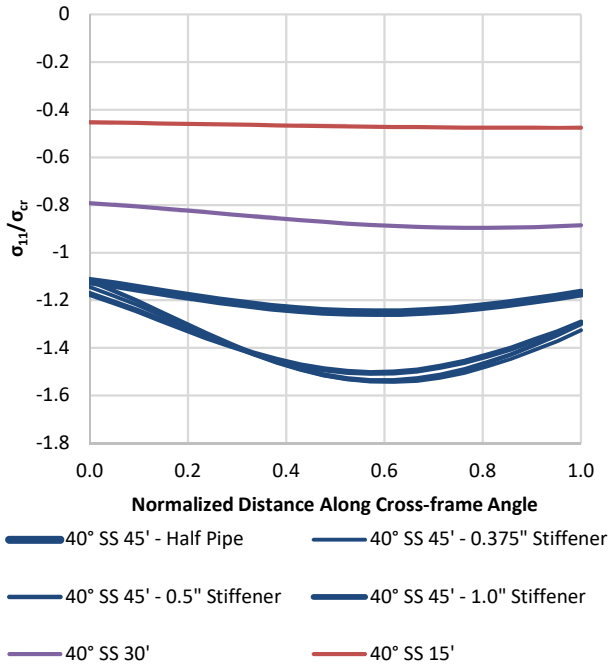

a) 40° skewed-staggered

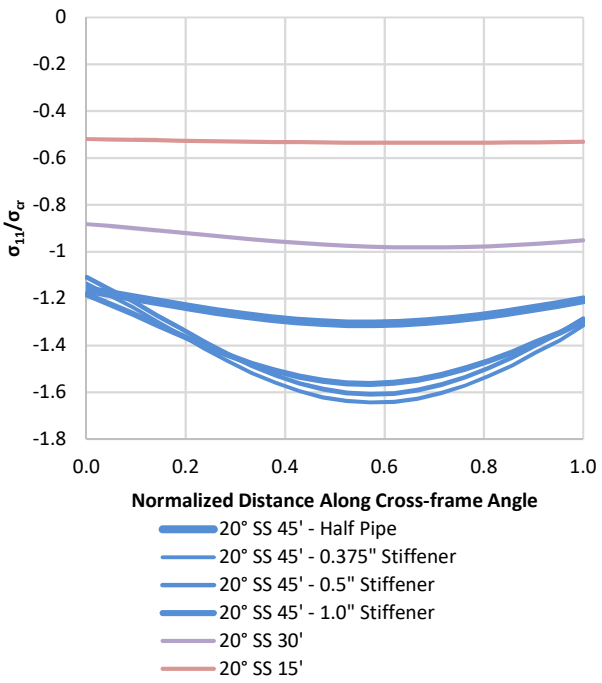

b) 20° skewed-staggered

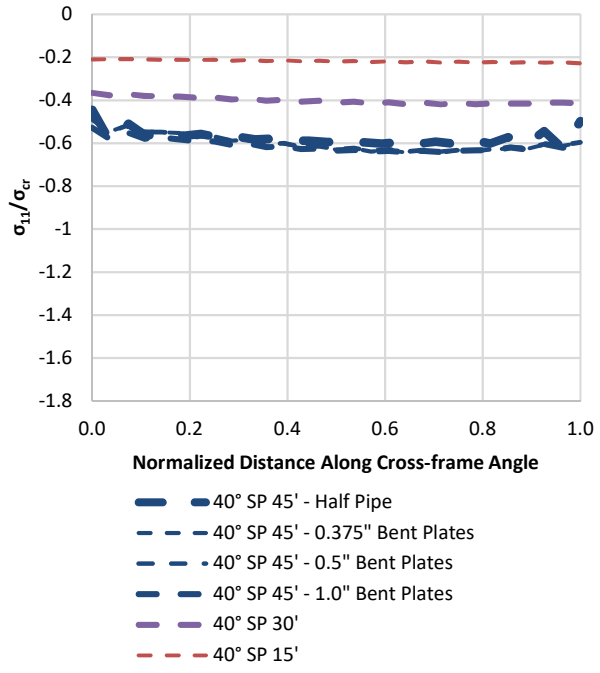

c) **40° skewed-parallel**

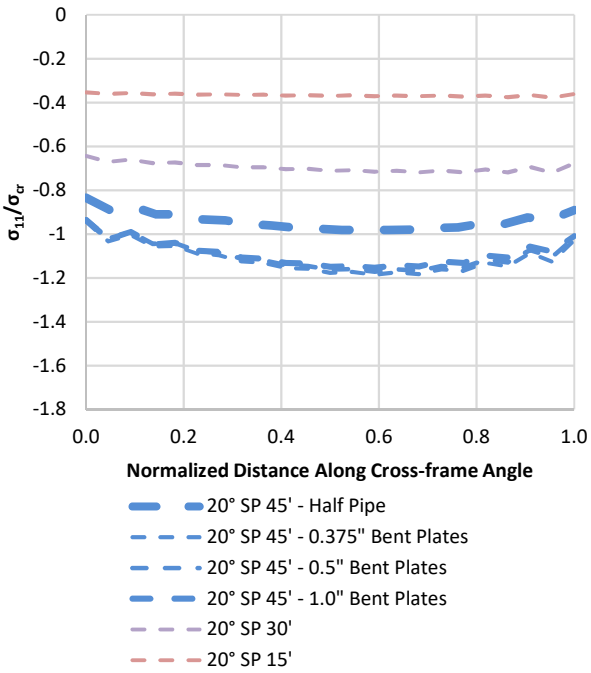

d) **20° skewed-parallel**

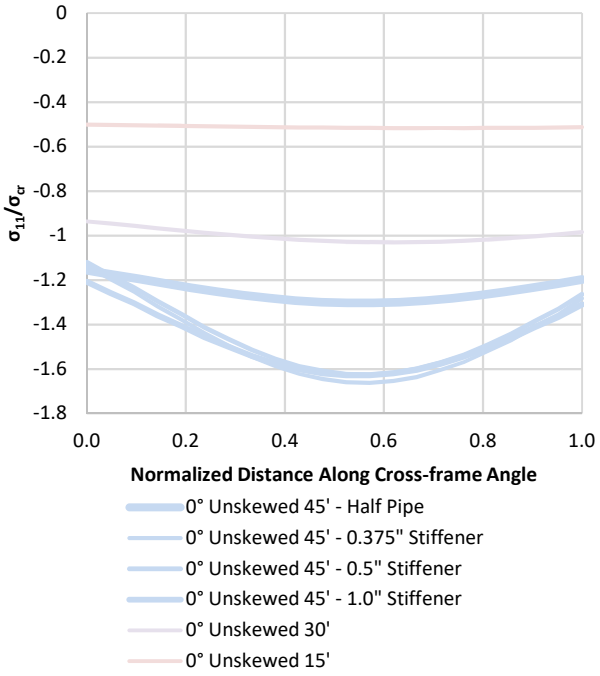

e) **Non-skewed bridge**

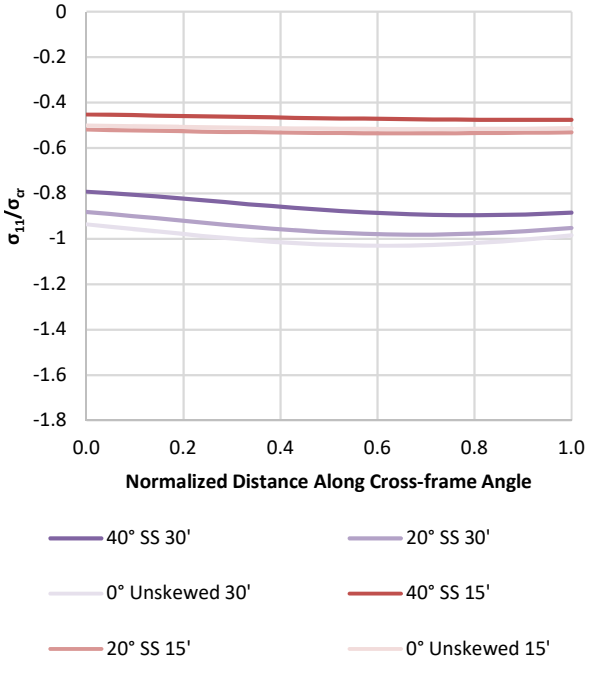

f) **Skewed-staggered, 9.14 m [30 ft] and 4.57 m [15 ft] spacing**

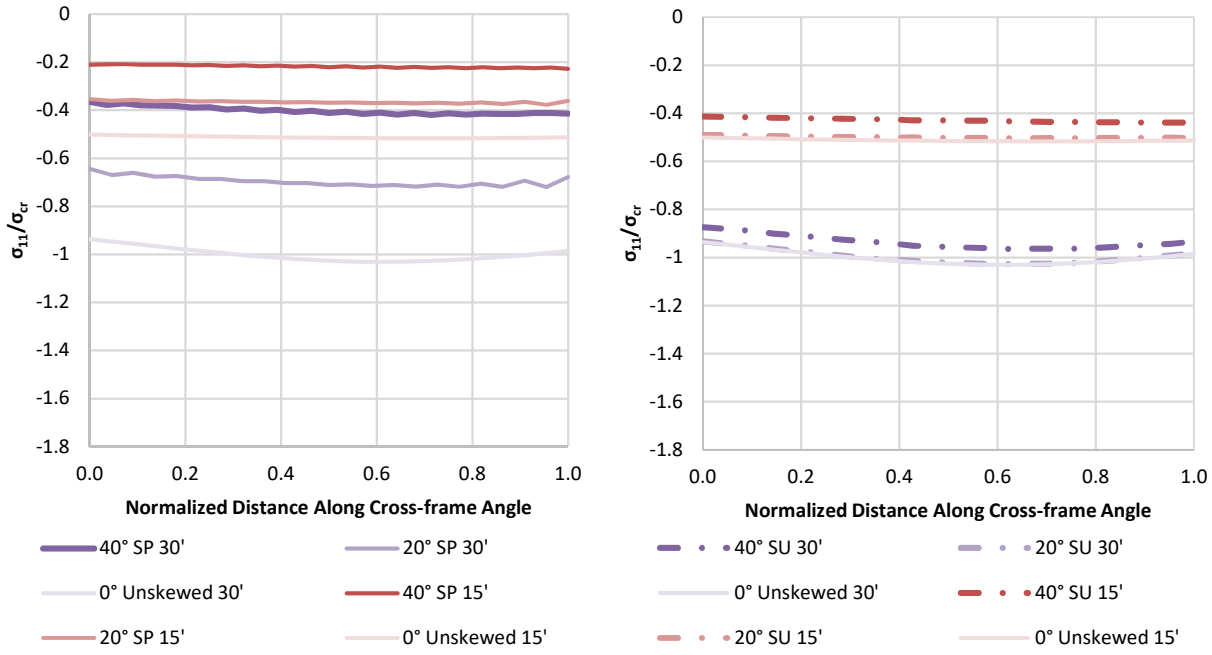

g) Skewed-parallel, 9.14 m [30 ft] and 4.57 m [15 ft] spacing

h) Skewed-unstaggered, 9.14 m [30 ft] and 4.57 m [15 ft] spacing

Figure 3.23 Cross-frame angle σ_{11} normalized by critical buckling stress in member C, grouped by skew angle and configuration

Figure 3.24 (a) through (d) shows the peak cross-frame angle member σ_{11} in Member C normalized by the critical buckling stress, *grouped by connection type* for the 13.7 m [45 ft] cross-frame spacing models. All skewed-staggered and non-skewed models were beyond the critical buckling stress, with the 20 degree and 0 degree skew angle models producing the largest cross-frame angle member stress ratios. Smaller skew angles produced larger stresses for the same configuration and connection type. The skewed-parallel configuration produced much smaller stress ratios compared to the skewed-staggered configuration, with the 40° skewed-parallel bridge with 13.7 m [45 ft] cross-frame spacing having the smaller stress ratio at around 60 percent for all connection types.

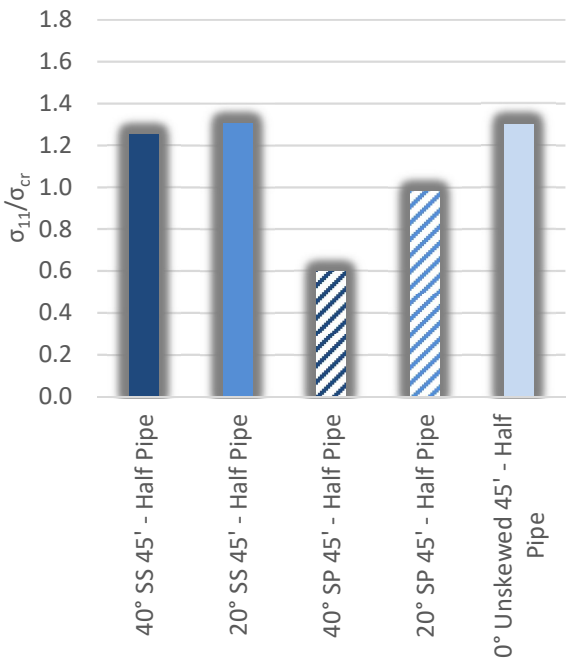

a) **Half-pipe connection, 13.7 m [45 ft] cross-frame spacing**

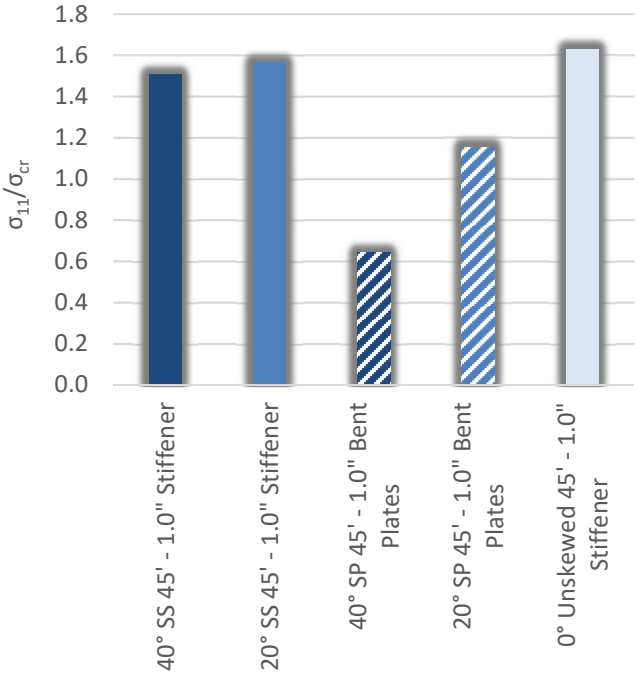

b) **25.4mm [1.0 in] stiffener connection, 13.7 m [45 ft] cross-frame spacing**

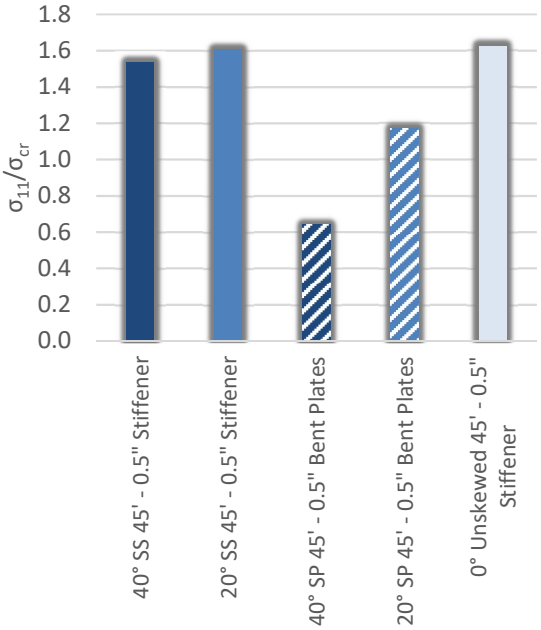

c) **12.7mm [1/2 in] stiffener connection, 13.7 m [45 ft] cross-frame spacing**

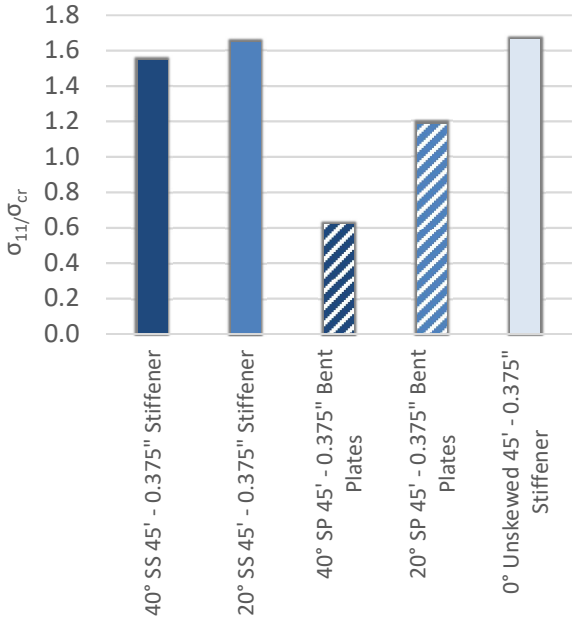

d) **9.53mm [3/8 in] stiffener connection, 13.7 m [45 ft] cross-frame spacing**

Figure 3.24 Peak cross-frame angle σ_{11} normalized by critical buckling stress in member C, grouped by connection type

Figure 3.25 (a) through (e) shows the peak cross-frame angle Member C σ_{11} normalized by the critical buckling stress, *grouped by skew angle and configuration* for the 13.7 m [45 ft] cross-frame spacing models. The half-pipe connection produced smaller stress ratios compared to stiffener connections of any thickness. While stress ratios typically decreased with increasing stiffener thickness, the differences in stress ratios between varying stiffener thicknesses were not significant. The 40° skewed-parallel bridge with 13.7 m [45 ft] cross-frame spacing produced the smallest stress ratio and stress variations in the cross-frame member for different connection types were minimal.

Figure 3.25 (f) and (g) groups peak cross-frame angle member stress ratios by configuration for the 4.57 m [15 ft] and 9.14 m [30 ft] cross-frame spacing models. Stress ratios increased with decreasing skew angle for these shorter cross-frame spacing models. The exception was the non-skewed bridge with 4.57 m [15 ft] cross-frame spacing, which had almost the same stress ratio as the 20° skewed-staggered model with the same cross-frame spacing. This stress increase for decreasing skew angle was more pronounced for the skewed-parallel configuration than for the skewed-staggered configuration even though the magnitude of the stress ratios were smaller for the skewed-parallel configuration.

While finite element analysis can generally reproduce trends in the variation of stress values, the magnitudes may not be reliably predicted. A course meshing for the cross-frame members was chosen to efficiently run these bridge models using large displacement theory. A more detailed modeling of cross-frame members and connections is recommended in future simulations to more accurately model the stress gradients within the members and restraints provided by the physical cross-frames.

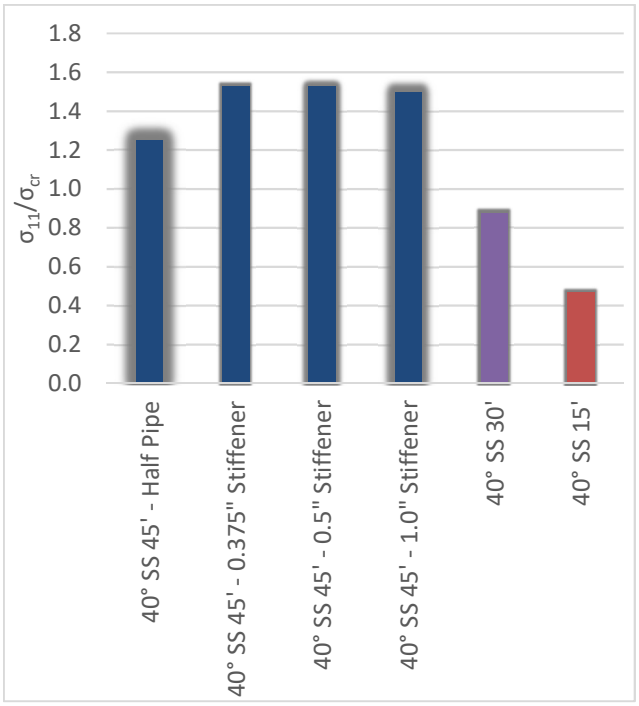

a) 40° skewed-staggered

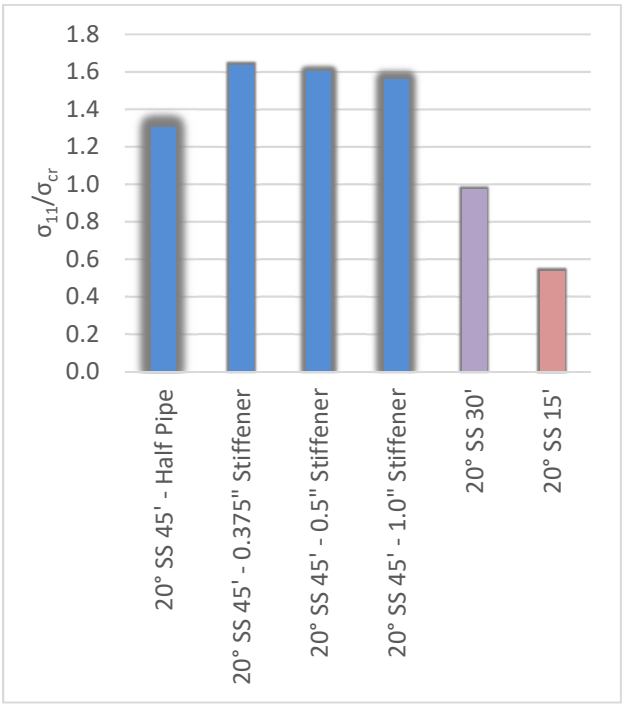

b) 20° skewed-staggered

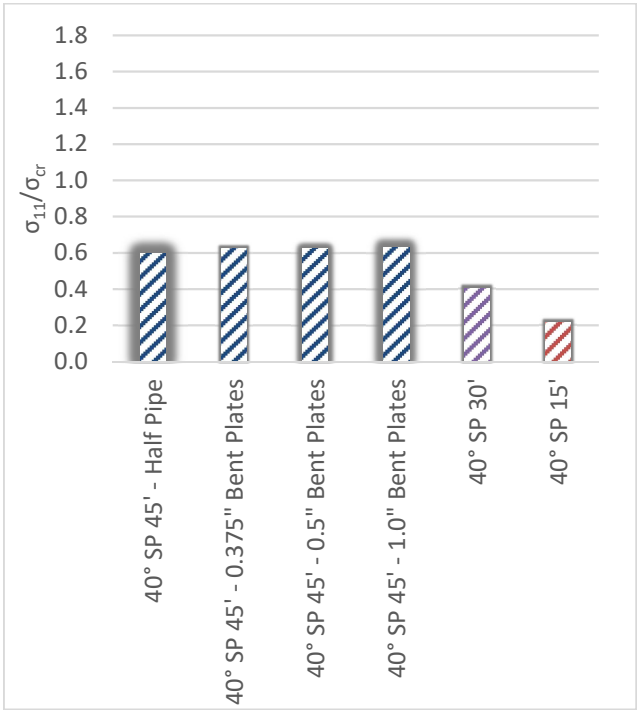

c) 40° skewed-parallel

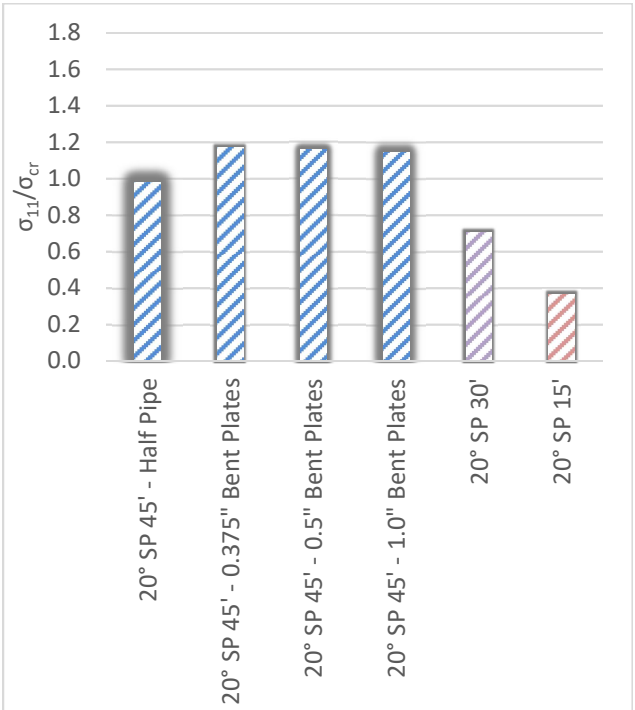

d) 20° skewed-parallel

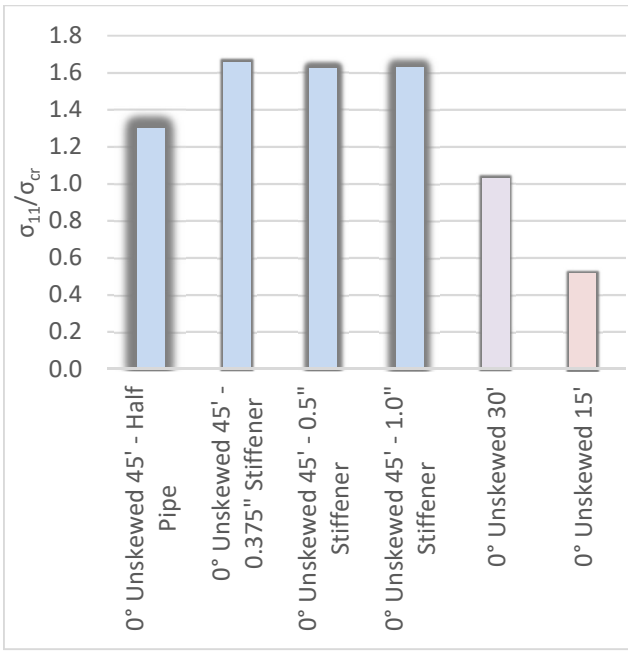

e) Non-skewed bridge

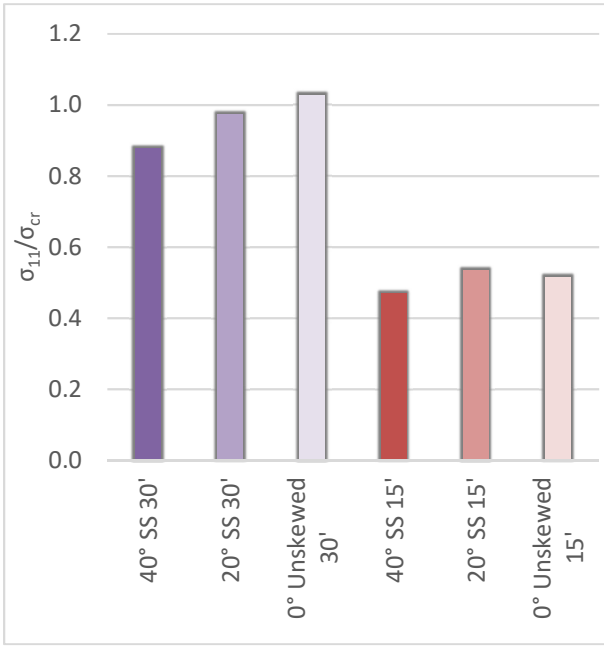

f) Skewed-staggered, 9.14 m [30 ft] and 4.57 m [15 ft] spacing

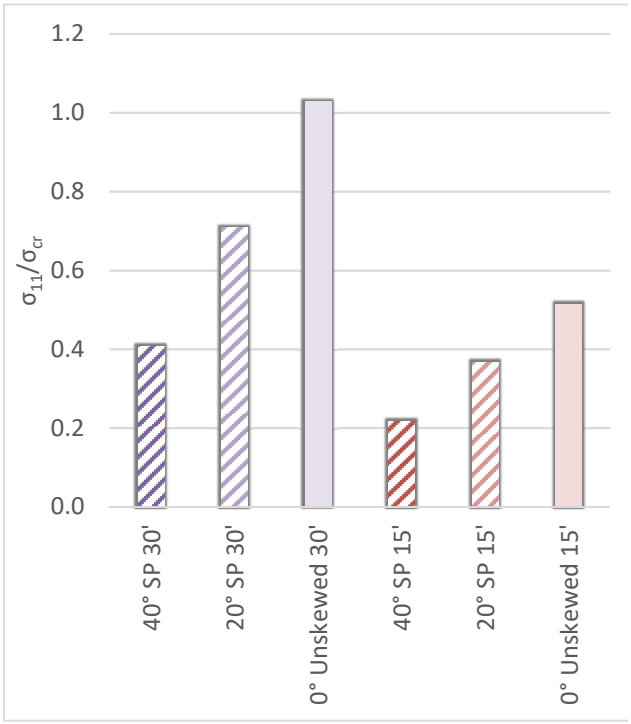

g) Skewed-parallel, 9.14 m [30 ft] and 4.57 m [15 ft] spacing

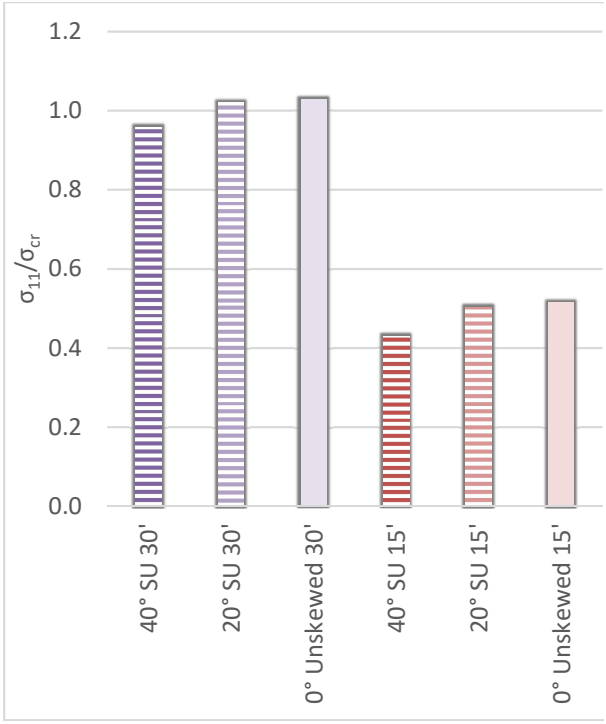

h) Skewed-unstaggered, 9.14 m [30 ft] and 4.57 m [15 ft] spacing

Figure 3.25 Peak cross-frame angle σ_{11} normalized by critical buckling stress in member C, grouped by skew angle and configuration

Deformed Shapes of the Bridge FE Models, and Cross-Frame Effectiveness

Figure 3.26, Figure 3.27, Figure 3.28, and Figure 3.29 present views of the deformed configurations for a 40° and 20° bridge system in both the skewed-parallel and skewed-staggered configuration. Overall, it can be seen that the cross-frames functioned as effective brace members for all connections, configurations, and spacing. This is apparent in that there is no apparent girder deflection at the brace points, showing that the braces are effective in producing the expected mode of girder buckling. Appendix A of this report also presents deformed shapes for every model in the parametric analyses.

Figure 3.26 shows the 40° skewed-parallel bridge with 13.7 m [45 ft] cross-frame spacing and stiffener connections in plan view. Only the cross-frames, webs, and bottom flanges are shown. The image is scaled to twice the actual deformation, with the color map showing Mises stresses from 0 MPa [0 ksi] in dark blue to 345 MPa [50 ksi] in red. Both the first and second unbraced lengths of the exterior girder in Span 1, better shown in Figure 3.27, are buckled and exhibiting roll-over behavior. Even with high stresses in the cross-frame members and stiffeners, these images show that the cross-frames are effectively bracing the girder and producing an inflection point between the two unbraced lengths.

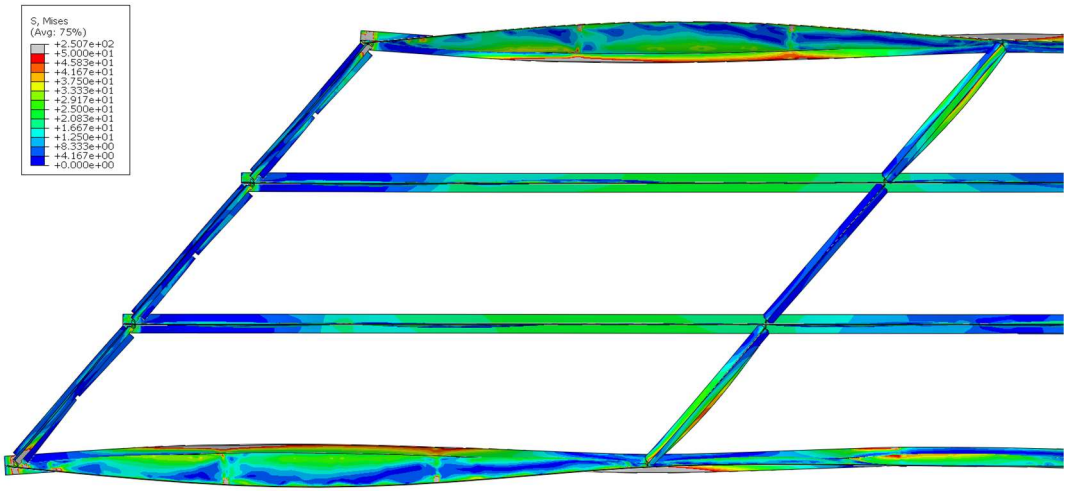

Figure 3.26 Deformed shape of the 40° skewed-parallel bridge with 13.7 m [45 ft] cross-frame spacing (plan view)

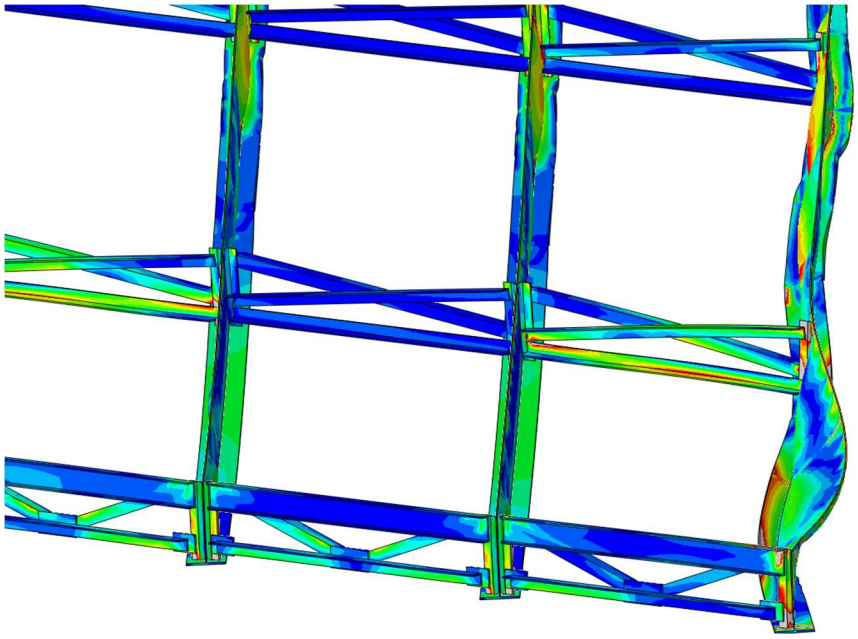

Figure 3.27 Deformed shape of the 40° skewed-parallel bridge with 13.7 m [45 ft] cross-frame spacing in Span 1 (plan view)

Figure 3.28 show the 20° skewed-staggered bridge with 13.7 m [45 ft] cross-frame spacing and half-pipe connections in plan view. Again, only the cross-frames, webs, and bottom flanges are shown. The image is scaled to twice the actual deformation, with the color map showing Mises stresses from 0 MPa [0 ksi] in dark blue to 345 MPa [50 ksi] in red. Not only does the half-pipe connection brace the girders better than the stiffener connections, but there are smaller stresses in the half-pipe connection itself, as shown in Figure 3.29.

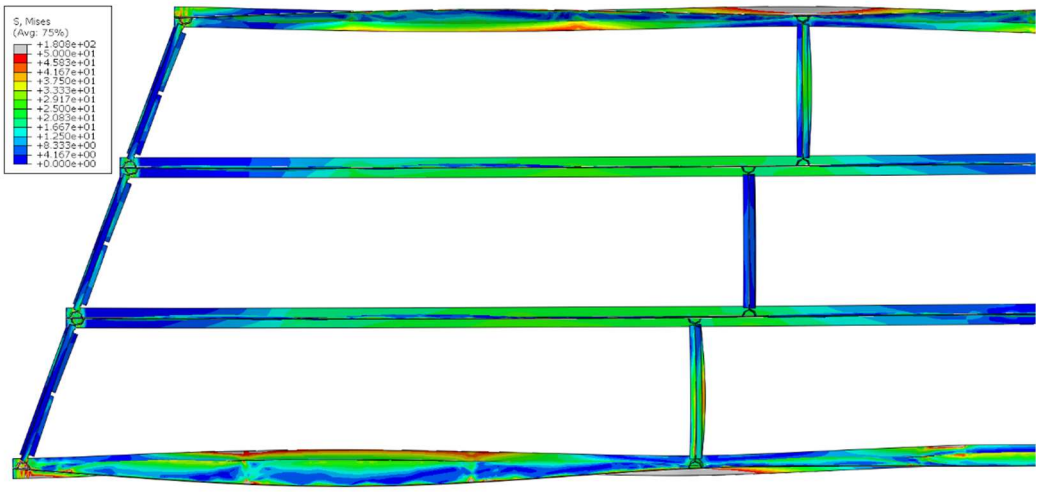

Figure 3.28 Deformed shape of the 20° skewed-staggered bridge with 13.7 m [45 ft] cross-frame spacing in plan view

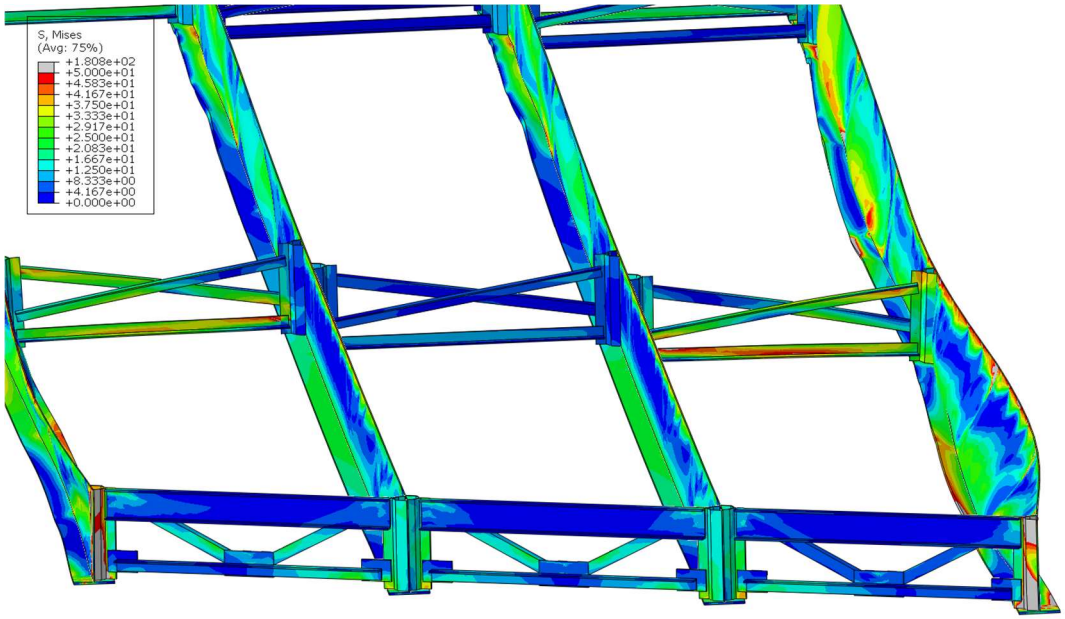

Figure 3.29 Deformed shape of the 20° skewed-staggered bridge with 13.7 m [45 ft] cross-frame spacing in Span 1

INTERIOR GIRDER (G3) IN-PLANE AND OUT-OF-PLANE BENDING STRESSES

Figure 3.30, Figure 3.31, Figure 3.32, and Figure 3.33 present strong-axis bending stress, weak-axis bending stress, top flange out-of-plane bending stress, and bottom flange out-of-plane

bending stress respectively for interior Girder 3, grouped by connection type, for the 4.57 m [15 ft] and 9.14 m [30 ft] cross-frame spacing models. Girder strong-axis and weak-axis bending stresses were calculated from both the top and bottom flanges. Results from a simple beam-line analysis of the respective girders are presented with strong-axis sectional stresses.

In Figure 3.30, the strong-axis sectional stresses for bridges with 4.57 m [15 ft] and 9.14 m [30 ft] cross-frame spacings were almost the same for all three configurations. For bridges with cross-frames spaced less than 9.14 m [30 ft], skew angle and cross-frame placement had little effect on the vertical bending stress in the interior girder. Strong-axis sectional stress calculated from the top flange in the interior girder matched relatively closely with results calculated from beam analysis as well. Strong-axis sectional stress calculated from the bottom flange resulted in lower values compared to those calculated from the top flange. Maximum strong-axis stress was 253 MPa [36.7 ksi], calculated from the top flange of the 0 degree non-skewed bridge with 4.57 m [15 ft] cross-frame spacing.

In Figure 3.31, the weak-axis sectional stresses for bridges with 4.57 m [15 ft] and 9.14 m [30 ft] cross-frame spacings were low for all three configurations. A maximum value of 37.0 MPa [5.37 ksi] was produced by the 40° skewed-staggered bridge with 4.57 m [15 ft] cross-frame spacing. The skewed-staggered configuration produced the highest peak weak-axis sectional stress value and the skewed-parallel configuration produced the lowest peak weak-axis sectional stress value for the same skew angle and cross-frame spacing. The skewed-staggered configurations produced stresses almost twice that found in the skewed-parallel configurations. For the skewed-parallel configuration, lateral bending loads are transferred directly from the cross-frame on one side of the girder to the cross-frame on the other side. However in the skewed-staggered configuration, the same loads must be transferred through bending in the

girder. For skewed-unstaggered configuration, weak-axis stress values were between that of the skewed-parallel and skewed-staggered configuration. While cross-frames are balanced on opposite sides of the girder, the cross-frame skew angle is not aligned with the abutment skew angle.

Figure 3.32 shows top flange out-of-plane bending stresses in Girder 3. Similar to weak-axis sectional stresses, the skewed-staggered configuration typically produced the highest maximum stress values while the skewed-parallel configuration typically produced the lowest maximum stress values. The maximum stress value had a magnitude of 42.0 MPa [6.09 ksi], found in the 40 degree skewed-staggered configuration with 9.14 m [30 ft] cross-frame spacing. Larger skew angles typically corresponded with higher stress values compared to smaller skew angles for bridges with the same cross-frame spacing and configuration.

Bottom flange out-of-plane bending stresses, shown in Figure 3.33, were much higher compared to top flange out-of-plane bending stresses. Again, the skewed-staggered configuration produced the highest maximum stress values and the skewed-parallel configuration produced the lowest maximum stress values. The highest magnitude stress of 65.5 MPa [9.50 ksi] was found in the 40 degree skewed-staggered configuration with 4.57 m [15 ft] cross-frame spacing.

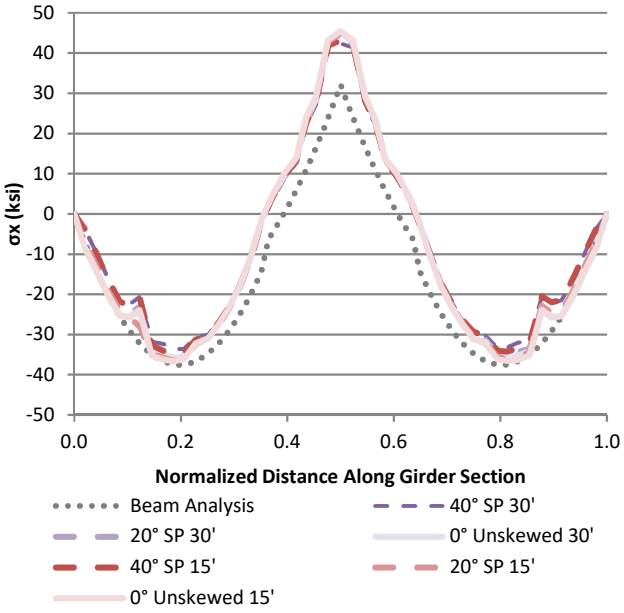

a) Skewed-parallel – Top Flange

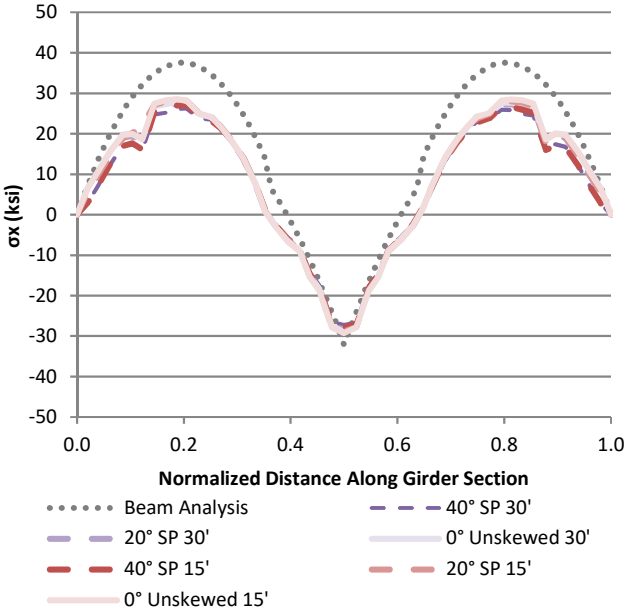

b) Skewed-parallel – Bottom Flange

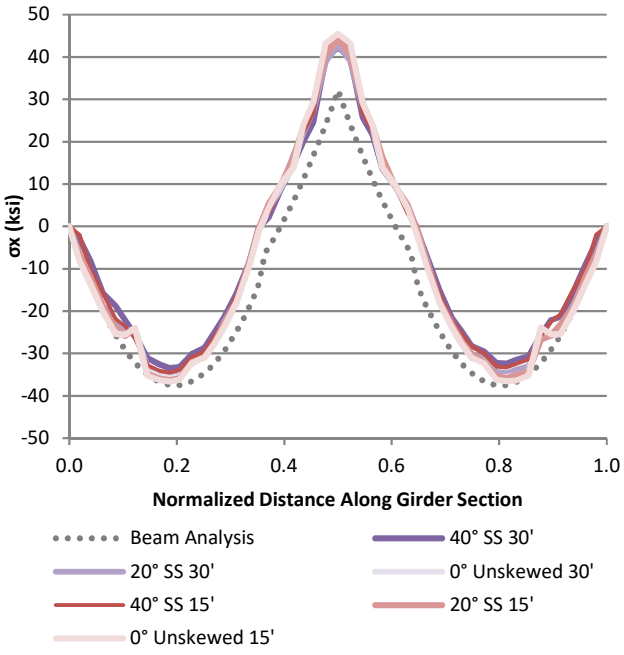

c) Skewed-staggered – Top Flange

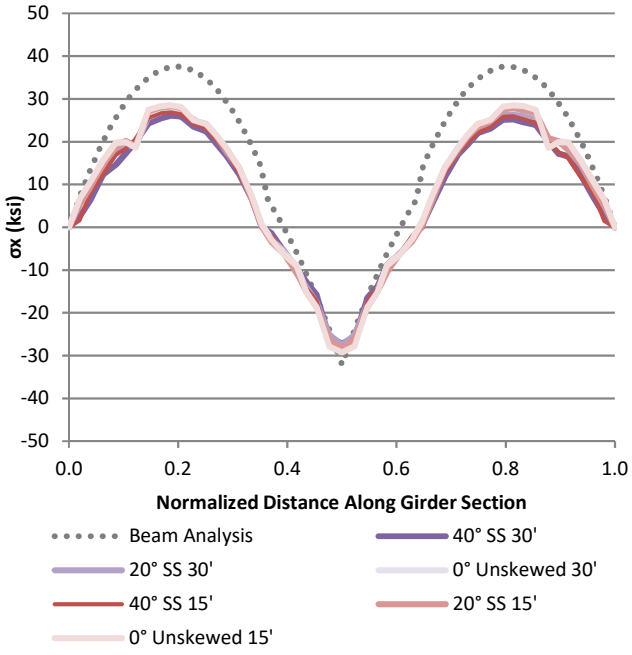

d) Skewed-staggered – Bottom Flange

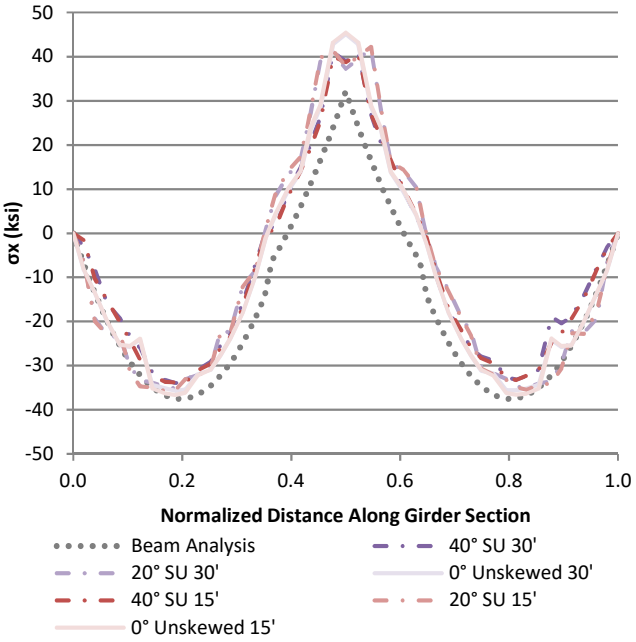

e) **Skewed-unstaggered – Top Flange**

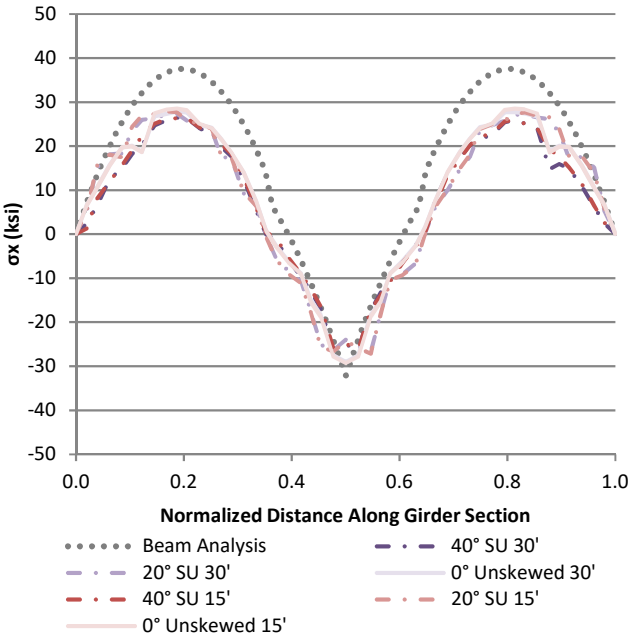

f) **Skewed-unstaggered – Bottom Flange**

Figure 3.30 Girder 3 strong-axis sectional stresses for bridges with 4.57 m [15 ft] and 9.14 m [30 ft] cross-frame spacings, grouped by configuration

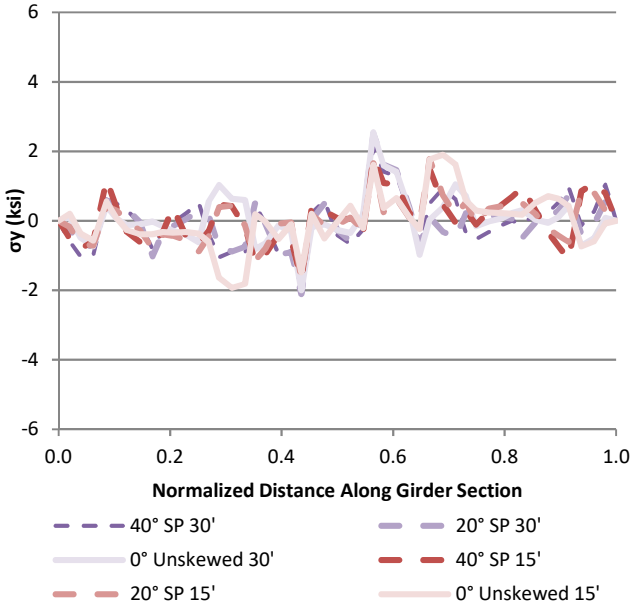

a) Skewed-parallel – Top Flange

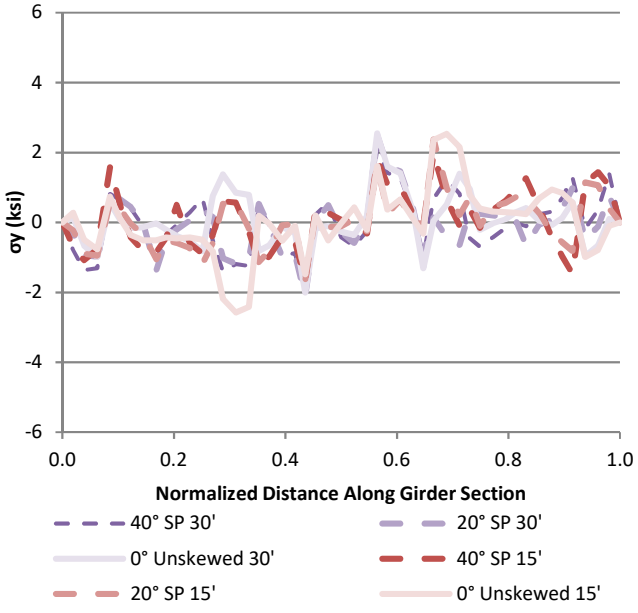

b) Skewed-parallel - Bottom Flange

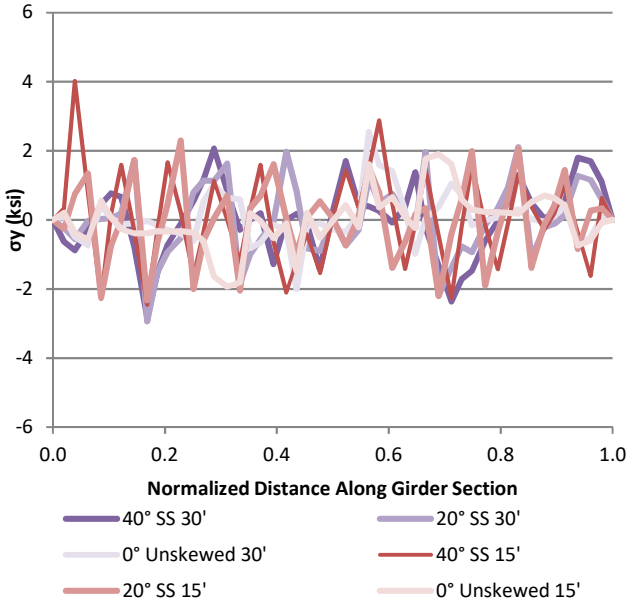

c) Skewed-staggered - Top Flange

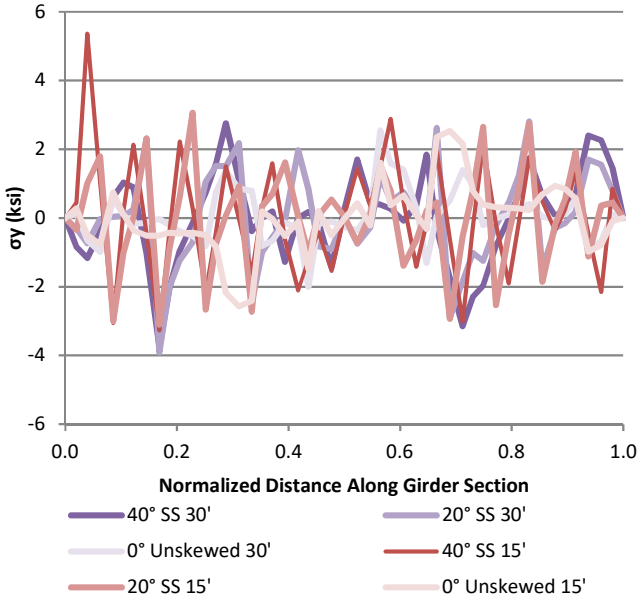

d) Skewed-staggered - Bottom Flange

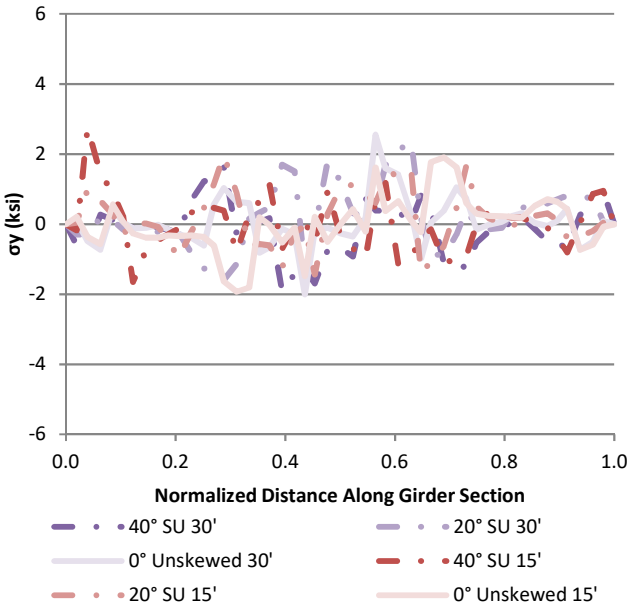

e) Skewed-unstaggered - Top Flange

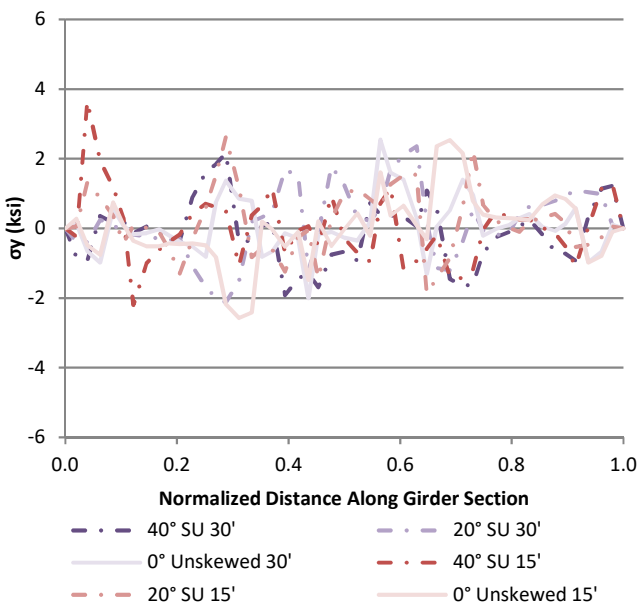

f) Skewed-unstaggered - Bottom Flange

Figure 3.31 Girder 3 weak-axis sectional stresses for bridges with 4.57 m [15 ft] and 9.14 m [30 ft] cross-frame spacings, grouped by configuration

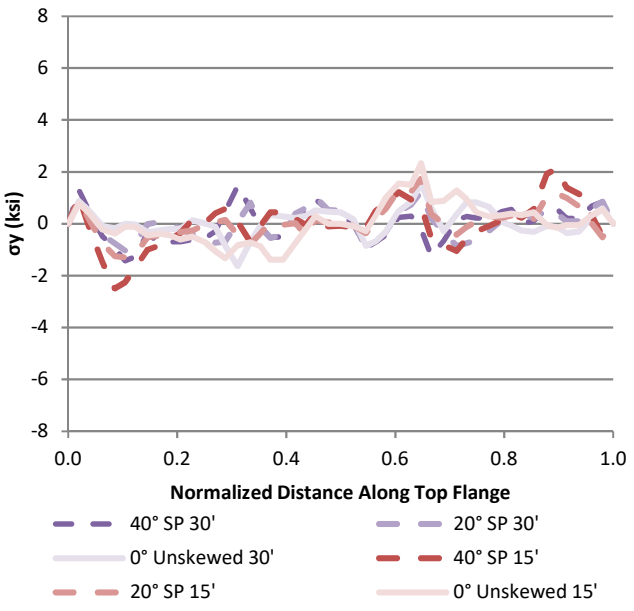

a) Skewed-parallel

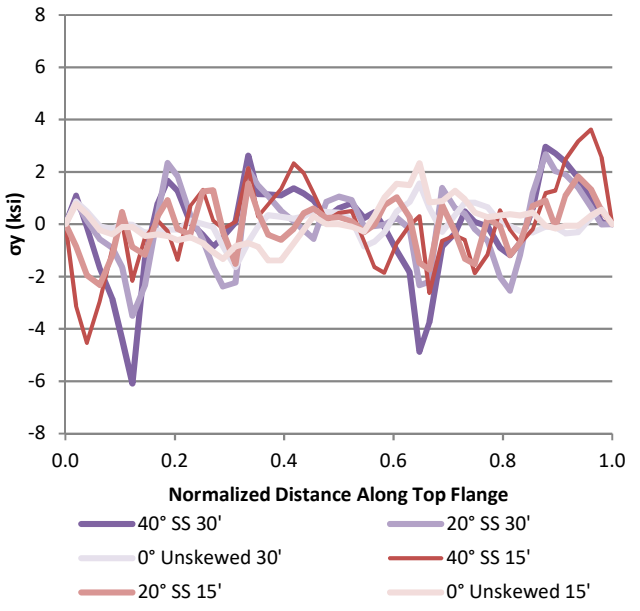

b) Skewed-staggered

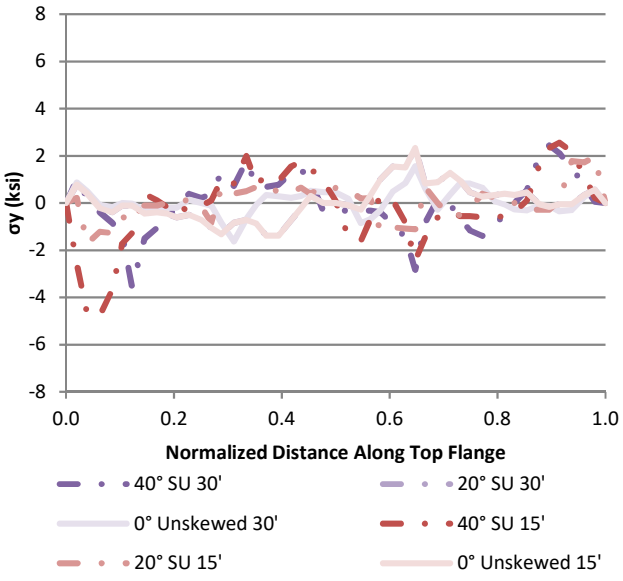

c) Skewed-unstaggered

Figure 3.32 Girder 3 top flange out-of-plane stresses for bridges with 4.57 m [15 ft] and 9.14 m [30 ft] cross-frame spacings, grouped by configuration

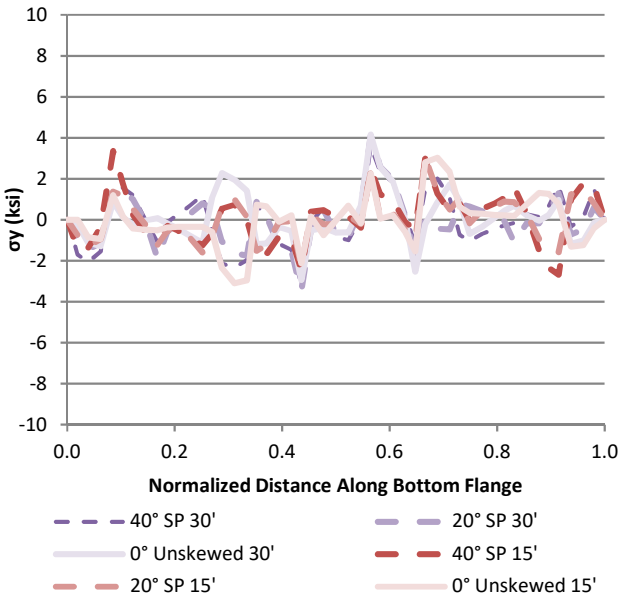

a) Skewed-parallel

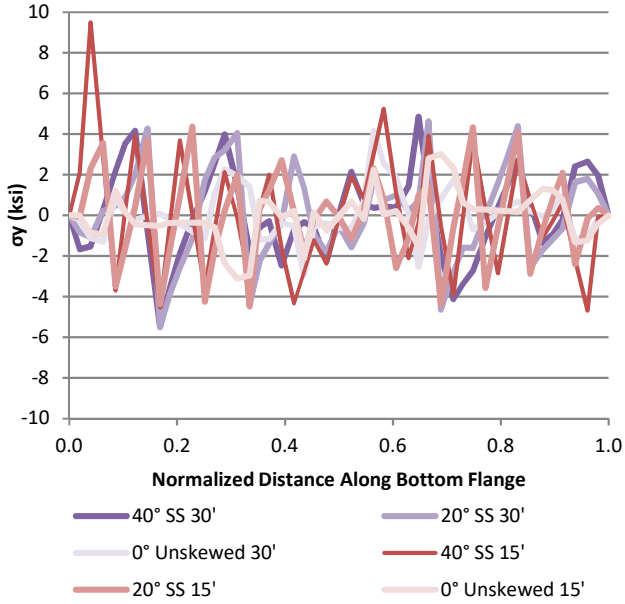

b) Skewed-staggered

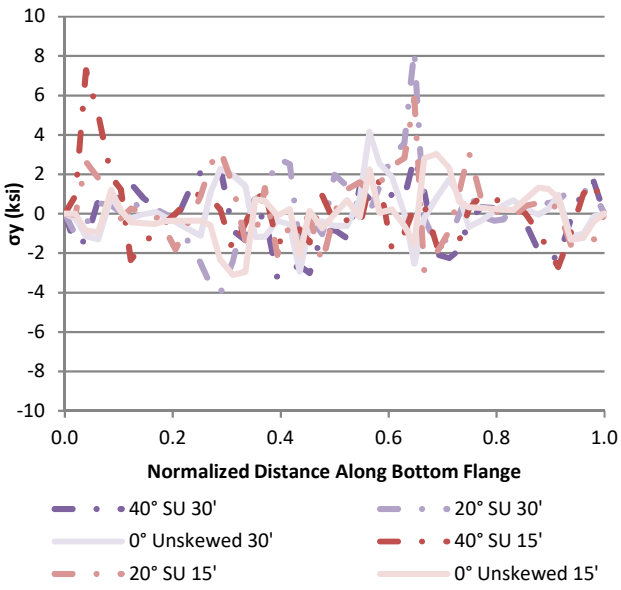

c) Skewed-unstaggered

Figure 3.33 Girder 3 bottom flange out-of-plane stresses for bridges with 4.57 m [15 ft] and 9.14 m [30 ft] cross-frame spacings, grouped by configuration

through Figure 3.37 present strong-axis bending stress, weak-axis bending stress, top flange out-of-plane bending stress, and bottom flange out-of-plane bending stress respectively for interior Girder 3, grouped by connection type, for the 13.7 m [45 ft] cross-frame spacing models. It was found that the skewed-staggered configuration produced significantly larger out-of-plane stresses in the interior girder near mid-span compared to the skewed-parallel configuration. This is due to unbalanced, lateral cross-frame forces from the exterior girder being transferred as bending in the interior girder. Not only is there a larger component of the lateral load transferred through the cross-frames between girders for the skewed-staggered configuration, that load must also be transferred through weak-axis bending of the interior girder to reach the brace on the opposite side of the girder.

Results from a simple beam-line analysis of the respective girders are again presented with strong-axis sectional stresses. The data shows that all out-of-plane stresses for Girder 3 were significantly smaller than out-of-plane exterior girder stresses due to the bracket overhang loading on the exterior girder. The maximum out-of-plane weak-axis sectional stress was less than 68.9 MPa [10 ksi]. Strong-axis girder stresses for the interior girder were also smaller compared to the exterior girder. As a result, lateral torsional buckling will likely occur in the exterior girders prior to it occurring in the interior girders due to the significant eccentricity coming from the overhang brackets.

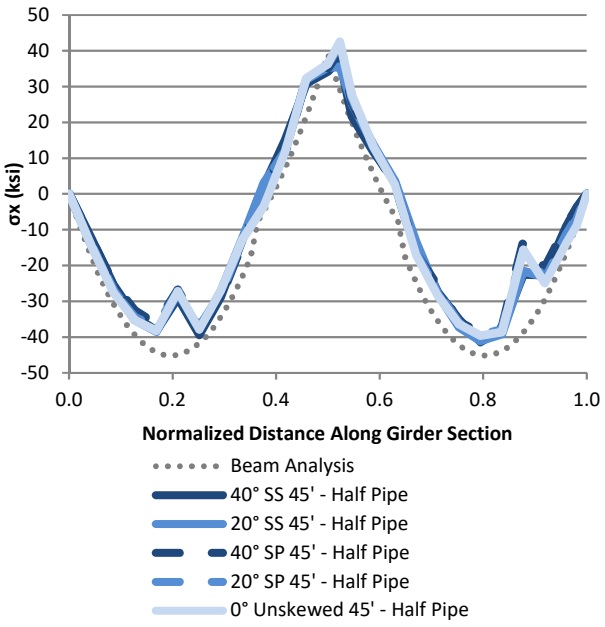

a) Half-pipe connection – Top Flange

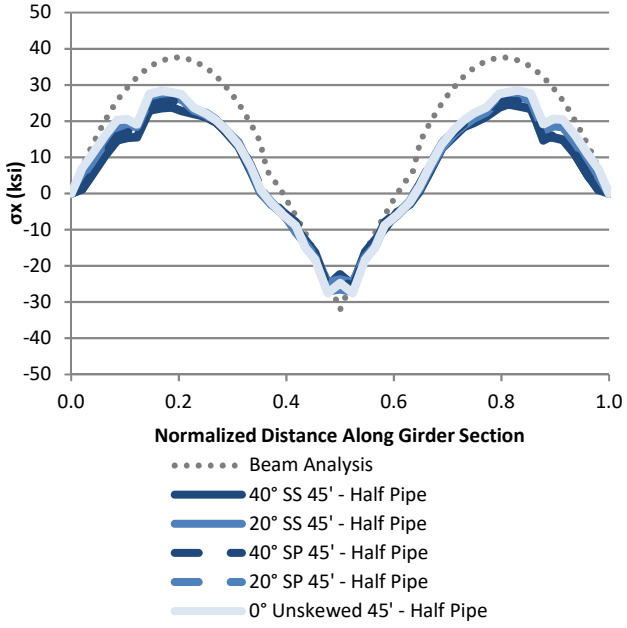

b) Half-pipe connection – Bottom Flange

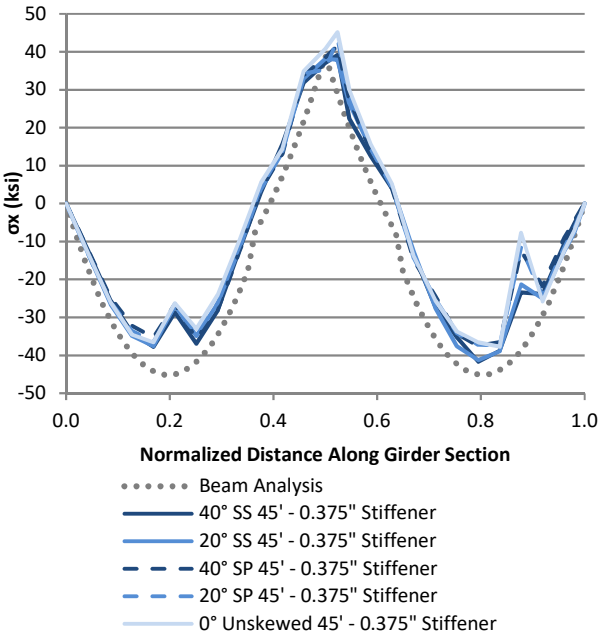

c) 9.53mm [3/8 in] stiffener connection – Top Flange

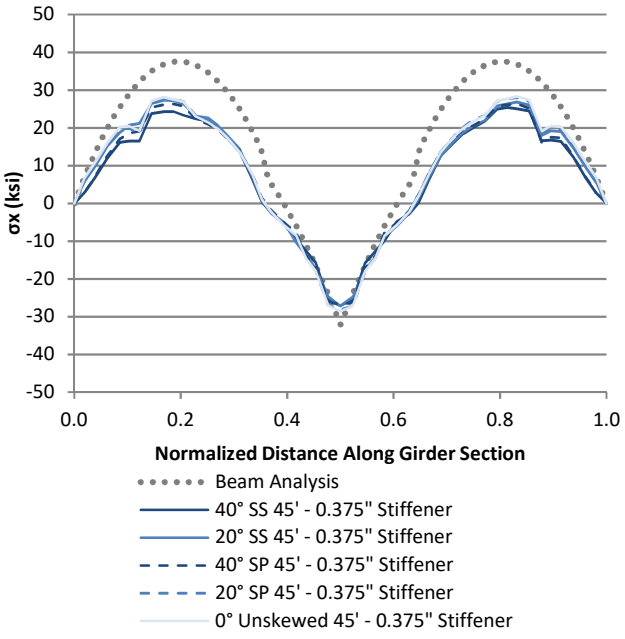

d) 9.53mm [3/8 in] stiffener connection – Bottom Flange

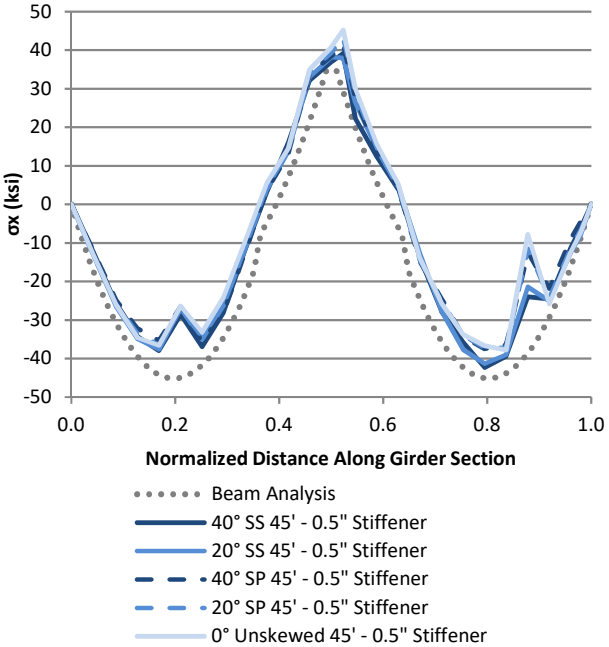

a) 12.7mm [1/2 in] stiffener connection – Top Flange

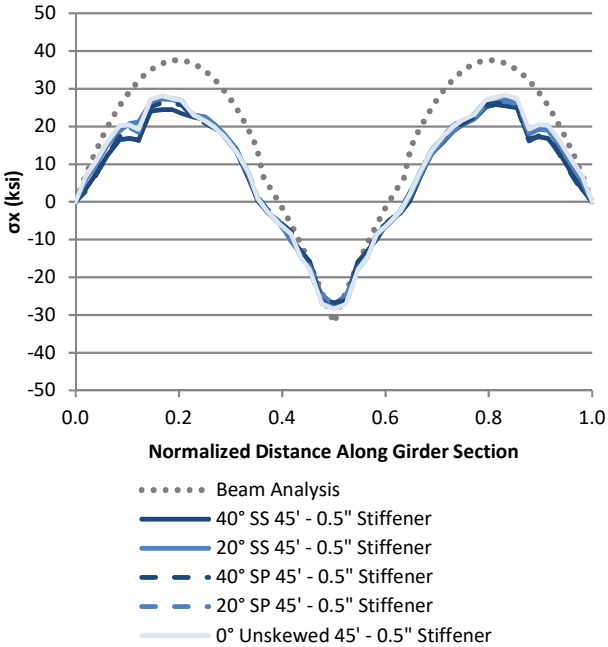

b) 12.7mm [1/2 in] stiffener connection – Bottom Flange

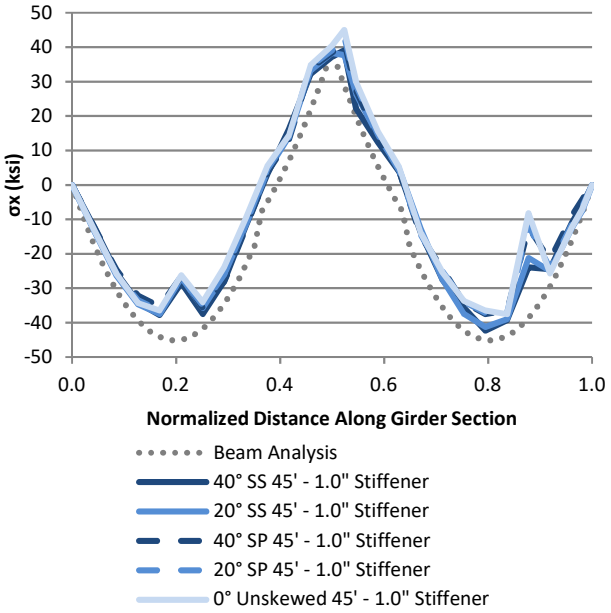

c) **25.4mm [1.0 in] stiffener connection – Top Flange**

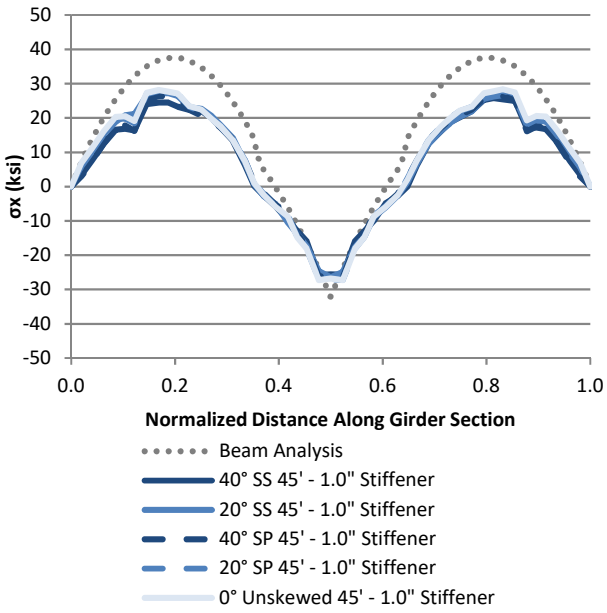

d) **25.4mm [1.0 in] stiffener connection – Bottom Flange**

Figure 3.34 Strong-axis sectional stresses for bridges with 13.7 m [45 ft] cross-frame spacing, grouped by connection type – interior girder (G3)

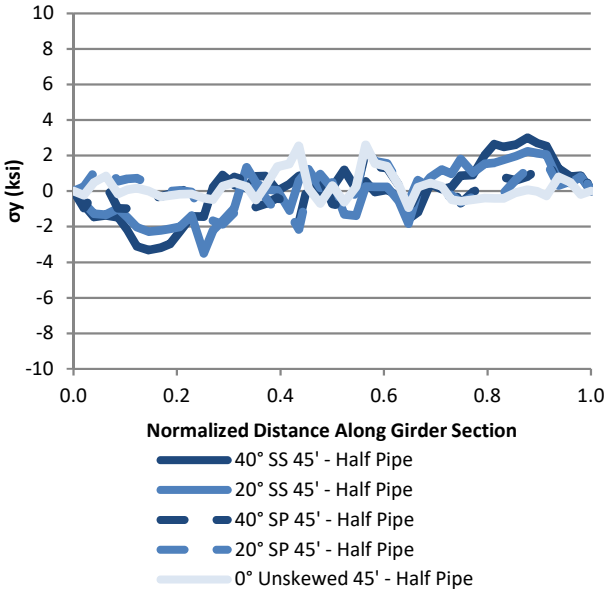

a) **Half-pipe connection – Top Flange**

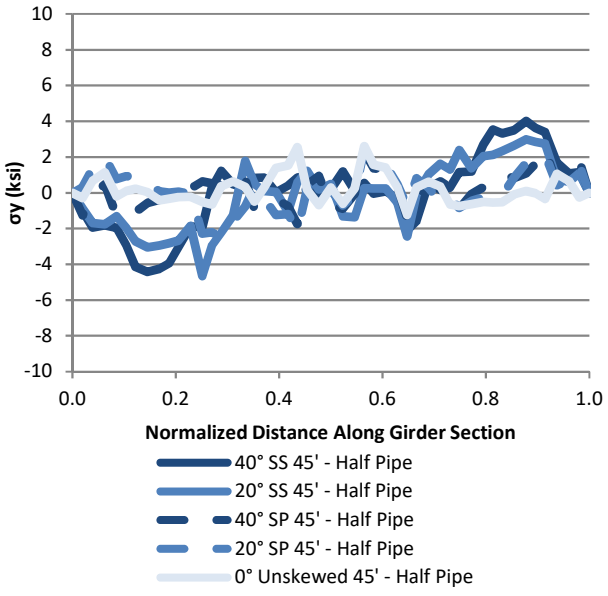

b) **Half-pipe connection - Bottom Flange**

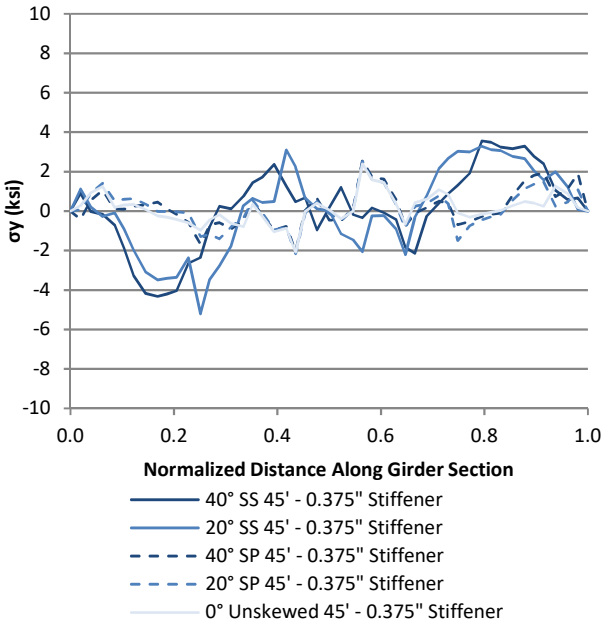

c) 9.53mm [3/8 in] stiffener connection - Top Flange

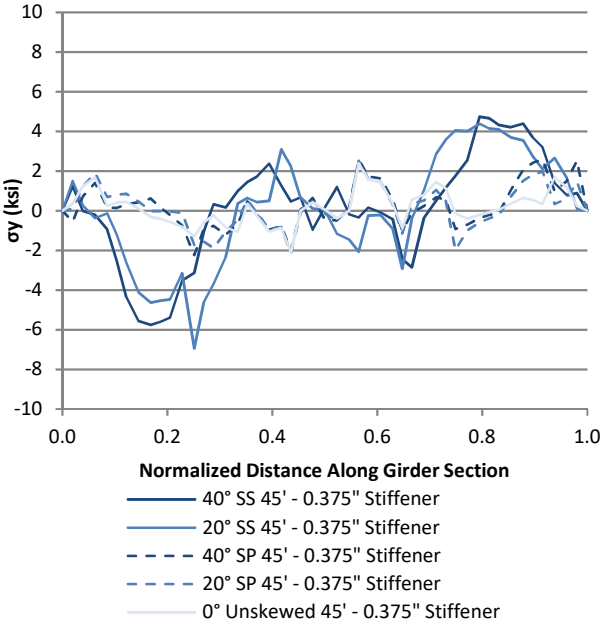

d) 9.53mm [3/8 in] stiffener connection - Bottom Flange

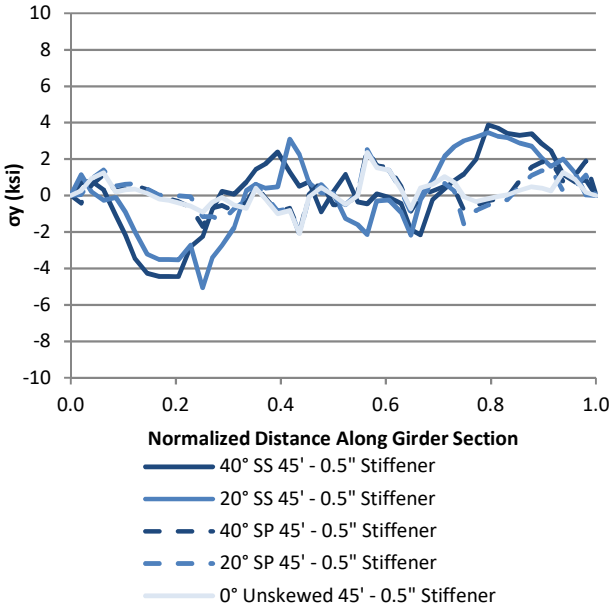

a) 12.7mm [1/2 in] stiffener connection - Top Flange

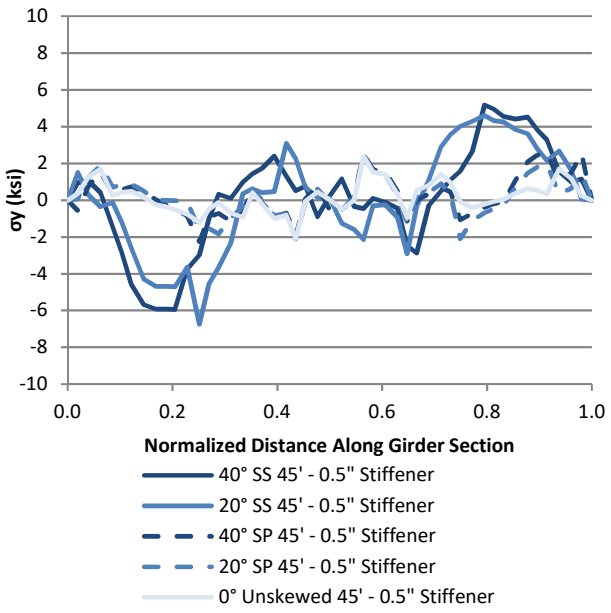

b) 12.7mm [1/2 in] stiffener connection - Bottom Flange

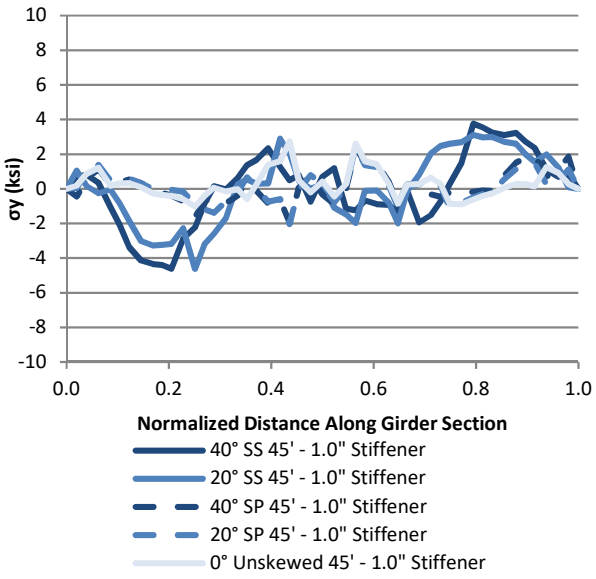

c) **25.4mm [1.0 in] stiffener connection - Top Flange**

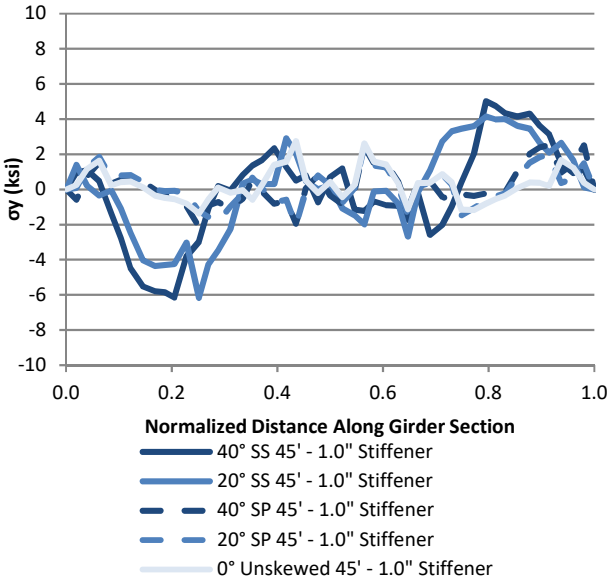

d) **25.4mm [1.0 in] stiffener connection - Bottom Flange**

Figure 3.35 Weak-axis sectional stresses for bridges with 13.7 m [45 ft] cross-frame spacing, grouped by connection type – interior girder (G3)

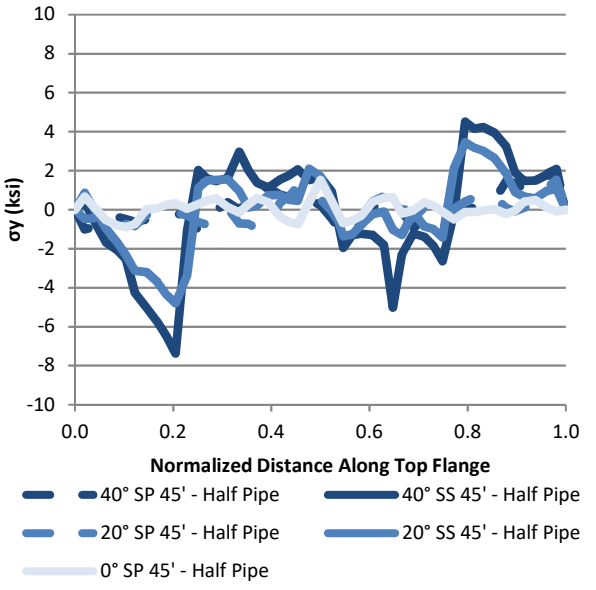

a) **Half-pipe connection**

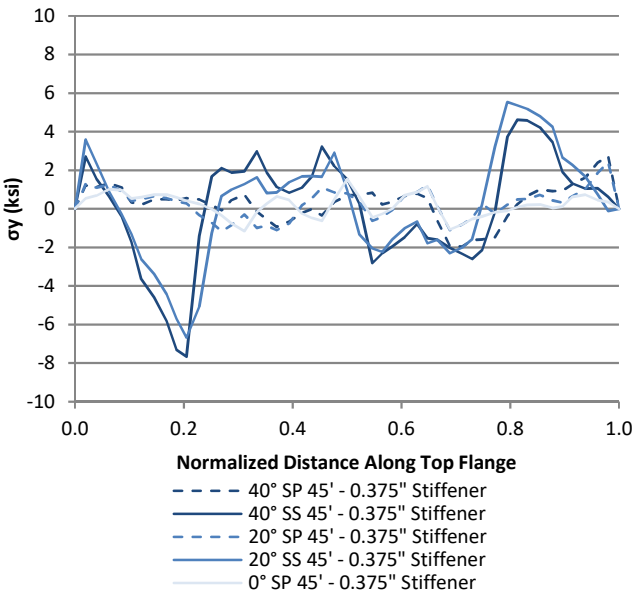

b) **9.53mm [3/8 in] stiffener connection**

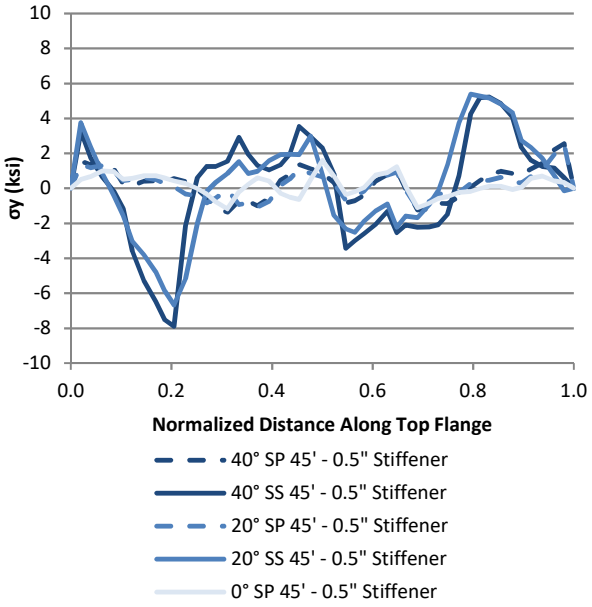

c) 12.7mm [1/2 in] stiffener connection

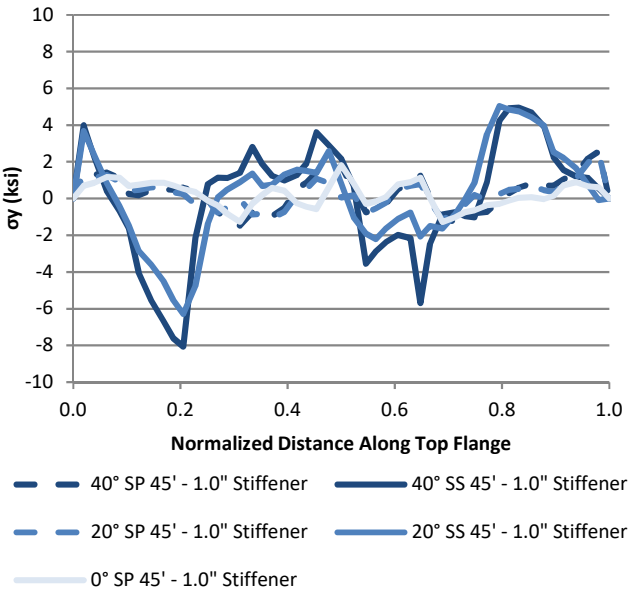

d) 25.4mm [1.0 in] stiffener connection

Figure 3.36 Top flange out-of-plane stresses for bridges with 13.7 m [45 ft] cross-frame spacing, grouped by connection type – interior girder (G3)

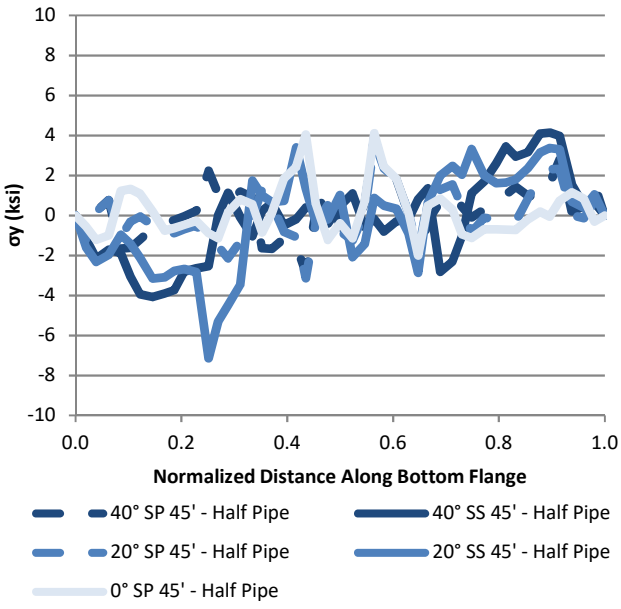

a) Half-pipe connection

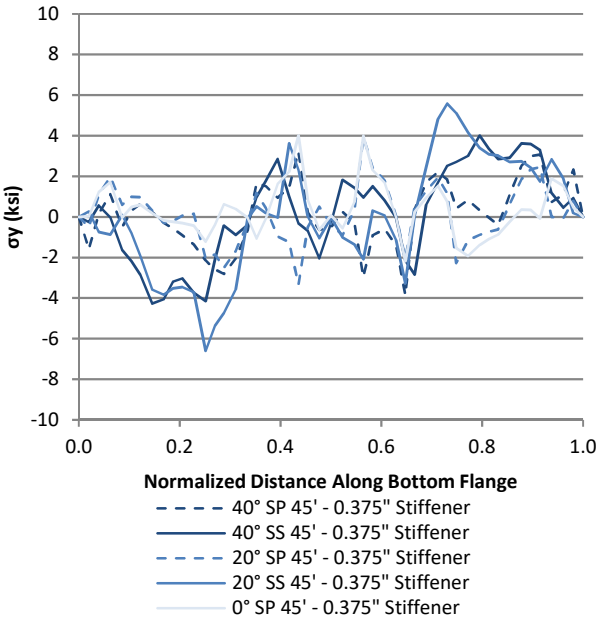

b) 9.53mm [3/8 in] stiffener connection

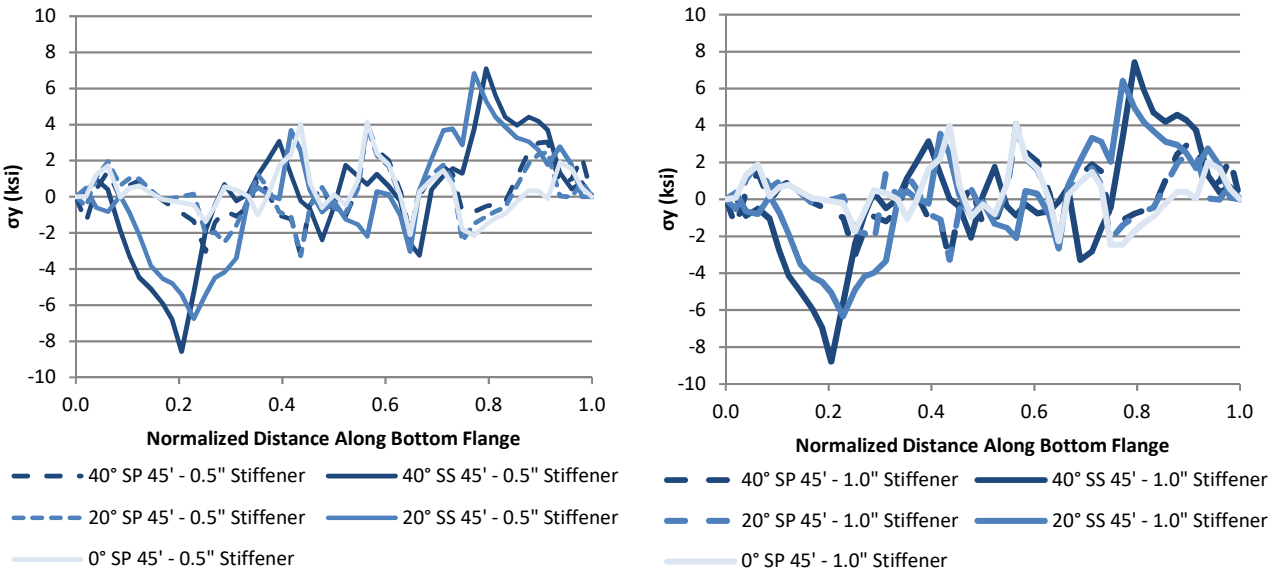

c) 12.7mm [1/2 in] stiffener connection **d) 25.4mm [1.0 in] stiffener connection**

Figure 3.37 Bottom flange out-of-plane stresses for bridges with 13.7 m [45 ft] cross-frame spacing, grouped by connection type – interior girder (G3)

Exterior Girder (G4) In-plane and Out-of-plane Bending Stresses

Figure 3.38 through Figure 3.41 present strong-axis bending stress, weak-axis bending stress, top flange out-of-plane bending stress, and bottom flange out-of-plane bending stress respectively for exterior Girder 4, grouped by connection type, for the 4.57 m [15 ft] and 9.14 m [30 ft] cross-frame spacing models. As before, girder strong-axis and weak-axis stresses were calculated from both the top and bottom flanges. Results from a simple beam-line analysis of the respective girders are presented with strong-axis sectional stresses.

Strong-axis bending stresses shown in Figure 3.38 have similar magnitudes in the exterior girders as were in the interior girders. Likewise, the strong-axis sectional stresses for bridges with 4.57 m [15 ft] and 9.14 m [30 ft] cross-frame spacings were almost the same for all three configurations. Strong-axis sectional stresses calculated from the top flange in the exterior

girder matched relatively closely with results calculated from beam analysis as well. Strong-axis sectional stresses calculated from the bottom flange resulted in lower values compared to those calculated using the distance to the top flange. For bridges with cross-frames spaced less than 9.14 m [30 ft], skew angle and cross-frame placement had little effect on the vertical bending stress in the exterior girder. Maximum stress was 282 MPa [40.9 ksi], calculated from the top flange of the 0 degree non-skewed bridge with 4.57 m [15 ft] cross-frame spacing.

Weak-axis sectional stress magnitudes, shown in Figure 3.39, are much higher in the exterior girder compared to the interior girder due to the placement of the bracket overhangs. The skewed-staggered configuration produced the highest stresses while the skewed-parallel configuration produced the lowest stresses. A maximum stress of 116 MPa [16.8 ksi] in the 40° skewed-staggered bridge with 9.14 m [30 ft] cross-frame spacing was produced, calculated from the bottom flange. For bridges with 4.57 m [15 ft] cross-frame spacings, a maximum stress of 55.0 MPa [7.97 ksi] was produced by the 0 degree unskewed bridge. There was a significant difference in stress levels between bridge with 4.57 m [15 ft] and 9.14 m [30 ft] cross-frame spacings. Skew angle, on the other hand, did not produce significant differences in weak-axis stress values. Stresses calculated from the bottom flange resulted in higher values than stresses calculated from the top flange.

The top flange bending stresses, shown in Figure 3.40, in Span 1 of the exterior girder were very similar for the three different bridge configurations. The 20° skewed-parallel bridge with 9.14 m [30 ft] cross-frame spacing produced a maximum stress magnitude of 112 MPa [16.3 ksi] and the 40° skewed-staggered bridge with 9.14 m [30 ft] cross-frame spacing produced a maximum stress magnitude of 112 MPa [16.3 ksi]. Similar to weak-axis sectional stresses, top

flange bending stresses were effected by cross-frame spacing more than skew angle for the exterior girder.

Girder 4 bottom flange out-of-plane bending stresses are presented in Figure 3.41. Similar to the interior girder, bottom flange out-of-plane bending stresses were much higher compared to top flange out-of-plane bending stresses. As such the stress difference between bridges with 9.14 m [30 ft] cross-frame spacings and 4.57 m [15 ft] cross-frame spacings were even more exaggerated. Again, the skewed-staggered configuration produced the highest maximum stress values and the skewed-parallel and skewed-unstaggered configurations produced the lowest maximum stress values. The highest magnitude stress of 198 MPa [28.7 ksi] was found in the 40° skewed-staggered configuration with 9.14 m [30 ft] cross-frame spacing.

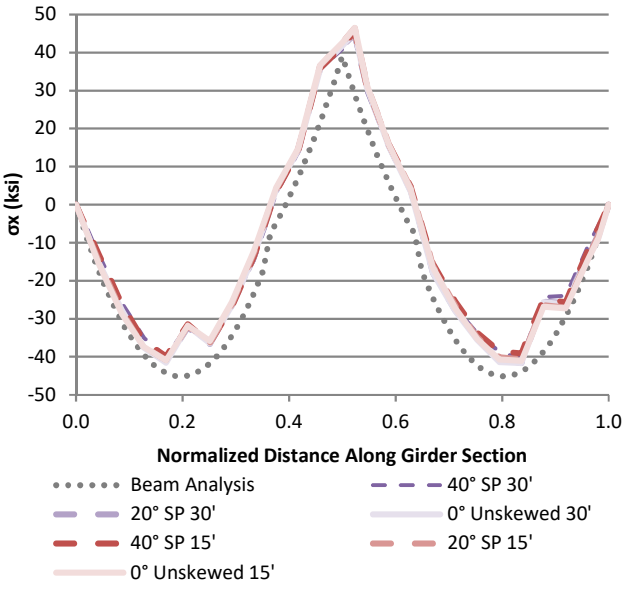

a) **Skewed-parallel – Top Flange**

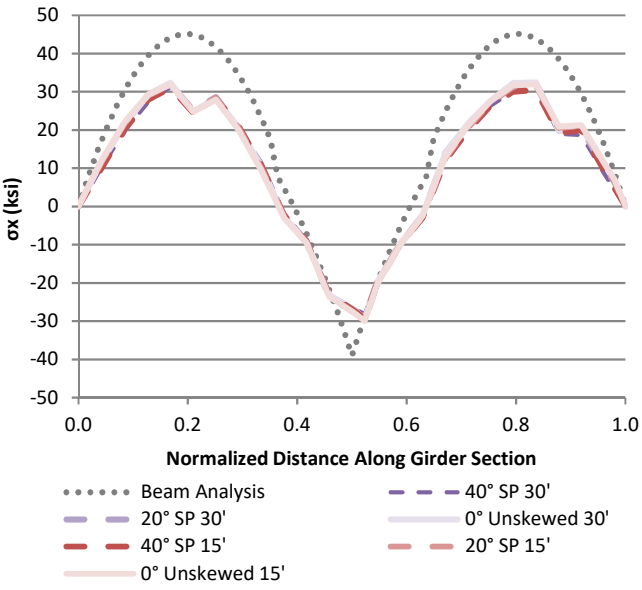

b) **Skewed-parallel – Bottom Flange**

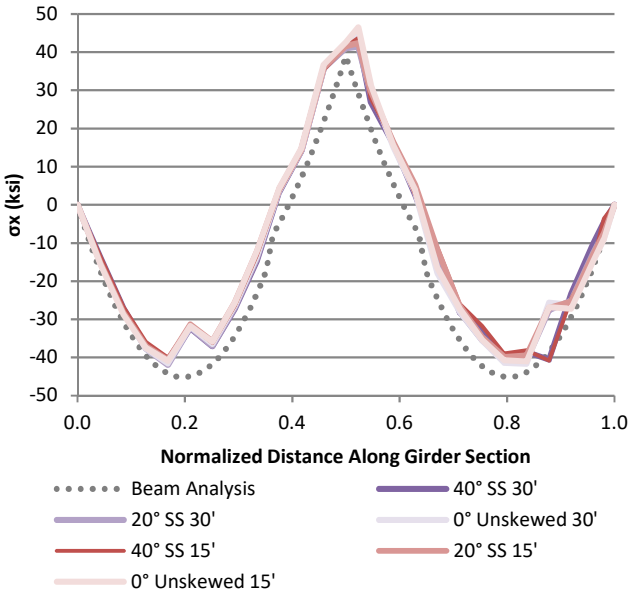

c) Skewed-staggered – Top Flange

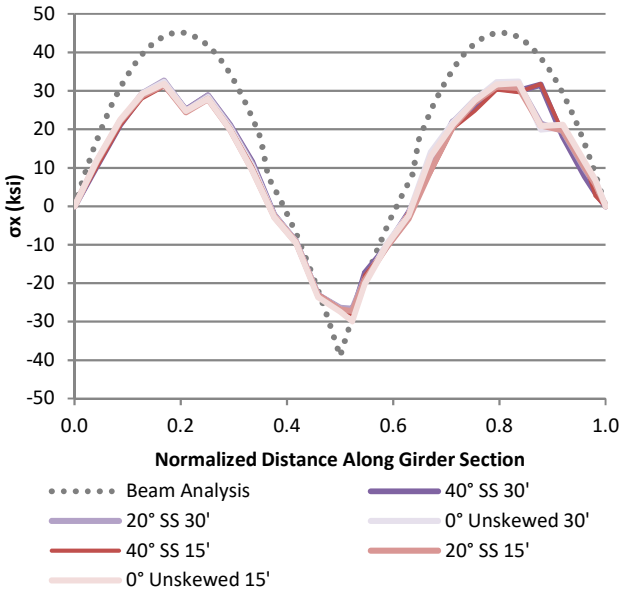

d) Skewed-staggered – Bottom Flange

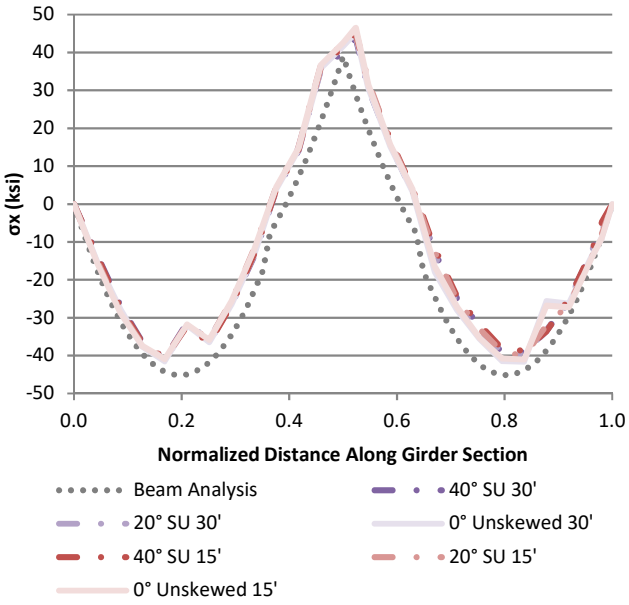

e) Skewed-unstaggered – Top Flange

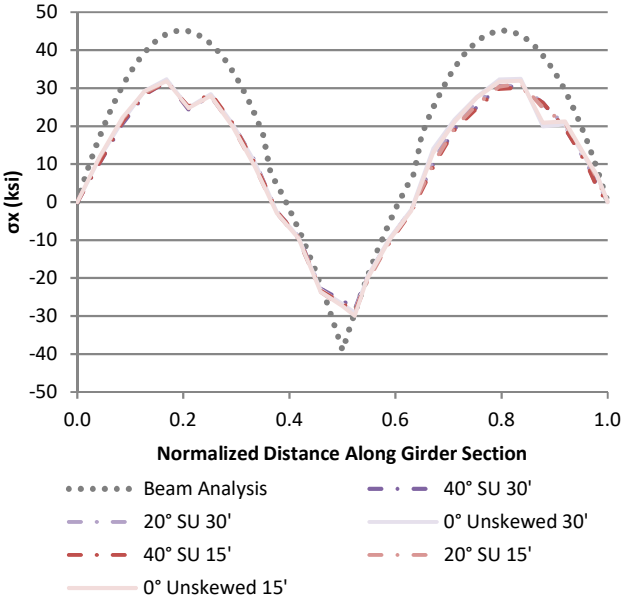

f) Skewed-unstaggered – Bottom Flange

Figure 3.38 Girder 4 strong-axis sectional stresses for bridges with 4.57 m [15 ft] and 9.14 m [30 ft] cross-frame spacings, grouped by configuration

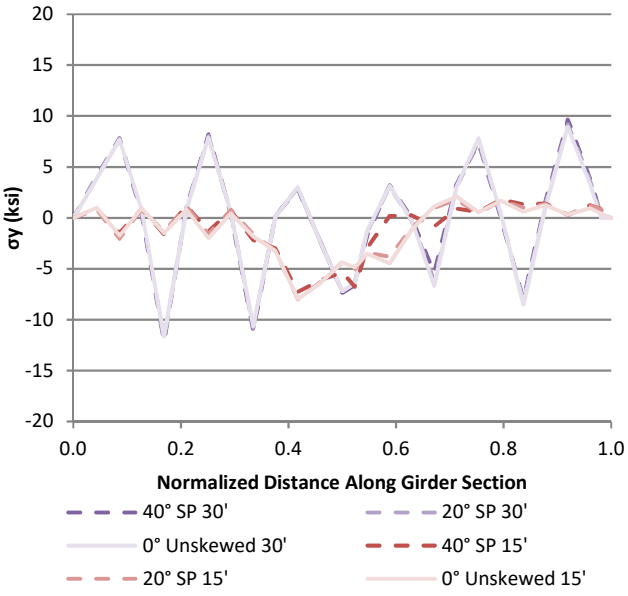

a) **Skewed-parallel – Top Flange**

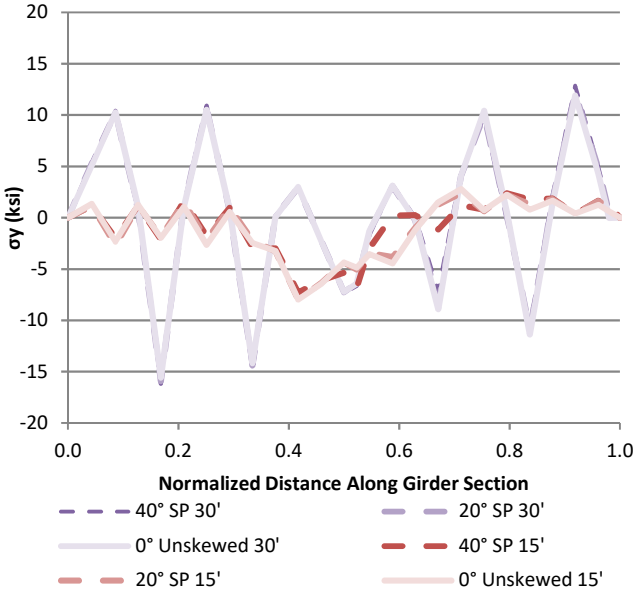

b) **Skewed-parallel - Bottom Flange**

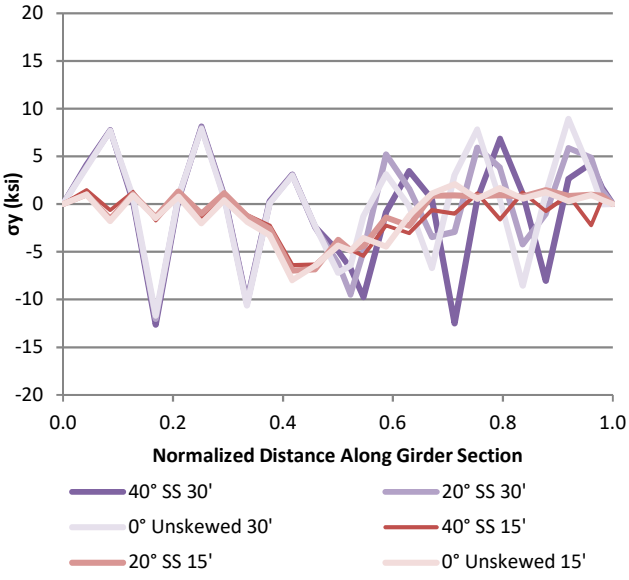

c) **Skewed-staggered - Top Flange**

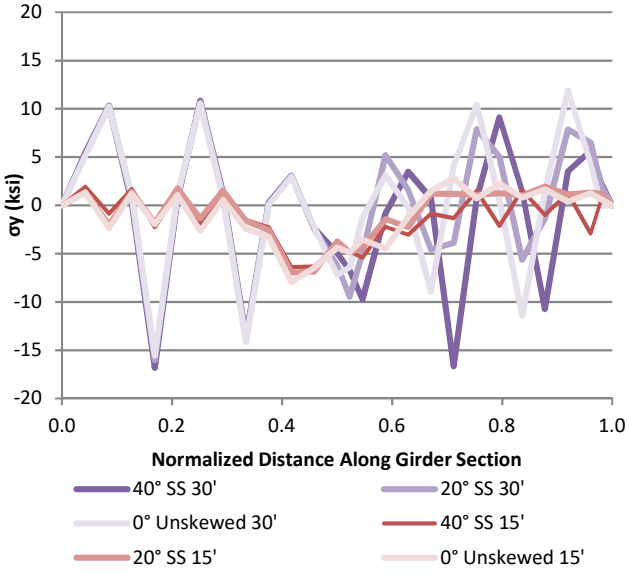

d) **Skewed-staggered - Bottom Flange**

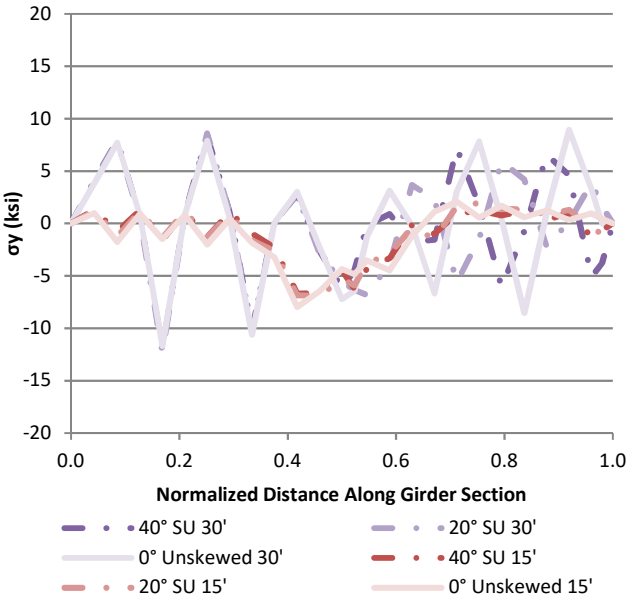

e) Skewed-unstaggered - Top Flange

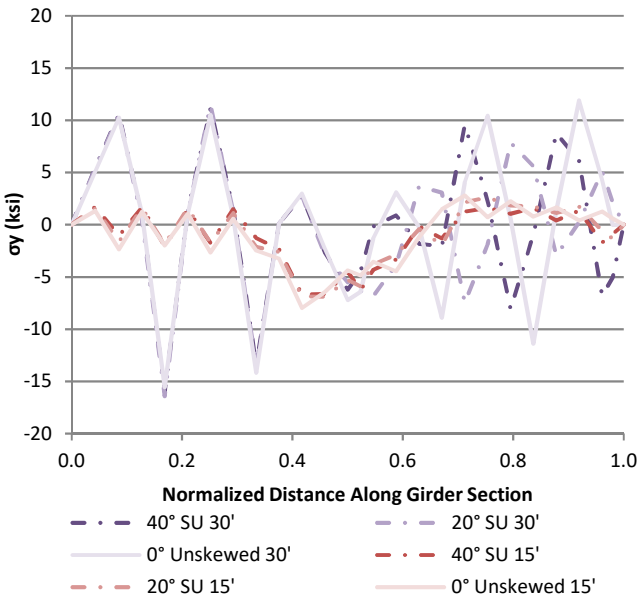

f) Skewed-unstaggered - Bottom Flange

Figure 3.39 Girder 4 weak-axis sectional stresses for bridges with 4.57 m [15 ft] and 9.14 m [30 ft] cross-frame spacings, grouped by configuration

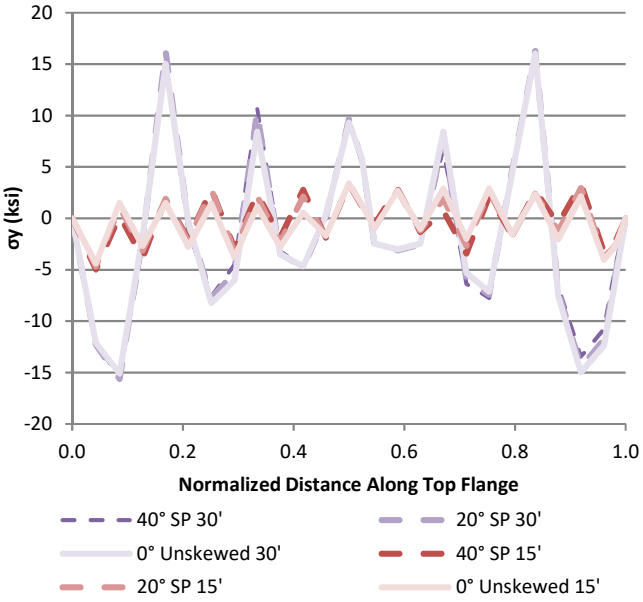

a) Skewed-parallel

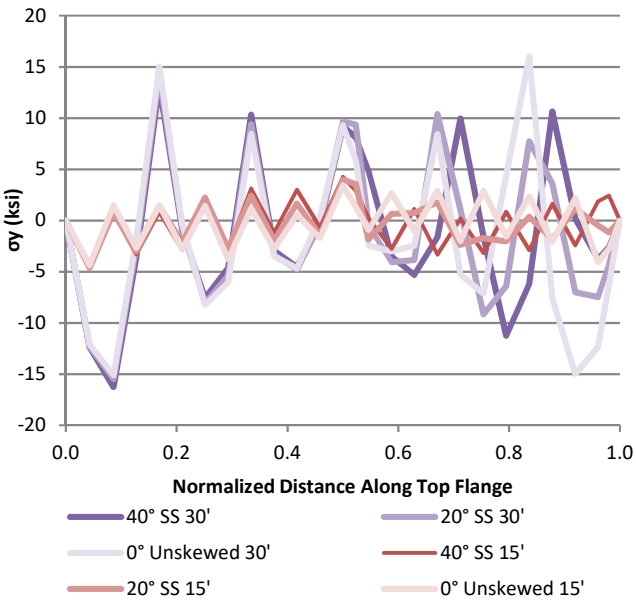

b) Skewed-staggered

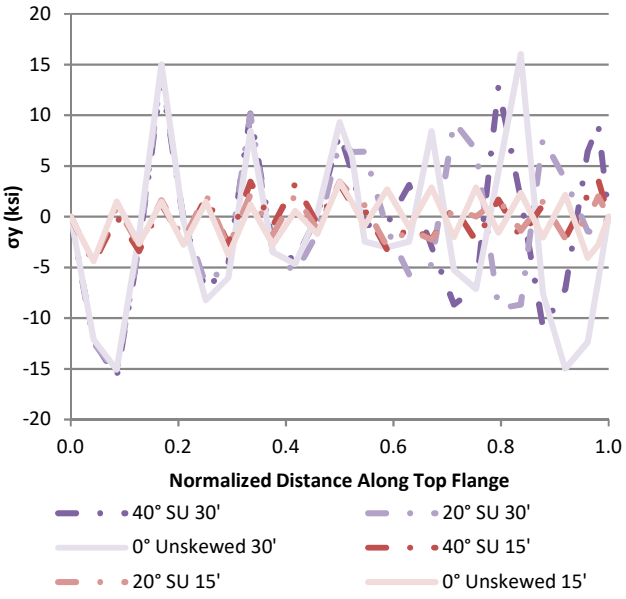

c) Skewed-unstaggered

Figure 3.40 Girder 4 top flange out-of-plane stresses for bridges with 4.57 m [15 ft] and 9.14 m [30 ft] cross-frame spacings, grouped by configuration

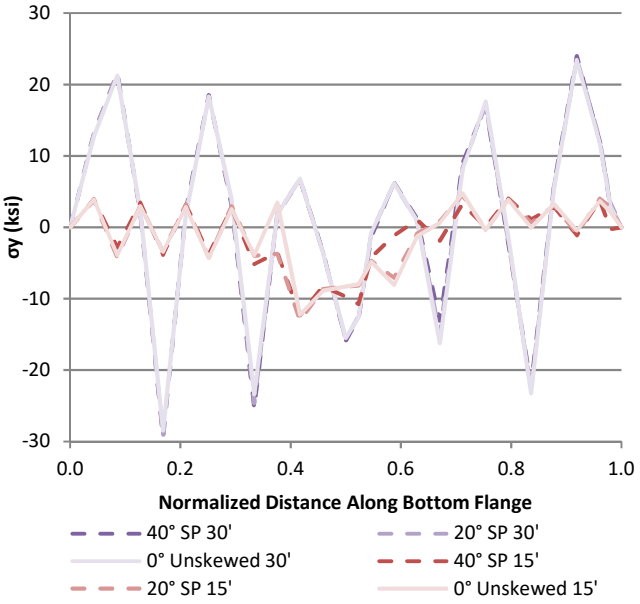

a) Skewed-parallel

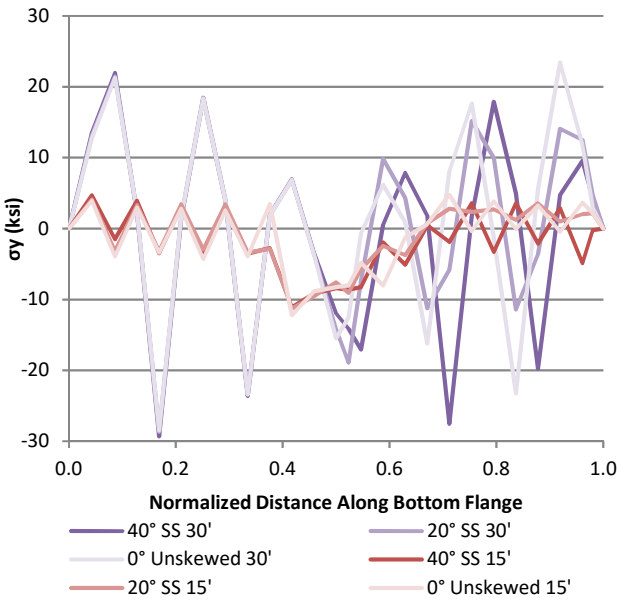

b) Skewed-staggered

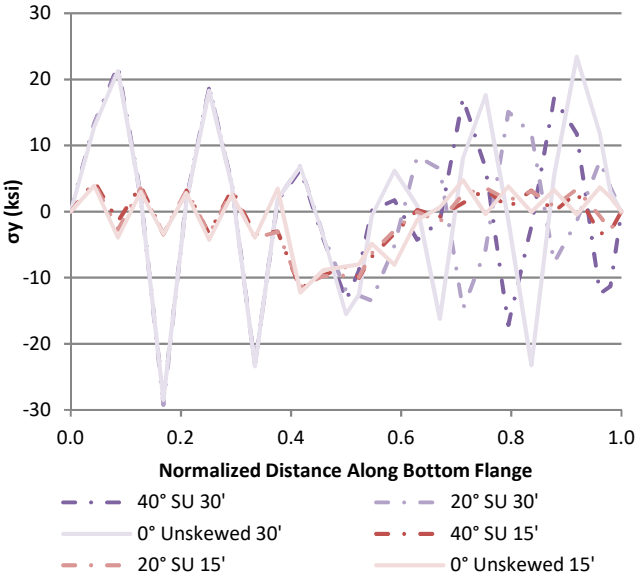

c) Skewed-unstaggered

Figure 3.41 Girder 4 bottom flange out-of-plane stresses for bridges with 4.57 m [15 ft] and 9.14 m [30 ft] cross-frame spacings, grouped by configuration

Figure 3.42 shows strong-axis Girder 4 bending stress calculated for the top and bottom flanges for bridges with 13.7 m [45 ft] cross-frame spacing, grouped by connection type. Results from a simple beam-line analysis of the respective girders are also presented with strong-axis bending stresses. The non-skewed configuration yielded the smallest strong-axis sectional stress followed by the 40° skewed-parallel configuration for any given connection type. The 20° skewed-parallel configuration produced the largest strong-axis sectional stress of the three skewed-parallel configurations. Both the 20° and 40° skewed-staggered configurations had similar magnitudes and resulted in the largest in-plane sectional stresses, with a maximum value of 290 MPa [42 ksi].

, Figure 3.44, and Figure 3.45 show the weak-axis bending stress, top flange out-of-plane bending stress, and bottom flange out-of-plane bending stress respectively for Girder 4 of the 13.7 m [45 ft] cross-frame spacing models, also grouped by connection type. Weak-axis bending stresses were plotted based on *c* values for the top flange and bottom flange. Strong-axis bending stresses were calculated for *c* values from the top flange and bottom flange. Results for the out-of-plane stresses were similar to the variation in lateral deflections for any given connection type. That is, larger skew angles produced smaller weak-axis sectional and out-of-plane flange stresses. The skewed-staggered configuration also exhibited larger out-of-plane stresses compared to the skewed-parallel configuration for any given skew angle and connection type. Peak bottom flange out-of-plane bending stresses were almost the same across all skew angles and configurations for any given connection type. Weak-axis sectional stresses in the exterior girder had a maximum value of 250 MPa [36 ksi], top flange out-of-plane bending stresses had a maximum value of 560 MPa [81 ksi], and bottom flange out-of-plane bending stresses had a maximum value of 500 MPa [73 ksi] in Girder 4.

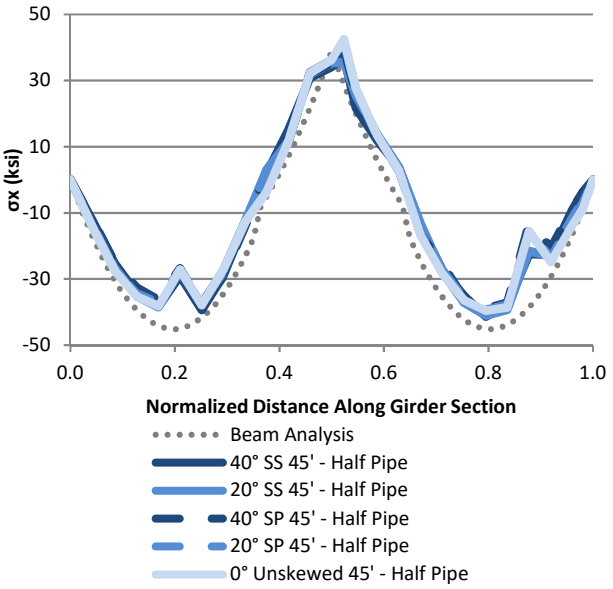

a) **Half-pipe connection – Top Flange**

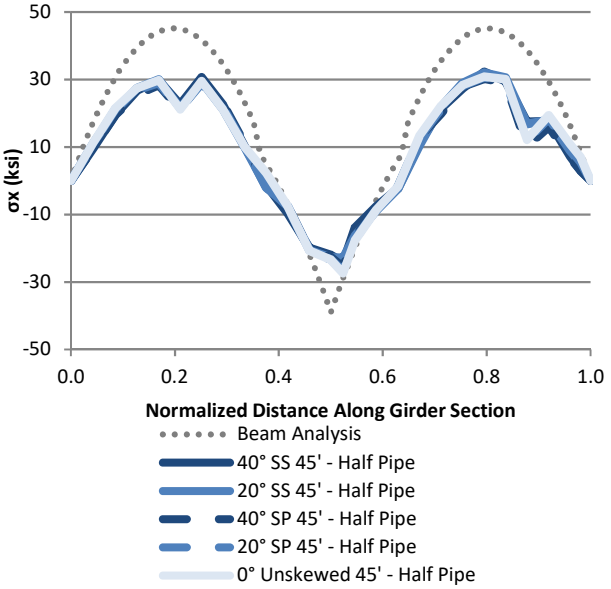

b) **Half-pipe connection – Bottom Flange**

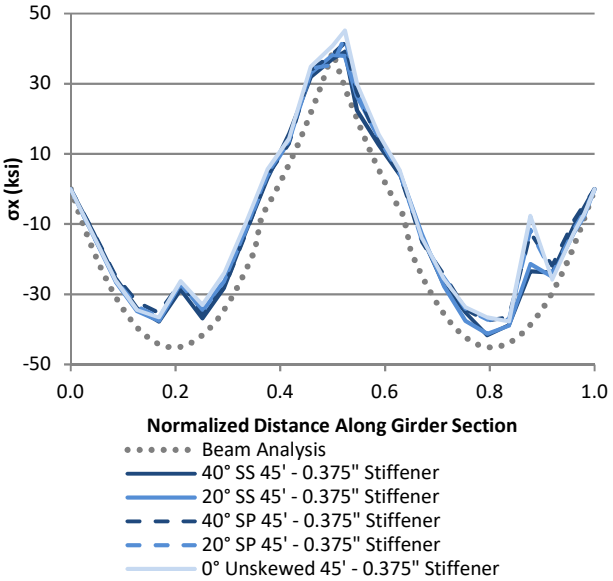

c) **9.53mm [3/8 in] stiffener connection – Top Flange**

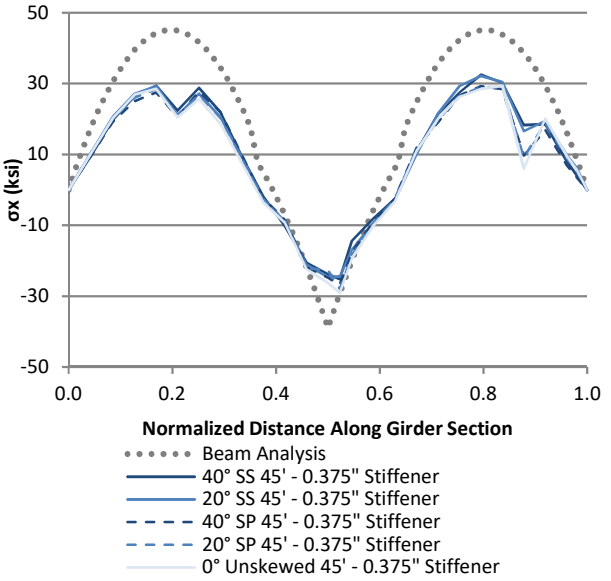

d) **9.53mm [3/8 in] stiffener connection – Bottom Flange**

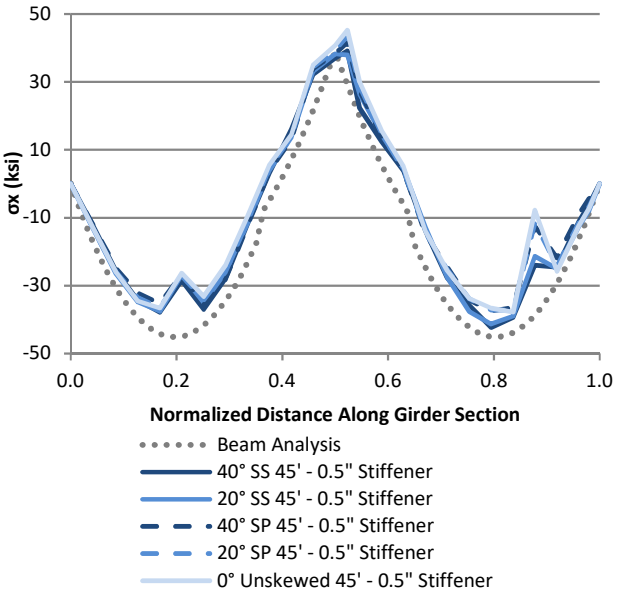

e) 12.7mm [1/2 in] stiffener connection – Top Flange

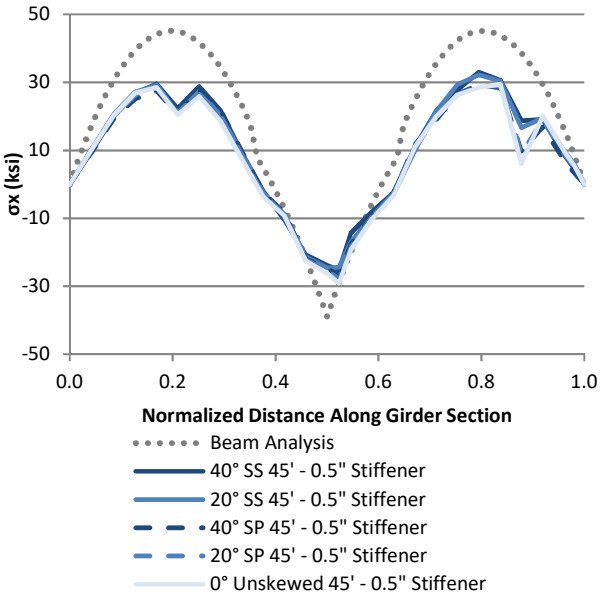

f) 12.7mm [1/2 in] stiffener connection – Bottom Flange

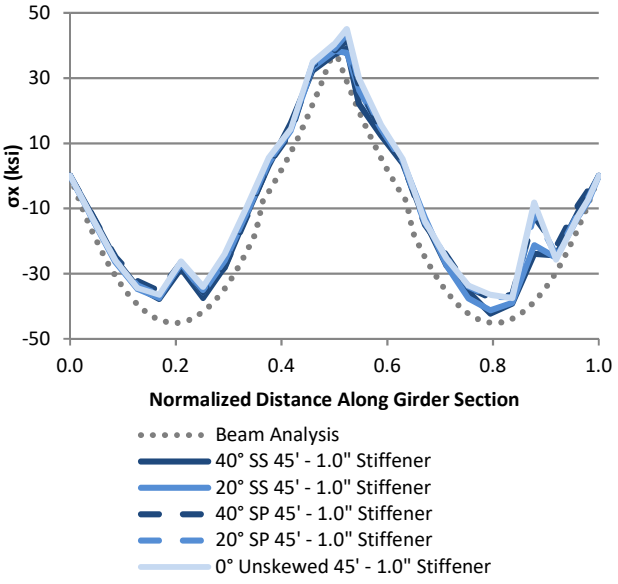

g) 25.4mm [1.0 in] stiffener connection – Top Flange

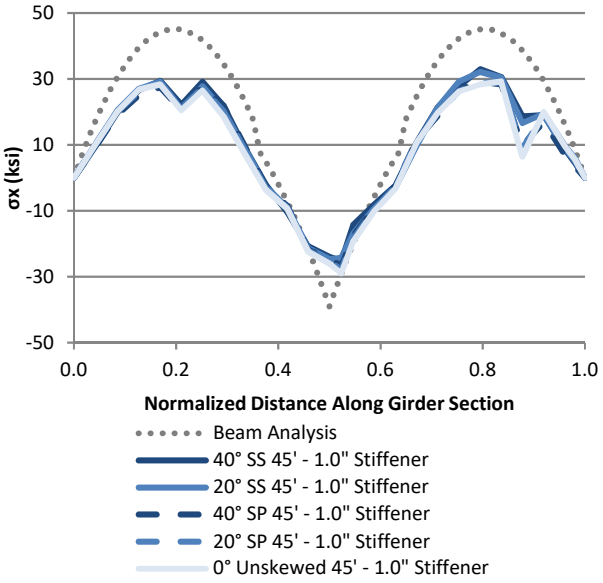

h) 25.4mm [1.0 in] stiffener connection – Bottom Flange

Figure 3.42 Strong-axis sectional stresses for bridges with 13.7 m [45 ft] cross-frame spacing, grouped by connection type – exterior girder (G4)

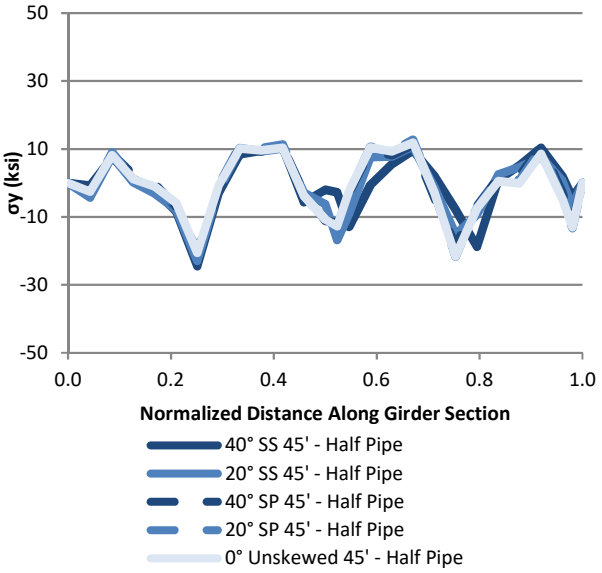

a) Half-pipe connection – Top Flange

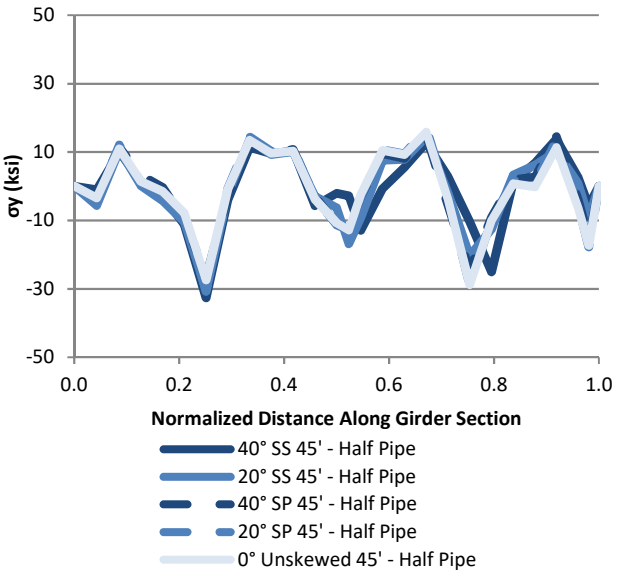

b) Half-pipe connection - Bottom Flange

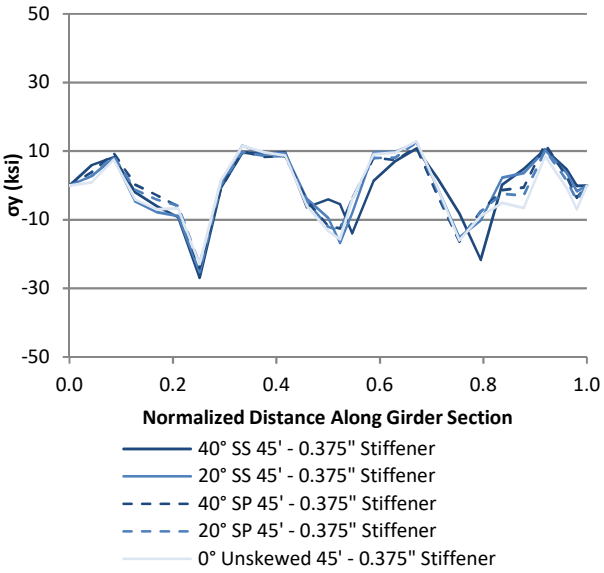

c) 9.53mm [3/8 in] stiffener connection - Top Flange

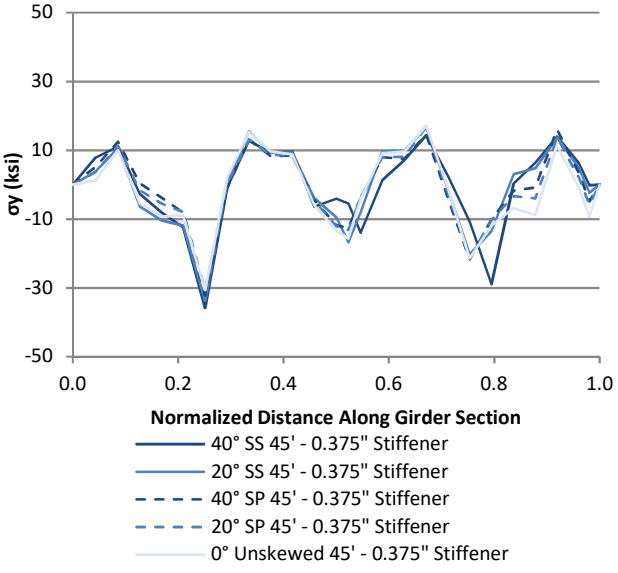

d) 9.53mm [3/8 in] stiffener connection - Bottom Flange

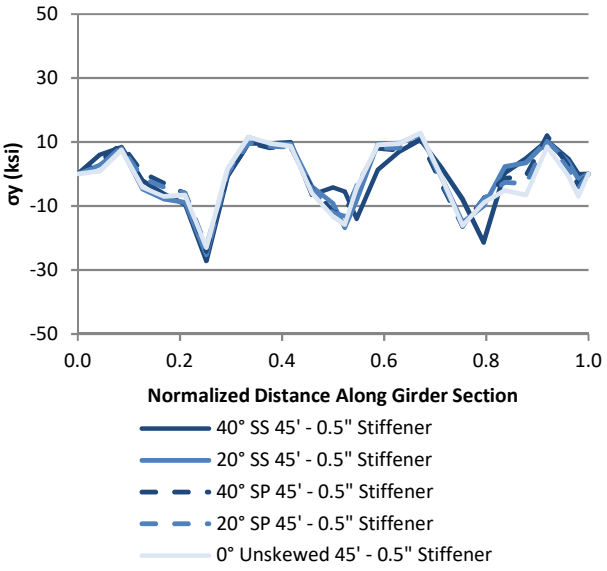

e) 12.7mm [1/2 in] stiffener connection - Top Flange

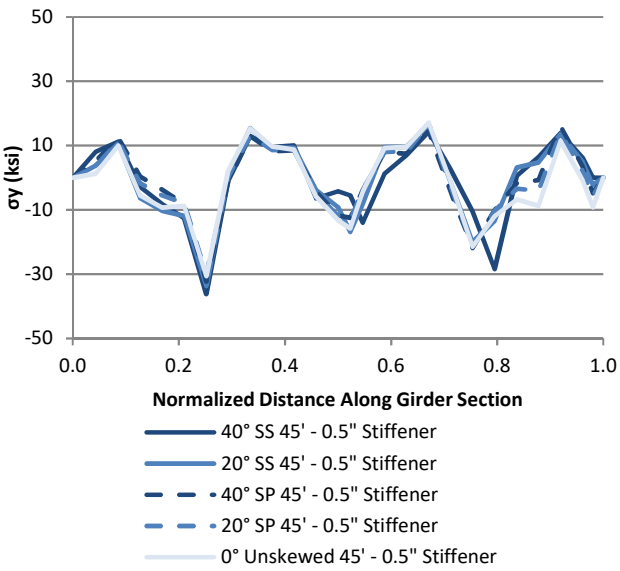

f) 12.7mm [1/2 in] stiffener connection - Bottom Flange

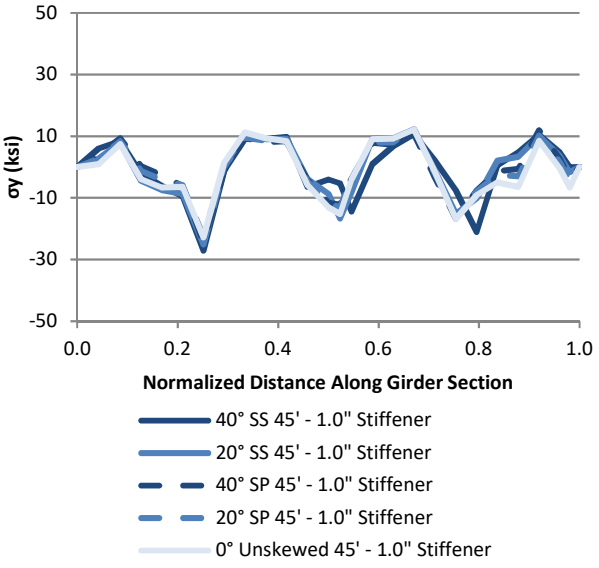

g) 25.4mm [1.0 in] stiffener connection - Top Flange

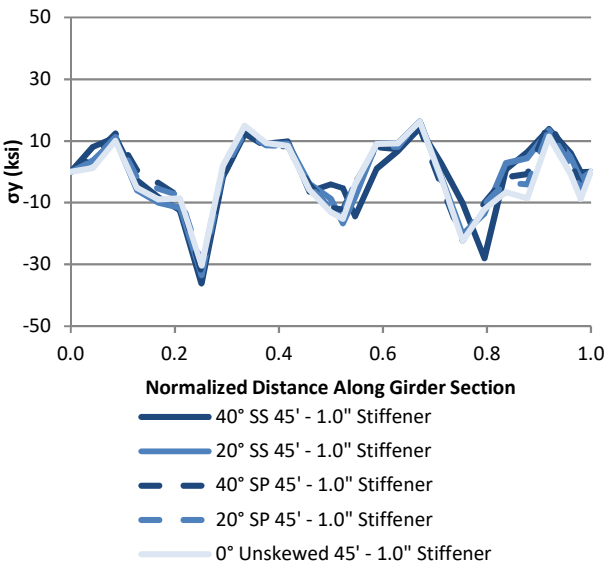

h) 25.4mm [1.0 in] stiffener connection - Bottom Flange

Figure 3.43 Girder 4 weak-axis sectional stresses for bridges with 13.7 m [45 ft] cross-frame spacing, grouped by connection type – exterior girder (G4)

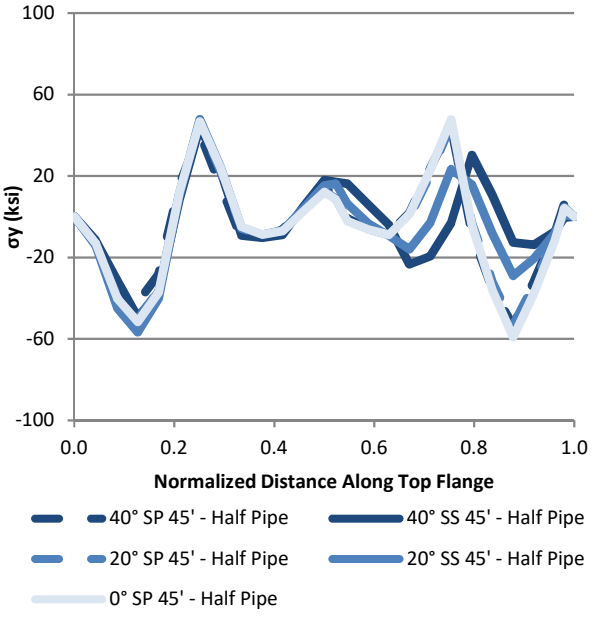

a) Half-pipe connection

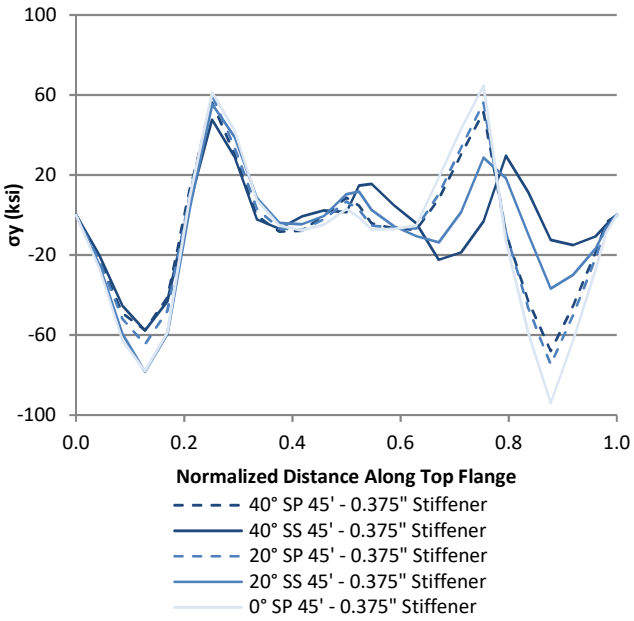

b) 9.53mm [3/8 in] stiffener connection

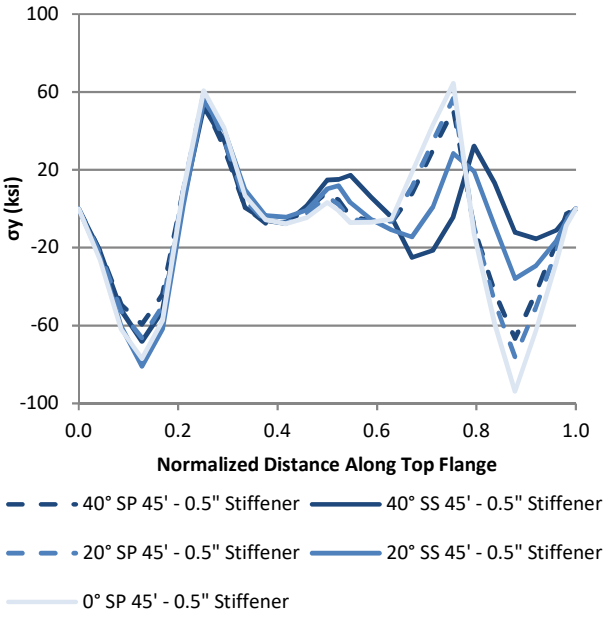

c) 12.7mm [1/2 in] stiffener connection

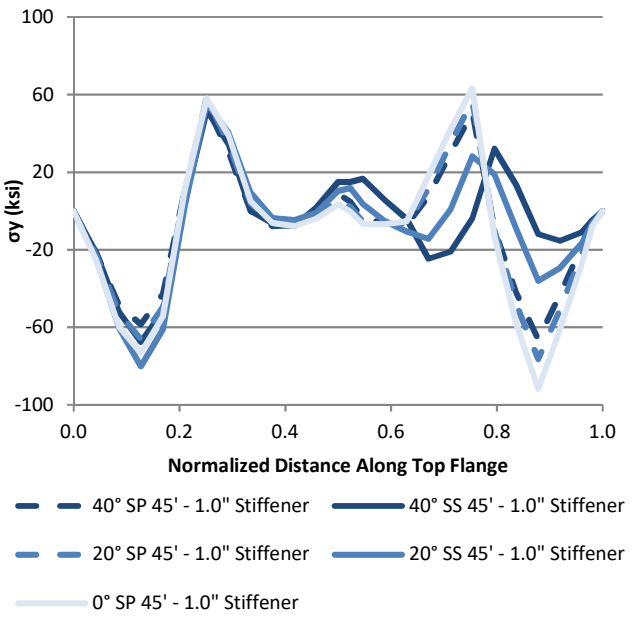

d) 25.4mm [1.0 in] stiffener connection

Figure 3.44 Top flange out-of-plane stresses for bridges with 13.7 m [45 ft] cross-frame spacing, grouped by connection type – exterior girder (G4)

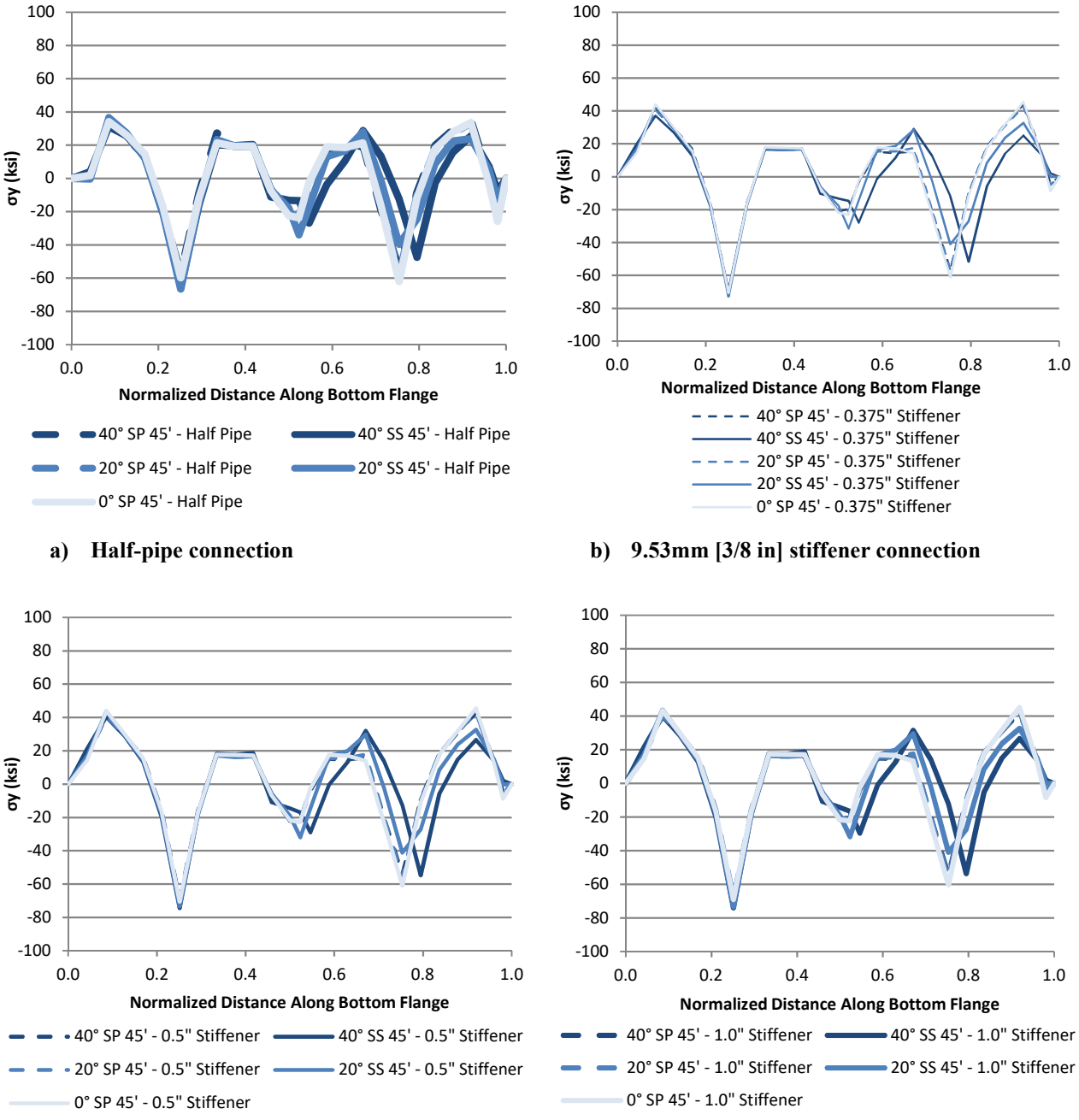

a) Half-pipe connection

b) 9.53mm [3/8 in] stiffener connection

c) 12.7mm [1/2 in] stiffener connection

d) 25.4mm [1.0 in] stiffener connection

Figure 3.45 Bottom flange out-of-plane stresses for bridges with 13.7 m [45 ft] cross-frame spacing, grouped by connection type – exterior girder (G4)

HORIZONTAL LOAD FROM EXTERIOR GIRDER CARRIED BY CROSS-FRAMES

While vertical loads are mainly carried by the girders and only a small percentage of the vertical force is transmitted through the cross-frames, the primary load path for lateral loads is through the cross-frame members. As the largest lateral force of the modeled constructions loads comes from the overhang brackets, the force in the exterior cross-frames relative to the applied overhang load is measured to determine the efficiency and effectiveness of the cross-frame at carrying horizontal load.

For the 13.7 m [45 ft] and 9.14 m [30 ft] cross-frame spacing models, the first interior cross-frame in Span 1, shown in Figure 3.19, was selected because the peak lateral deflection occurred near that location and maximum stresses were found in that cross-frame. For the 4.16 m [15 ft] cross-frame spacing models, the cross-frame at mid-span of Span 1 was selected because it produced the maximum stresses and it matches the location of the cross-frame selected for the 13.7 m [45 ft] spacing models.

As each top and bottom plate load of the overhang bracket force is 16.0 kN [3.61 kips], with the load multiplied by the 1.75 Strength I load factor to equal 28.1 kN [6.31 kips]. The brackets are spaced 101.6 cm [40 in] on center. This results in an overhang force of 27.6 kN/m [8.421 kips/ft]. Therefore each cross-frame carries 126 kN [28.4 kips] of overhang load with 4.16 m [15 ft] cross-frame spacing, 253 kN [56.8 kips] of overhang load with 9.14 m [30 ft] cross-frame spacing, and 379 kN [85.2 kips] of overhang load with 13.7 m [45 ft] cross-frame spacing.

Figure 3.46 shows the equation of calculating forces as stress in the local member axial direction multiplied by the area of the member. Element sectional stresses are obtained at the mid-brace location nearest the applied overhang load, which is the ¾ point for the diagonal

members and the ½ location for the bottom chord. The horizontal force component of each member is then calculated based on the member angle relative the horizontal plane of the bridge, as shown in Figure 3.47. The component of the force perpendicular to the girder line is also incorporated for cross-frames place parallel to skew, as demonstrated in Figure 3.48.

Figure 3.49 and Figure 3.50 shows a sample calculation of the horizontal force over the overhang load for the 40° skewed-parallel bridge with 13.7 m [45 ft] cross-frame spacing and 9.53 mm [0.375 in] thick stiffeners. Member B is in tension and Member A and C are combined to form the compression force in the cross-frame. The total tension and compression forces are divided by the overhang load for the cross-frame tributary length, given in Figure 3.50. The difference between tension and compression force ratios indicate bending in the cross-frame.

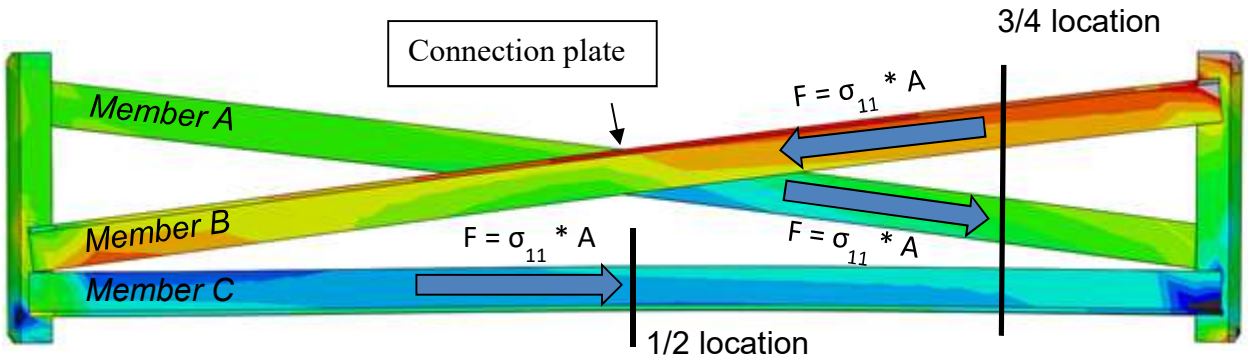

Figure 3.46 Cross-frame member force calculation

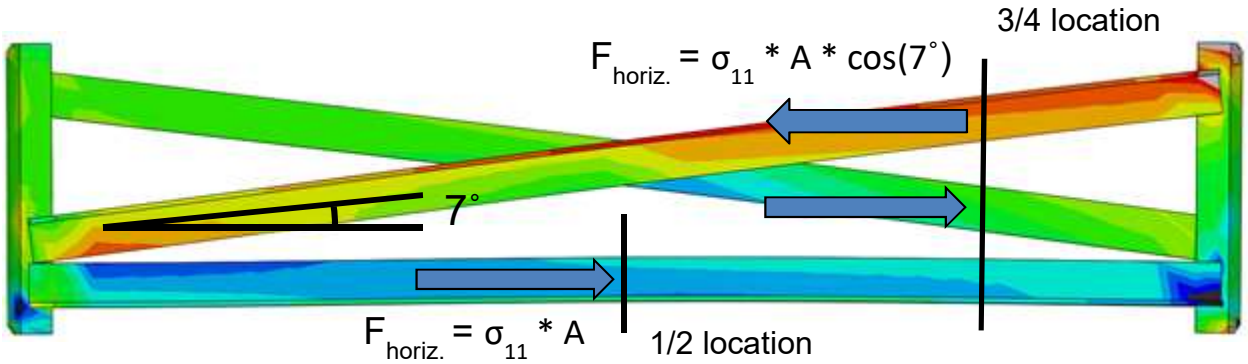

Figure 3.47 Cross-frame horizontal force component calculation

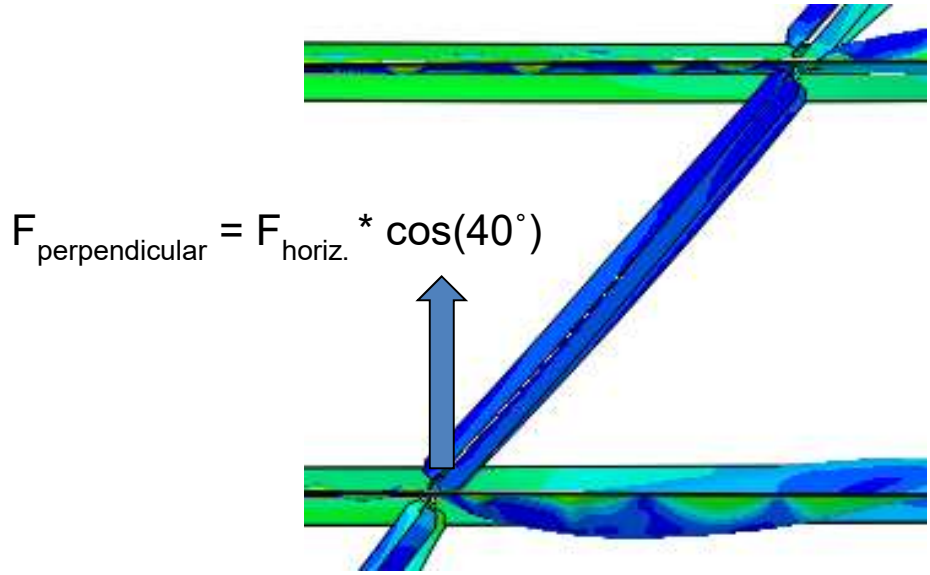

Figure 3.48 Cross-frame perpendicular force component calculation for the 40° skewed-parallel configurations

$A_{angle} = 6.48\ in^2$

Total Tension Force = 85.29*cos(40˚) = **65.34k**

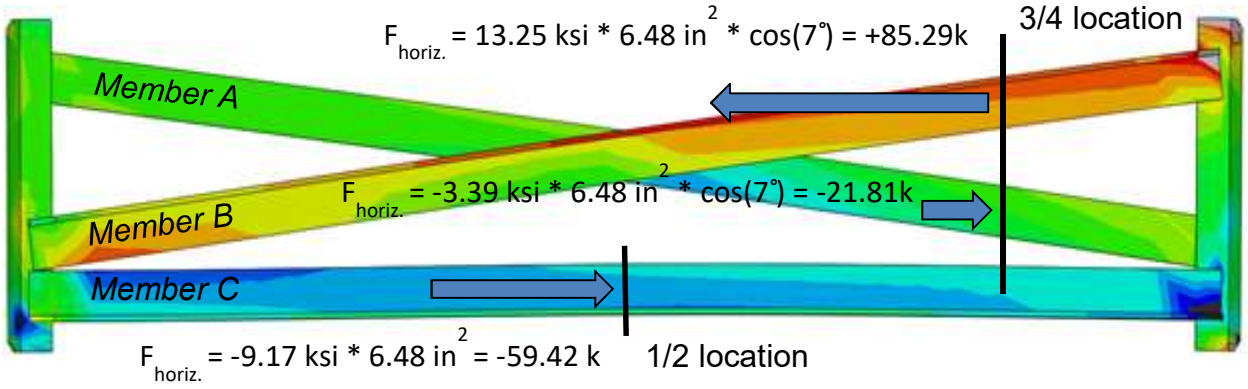

Figure 3.49 Cross-frame members horizontal force component sample calculation for the 40° skewed-parallel bridge with 13.7 m [45 ft] cross-frame spacing and 9.53 mm [0.375 in] thick stiffeners

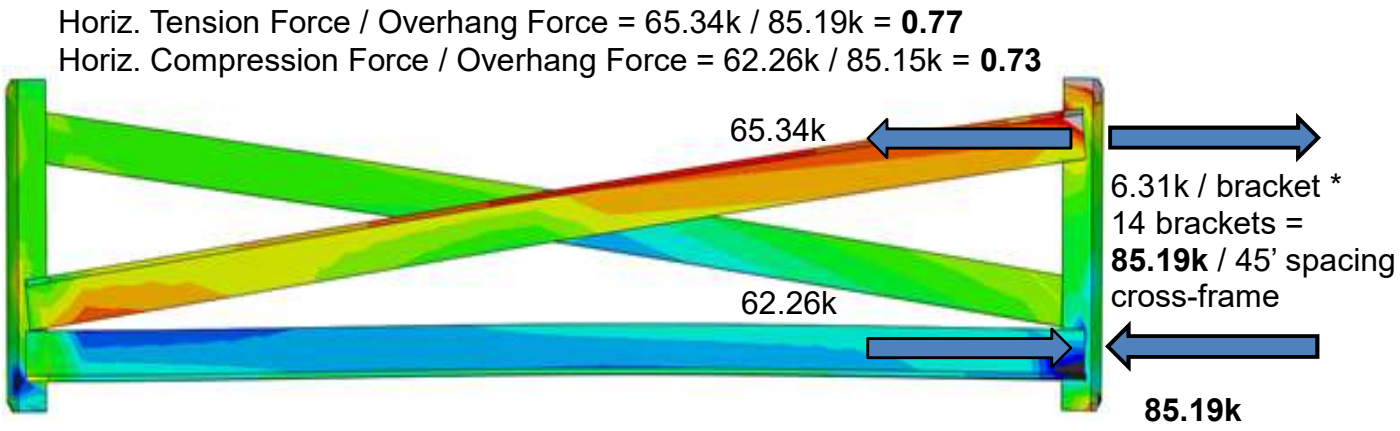

Figure 3.50 Cross-frame horizontal tension and compression force as a ratio of the overhang bracket force sample calculation for the 40° skewed-parallel bridge with 13.7 m [45 ft] cross-frame spacing and 9.53 mm [0.375 in] thick stiffeners

Figure 3.51 (a) through (d) shows horizontal tension and compression forces in the cross-frames as a ratio of the overhang load grouped by connection type. The difference between tension and compression force ratios may indicate bending in the cross-frame, which is relatively low for all connection types. Cross-frames placed perpendicular to the girder line, including skewed-staggered and unskewed configurations, produced the largest ratio of forces. In stiffer connections, as in the half-pipe and 25.4 mm [1.0 in] thick stiffener connections, these magnitudes were relatively similar. For less stiff connections, as in the cross-frames with 12.7 mm [0.5 in] and 9.53 mm [0.375 in] thick stiffeners, the force ratio slightly increased with decreasing skew angle. Skew angle did not affect the horizontal force transfer of loads in skewed-staggered and unskewed configurations.

The 40° skewed-parallel configuration produced the smallest tension and compression forces in the cross-frames, followed by the 20° skewed-parallel configuration. The 40° skewed-parallel configuration produced forces about half that of the skewed-staggered and unskewed

configuration. This is due to the fact that the lateral force component of the load decreases with increasing skew angle.

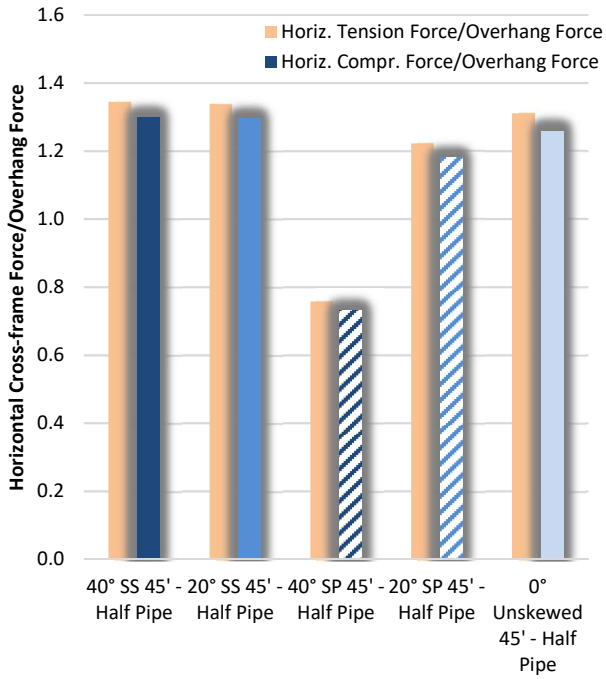

a) Half-pipe connection, 13.7 m [45 ft] cross-frame spacing

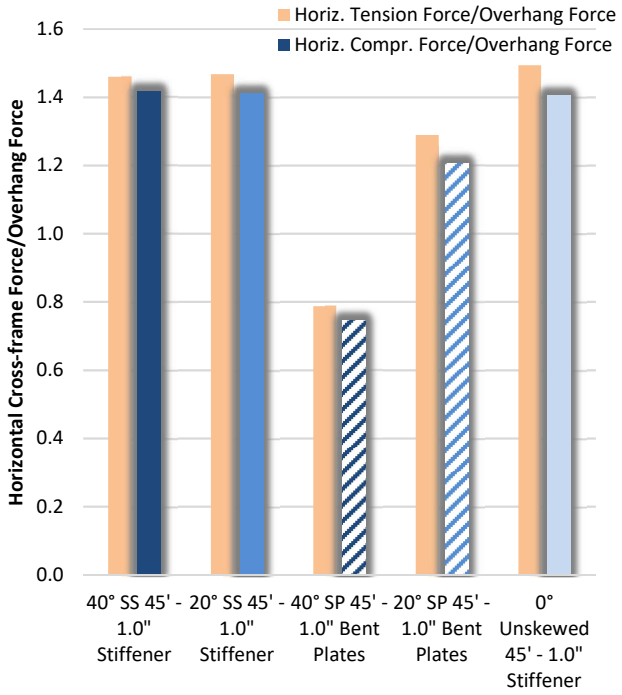

b) 25.4mm [1.0 in] stiffener connection, 13.7 m [45 ft] cross-frame spacing

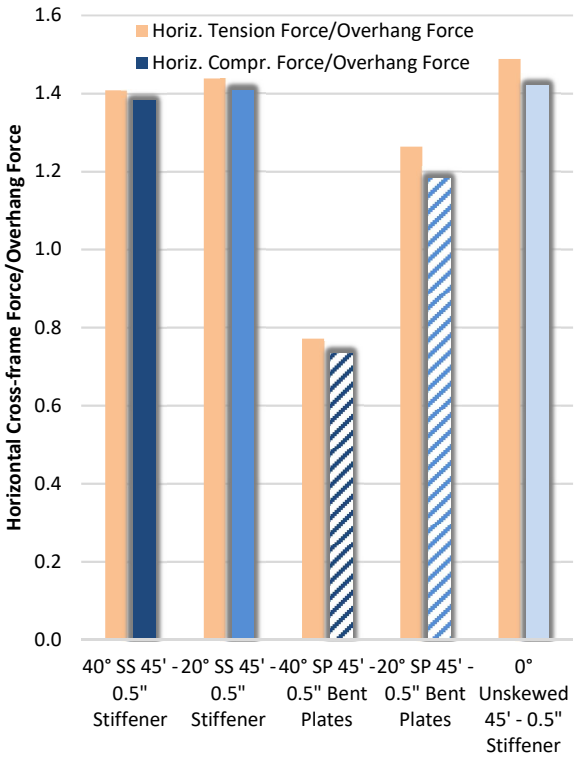

c) 12.7mm [1/2 in] stiffener connection, 13.7 m [45 ft] cross-frame spacing

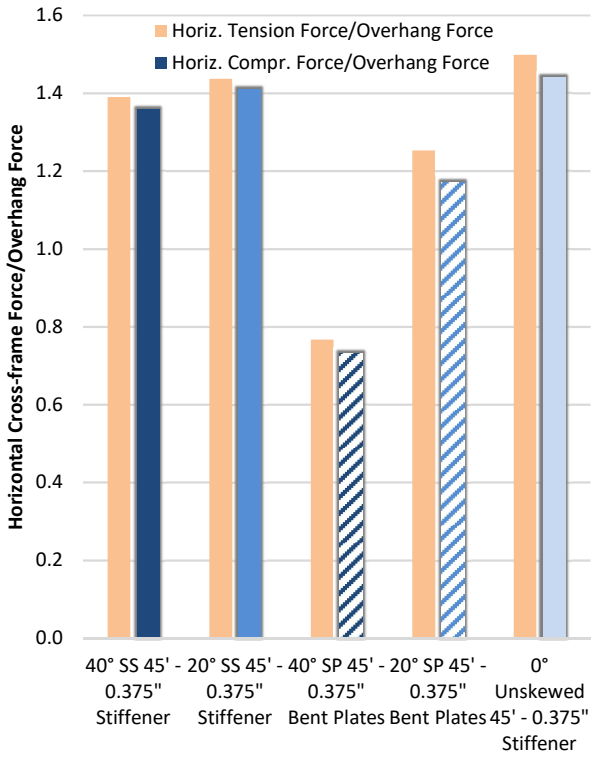

d) 9.53mm [3/8 in] stiffener connection, 13.7 m [45 ft] cross-frame spacing

Figure 3.51 Cross-frame horizontal tension and compression force as a ratio of the overhang load, grouped by connection type

Figure 3.52 (a) through (e) shows cross-frame horizontal tension and compression forces normalized by the overhang load, grouped by skew angle. Again, the difference between tension and compression force ratios may indicate bending in the cross-frame, which is low for all skew angles. For the skewed-staggered configuration, the half-pipe connection produced the smallest force ratio and thicker stiffeners attracted more lateral force in bridges with 13.7 m [45 ft] cross-frame spacing. Horizontal forces also increased with increasing cross-frame spacing in the skewed-staggered configuration. For the skewed-parallel configuration, the horizontal force ratio was relatively similar across varying connection types in bridges with cross-frames spaced at

13.7 m [45 ft]. Bridges with 4.57 m [15 ft] and 9.14 m [30 ft] cross-frame spacings also had relatively similar forces in the skewed-parallel configuration.

For the unskewed configuration, the half-pipe connection had the smallest lateral forces in the cross-frames of bridges with 13.7 m [45 ft] cross-frame spacing. The force ratio slightly decreased with increasing stiffener thickness in the unskewed configuration. For the unskewed configuration, the horizontal force in the bridge with 4.57 m [15 ft] cross-frame spacing was slightly larger than the cross-frame force found in the bridge with 9.14 m [30 ft] cross-frame spacing.

Figure 3.52 (f) through (h) shows cross-frame horizontal tension and compression force ratios grouped by configuration for the 4.57 m [15 ft] and 9.14 m [30 ft] cross-frame spacings. Cross-frame spacing had a minor effect on lateral forces, with cross-frames spaced 4.57 m [15 ft] producing slightly smaller magnitudes than cross-frames spaced 9.14 m [30 ft]. Skew angle had very little effect on the forces produced by the skewed-staggered and skewed-unstaggered configurations. For the skewed-parallel configuration, larger skew angles produced smaller lateral forces in the cross-frames due to the smaller horizontal force component.

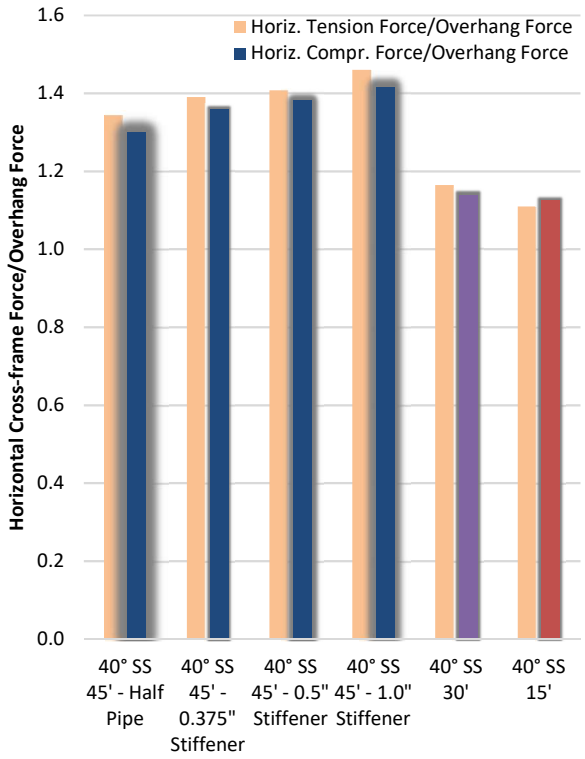

a) 40° skewed-staggered

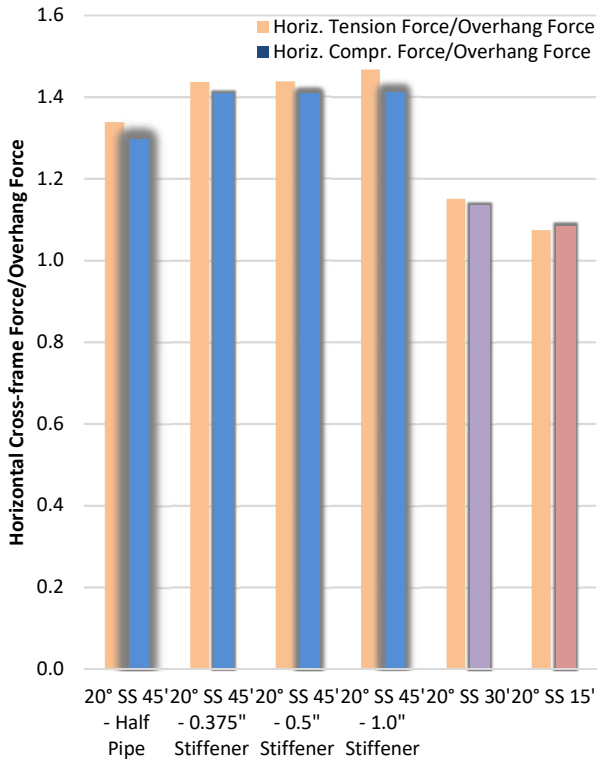

b) 20° skewed-staggered

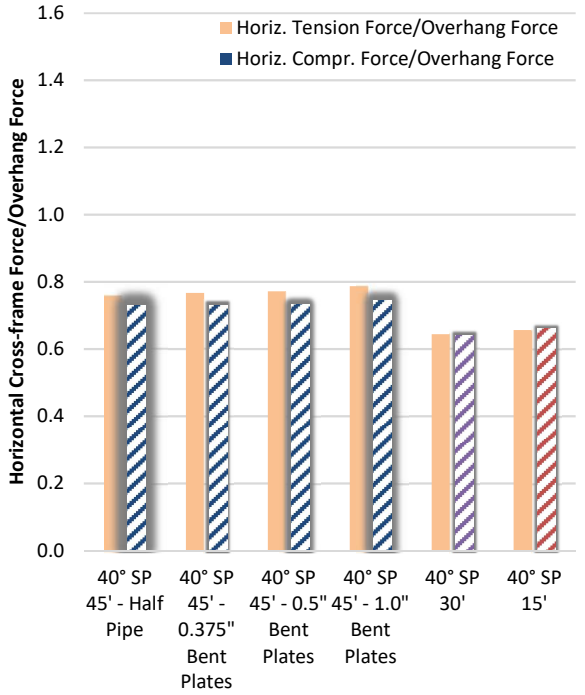

c) 40° skewed-parallel

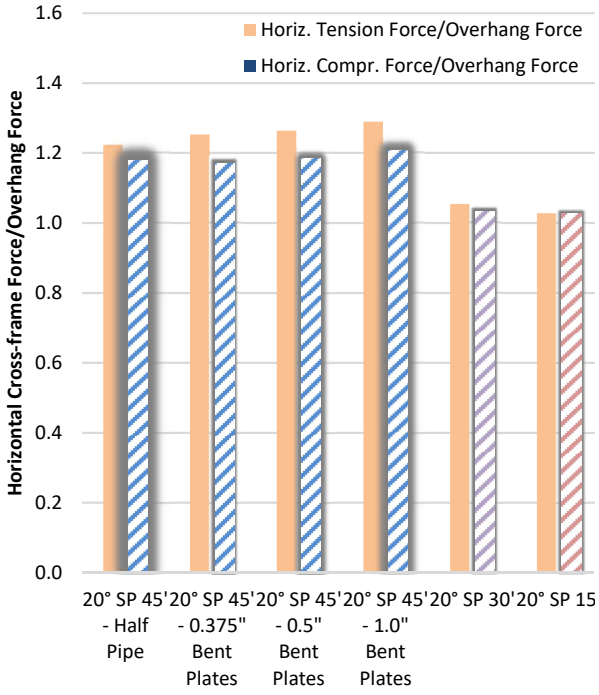

d) 20° skewed-parallel

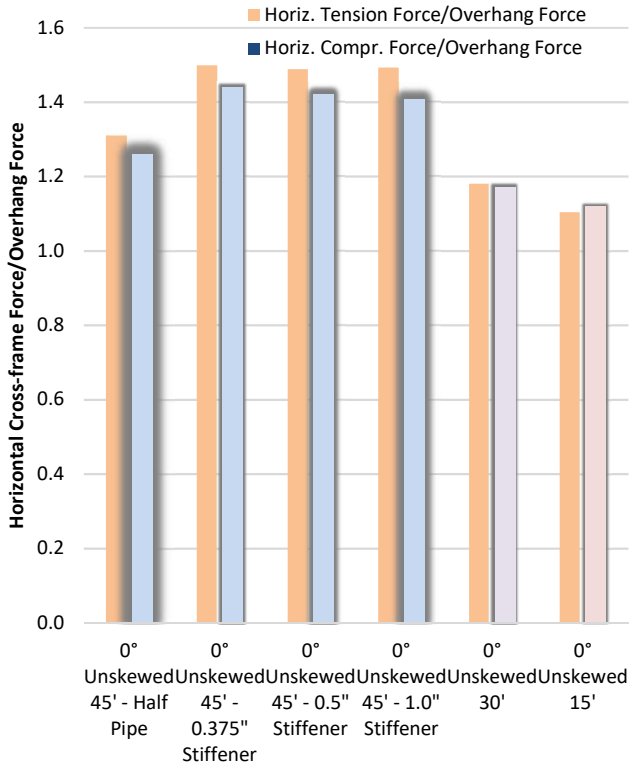

e) Non-skewed

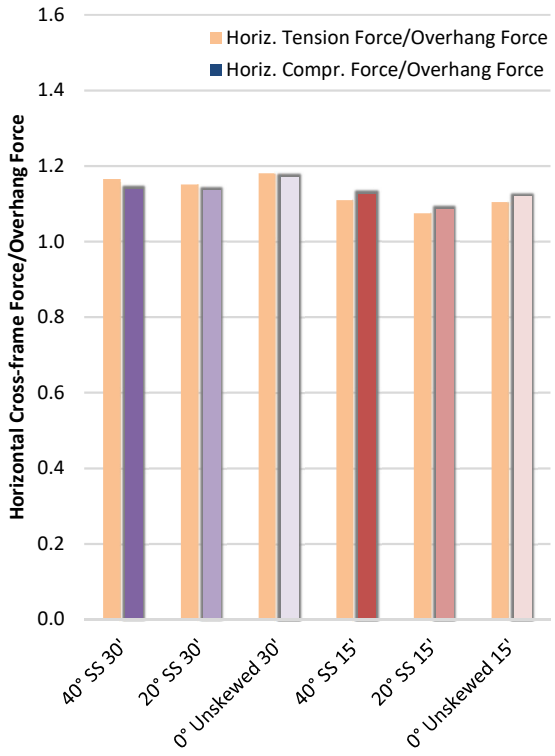

f) Skewed-staggered, 9.14 m [30 ft] and 4.57 m [15 ft] spacing

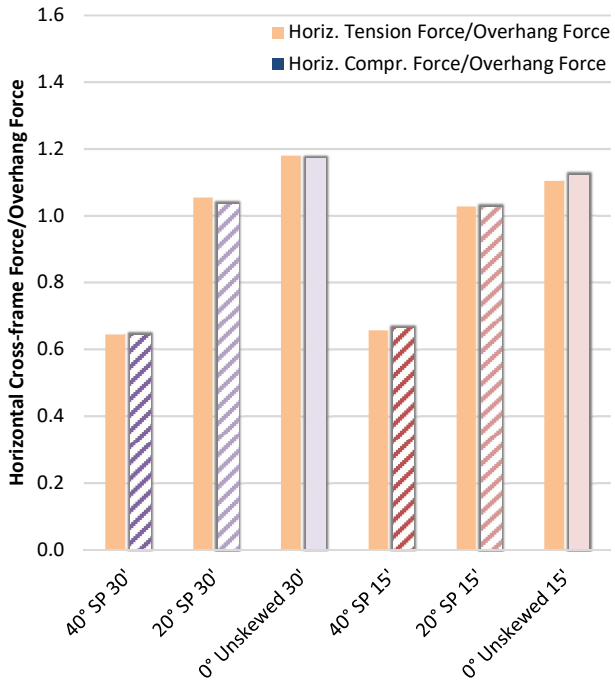

g) Skewed-parallel, 9.14 m [30 ft] and 4.57 m [15 ft] spacing

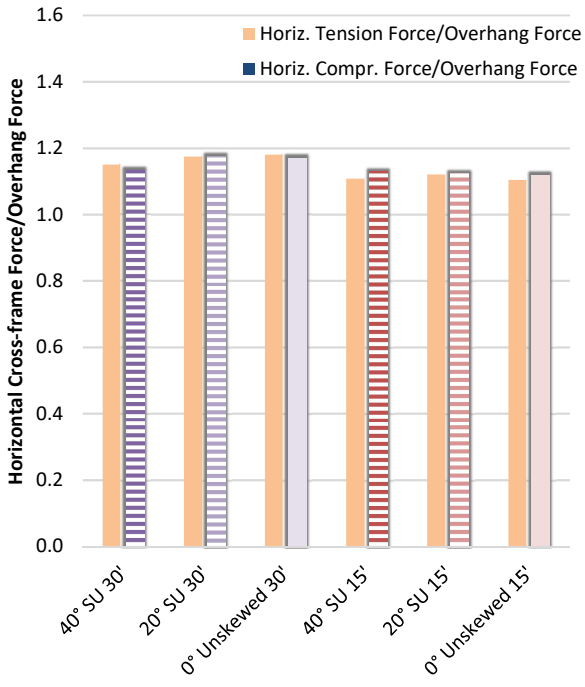

h) Skewed-unstaggered, 9.14 m [30 ft] and 4.57 m [15 ft] spacing

Figure 3.52 Cross-frame horizontal tension and compression force as a ratio of the overhang load, grouped by skew angle and configuration

Figure 3.53 (a) through (d) shows horizontal compression forces in the cross-frame bottom chord as a ratio of the overhang load, grouped by connection type. The bottom chord carries a large portion of the overall cross-frames forces and has the longest unbraced length. Members A and B were connected at the midpoint and thus have a shorter unbraced length. The 40° skewed-parallel configuration produced the smallest tension and compression forces in the bottom chord. The unskewed configuration typically produced the largest member forces. Unlike overall cross-frame forces, the 20° skewed-parallel and skewed-staggered configurations produced relatively similar force magnitudes in the bottom chord. The 40° skewed-staggered configuration had slightly smaller forces than the 20° skewed-staggered configuration. The skew angle had a larger effect on horizontal force transfer relative to the overall cross-frame system.

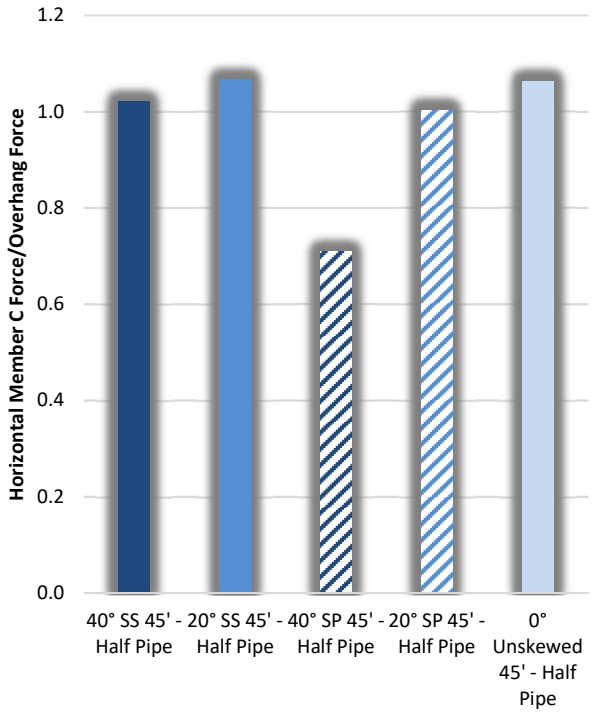

a) Half-pipe connection, 13.7 m [45 ft] cross-frame spacing

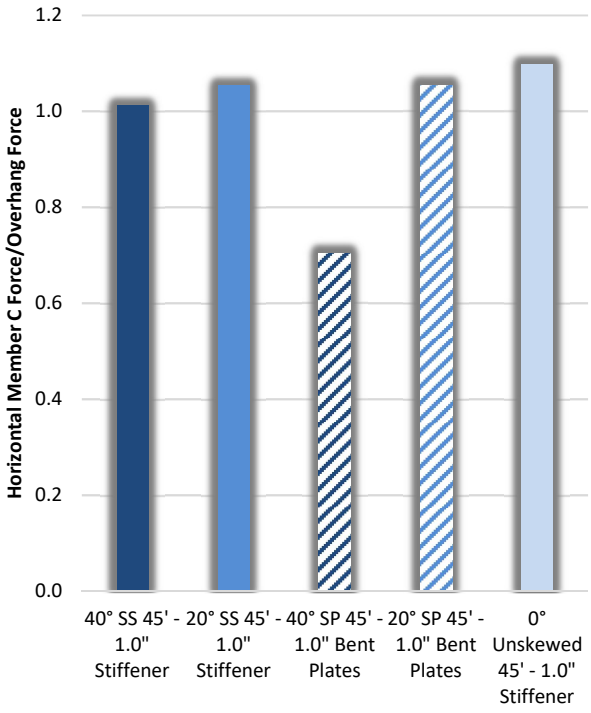

b) 25.4mm [1.0 in] stiffener connection, 13.7 m [45 ft] cross-frame spacing

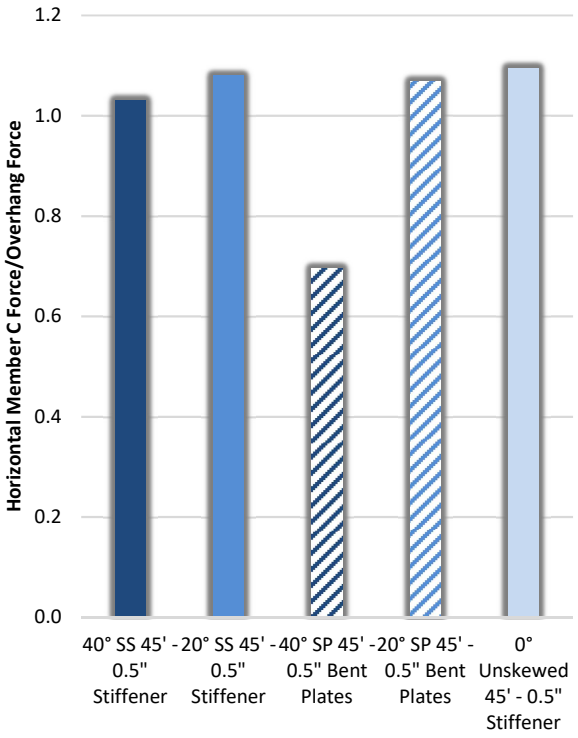

c) 12.7mm [1/2 in] stiffener connection, 13.7 m [45 ft] cross-frame spacing

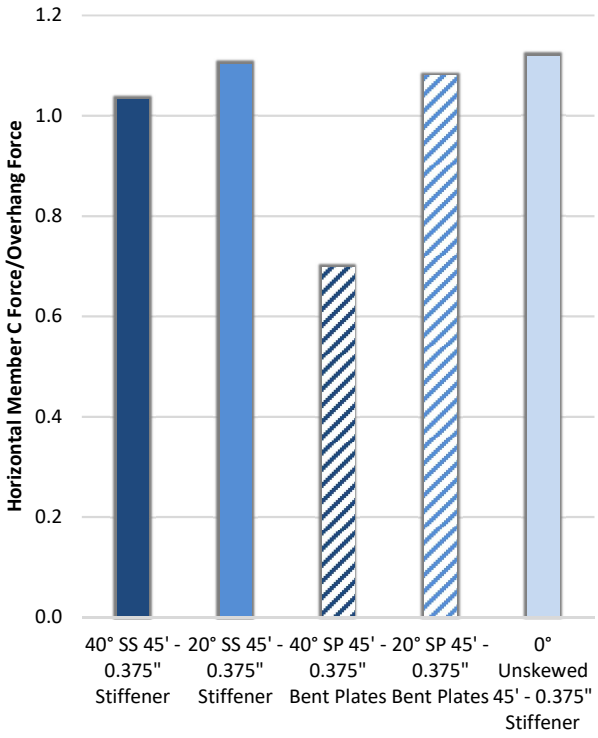

d) 9.53mm [3/8 in] stiffener connection, 13.7 m [45 ft] cross-frame spacing

Figure 3.53 Cross-frame member C horizontal tension and compression force as a ratio of the overhang load, grouped by connection type

Figure 3.54 (a) through (e) shows cross-frame bottom chord horizontal compression forces normalized by the overhang load, grouped by skew angle. For the skewed-staggered configuration, the half-pipe connection produced relatively similar forces as stiffener connections in bridges with 13.7 m [45 ft] cross-frame spacing. Thicker stiffeners attracted the same or less lateral force in the bottom chord. While bridges with 9.14 m [30 ft] cross-frame spacings produced the smallest force ratios, bridges with 4.57 m [15 ft] cross-frame spacings produced forces similar to bridges with 13.7 m [45 ft] spacings for the skewed-staggered configuration. For the skewed-parallel configuration, the horizontal force ratio was relatively similar across all

connection types and cross-frame spacings, with the 9.14 m [30 ft] cross-frame spacing models producing forces slightly smaller than the 4.57 m [15 ft] or 13.7 m [45 ft] spacing bridges.

For the unskewed configuration, the half-pipe connection had slightly smaller lateral forces in the bottom chord compared to stiffener connections of bridges with 13.7 m [45 ft] cross-frame spacing. The force ratio between varying stiffener thicknesses of bridges with 13.7 m [45 ft] cross-frame spacing was almost the same. For the unskewed configuration, the horizontal forces in the bridge with 4.57 m [15 ft] cross-frame spacing was exactly the same as that found in the bridge with 9.14 m [30 ft] cross-frame spacing.

Figure 3.54 (f) through (h) shows horizontal compression force ratios in the bottom chord, grouped by configuration for the 4.57 m [15 ft] and 9.14 m [30 ft] cross-frame spacings. Bottom chord forces increased with decreasing skew angle in all three configurations except for the 0° skewed-staggered bridge with 4.57 m [15 ft] cross-frame spacing having a slightly smaller value compared to the 20° skewed-staggered bridge with 4.57 m [15 ft] cross-frame spacing. Cross-frame spacing did not affect the unskewed configuration, as both 4.57 m [15 ft] and 9.14 m [30 ft] cross-frame spacings produced almost the same results in the bottom chord. In the skewed-staggered and skewed-parallel configuration, the 4.57 m [15 ft] spacing models had larger forces in the bottom chord compared to the 9.14 m [30 ft] cross-frame spacing models. In the skewed-unstaggered configuration, bridges with 4.57 m [15 ft] spacings had slightly smaller force ratios relative bridges with 9.14 m [30 ft] cross-frame spacings. Overall, skew angle had a much greater effect on lateral forces transferred through the bottom chord than across the cross-frame as a whole.

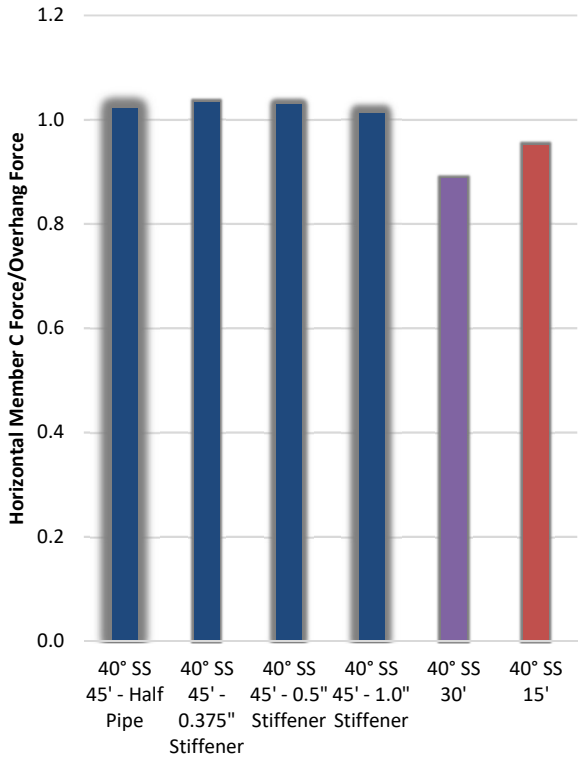

a) 40° skewed-staggered

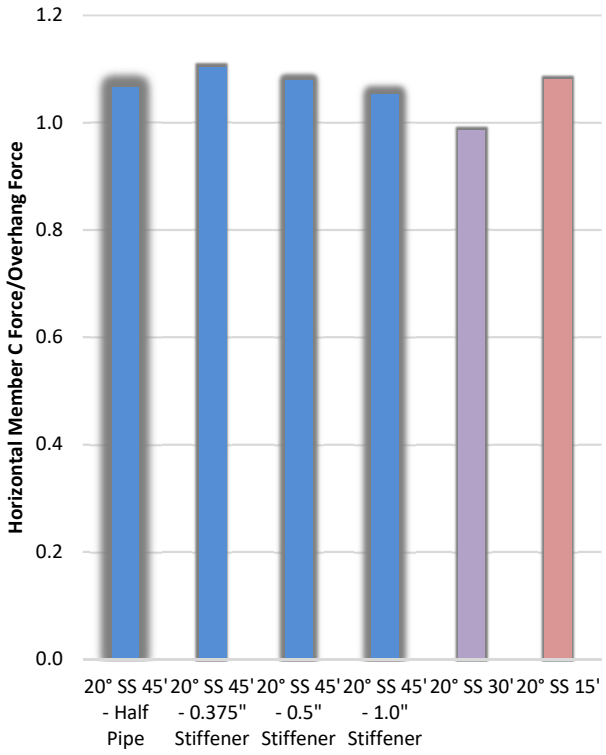

b) 20° skewed-staggered

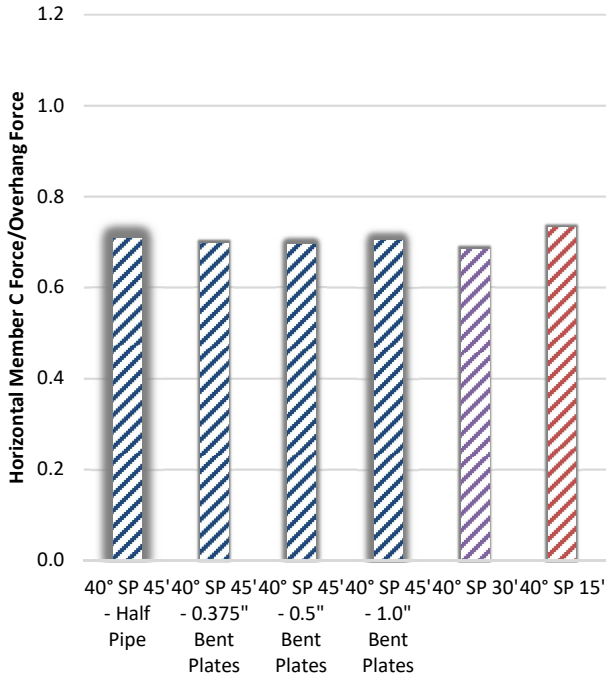

c) 40° skewed-parallel

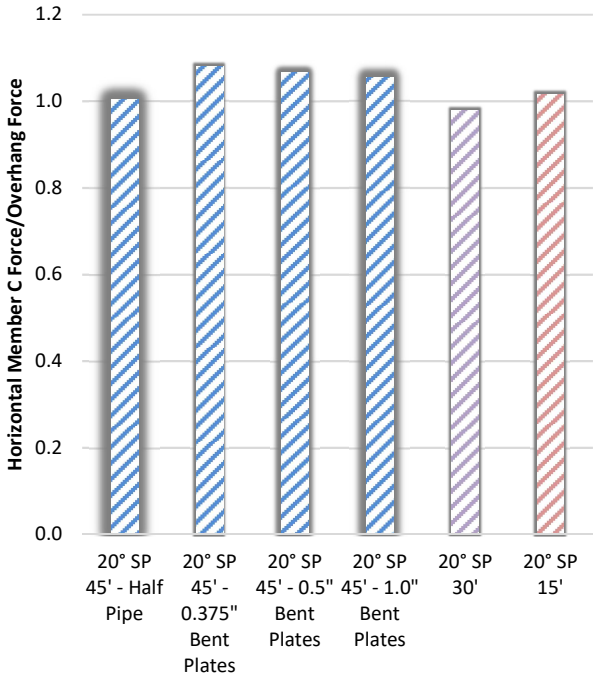

d) 20° skewed-parallel

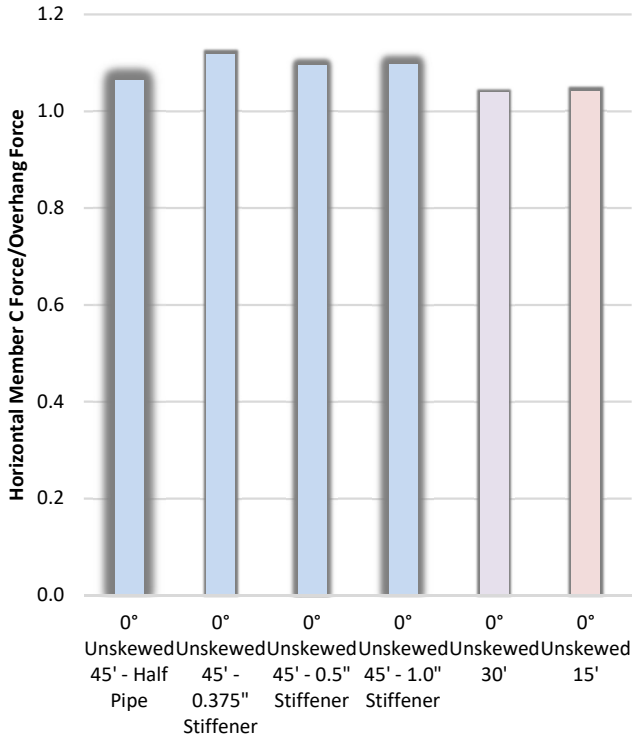

e) Non-skewed

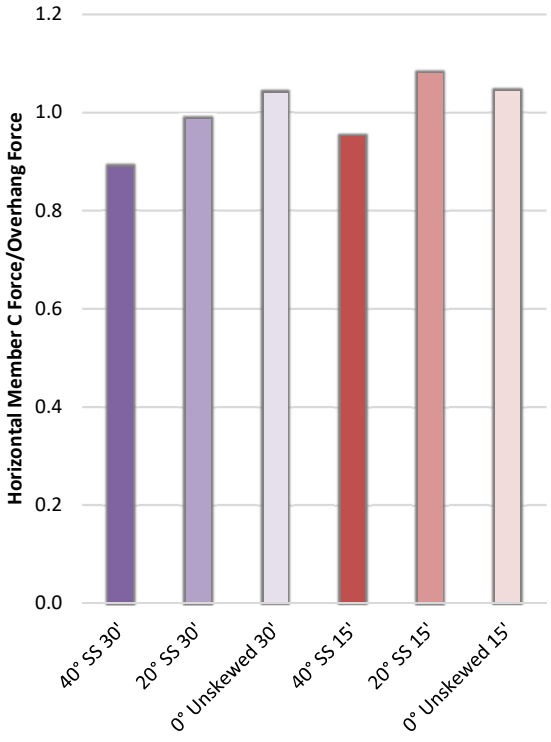

f) Skewed-staggered, 9.14 m [30 ft] and 4.57 m [15 ft] spacing

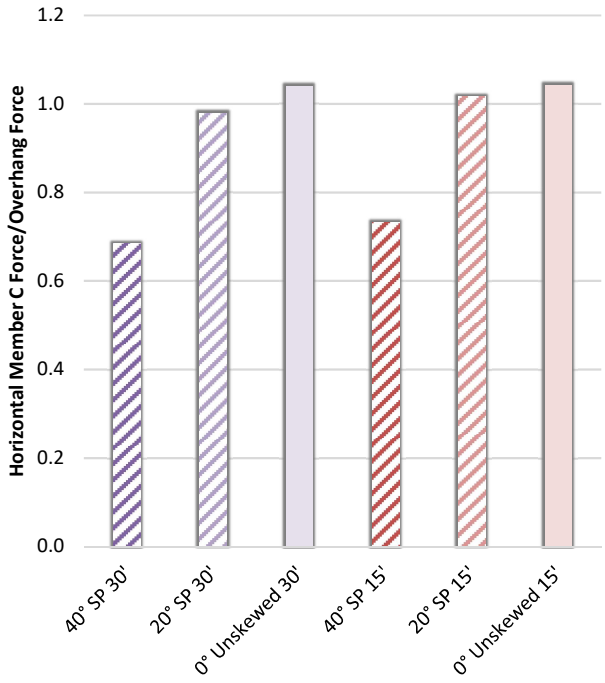

g) Skewed-parallel, 9.14 m [30 ft] and 4.57 m [15 ft] spacing

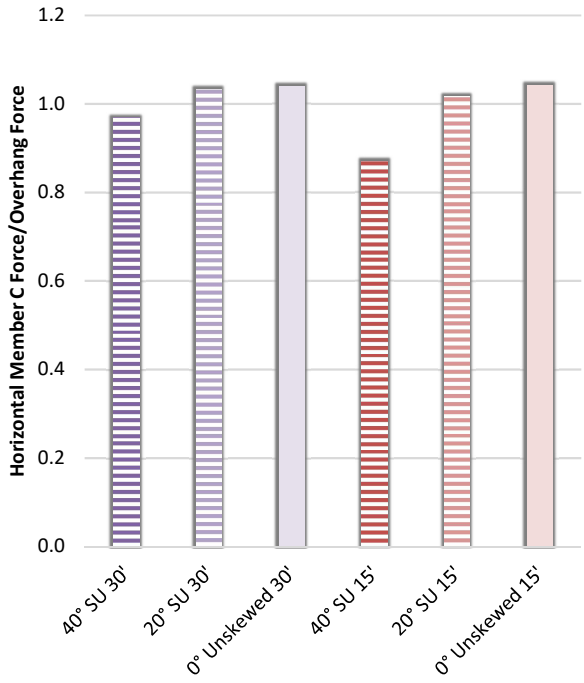

h) Skewed-unstaggered, 9.14 m [30 ft] and 4.57 m [15 ft] spacing

Figure 3.54 Cross-frame member C horizontal tension and compression force as a ratio of the overhang load, grouped by skew angle and configuration

CONCLUSIONS

This report has presented a study of a bridge system where bridge configuration, skew angle, cross-frame spacing, and cross-frame connection stiffness were varied to examine the implications on stability and lateral flange bending stresses.

The results were examined in terms of lateral displacement of the top (compression) flange in the positive flexure region, which produced the largest lateral deflections; girder stresses extracted from the interior and exterior girders; and stresses in the cross-frame angles to determine the lateral force transfer in the members and its susceptibility to buckling. Bridge configuration, cross-frame spacing skew angle, and connection type all affected the susceptibility of the bridge to lateral torsional buckling. From these data, the following conclusions can be drawn:

- The skewed-staggered configuration produced larger exterior top flange lateral displacements and larger out-of-plane girder stresses than the skewed-parallel configuration for the 13.7 m [45 ft] cross-frame spacing models.
- The exterior top flange lateral displacements for the 4.57 m [15 ft] and 9.14 m [30 ft] cross-frame spacing models had a maximum deflection of 45.2 mm [1.78 in] found in the 40° skewed-staggered bridge with 9.14 m [30 ft] cross-frame spacing. As would be expected, the lateral deflections in systems with larger cross-frame spacing (13.7 m [45 ft]) became extremely large. Therefore, even *if* the braces in such a system were found to be effective from a strength and stiffness standpoint, and *if* the girder was able to remain stable for such a long unbraced length, the lateral displacements in the girders would be untenable. This observation was not unexpected, as the goal of examining a system with

such long unbraced lengths was to amplify differences between the various connection stiffness parameters examined, and it is reiterated here for clarity.

- Larger skew angles produced smaller exterior top flange lateral displacements and smaller lateral flange bending stresses than smaller skew angles for the 13.7 m [45 ft] cross-frame spacing models.
- Smaller skew angles produced smaller exterior top flange lateral displacements than larger skew angles for 4.57 m [15 ft] and 9.14 m [30 ft] cross-frame spacing models, with the exception of the 0° non-skewed bridge with 4.57 m [15 ft] cross-frame spacing, which resulted in slightly larger displacements than the 20° bridge with the same configuration and cross-frame spacing.
- The skewed-staggered configuration resulted in larger cross-frame stresses in the bottom horizontal angle member, Member C, than the skewed-parallel configuration for any given skew angle, connection type, and cross-frame spacing.
- Smaller skew angles corresponded with larger cross-frame stresses in Member C.
- Variations in stiffener thicknesses produced very small or insignificant differences in lateral displacements of the compression flange or cross-frame stresses.
- The half-pipe connection produced the smallest lateral displacements, out-of-plane girder stresses, and cross-frame stresses, in all systems examined.
- Cross-frame spacing had a great effect on girder lateral displacements than skew angle, cross-frame configuration (SS vs SP), or connection stiffness.

- Cross-frames placed perpendicular to skew carried a larger portion of the lateral overhang force compared to cross-frames placed parallel to skew, which carried a smaller horizontal component of the load as skew angle increased.

For the cross-frames / diaphragms carried parallel to skew, the data showed that as the cross-frame forces are balanced on the opposite side of the girder cross-section, generally smaller lateral deflections and smaller cross-frame stresses were produced. The results showed that stiffener thickness had little effect on cross-frame stresses, but did result in noticeable differences in terms of peak lateral displacements. Even with an unusually long cross-frame spacing of 13.7 m [45 ft], cross-frames in all skew angles and configurations effectively braced the girders (although the girders themselves did exhibit extremely large lateral displacements when too few cross-frames were present).

For cross-frames spaced within KDOT's maximum requirement of 7.62 m [25 ft], lateral torsional buckling was not a significant problem for any skew angle or configuration tested. Stiffener thickness and cross-frame orientation had very little effect on lateral deflections overall. For the 13.7 m [45 ft] cross-frame spacing models, the skewed-staggered models produced larger deflections than the skewed-parallel models for the same skew angle. However, these deflections were on the order of 30 cm [12 in] so small differences between the varying orientations are out-weight by the scale of deflections. For the 9.14 m [30 ft] cross-frame spacing models, larger skew angles produced slightly larger lateral deflections. As cross-frame spacing reduced, global effects played a larger role for cross-frames spaced at 4.57 m [15 ft], as deflections were relatively similar between different skew angles and orientations with variations in the position of the peak deflections.

Finally, the data showed that cross-frame placed parallel to skew up to an angle of 40° performed similar or better than cross-frames oriented perpendicular to skew for every given skew angle and connection type. However, as skew angles become larger, designers will have to consider the increased fabrication cost of using longer, heavier members for a skewed-parallel configuration with reduced fit-up costs and better fatigue performance. Cross-frames placed parallel to skew for larger skew angles also increases connection flexibility and lowers brace stiffness, which increases fabrication and construction costs. It is stressed that in all cases studied the longer (more flexible) cross-frames used in the skewed-parallel systems remained sufficient to restrain the girder; this must be ensured by designing the cross-frames to have sufficient strength and stiffness to restrain girder buckling, otherwise the results of this study may not translate to practice.

REFERENCES

AASHTO (2010). “LRFD Bridge Design Specifications.” *American Association of State Highway and Transportation Officials,* Washington, D.C.

AISC (2010). “Steel Construction Manual, 14th Ed.” *American Institute of Steel Construction*, Chicago, IL.

AISI Example 2: Two-Span Continuous Composite I Girder (1997). *American Iron and Steel Institute*.

Bishara, A. and Elmir, W. (1990). "*Interaction between Cross Frames and Girders*." J. Struct. Eng., 10.1061/(ASCE)0733-9445(1990)116:5(1319), 1319-1333.

Gupta, Y.P., Kumar, A. (1983). “Structural Behaviour of Interconnected Skew Slab-Girder Bridges,” Journal of the Institution of Engineers (India), Civil Engineering Division, 64, 119-124.

Hassel, H. (2011). “An Analytical Evaluation of Distortion-Induced Fatigue in Steel Bridges,” thesis, presented to University of Kansas, at Lawrence, KS in partial fulfillment of the requirements for the° of Master of Civil Engineering.

Hassel, H., Bennett, C., Matamoros, A., and Rolfe, S. (2012). “Parametric analysis of cross-frame layout on distortion-induced fatigue in skewed steel bridges.” J. Bridge Eng., 10.1061/(ASCE)BE.19435592.0000388, 601–611.

KDOT. (2010). “Design Manual: Volume III – Bridge Selection.” *Kansas Department of Transportation*.

Krupicka, G., and Poellot, B. (1993). “Nuisance Stiffness,” HDR Engineering, Inc., Bridgeline, 4(1), 3.

McConnell, J., Ambrose, K., and Radovic, M. (2013). “Cross-Frame Forces in Skewed Steel I-Girder Bridges: Field Testing and Applications to System-Capacity”, Presented at 2013 ASCE / SEI Structures Congress, Pittsburgh, PA, May 2-4, 2013.

McConnell, J., Radovic, M. (2014). “Evaluation of Cross-frame Designs for Highly Skewed Steel I-Girder Bridges.” Presented at 31st Annual International Bridge Conference, Engineers Society of Western Pennsylvania, Pittsburg, PA, IBC 14-47.

McConnell, J., Radovic, M., and Ambrose, K. (2014). “Cross-Frame Forces in Skewed Steel I-Girder Bridges: Field Measurements and Finite Element Analysis”, University of Delaware Center for Bridge Engineering, Final Report to Delaware Department of Transportation.

Ozgur, C. (2011). “Influence Of Cross-Frame Detailing On Curved And Skewed Steel I-Girder Bridges”, Doctoral Dissertation, Georgia Institute of Technology.

Quadrato, C., Battistini, A., Frank, K., Helwig, T., & Engelhardt, M. (2010). Improved cross-frame connection details for steel bridges with skewed supports. Transportation Research Record: Journal of the Transportation Research Board, (2200), 29-35.

Simulia. (2010). ABAQUS FEA Version 6.10-2. Providence, RI. http://www.simulia.com.

Wang, L. and Helwig, T.A. (2008). “Stability Bracing Requirements for Steel Bridge Girders with Skewed Supports.” *Journal of Bridge Engineering*, 13(2), 149-157.

Yura, J. A., Phillips, B., Raju, S., and Webb, S. (1992), "Bracing of Steel Beams in Bridges," Report No. 1239-4F, Center for Transportation Research, University of Texas at Austin, October, 80 p.

Yura, J. (2001). "Fundamentals of Beam Bracing." *Engineering Journal*, AISC, First Quarter, 11-26.

Winter, G. (1958). "Lateral Bracing of Columns and Beams." J. Struct. Div., Vol. 84(ST2), 1-22.

Zhou, J., Bennett, C., Matamoros, A., Li, J., and Rolfe, S. "Skewed Steel Bridges, Part I: Effect of Cross-Frame Layout on Lateral Flange Bending Stresses," Final Report to the Kansas Department of Transportation, Project KTRAN KU-13-3, September, 2015.

Appendices

APPENDIX A: DEFORMED SHAPES OF ALL FINITE ELEMENT MODELS INCLUDED IN THE PARAMETRIC STUDY

Figure A.1 through Figure A.102 presents views of the deformed shapes for the 40°, 20°, and 0° bridge systems. Skewed-parallel, skewed-staggered, and skewed-unstaggered configurations are shown for bridges with 4.2 m [15 ft], 9.14 m [30 ft], and 13.7 m [45 ft] cross-frame spacings where applicable. For bridges with a 13.7 m [45 ft] cross-frame spacing, cross-frames with 9.5 mm [3/8 in], 13 mm [1/2 in], 26 mm [1.0 in], and half-pipe connections are shown. For bridges with 4.2 m [15 ft] and 9.14 m [30 ft] cross-frame spacings, cross-frames have 9.5 mm [3/8 in] connection stiffeners.

40° SKEWED-PARALLEL BRIDGE

45 FT CROSS-FRAME SPACING;

3/8" THICK STIFFENERS

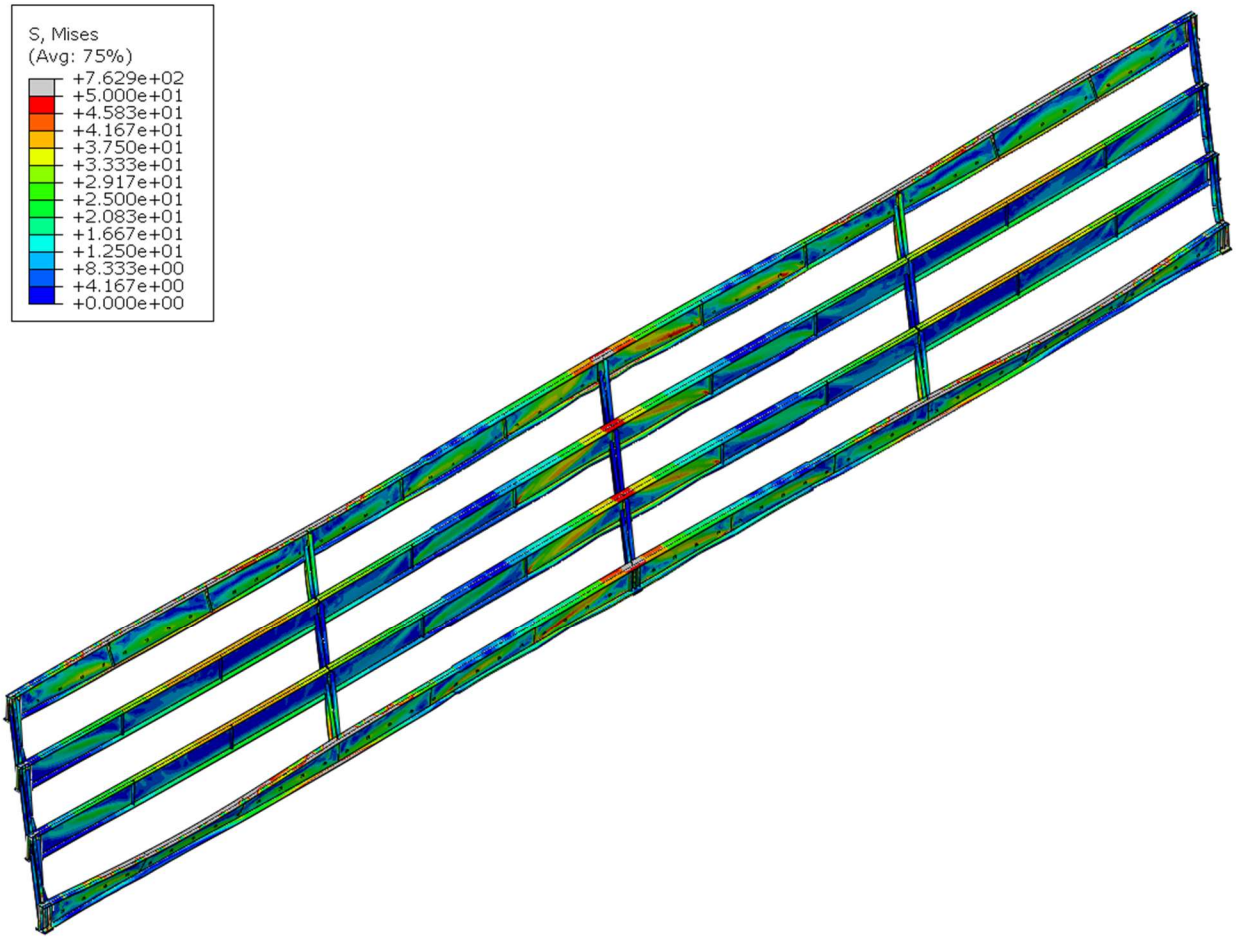

Figure A.1 Deformed shaped of the 40° skewed-parallel bridge with 13.7 m [45 ft] cross-frame spacing and 9.53 mm [3/8 in] thick stiffeners in isotropic view

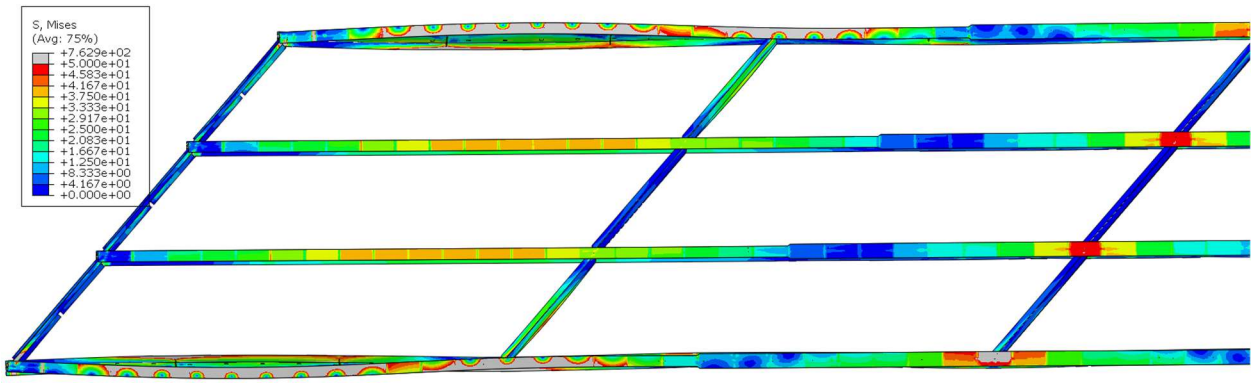

Figure A.2 Deformed shape of the 40° skewed-parallel bridge in Span 1 with 13.7 m [45 ft] cross-frame spacing and 9.53 mm [3/8 in] thick stiffeners in plan view

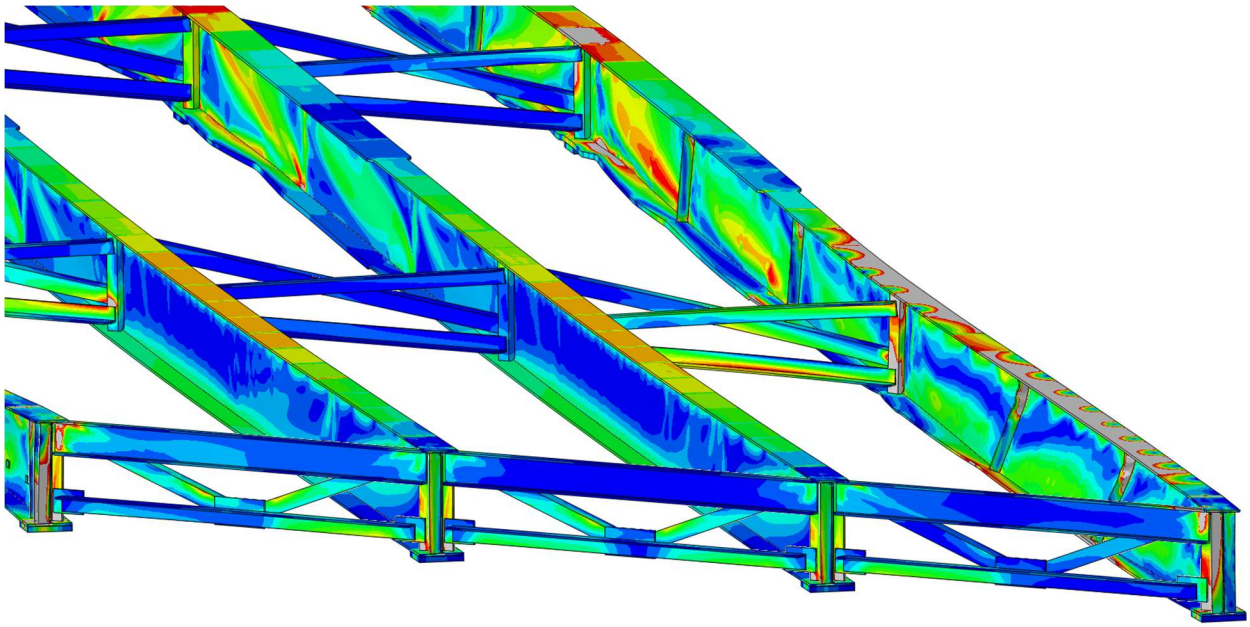

Figure A.3 Girder deformation of the 40° skewed-parallel bridge with 13.7 m [45 ft] cross-frame spacing and 9.53 mm [3/8 in] thick stiffeners

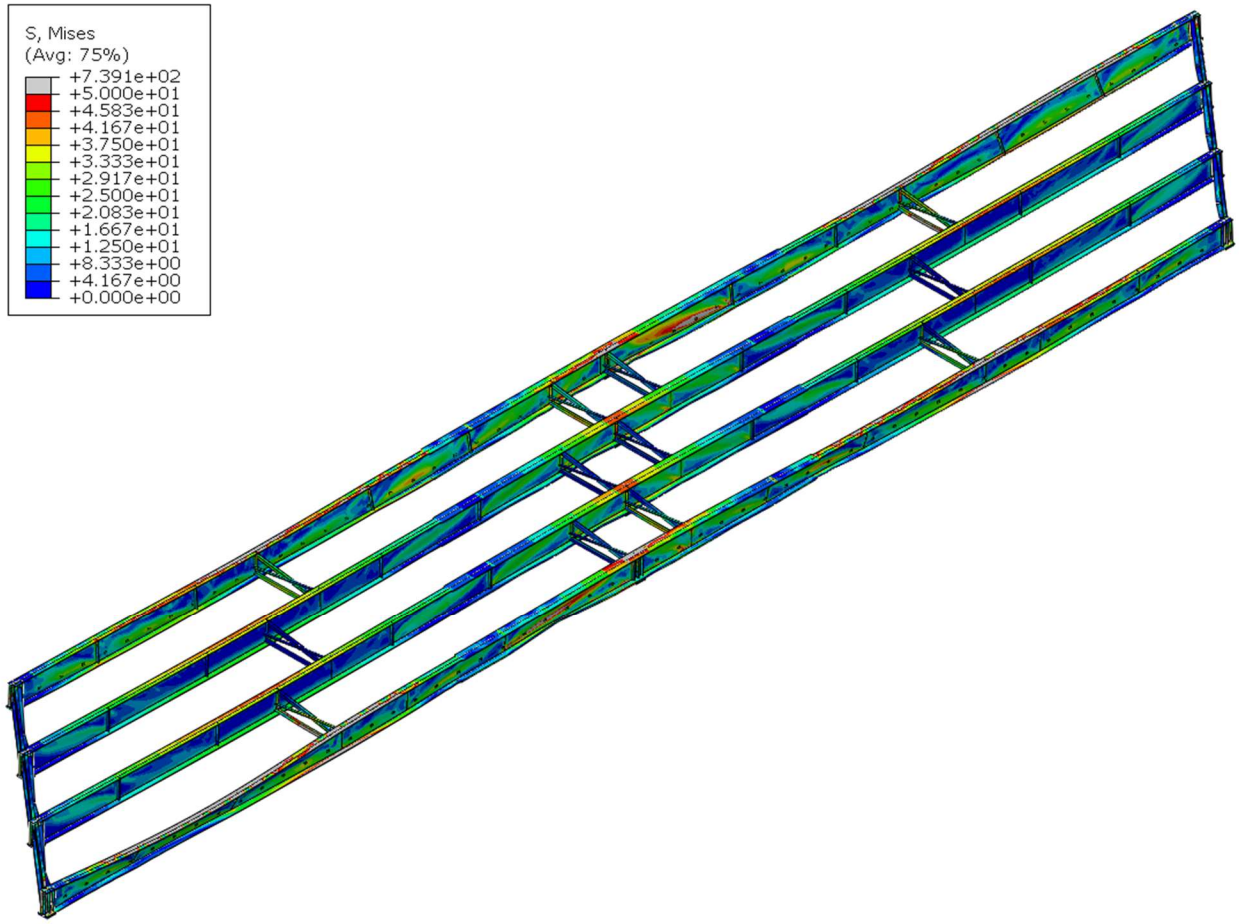

Figure A.4 Deformed shaped of the 40° skewed-staggered bridge with 13.7 m [45 ft] cross-frame spacing and 9.53 mm [3/8 in] thick stiffeners in isotropic view

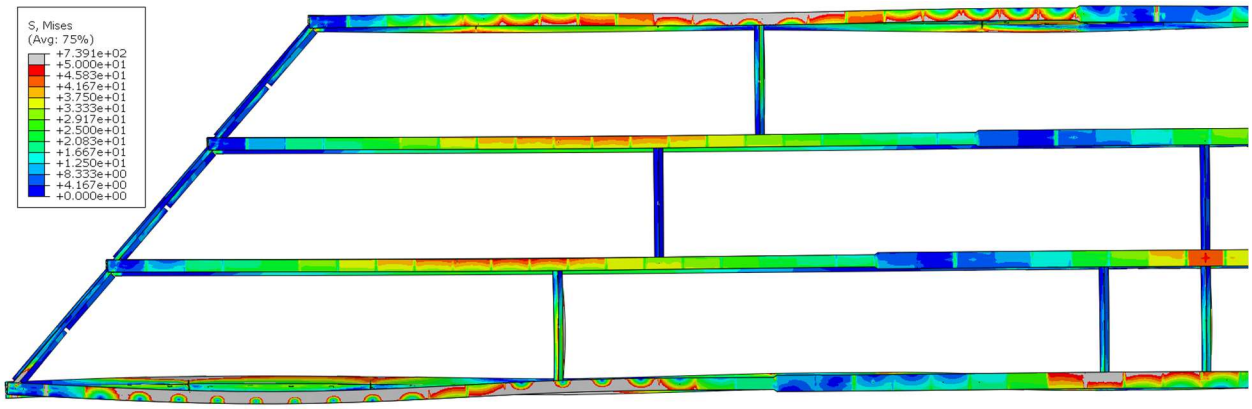

Figure A.5 Deformed shape of the 40° skewed-staggered bridge in Span 1 with 13.7 m [45 ft] cross-frame spacing and 9.53 mm [3/8 in] thick stiffeners in plan view

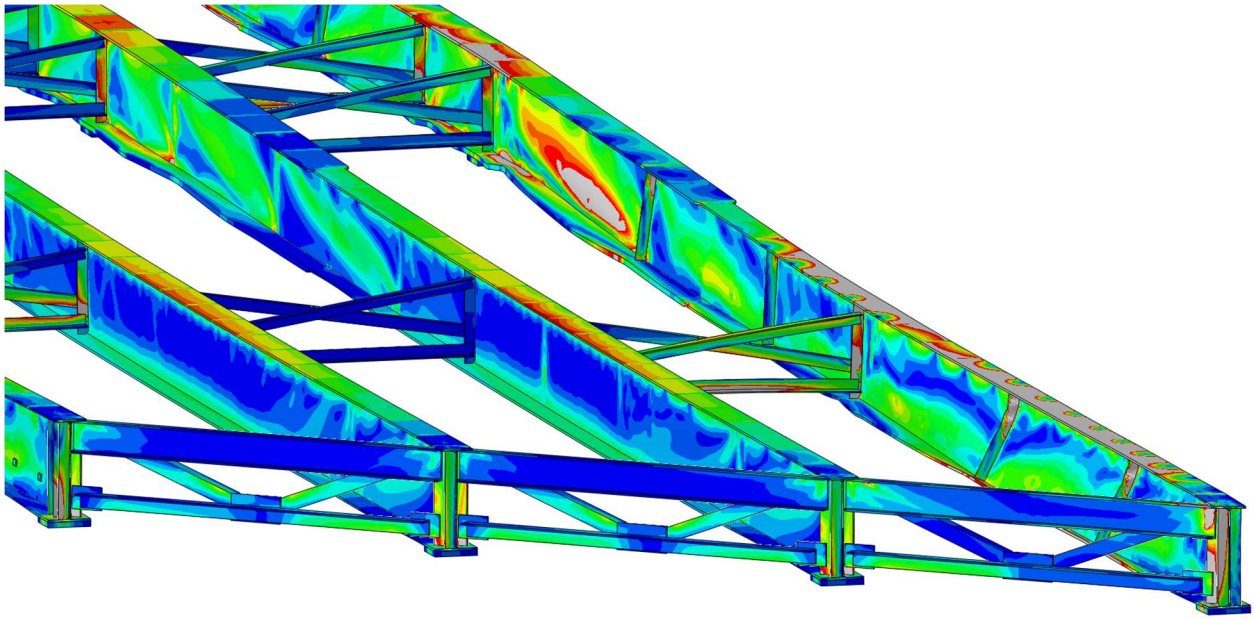

Figure A.6 Girder deformation of the 40° skewed-staggered bridge with 13.7 m [45 ft] cross-frame spacing and 9.53 mm [3/8 in] thick stiffeners

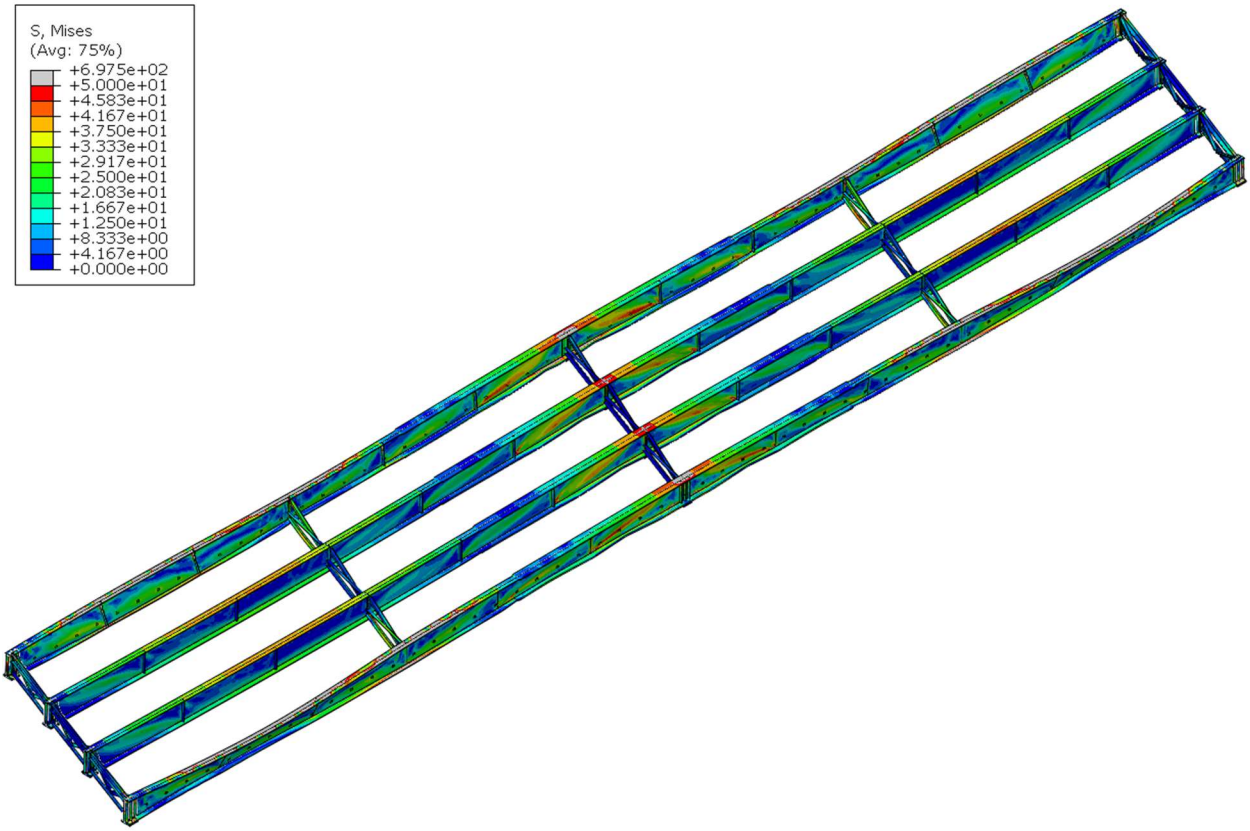

Figure A.7 Deformed shaped of the 20° skewed-parallel bridge with 13.7 m [45 ft] cross-frame spacing and 9.53 mm [3/8 in] thick stiffeners in isotropic view

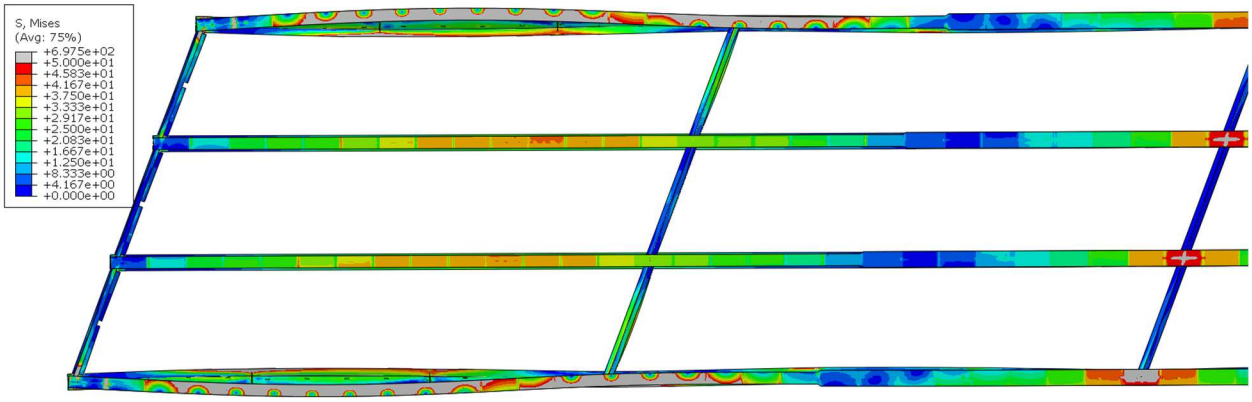

Figure A.8 Deformed shape of the 20° skewed-parallel bridge in Span 1 with 13.7 m [45 ft] cross-frame spacing and 9.53 mm [3/8 in] thick stiffeners in plan view

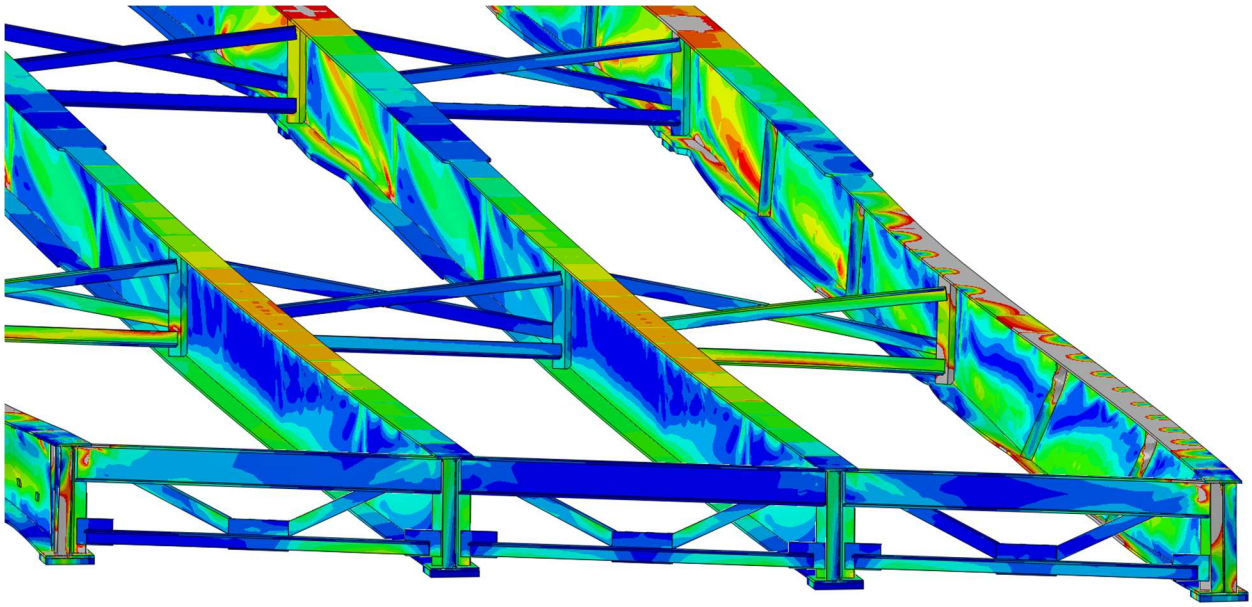

Figure A.9 Girder deformation of the 20° skewed-parallel bridge with 13.7 m [45 ft] cross-frame spacing and 9.53 mm [3/8 in] thick stiffeners

20° SKEWED-STAGGERED BRIDGE

45 FT CROSS-FRAME SPACING;

3/8" THICK STIFFENERS

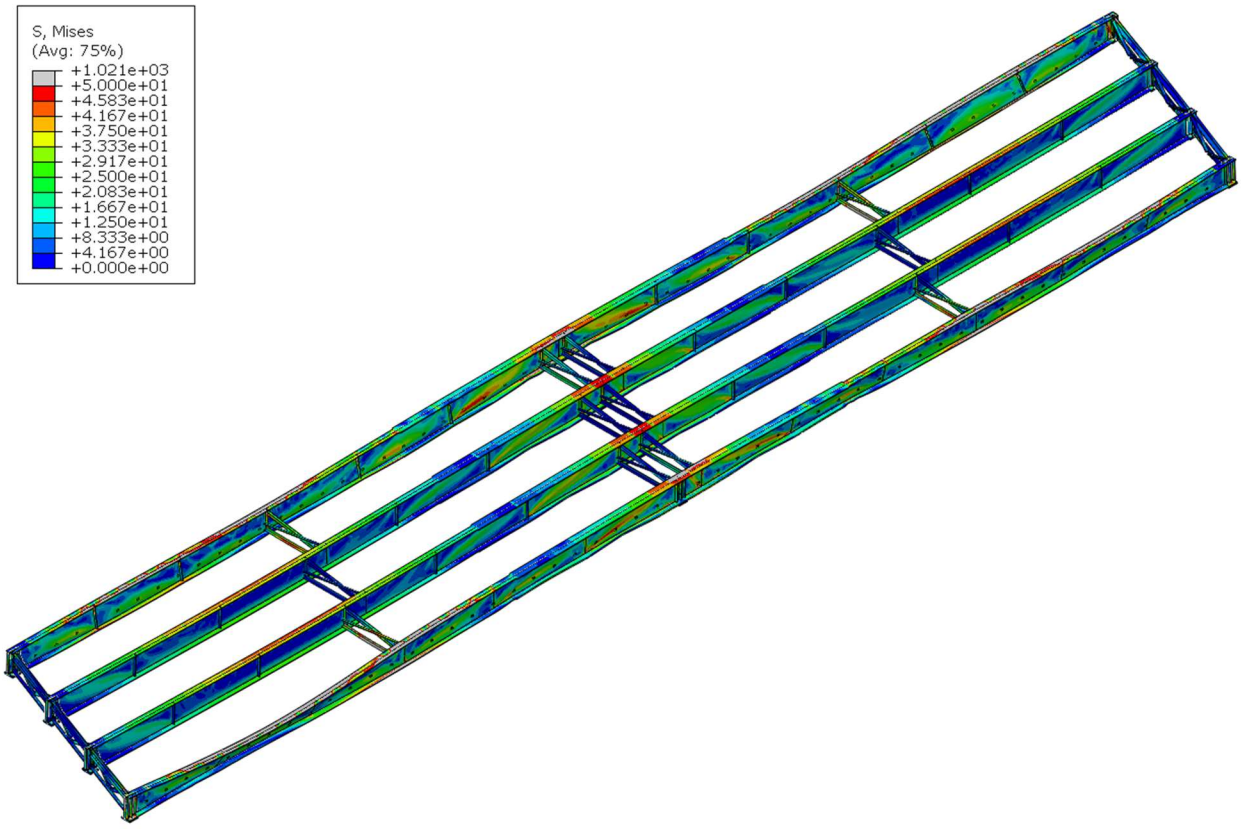

Figure A.10 Deformed shaped of the 20° skewed-staggered bridge with 13.7 m [45 ft] cross-frame spacing and 9.53 mm [3/8 in] thick stiffeners in isotropic view

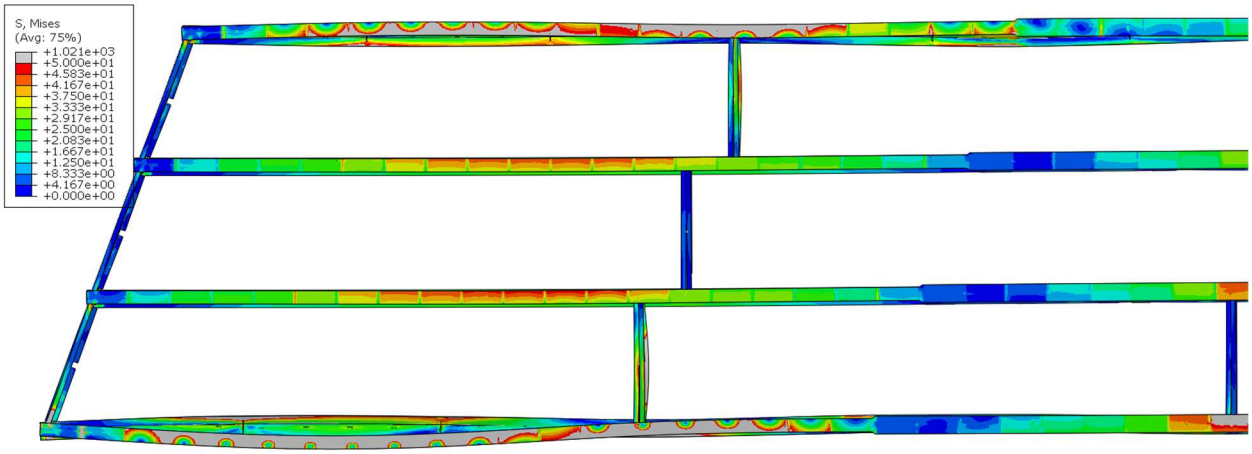

Figure A.11 Deformed shape of the 20° skewed-staggered bridge in Span 1 with 13.7 m [45 ft] cross-frame spacing and 9.53 mm [3/8 in] thick stiffeners in plan view

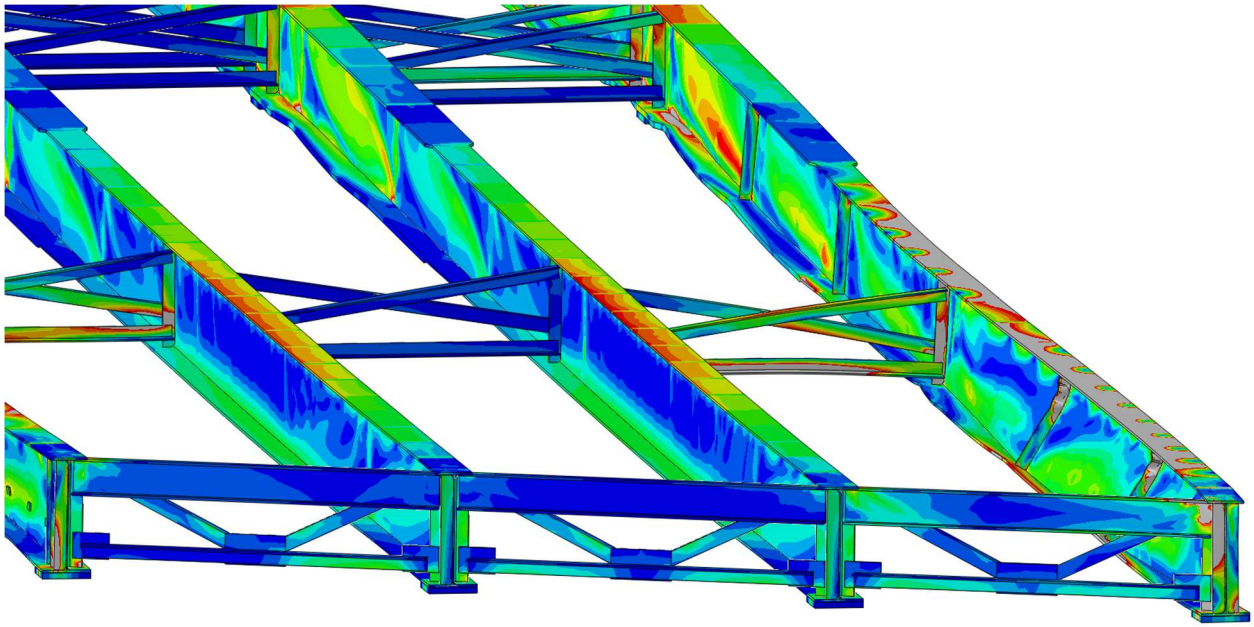

Figure A.12 Girder deformation of the 20° skewed-staggered bridge with 13.7 m [45 ft] cross-frame spacing and 9.53 mm [3/8 in] thick stiffeners

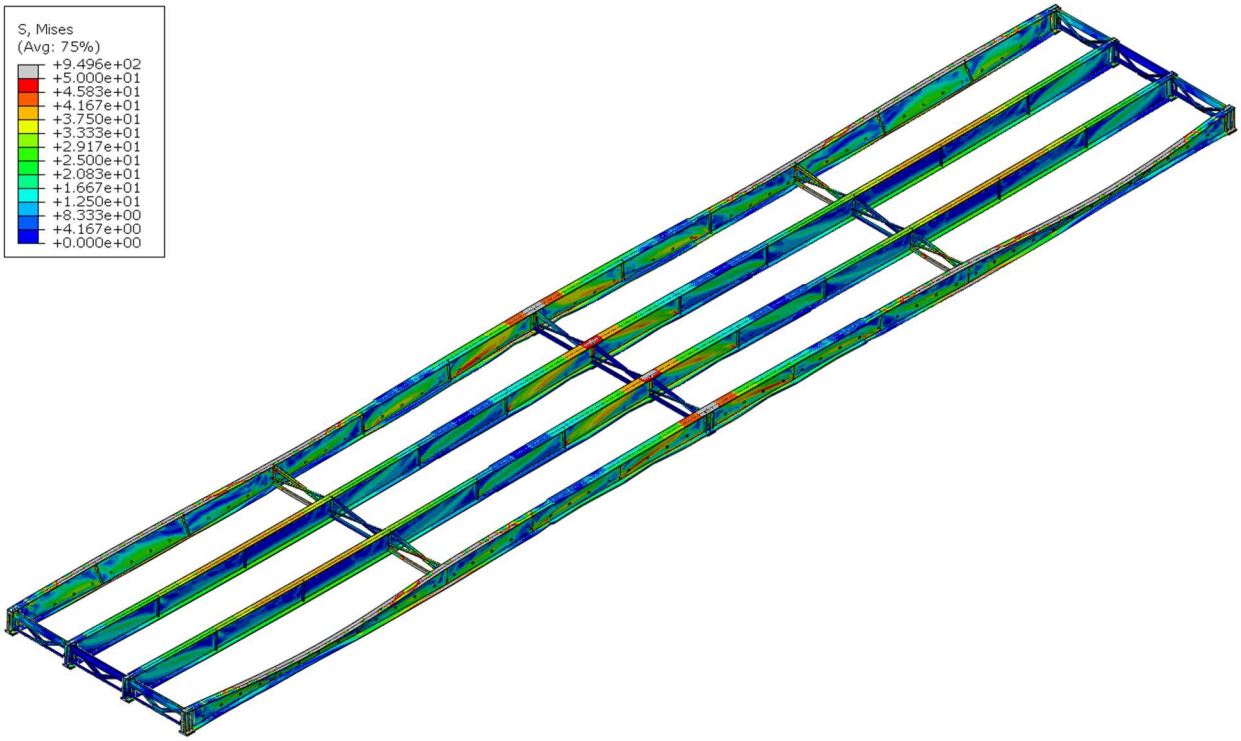

Figure A.13 Deformed shaped of the non-skewed bridge with 13.7 m [45 ft] cross-frame spacing and 9.53 mm [3/8 in] thick stiffeners in isotropic view

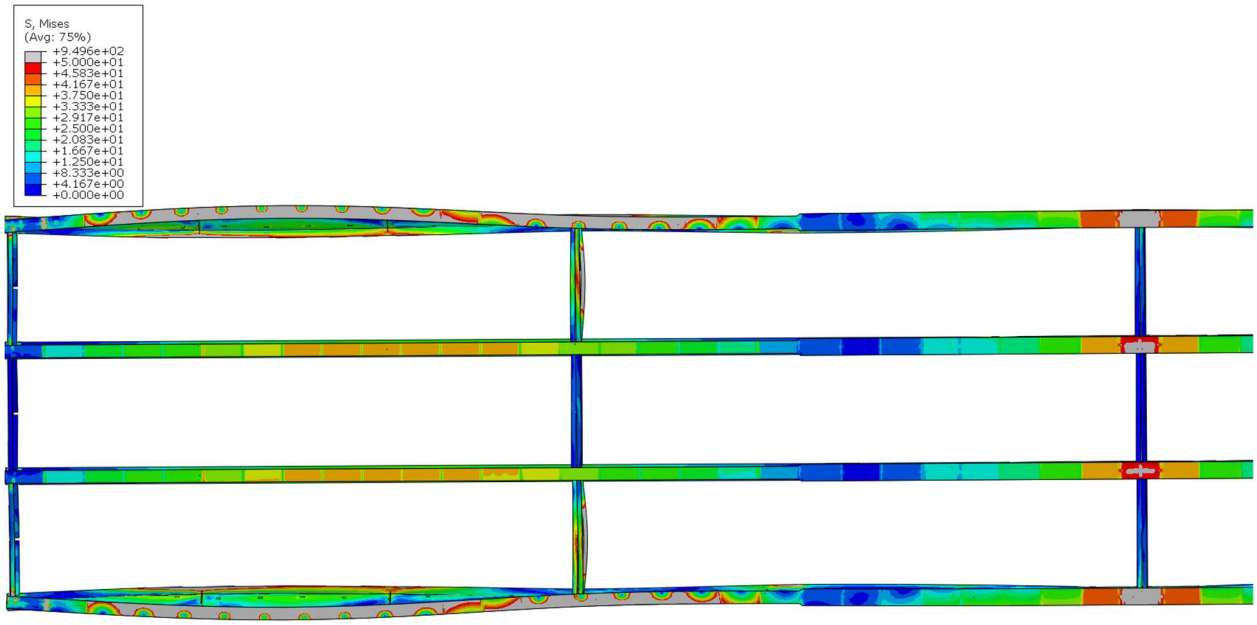

Figure A.14 Deformed shape of the non-skewed bridge in Span 1 with 13.7 m [45 ft] cross-frame spacing and 9.53 mm [3/8 in] thick stiffeners in plan view

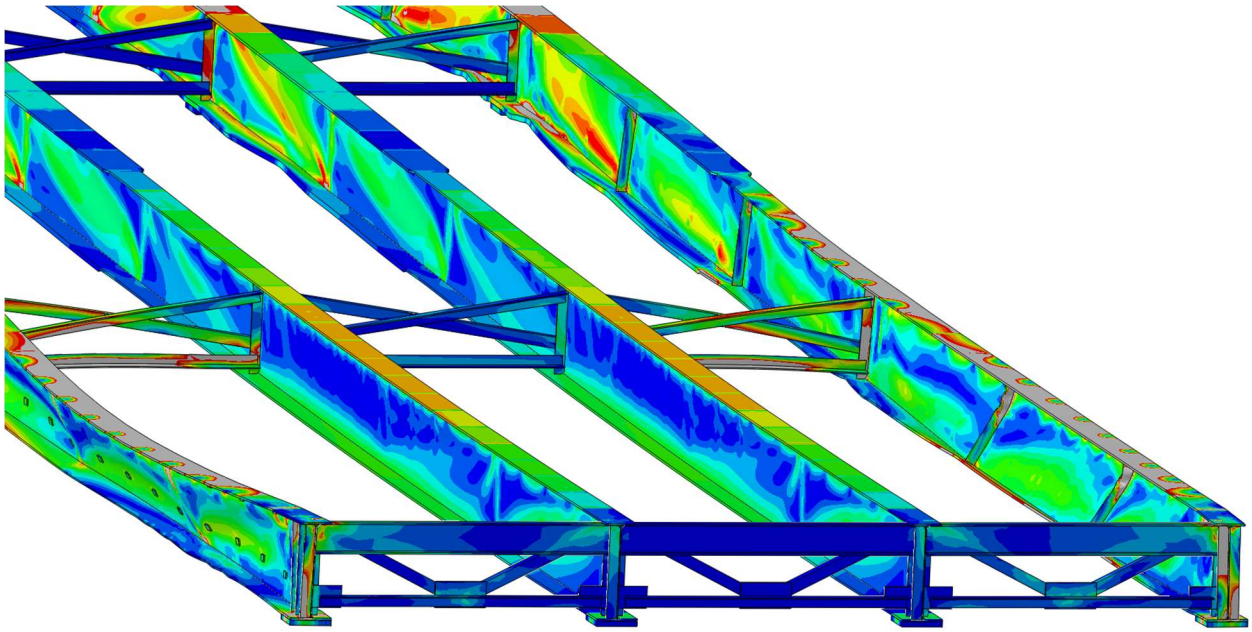

Figure A.15 Girder deformation of the non-skewed bridge with 13.7 m [45 ft] cross-frame spacing and 9.53 mm [3/8 in] thick stiffeners

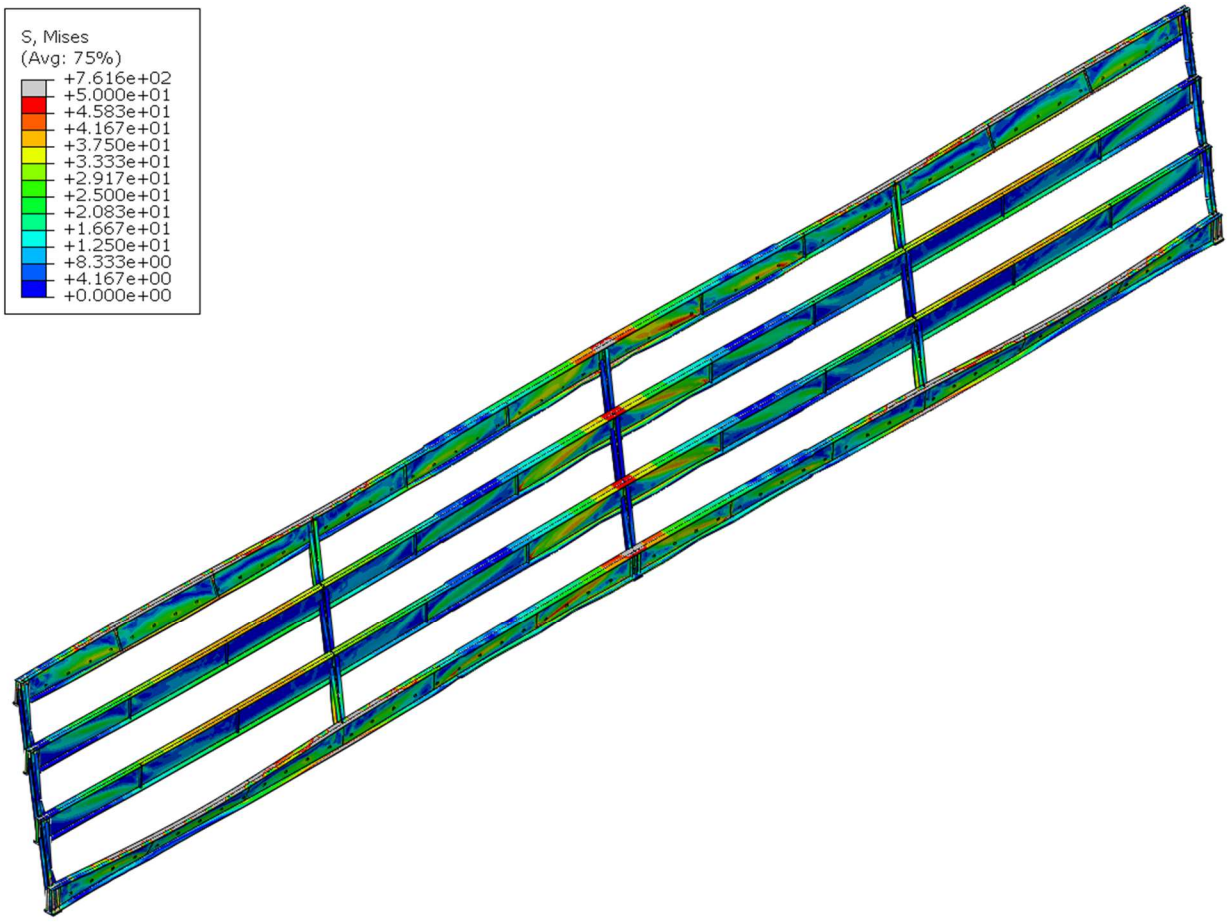

Figure A.16 Deformed shaped of the 40° skewed-parallel bridge with 13.7 m [45 ft] cross-frame spacing and 12.7 mm [1/2 in] thick stiffeners in isotropic view

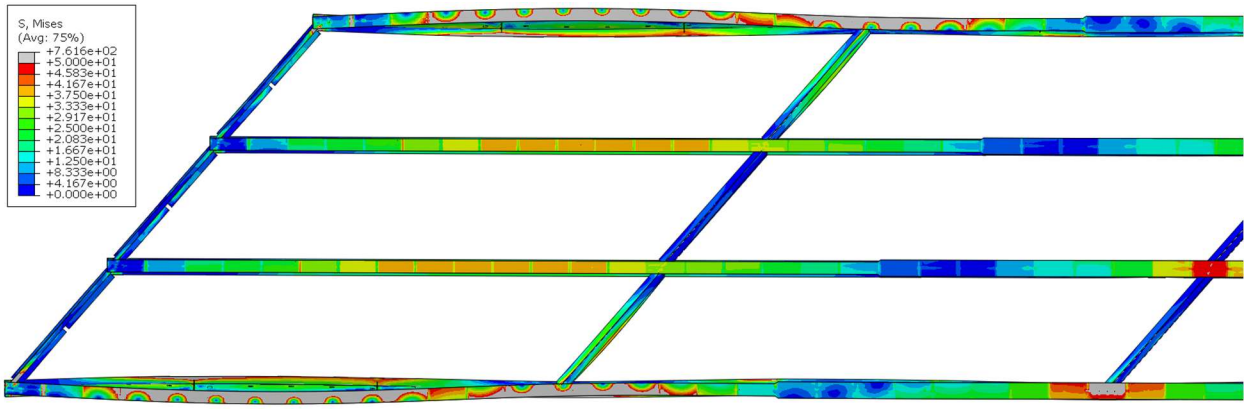

Figure A.17 Deformed shape of the 40° skewed-parallel bridge in Span 1 with 13.7 m [45 ft] cross-frame spacing and 12.7 mm [1/2 in] thick stiffeners in plan view

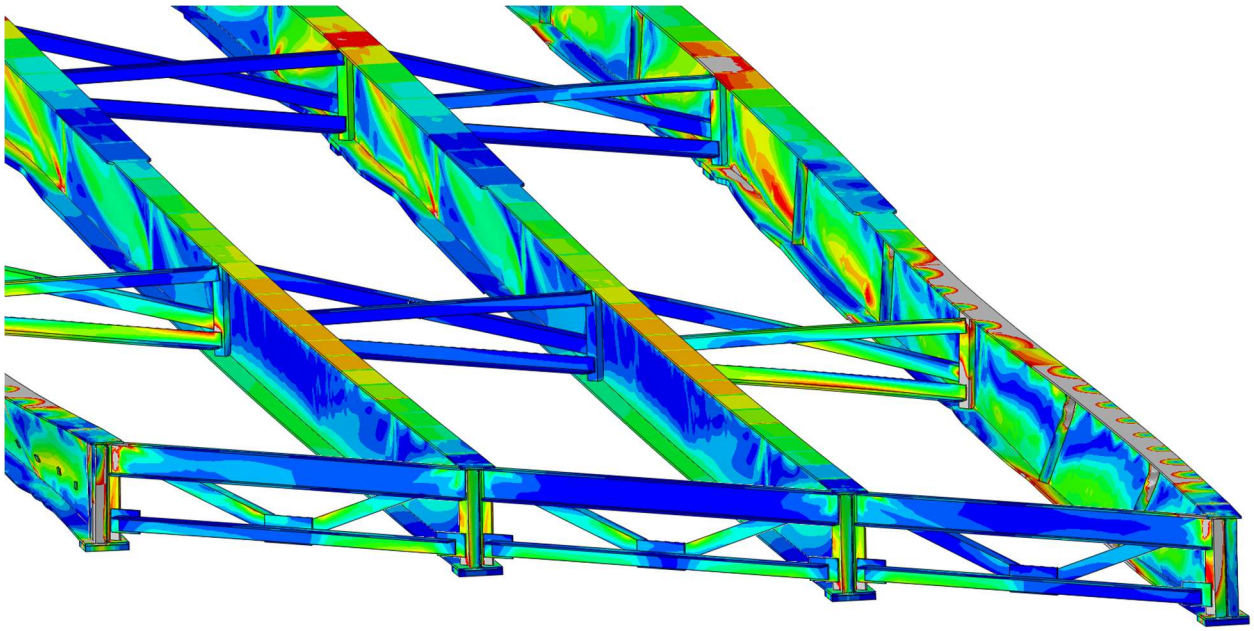

Figure A.18 Girder deformation of the 40° skewed-parallel bridge with 13.7 m [45 ft] cross-frame spacing and 12.7 mm [1/2 in] thick stiffeners

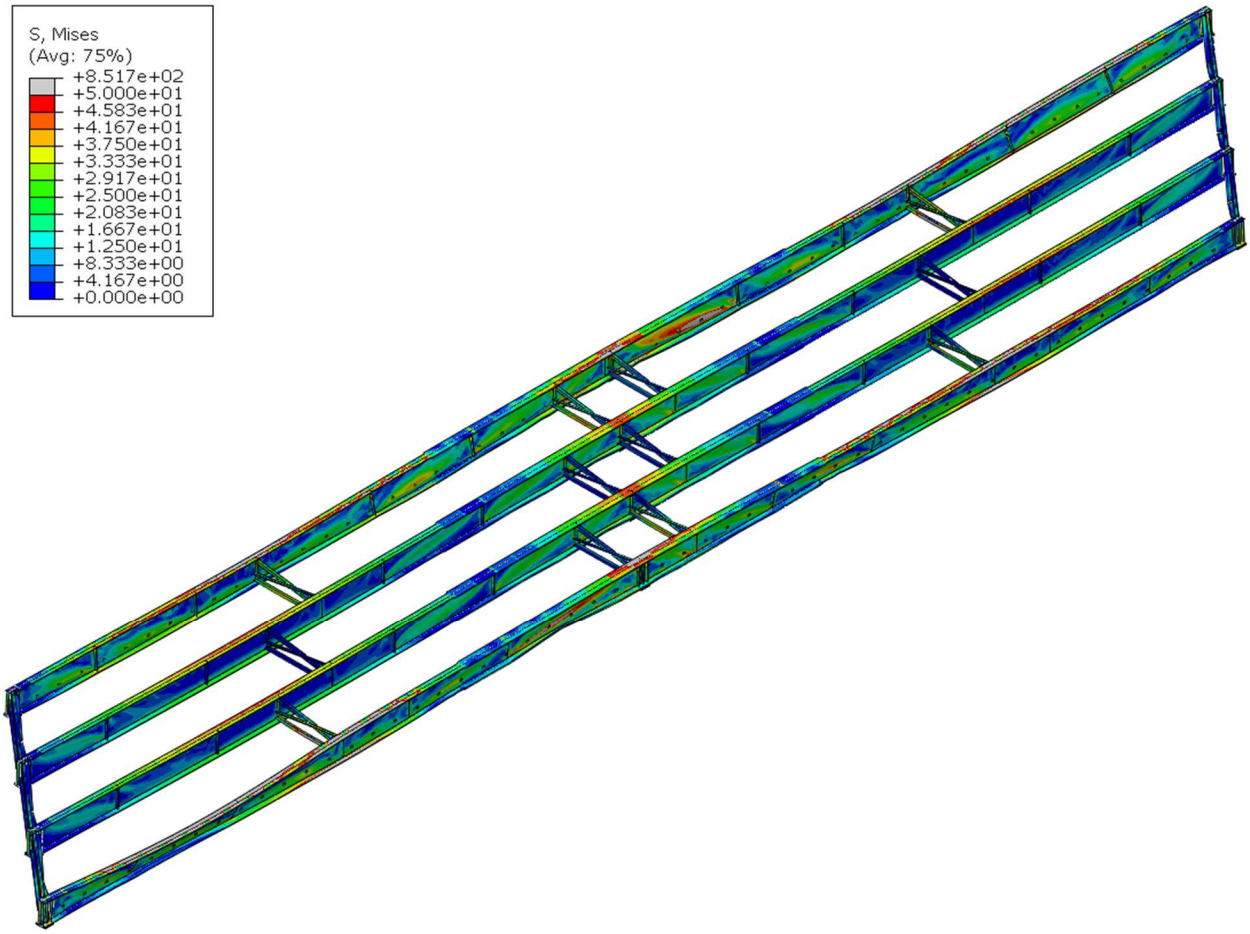

Figure A.19 Deformed shaped of the 40° skewed-staggered bridge with 13.7 m [45 ft] cross-frame spacing and 12.7 mm [1/2 in] thick stiffeners in isotropic view

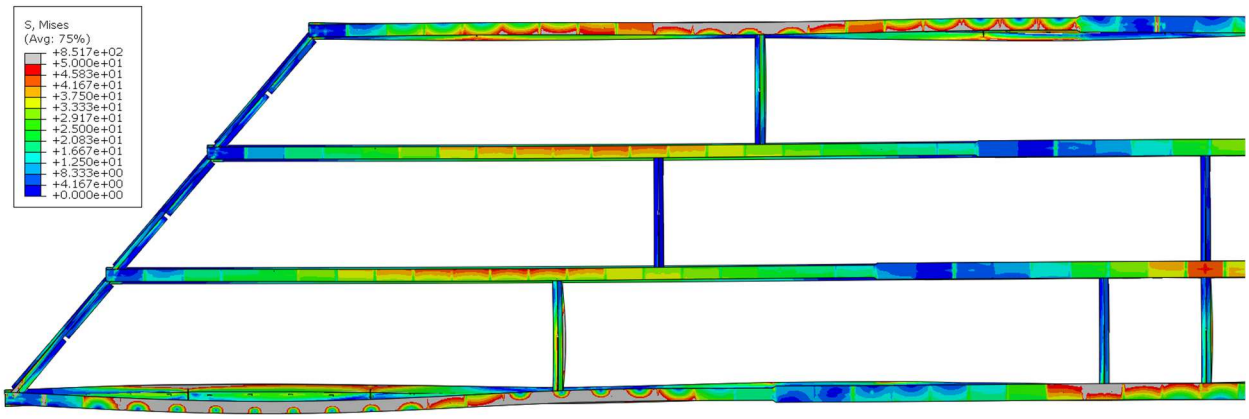

Figure A.20 Deformed shape of the 40° skewed-staggered bridge in Span 1 with 13.7 m [45 ft] cross-frame spacing and 12.7 mm [1/2 in] thick stiffeners in plan view

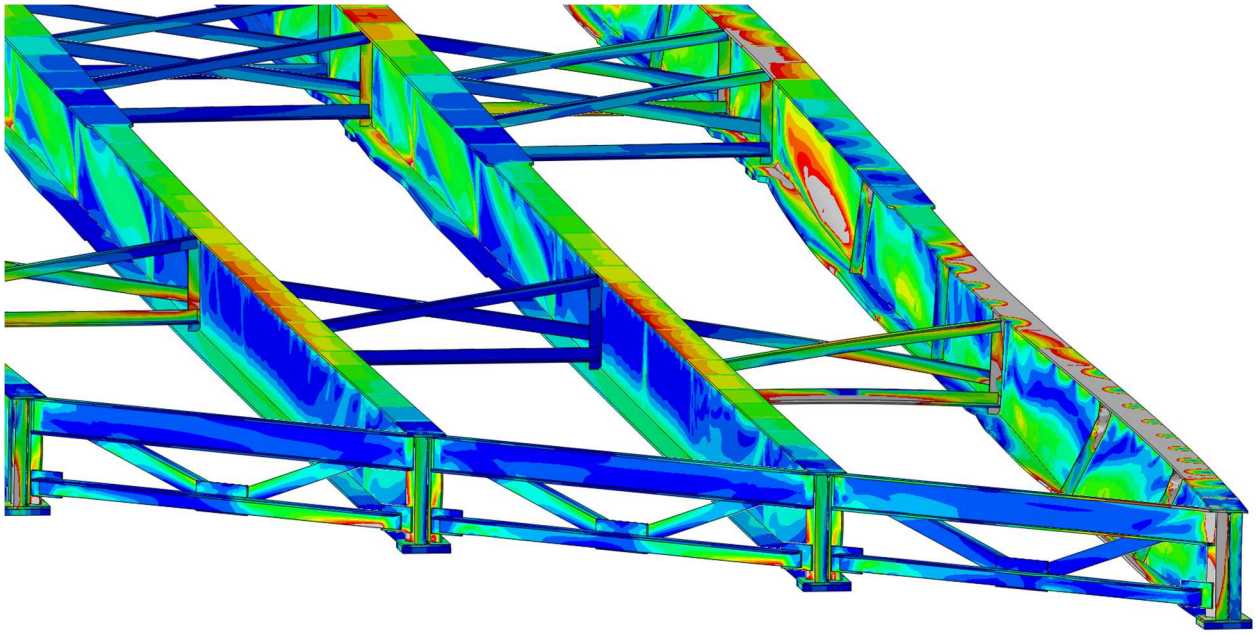

Figure A.21 Girder deformation of the 40° skewed-staggered bridge with 13.7 m [45 ft] cross-frame spacing and 12.7 mm [1/2 in] thick stiffeners

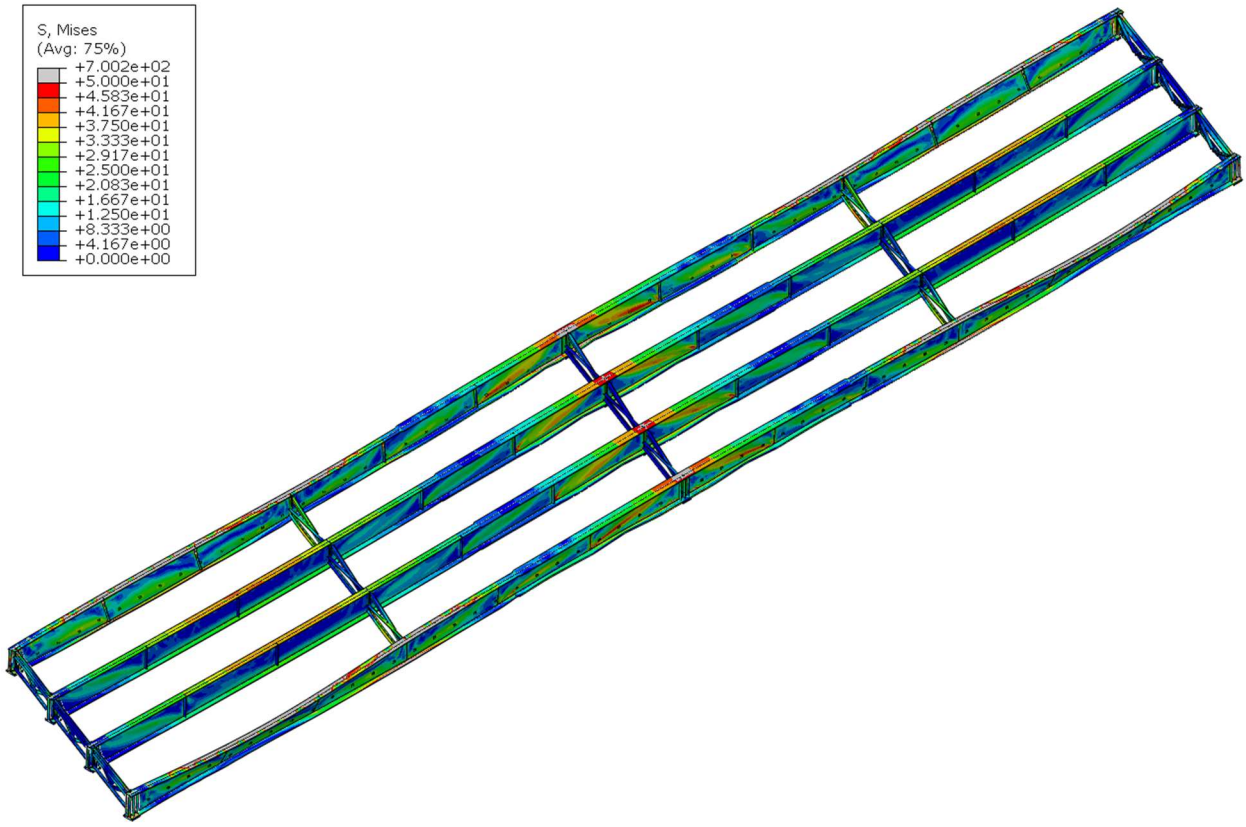

Figure A.22 Deformed shaped of the 20° skewed-parallel bridge with 13.7 m [45 ft] cross-frame spacing and 12.7 mm [1/2 in] thick stiffeners in isotropic view

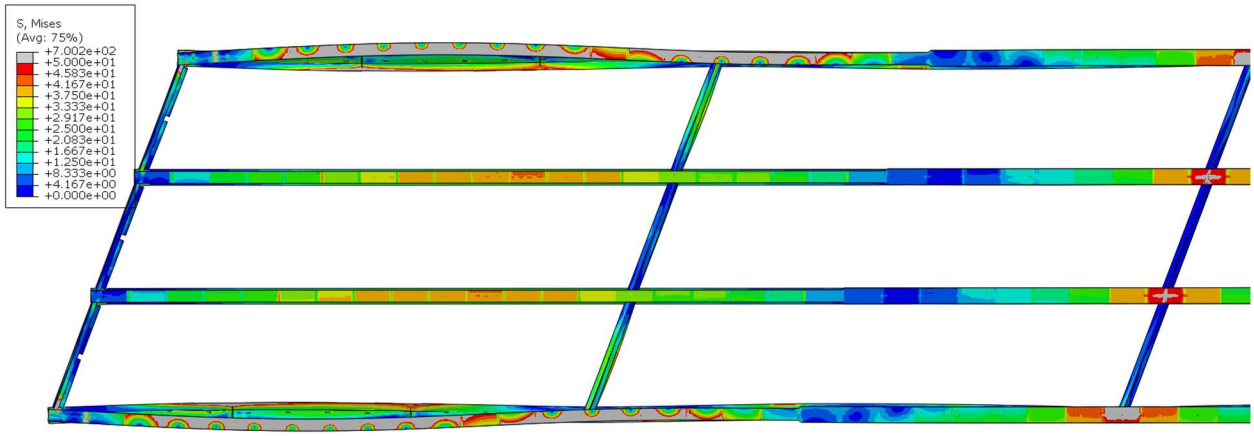

Figure A.23 Deformed shape of the 20° skewed-parallel bridge in Span 1 with 13.7 m [45 ft] cross-frame spacing and 12.7 mm [1/2 in] thick stiffeners in plan view

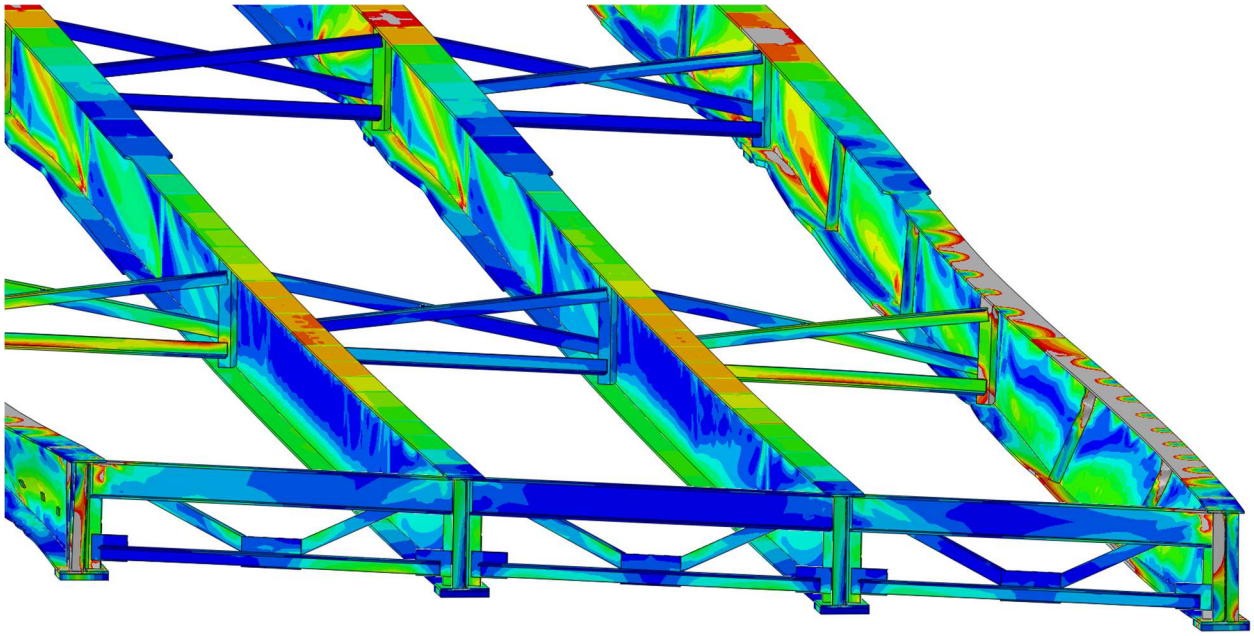

Figure A.24 Girder deformation of the 20° skewed-parallel bridge with 13.7 m [45 ft] cross-frame spacing and 12.7 mm [1/2 in] thick stiffeners

20° SKEWED-STAGGERED BRIDGE

45 FT CROSS-FRAME SPACING;

1/2" THICK STIFFENERS

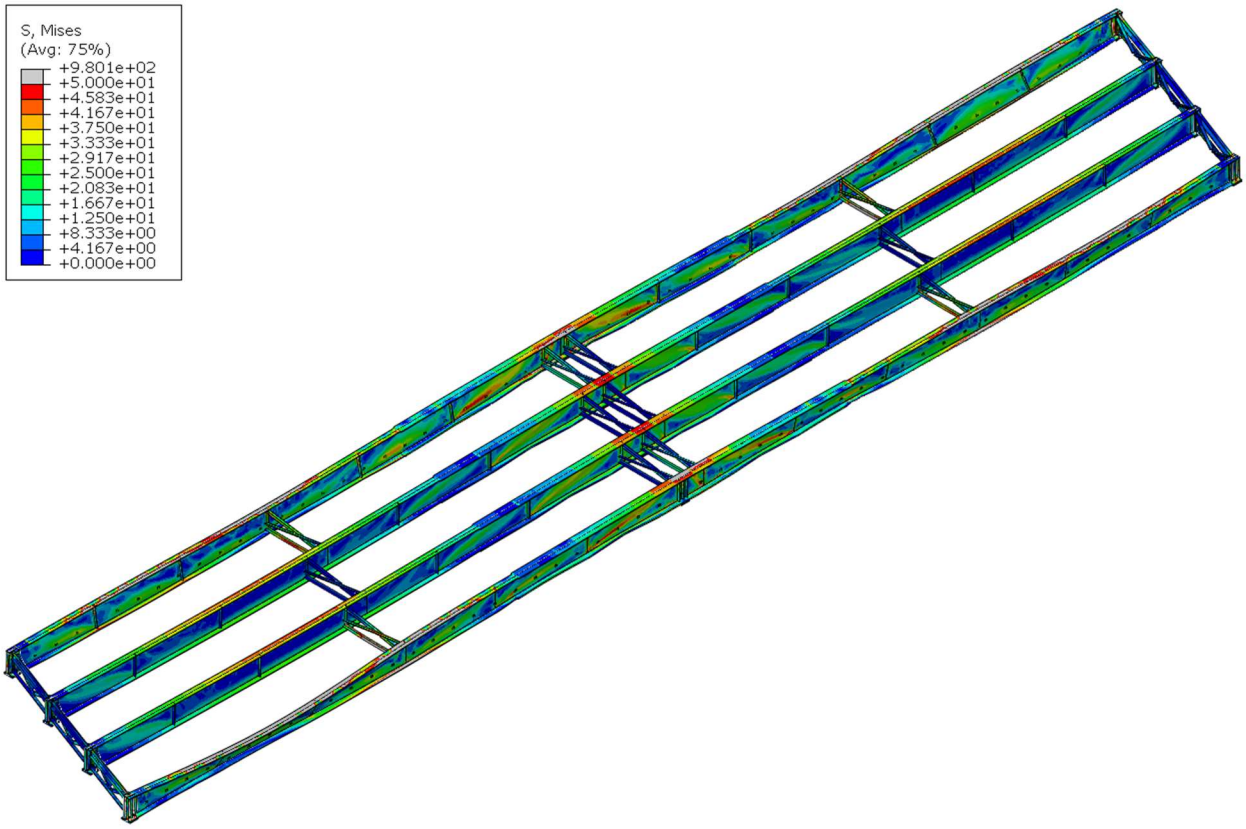

Figure A.25 Deformed shaped of the 20° skewed-staggered bridge with 13.7 m [45 ft] cross-frame spacing and 12.7 mm [1/2 in] thick stiffeners in isotropic view

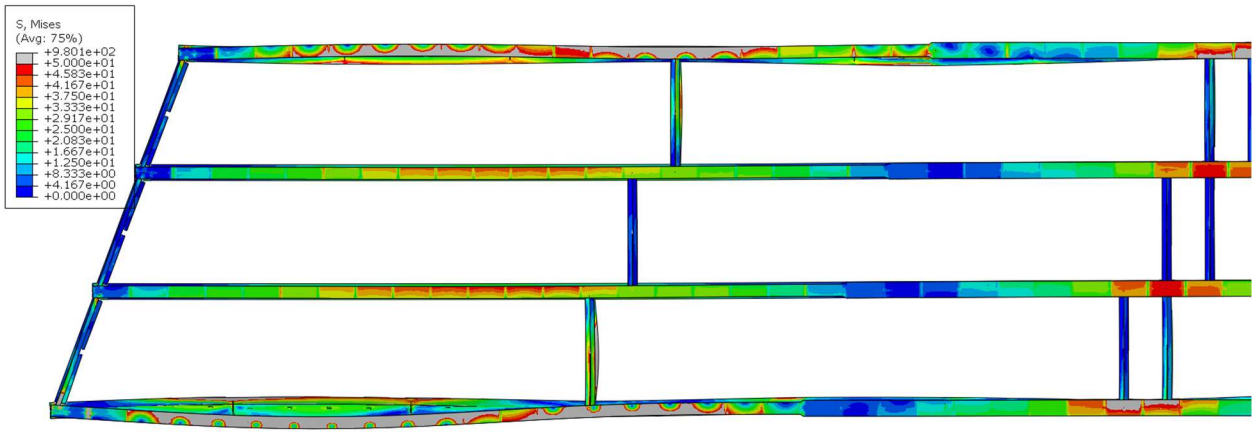

Figure A.26 Deformed shape of the 20° skewed-staggered bridge in Span 1 with 13.7 m [45 ft] cross-frame spacing and 12.7 mm [1/2 in] thick stiffeners in plan view

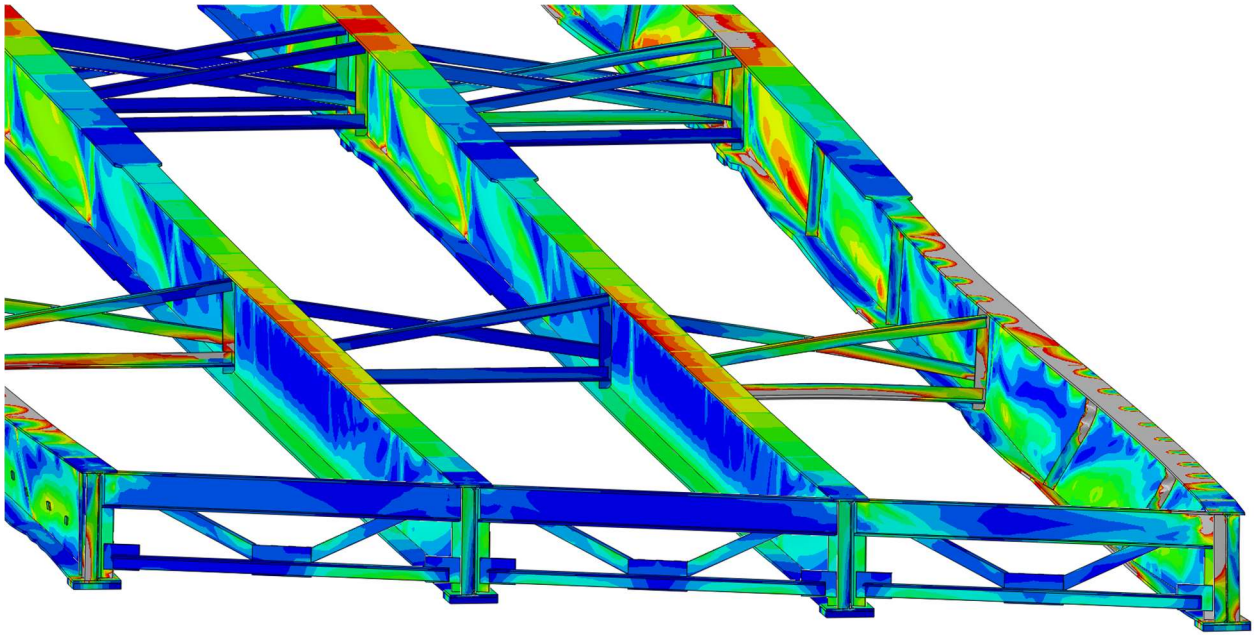

Figure A.27 Girder deformation of the 20° skewed-staggered bridge with 13.7 m [45 ft] cross-frame spacing and 12.7 mm [1/2 in] thick stiffeners

NON-SKEWED BRIDGE

45 FT CROSS-FRAME SPACING;

1/2" THICK STIFFENERS

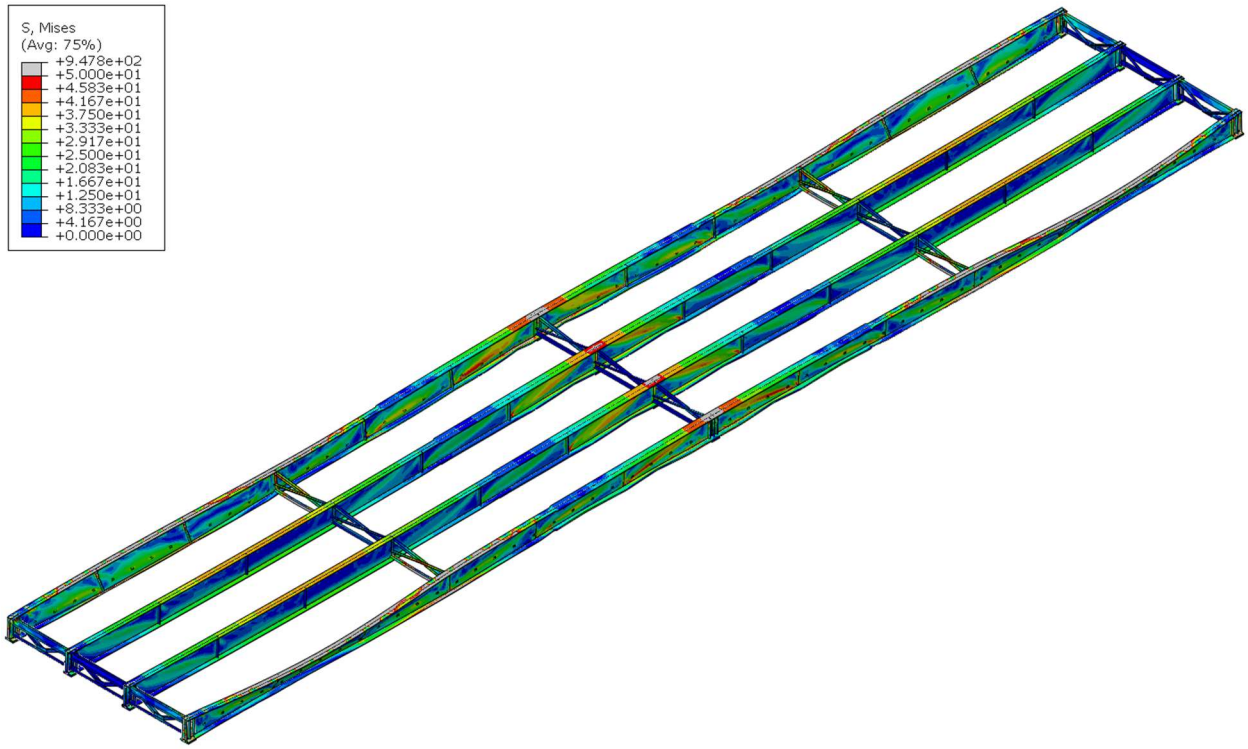

Figure A.28 Deformed shaped of the non-skewed bridge with 13.7 m [45 ft] cross-frame spacing and 12.7 mm [1/2 in] thick stiffeners in isotropic view

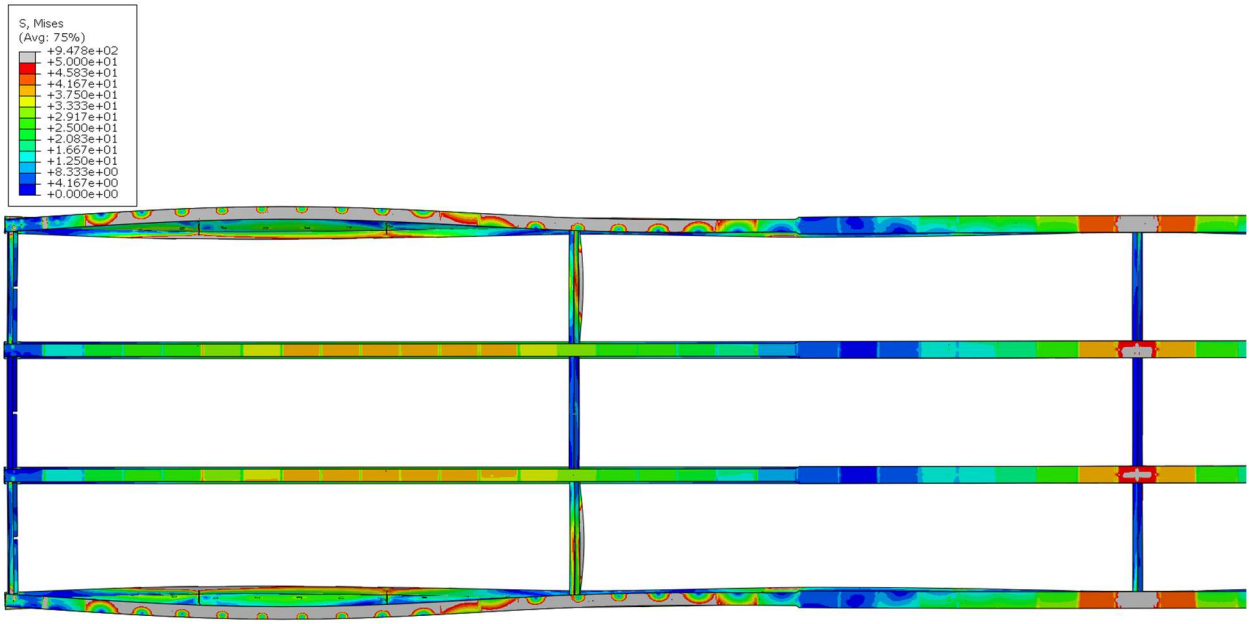

Figure A.29 Deformed shape of the non-skewed bridge in Span 1 with 13.7 m [45 ft] cross-frame spacing and 12.7 mm [1/2 in] thick stiffeners in plan view

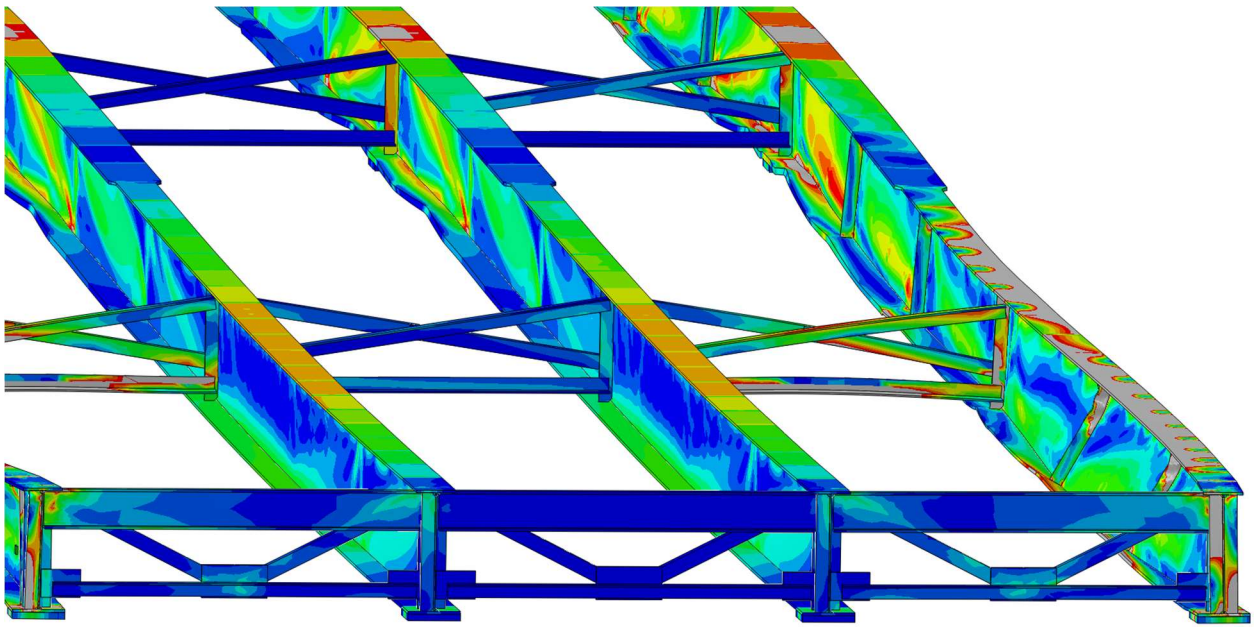

Figure A.30 Girder deformation of the non-skewed bridge with 13.7 m [45 ft] cross-frame spacing and 12.7 mm [1/2 in] thick stiffeners

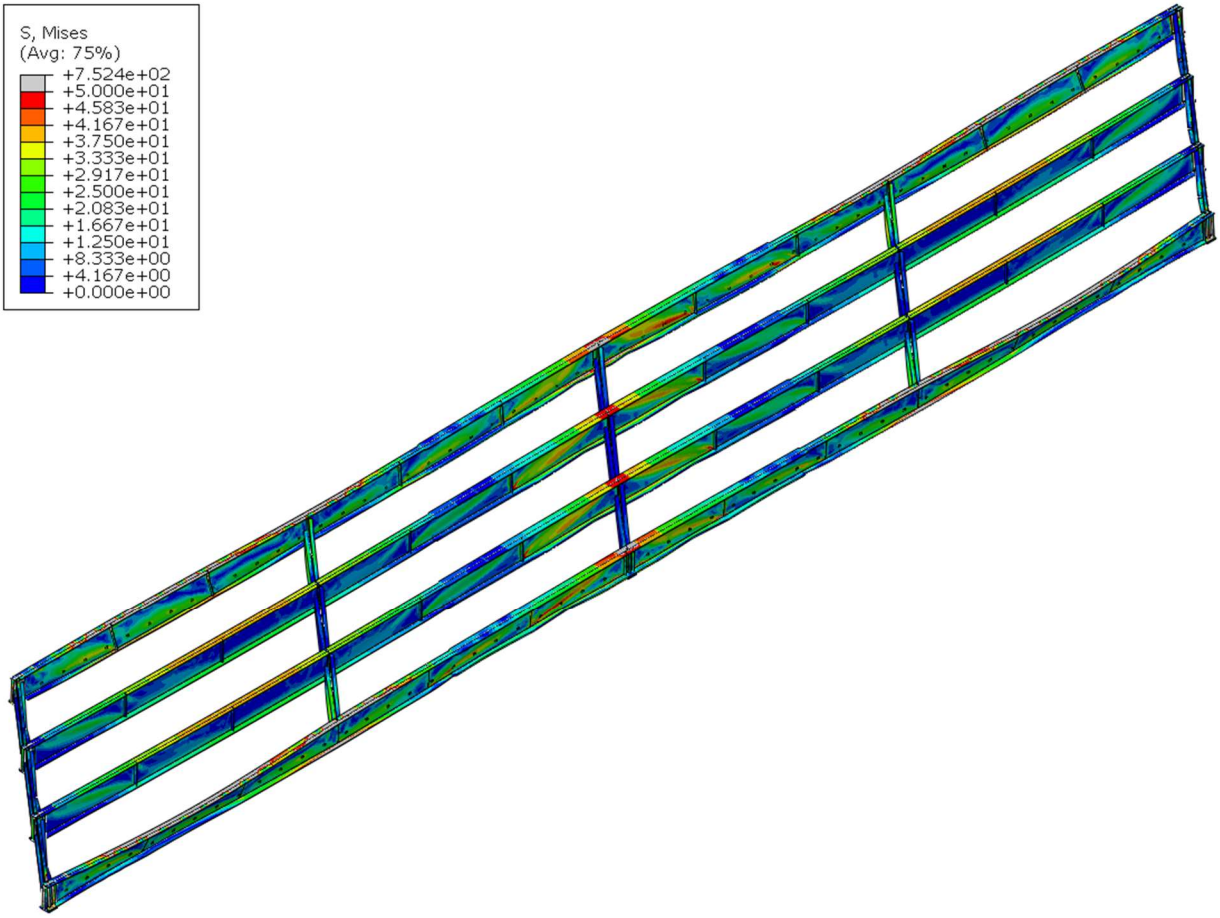

Figure A.31 Deformed shaped of the 40° skewed-parallel bridge with 13.7 m [45 ft] cross-frame spacing and 25.4 mm [1.0 in] thick stiffeners in isotropic view

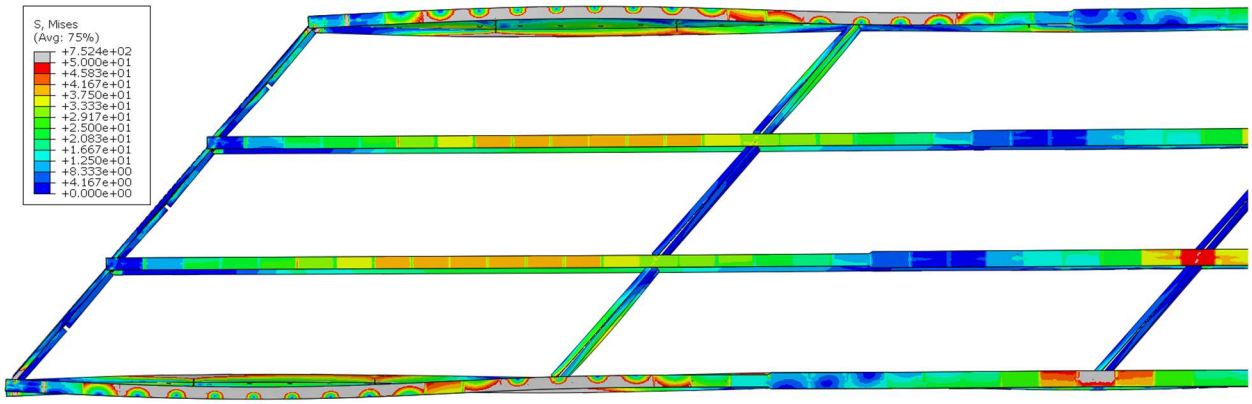

Figure A.32 Deformed shape of the 40° skewed-parallel bridge in Span 1 with 13.7 m [45 ft] cross-frame spacing and 25.4 mm [1.0 in] thick stiffeners in plan view

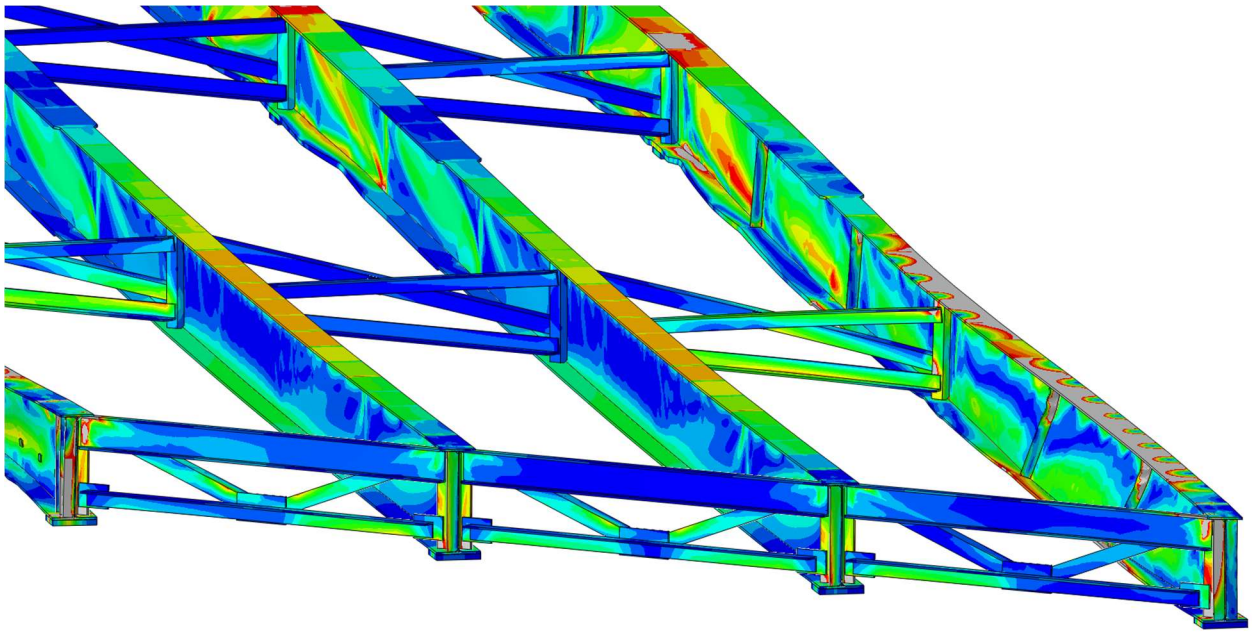

Figure A.33 Girder deformation of the 40° skewed-parallel bridge with 13.7 m [45 ft] cross-frame spacing and 25.4 mm [1.0 in] thick stiffeners

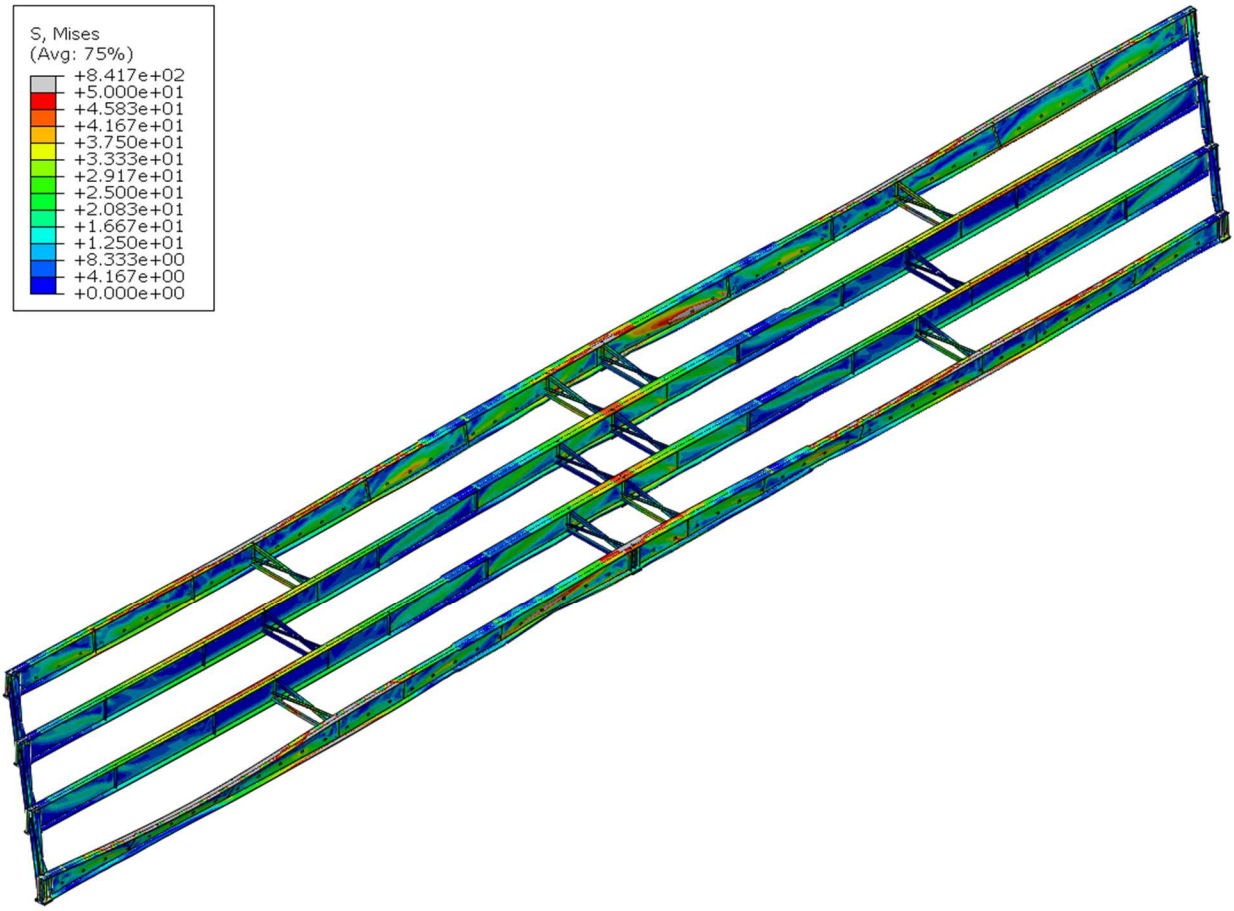

Figure A.34 Deformed shaped of the 40° skewed-staggered bridge with 13.7 m [45 ft] cross-frame spacing and 25.4 mm [1.0 in] thick stiffeners in isotropic view

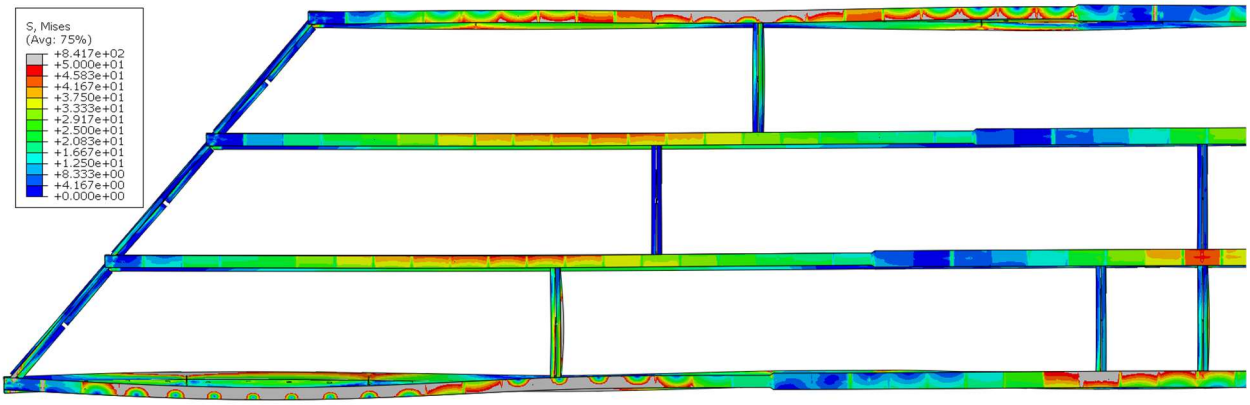

Figure A.35 Deformed shape of the 40° skewed-staggered bridge in Span 1 with 13.7 m [45 ft] cross-frame spacing and 25.4 mm [1.0 in] thick stiffeners in plan view

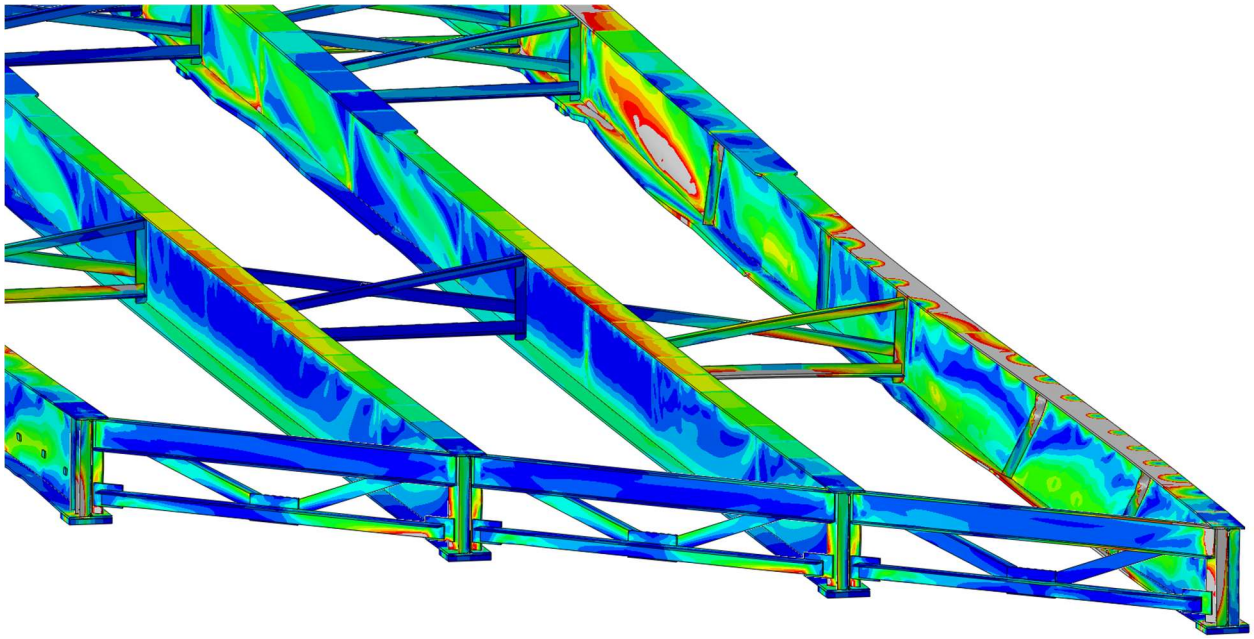

Figure A.36 Girder deformation of the 40° skewed-staggered bridge with 13.7 m [45 ft] cross-frame spacing and 25.4 mm [1.0 in] thick stiffeners

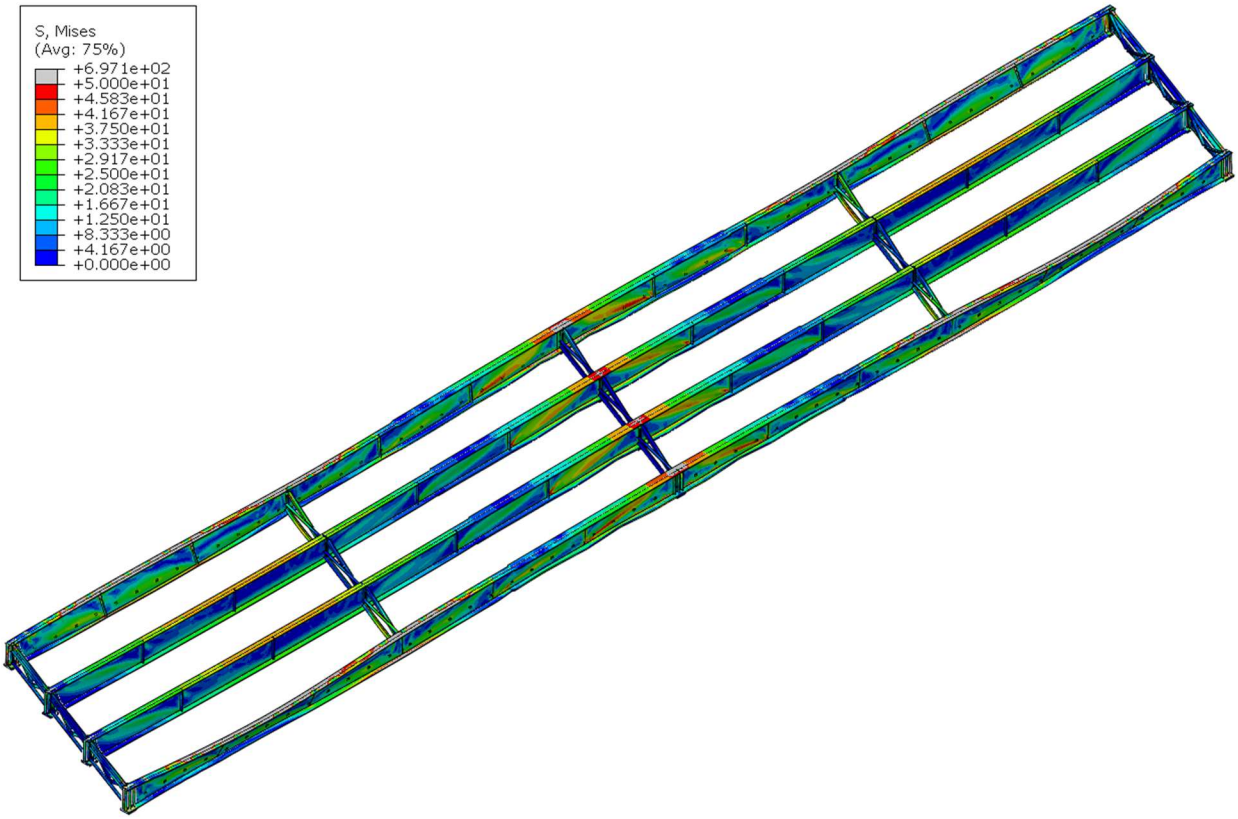

Figure A.37 Deformed shaped of the 20° skewed-parallel bridge with 13.7 m [45 ft] cross-frame spacing and 25.4 mm [1.0 in] thick stiffeners in isotropic view

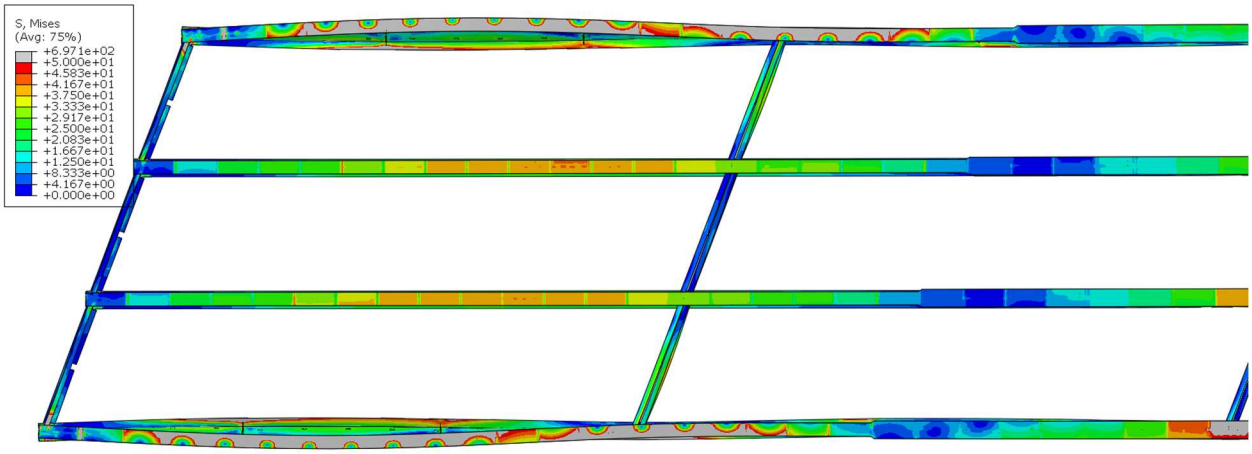

Figure A.38 Deformed shape of the 20° skewed-parallel bridge in Span 1 with 13.7 m [45 ft] cross-frame spacing and 25.4 mm [1.0 in] thick stiffeners in plan view

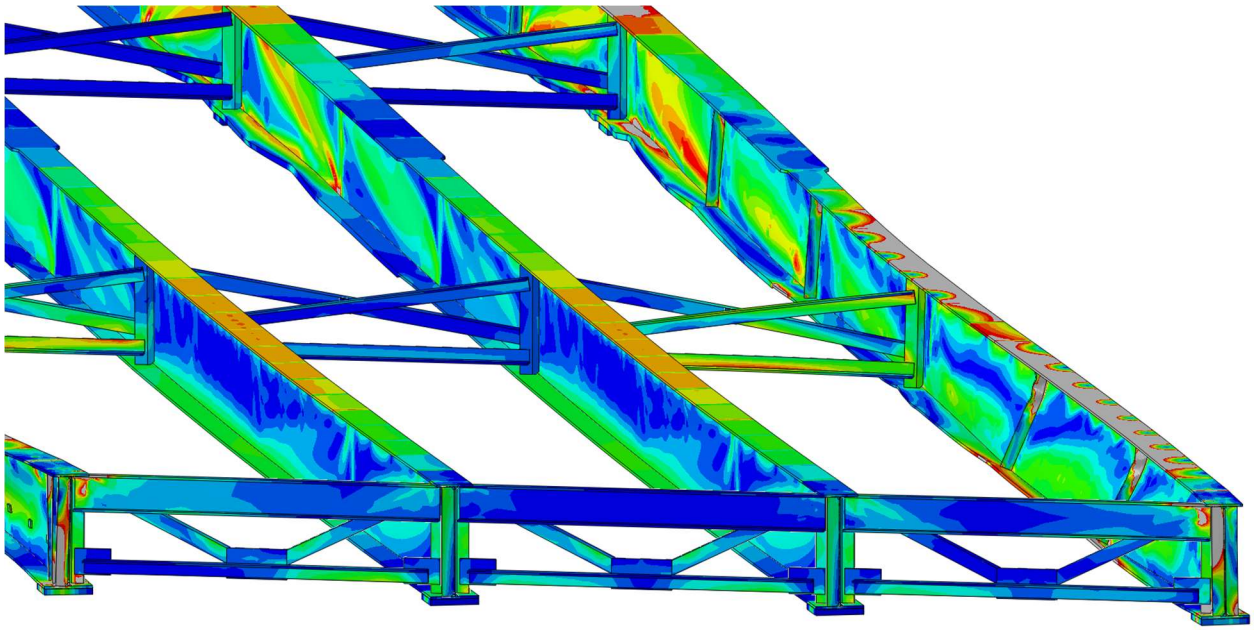

Figure A.39 Girder deformation of the 20° skewed-parallel bridge with 13.7 m [45 ft] cross-frame spacing and 25.4 mm [1.0 in] thick stiffeners

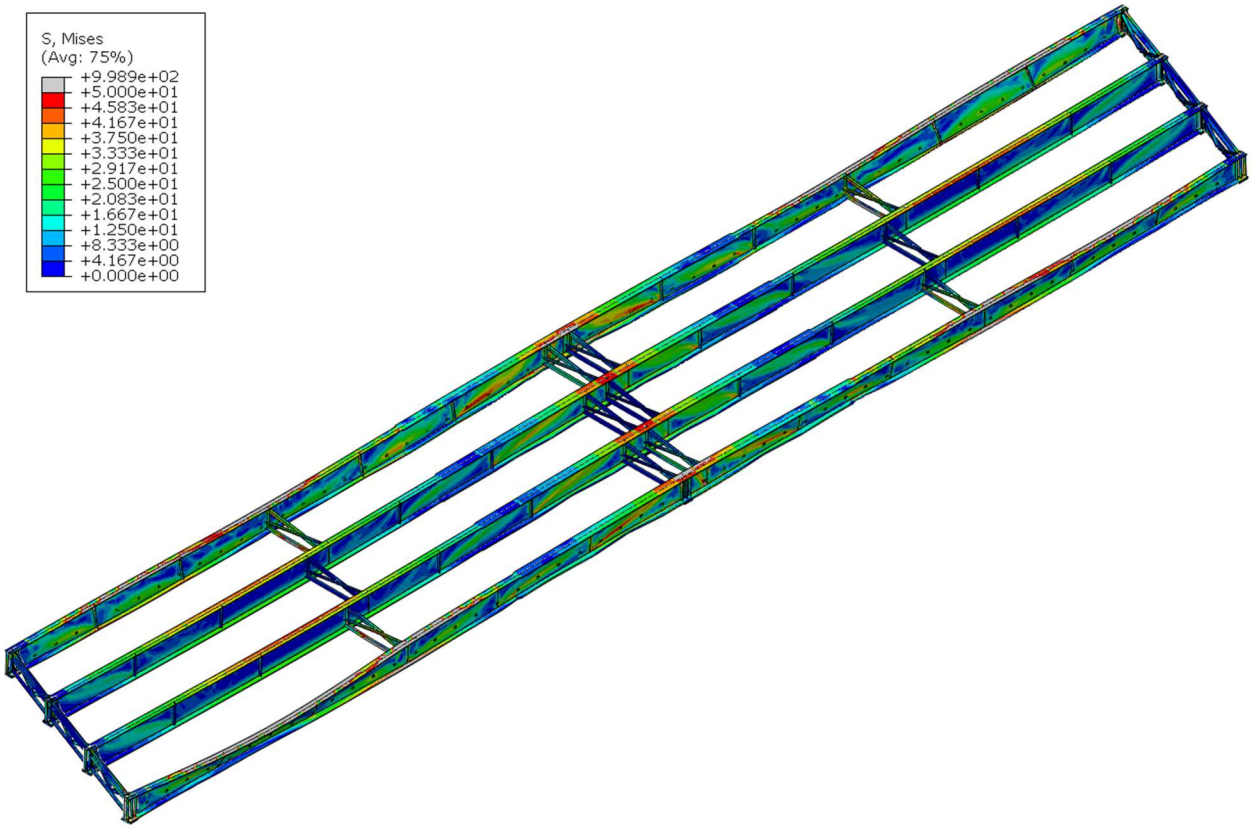

Figure A.40 Deformed shaped of the 20° skewed-staggered bridge with 13.7 m [45 ft] cross-frame spacing and 25.4 mm [1.0 in] thick stiffeners in isotropic view

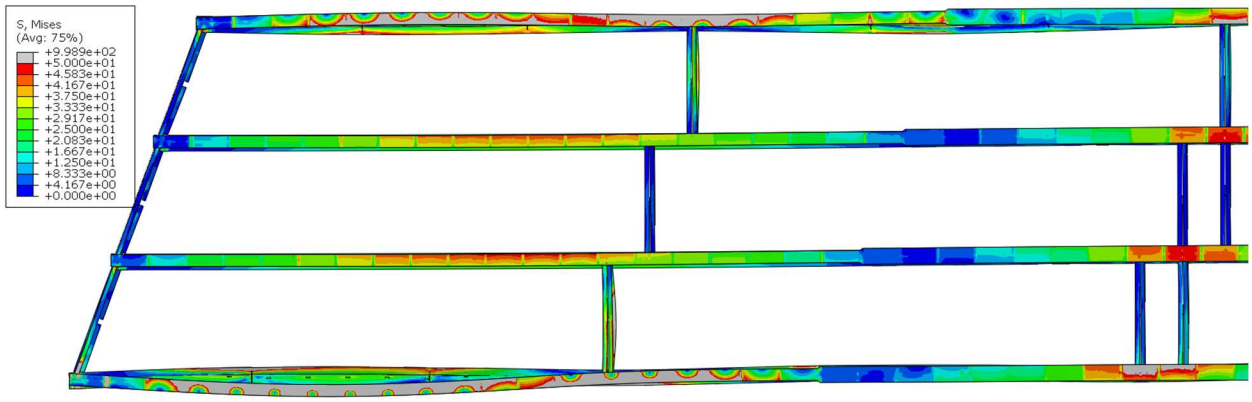

Figure A.41 Deformed shape of the 20° skewed-staggered bridge in Span 1 with 13.7 m [45 ft] cross-frame spacing and 25.4 mm [1.0 in] thick stiffeners in plan view

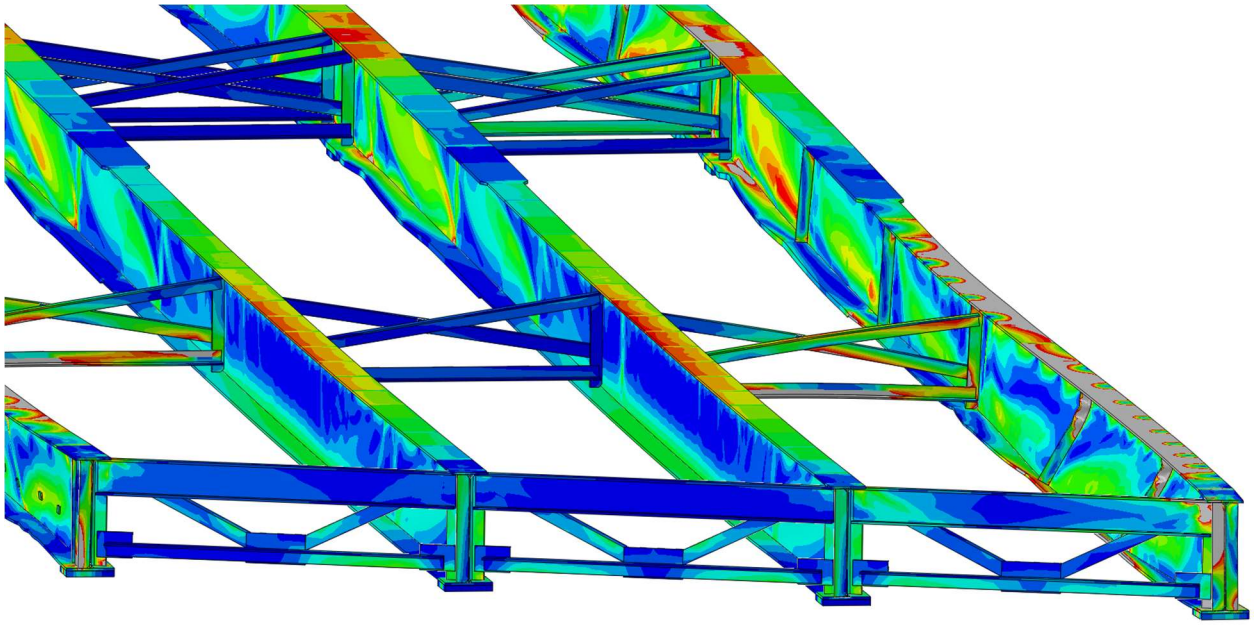

Figure A.42 Girder deformation of the 20° skewed-staggered bridge with 13.7 m [45 ft] cross-frame spacing and 25.4 mm [1.0 in] thick stiffeners

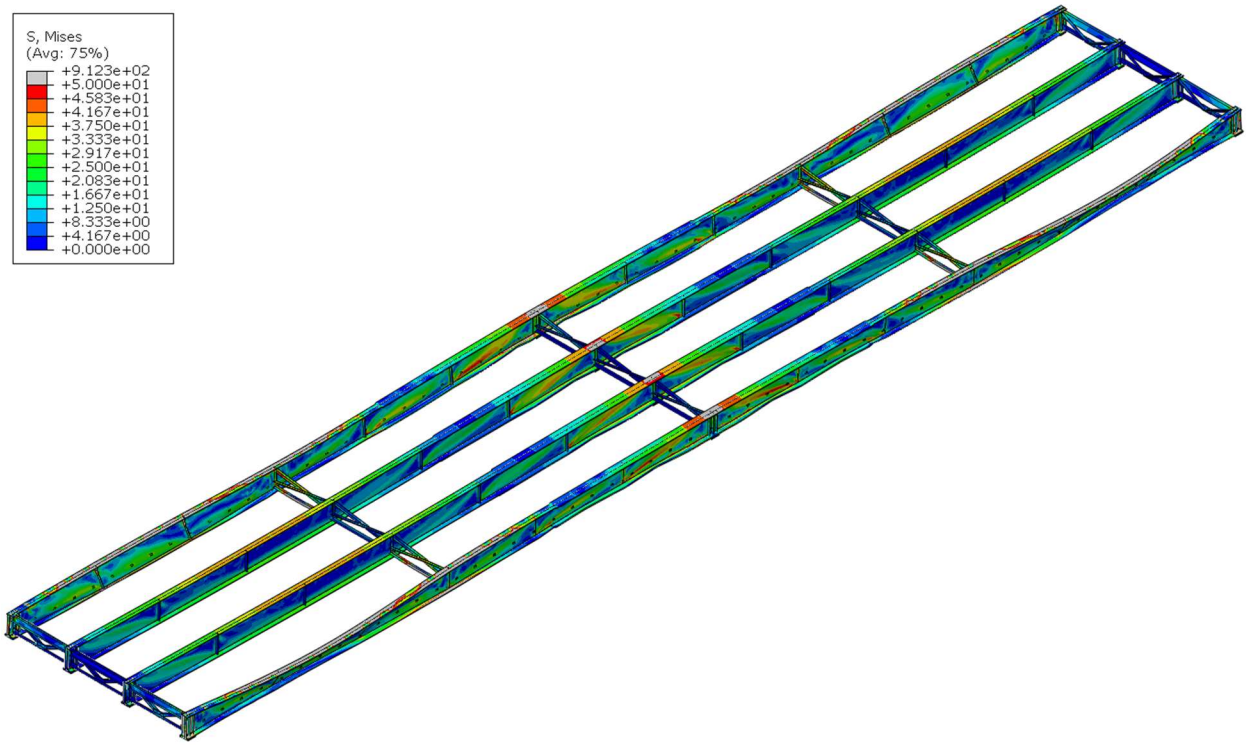

Figure A.43 Deformed shaped of the non-skewed bridge with 13.7 m [45 ft] cross-frame spacing and 25.4 mm [1.0 in] thick stiffeners in isotropic view

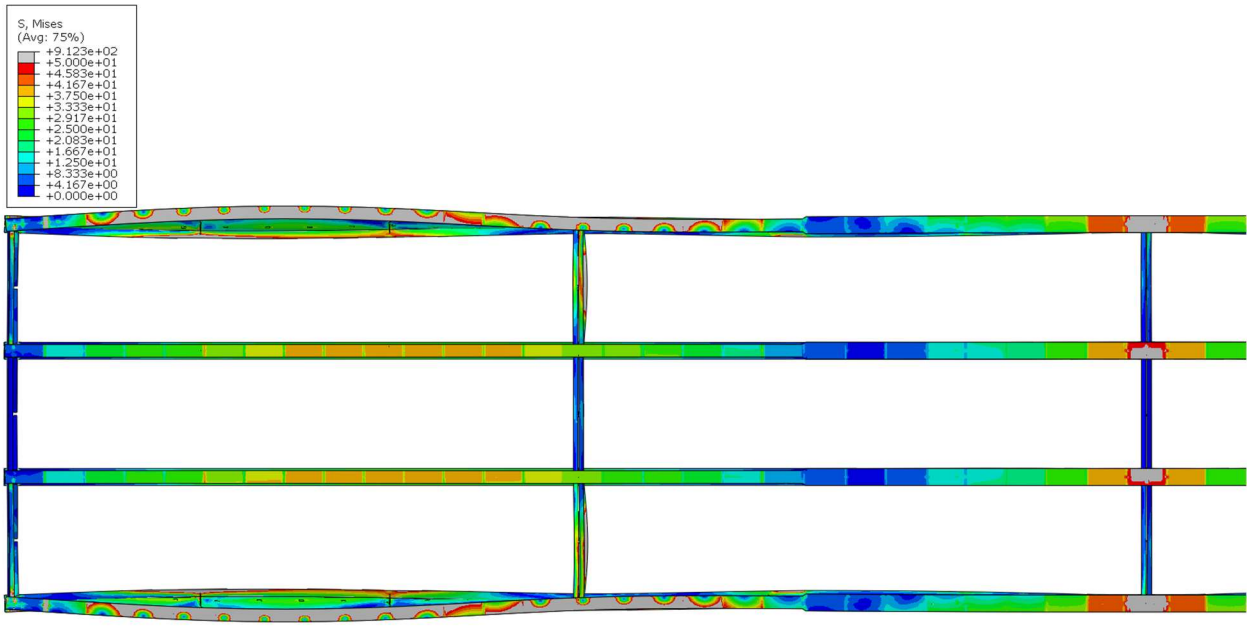

Figure A.44 Deformed shape of the non-skewed bridge in Span 1 with 13.7 m [45 ft] cross-frame spacing and 25.4 mm [1.0 in] thick stiffeners in plan view

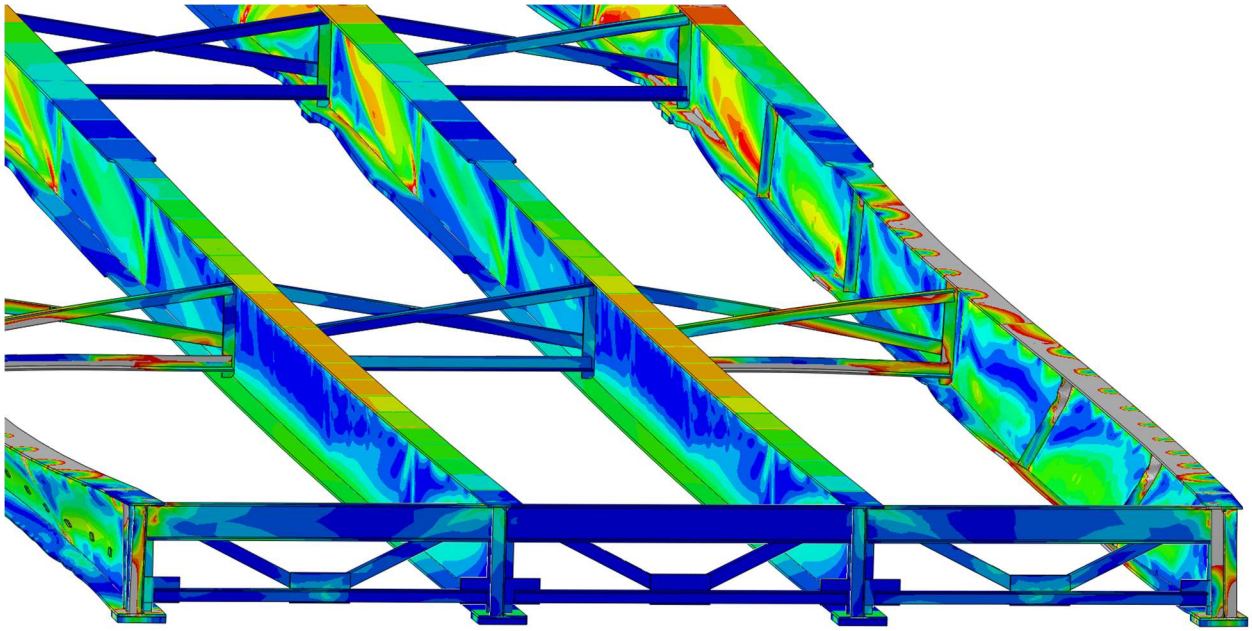

Figure A.45 Girder deformation of the non-skewed bridge with 13.7 m [45 ft] cross-frame spacing and 25.4 mm [1.0 in] thick stiffeners

40° SKEWED-PARALLEL BRIDGE

45 FT CROSS-FRAME SPACING;

HALF-PIPE STIFFENERS

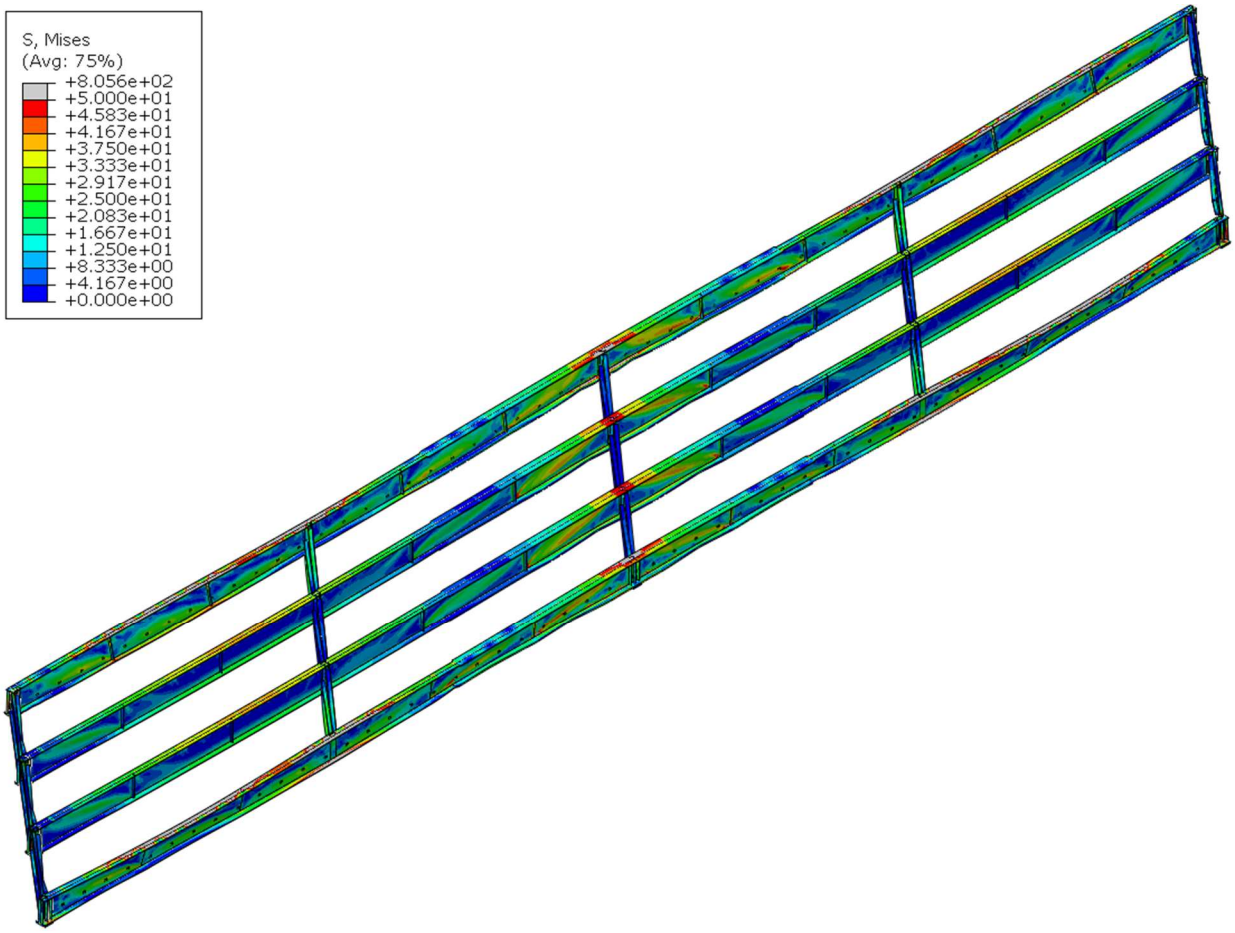

Figure A.46 Deformed shaped of the 40° skewed-parallel bridge with 13.7 m [45 ft] cross-frame spacing and half-pipe connection in isotropic view

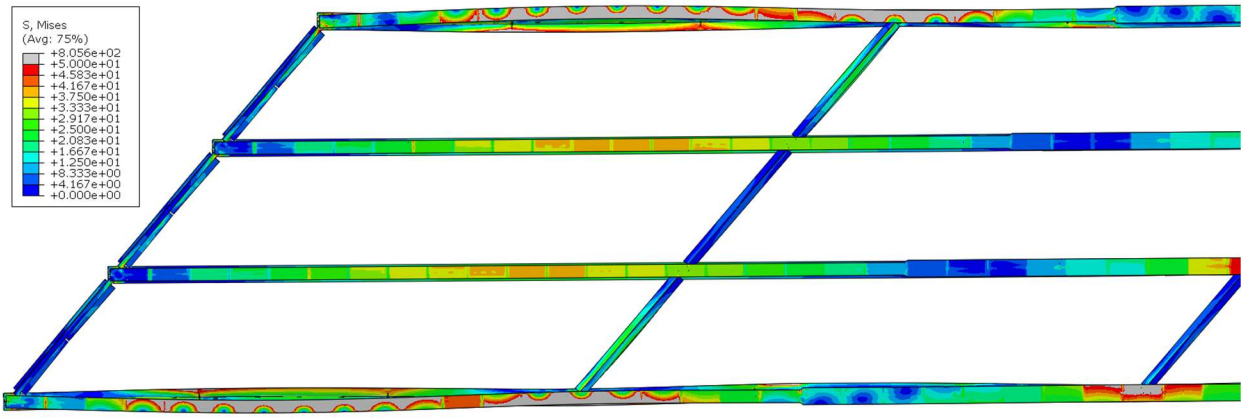

Figure A.47 Deformed shape of the 40° skewed-parallel bridge in Span 1 with 13.7 m [45 ft] cross-frame spacing and half-pipe connection in plan view

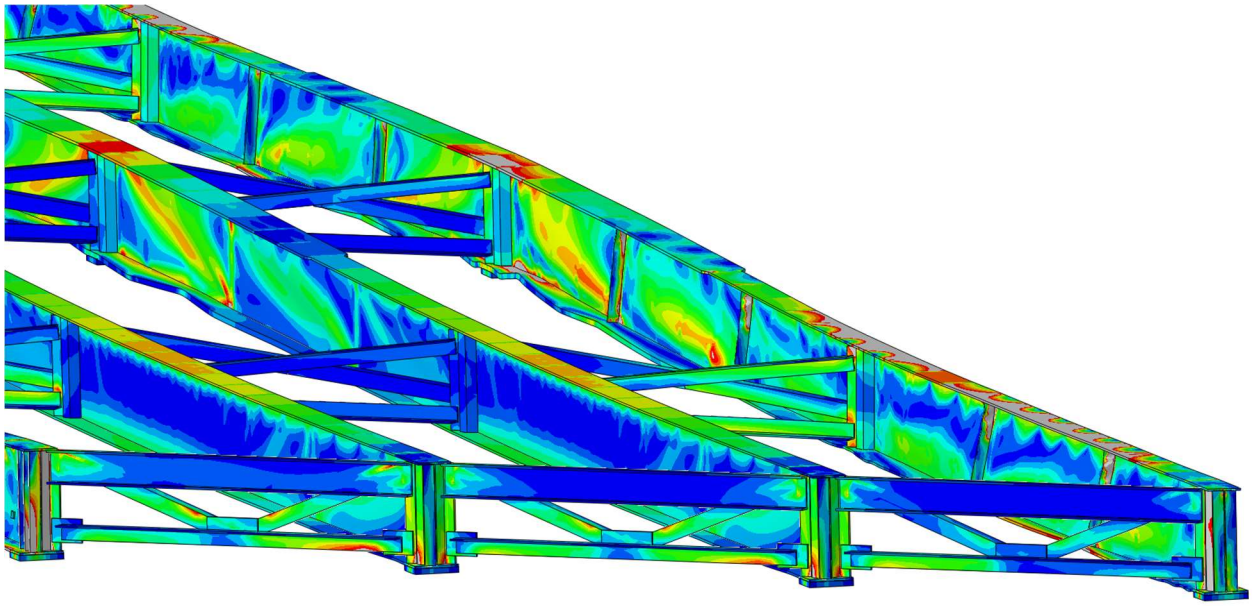

Figure A.48 Girder deformation of the 40° skewed-parallel bridge with 13.7 m [45 ft] cross-frame spacing and half-pipe connection

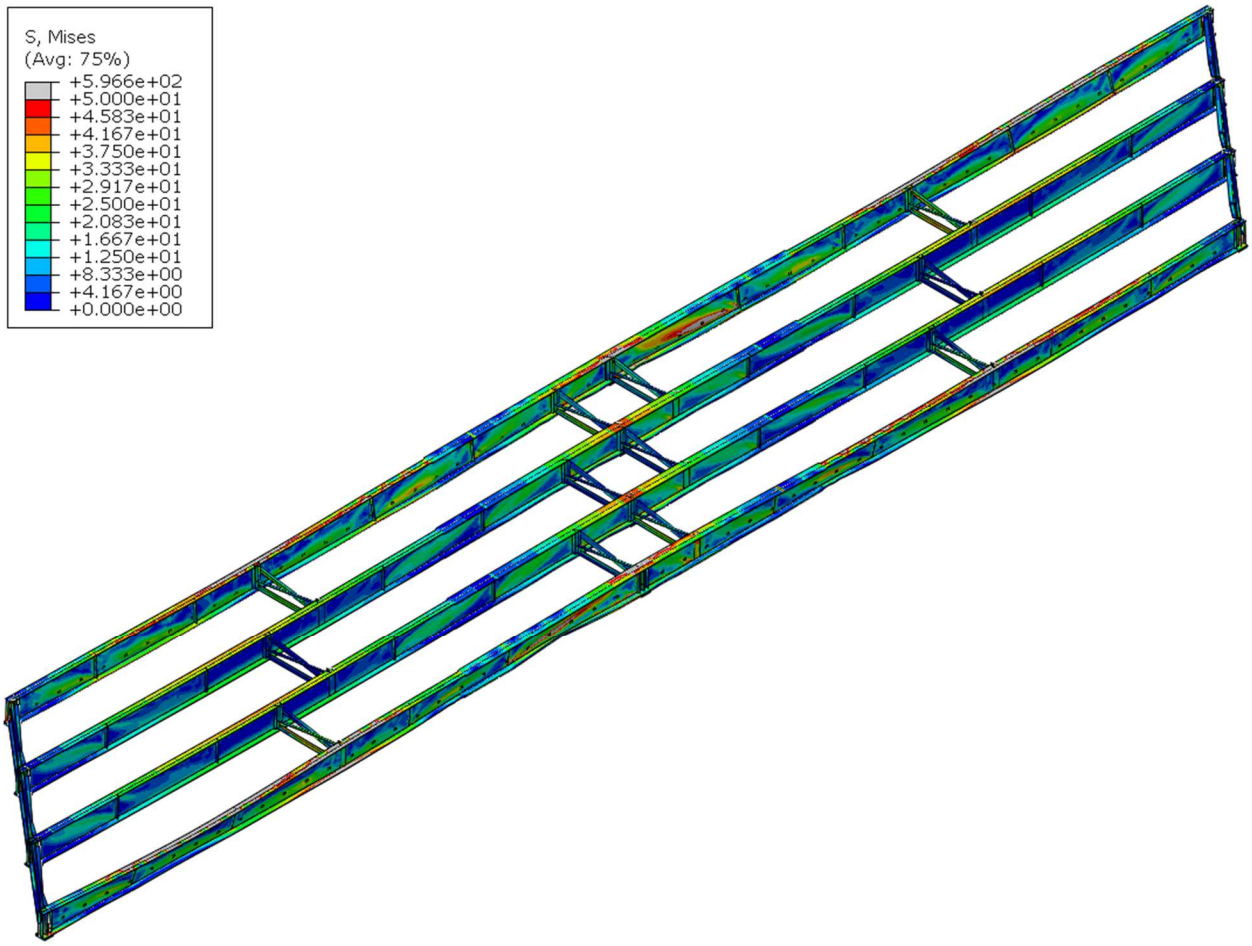

Figure A.49 Deformed shaped of the 40° skewed-staggered bridge with 13.7 m [45 ft] cross-frame spacing and half-pipe connection in isotropic view

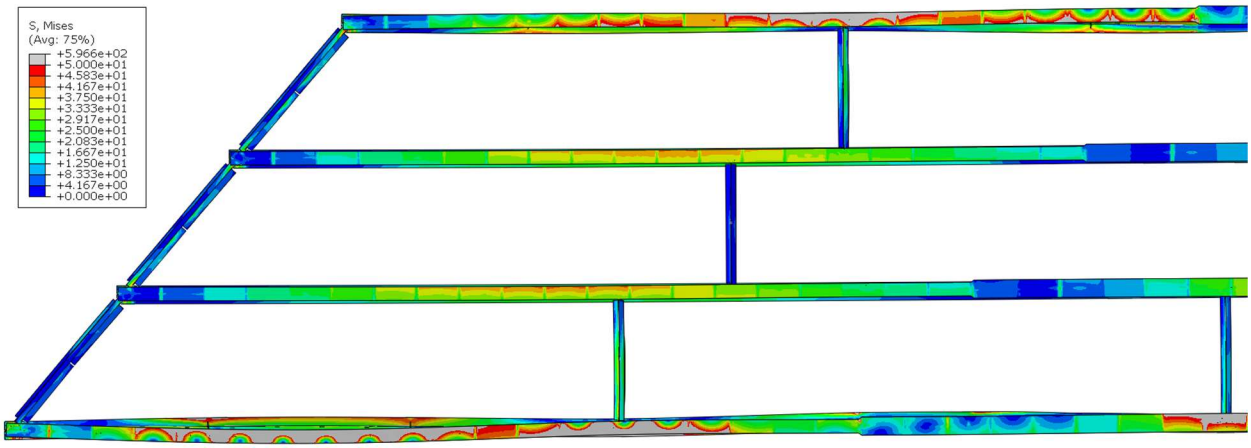

Figure A.50 Deformed shape of the 40° skewed-staggered bridge in Span 1 with 13.7 m [45 ft] cross-frame spacing and half-pipe connection in plan view

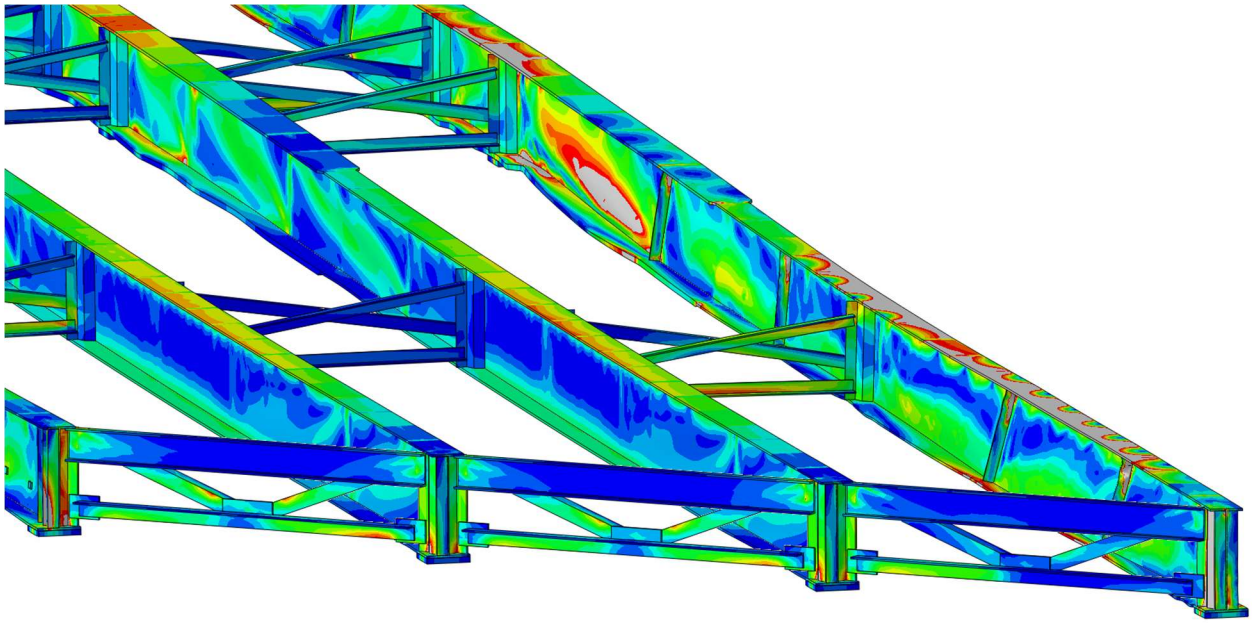

Figure A.51 Girder deformation of the 40° skewed-staggered bridge with 13.7 m [45 ft] cross-frame spacing and half-pipe connection

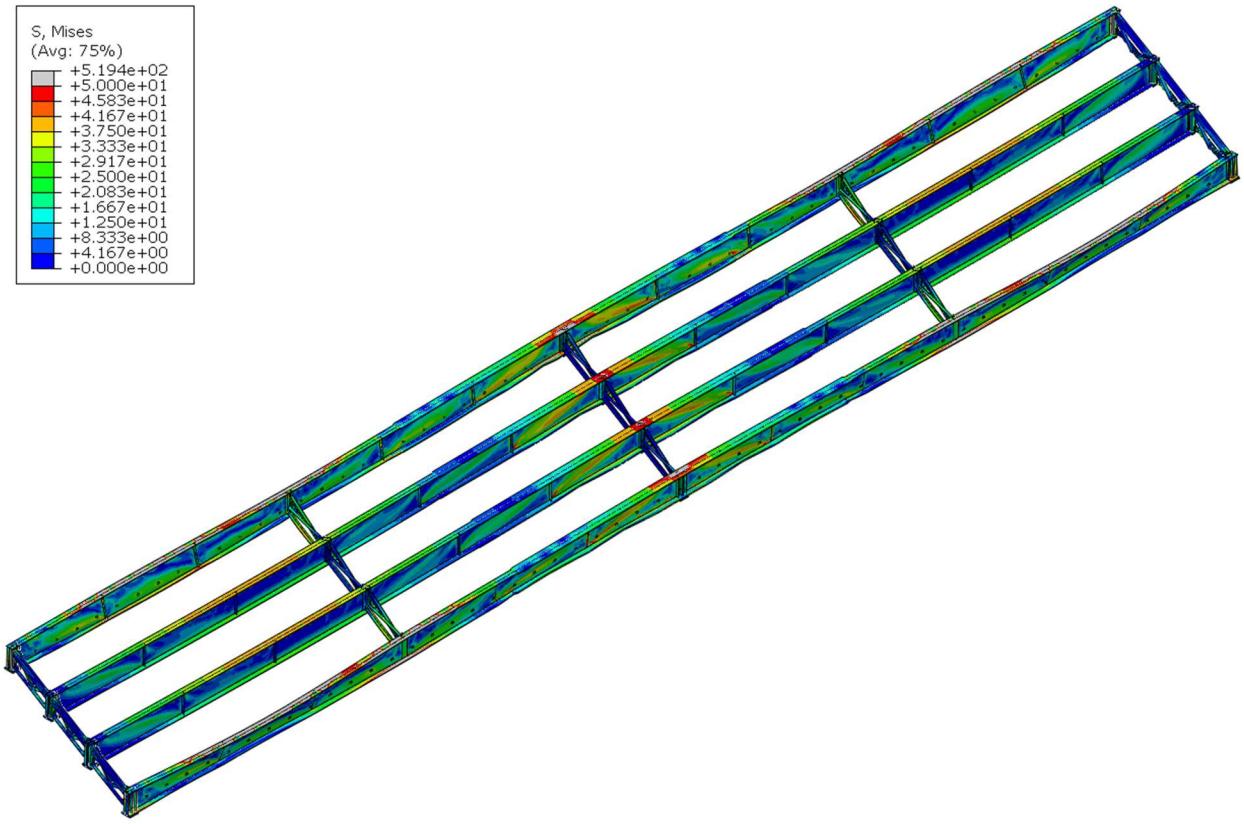

Figure A.52 Deformed shaped of the 20° skewed-parallel bridge with 13.7 m [45 ft] cross-frame spacing and half-pipe connection in isotropic view

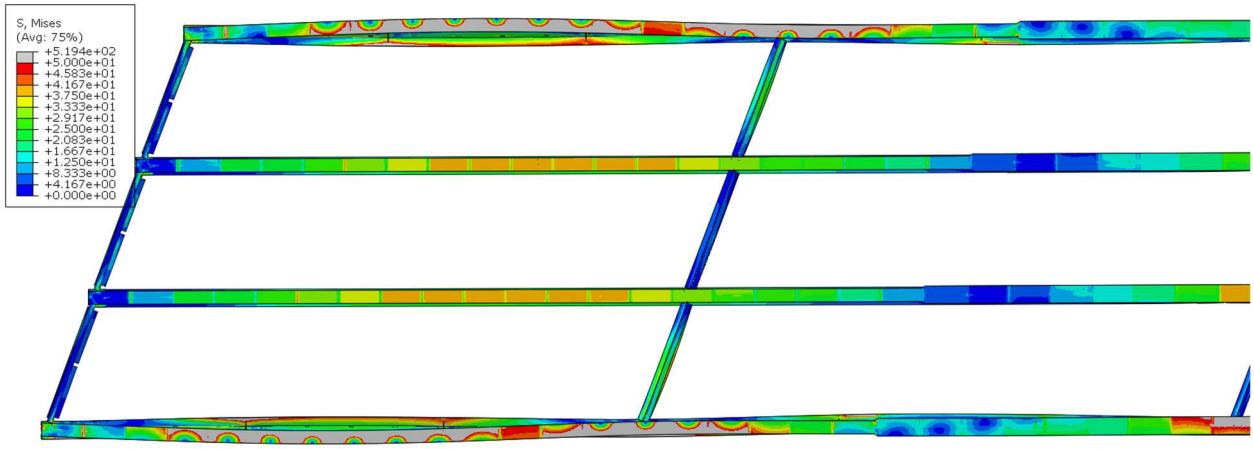

Figure A.53 Deformed shape of the 20° skewed-parallel bridge in Span 1 with 13.7 m [45 ft] cross-frame spacing and half-pipe connection in plan view

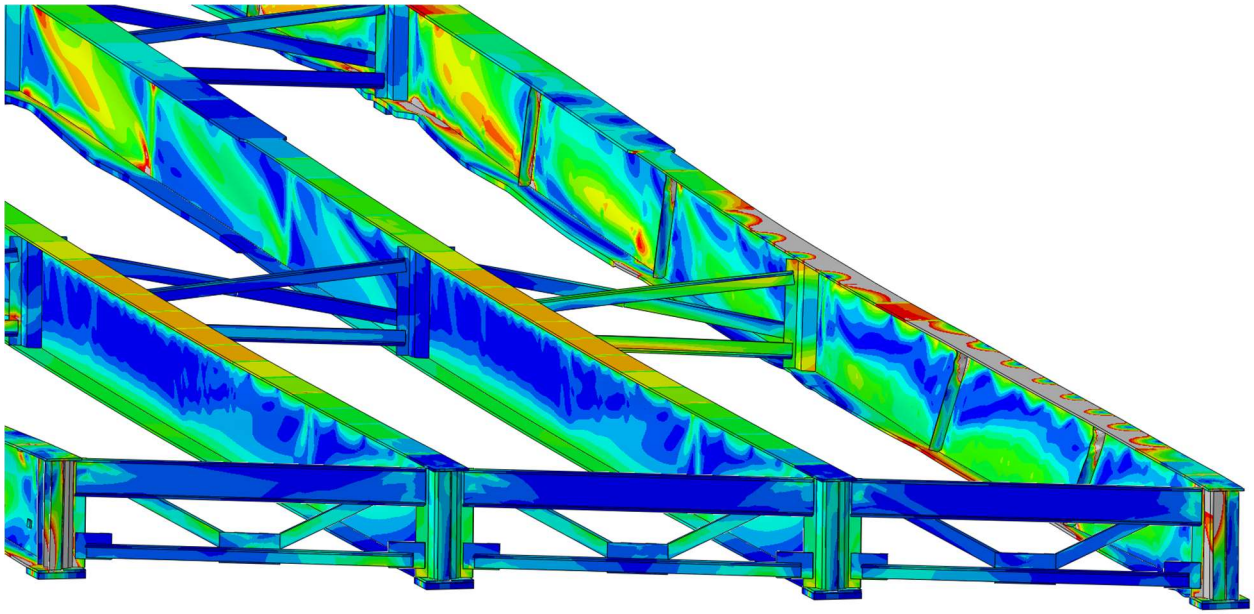

Figure A.54 Girder deformation of the 20° skewed-parallel bridge with 13.7 m [45 ft] cross-frame spacing and half-pipe connection

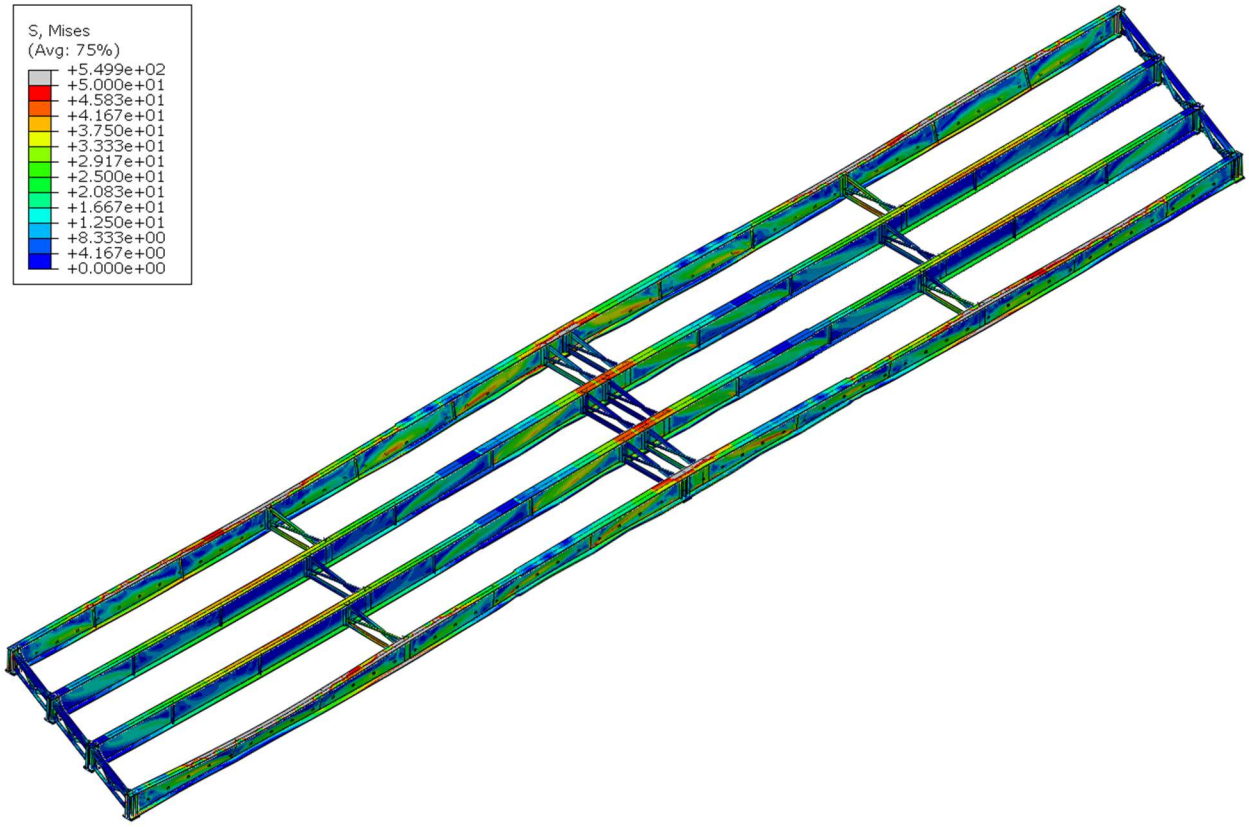

Figure A.55 Deformed shaped of the 20° skewed-staggered bridge with 13.7 m [45 ft] cross-frame spacing and half-pipe connection in isotropic view

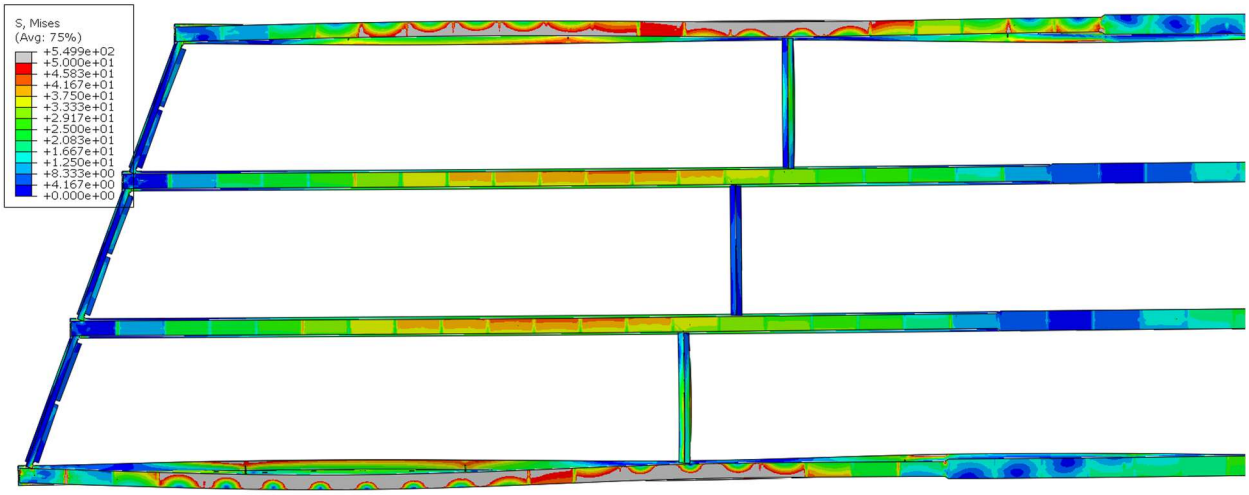

Figure A.56 Deformed shape of the 20° skewed-staggered bridge in Span 1 with 13.7 m [45 ft] cross-frame spacing and half-pipe connection in plan view

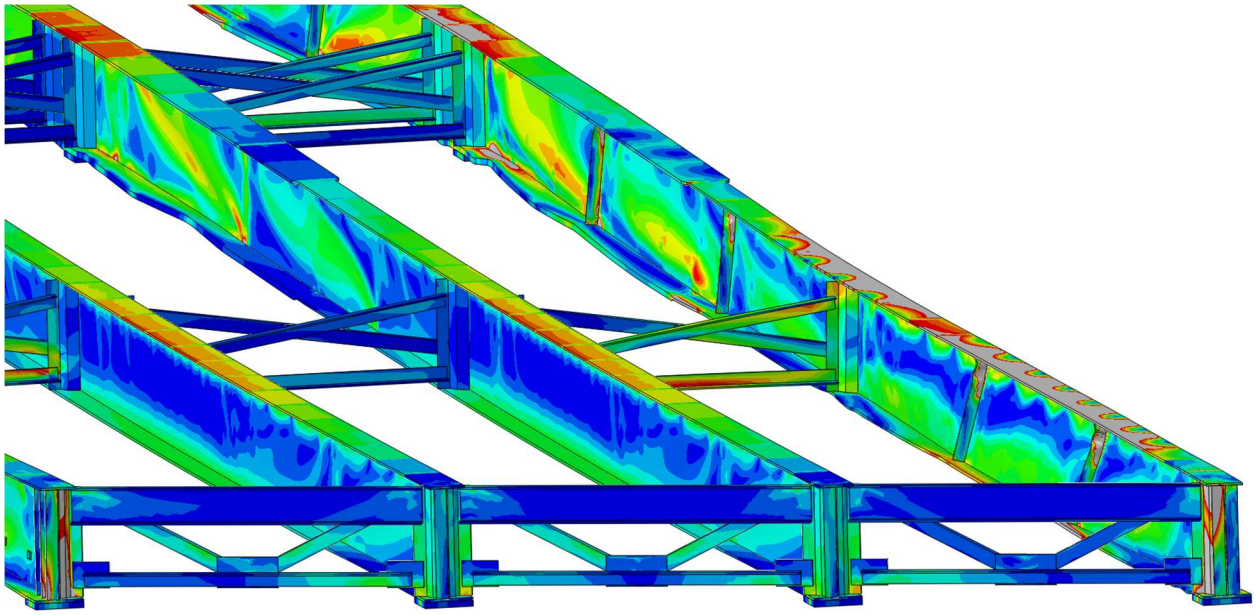

Figure A.57 Girder deformation of the 20° skewed-staggered bridge with 13.7 m [45 ft] cross-frame spacing and half-pipe connection

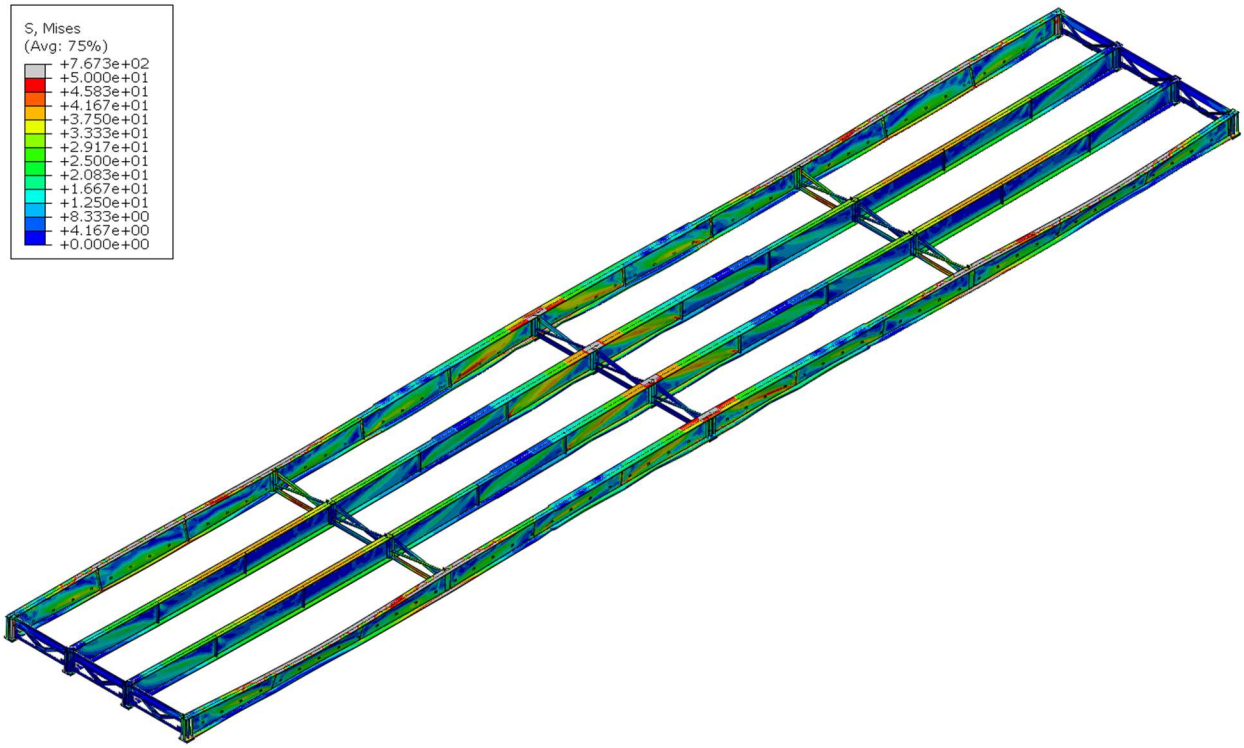

Figure A.58 Deformed shaped of the non-skewed bridge with 13.7 m [45 ft] cross-frame spacing and half-pipe connection in isotropic view

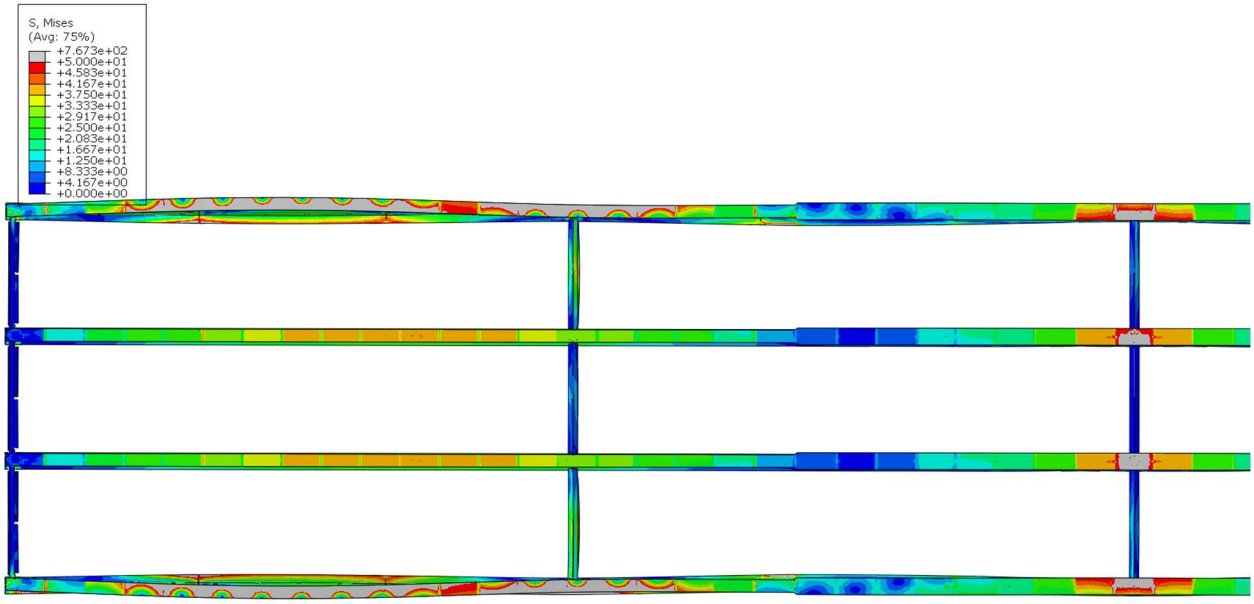

Figure A.59 Deformed shape of the non-skewed bridge in Span 1 with 13.7 m [45 ft] cross-frame spacing and half-pipe connection in plan view

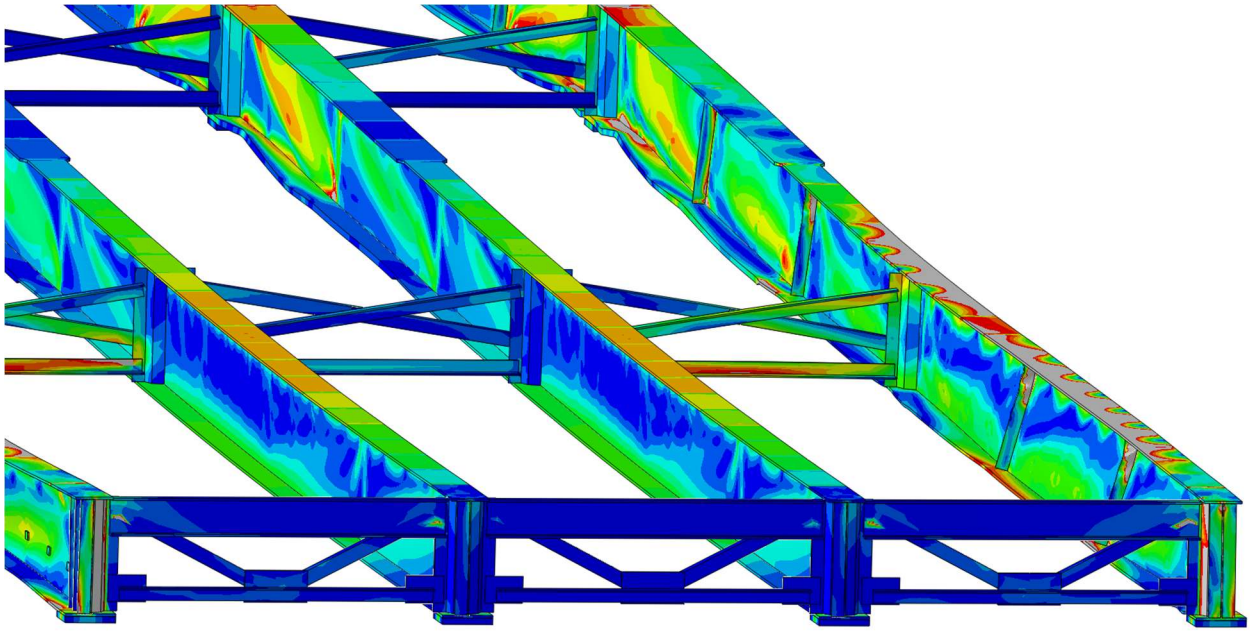

Figure A.60 Girder deformation of the non-skewed bridge with 13.7 m [45 ft] cross-frame spacing and half-pipe connection

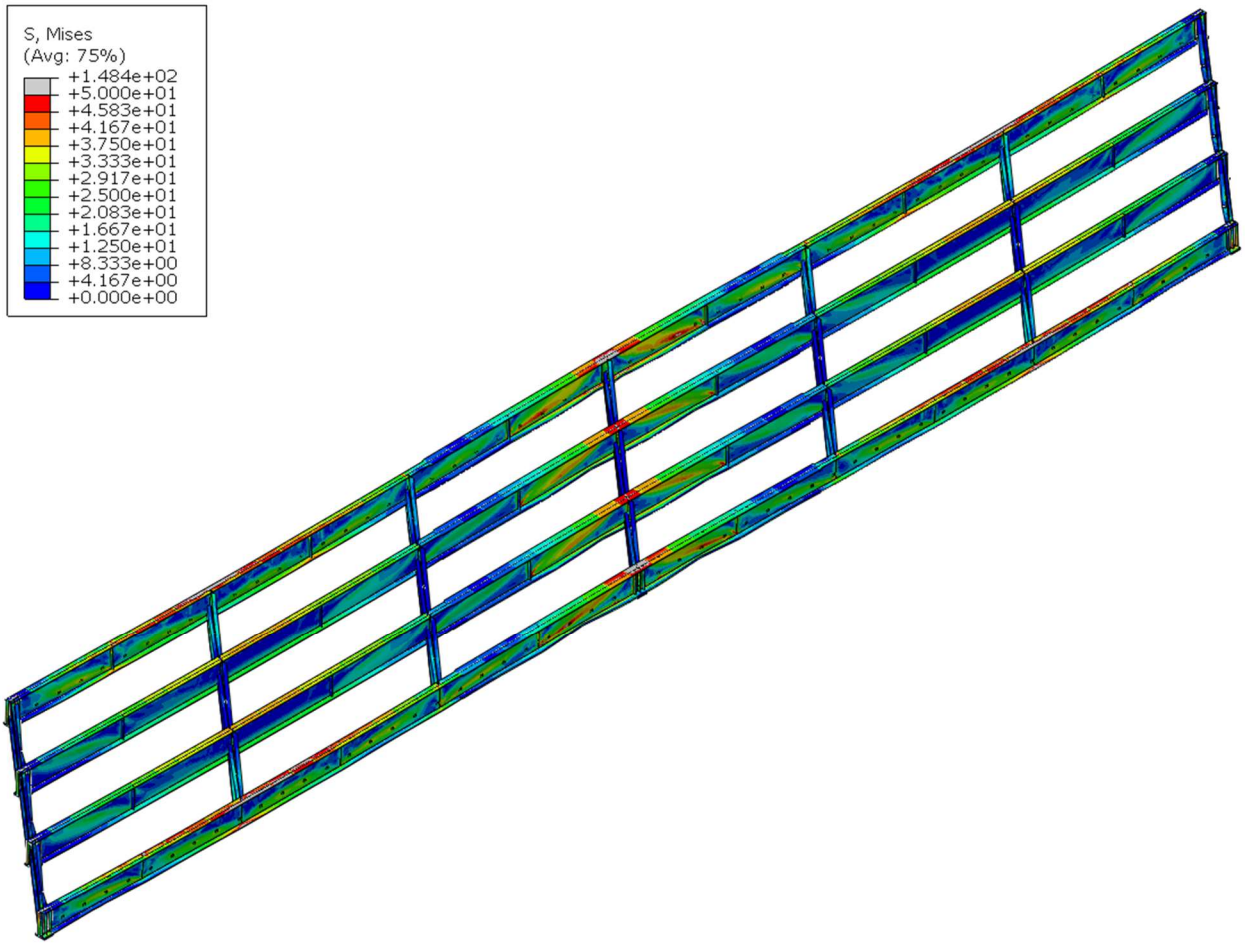

Figure A.61 Deformed shaped of the 40° skewed-parallel bridge with 9.14 m [30 ft] cross-frame spacing in isotropic view

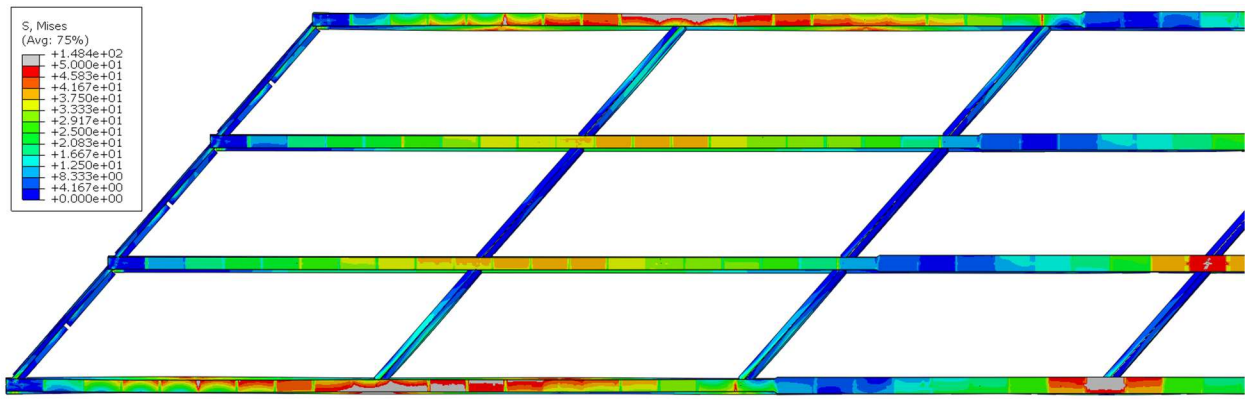

Figure A.62 Deformed shape of the 40° skewed-parallel bridge in Span 1 with 9.14 m [30 ft] cross-frame spacing in plan view

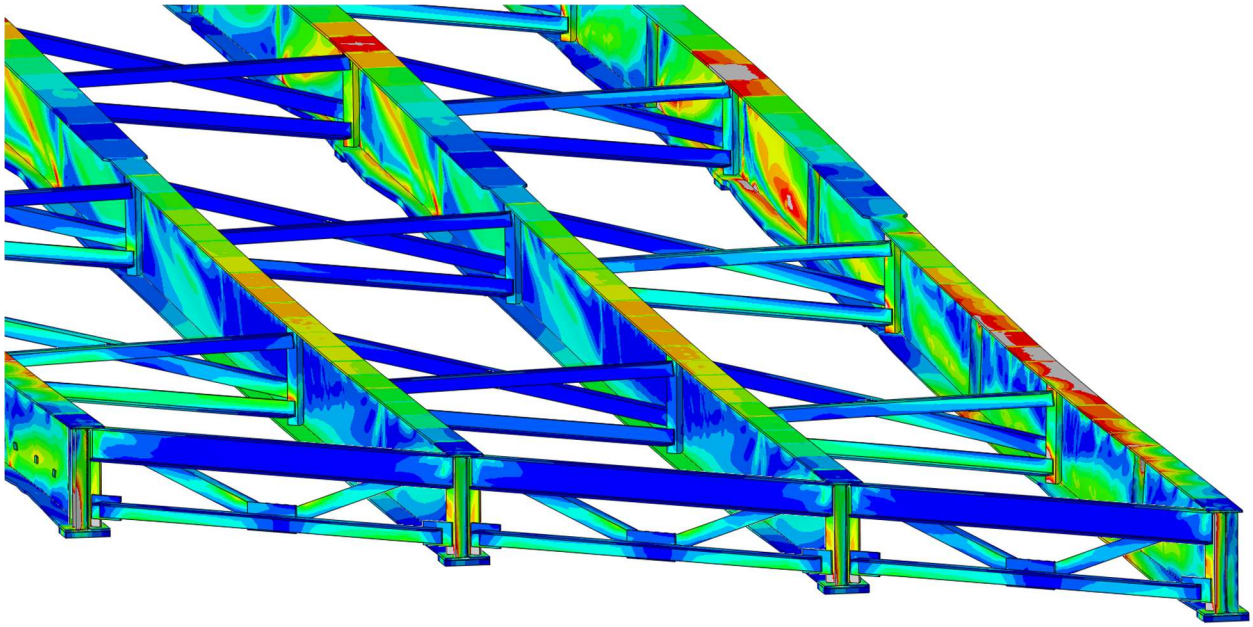

Figure A.63 Girder deformation of the 40° skewed-parallel bridge with 9.14 m [30 ft] cross-frame spacing

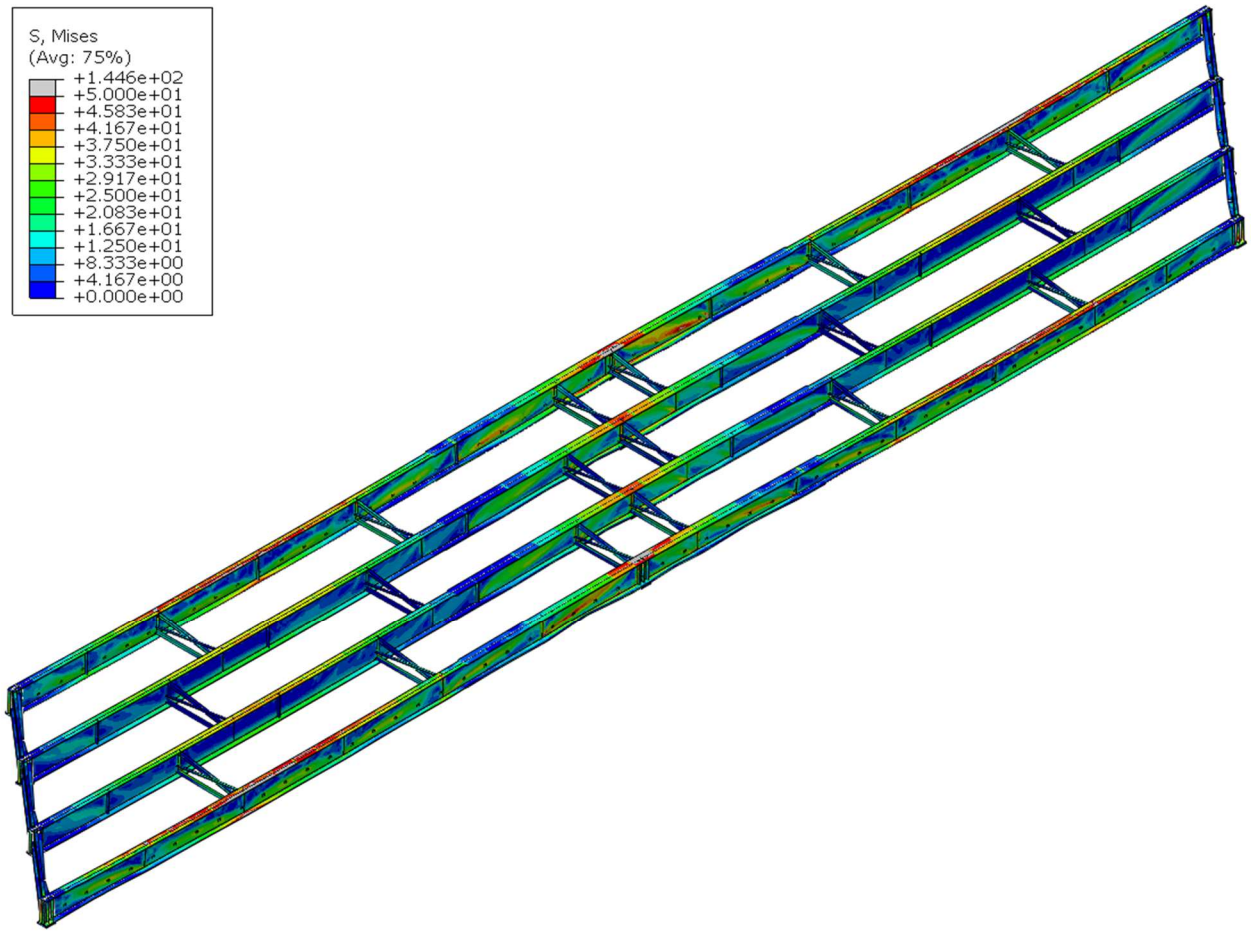

Figure A.64 Deformed shaped of the 40° skewed-staggered bridge with 9.14 m [30 ft] cross-frame spacing in isotropic view

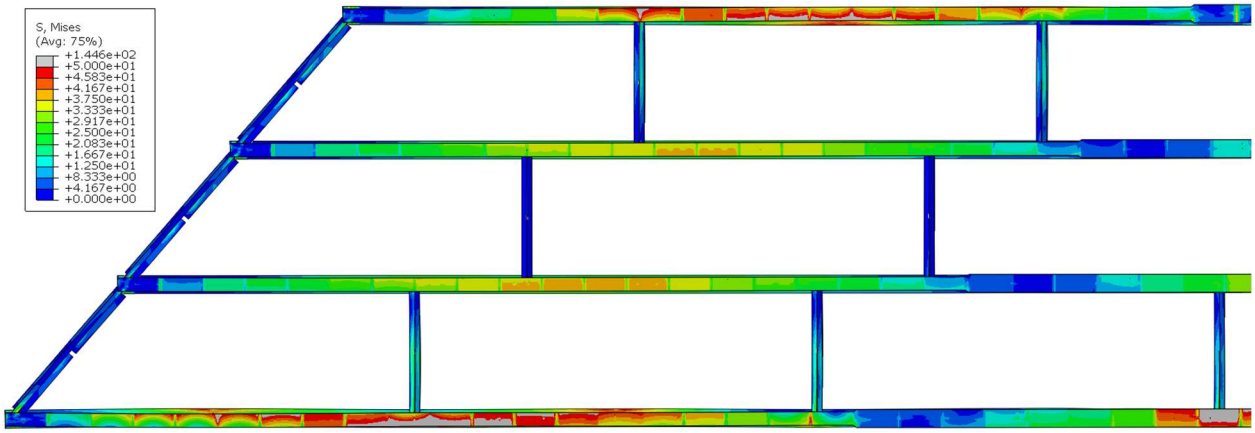

Figure A.65 Deformed shape of the 40° skewed-staggered bridge in Span 1 with 9.14 m [30 ft] cross-frame spacing in plan view

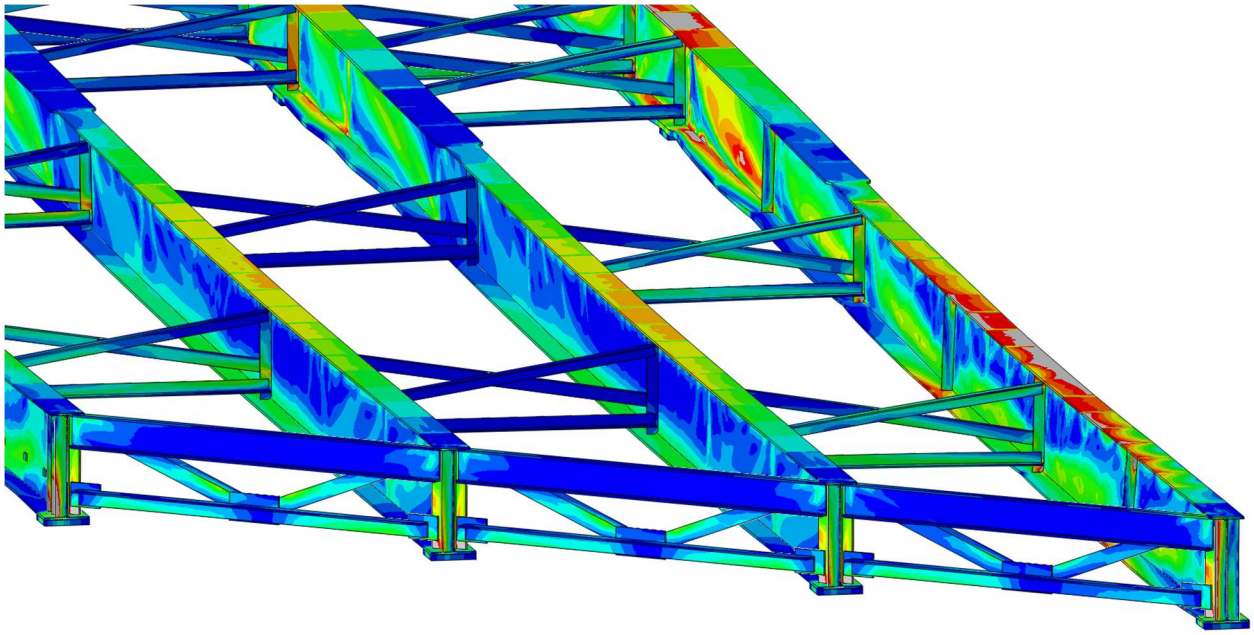

Figure A.66 Girder deformation of the 40° skewed-staggered bridge with 9.14 m [30 ft] cross-frame spacing

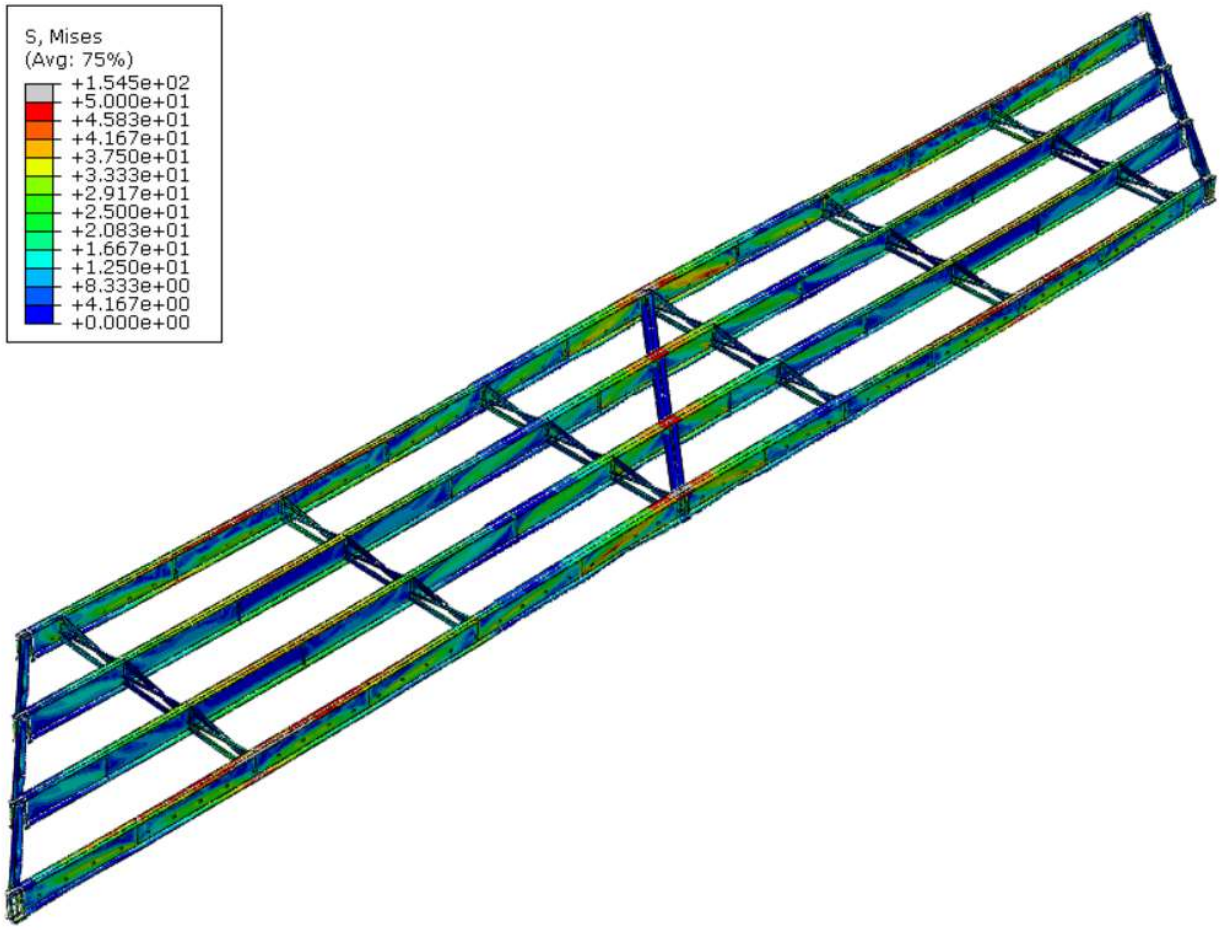

Figure A.67 Deformed shaped of the 40° skewed-unstaggered bridge with 9.14 m [30 ft] cross-frame spacing in isotropic view

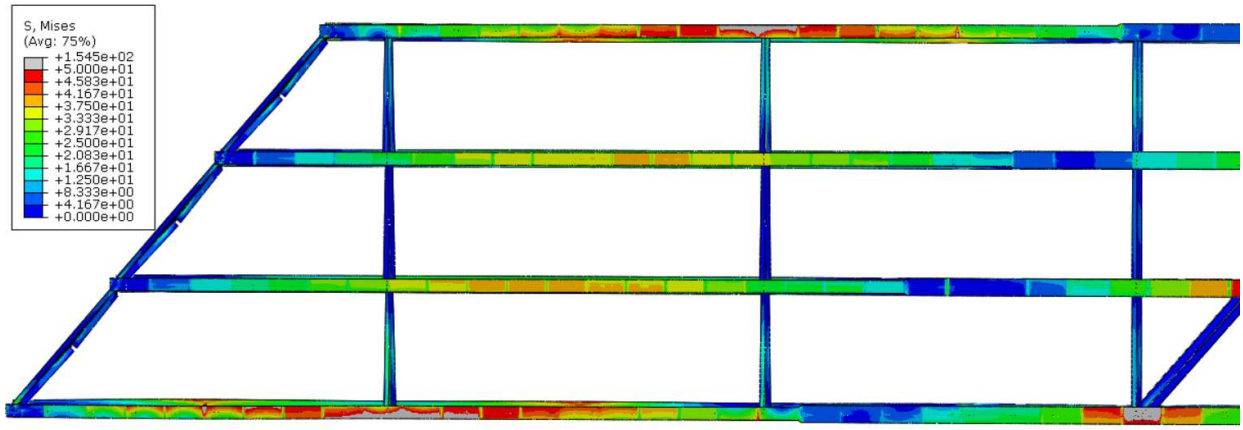

Figure A.68 Deformed shape of the 40° skewed-unstaggered bridge in Span 1 with 9.14 m [30 ft] cross-frame spacing in plan view

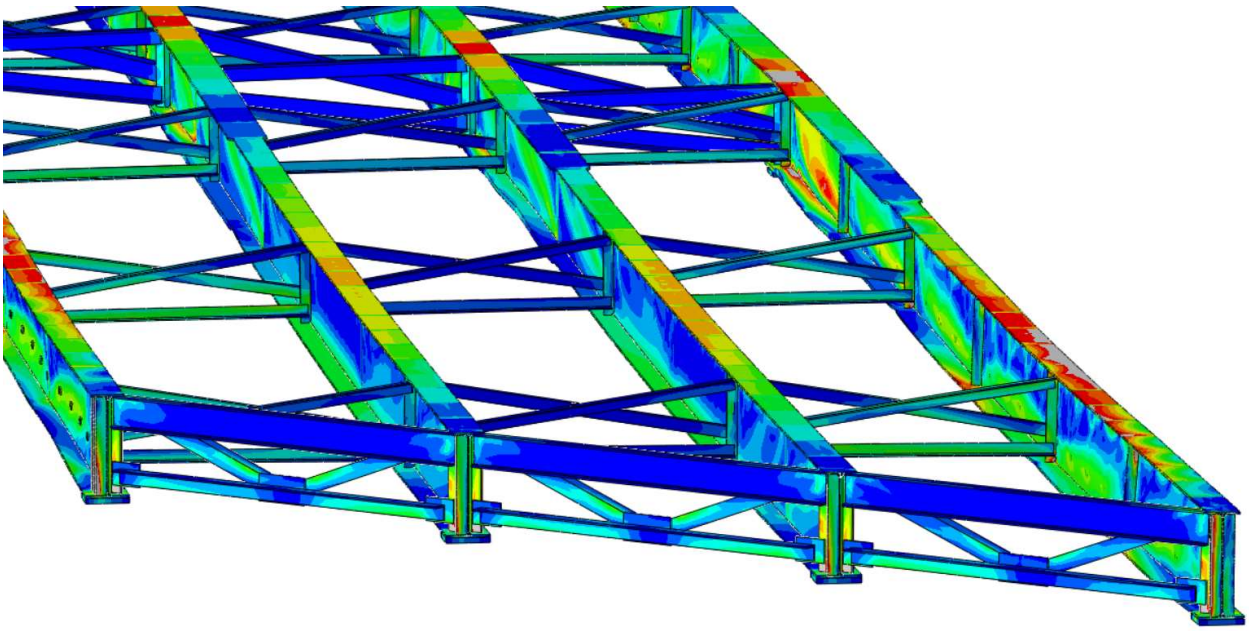

Figure A.69 Girder deformation of the 40° skewed-unstaggered bridge with 9.14 m [30 ft] cross-frame spacing

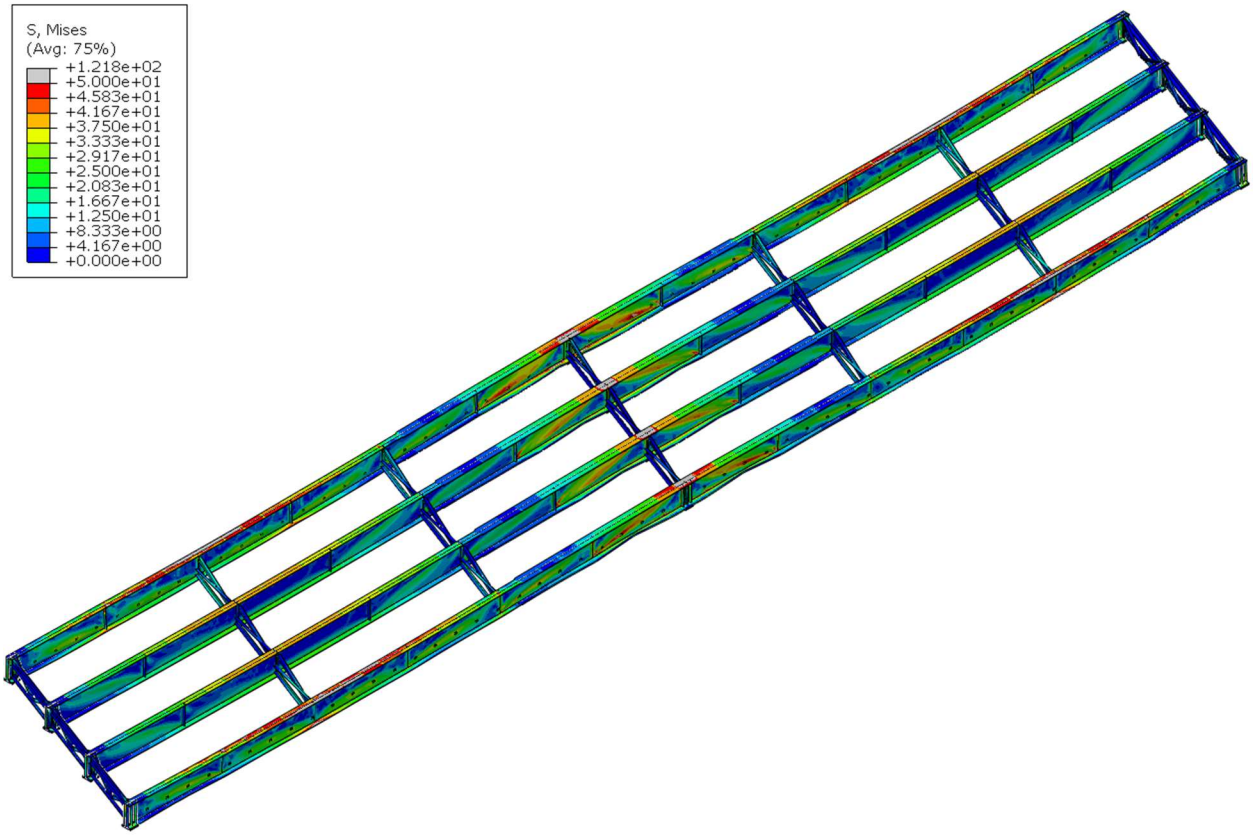

Figure A.70 Deformed shaped of the 20° skewed-parallel bridge with 9.14 m [30 ft] cross-frame spacing in isotropic view

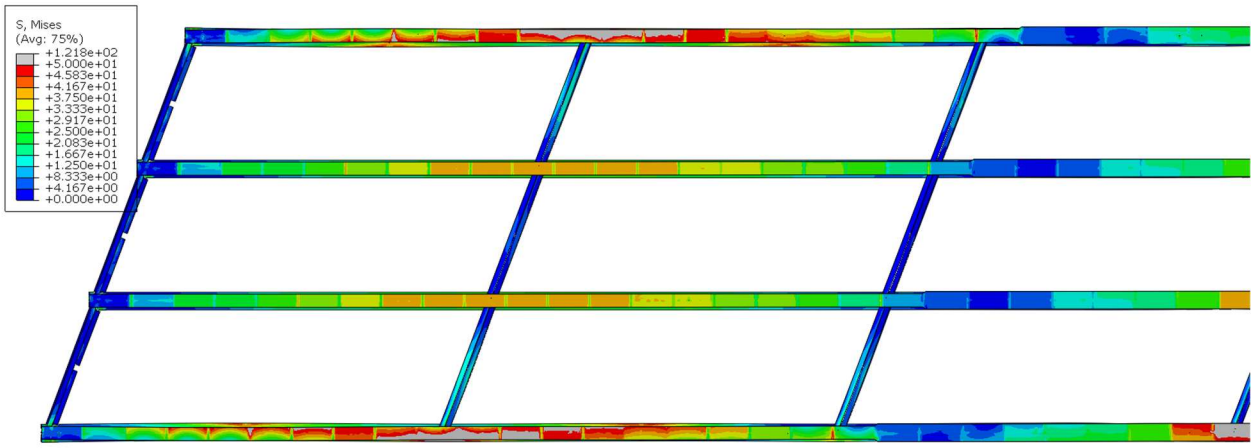

Figure A.71 Deformed shape of the 20° skewed-parallel bridge in Span 1 with 9.14 m [30 ft] cross-frame spacing in plan view

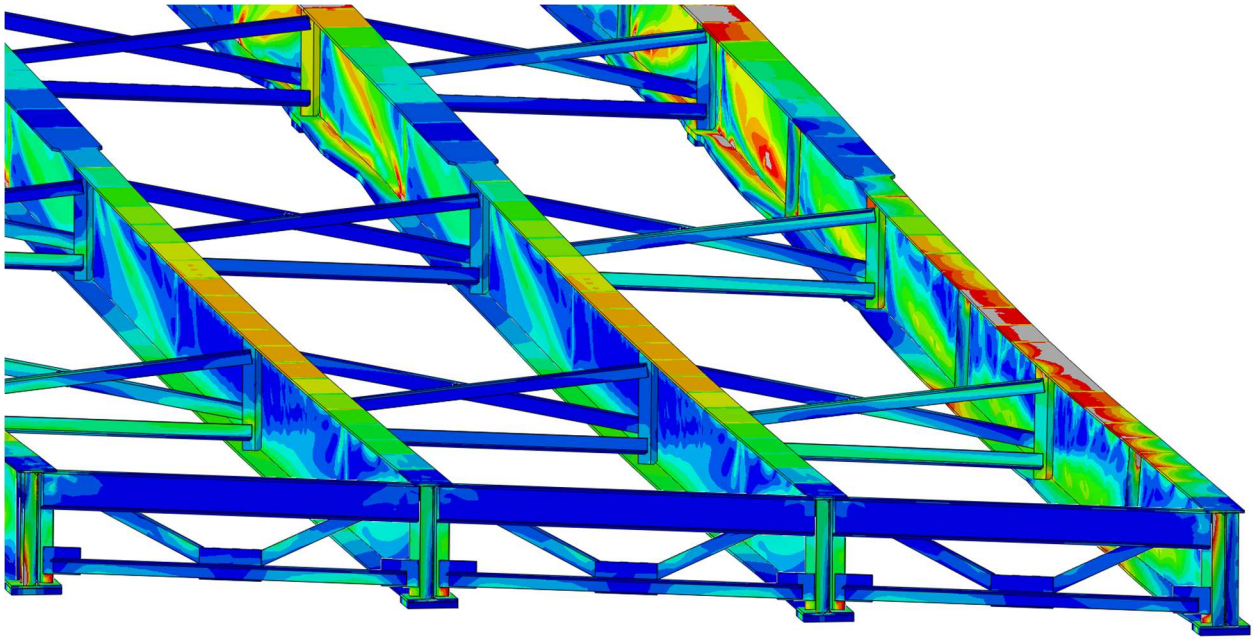

Figure A.72 Girder deformation of the 20° skewed-parallel bridge with 9.14 m [30 ft] cross-frame spacing

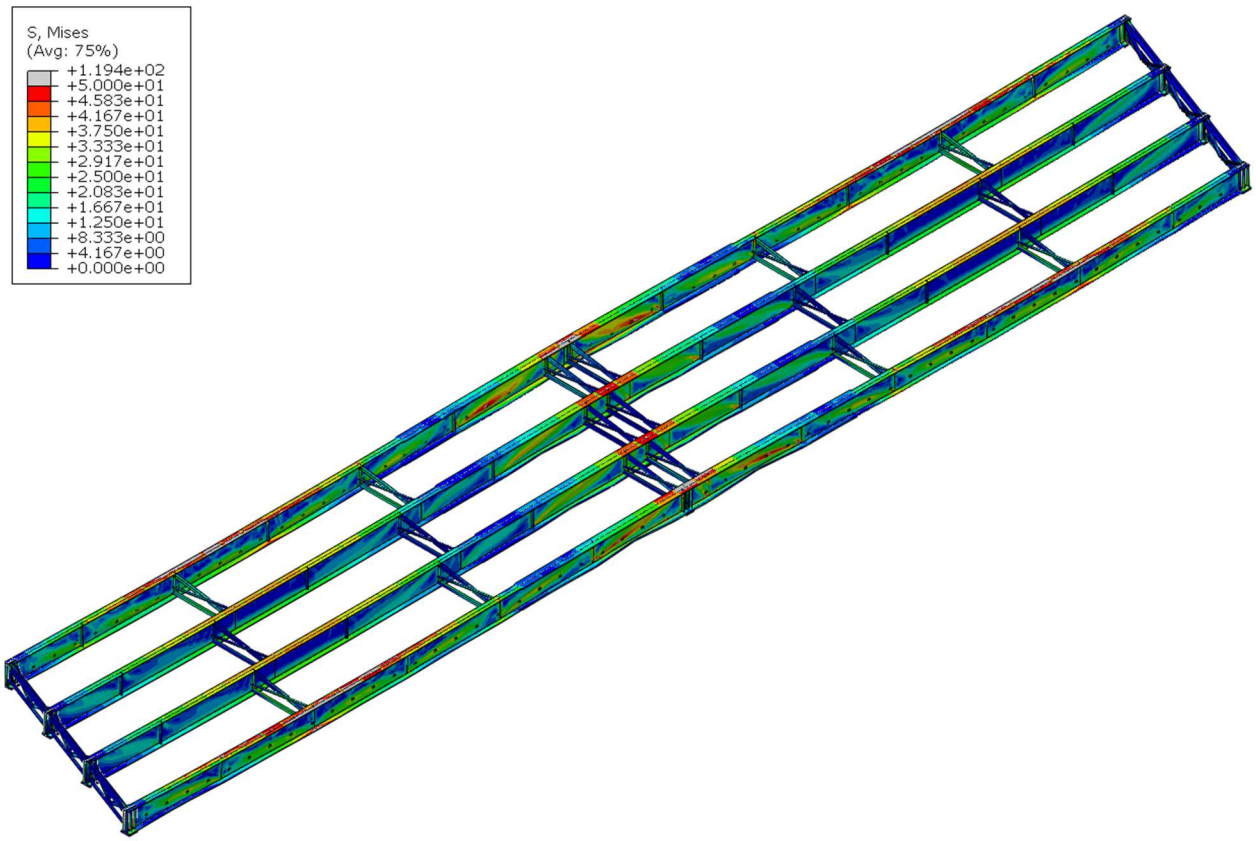

Figure A.73 Deformed shaped of the 20° skewed-staggered bridge with 9.14 m [30 ft] cross-frame spacing in isotropic view

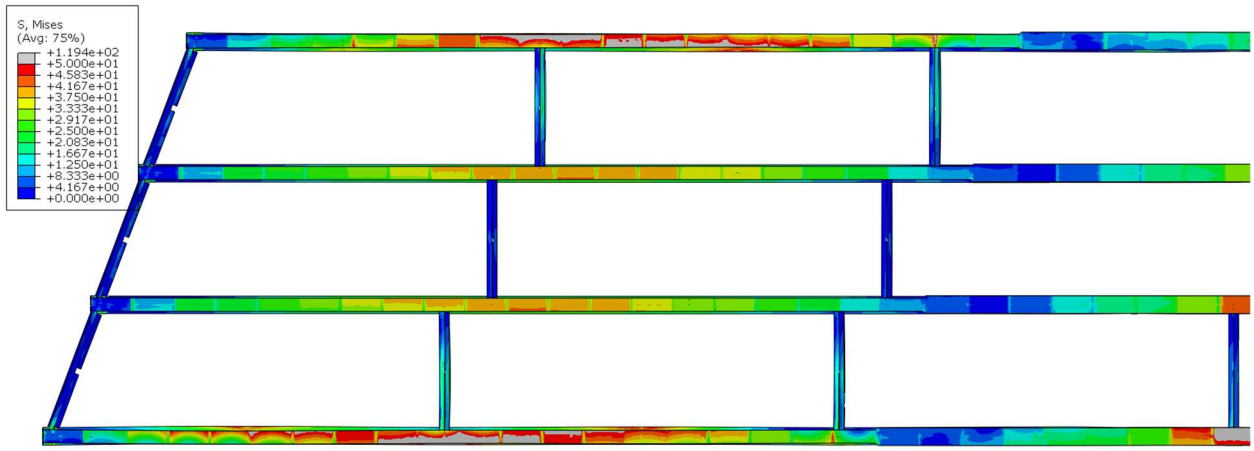

Figure A.74 Deformed shape of the 20° skewed-staggered bridge in Span 1 with 9.14 m [30 ft] cross-frame spacing in plan view

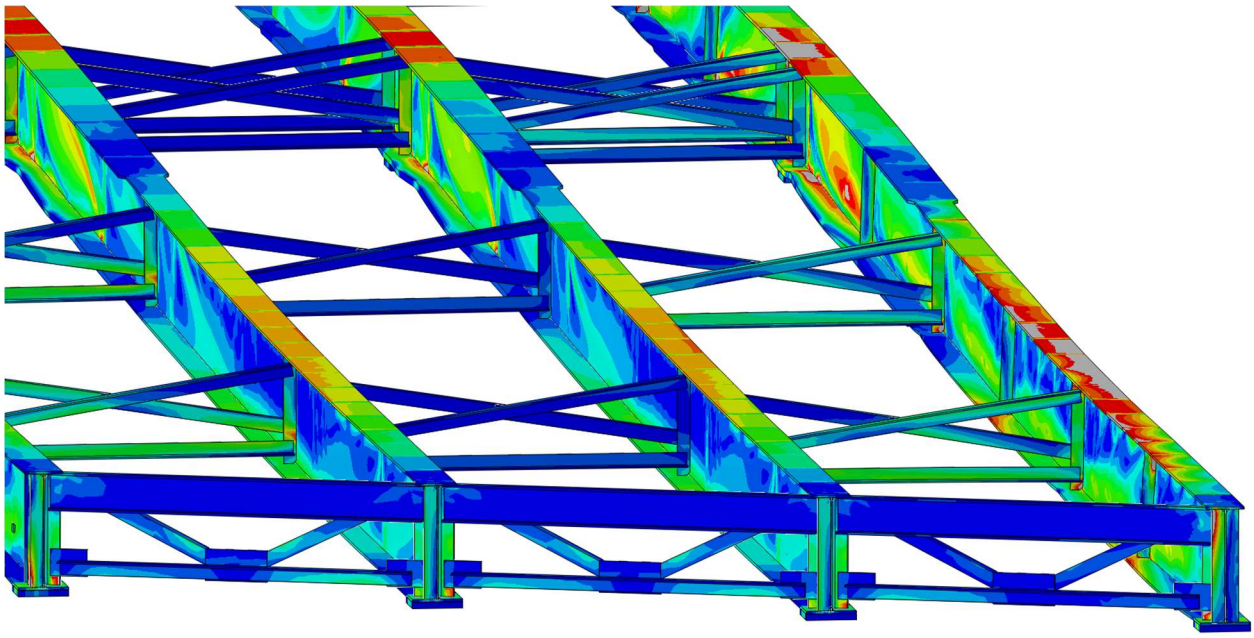

Figure A.75 Girder deformation of the 20° skewed-staggered bridge with 9.14 m [30 ft] cross-frame spacing

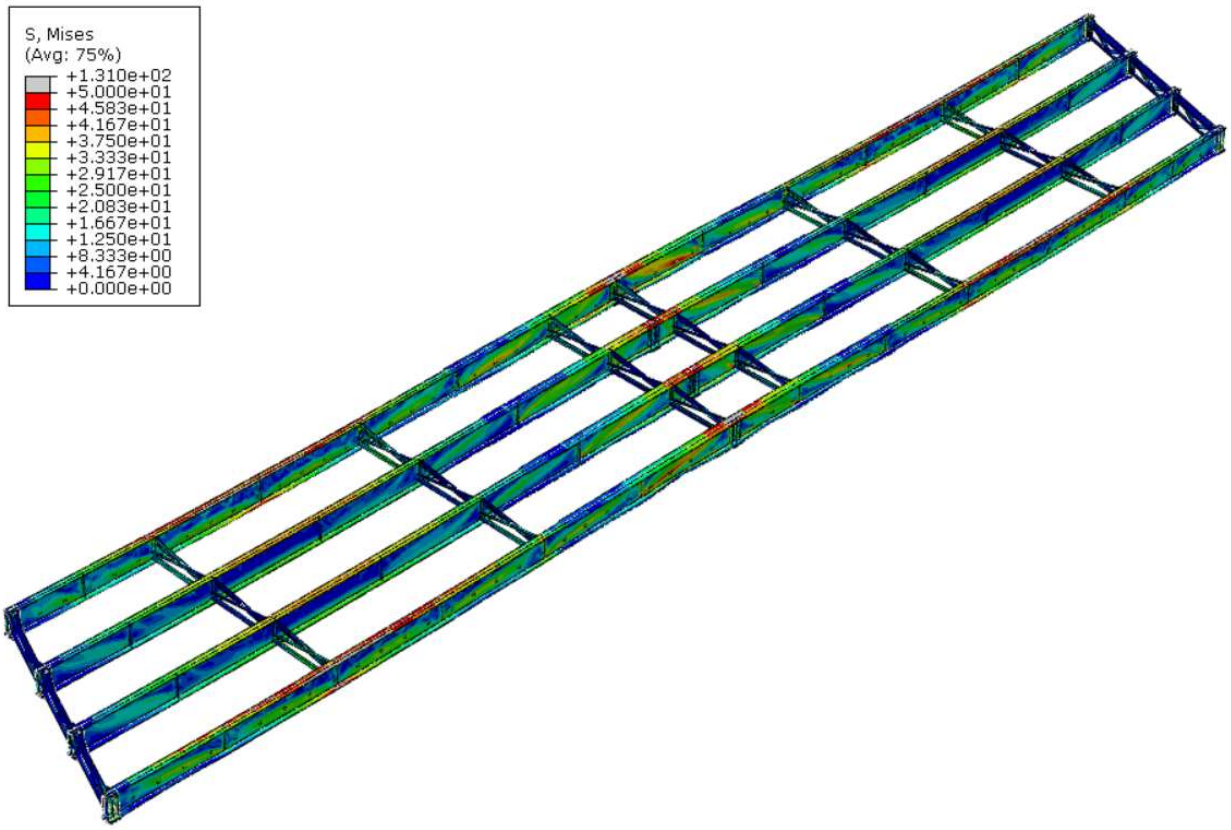

Figure A.76 Deformed shaped of the 20° skewed-unstaggered bridge with 9.14 m [30 ft] cross-frame spacing in isotropic view

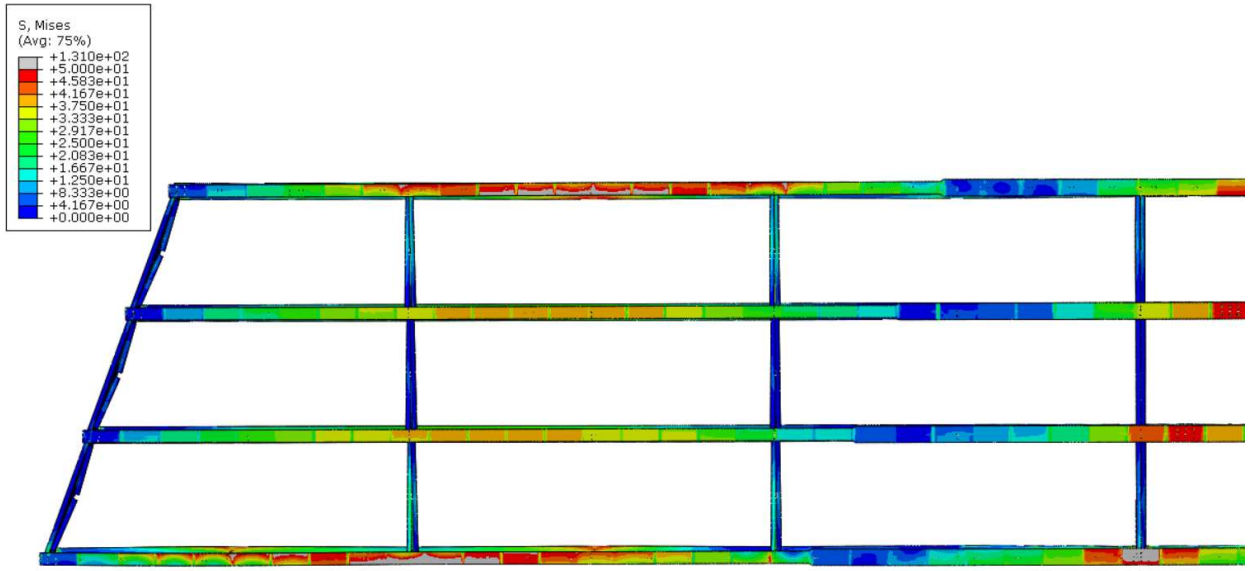

Figure A.77 Deformed shape of the 20° skewed-unstaggered bridge with 9.14 m [30 ft] cross-frame spacing in plan view

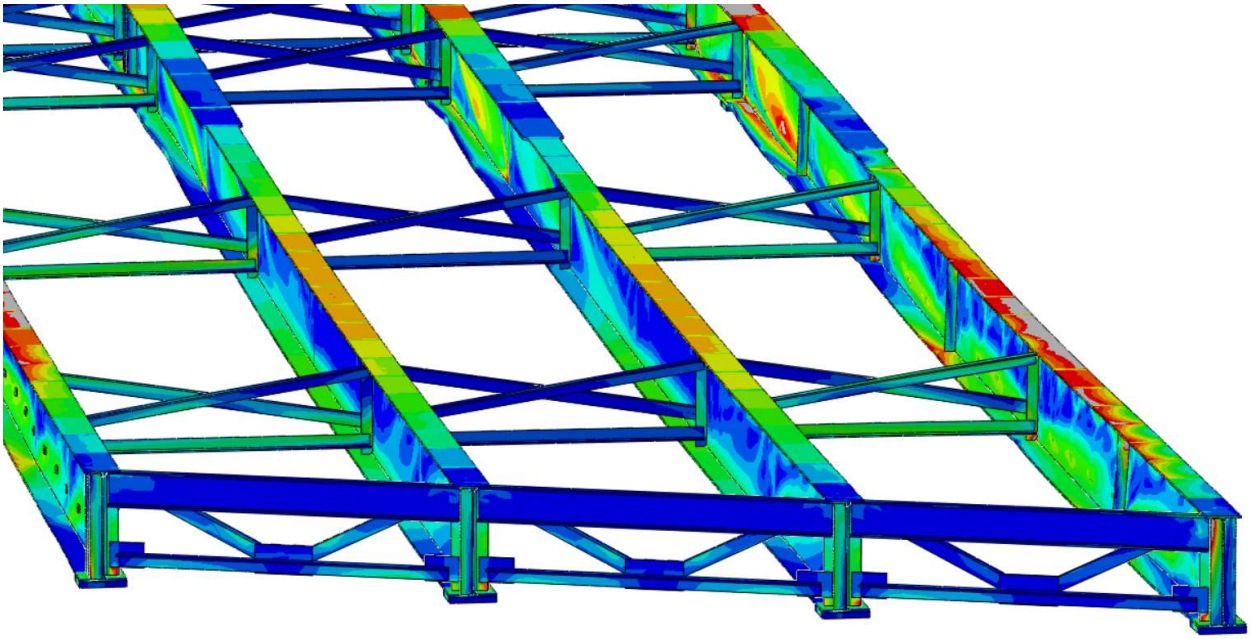

Figure A.78 Girder deformation of the 20° skewed-unstaggered bridge with 9.14 m [30 ft] cross-frame spacing

NON-SKEWED BRIDGE

30 FT CROSS-FRAME SPACING;

3/8" THICK STIFFENERS

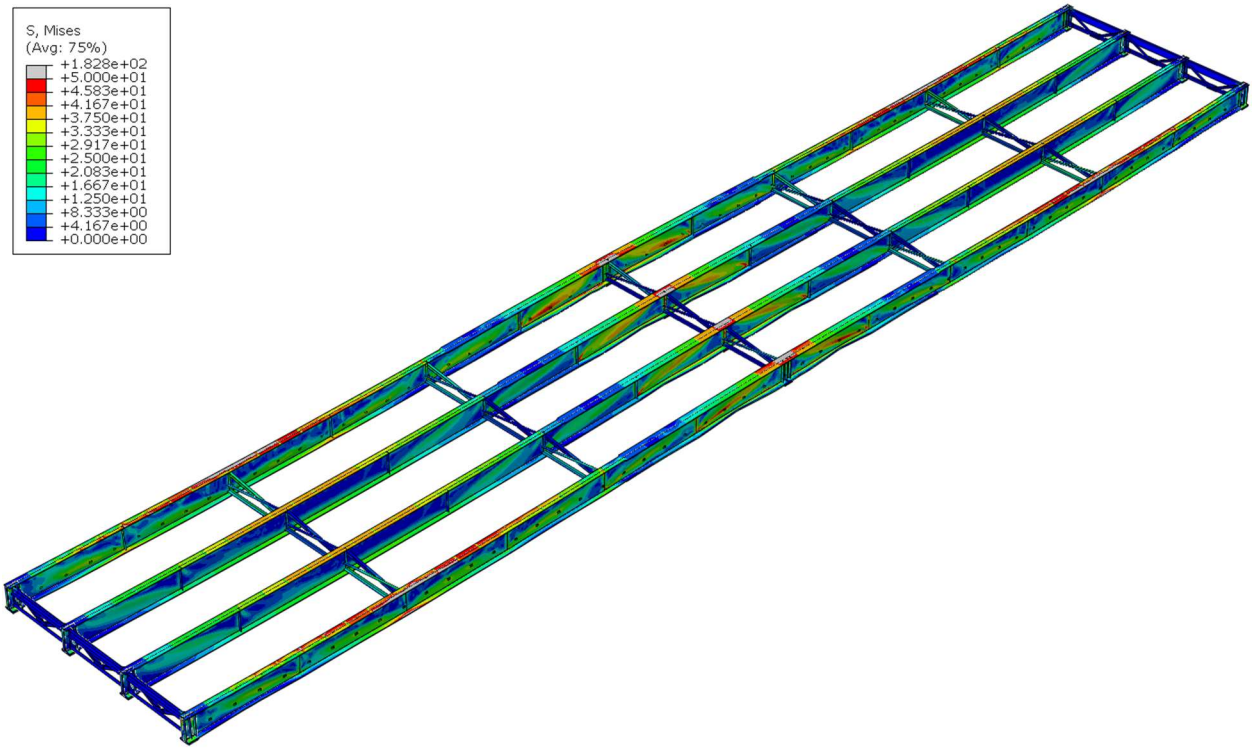

Figure A.79 Deformed shaped of the non-skewed bridge with 9.14 m [30 ft] cross-frame spacing in isotropic view

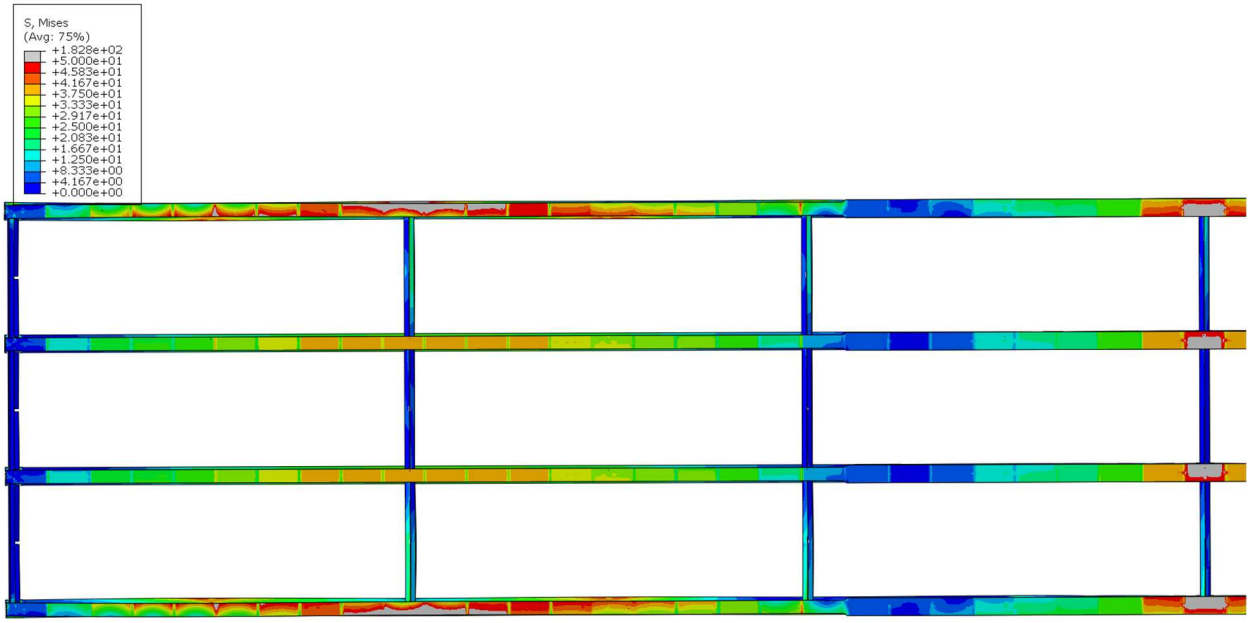

Figure A.80 Deformed shape of the non-skewed bridge in Span 1 with 9.14 m [30 ft] cross-frame spacing in plan view

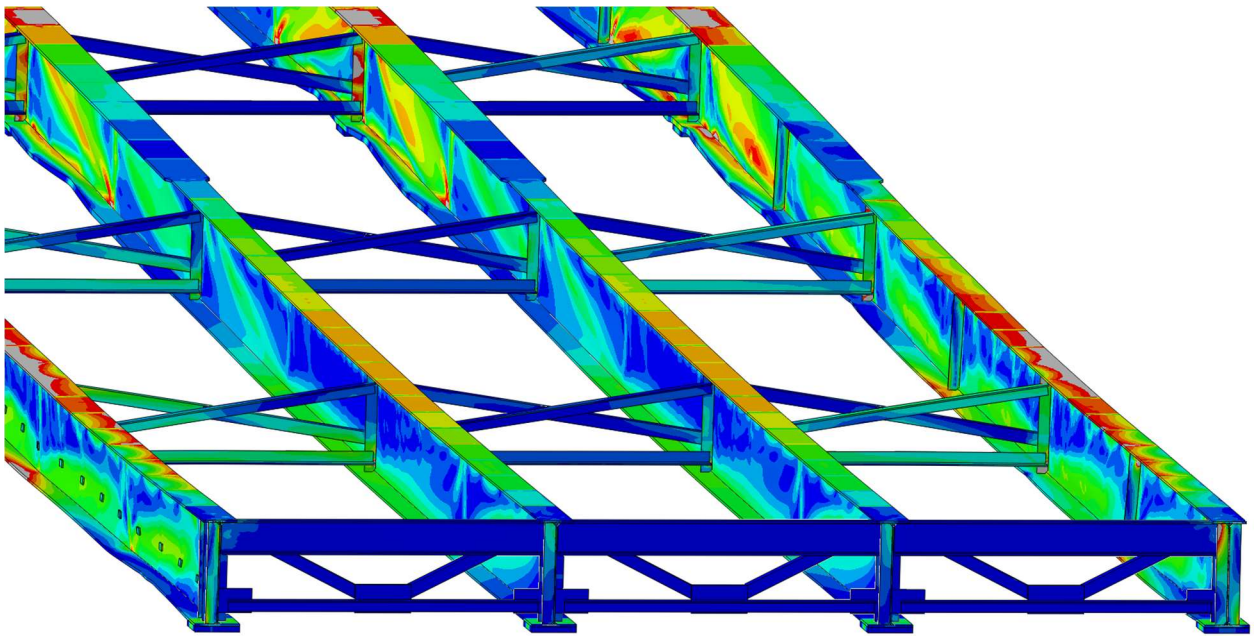

Figure A.81 Girder deformation of the non-skewed bridge with 9.14 m [30 ft] cross-frame spacing

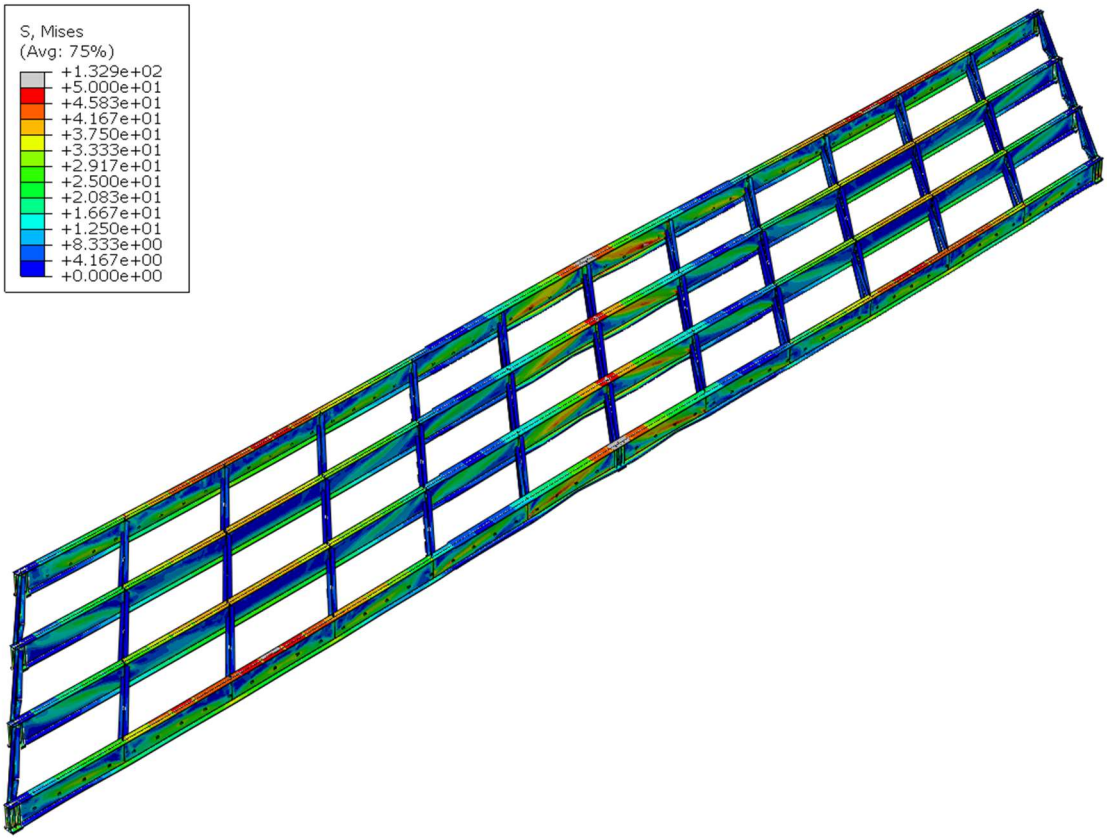

Figure A.82 Deformed shaped of the 40° skewed-parallel bridge with 4.57 m [15 ft] cross-frame spacing in isotropic view

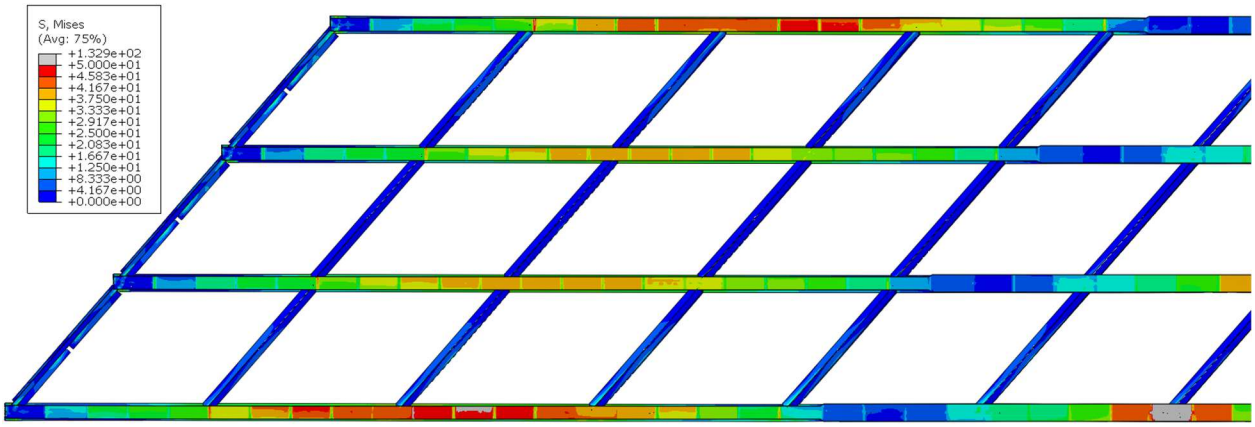

Figure A.83 Deformed shape of the 40° skewed-parallel bridge in Span 1 with 4.57 m [15 ft] cross-frame spacing in plan view

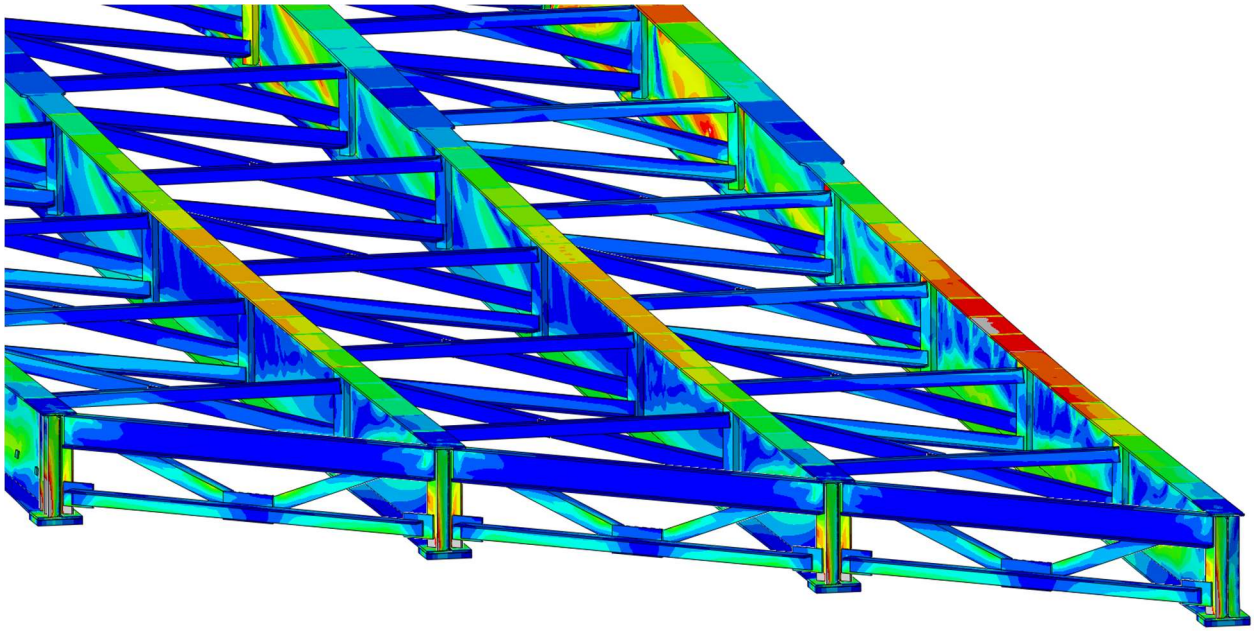

Figure A.84 Girder deformation of the 40° skewed-parallel bridge with 4.57 m [15 ft] cross-frame spacing

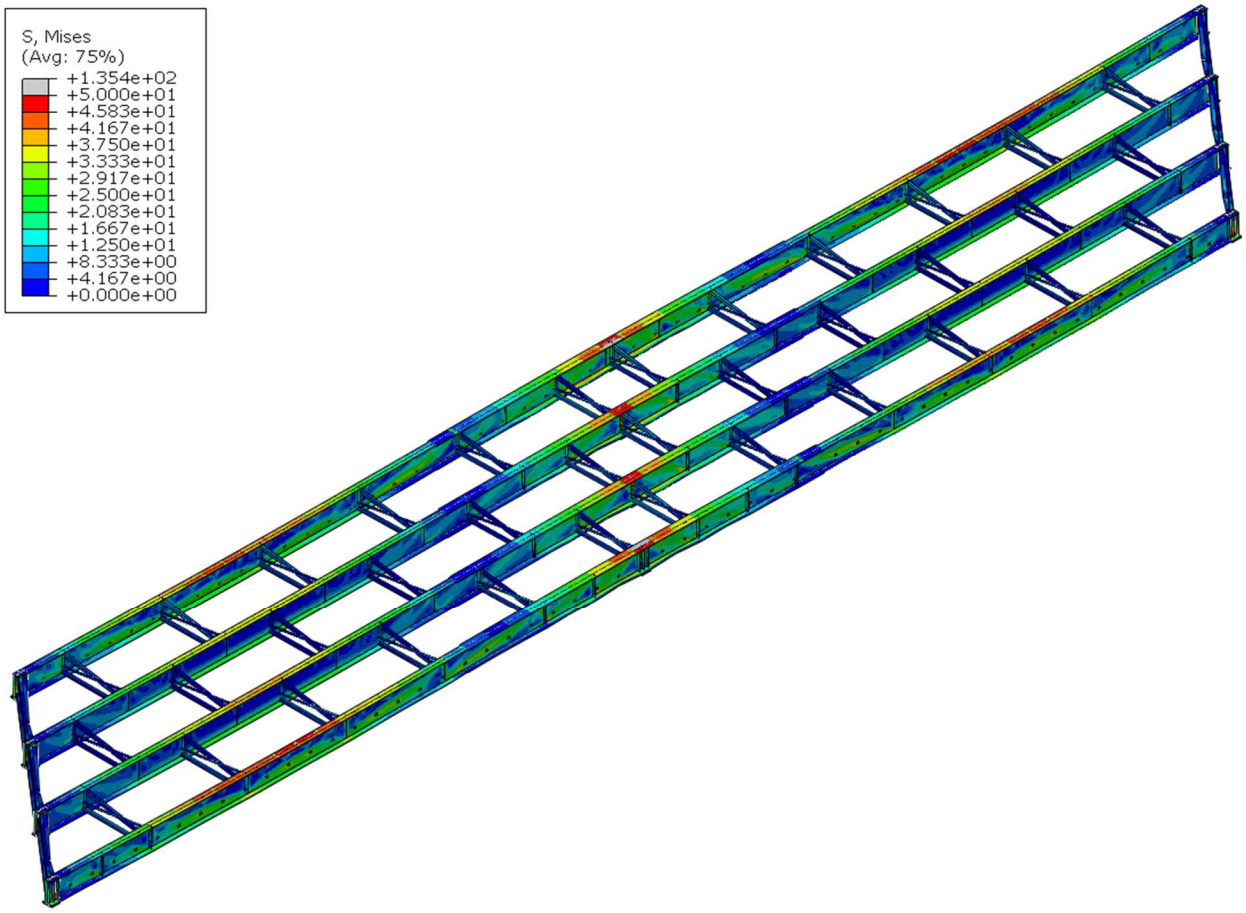

Figure A.85 Deformed shaped of the 40° skewed-staggered bridge with 4.57 m [15 ft] cross-frame spacing in isotropic view

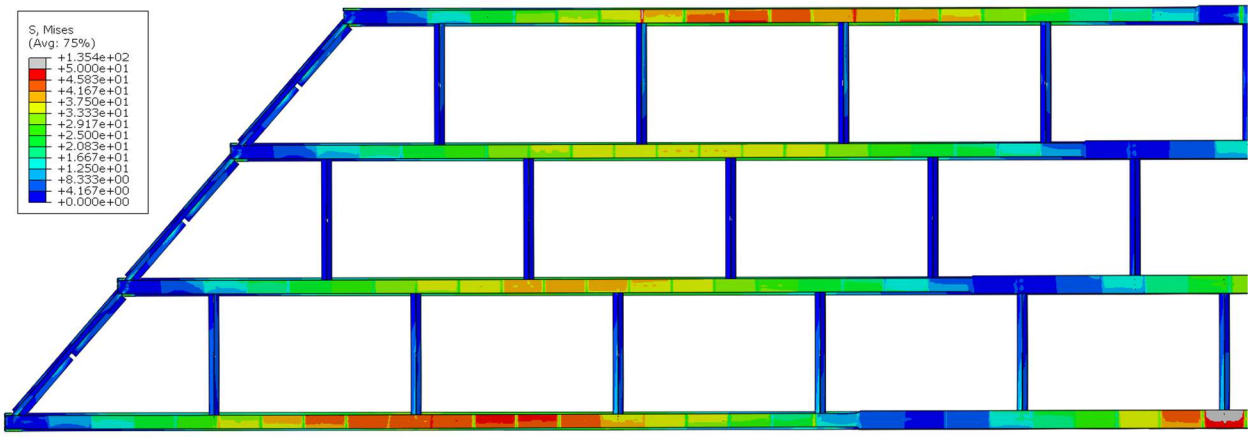

Figure A.86 Deformed shape of the 40° skewed-staggered bridge in Span 1 with 4.57 m [15 ft] cross-frame spacing in plan view

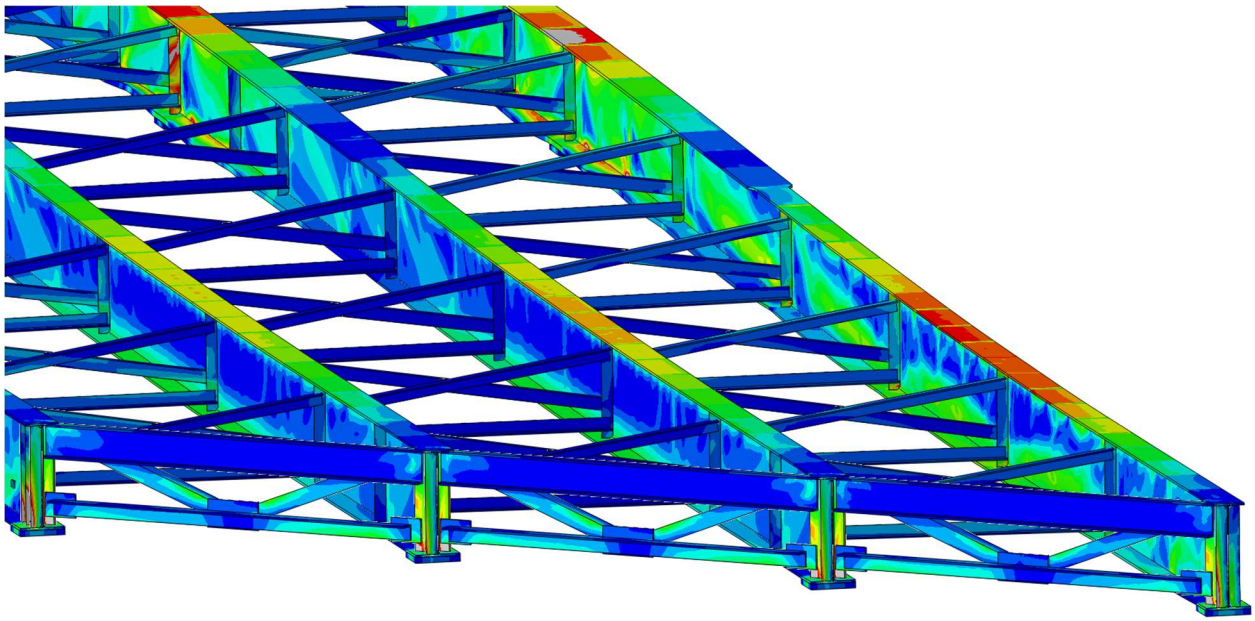

Figure A.87 Girder deformation of the 40° skewed-staggered bridge with 4.57 m [15 ft] cross-frame spacing

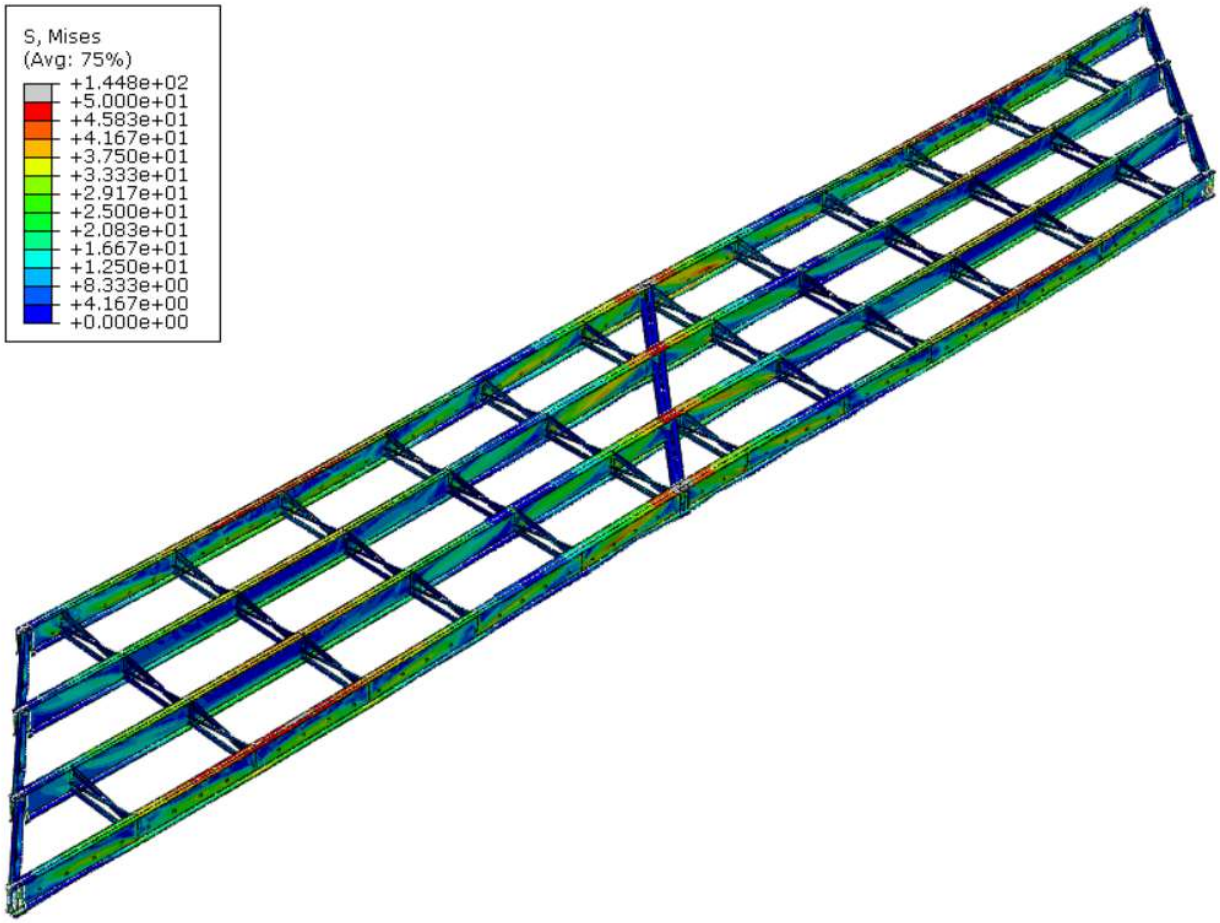

Figure A.88 Deformed shaped of the 40° skewed-unstaggerd bridge with 4.57 m [15 ft] cross-frame spacing in isotropic view

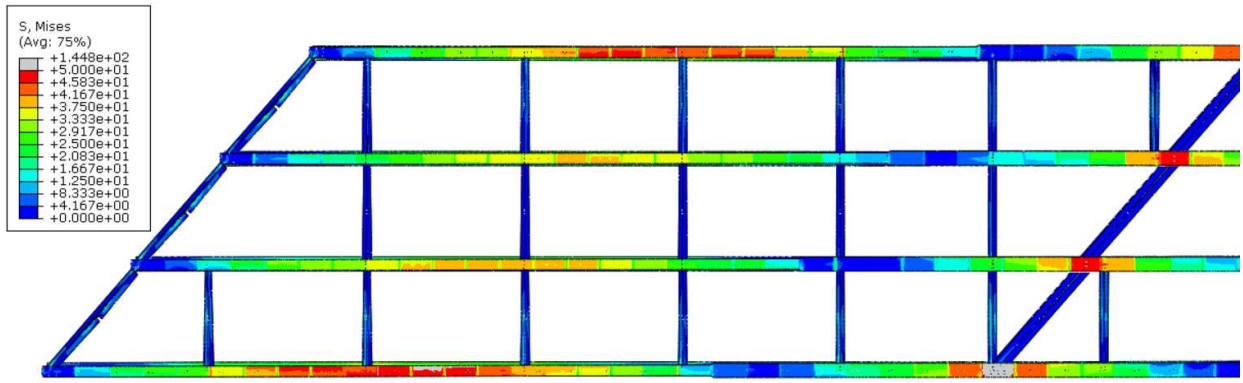

Figure A.89 Deformed shape of the 40° skewed-unstaggered bridge in Span 1 with 4.57 m [15 ft] cross-frame spacing in plan view

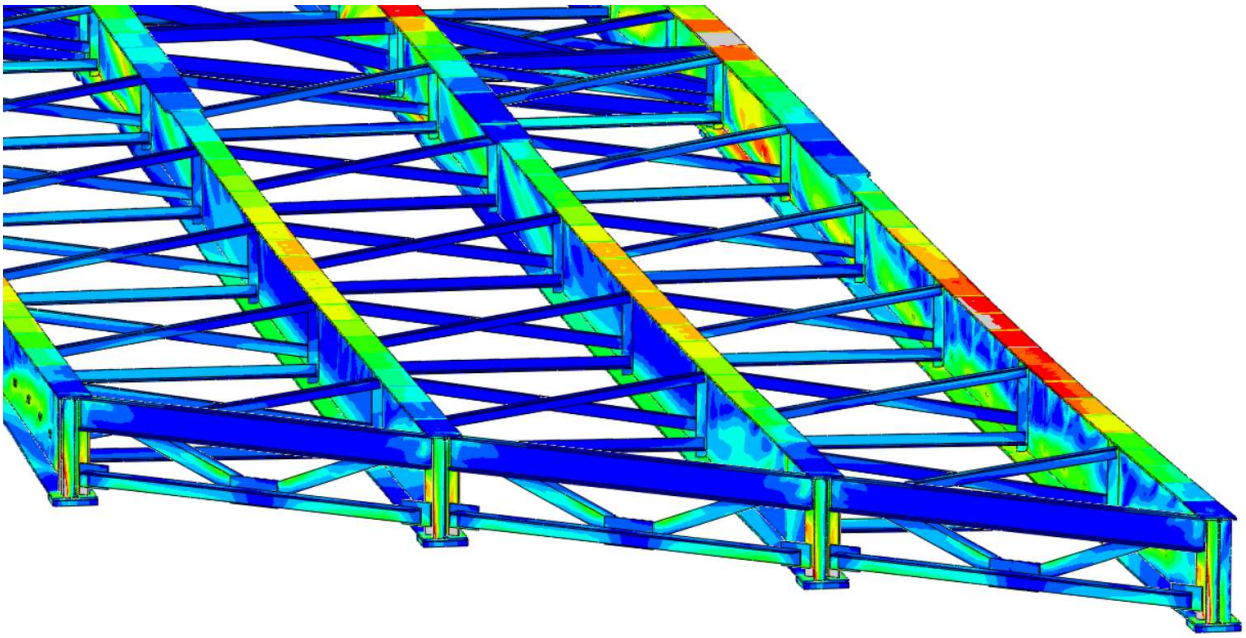

Figure A.90 Girder deformation of the 40° skewed-unstaggered bridge with 4.57 m [15 ft] cross-frame spacing

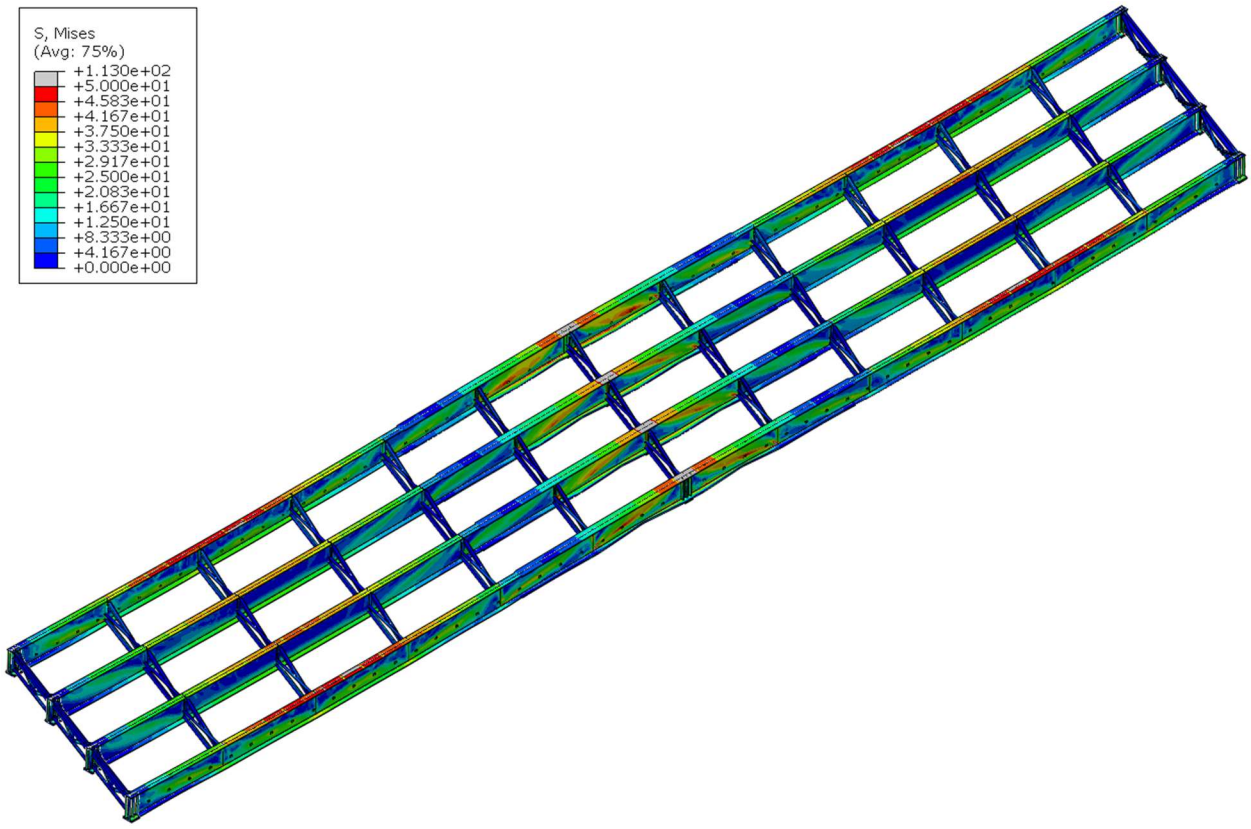

Figure A.91 Deformed shaped of the 20° skewed-parallel bridge with 4.57 m [15 ft] cross-frame spacing in isotropic view

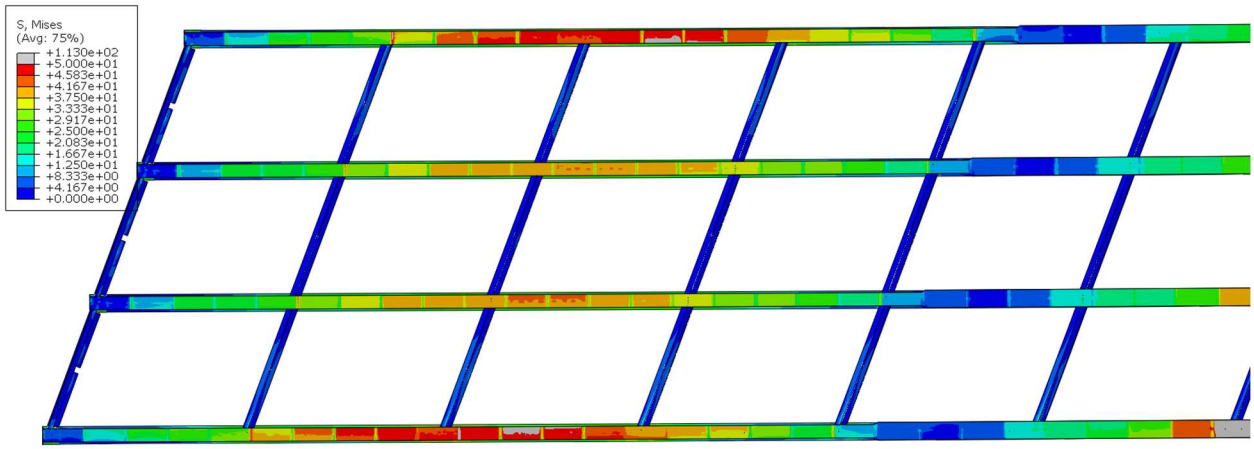

Figure A.92 Deformed shape of the 20° skewed-parallel bridge in Span 1 with 4.57 m [15 ft] cross-frame spacing in plan view

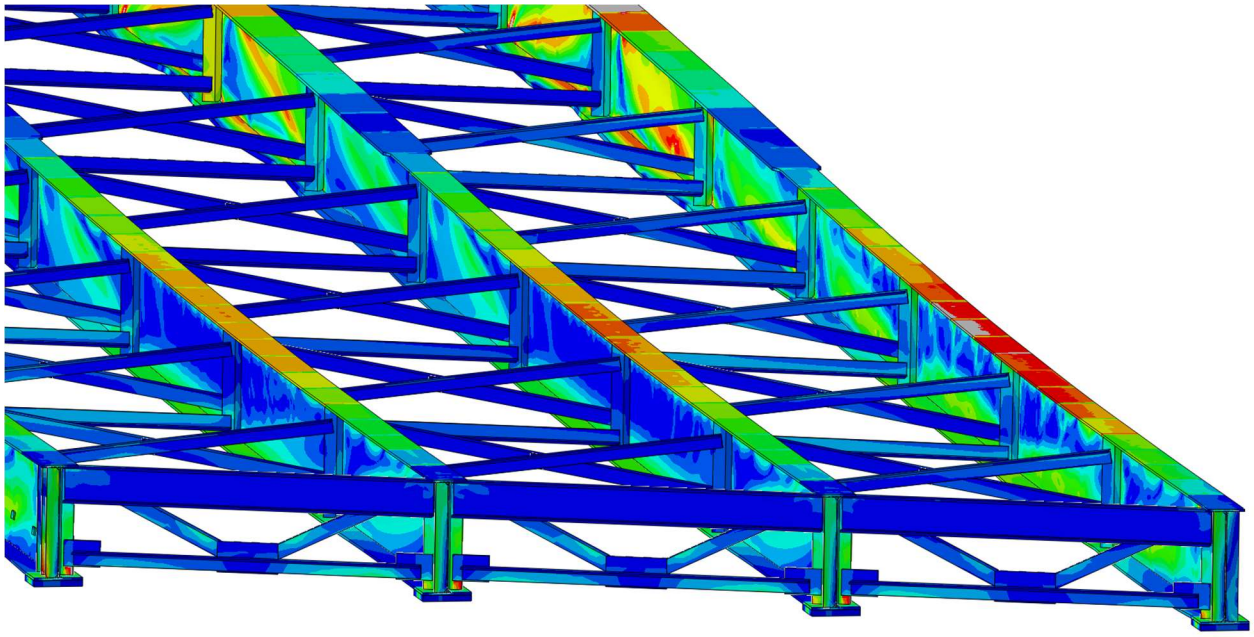

Figure A.93 Girder deformation of the 20° skewed-parallel bridge with 4.57 m [15 ft] cross-frame spacing

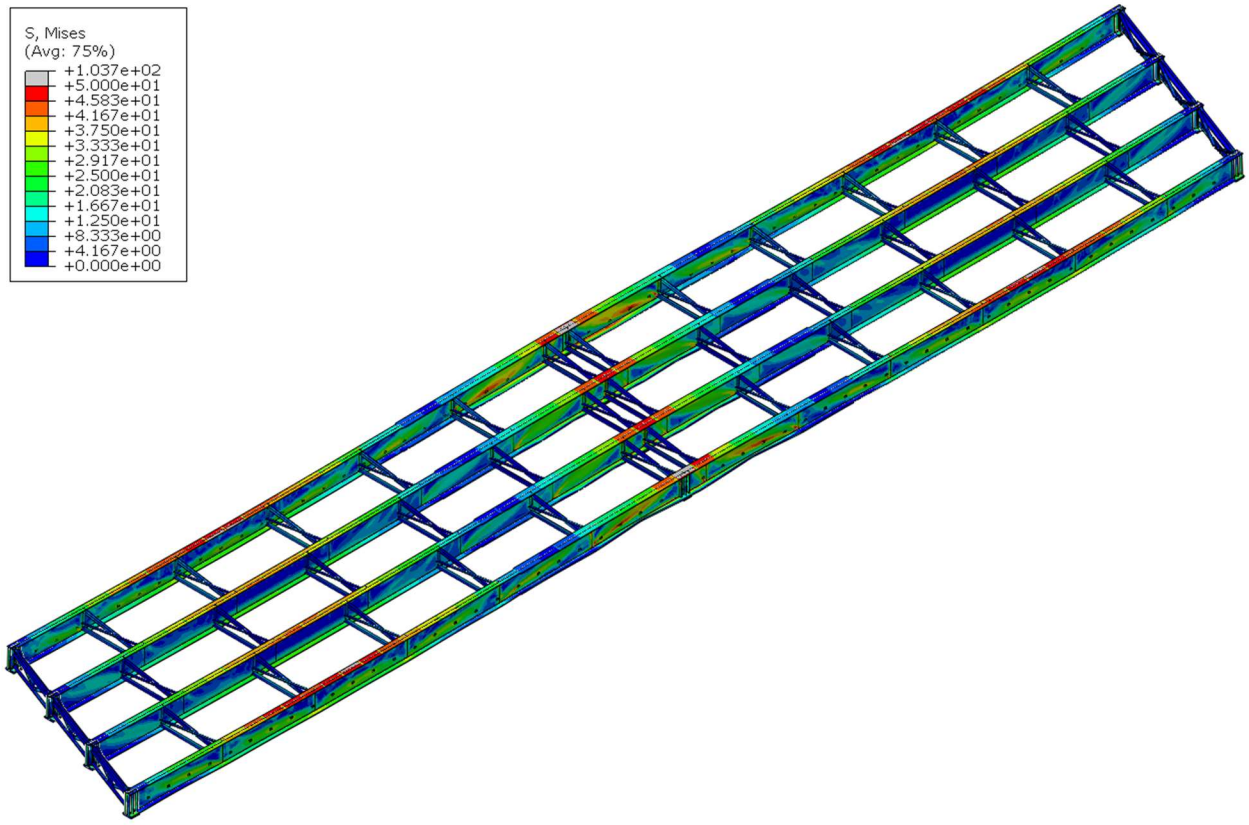

Figure A.94 Deformed shaped of the 20° skewed-staggered bridge with 4.57 m [15 ft] cross-frame spacing in isotropic view

.

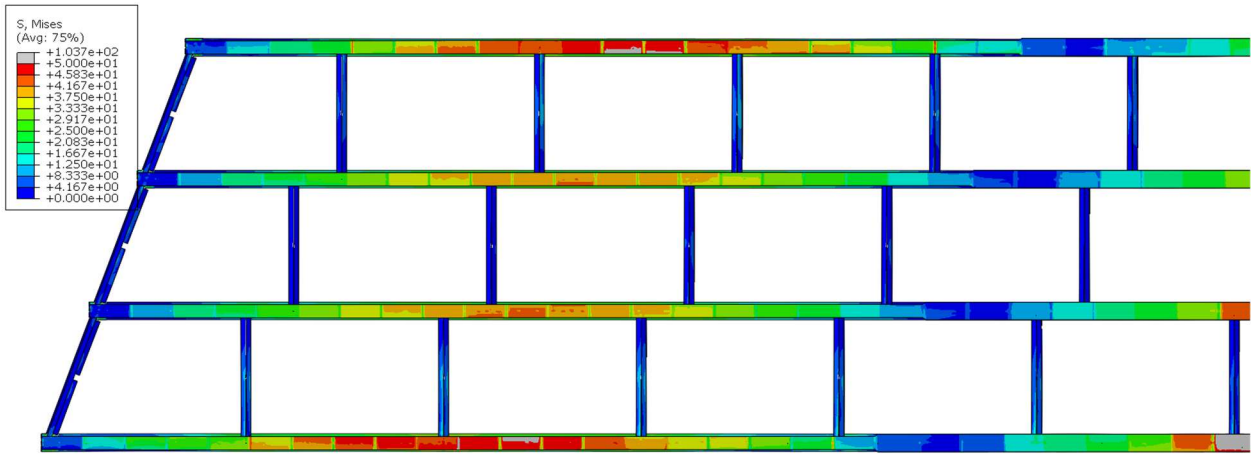

Figure A.95 Deformed shape of the 20° skewed-staggered bridge in Span 1 with 4.57 m [15 ft] cross-frame spacing in plan view

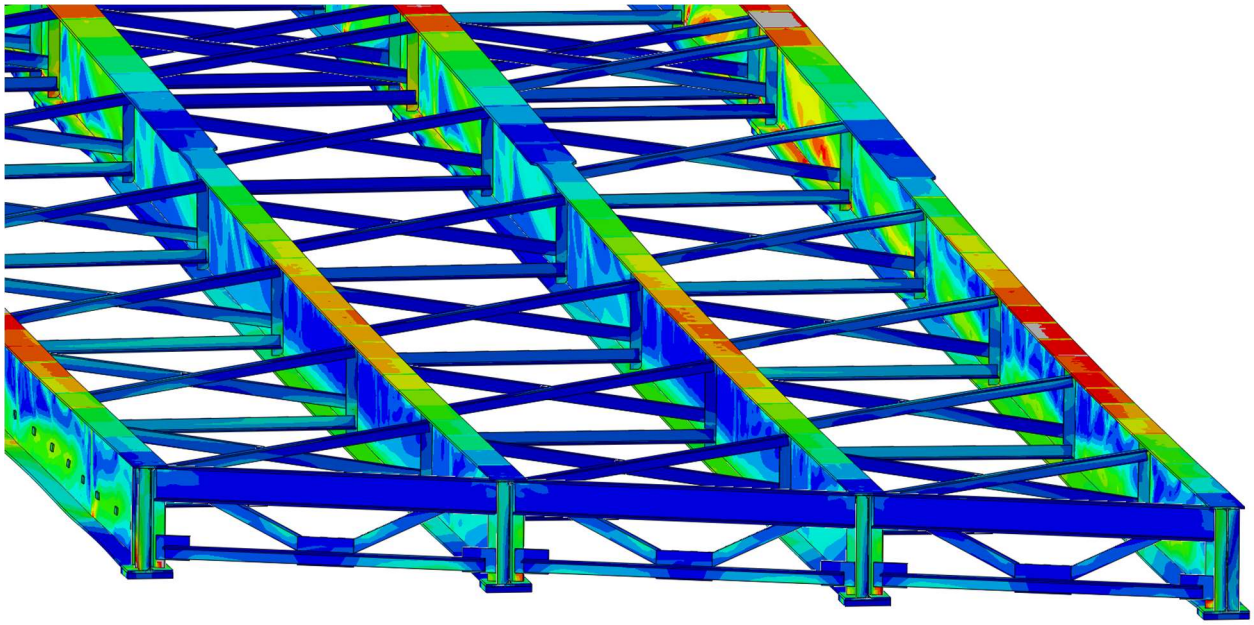

Figure A.96 Girder deformation of the 20° skewed-staggered bridge with 4.57 m [15 ft] cross-frame spacing

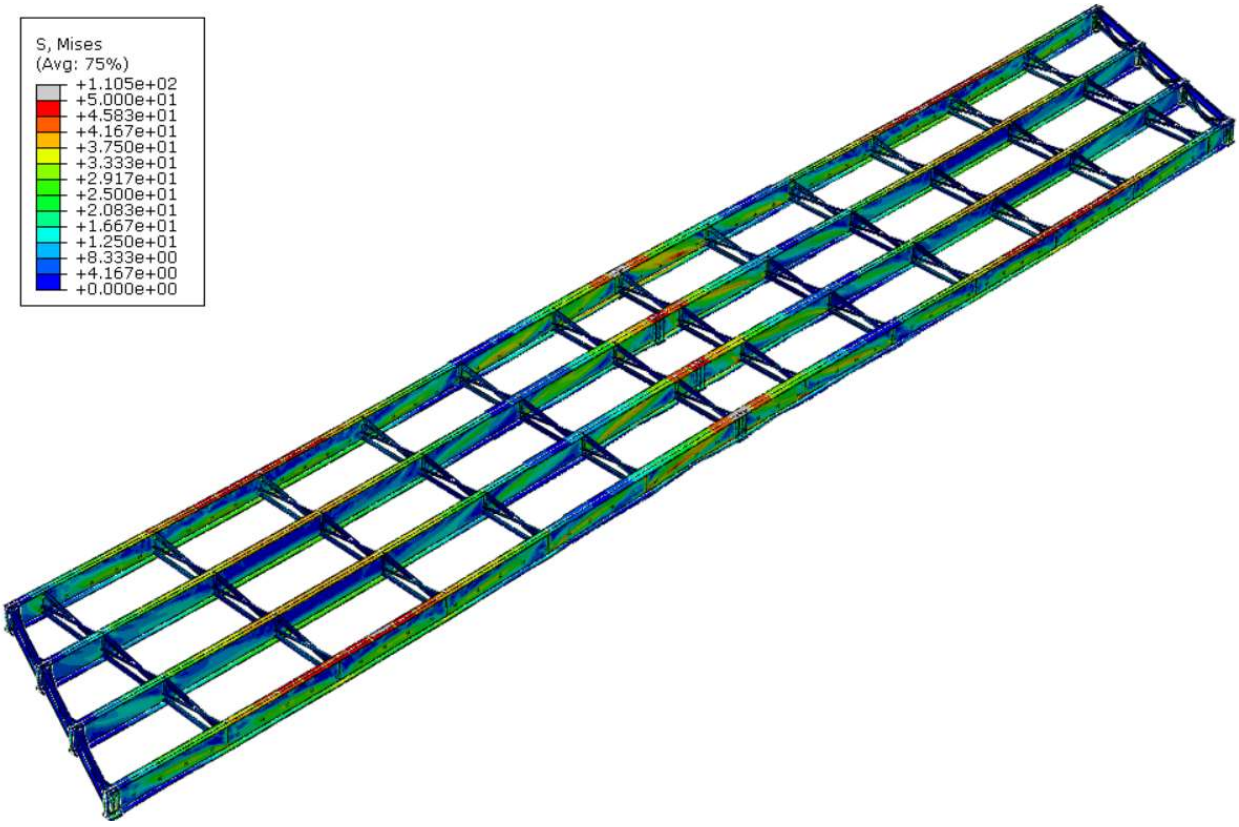

Figure A.97 Deformed shaped of the 20° skewed-unstaggered bridge with 4.57 m [15 ft] cross-frame spacing in isotropic view

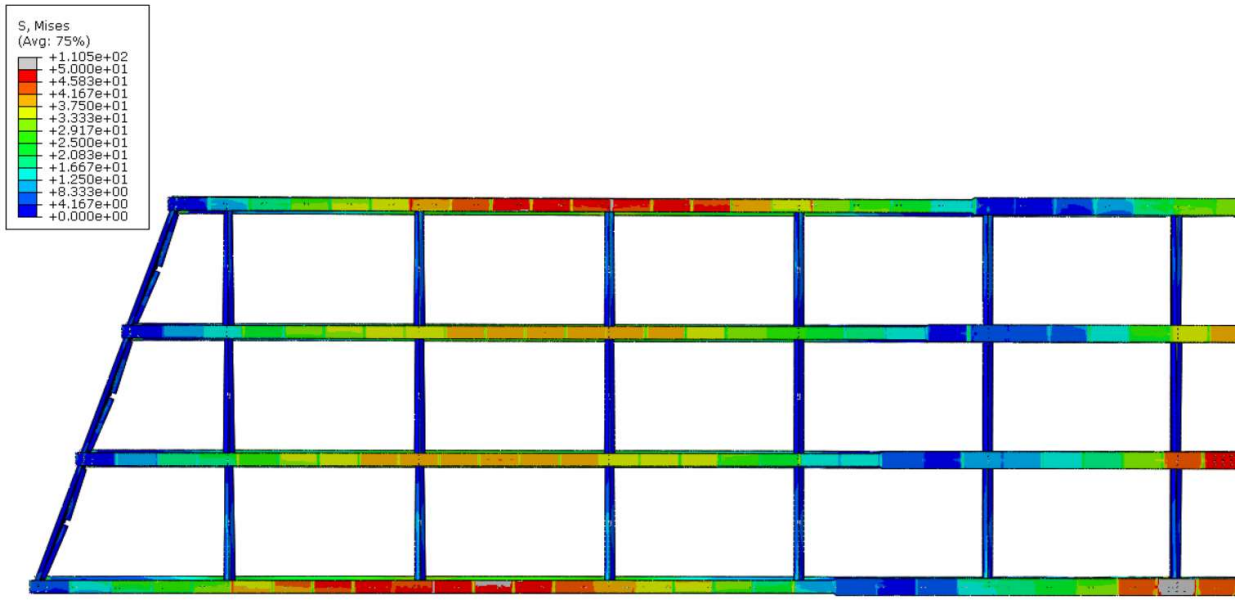

Figure A.98 Deformed shape of the 20° skewed-unstaggered bridge in Span 1 with 4.57 m [15 ft] cross-frame spacing in plan view

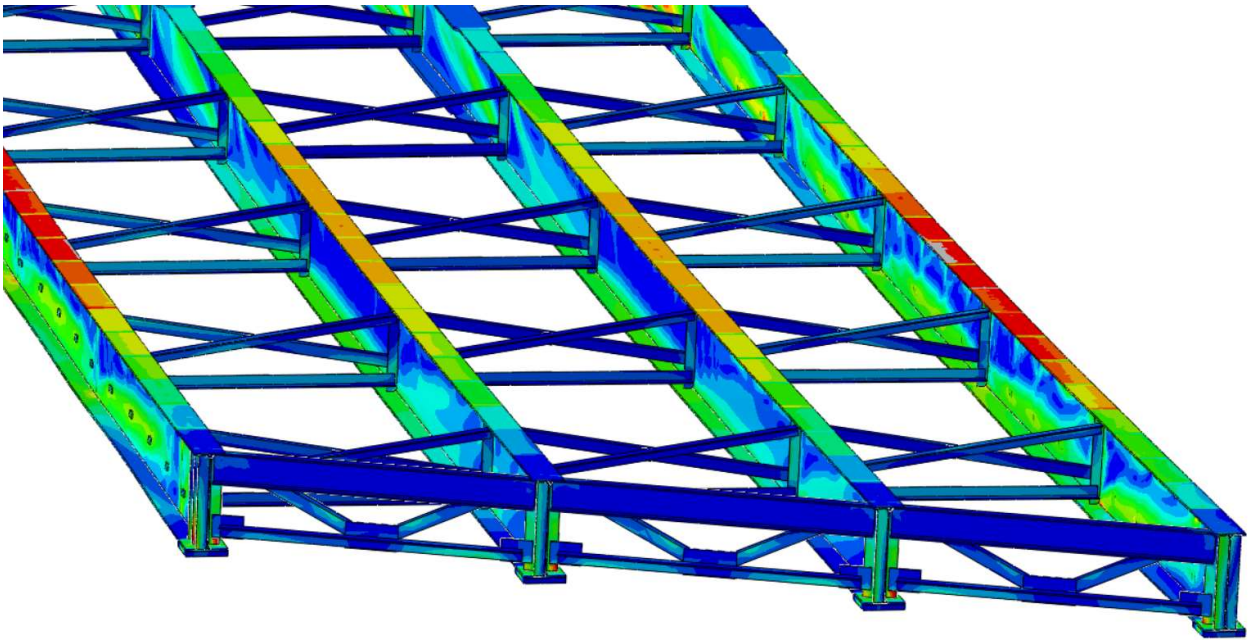

Figure A.99 Girder deformation of the 20° skewed-unstaggered bridge with 4.57 m [15 ft] cross-frame spacing

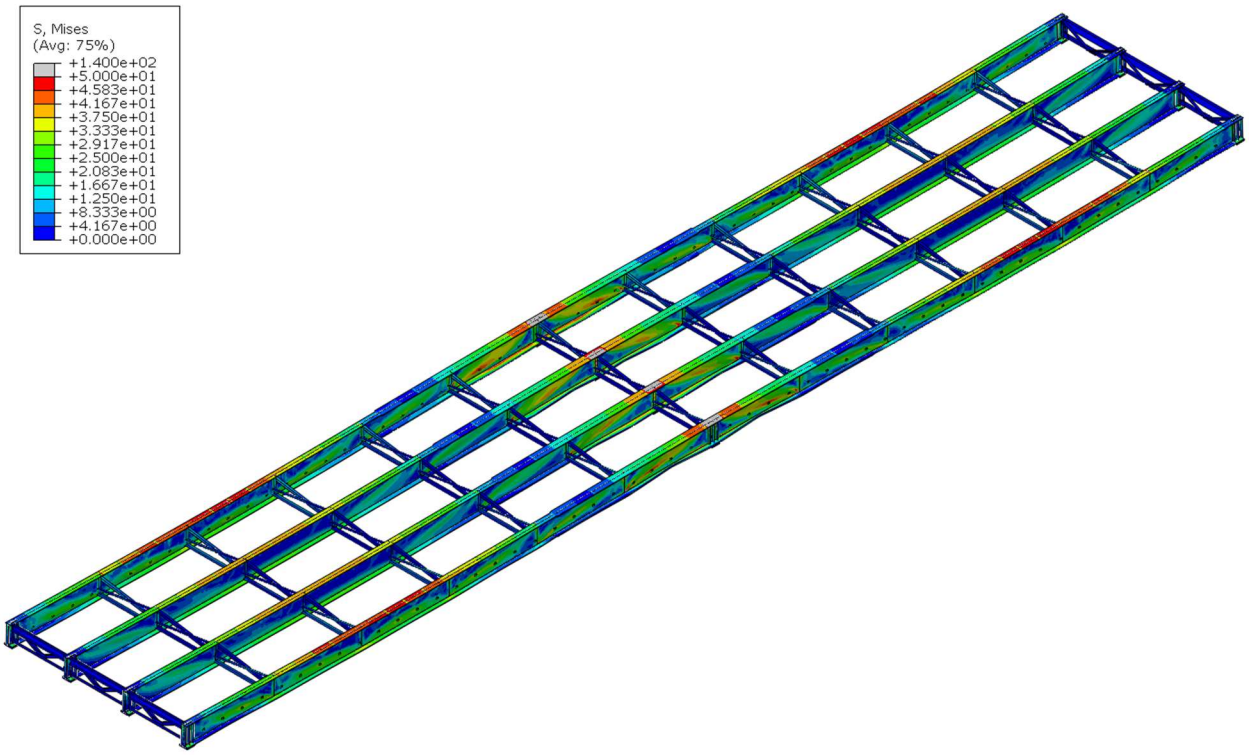

Figure A.100 Deformed shaped of the non-skewed bridge with 4.57 m [15 ft] cross-frame spacing in isotropic view

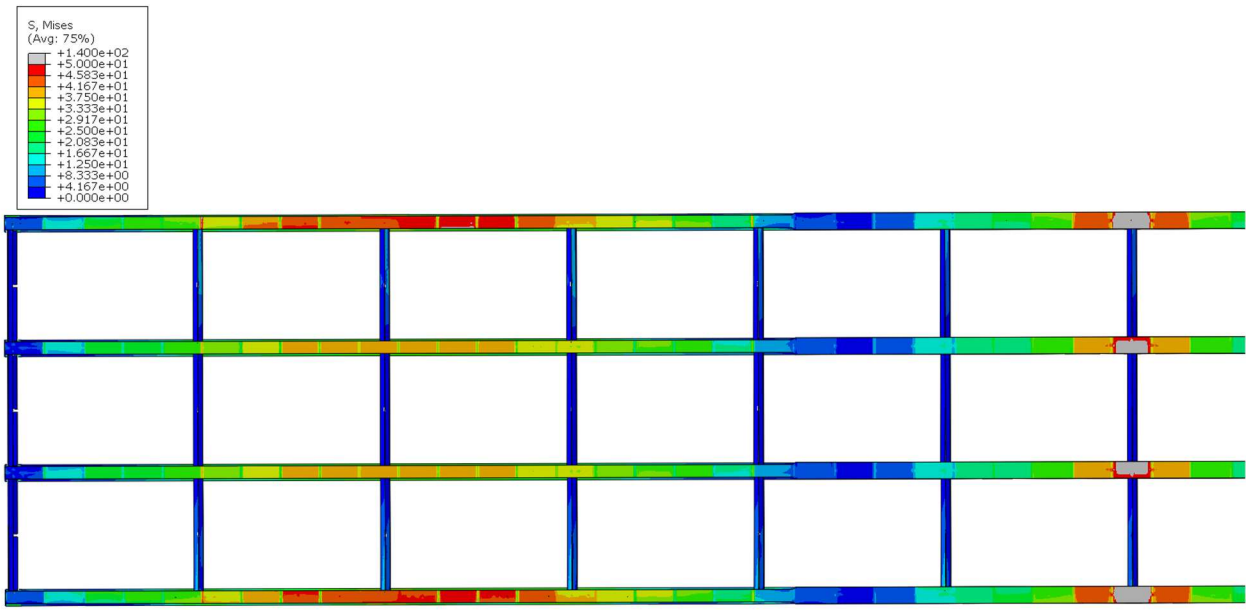

Figure A.101 Deformed shape of the non-skewed bridge in Span 1 with 4.57 m [15 ft] cross-frame spacing in plan view

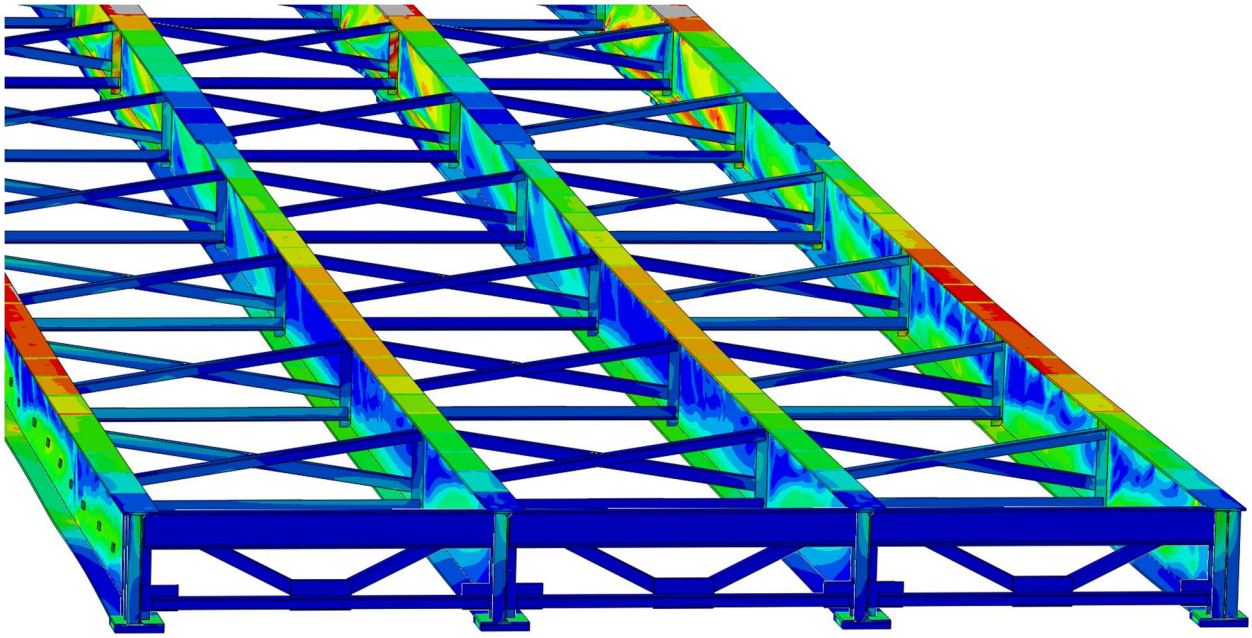

Figure A.102 Girder deformation of the non-skewed bridge with 4.57 m [15 ft] cross-frame spacing

APPENDIX B: AASHTO-PREDICTED CAPACITY CALCULATIONS

AASHTO girder section capacity calculations are presented in Appendix B for the interior and exterior girders in the positive and negative flexure regions (AASHTO 2010). Girder section properties are shown in Figure B.1, Figure B.2, Figure B.4, and Figure B.5 for each respective girder region. Bending moment diagrams, shown in Figure B.3 and Figure B.6 for the exterior and interior girders, respectively, were computed using Mastan2 (Ziemian and Mcguire 2000). Compression flange local buckling, tension flange yielding, and compression flange lateral-torsional buckling for the 4.2 m [15 ft], 9.14 m [30 ft], and 13.7 m [45 ft] cross-frame spacings are presented. Expected governing strengths for interior and exterior girders were calculated to provide a basis for comparison with values found in the 3D FEA bridge models.

Exterior Girder Check - Positive Flexure Region

b_{fc} = 12”
t_{fc} = 0.75”
D = 36”
t_w = 0.4375”
b_{ft} = 16”
t_{ft} = 0.875”
A = 38.75 in^2
$C_{y,top}$ = 21.145”
$C_{y,bot}$ = 16.48”
I_x = 9278.26 in^4
I_y = 406.92 in^4
S_{xt} = 562.95 in^3
S_{xc} = 438.79 in^3

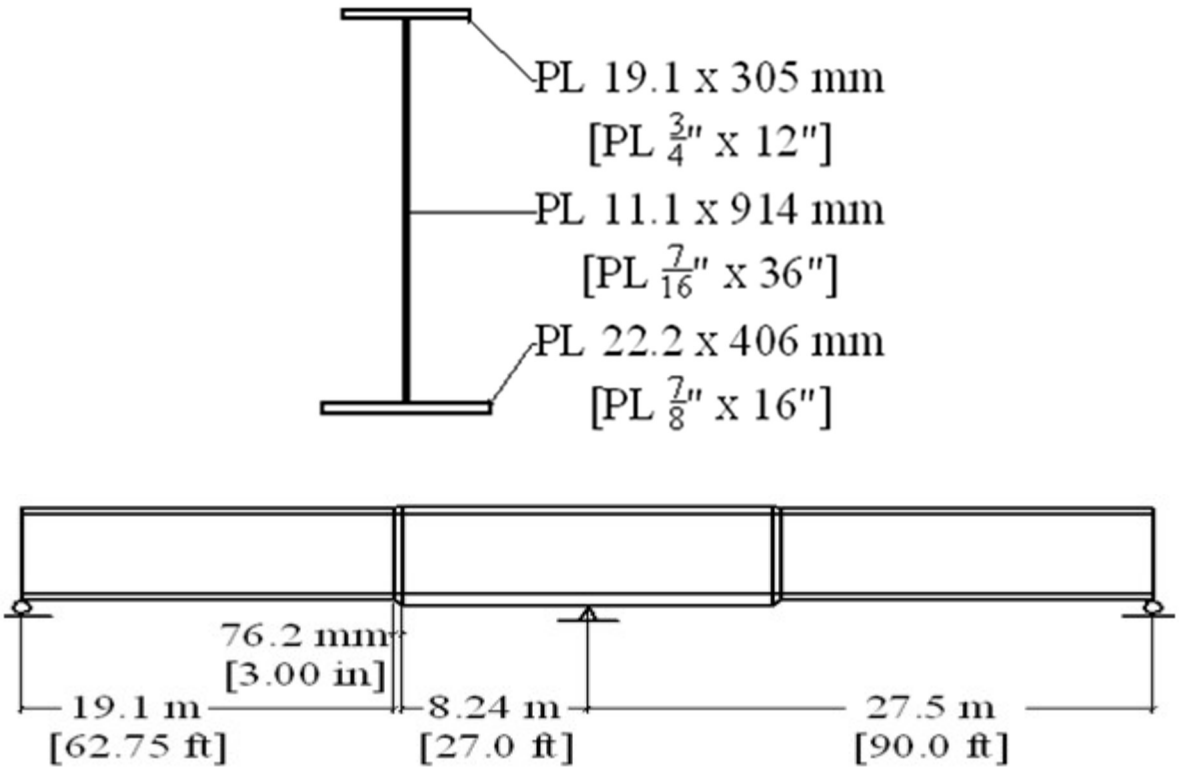

$S_y = 50.86\ in^3$

$r_x = 15.47$”

$r_y = 3.24$”

Figure B.1 Exterior girder positive flexure region section properties

Determine Classification of the Section:

Check $\frac{2D_c}{t_w} \leq 5.7\sqrt{\frac{E}{F_{yc}}}$ *(AASHTO 2010 6.10.6.2.3-1)*

$D_c = D + t_{ft} - C_y = 36 + {}^{7}/_{8}" - 16.48 = 20.40"$

Check $\frac{(2)(19")}{{}^{1}/_{2}"} = 93.23 \leq 5.7\sqrt{\frac{29{,}000\ ksi}{50\ ksi}} = 137.3$ OK, ∴ web is non-slender

Check $\frac{I_{yc}}{I_{yt}} \geq 0.3$

$I_{yc} = \frac{1}{12}bh^3 + Ad^2$

$I_{yc} = \frac{1}{12}(12")({}^{3}/_{4}")^3 + (9\ in^2)(20.77")^2 = 3{,}883\ in^4$

$I_{yt} = \frac{1}{12}(16")({}^{7}/_{8}")^3 + (14\ in^2)(16.04")^2 = 3{,}604\ in^4$

Check $\frac{I_{yc}}{I_{yt}} = \frac{3{,}883 in^4}{3{,}604 in^4} = 1.1 \geq 0.3$ OK

Check Compression Flange Local Buckling:

$\lambda_f = \frac{b_{fc}}{2t_{fc}} = \frac{12"}{(2)({}^{3}/_{4}")} = 8$ *(AASHTO 2010 6.10.8.2.2-3)*

$\lambda_{pf} = 0.38\sqrt{\frac{E}{F_{yc}}} = 0.38\sqrt{\frac{29{,}000\ ksi}{50\ ksi}} = 9.152$ *(AASHTO 2010 6.10.8.2.2-4)*

$\lambda_f < \lambda_{pf}$ ∴ compact flange

$F_{nc} = R_b R_h F_{yc}$ *(AASHTO 2010 6.10.8.2.2-1)*

R_b = 1.0 since web is non-slender

R_h = 1.0 since section is non-hybrid

$F_{nc} = R_b R_h F_{yc} = (1.0)(1.0)(50\ ksi) = \ 50\ ksi$

Check Compression Flange Lateral-Torsional Buckling:

Check unbraced length of the beam, **L_b = 45' = 540"**

$$r_t = \frac{b_{fc}}{\sqrt{12\left(1+\frac{1}{3}\frac{D_c t_w}{b_{fc} t_{fc}}\right)}} = \frac{12}{\sqrt{12\left(1+\frac{1}{3}\frac{(20.395")(7/16")}{(12")(3/4")}\right)}} = 3.003"$$ *(AASHTO 2010 6.10.8.2.3-9)*

$$L_p = 1.0 r_t \sqrt{\frac{E}{F_{yc}}} = (1.0)(3.003")\sqrt{\frac{29{,}000^{ksi}}{50^{ksi}}} = 72.33"$$ *(AASHTO 2010 6.10.8.2.3-4)*

$F_{yr} = \min\left(0.7F_{yc}, F_{yw}\right) \geq 0.5F_{yc}$ *(AASHTO 2010 pg6-145)*

$F_{yr} = (0.7)\left(50^{ksi}\right) = 35^{ksi} > 25ksi$

$$L_r = \pi r_t \sqrt{\frac{E}{F_{yr}}} = (\pi)(3.003")\sqrt{\frac{29{,}000^{ksi}}{35^{ksi}}} = 271.6"$$ *(AASHTO 2010 6.10.8.2.3-5)*

Since $L_p = 72.33" < L_r = 271.6" <$ L_b=540.0", Elastic LTB must be investigated.

$F_{nc} = F_{cr} \leq R_b R_h F_{yc}$ *(AASHTO 2010 6.10.8.2.3-3)*

$$F_{cr} = \frac{C_b R_b \pi^2 E}{(\frac{L_b}{r_t})^2}$$ *(AASHTO 2010 6.10.8.2.3-8)*

R_b = 1.0 since web is non-slender

R_h = 1.0 since section is non-hybrid

Compute the Moment Gradient Factor, Cb, for the Positive Flexure Critical Segment:

$$M_{mid} = 17{,}400^{k-in} \rightarrow f_{mid} = \frac{17{,}400^{k-in}}{438.8\ in^3} = 39.65\ ksi$$

$$M_2 = 16{,}020^{k-in} \rightarrow f_2 = \frac{16{,}020^{k-i}}{438.8\ in^3} = 36.51\ ksi$$

$$f_{mid}/f_2 > 1$$

$$C_b = 1 \qquad \textit{(AASHTO 2010 6.10.8.2.3-6)}$$

$$F_{cr} = \frac{(1.0)(1.0)\pi^2(29{,}000\ ksi)}{(\frac{540"}{3.003})^2} = 8.85\ ksi < 50\ ksi\ max \rightarrow F_{cr} = 8.85\ ksi$$

Check Compression Flange Lateral-Torsional Buckling:

Check unbraced length of the beam, **L_b = 30' = 360"**

$$r_t = \frac{b_{fc}}{\sqrt{12\left(1+\frac{1}{3}\frac{D_c t_w}{b_{fc} t_{fc}}\right)}} = \frac{12}{\sqrt{12\left(1+\frac{1}{3}\frac{(20.395")(7/16")}{(12")(3/4")}\right)}} = 3.003" \qquad \textit{(AASHTO 2010 6.10.8.2.3-9)}$$

$$L_p = 1.0 r_t \sqrt{\frac{E}{F_{yc}}} = (1.0)(3.003")\sqrt{\frac{29{,}000^{ksi}}{50^{ksi}}} = 72.33" \qquad \textit{(AASHTO 2010 6.10.8.2.3-4)}$$

$$F_{yr} = \min\left(0.7F_{yc}, F_{yw}\right) \geq 0.5F_{yc} \qquad \textit{(AASHTO 2010 pg6-145)}$$

$$F_{yr} = (0.7)\left(50^{ksi}\right) = 35^{ksi} > 25ksi$$

$$L_r = \pi r_t \sqrt{\frac{E}{F_{yr}}} = (\pi)(3.003")\sqrt{\frac{29{,}000^{ksi}}{35^{ksi}}} = 271.6" \qquad \textit{(AASHTO 2010 6.10.8.2.3-5)}$$

Since $L_p = 72.33" < L_r = 271.6" <$ L_b=360.0", Elastic LTB must be investigated.

$$F_{nc} = F_{cr} \leq R_b R_h F_{yc} \qquad \textit{(AASHTO 2010 6.10.8.2.3-3)}$$

$$F_{cr} = \frac{C_b R_b \pi^2 E}{(\frac{L_b}{r_t})^2} \qquad \textit{(AASHTO 2010 6.10.8.2.3-8)}$$

R_b = 1.0 since web is non-slender

R_h = 1.0 since section is non-hybrid

Compute the Moment Gradient Factor, Cb, for the Positive Flexure Critical Segment:

$$C_b = 1.75 - 1.05\left(\frac{f_1}{f_2}\right) + 0.3\left(\frac{f_1}{f_2}\right)^2 \leq 2.3$$ *(AASHTO 2010 6.10.8.2.3-7)*

$$M_2 = 17{,}400^{k-in} \rightarrow f_2 = \frac{17{,}400^{k-in}}{438.8\ in^3} = 39.65\ ksi$$

$$M_0 = 0^{k-in} \rightarrow f_0 = 0\ ksi$$

$$M_{mid} = 12{,}890^{k-in} \rightarrow f_{mid} = \frac{12{,}890^{k-in}}{438.8\ in^3} = 29.38\ ksi$$

Since the bending moment diagram is not concave,

$$f_1 = 2f_{mid} - f_2 \geq f_0$$ *(AASHTO 2010 6.10.8.2.3-11)*

$$(2)(29.38) - (39.65^{ksi}) = 19.11\ ksi \geq 0\ ksi$$

$$C_b = 1.75 - 1.05\left(\frac{19.11}{39.65}\right) + 0.3\left(\frac{19.11}{39.65}\right)^2 = 1.314 \leq 2.3 \rightarrow C_b = 1.314$$

$$F_{cr} = \frac{(1.314)(1.0)\pi^2(29{,}000\ ksi)}{(\frac{360"}{3.003})^2} = 26.17\ ksi < 50\ ksi\ max \rightarrow F_{cr} = 26.17\ ksi$$

<u>Check Compression Flange Lateral-Torsional Buckling:</u>

Check unbraced length of the beam, **L_b = 15' = 180"**

$$r_t = \frac{b_{fc}}{\sqrt{12\left(1+\frac{1}{3}\frac{D_c t_w}{b_{fc} t_{fc}}\right)}} = \frac{12}{\sqrt{12\left(1+\frac{1}{3}\frac{(20.395")(7/16")}{(12")(3/4")}\right)}} = 3.003"$$ *(AASHTO 2010 6.10.8.2.3-9)*

$$L_p = 1.0 r_t \sqrt{\frac{E}{F_{yc}}} = (1.0)(3.003")\sqrt{\frac{29{,}000^{ksi}}{50^{ksi}}} = 72.33"$$ *(AASHTO 2010 6.10.8.2.3-4)*

$$F_{yr} = \min\left(0.7F_{yc}, F_{yw}\right) \geq 0.5F_{yc}$$ *(AASHTO 2010 pg6-145)*

$$F_{yr} = (0.7)\left(50^{ksi}\right) = 35^{ksi} > 25ksi$$

$$L_r = \pi r_t \sqrt{\frac{E}{F_{yr}}} = (\pi)(3.003")\sqrt{\frac{29{,}000^{ksi}}{35^{ksi}}} = 271.6"$$ *(AASHTO 2010 6.10.8.2.3-5)*

Since $L_p = 72.33" < L_b = 180.0" < L_r = 271.6"$, Inelastic LTB must be investigated.

$$F_{nc(LTB)} = C_b[1 - \left(1 - \frac{F_{yr}}{R_h F_{yc}}\right)\left(\frac{L_b - L_p}{L_r - L_p}\right)]R_b R_h F_{yc} \leq R_b R_h F_{yc} \qquad \textit{(AASHTO 2010 6.10.8.2.3-2)}$$

$R_b = 1.0$ since web is non-slender

$R_h = 1.0$ since section is non-hybrid

Compute the Moment Gradient Factor, Cb, for the Abutment Segment:

$$C_b = 1.75 - 1.05\left(\frac{f_1}{f_2}\right) + 0.3\left(\frac{f_1}{f_2}\right)^2 \leq 2.3 \qquad \textit{(AASHTO 2010 6.10.8.2.3-7)}$$

$$M_2 = 12{,}890^{k-in} \rightarrow f_2 = \frac{12{,}890^{k-in}}{438.8\ in^3} = 29.38\ ksi$$

$$M_0 = 0^{k-in} \rightarrow f_0 = 0\ ksi$$

$$M_{mid} = 7{,}699^{k-i} \rightarrow f_{mid} = \frac{7{,}699^{k-in}}{438.8\ in^3} = 17.55\ ksi$$

Since the bending moment diagram is not concave,

$$f_1 = 2f_{mid} - f_2 \geq f_0 \qquad \textit{(AASHTO 2010 6.10.8.2.3-11)}$$

$$(2)\left(17.55^{ksi}\right) - (29.38^{ksi}) = 5.720^{ksi} \geq 0\ ksi$$

$$C_b = 1.75 - 1.05\left(\frac{5.720}{29.38}\right) + 0.3\left(\frac{5.720}{29.38}\right)^2 = 1.557 \leq 2.3 \rightarrow C_b = 1.557$$

Compute the Moment Gradient Factor, Cb, for the Mid-span Segment:

$$M_2 = 17{,}400^{k-in} \rightarrow f_2 = \frac{17{,}400^{k-in}}{438.8\ in^3} = 39.65\ ksi$$

$$M_0 = 12{,}890^{k-in} \rightarrow f_0 = \frac{12{,}890^{k-in}}{438.8\ in^3} = 29.38\ ksi$$

$$M_{mid} = 16{,}130^{k-in} \rightarrow f_{mid} = \frac{16{,}130^{k-in}}{438.8\ in^3} = 36.76\ ksi$$

Since the bending moment diagram is not concave,

$$f_1 = 2f_{mid} - f_2 \geq f_0 \qquad \textit{(AASHTO 2010 6.10.8.2.3-11)}$$

$(2)\left(36.76^{ksi}\right) - (39.65^{ksi}) = 33.87^{ksi} \geq f_0 = 29.38 \rightarrow f_1 = 33.87\ ksi$

$C_b = 1.75 - 1.05\left(\frac{33.87}{39.65}\right) + 0.3\left(\frac{33.87}{39.65}\right)^2 = 1.072 \leq 2.3 \quad \rightarrow C_b = 1.557$ Controls

$$F_{nc(LTB)} = 1.557\left[1 - \left(1 - \frac{35^{ksi}}{(1.00)(50^{ksi})}\right)\left(\frac{180.0" - 72.33"}{271.56" - 72.33"}\right)\right](1.0)(1.0)\left(50^{ksi}\right)$$

$$\leq (1.0)(1.0)\left(50^{ksi}\right)$$

$F_{nc(LTB)} = 65.23\ ksi \leq 50\ ksi\ max \rightarrow F_{nc(LTB)} = 50\ ksi$

The governing strength for the compression flange is the smaller of $F_{nc(FLB)}\ and\ F_{nc(LTB)}$:

For **L_b = 45'**, $F_{nc(LTB)} = 8.85^{ksi} < F_{nc(FLB)} = 50^{ksi}$, LTB governs the strength of the compression flange.

$F_{nc} = F_{nc(LTB)} = 8.85\ ksi$

$\Phi F_{nc} = (1.0)(8.85) = 8.85\ ksi$ *(AASHTO 2010 6.10.8.1.1-1)*

For **L_b = 30'**, $F_{nc(LTB)} = 26.15^{ksi} < F_{nc(FLB)} = 50^{ksi}$, LTB governs the strength of the compression flange.

$F_{nc} = F_{nc(LTB)} = 26.15\ ksi$

$\Phi F_{nc} = (1.0)(26.15) = 26.15\ ksi$ *(AASHTO 2010 6.10.8.1.1-1)*

For **L_b = 15'**, $F_{nc(LTB)} = F_{nc(FLB)} = 50\ ksi$, yielding governs the strength of the compression flange.

$F_{nc} = F_{yc} = 50\ ksi$

$\Phi F_{nc} = (1.0)\left(50^{ksi}\right) = 50\ ksi$ *(AASHTO 2010 6.10.8.1.1-1)*

Investigate the Strength of the Tension Flange:

$F_{nt} = R_h F_{yt} = (1.0)\left(50^{ksi}\right) = 50^{ksi}$ *(AASHTO 2010 6.10.8.3-1)*

$\Phi F_{nt} = (1.0)\left(50^{ksi}\right) = 50^{ksi}$

Exterior Girder Check - Negative Flexure Region

b_{fc} = 16”

t_{fc} = 2.0”

D = 36”

t_w = 0.5”

b_{ft} = 16”

t_{ft} = 1.0”

A = 66 in^2

C_y = 15.27”

I_x = 17510 in^4

I_y = 1024 in^4

S_{xt} = 737.88 in^3

S_{xc} = 1146 in^3

S_y = 128.1 in^3

r_x = 16.29”

r_y = 3.94”

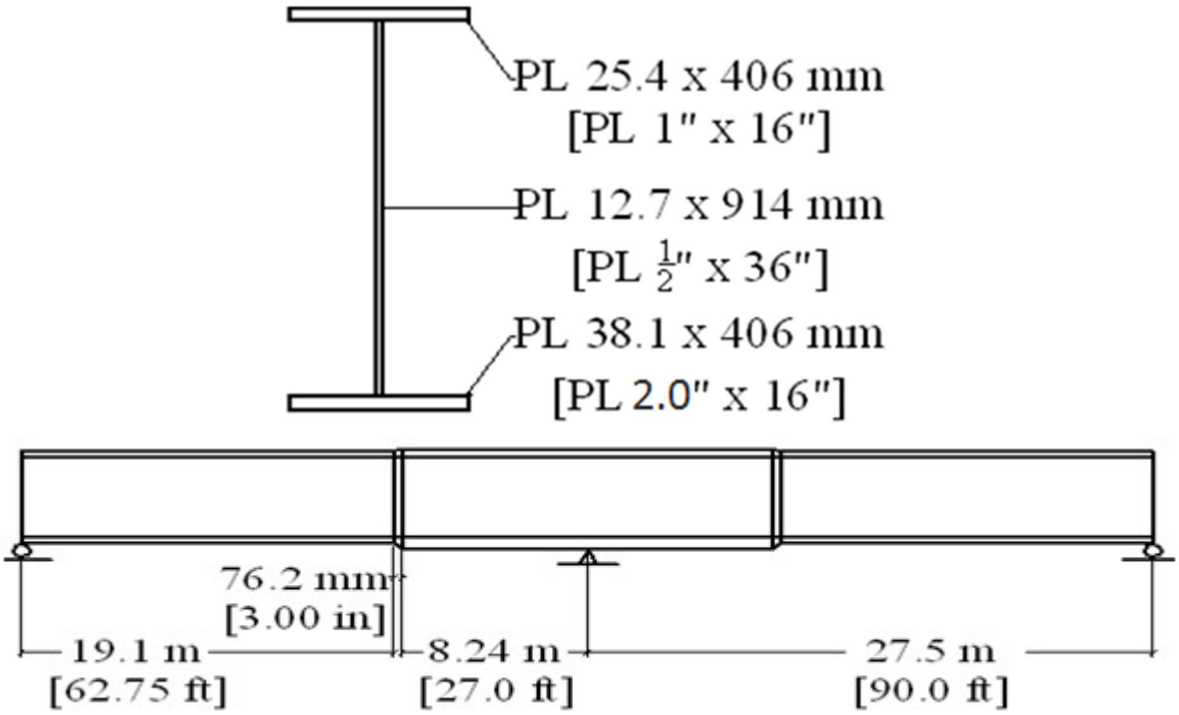

Figure B.2 Exterior girder negative flexure region section properties

Determine Classification of the Section:

Check $\frac{2D_c}{t_w} \leq 5.7\sqrt{\frac{E}{F_{yc}}}$ *(AASHTO 2010 6.10.6.2.3-1)*

$D_c = C_y - t_{fc} = 15.27 + 2.0" = 13.27"$

Check $\frac{(2)(19")}{1/2"} = 53.08 \leq 5.7\sqrt{\frac{29{,}000\ ksi}{50\ ksi}} = 137.3$ OK, ∴ web is non-slender

Check $\frac{I_{yc}}{I_{yt}} \geq 0.3$

$I_{yc} = \frac{1}{12}bh^3 + Ad^2$

$I_{yc} = \frac{1}{12}(16")(2.0")^3 + (32\ in^2)(14.27")^2 = 6{,}527\ in^4$

$$I_{yt} = \frac{1}{12}(16")(1.0")^3 + (16\ in^2)(23.23")^2 = 8{,}635\ in^4$$

Check $\frac{I_{yc}}{I_{yt}} = \frac{6{,}527\ in^4}{8{,}635\ in^4} = 0.76 \geq 0.3$ OK

Check Compression Flange Local Buckling:

$$\lambda_f = \frac{b_{fc}}{2t_{fc}} = \frac{16"}{(2)(2.0")} = 4.0$$ *(AASHTO 2010 6.10.8.2.2-3)*

$$\lambda_{pf} = 0.38\sqrt{\frac{E}{F_{yc}}} = 0.38\sqrt{\frac{29{,}000\ ksi}{50\ ksi}} = 9.152$$ *(AASHTO 2010 6.10.8.2.2-4)*

$\lambda_f < \lambda_{pf}$ ∴ compact flange

$$F_{nc} = R_b R_h F_{yc}$$ *(AASHTO 2010 6.10.8.2.2-1)*

R_b = 1.0 since web is non-slender

R_h = 1.0 since section is non-hybrid

$$F_{nc} = R_b R_h F_{yc} = (1.0)(1.0)(50\ ksi) = 50\ ksi$$

Check Compression Flange Lateral-Torsional Buckling:

Check unbraced length of the beam, **L_b = 45' = 540"**

$$r_t = \frac{b_{fc}}{\sqrt{12\left(1+\frac{1}{3}\frac{D_c t_w}{b_{fc} t_{fc}}\right)}} = \frac{16}{\sqrt{12\left(1+\frac{1}{3}\frac{(13.27")(1/2")}{(16")(2.0"}\right)}} = 4.566"$$ *(AASHTO 2010 6.10.8.2.3-9)*

$$L_p = 1.0 r_t \sqrt{\frac{E}{F_{yc}}} = (1.0)(4.566")\sqrt{\frac{29{,}000^{ksi}}{50^{ksi}}} = 110.0"$$ *(AASHTO 2010 6.10.8.2.3-4)*

$$F_{yr} = \min\left(0.7F_{yc}, F_{yw}\right) \geq 0.5F_{yc}$$ *(AASHTO 2010 pg6-145)*

$$F_{yr} = (0.7)\left(50^{ksi}\right) = 35^{ksi} > 25ksi$$

$$L_r = \pi r_t \sqrt{\frac{E}{F_{yr}}} = (\pi)(4.566")\sqrt{\frac{29{,}000^{ksi}}{35^{ksi}}} = 412.9"$$ *(AASHTO 2010 6.10.8.2.3-5)*

Since $L_p = 110.0" < L_r = 412.9" <$ L_b=540.0", Elastic LTB must be investigated.

$F_{nc} = F_{cr} \leq R_b R_h F_{yc}$ *(AASHTO 2010 6.10.8.2.3-3)*

$F_{cr} = \frac{C_b R_b \pi^2 E}{(\frac{L_b}{r_t})^2}$ *(AASHTO 2010 6.10.8.2.3-8)*

R_b = 1.0 since web is non-slender

R_h = 1.0 since section is non-hybrid

Compute the Moment Gradient Factor, Cb, for the Positive Flexure Critical Segment:

$C_b = 1.75 - 1.05\left(\frac{f_1}{f_2}\right) + 0.3\left(\frac{f_1}{f_2}\right)^2 \leq 2.3$ *(AASHTO 2010 6.10.8.2.3-7)*

$M_{mid} = -5{,}646^{k-in} \rightarrow f_{mid} = \frac{5{,}646^{k-in}}{1{,}146\ in^3} = 4.93\ ksi$

$M_2 = -43{,}920^{k-in} \rightarrow f_2 = \frac{43{,}920^{k-in}}{1{,}146\ in^3} = 38.32\ ksi$

$M_0 = 0^{k-in} \rightarrow f_0 = 0\ ksi$

Since the bending moment diagram is concave,

$f_1 = f_0 = 0\ ksi$ *(AASHTO 2010 6.10.8.2.3-10)*

$C_b = 1.75 - 1.05\left(\frac{0}{38.32}\right) + 0.3\left(\frac{0}{38.32}\right)^2 = 1.75 \leq 2.3 \rightarrow C_b = 1.75$

$F_{cr} = \frac{(1.75)(1.0)\pi^2(29{,}000\ ksi)}{(\frac{540"}{4.566})^2} = 35.81\ ksi < 50\ ksi\ max \rightarrow F_{cr} = 35.81\ ksi$

<u>Check Compression Flange Lateral-Torsional Buckling:</u>

Check unbraced length of the beam, **L_b = 30' = 360"**

$$r_t = \frac{b_{fc}}{\sqrt{12\left(1+\frac{1}{3}\frac{D_c t_w}{b_{fc} t_{fc}}\right)}} = \frac{16}{\sqrt{12\left(1+\frac{1}{3}\frac{(13.27")(1/2")}{(16")(2.0"}\right)}} = 4.566"$$ *(AASHTO 2010 6.10.8.2.3-9)*

$$L_p = 1.0 r_t \sqrt{\frac{E}{F_{yc}}} = (1.0)(4.566")\sqrt{\frac{29{,}000^{ksi}}{50^{ksi}}} = 110.0"$$ *(AASHTO 2010 6.10.8.2.3-4)*

$$F_{yr} = \min\left(0.7F_{yc}, F_{yw}\right) \geq 0.5F_{yc}$$ *(AASHTO 2010 pg6-145)*

$$F_{yr} = (0.7)\left(50^{ksi}\right) = 35^{ksi} > 25ksi$$

$$L_r = \pi r_t \sqrt{\frac{E}{F_{yr}}} = (\pi)(4.566")\sqrt{\frac{29{,}000^{ksi}}{35^{ksi}}} = 412.9"$$ *(AASHTO 2010 6.10.8.2.3-5)*

Since $L_p = 110.0" < L_b = 360.0" <$ L_b=412.9", Inelastic LTB must be investigated.

$$F_{nc(LTB)} = C_b[1 - \left(1 - \frac{F_{yr}}{R_h F_{yc}}\right)\left(\frac{L_b - L_p}{L_r - L_p}\right)]R_b R_h F_{yc} \leq R_b R_h F_{yc}$$ *(AASHTO 2010 6.10.8.2.3-2)*

R_b = 1.0 since web is non-slender

R_h = 1.0 since section is non-hybrid

Compute the Moment Gradient Factor, Cb, for the Negative Flexure Critical Segment:

$$C_b = 1.75 - 1.05\left(\frac{f_1}{f_2}\right) + 0.3\left(\frac{f_1}{f_2}\right)^2 \leq 2.3$$ *(AASHTO 2010 6.10.8.2.3-7)*

$$M_2 = -43{,}920^{k-in} \rightarrow f_2 = \frac{43{,}920^{k-in}}{1{,}146\ in^3} = 38.32\ ksi$$

$$M_0 = 0^{k-in} \rightarrow f_0 = 0\ ksi$$

$$M_{mid} = -16{,}290^{k-in} \rightarrow f_{mid} = \frac{16{,}290^{k-in}}{1{,}146\ in^3} = 14.21\ ksi$$

Since the bending moment diagram is concave,

$$f_1 = f_0 = 0\ ksi$$ *(AASHTO 2010 6.10.8.2.3-10)*

$$C_b = 1.75 - 1.05\left(\frac{0}{38.32}\right) + 0.3\left(\frac{0}{38.32}\right)^2 = 1.75 \leq 2.3 \rightarrow C_b = 1.75$$

$$F_{nc(LTB)} = 1.75\left[1 - \left(1 - \frac{35^{ksi}}{(1.00)(50^{ksi})}\right)\left(\frac{360.0" - 110.0"}{412.9" - 110.0"}\right)\right](1.0)(1.0)\left(50^{ksi}\right)$$

$$\leq (1.0)(1.0)\left(50^{ksi}\right)$$

$$F_{nc(LTB)} = 65.83\ ksi \leq 50\ ksi\ max \rightarrow F_{nc(LTB)} = 50\ ksi$$

Check Compression Flange Lateral-Torsional Buckling:

Check unbraced length of the beam, **L_b = 15' = 180"**

$$r_t = \frac{b_{fc}}{\sqrt{12\left(1+\frac{1}{3}\frac{D_c t_w}{b_{fc} t_{fc}}\right)}} = \frac{16}{\sqrt{12\left(1+\frac{1}{3}\frac{(13.27")(1/2")}{(16")(2.0"}\right)}} = 4.566"$$ *(AASHTO 2010 6.10.8.2.3-9)*

$$L_p = 1.0 r_t \sqrt{\frac{E}{F_{yc}}} = (1.0)(4.566")\sqrt{\frac{29{,}000^{ksi}}{50^{ksi}}} = 110.0"$$ *(AASHTO 2010 6.10.8.2.3-4)*

$$F_{yr} = \min\left(0.7F_{yc}, F_{yw}\right) \geq 0.5F_{yc}$$ *(AASHTO 2010 pg6-145)*

$$F_{yr} = (0.7)\left(50^{ksi}\right) = 35^{ksi} > 25ksi$$

$$L_r = \pi r_t \sqrt{\frac{E}{F_{yr}}} = (\pi)(4.566")\sqrt{\frac{29{,}000^{ksi}}{35^{ksi}}} = 412.9"$$ *(AASHTO 2010 6.10.8.2.3-5)*

Since $L_p = 110.0" < L_b = 180.0" <$ L_b=412.9", Inelastic LTB must be investigated.

$$F_{nc(LTB)} = C_b[1 - \left(1 - \frac{F_{yr}}{R_h F_{yc}}\right)\left(\frac{L_b - L_p}{L_r - L_p}\right)]R_b R_h F_{yc} \leq R_b R_h F_{yc}$$ *(AASHTO 2010 6.10.8.2.3-2)*

R_b = 1.0 since web is non-slender

R_h = 1.0 since section is non-hybrid

Compute the Moment Gradient Factor, Cb, for the Transition Region Segment:

$$C_b = 1.75 - 1.05\left(\frac{f_1}{f_2}\right) + 0.3\left(\frac{f_1}{f_2}\right)^2 \leq 2.3$$ *(AASHTO 2010 6.10.8.2.3-7)*

$$M_2 = -16{,}290^{k-in} \rightarrow f_2 = \frac{16{,}290^{k-in}}{1{,}146\ in^3} = 14.21\ ksi$$

$M_0 = 0^{k-in} \rightarrow f_0 = 0\ ksi$

$M_{mid} = -5{,}646^{k-in} \rightarrow f_{mid} = \dfrac{5{,}646^{k-in}}{1{,}146\ in^3} = 4.93\ ksi$

Since the bending moment diagram is concave,

$f_1 = f_0 = 0\ ksi$ *(AASHTO 2010 6.10.8.2.3-10)*

$C_b = 1.75 - 1.05\left(\frac{0}{14.21}\right) + 0.3\left(\frac{0}{14.21}\right)^2 = 1.75 \leq 2.3 \ \rightarrow C_b = 1.75$

Compute the Moment Gradient Factor, Cb, for Center Pier Segment:

$M_2 = -43{,}920^{k-in} \rightarrow f_2 = \dfrac{43{,}920^{k-in}}{1{,}146\ in^3} = 38.32\ ksi$

$M_0 = -16{,}290^{k-in} \rightarrow f_0 = \dfrac{16{,}290^{k-in}}{1{,}146\ in^3} = 14.21\ ksi$

$M_{mid} = -29{,}050^{k-in} \rightarrow f_{mid} = \dfrac{29{,}050^{k-in}}{1{,}146\ in^3} = 25.35\ ksi$

Since the bending moment diagram is concave,

$f_1 = f_0 = 14.21\ ksi$ *(AASHTO 2010 6.10.8.2.3-10)*

$C_b = 1.75 - 1.05\left(\frac{14.21}{38.32}\right) + 0.3\left(\frac{14.21}{38.32}\right)^2 = 1.40 \leq 2.3 \ \rightarrow C_b = 1.75$ Controls

$$F_{nc(LTB)} = 1.75\left[1 - \left(1 - \frac{35^{ksi}}{(1.00)(50^{ksi})}\right)\left(\frac{180.0" - 110.0"}{412.9" - 110.0"}\right)\right](1.0)(1.0)\left(50^{ksi}\right)$$

$$\leq (1.0)(1.0)\left(50^{ksi}\right)$$

$F_{nc(LTB)} = 81.43\ ksi \leq 50\ ksi\ max \rightarrow F_{nc(LTB)} = 50\ ksi$

The governing strength for the compression flange is the smaller of $F_{nc(FLB)}\ and\ F_{nc(LTB)}$:

For **L_b = 45'**, $F_{nc(LTB)} = 35.81^{ksi} < F_{nc(FLB)} = 50^{ksi}$, LTB governs the strength of the compression flange.

$F_{nc} = F_{nc(LTB)} = 35.81\ ksi$

$\Phi F_{nc} = (1.0)(35.81) = 35.81\ ksi$ *(AASHTO 2010 6.10.8.1.1-1)*

For **L_b = 30'**, $F_{nc(LTB)} = 50^{ksi} < F_{nc(FLB)} =$

50^{ks} , yielding governs the strength of the compression flange.

$F_{nc} = F_{yc} = 50\ ksi$

$\Phi F_{nc} = (1.0)(50) = 50\ ksi$ *(AASHTO 2010 6.10.8.1.1-1)*

For **L_b = 15'**, $F_{nc(LTB)} = F_{nc(FLB)} =$

$50\ ksi$, yielding governs the strength of the compression flange.

$F_{nc} = F_{yc} = 50\ ksi$

$\Phi F_{nc} = (1.0)\left(50^{ksi}\right) = 50\ ksi$ *(AASHTO 2010 6.10.8.1.1-1)*

Investigate the Strength of the Tension Flange:

$F_{nt} = R_h F_{yt} = (1.0)\left(\ 50^{ksi}\right) = 50^{ksi}$ *(AASHTO 2010 6.10.8.3-1)*

$\Phi F_{nt} = (1.00)\ \left(\ 50^{ksi}\right) = 50^{ksi}$

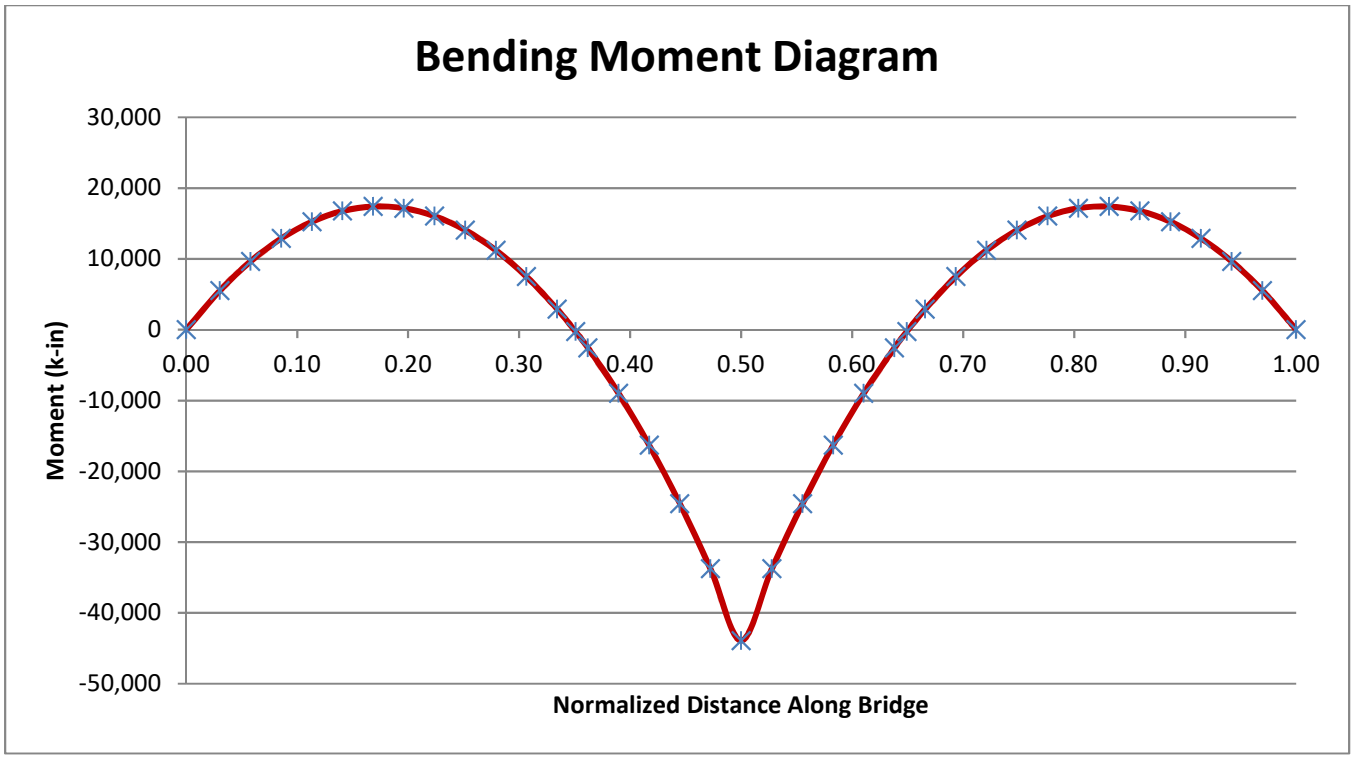

Figure B.3 Exterior girder bending moment diagram

Table B.1 Exterior girder moment and stress along bridge

Normalized Position	Position (in)	M_z (k-in)	σ_z (ksi)
0.00	0	0	0
0.03	66	5532.5	9.83
0.06	126	9647.7	17.14
0.09	186	12892	22.90
0.11	246	15266	27.12
0.14	306	16768	29.78
0.17	366	17400	30.91
0.20	426	17161	30.48
0.22	486	16051	28.51
0.25	546	14071	24.99
0.28	606	11219	19.93
0.31	666	7496.8	13.32
0.33	726	2903.6	5.16
0.35	762	-270.35	-0.48
0.36	786	-2565.8	-4.56
0.39	846	-8960.8	-15.92
0.42	906	-16293	-28.94
0.44	966	-24563	-43.63
0.47	1026	-33771	-59.98
0.50	1086	-43916	-78.00
0.53	1146	-33771	-59.98
0.56	1206	-24563	-43.63
0.58	1266	-16293	-28.94
0.61	1326	-8960.8	-15.92
0.64	1386	-2565.8	-4.56
0.65	1410	-270.35	-0.48
0.67	1446	2903.6	5.16
0.69	1506	7496.8	13.32
0.72	1566	11219	19.93
0.75	1626	14071	24.99
0.78	1686	16051	28.51
0.80	1746	17161	30.48
0.83	1806	17400	30.91
0.86	1866	16768	29.78
0.89	1926	15266	27.12
0.91	1986	12892	22.90
0.94	2046	9647.7	17.14
0.97	2106	5532.5	9.83
1.00	2172	0	0

Interior Girder Check - Positive Flexure Region

b_{fc} = 12”

t_{fc} = 0.75”

D = 36”

t_w = 0.4375”

b_{ft} = 16”

t_{ft} = 0.875”

A = 38.75 in^2

$C_{y,top}$ = 21.145”

$C_{y,bot}$ = 16.48”

I_x = 9278.26 in^4

I_y = 406.92 in^4

S_{xt} = 562.95 in^3

S_{xc} = 438.79 in^3

S_y = 50.86 in^3

r_x = 15.47”

r_y = 3.24”

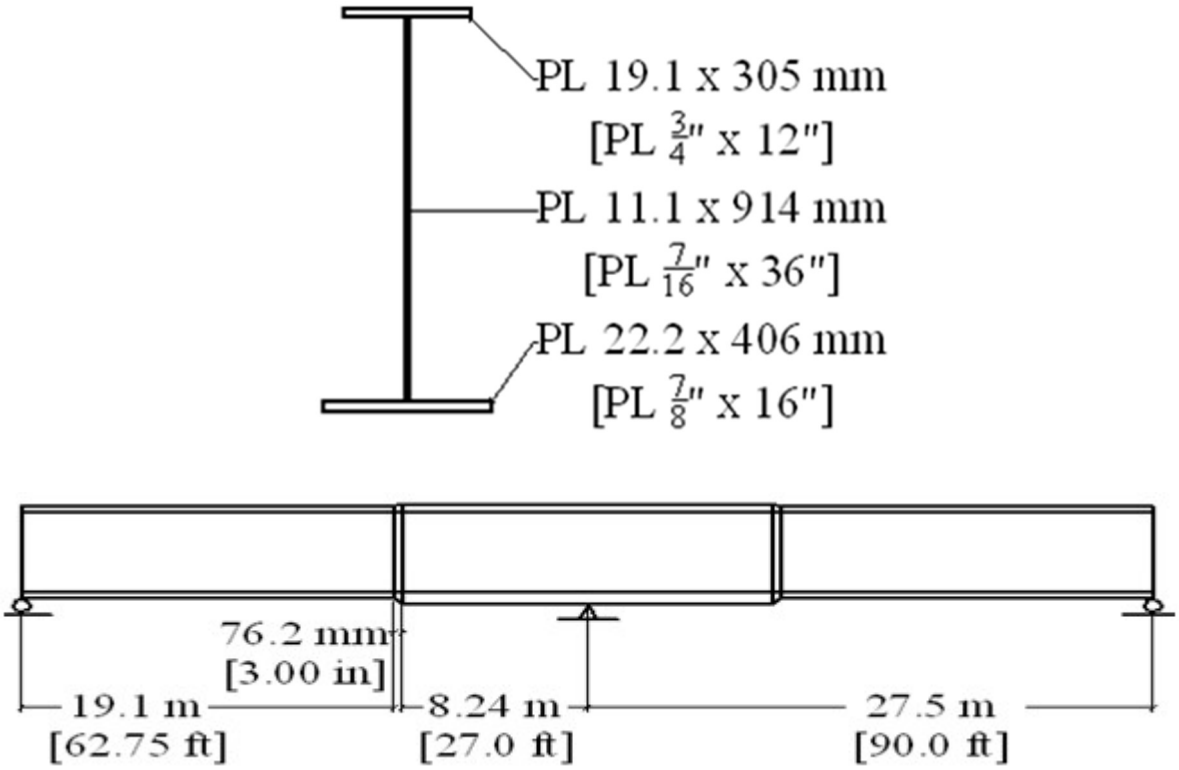

Figure B.4 Interior girder positive flexure region section properties

Determine Classification of the Section:

Check $\frac{2D_c}{t_w} \leq 5.7\sqrt{\frac{E}{F_{yc}}}$ *(AASHTO 2010 6.10.6.2.3-1)*

$D_c = D + t_{ft} - C_y = 36 + {}^{7}/_{8}" - 16.48 = 20.40"$

Check $\frac{(2)(19")}{{}^{1}/_{2}"} = 93.23 \leq 5.7\sqrt{\frac{29{,}000\ ksi}{50\ ksi}} = 137.3$ OK, ∴ web is non-slender

Check $\frac{I_{yc}}{I_{yt}} \geq 0.3$

$I_{yc} = \frac{1}{12}bh^3 + Ad^2$

$$I_{yc} = \frac{1}{12}(12")({}^{3}/_{4}")^3 + (9\ in^2)(20.77")^2 = 3{,}883\ in^4$$

$$I_{yt} = \frac{1}{12}(16")({}^{7}/_{8}")^3 + (14\ in^2)(16.04")^2 = 3{,}604\ in^4$$

Check $\frac{I_{yc}}{I_{yt}} = \frac{3{,}883 in^4}{3{,}604 in^4} = 1.1 \geq 0.3$ OK

Check Compression Flange Local Buckling:

$\lambda_f = \frac{b_{fc}}{2t_{fc}} = \frac{12"}{(2)({}^{3}/_{4}")} = 8$ *(AASHTO 2010 6.10.8.2.2-3)*

$\lambda_{pf} = 0.38\sqrt{\frac{E}{F_{yc}}} = 0.38\sqrt{\frac{29{,}000\ ksi}{50\ ksi}} = 9.152$ *(AASHTO 2010 6.10.8.2.2-4)*

$\lambda_f < \lambda_{pf}$ ∴ compact flange

$F_{nc} = R_b R_h F_{yc}$ *(AASHTO 2010 6.10.8.2.2-1)*

R_b = 1.0 since web is non-slender

R_h = 1.0 since section is non-hybrid

$F_{nc} = R_b R_h F_{yc} = (1.0)(1.0)(50\ ksi) = 50\ ksi$

Check Compression Flange Lateral-Torsional Buckling:

Check unbraced length of the beam, **L_b = 45' = 540"**

$r_t = \frac{b_{fc}}{\sqrt{12\left(1+\frac{1}{3}\frac{D_c t_w}{b_{fc} t_{fc}}\right)}} = \frac{12}{\sqrt{12\left(1+\frac{1}{3}\frac{(20.395")({}^{7}/_{16}")}{(12")({}^{3}/_{4}")}\right)}} = 3.003"$ (AASHTO 2010 6.10.8.2.3-9)

$L_p = 1.0 r_t \sqrt{\frac{E}{F_{yc}}} = (1.0)(3.003")\sqrt{\frac{29{,}000^{ksi}}{50^{ksi}}} = 72.33"$ *(AASHTO 2010 6.10.8.2.3-4)*

$F_{yr} = \min(0.7F_{yc}, F_{yw}) \geq 0.5F_{yc}$ *(AASHTO 2010 pg6-145)*

$F_{yr} = (0.7)\left(50^{ksi}\right) = 35^{ksi} > 25ksi$

$L_r = \pi r_t\sqrt{\frac{E}{F_{yr}}} = (\pi)(3.003")\sqrt{\frac{29{,}000^{ksi}}{35^{ksi}}} = 271.6"$ *(AASHTO 2010 6.10.8.2.3-5)*

Since $L_p = 72.33" < L_r = 271.6" <$ L_b=540.0", Elastic LTB must be investigated.

$F_{nc} = F_{cr} \leq R_b R_h F_{yc}$ *(AASHTO 2010 6.10.8.2.3-3)*

$F_{cr} = \frac{C_b R_b \pi^2 E}{(\frac{L_b}{r_t})^2}$ *(AASHTO 2010 6.10.8.2.3-8)*

R_b = 1.0 since web is non-slender

R_h = 1.0 since section is non-hybrid

Compute the Moment Gradient Factor, Cb, for the Positive Flexure Critical Segment:

$M_{mid} = 15{,}323^{k-in} \rightarrow f_{mid} = \frac{15{,}323^{k-in}}{438.8\ in^3} = 34.92\ ksi$

$M_2 = 13{,}432^{k-in} \rightarrow f_2 = \frac{13{,}432^{k-in}}{438.8\ in^3} = 32.07\ ksi$

$f_{mid}/f_2 > 1$

$C_b = 1$ *(AASHTO 2010 6.10.8.2.3-6)*

$F_{cr} = \frac{(1.0)(1.0)\pi^2(29{,}000\ ksi)}{(\frac{540"}{3.003})^2} = 8.85\ ksi < 50\ ksi\ max \rightarrow F_{cr} = 8.85\ ksi$

<u>Check Compression Flange Lateral-Torsional Buckling:</u>

Check unbraced length of the beam, **L_b = 30' = 360"**

$r_t = \frac{b_{fc}}{\sqrt{12\left(1+\frac{1}{3}\frac{D_c t_w}{b_{fc} t_{fc}}\right)}} = \frac{12}{\sqrt{12\left(1+\frac{1}{3}\frac{(20.395")(7/16")}{(12)(3/4")}\right)}} = 3.003"$ *(AASHTO 2010 6.10.8.2.3-9)*

$L_p = 1.0 r_t\sqrt{\frac{E}{F_{yc}}} = (1.0)(3.003")\sqrt{\frac{29{,}000^{ksi}}{50^{ksi}}} = 72.33"$ *(AASHTO 2010 6.10.8.2.3-4)*

$F_{yr} = \min\left(0.7F_{yc}, F_{yw}\right) \geq 0.5F_{yc}$ *(AASHTO 2010 pg6-145)*

$F_{yr} = (0.7)\left(50^{ksi}\right) = 35^{ksi} > 25ksi$

$L_r = \pi r_t \sqrt{\frac{E}{F_{yr}}} = (\pi)(3.003")\sqrt{\frac{29{,}000^{ksi}}{35^{ksi}}} = 271.6"$ *(AASHTO 2010 6.10.8.2.3-5)*

Since $L_p = 72.33" < L_r = 271.6" <$ L_b=360.0", Elastic LTB must be investigated.

$F_{nc} = F_{cr} \leq R_b R_h F_{yc}$ *(AASHTO 2010 6.10.8.2.3-3)*

$F_{cr} = \frac{C_b R_b \pi^2 E}{(\frac{L_b}{r_t})^2}$ *(AASHTO 2010 6.10.8.2.3-8)*

R_b = 1.0 since web is non-slender

R_h = 1.0 since section is non-hybrid

Compute the Moment Gradient Factor, Cb, for the Positive Flexure Critical Segment:

$C_b = 1.75 - 1.05\left(\frac{f_1}{f_2}\right) + 0.3\left(\frac{f_1}{f_2}\right)^2 \leq 2.3$ *(AASHTO 2010 6.10.8.2.3-7)*

$M_2 = 16{,}640^{k-in} \rightarrow f_2 = \frac{16{,}640^{k-in}}{438.8\ in^3} = 37.92\ ksi$

$M_0 = 0^{k-in} \rightarrow f_0 = 0\ ksi$

$M_{mid} = 12{,}340^{k-in} \rightarrow f_{mid} = \frac{12{,}340^{k-in}}{438.8\ in^3} = 28.12\ ksi$

Since the bending moment diagram is not concave,

$f_1 = 2f_{mid} - f_2 \geq f_0$ *(AASHTO 2010 6.10.8.2.3-11)*

$(2)(28.12) - (37.92^{ksi}) = 18.32\ ksi \geq 0\ ksi$

$C_b = 1.75 - 1.05\left(\frac{18.32}{37.92}\right) + 0.3\left(\frac{18.32}{37.92}\right)^2 = 1.313 \leq 2.3 \rightarrow C_b = 1.313$

$F_{cr} = \frac{(1.313)(1.0)\pi^2(29{,}000\ ksi)}{(\frac{360}{3.003})^2} = 26.15\ ksi < 50\ ksi\ max \rightarrow F_{cr} = 26.15\ ksi$

Check Compression Flange Lateral-Torsional Buckling:

Check unbraced length of the beam, **L_b = 15' = 180"**

$$r_t = \frac{b_{fc}}{\sqrt{12\left(1+\frac{1}{3}\frac{D_c t_w}{b_{fc} t_{fc}}\right)}} = \frac{12}{\sqrt{12\left(1+\frac{1}{3}\frac{(20.395")(7/16")}{(12)(3/4")}\right)}} = 3.003"$$ *(AASHTO 2010 6.10.8.2.3-9)*

$$L_p = 1.0 r_t \sqrt{\frac{E}{F_{yc}}} = (1.0)(3.003")\sqrt{\frac{29{,}000^{ksi}}{50^{ksi}}} = 72.33"$$ *(AASHTO 2010 6.10.8.2.3-4)*

$$F_{yr} = \min\left(0.7F_{yc}, F_{yw}\right) \geq 0.5F_{yc}$$ *(AASHTO 2010 pg6-145)*

$$F_{yr} = (0.7)\left(50^{ksi}\right) = 35^{ksi} > 25ksi$$

$$L_r = \pi r_t \sqrt{\frac{E}{F_{yr}}} = (\pi)(3.003")\sqrt{\frac{29{,}000^{ksi}}{35^{ksi}}} = 271.6"$$ *(AASHTO 2010 6.10.8.2.3-5)*

Since $L_p = 72.33" < L_b = 180.0" < L_r = 271.6"$, Inelastic LTB must be investigated.

$$F_{nc(LTB)} = C_b\left[1 - \left(1 - \frac{F_{yr}}{R_h F_{yc}}\right)\left(\frac{L_b - L_p}{L_r - L_p}\right)\right] R_b R_h F_{yc} \leq R_b R_h F_{yc}$$ *(AASHTO 2010 6.10.8.2.3-2)*

R_b = 1.0 since web is non-slender

R_h = 1.0 since section is non-hybrid

Compute the Moment Gradient Factor, Cb, for the Abutment Segment:

$$C_b = 1.75 - 1.05\left(\frac{f_1}{f_2}\right) + 0.3\left(\frac{f_1}{f_2}\right)^2 \leq 2.3$$ *(AASHTO 2010 6.10.8.2.3-7)*

$$M_2 = 12{,}340^{k-in} \rightarrow f_2 = \frac{12{,}340^{k-in}}{438.8\ in^3} = 28.12\ ksi$$

$$M_0 = 0^{k-in} \rightarrow f_0 = 0\ ksi$$

$$M_{mid} = 7{,}369^{k-in} \rightarrow f_{mid} = \frac{7{,}369^{k-in}}{438.8\ in^3} = 16.79\ ksi$$

Since the bending moment diagram is not concave,

$$f_1 = 2f_{mid} - f_2 \geq f_0$$ *(AASHTO 2010 6.10.8.2.3-11)*

$$(2)\left(16.79^{ksi}\right) - (28.12^{ksi}) = 5.460^{ksi} \geq 0\ ksi$$

$$C_b = 1.75 - 1.05\left(\frac{5.460}{28.12}\right) + 0.3\left(\frac{5.460}{28.12}\right)^2 = 1.557 \leq 2.3 \quad \rightarrow C_b = 1.557$$

Compute the Moment Gradient Factor, Cb, for the Mid-span Segment:

$$M_2 = 16{,}640^{k-in} \rightarrow f_2 = \frac{16{,}640^{k-in}}{438.8\ in^3} = 37.92\ ksi$$

$$M_0 = 12{,}340^{k-in} \rightarrow f_0 = \frac{12{,}340^{k-in}}{438.8\ in^3} = 28.12\ ksi$$

$$M_{mid} = 15{,}430^{k-in} \rightarrow f_{mid} = \frac{15{,}430^{k-in}}{438.8\ in^3} = 35.16\ ksi$$

Since the bending moment diagram is not concave,

$f_1 = 2f_{mid} - f_2 \geq f_0$ *(AASHTO 2010 6.10.8.2.3-11)*

$(2)\left(35.16^{ksi}\right) - (37.92^{ksi}) = 32.41^{ksi} \geq f_0 = 28.12 \rightarrow f_1 = 32.41\ ksi$

$C_b = 1.75 - 1.05\left(\frac{32.41}{37.92}\right) + 0.3\left(\frac{32.41}{37.92}\right)^2 = 1.072 \leq 2.3 \quad \rightarrow C_b = 1.557$ Controls

$$F_{nc(LTB)} = 1.557\left[1 - \left(1 - \frac{35^{ksi}}{(1.00)(50^{ksi})}\right)\left(\frac{180.0" - 72.33"}{271.56" - 72.33"}\right)\right](1.0)(1.0)\left(50^{ksi}\right)$$

$$\leq (1.0)(1.0)\left(50^{ksi}\right)$$

$F_{nc(LTB)} = 65.23\ ksi \leq 50\ ksi\ max \rightarrow F_{nc(LTB)} = 50\ ksi$

The governing strength for the compression flange is the smaller of $F_{nc(FLB)}\ and\ F_{nc(LTB)}$:

For **L_b = 45'**, $F_{nc(LTB)} = 8.85^{ksi} < F_{nc(FLB)} = 50^{ksi}$, LTB governs the strength of the compression flange.

$F_{nc} = F_{nc(LTB)} = 8.85\ ksi$

$\Phi F_{nc} = (1.0)(8.85) = 8.85\ ksi$ *(AASHTO 2010 6.10.8.1.1-1)*

For **L_b = 30'**, $F_{nc(LTB)} = 26.15^{ksi} < F_{nc(FLB)} =$

50^{ksi}, LTB governs the strength of the compression flange.

$F_{nc} = F_{nc(LTB)} = 26.15\ ksi$

$\Phi F_{nc} = (1.0)(26.15) = 26.15\ ksi$ *(AASHTO 2010 6.10.8.1.1-1)*

For **L_b = 15'**, $F_{nc(LTB)} = F_{nc(FLB)} =$

$50\ ksi$, yielding governs the strength of the compression flange.

$F_{nc} = F_{yc} = 50\ ksi$

$\Phi F_{nc} = (1.0)\left(50^{ksi}\right) = 50\ ksi$ *(AASHTO 2010 6.10.8.1.1-1)*

Investigate the Strength of the Tension Flange:

$F_{nt} = R_h F_{yt} = (1.0)\left(\ 50^{ksi}\right) = 50^{ksi}$ *(AASHTO 2010 6.10.8.3-1)*

$\Phi F_{nt} = (1.0)\ \left(\ 50^{ksi}\right) = 50^{ksi}$

Interior Girder Check - Negative Flexure Region

b_{fc} = 16”

t_{fc} = 2.0”

D = 36”

t_w = 0.5”

b_{ft} = 16”

t_{ft} = 1.0”

A = 66 in^2

C_y = 15.27”

I_x = 17,510 in^4

I_y = 1024 in^4

S_{xt} = 737.88 in^3

S_{xc} = 1146 in^3

S_y = 128.1 in^3

r_x = 16.29”

r_y = 3.94”

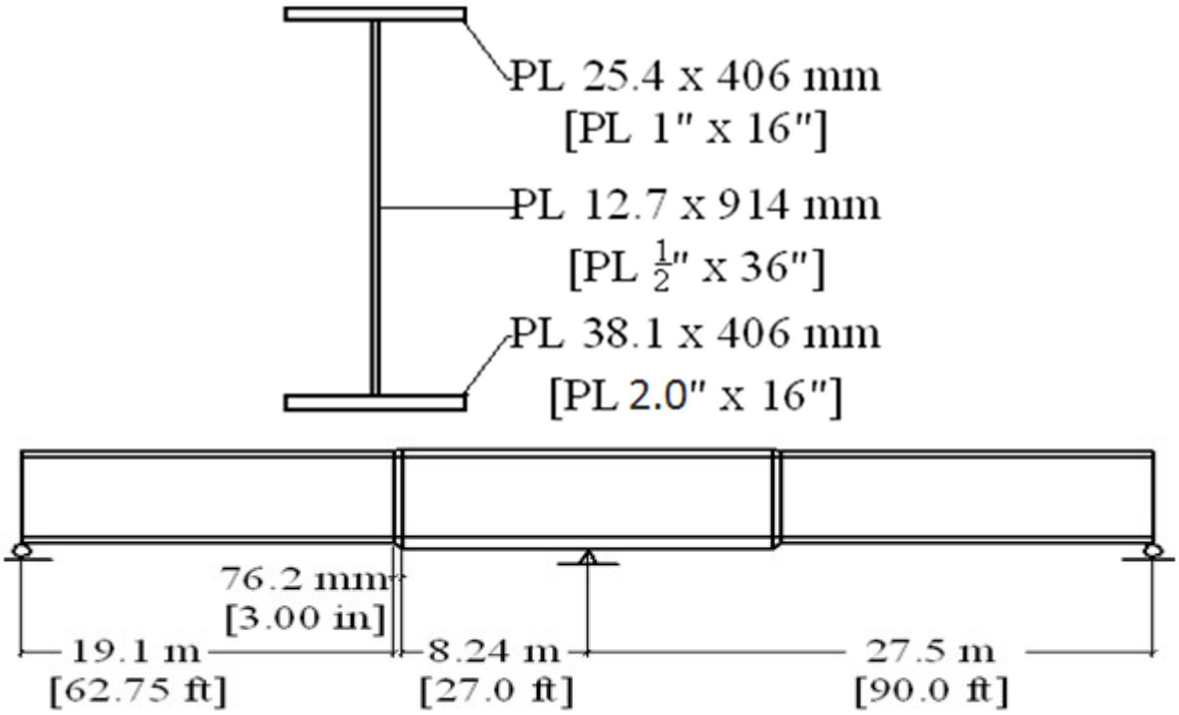

Figure B.5 Interior girder negative flexure region section properties

Determine Classification of the Section:

Check $\frac{2D_c}{t_w} \leq 5.7\sqrt{\frac{E}{F_{yc}}}$ *(AASHTO 2010 6.10.6.2.3-1)*

$D_c = C_y - t_{fc} = 15.27 + 2.0" = 13.27"$

Check $\frac{(2)(19")}{1/2"} = 53.08 \leq 5.7\sqrt{\frac{29{,}000\ ksi}{50\ ksi}} = 137.3$ OK, ∴ web is non-slender

Check $\frac{I_{yc}}{I_{yt}} \geq 0.3$

$I_{yc} = \frac{1}{12}bh^3 + Ad^2$

$I_{yc} = \frac{1}{12}(16")(2.0")^3 + (32\ in^2)(14.27")^2 = 6{,}527\ in^4$

$$I_{yt} = \frac{1}{12}(16")(1.0")^3 + (16\ in^2)(23.23")^2 = 8{,}635\ in^4$$

Check $\frac{I_{yc}}{I_{yt}} = \frac{6{,}527\ in^4}{8{,}635\ in^4} = 0.76 \geq 0.3$ OK

Check Compression Flange Local Buckling:

$$\lambda_f = \frac{b_{fc}}{2t_{fc}} = \frac{16"}{(2)(2.0")} = 4.0$$ *(AASHTO 2010 6.10.8.2.2-3)*

$$\lambda_{pf} = 0.38\sqrt{\frac{E}{F_{yc}}} = 0.38\sqrt{\frac{29{,}000\ ksi}{50\ ksi}} = 9.152$$ *(AASHTO 2010 6.10.8.2.2-4)*

$\lambda_f < \lambda_{pf}$ ∴ compact flange

$$F_{nc} = R_b R_h F_{yc}$$ *(AASHTO 2010 6.10.8.2.2-1)*

R_b = 1.0 since web is non-slender

R_h = 1.0 since section is non-hybrid

$$F_{nc} = R_b R_h F_{yc} = (1.0)(1.0)(50\ ksi) = 50\ ksi$$

Check Compression Flange Lateral-Torsional Buckling:

Check unbraced length of the beam, **L_b = 45' = 540"**

$$r_t = \frac{b_{fc}}{\sqrt{12\left(1+\frac{1}{3}\frac{D_c t_w}{b_{fc} t_{fc}}\right)}} = \frac{16}{\sqrt{12\left(1+\frac{1}{3}\frac{(13.27")(1/2")}{(16)(2.0")}\right)}} = 4.566"$$ *(AASHTO 2010 6.10.8.2.3-9)*

$$L_p = 1.0 r_t \sqrt{\frac{E}{F_{yc}}} = (1.0)(4.566")\sqrt{\frac{29{,}000^{ksi}}{50^{ksi}}} = 110.0"$$ *(AASHTO 2010 6.10.8.2.3-4)*

$$F_{yr} = \min\left(0.7F_{yc}, F_{yw}\right) \geq 0.5F_{yc}$$ *(AASHTO 2010 pg6-145)*

$$F_{yr} = (0.7)\left(50^{ksi}\right) = 35^{ksi} > 25ksi$$

$$L_r = \pi r_t \sqrt{\frac{E}{F_{yr}}} = (\pi)(4.566")\sqrt{\frac{29{,}000^{ksi}}{35^{ksi}}} = 412.9"$$ *(AASHTO 2010 6.10.8.2.3-5)*

Since $L_p = 110.0" < L_r = 412.9" <$ L_b=540.0", Elastic LTB must be investigated.

$F_{nc} = F_{cr} \leq R_b R_h F_{yc}$ *(AASHTO 2010 6.10.8.2.3-3)*

$F_{cr} = \frac{C_b R_b \pi^2 E}{(\frac{L_b}{r_t})^2}$ *(AASHTO 2010 6.10.8.2.3-8)*

R_b = 1.0 since web is non-slender

R_h = 1.0 since section is non-hybrid

Compute the Moment Gradient Factor, Cb, for the Positive Flexure Critical Segment:

$C_b = 1.75 - 1.05\left(\frac{f_1}{f_2}\right) + 0.3\left(\frac{f_1}{f_2}\right)^2 \leq 2.3$ *(AASHTO 2010 6.10.8.2.3-7)*

$M_{mid} = -7{,}344^{k-in} \rightarrow f_{mid} = \frac{7{,}344^{k-in}}{1{,}146\ in^3} = 6.41\ ksi$

$M_2 = -41{,}700^{k-in} \rightarrow f_2 = \frac{41{,}700^{k-in}}{1{,}146\ in^3} = 36.37\ ksi$

$M_0 = 0^{k-in} \rightarrow f_0 = 0\ ksi$

Since the bending moment diagram is concave,

$f_1 = f_0 = 0\ ksi$ *(AASHTO 2010 6.10.8.2.3-10)*

$C_b = 1.75 - 1.05\left(\frac{0}{36.37}\right) + 0.3\left(\frac{0}{36.37}\right)^2 = 1.75 \leq 2.3 \rightarrow C_b = 1.75$

$F_{cr} = \frac{(1.75)(1.0)\pi^2(29{,}000\ ksi)}{(\frac{540"}{4.566})^2} = 35.81\ ksi < 50\ ksi\ max \rightarrow F_{cr} = 35.81\ ksi$

<u>Check Compression Flange Lateral-Torsional Buckling:</u>

Check unbraced length of the beam, **L_b = 30' = 360"**

$$r_t = \frac{b_{fc}}{\sqrt{12\left(1+\frac{1}{3}\frac{D_c t_w}{b_{fc} t_{fc}}\right)}} = \frac{16}{\sqrt{12\left(1+\frac{1}{3}\frac{(13.27")(1/2")}{(16)(2.0")}\right)}} = 4.566"$$ *(AASHTO 2010 6.10.8.2.3-9)*

$$L_p = 1.0 r_t \sqrt{\frac{E}{F_{yc}}} = (1.0)(4.566")\sqrt{\frac{29{,}000^{ksi}}{50^{ksi}}} = 110.0"$$ *(AASHTO 2010 6.10.8.2.3-4)*

$$F_{yr} = \min\left(0.7F_{yc}, F_{yw}\right) \geq 0.5F_{yc}$$ *(AASHTO 2010 pg6-145)*

$$F_{yr} = (0.7)\left(50^{ksi}\right) = 35^{ksi} > 25ksi$$

$$L_r = \pi r_t \sqrt{\frac{E}{F_{yr}}} = (\pi)(4.566")\sqrt{\frac{29{,}000^{ksi}}{35^{ksi}}} = 412.9"$$ *(AASHTO 2010 6.10.8.2.3-5)*

Since $L_p = 110.0" < L_b = 360.0" <$ L_b=412.9", Inelastic LTB must be investigated.

$$F_{nc(LTB)} = C_b\left[1 - \left(1 - \frac{F_{yr}}{R_h F_{yc}}\right)\left(\frac{L_b - L_p}{L_r - L_p}\right)\right]R_b R_h F_{yc} \leq R_b R_h F_{yc}$$ *(AASHTO 2010 6.10.8.2.3-2)*

R_b = 1.0 since web is non-slender

R_h = 1.0 since section is non-hybrid

Compute the Moment Gradient Factor, Cb, for the Negative Flexure Critical Segment:

$$C_b = 1.75 - 1.05\left(\frac{f_1}{f_2}\right) + 0.3\left(\frac{f_1}{f_2}\right)^2 \leq 2.3$$ *(AASHTO 2010 6.10.8.2.3-7)*

$$M_2 = -41{,}700^{k-in} \rightarrow f_2 = \frac{41{,}700^{k-in}}{1{,}146\ in^3} = 36.37\ ksi$$

$$M_0 = 0^{k-in} \rightarrow f_0 = 0\ ksi$$

$$M_{mid} = -15{,}600^{k-in} \rightarrow f_{mid} = \frac{15{,}600^{k-in}}{1{,}146\ in^3} = 13.61\ ksi$$

Since the bending moment diagram is concave,

$$f_1 = f_0 = 0\ ksi$$ *(AASHTO 2010 6.10.8.2.3-10)*

$$C_b = 1.75 - 1.05\left(\frac{0}{36.37}\right) + 0.3\left(\frac{0}{36.37}\right)^2 = 1.75 \leq 2.3 \rightarrow C_b = 1.75$$

$$F_{nc(LTB)} = 1.75\left[1 - \left(1 - \frac{35^{ksi}}{(1.00)(50^{ksi})}\right)\left(\frac{360.0" - 110.0"}{412.9" - 110.0"}\right)\right](1.0)(1.0)\left(50^{ksi}\right)$$

$$\leq (1.0)(1.0)\left(50^{ksi}\right)$$

$$F_{nc(LTB)} = 65.83\ ksi \leq 50\ ksi\ max \rightarrow F_{nc(LTB)} = 50\ ksi$$

Check Compression Flange Lateral-Torsional Buckling:

Check unbraced length of the beam, **L_b = 15' = 180"**

$$r_t = \frac{b_{fc}}{\sqrt{12\left(1+\frac{1}{3}\frac{D_c t_w}{b_{fc} t_{fc}}\right)}} = \frac{16}{\sqrt{12\left(1+\frac{1}{3}\frac{(13.27")(1/2")}{(16)(2.0")}\right)}} = 4.566"$$ *(AASHTO 2010 6.10.8.2.3-9)*

$$L_p = 1.0 r_t \sqrt{\frac{E}{F_{yc}}} = (1.0)(4.566")\sqrt{\frac{29{,}000^{ksi}}{50^{ksi}}} = 110.0"$$ *(AASHTO 2010 6.10.8.2.3-4)*

$$F_{yr} = \min\left(0.7F_{yc}, F_{yw}\right) \geq 0.5F_{yc}$$ *(AASHTO 2010 pg6-145)*

$$F_{yr} = (0.7)\left(50^{ksi}\right) = 35^{ksi} > 25ksi$$

$$L_r = \pi r_t \sqrt{\frac{E}{F_{yr}}} = (\pi)(4.566")\sqrt{\frac{29{,}000^{ksi}}{35^{ksi}}} = 412.9"$$ *(AASHTO 2010 6.10.8.2.3-5)*

Since $L_p = 110.0" < L_b = 180.0" <$ L_b=412.9", Inelastic LTB must be investigated.

$$F_{nc(LTB)} = C_b[1 - \left(1 - \frac{F_{yr}}{R_h F_{yc}}\right)\left(\frac{L_b - L_p}{L_r - L_p}\right)]R_b R_h F_{yc} \leq R_b R_h F_{yc}$$ *(AASHTO 2010 6.10.8.2.3-2)*

R_b = 1.0 since web is non-slender

R_h = 1.0 since section is non-hybrid

Compute the Moment Gradient Factor, Cb, for the Transition Region Segment:

$$C_b = 1.75 - 1.05\left(\frac{f_1}{f_2}\right) + 0.3\left(\frac{f_1}{f_2}\right)^2 \leq 2.3$$ *(AASHTO 2010 6.10.8.2.3-7)*

$$M_2 = -15{,}600^{k-in} \rightarrow f_2 = \frac{15{,}600^{k-in}}{1{,}146\ in^3} = 13.61\ ksi$$

$M_0 = 0^{k-in} \rightarrow f_0 = 0\ ksi$

$M_{mid} = -7{,}344^{k-in} \rightarrow f_{mid} = \dfrac{7{,}344^{k-in}}{1{,}146\ in^3} = 6.41\ ksi$

Since the bending moment diagram is concave,

$f_1 = f_0 = 0\ ksi$ *(AASHTO 2010 6.10.8.2.3-10)*

$C_b = 1.75 - 1.05\left(\frac{0}{13.61}\right) + 0.3\left(\frac{0}{13.61}\right)^2 = 1.75 \leq 2.3 \ \rightarrow C_b = 1.75$

Compute the Moment Gradient Factor, Cb, for Center Pier Segment:

$M_2 = -41{,}700^{k-in} \rightarrow f_2 = \dfrac{41{,}700^{k-in}}{1{,}146\ in^3} = 36.37\ ksi$

$M_0 = -15{,}600^{k-in} \rightarrow f_0 = \dfrac{15{,}600^{k-in}}{1{,}146\ in^3} = 13.61\ ksi$

$M_{mid} = -27{,}680^{k-in} \rightarrow f_{mid} = \dfrac{27{,}680^{k-in}}{1{,}146\ in^3} = 24.14\ ksi$

Since the bending moment diagram is concave,

$f_1 = f_0 = 13.61\ ksi$ *(AASHTO 2010 6.10.8.2.3-10)*

$C_b = 1.75 - 1.05\left(\frac{13.61}{36.37}\right) + 0.3\left(\frac{13.61}{36.37}\right)^2 = 1.40 \leq 2.3 \ \rightarrow C_b = 1.75$ Controls

$$F_{nc(LTB)} = 1.75\left[1 - \left(1 - \frac{35^{ksi}}{(1.00)(50^{ksi})}\right)\left(\frac{180.0" - 110.0"}{412.9" - 110.0"}\right)\right](1.0)(1.0)\left(50^{ksi}\right)$$

$$\leq (1.0)(1.0)\left(50^{ksi}\right)$$

$F_{nc(LTB)} = 81.43\ ksi \leq 50\ ksi\ max \rightarrow F_{nc(LTB)} = 50\ ksi$

The governing strength for the compression flange is the smaller of $F_{nc(FLB)}\ and\ F_{nc(LTB)}$:

For **L_b = 45'**, $F_{nc(LTB)} = 35.81^{ksi} < F_{nc(FLB)} = 50^{ksi}$, LTB governs the strength of the compression flange.

$F_{nc} = F_{nc(LTB)} = 35.81\ ksi$

$\Phi F_{nc} = (1.0)(35.81) = 35.81\ ksi$ *(AASHTO 2010 6.10.8.1.1-1)*

For **L_b = 30'**, $F_{nc(LTB)} = 50^{ksi} < F_{nc(FLB)} =$

50^{ksi}, yielding governs the strength of the compression flange.

$F_{nc} = F_{yc} = 50\ ksi$

$\Phi F_{nc} = (1.0)(50) = 50\ ksi$ *(AASHTO 2010 6.10.8.1.1-1)*

For **L_b = 15'**, $F_{nc(LTB)} = F_{nc(FLB)} =$

$50\ ksi$, yielding governs the strength of the compression flange.

$F_{nc} = F_{yc} = 50\ ksi$

$\Phi F_{nc} = (1.0)\left(50^{ksi}\right) = 50\ ksi$ *(AASHTO 2010 6.10.8.1.1-1)*

Investigate the Strength of the Tension Flange:

$F_{nt} = R_h F_{yt} = (1.0)\left(\ 50^{ksi}\right) = 50^{ksi}$ *(AASHTO 2010 6.10.8.3-1)*

$\Phi F_{nt} = (1.00)\ \left(\ 50^{ksi}\right) = 50^{ksi}$

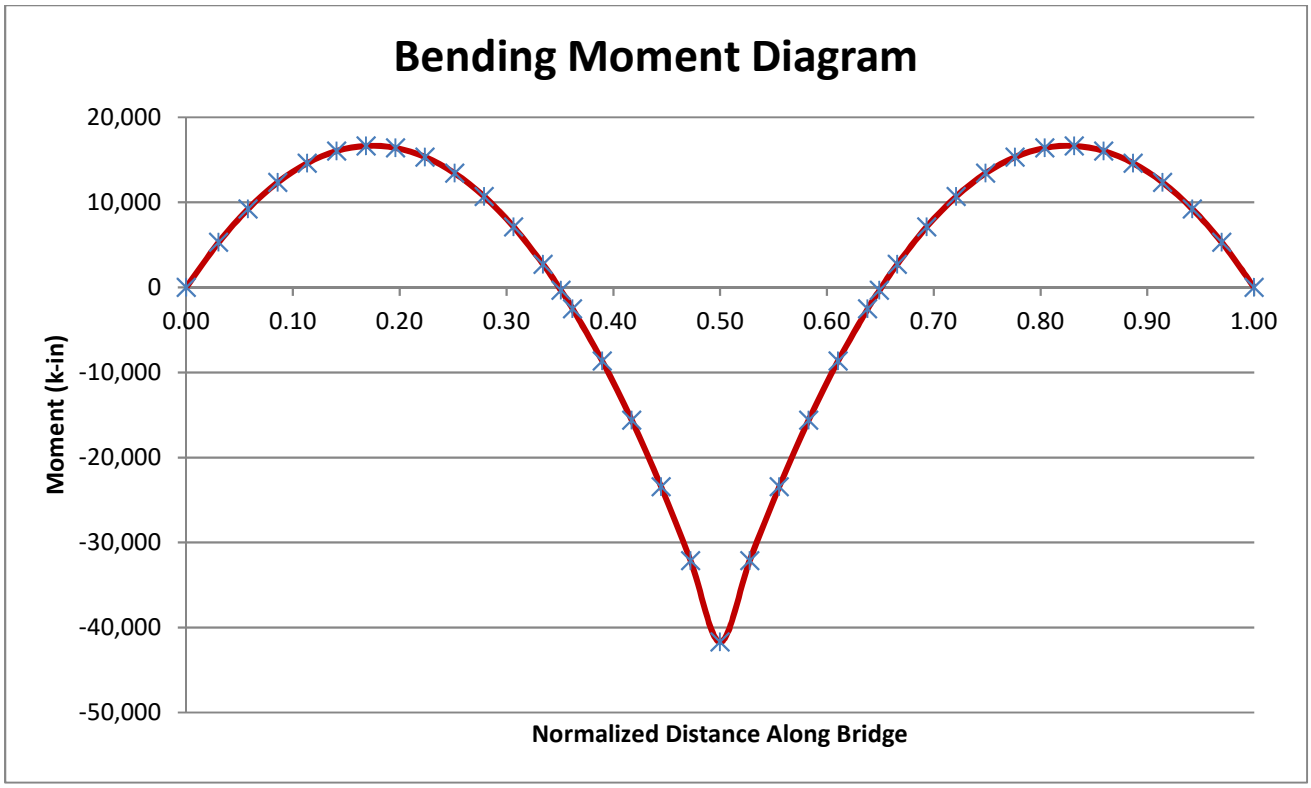

Figure B.6 Interior girder bending moment diagram

Table B.2 Interior girder moment and stress along bridge

Normalized Position	Position (in)	M_z (k-in)	σ_z (ksi)	
0.00	0	0.00	0.00	
0.03	66	5295.5	9.41	
0.06	126	9233.4	16.40	
0.09	186	12337	21.91	
0.11	246	14606	25.94	
0.14	306	16040	28.49	
0.17	366	16640	29.56	
0.20	426	16405	29.14	
0.22	486	15336	27.24	
0.25	546	13432	23.86	
0.28	606	10694	18.99	
0.31	666	7121.6	12.65	
0.33	726	2714.4	4.82	
0.35	762	-330.48	-0.59	← Transition
`0.36	786	-2529.8	-4.49	
0.39	846	-8633.8	-15.34	
0.42	906	-15603	-27.71	
0.44	966	-23438	-41.63	
0.47	1026	-32139	-57.09	
0.50	1086	-41704	-74.07	
0.53	1146	-32139	-57.09	
0.56	1206	-23438	-41.63	
0.58	1266	-15603	-27.71	
0.61	1326	-8633.8	-15.34	
0.64	1386	-2529.8	-4.49	
0.65	1410	-330.48	-0.59	← Transition
0.67	1446	2714.4	4.82	
0.69	1506	7121.6	12.65	
0.72	1566	10694	18.99	
0.75	1626	13432	23.86	
0.78	1686	15336	27.24	
0.80	1746	16405	29.14	
0.83	1806	16640	29.56	
0.86	1866	16040	28.49	
0.89	1926	14606	25.94	
0.91	1986	12337	21.91	
0.94	2046	9233.4	16.40	
0.97	2106	5295.5	9.41	
1.00	2172	0.00	0.00	

REFERENCES

AASHTO (2010). “LRFD Bridge Design Specifications.” *American Association of State Highway and Transportation Officials,* Washington, D.C.

Ziemian, R. D. and Mcguire, W. (2000). Mastan2 Version 3.5. http://www.mastan2.com

APPENDIX C: GIRDER SHELL ELEMENTS MODELING AND DYNAMIC ANALYSIS

The objective of these parametric studies was to provide guidance concerning the design of the girder elements and analysis technique used that will offer accurate results at the least computation cost. Given the length of run-time required for each full-sized bridge model, up to 100 hours depending on the processor speed for a solid elements model, and the number of models needed to capture all parameters, computational efficiently is of major concern. Conventional and continuum shell elements were used to model both the girder web alone and the entire girder to determine their effectiveness relative to solid elements. Dynamic implicit and explicit analysis techniques were used to determine their computational efficiency relative to a static analysis and ability to arrive at a convergent solution. The results showed that both conventional shell elements and continuum shell elements were unable capture girder buckling or higher order buckling modes. Dynamic implicit analysis did not improve computation time and had convergence issues. Dynamic explicit analysis required specific knowledge of the mass scale and load amplitude of any give bridge model. Therefore solid elements were chosen to model all bridge parts combined with a static analysis technique for the main study of the paper.

In order to compare the efficiency of solid elements to shell elements and the ability for geometrically non-linear models to reach a convergent solution using static or dynamic analysis, three-dimensional finite element (FE) models of the bridge were constructed using Abaqus v.6.10-2 (Simulia, 2010). The bridge geometry used within this study consists of a single 9.14 m [30 ft] span, composed of three girders spaced at 3.1 m [10 ft] as represented in **Error! Reference source not found.**. Girders were composed of a PL19.1 x 305 mm [PL0.75 x 12 in] top flange, a PL11.1 x 914 mm [PL0.4375 x 36 in] web, and a PL22.2 x 406 mm [PL0.875 x 16

in] bottom flange. Triangular welds attach the top and bottom flanges to the web through a tie connection.

Cross-frames consist of L108x108x12.7 mm [L4.25x4.25x0.5 in] diagonals and L138x138x12.7 mm [L5.42x5.42x0.5 in] bottom chord attached to a 102x912x9.53 mm [4x35.9x0.375 in] stiffener plate. Stiffeners had a 25.4 mm [1.0 in] by 25.4 mm [1.0 in] cope allowing for the girder welds and were tied directly to the webs. The cross-frame angles and stiffeners were merged in Abaqus, retaining intersecting boundaries. A 108x108x9.53 mm [4.25x4.25x0.375 in] connection plate was placed between the intersection of the two diagonal angles. C3D8R brick elements were used in the cross-frames, but C3D4 tetrahedral and C3D6 wedge elements were used to transition between mesh sizes where needed. Cross-frames were spaced at 4.57 m [15 ft] or 9.14 m [30 ft].

Geometric nonlinearity was considered for all analyses were applicable. All elements were steel material modeled to have a modulus of elasticity of 200,000 MPa [29,000 ksi] and Poisson's ratio of 0.3. A mesh size of 25.4 mm [1.0 in] was used for cross-frame, web, flange, and weld elements. Surface-to-surface tie constraints were used to attach parts within models. Girder boundary conditions were modeled by applying a translational constraint over a 152 mm [6.0 in] strip of the bearing plate at support locations. Pinned support conditions were used to represent the abutment pier on one side while fixed support conditions were used to represent the other abutment pier bearings.

A vertical load was applied to the center of the middle beam at mid-span over a 152 mm [6.0 in] by 12.7 mm [0.5 in] surface, as shown in Unskewed single span bridge model with vertical load and out-of-plane load applied. The magnitude of the applied load is arbitrary and only needs to cause buckling of the girder. Applied force magnitudes are labeled with their

respective figures. An out-of-plane load was applied in conjunction with the vertical load along the top flange of the middle beam at mid-span where designated. This load was applied along the 19.1 mm [0.75 in] width of the top flange over the same 152 mm [6.0 in] length as the vertical load, as shown in Figure C.1. The out-of-plane load was set at a constant 0.41 MPa [0.06 ksi], which converts to a 0.80 kN [0.18 kips] force.

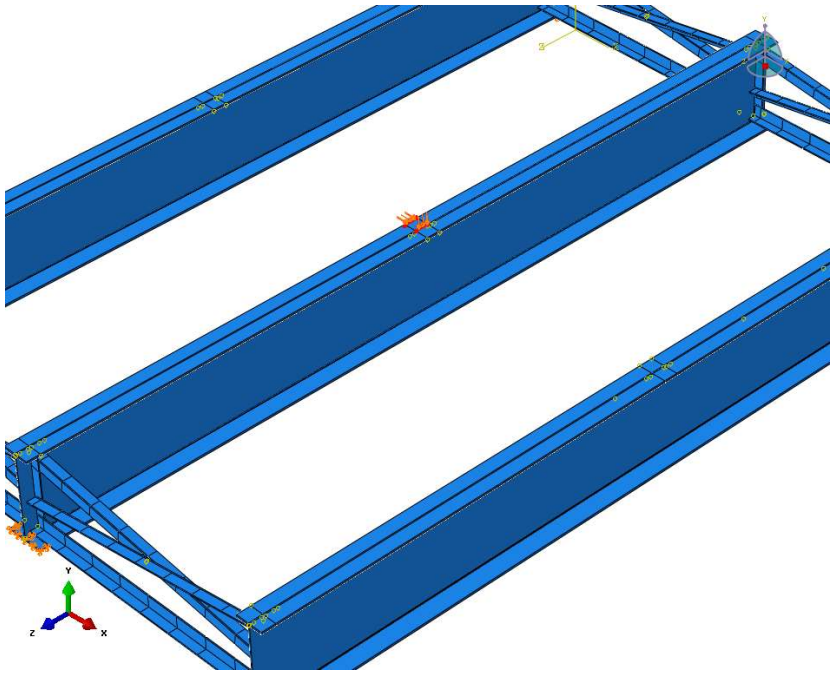

Figure C.1 Unskewed single span bridge model with vertical load and out-of-plane load applied – 3D solid elements

Figure 2 through Figure 4 shows the single span bridge model with solid elements for all parts. Figure 5 and Figure 6 shows the single span bridge model with conventional shell elements used for the webs. Figure 7 through Figure 9 shows the single span bridge model with conventional shell elements used for both the webs and flanges. Cross-frames were spaced at 4.57 m [15 ft]. An 80.1 kN [18 kips] vertical load was applied to the center girder at mid-span. The scale was set to 300 times and the Mises stress range was from 0 MPa [0 ksi] to 34.5 MPa [5 ksi]. For all models, the deflections and stresses were low, and bucking of the girders did not occur.

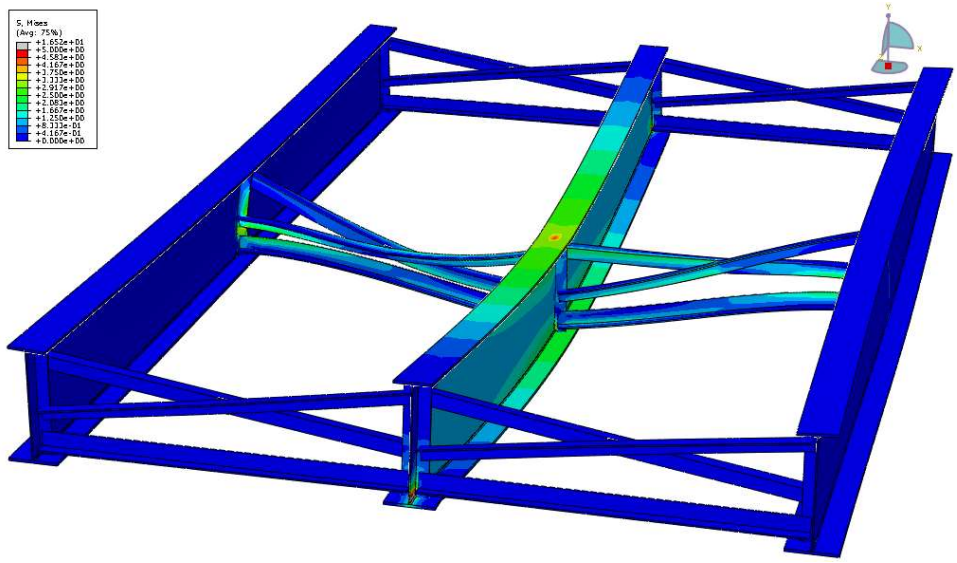

Figure C.2 Side view of the unskewed single span bridge model with 4.57 m [15 ft] cross-frame spacing and 80.1 kN [18 kips] center load – 3D solid elements

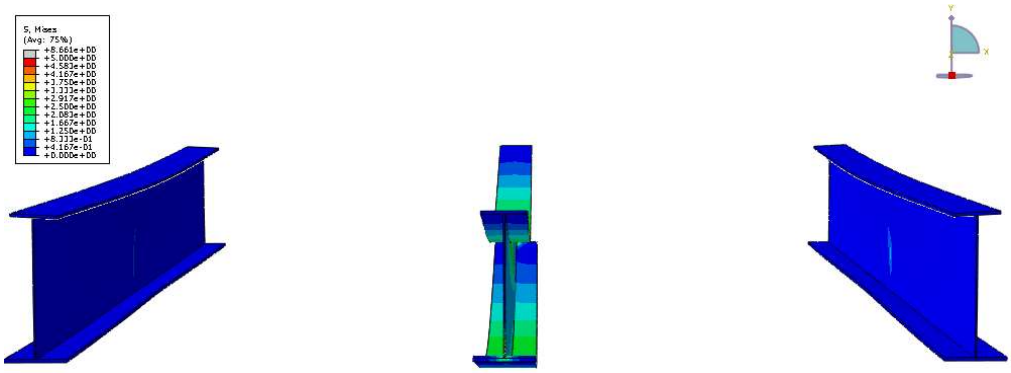

Figure C.3 Girder view of the unskewed single span bridge model with 4.57 m [15 ft] cross-frame spacing, solid elements, and 80.1 kN [18 kips] center load – 3D solid elements

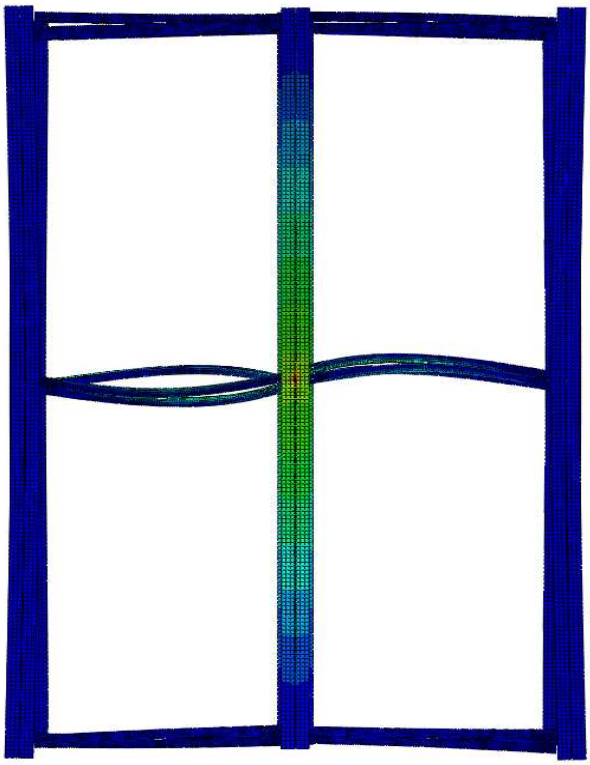

Figure C.4 Plan view of the unskewed single span bridge model with 4.57 m [15 ft] cross-frame spacing and 80.1 kN [18 kips] center load – 3D solid elements

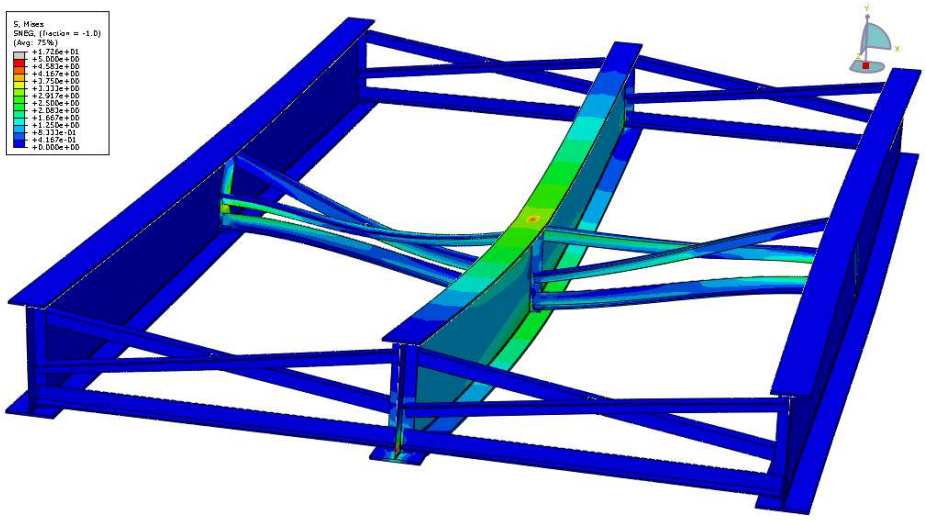

Figure C.5 Side view of the unskewed single span bridge model with 4.57 m [15 ft] cross-frame spacing and 80.1 kN [18 kips] center load - conventional web shell elements

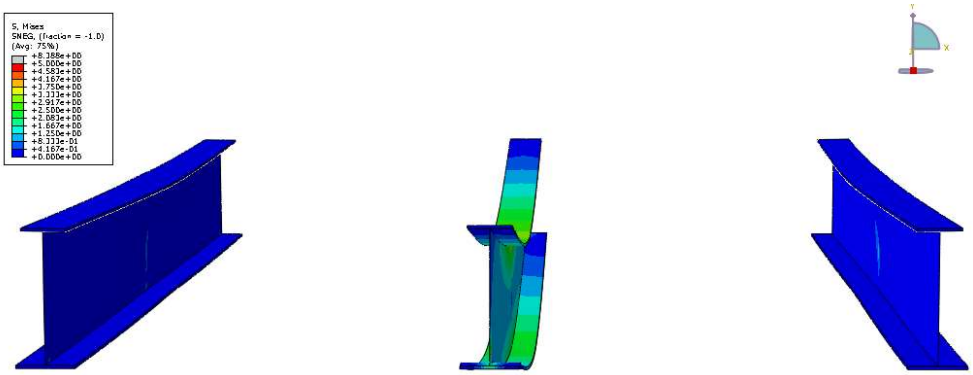

Figure C.6 Girder view of the unskewed single span bridge model with 4.57 m [15 ft] cross-frame spacing and 80.1 kN [18 kips] center load - conventional web shell elements

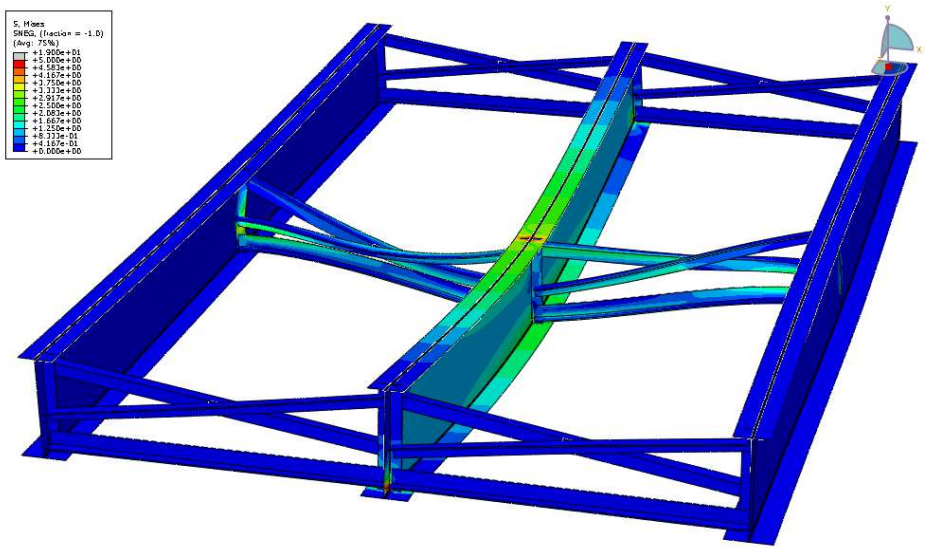

Figure C.7 Side view of the unskewed single span bridge model with 4.57 m [15 ft] cross-frame spacing and 80.1 kN [18 kips] center load - conventional web and flange shell elements

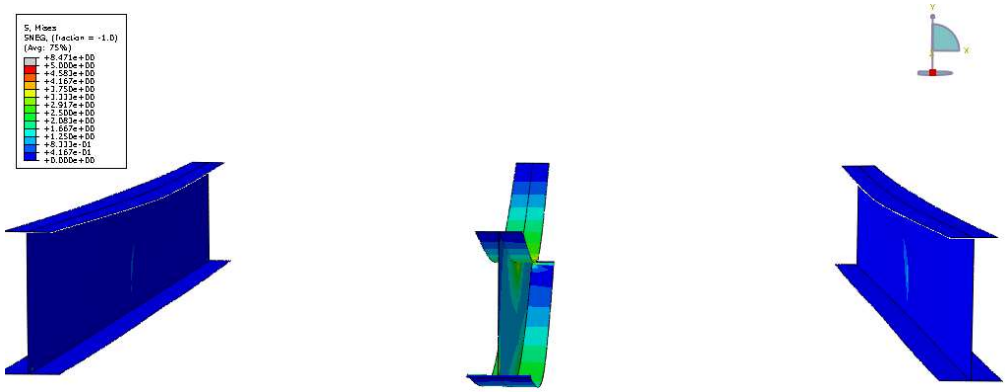

Figure C.8 Girder view of the unskewed single span bridge model with 4.57 m [15 ft] cross-frame spacing and 80.1 kN [18 kips] center load - conventional web and flange shell elements

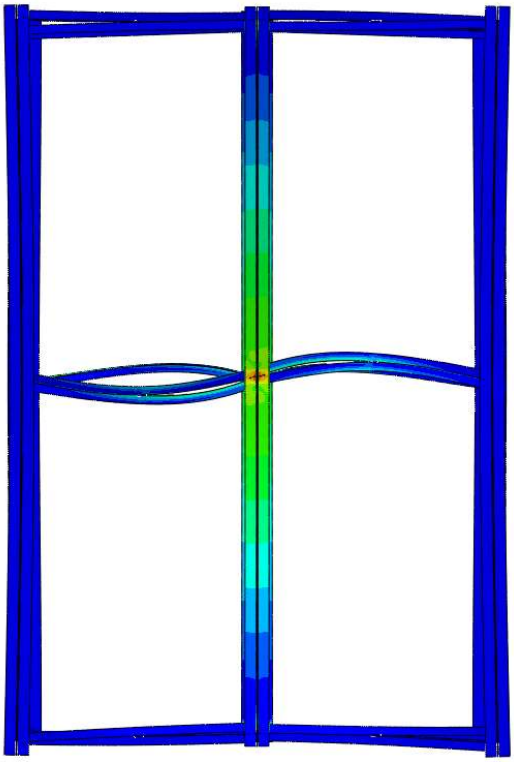

Figure C.9 Plan view of the unskewed single span bridge model with 4.57 m [15 ft] cross-frame spacing and 80.1 kN [18 kips] center load - conventional web and flange shell elements

Figure 10 through Figure 12 shows the single span bridge model with solid elements used for all parts. Figure 13 through Figure 15 shows the single span bridge model with continuum shell elements used for the girders. Figure 16 through Figure 18 shows the single span bridge model with conventional shell elements used for girder webs and flanges. Cross-frames were spaced at 9.14 m [30 ft]. An 80.1 kN [18 kips] vertical load was applied to the center girder at midspan. The scale was set to 300 times and the Mises stress range was from 0 MPa [0 ksi] to 34.5 MPa [5 ksi]. Deflections and stresses were low, but second order local buckling effects were beginning to show in the girder webs using solid elements. For girders utilizing shell elements, deflections and stress levels were similar to that of the solid element model, but second order effects did not appear.

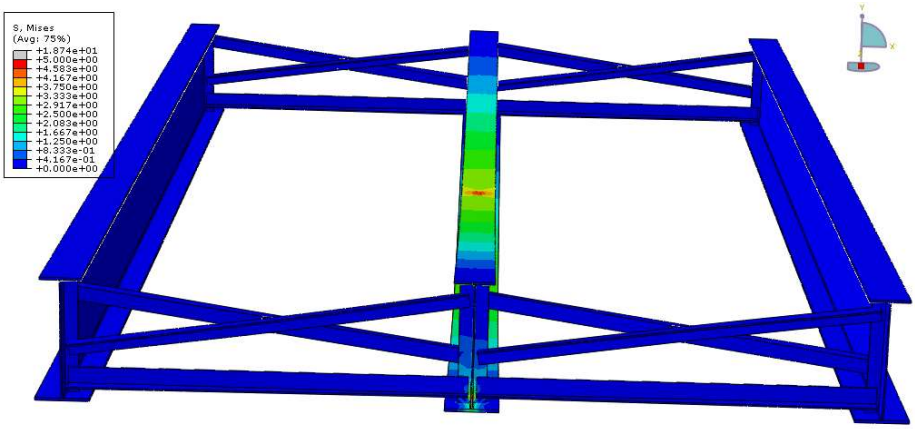

Figure C.10 Front view of the unskewed single span bridge model with 9.14 m [30 ft] cross-frame spacing and 80.1 kN [18 kips] center load – 3D solid elements

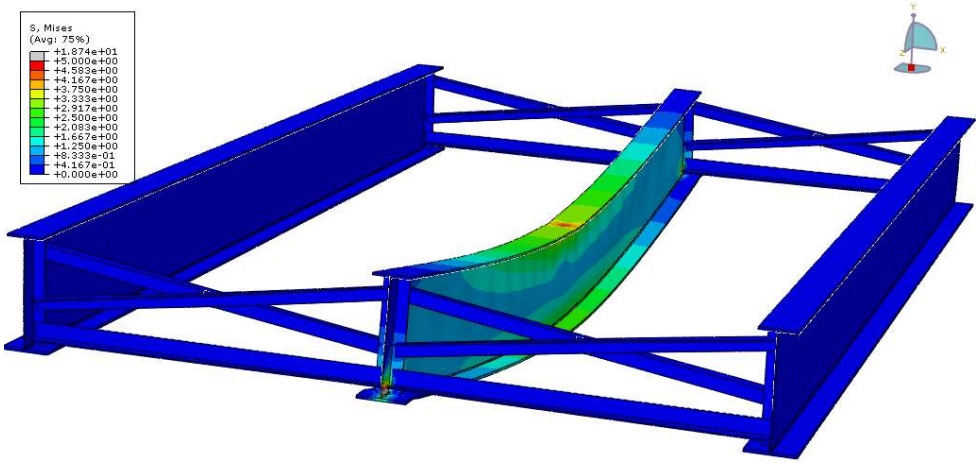

Figure C.11 Side view of the unskewed single span bridge model with 9.14 m [30 ft] cross-frame spacing and 80.1 kN [18 kips] center load – 3D solid elements

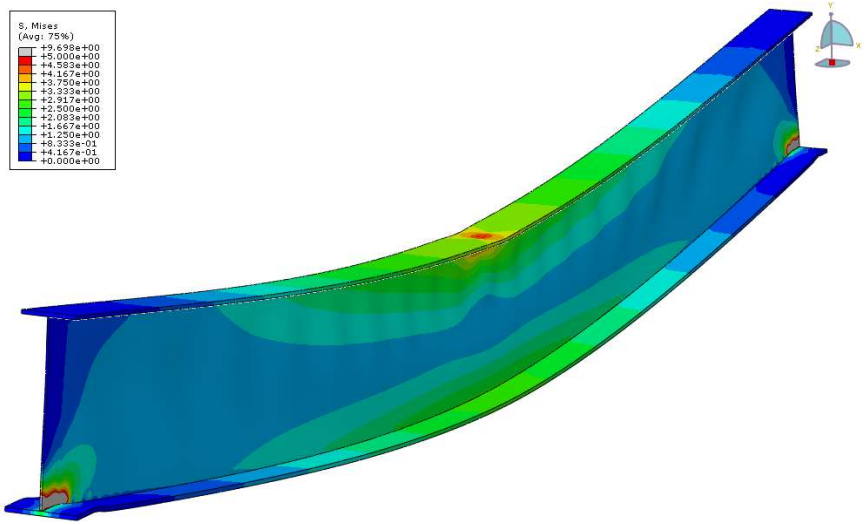

Figure C.12 Center girder view of the unskewed single span bridge model with 9.14 m [30 ft] cross-frame spacing and 80.1 kN [18 kips] center load – 3D solid elements

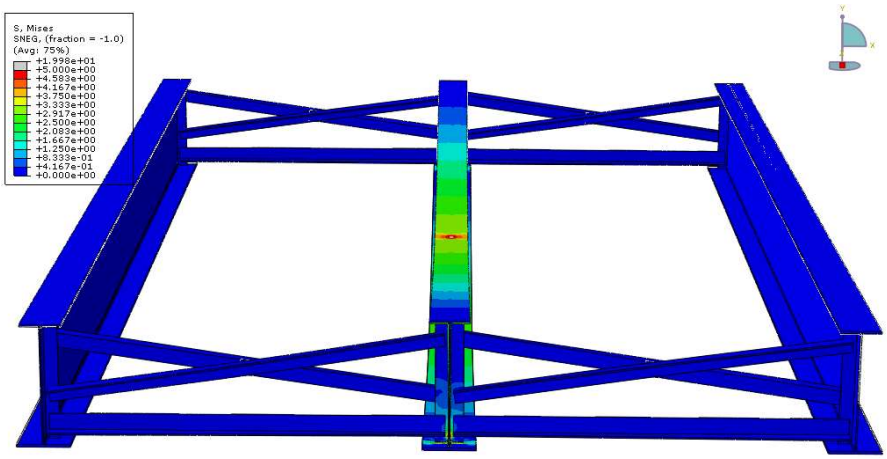

Figure C.13 Front view of the unskewed single span bridge model with 9.14 m [30 ft] cross-frame spacing and 80.1 kN [18 kips] center load - continuum girder shell elements

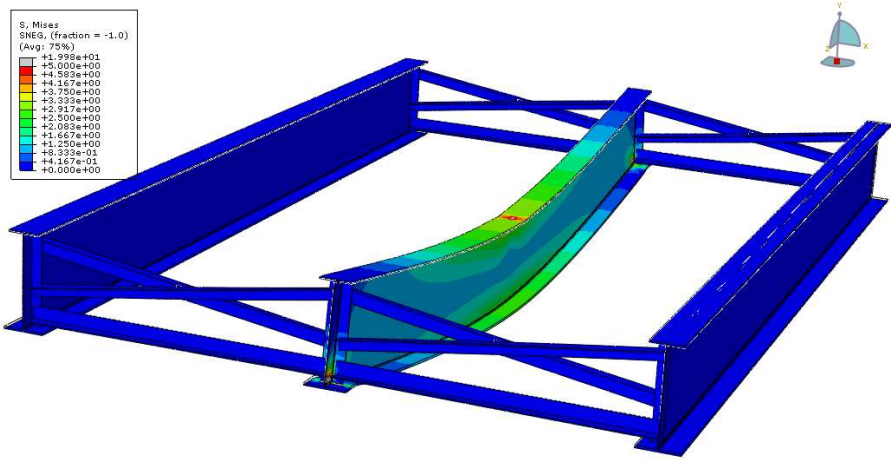

Figure C.14 Side view of the unskewed single span bridge model with 9.14 m [30 ft] cross-frame spacing and 80.1 kN [18 kips] center load - continuum girder shell elements

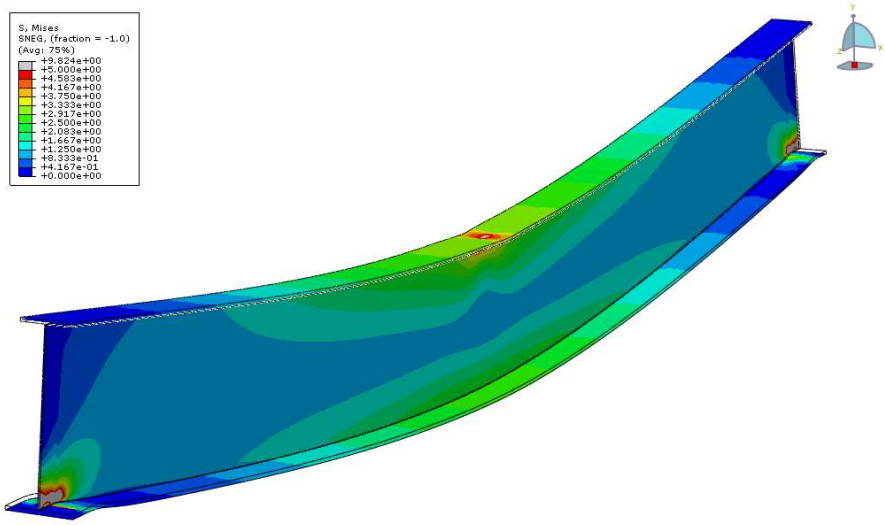

Figure C.15 Center girder view of the unskewed single span bridge model with 9.14 m [30 ft] cross-frame spacing and 80.1 kN [18 kips] center load - continuum girder shell elements

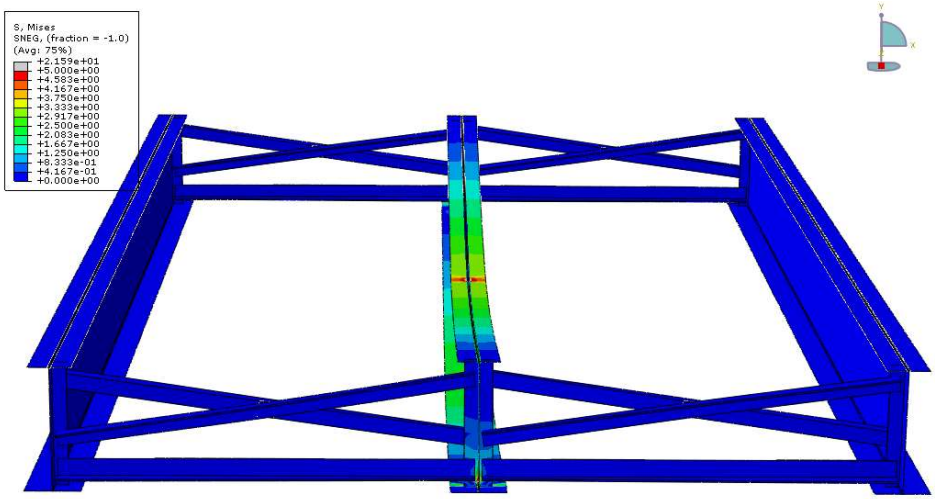

Figure C.16 Front view of the unskewed single span bridge model with 9.14 m [30 ft] cross-frame spacing and 80.1 kN [18 kips] center load - conventional girder shell elements

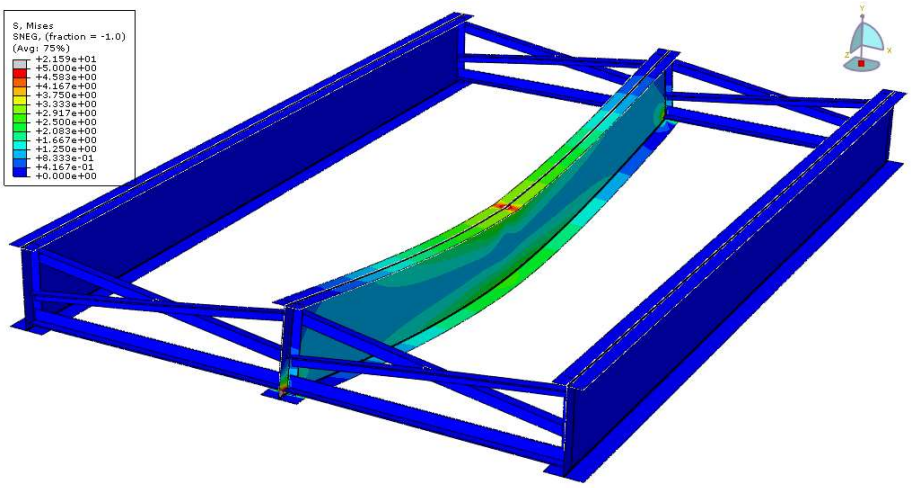

Figure C.17 Side view of the unskewed single span bridge model with 9.14 m [30 ft] cross-frame spacing and 80.1 kN [18 kips] center load - conventional girder shell elements

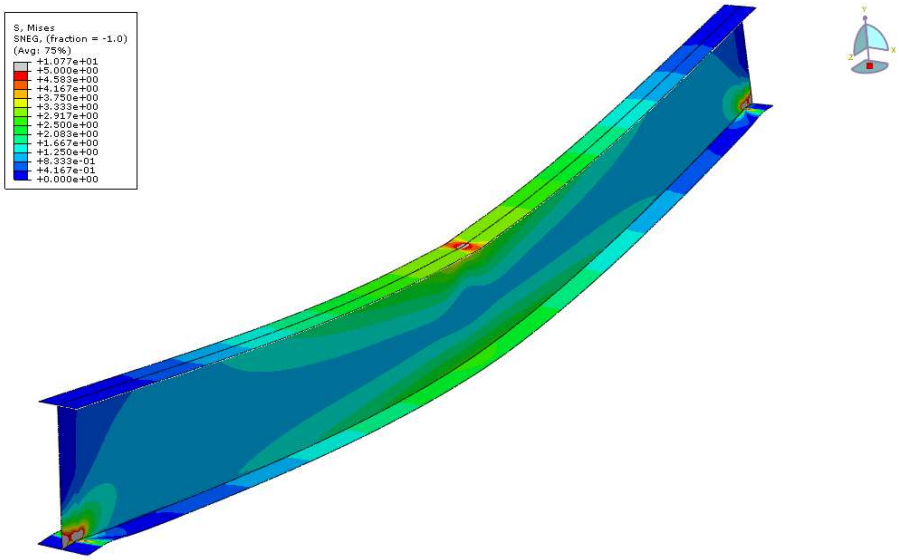

Figure C.18 Center girder view of the unskewed single span bridge model with 9.14 m [30 ft] cross-frame spacing and 80.1 kN [18 kips] center load - conventional girder shell elements

Error! Reference source not found. through

Figure C.21 shows the single span bridge model with continuum shell elements used for the girders. Cross-frames were spaced at 9.14 m [30 ft]. An 801 kN [180 kips] vertical load was applied to the center girder at midspan. The scale was set to 30 times and the Mises stress range was from 0 MPa [0 ksi] to 345 MPa [50 ksi]. Deflections and stresses increased in proportion

with the applied load. However, the girders only deflected vertically and buckling did not occur. Second order localized effects also were not present in the girder elements.

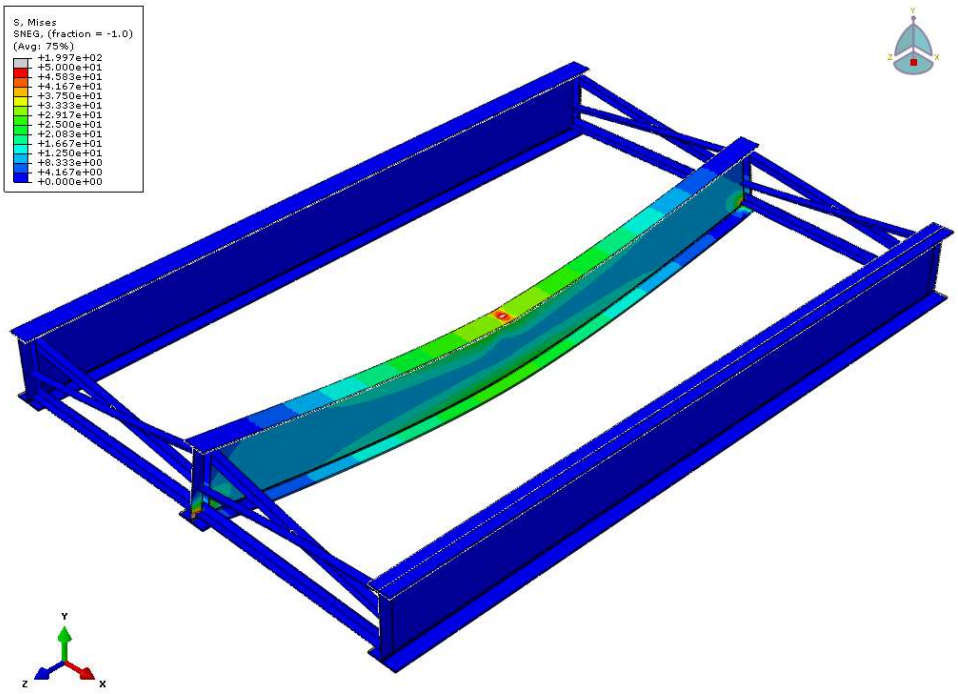

Figure C.19 Side view of the unskewed single span bridge model with 9.14 m [30 ft] cross-frame spacing and 801 kN [180 kips] center load - continuum girder shell elements

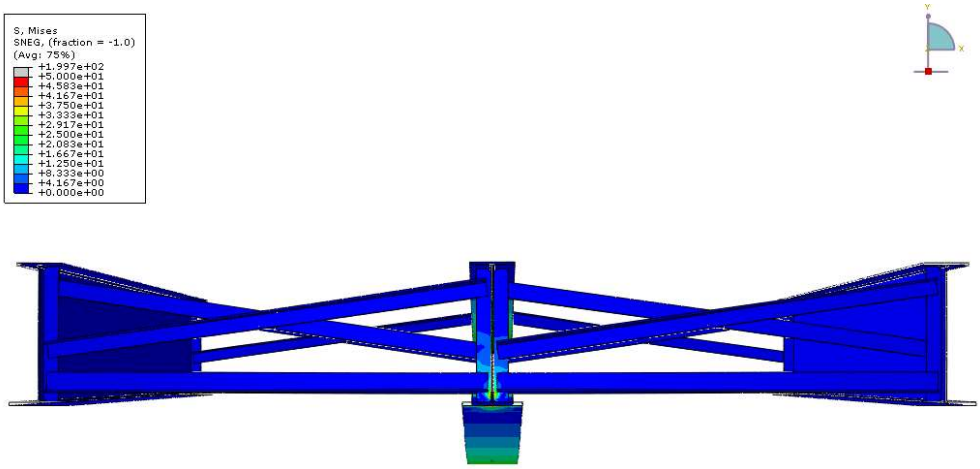

Figure C.20 Front elevation view of the unskewed single span bridge model with 9.14 m [30 ft] cross-frame spacing and 801 kN [180 kips] center load - continuum girder shell elements

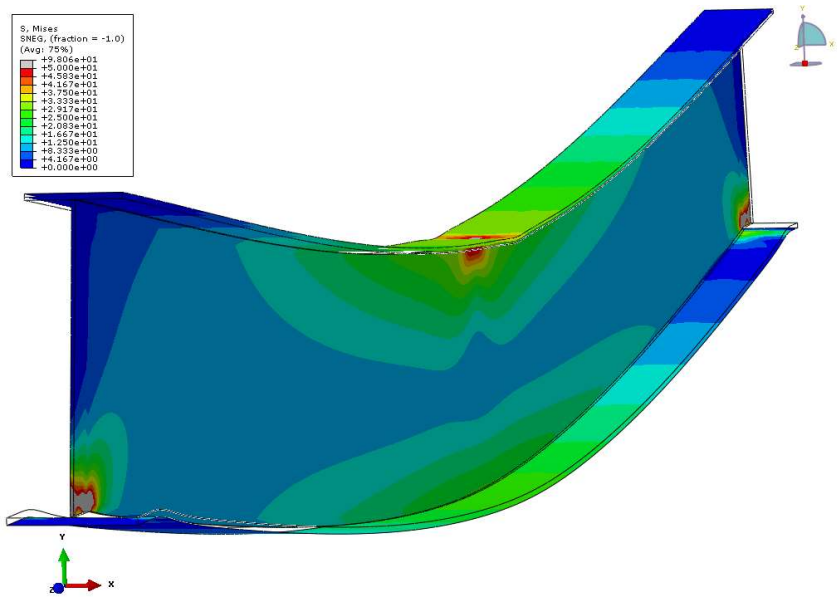

Figure C.21 Girder view of the unskewed single span bridge model with 9.14 m [30 ft] cross-frame spacing and 801 kN [180 kips] center load - continuum girder shell elements

Figure 22, Figure 23, Figure 24, and Figure 25 shows the center girder with continuum shell elements of the single span bridge model represented in Figure 19. Cross-frames were spaced at 9.14 m [30 ft] and an 801 kN [180 kips] vertical load was applied to the center girder at midspan. The displacement scale was set to 30 times. In Figure 22, the color map represents SF1, direct membrane force per unit width in local 1-direction, ranging from -97.9 kN [-22 kips] to 48.9 kN [11 kips]. The color map in Figure 23 shows SF2, direct membrane force per unit width in local 1-direction, ranging from -209 kN [-47 kips] to 182 kN [41 kips]. The color map in Figure 24 displays SM1, bending moment force per unit width in local 1-direction, ranging from -226 N-m [-2 k-in] to 452 N-m [4 k-in]. Finally, in Figure 25, the color map shows SM2, bending moment force per unit width in local 2-direction, ranging from -226 N-m [-2 k-in] to 678 N-m [6 k-in].

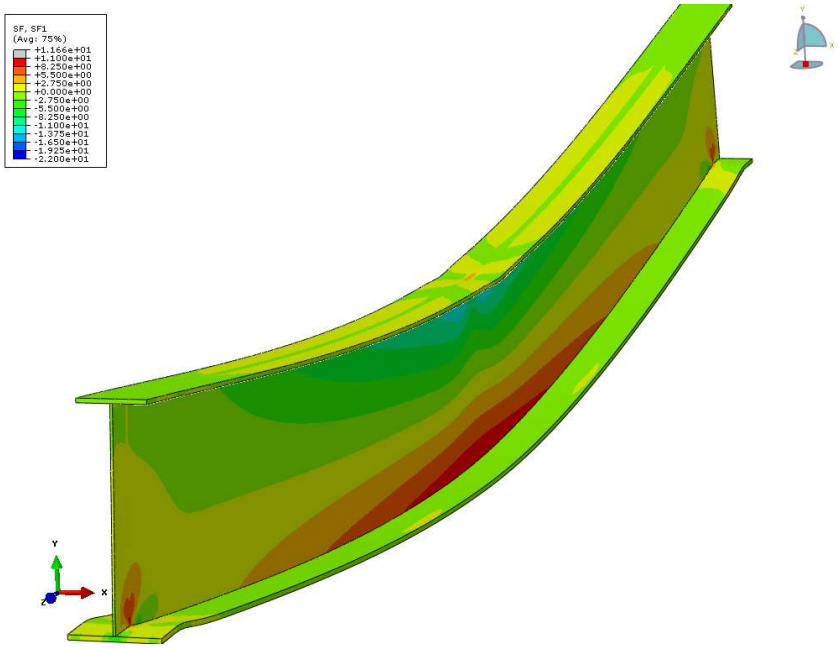

Figure C.22 SF1 (direct membrane force per unit width in local 1-direction) for the unskewed single span bridge model with 9.14 m [30 ft] cross-frame spacing and 801 kN [180 kips] center load - continuum girder shell elements

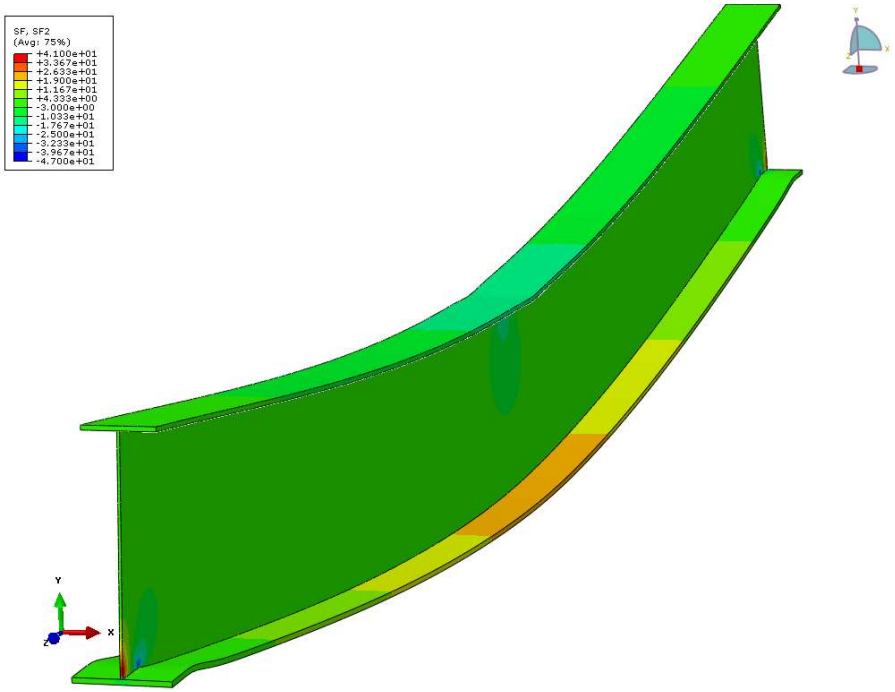

Figure C.23 SF2 (direct membrane force per unit width in local 2-direction) for the unskewed single span bridge model with 9.14 m [30 ft] cross-frame spacing and 801 kN [180 kips] center load - continuum girder shell elements

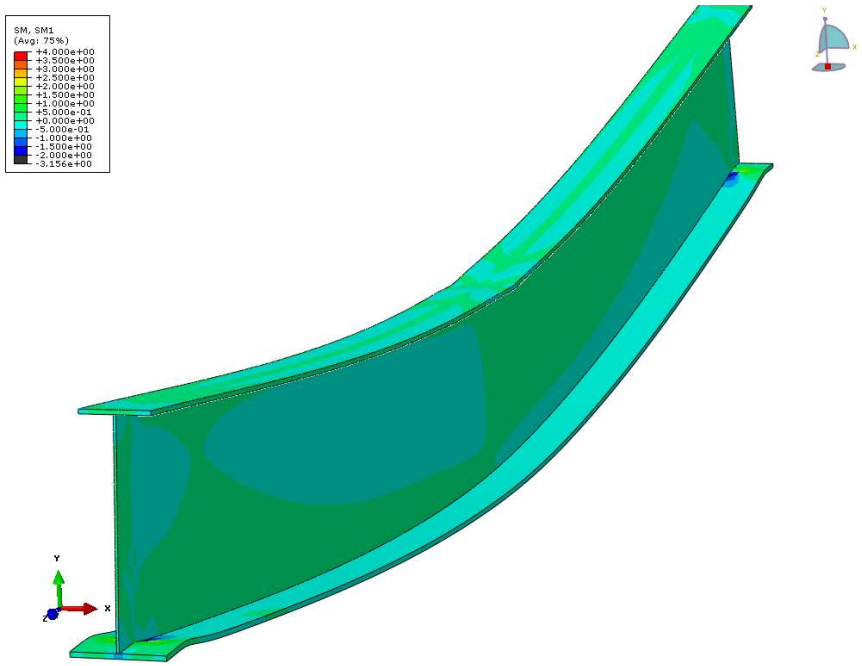

Figure C.24 SM1 (bending moment force per unit width in local 1-axis) for the unskewed single span bridge model with 9.14 m [30 ft] cross-frame spacing and 801 kN [180 kips] center load - continuum girder shell elements

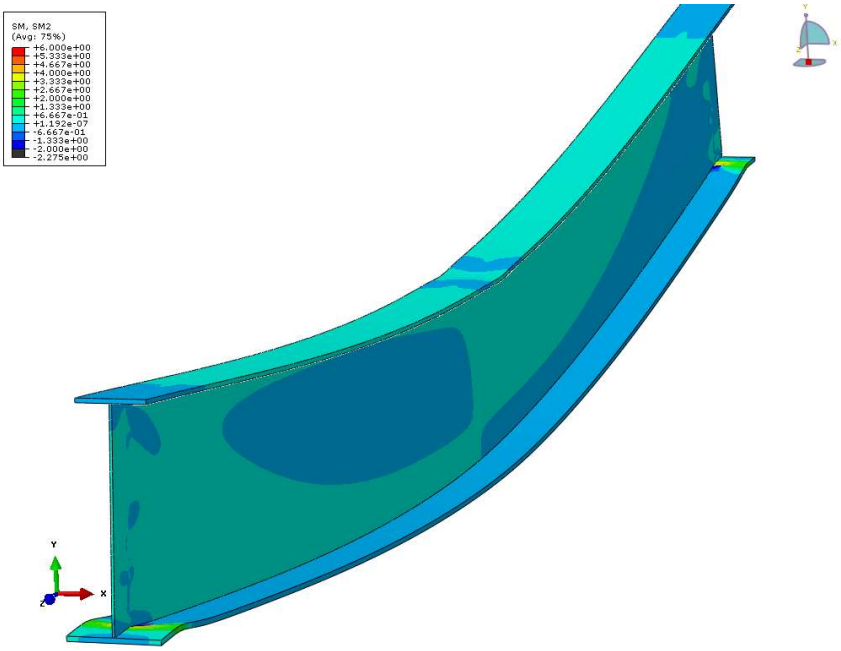

Figure C.25 SM2 (bending moment force per unit width in local 2-axis) for the unskewed single span bridge model with 9.14 m [30 ft] cross-frame spacing and 801 kN [180 kips] center load - continuum girder shell elements

Error! Reference source not found. through **Error! Reference source not found.** shows the single span bridge model with conventional shell elements used for the girders. Cross-

frames were spaced at 9.14 m [30 ft]. An 801 kN [180 kips] vertical load was applied to the center girder at midspan. The scale was set to 30 times and the Mises stress range was from 0 MPa [0 ksi] to 345 MPa [50 ksi]. Deflections and stresses increased in proportion with the applied load, but girders only deflected vertically and buckling did not occur. Second order localized effects were unable to form within the girder shell elements.

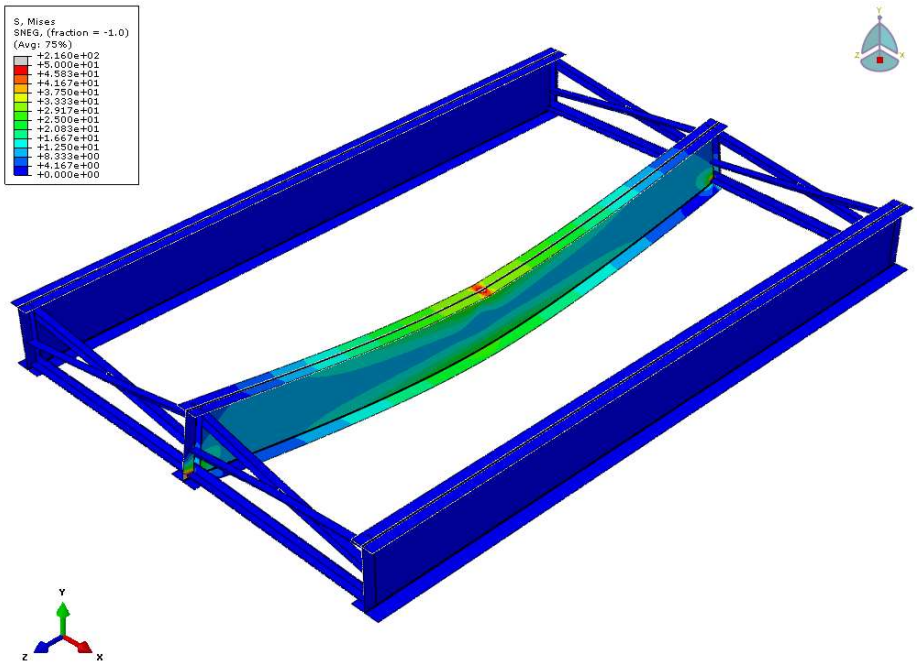

Figure C.26 Side view of the unskewed single span bridge model with 9.14 m [30 ft] cross-frame spacing and 801 kN [180 kips] center load - conventional girder shell elements

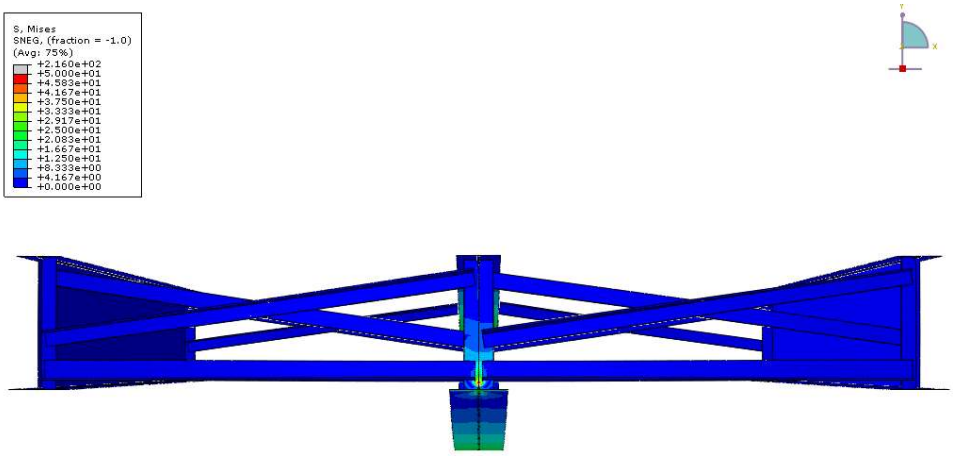

Figure C.27 Front elevation of the unskewed single span bridge model with 9.14 m [30 ft] cross-frame spacing and 801 kN [180 kips] center load - conventional girder shell elements

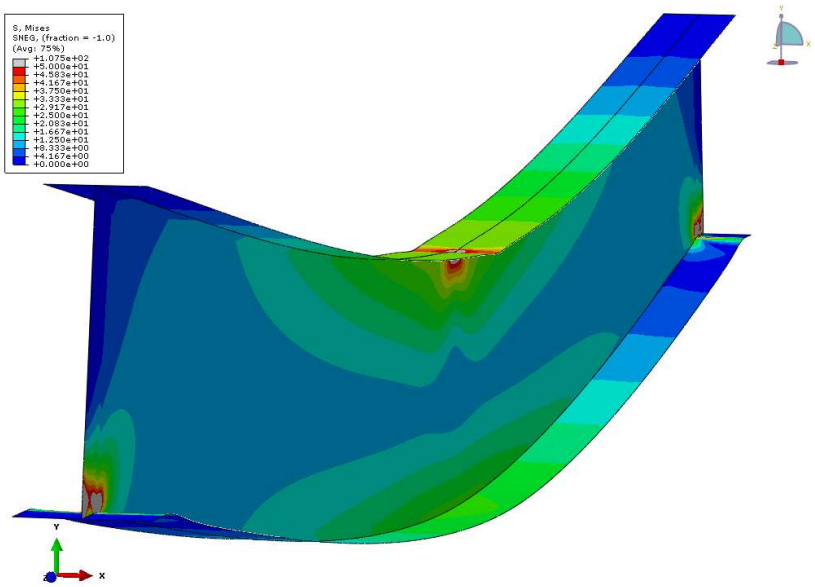

Figure C.28 Girder view of the unskewed single span bridge model with 9.14 m [30 ft] cross-frame spacing and 801 kN [180 kips] center load - conventional girder shell elements

Figure 29, Figure 30, Figure 31, and Figure 32 shows the center girder with conventional shell elements of the single span bridge model represented in Figure 26. Cross-frames were spaced at 9.14 m [30 ft] and an 801 kN [180 kips] vertical load was applied to the girder shown. The displacement scale was set to 30 times. In Figure 29, the color map represents SF1, direct membrane force per unit width in local 1-direction, ranging from -97.9 kN [-22 kips] to 48.9 kN [11 kips]. The color map in Figure 30 displays SF2, direct membrane force per unit width in local 2-direction, ranging from -209 kN [-47 kips] to 182 kN [41 kips]. In Figure 31, the color map presents SM1, bending moment force per unit width in local 1-direction, ranging from -226 N-m [-2 k-in] to 452 N-m [4 k-in]. The color map in Figure 32 shows SM2, bending moment force per unit width in local 2-direction, ranging from -678 N-m [-6 k-in] to 226 N-m [2 k-in].

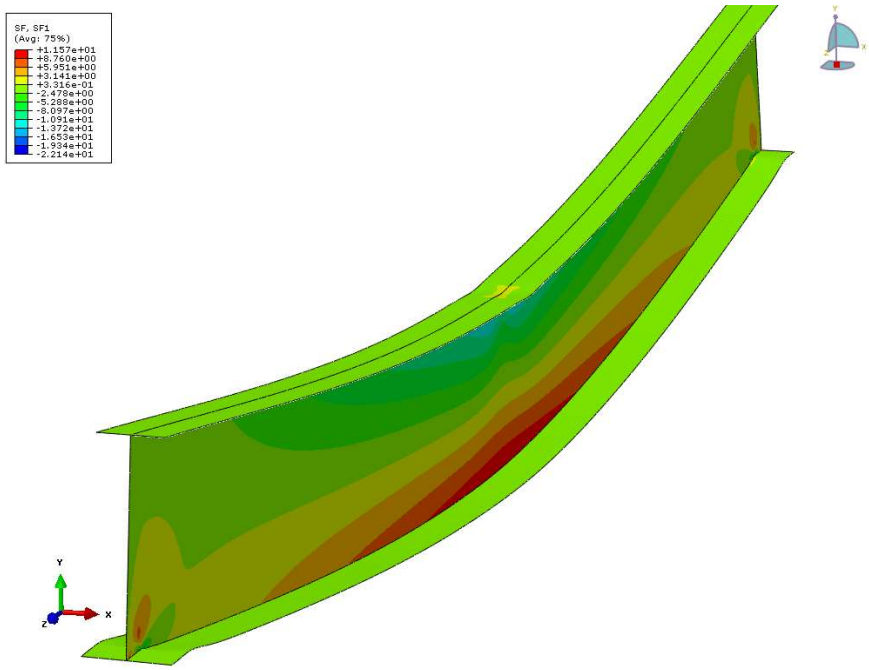

Figure C.29 SF1 (direct membrane force per unit width in local 1-direction) for the unskewed single span bridge model with 9.14 m [30 ft] cross-frame spacing and 801 kN [180 kips] center load - conventional girder shell elements

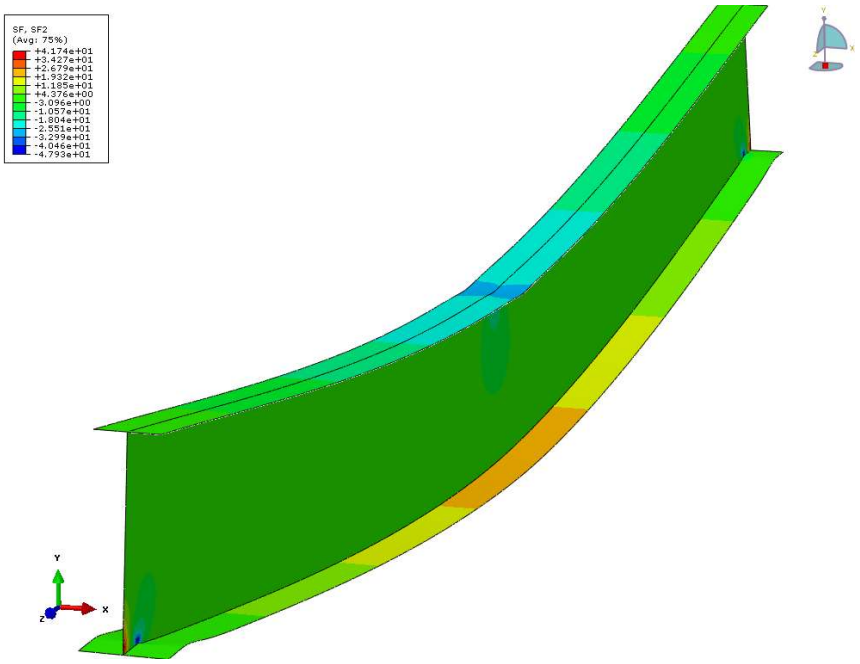

Figure C.30 SF2 (direct membrane force per unit width in local 2-direction) for the unskewed single span bridge model with 9.14 m [30 ft] cross-frame spacing and 801 kN [180 kips] center load - conventional girder shell elements

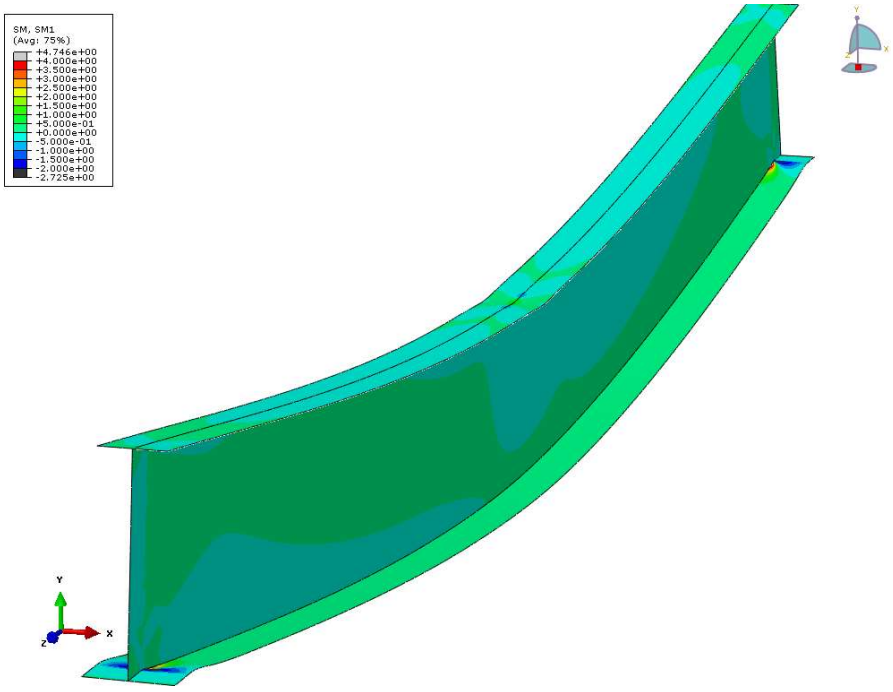

Figure C.31 SM1 (bending moment force per unit width in local 1-axis) for the unskewed single span bridge model with 9.14 m [30 ft] cross-frame spacing and 801 kN [180 kips] center load - conventional girder shell elements

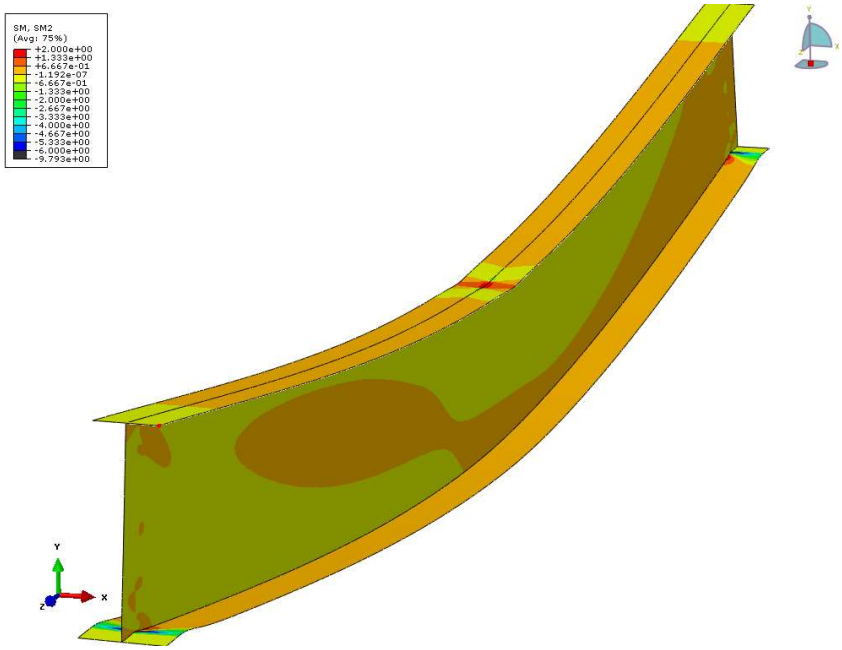

Figure C.32 SM2 (bending moment force per unit width in local 2-axis) for the unskewed single span bridge model with 9.14 m [30 ft] cross-frame spacing and 801 kN [180 kips] center load - conventional girder shell elements

Figure 33 through Figure 37 shows the single span bridge model with continuum shell elements used for the girders. Figure 38 through Figure 40 shows the single span bridge model with conventional shell elements used for the girders. Cross-frames were spaced at 9.14 m [30 ft]. An 80.1 kN [18 kips] vertical load was applied to the center girder at midspan along with a 0.80 kN [0.18 kip] out-of-plane load along the top flange at the same location. The scale was set to 100 times and the Mises stress range was from 0 MPa [0 ksi] to 34.5 MPa [5 ksi]. While the stresses and deflections were low, the girders deflected vertically and the top flange showed lateral bending. However, the deflections were more characteristic of bending rather than buckling of the girder. As previously confirmed, both continuum and conventional shell elements are unable to capture buckling or higher order local buckling modes.

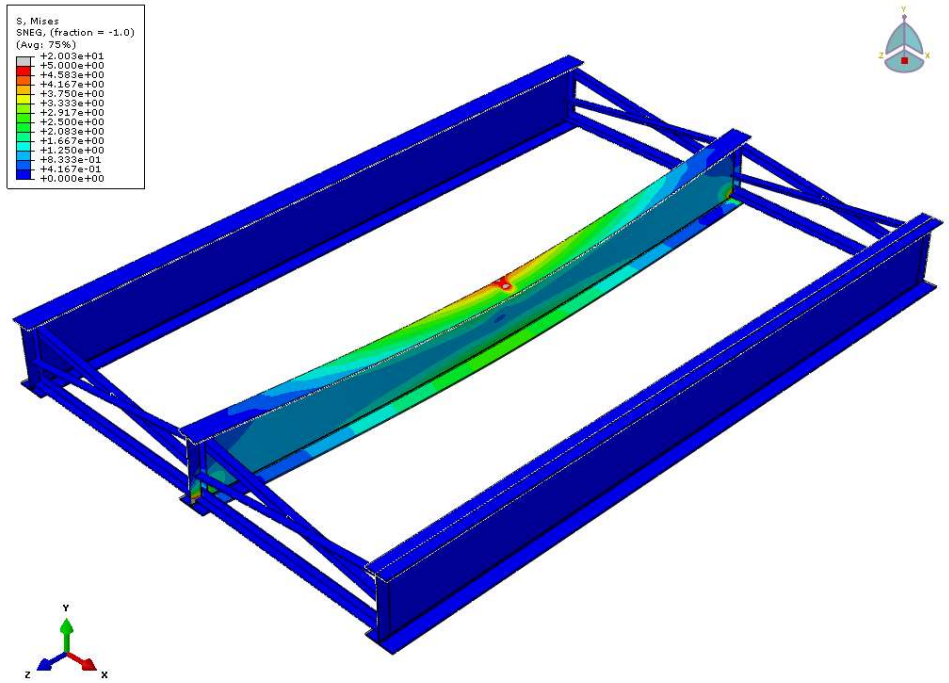

Figure C.33 Side view of the unskewed single span bridge model with 9.14 m [30 ft] cross-frame spacing, 80.1 kN [18 kips] center load, and 0.80 kN [0.18 kips] out-of-plane load - continuum girder shell elements

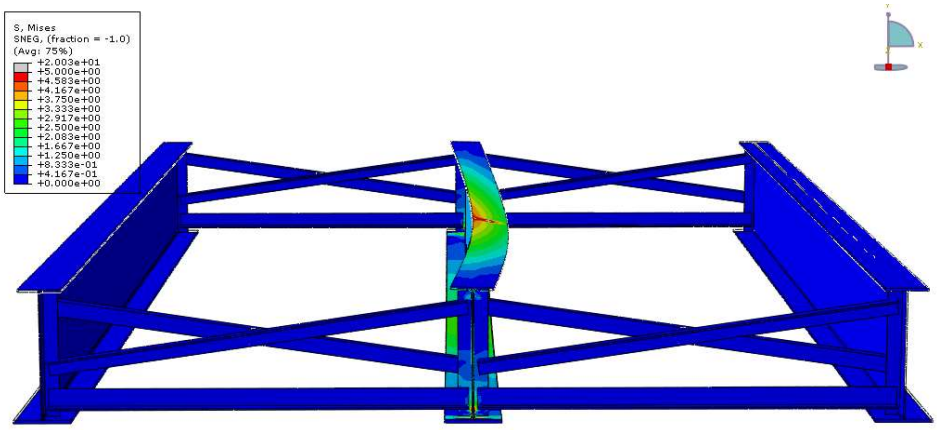

Figure C.34 Front view of the unskewed single span bridge model with 9.14 m [30 ft] cross-frame spacing, 80.1 kN [18 kips] center load, and 0.80 kN [0.18 kips] out-of-plane load - continuum girder shell elements

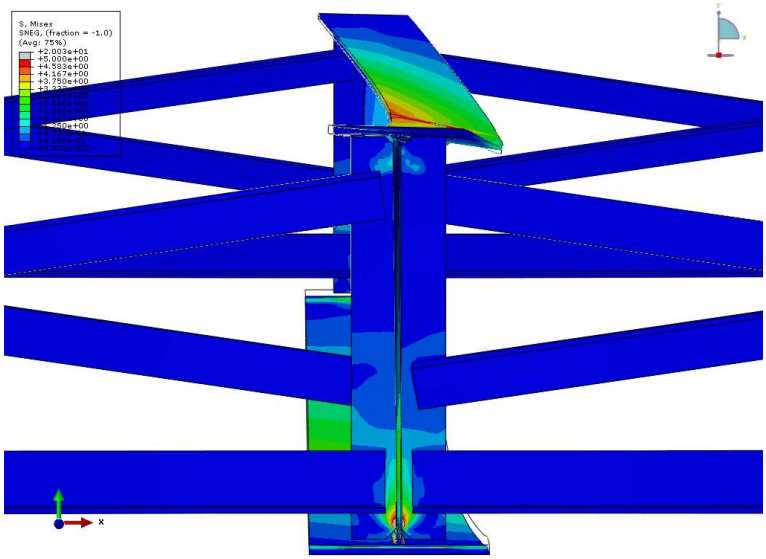

Figure C.35 Center girder elevation of the unskewed single span bridge model with 9.14 m [30 ft] cross-frame spacing, 80.1 kN [18 kips] center load, and 0.80 kN [0.18 kips] out-of-plane load - continuum girder shell elements

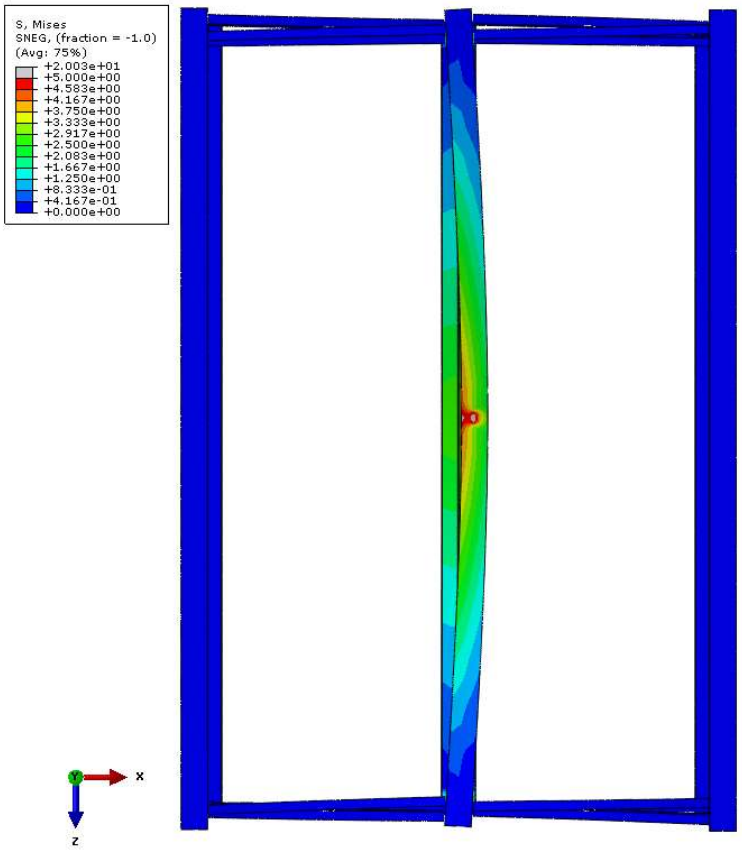

Figure C.36 Plan view of the unskewed single span bridge model with 9.14 m [30 ft] cross-frame spacing, 80.1 kN [18 kips] center load, and 0.80 kN [0.18 kips] out-of-plane load - continuum girder shell elements

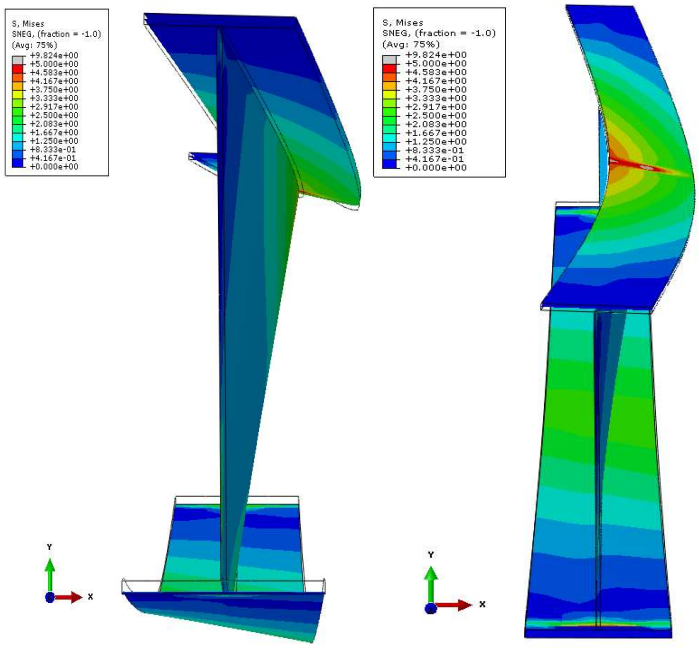

Figure C.37 Girder section of the unskewed single span bridge model with 9.14 m [30 ft] cross-frame spacing, 80.1 kN [18 kips] center load, and 0.80 kN [0.18 kips] out-of-plane load - continuum girder shell elements

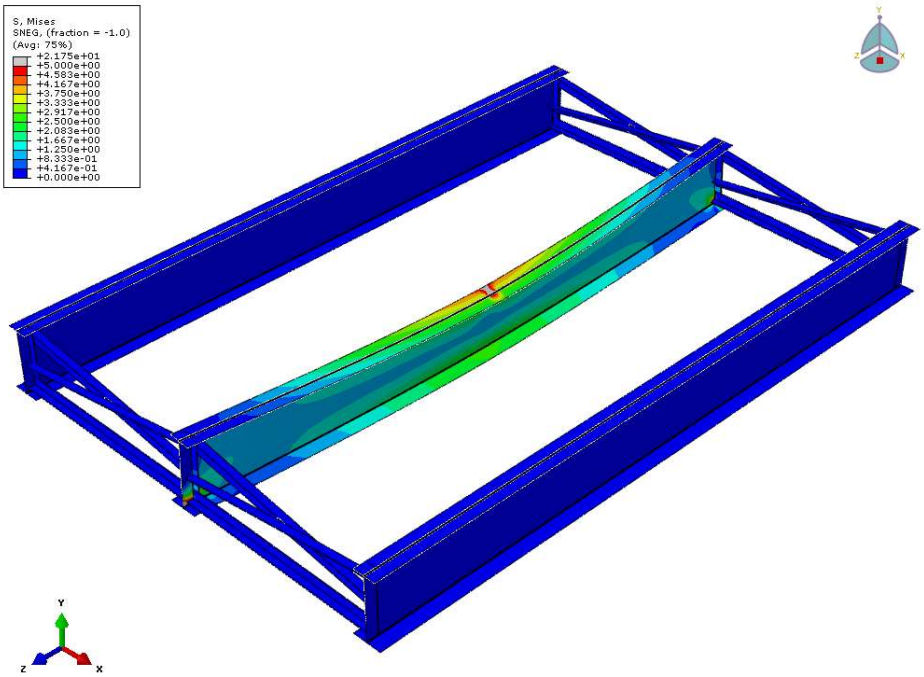

Figure C.38 Side view of the unskewed single span bridge model with 9.14 m [30 ft] cross-frame spacing, 80.1 kN [18 kips] center load, and 0.80 kN [0.18 kips] out-of-plane load - conventional girder shell elements

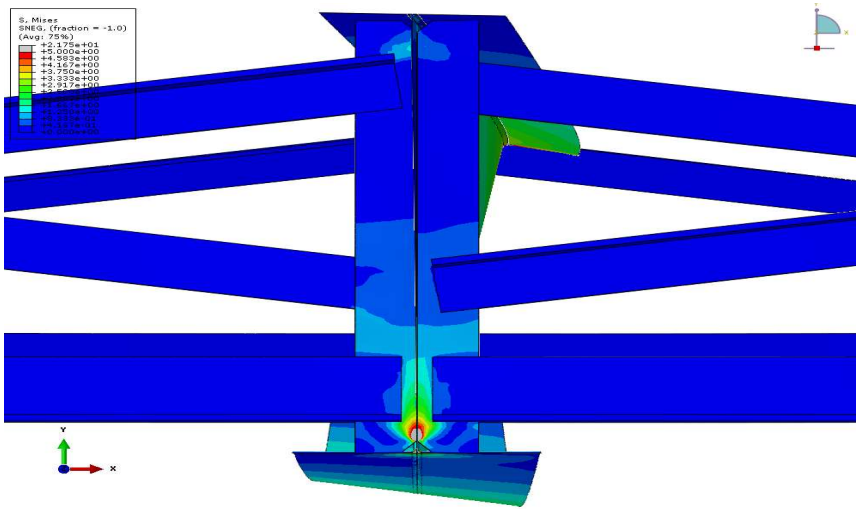

Figure C.39 Center girder elevation of the unskewed single span bridge model with 9.14 m [30 ft] cross-frame spacing, 80.1 kN [18 kips] center load, and 0.80 kN [0.18 kips] out-of-plane load - conventional girder shell elements

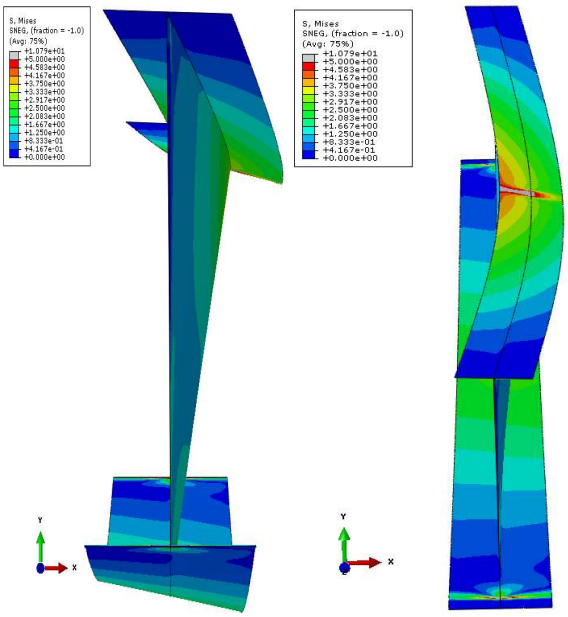

Figure C.40 Girder section of the unskewed single span bridge model with 9.14 m [30 ft] cross-frame spacing, 80.1 kN [18 kips] center load, and 0.80 kN [0.18 kips] out-of-plane load - conventional girder shell elements

Error! Reference source not found. through **Error! Reference source not found.** shows the full-scale model of the 40° skewed-staggered bridge with 4.57 m [15 ft] cross-frame spacing and conventional web shell elements. The bridge geometry, modeling methodology, and applied loads are described in Part 2 of this dissertation with the exception that the overhang brackets were modeled explicitly and the abutment cross-frames were composed of L152x152x25.4 mm [L6.0x6.0x1.0 in] angles with a 25.4 mm [1.0 in] thick stiffener. Due to convergence issues, the model achieved 77% run-time competition. The scale in the figures was set to 3 times and the Mises stress range was from 0 MPa [0 ksi] to 345 MPa [50 ksi]. Even at partial completion, localized yielding can be seen in the web and flanges. Stresses were low in the cross-frames and overhang brackets, suggesting lateral forces were small. While the girders do not show signs of lateral torsional buckling, likely due to the short unbraced length, the web was able to capture forces from the overhang bracket connections.

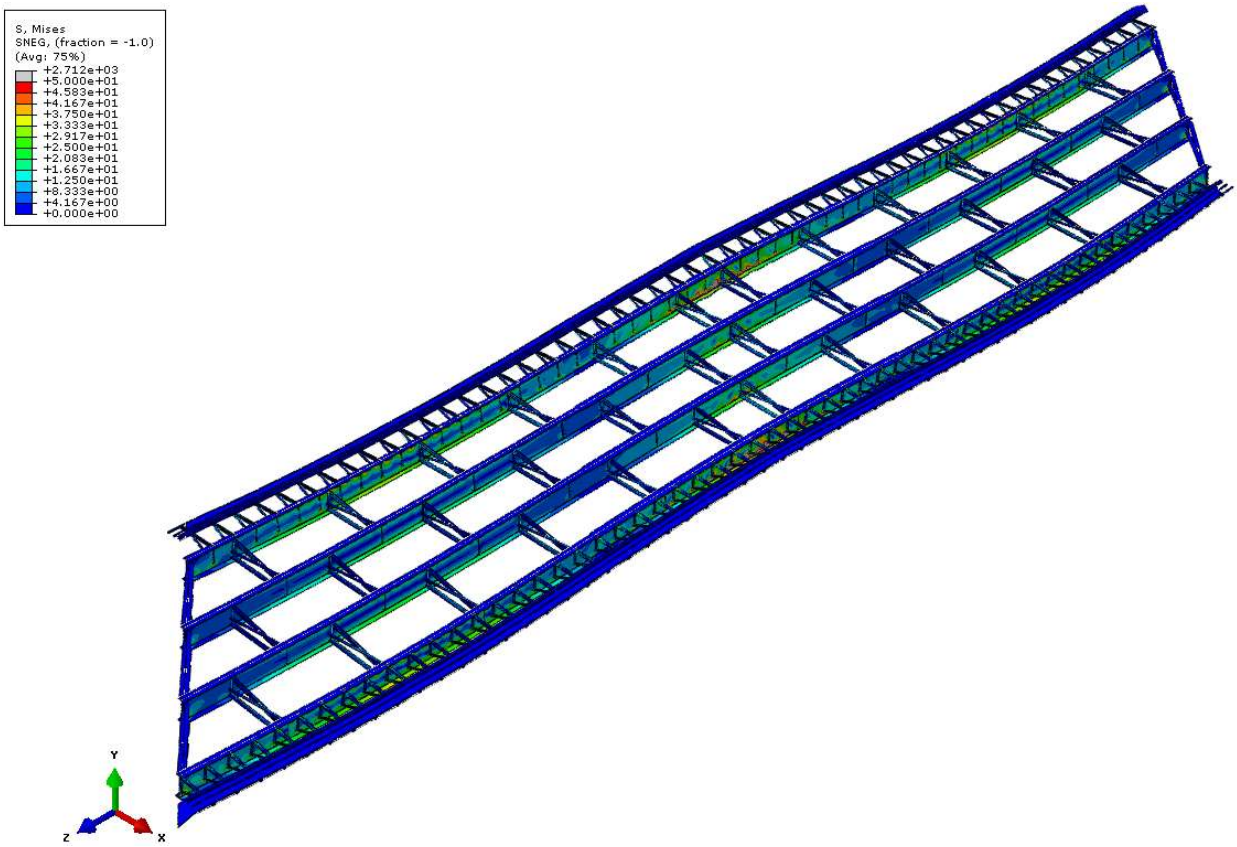

Figure C.41 Isotropic view of the 40° skewed-staggered bridge with 4.57 m [15 ft] cross-frame spacing - conventional web shell elements

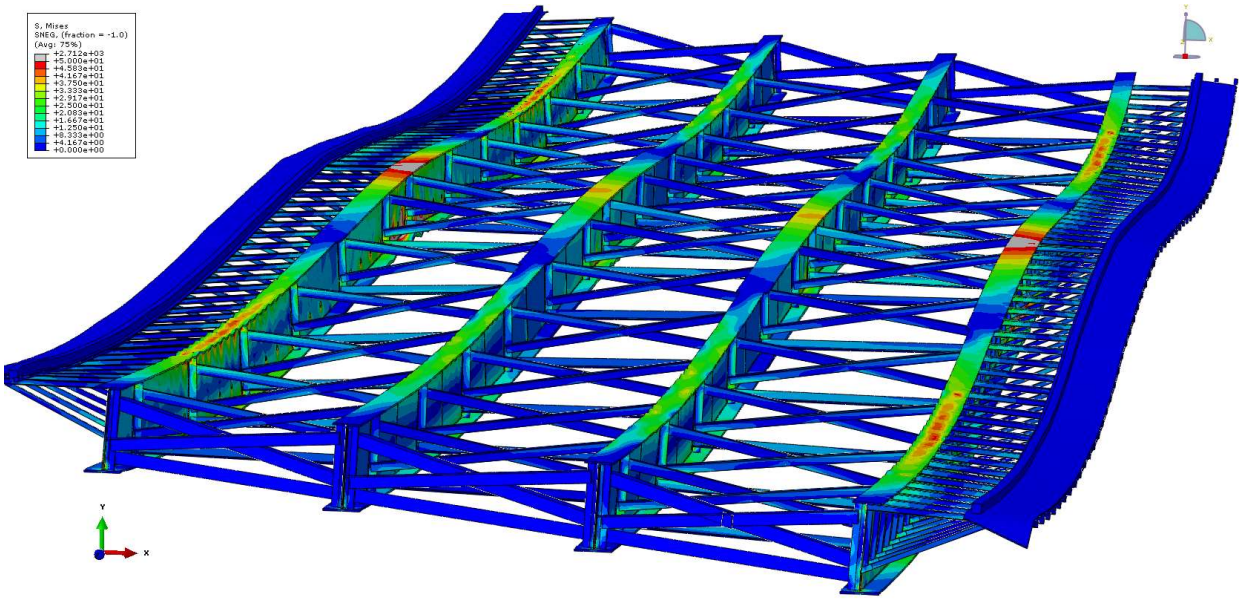

Figure C.42 Side view of the 40° skewed-staggered bridge with 4.57 m [15 ft] cross-frame spacing-conventional web shell elements

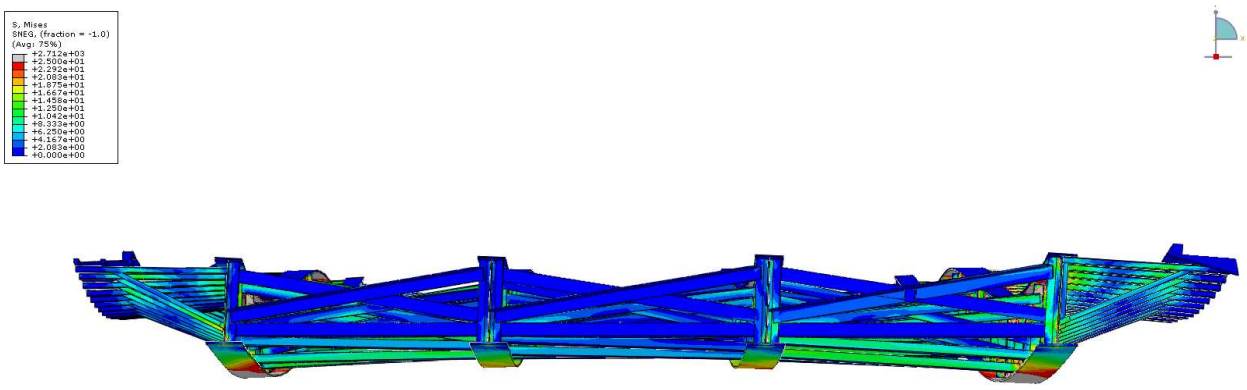

Figure C.43 Front elevation of the 40° skewed-staggered bridge with 4.57 m [15 ft] cross-frame spacing - conventional web shell elements

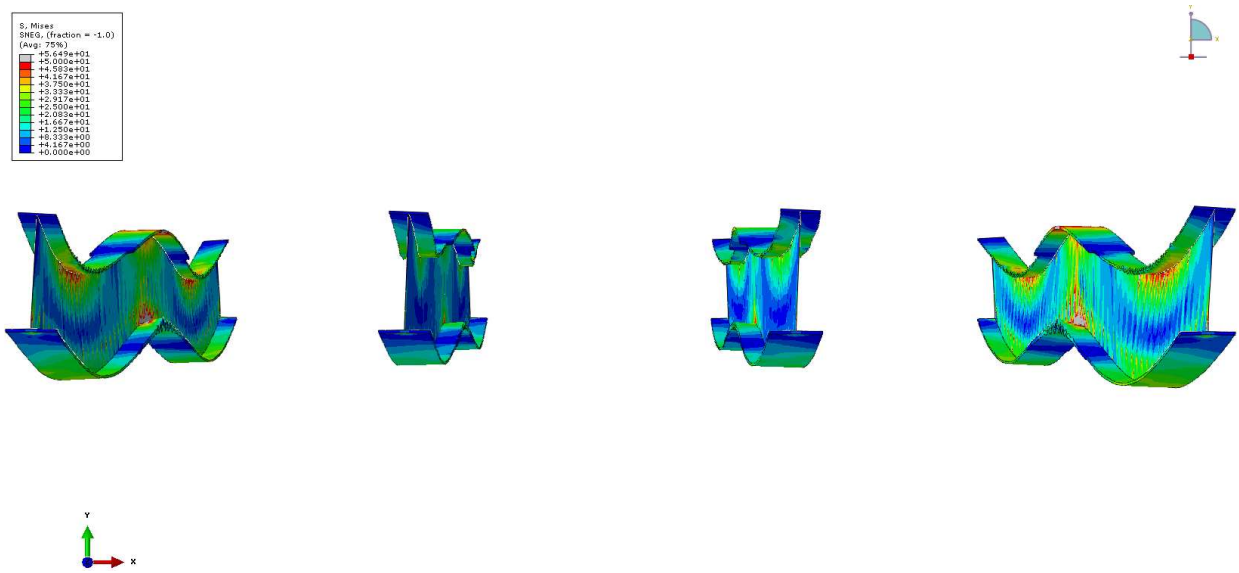

Figure C.44 Girder view of the 40° skewed-staggered bridge with 4.57 m [15 ft] cross-frame spacing - conventional web shell elements

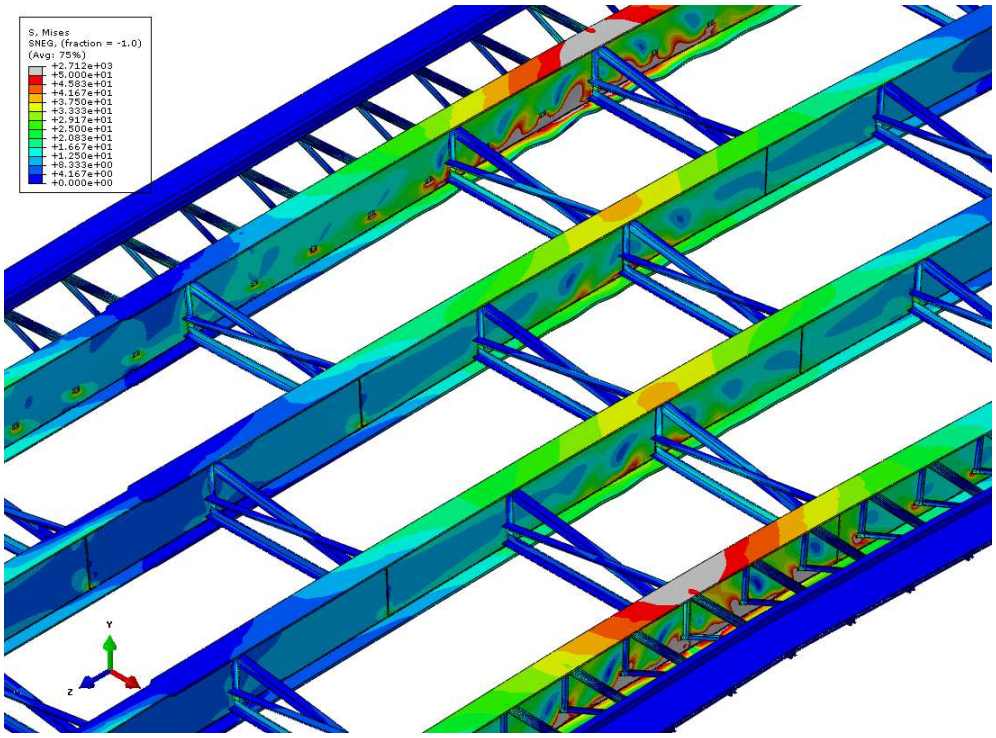

Figure C.45 Center span of the 40° skewed-staggered bridge with 4.57 m [15 ft] cross-frame spacing - conventional web shell elements

Error! Reference source not found. through **Error! Reference source not found.** shows the single span bridge model with solid elements used for the girders. Cross-frames were spaced at 9.14 m [30 ft]. An 80.1 kN [18 kips] vertical load was applied to the center girder at mid-span along with a 0.80 kN [0.18 kip] out-of-plane load along the top flange at the same location. The scale was set to 10 times and the Mises stress range was from 0 MPa [0 ksi] to 34.5 MPa [5 ksi]. The model completed to 89% run-time under a static analysis before erroring out. Due to the partial run-time, stresses and vertical deflections were low. However, the applied load was enough to cause buckling of the web and top flanges not seen with models using girder shell elements.

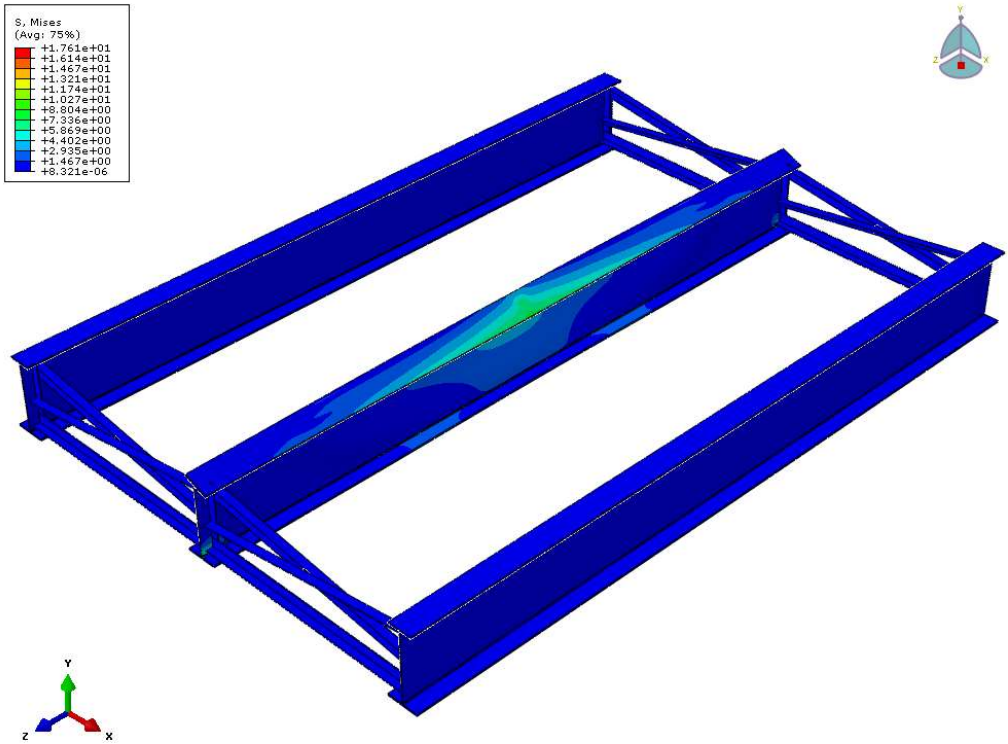

Figure C.46 Side view of the unskewed single span bridge model with 9.14 m [30 ft] cross-frame spacing, 80.1 kN [18 kips] center load, and 0.80 kN [0.18 kips] out-of-plane load – 3D solid elements

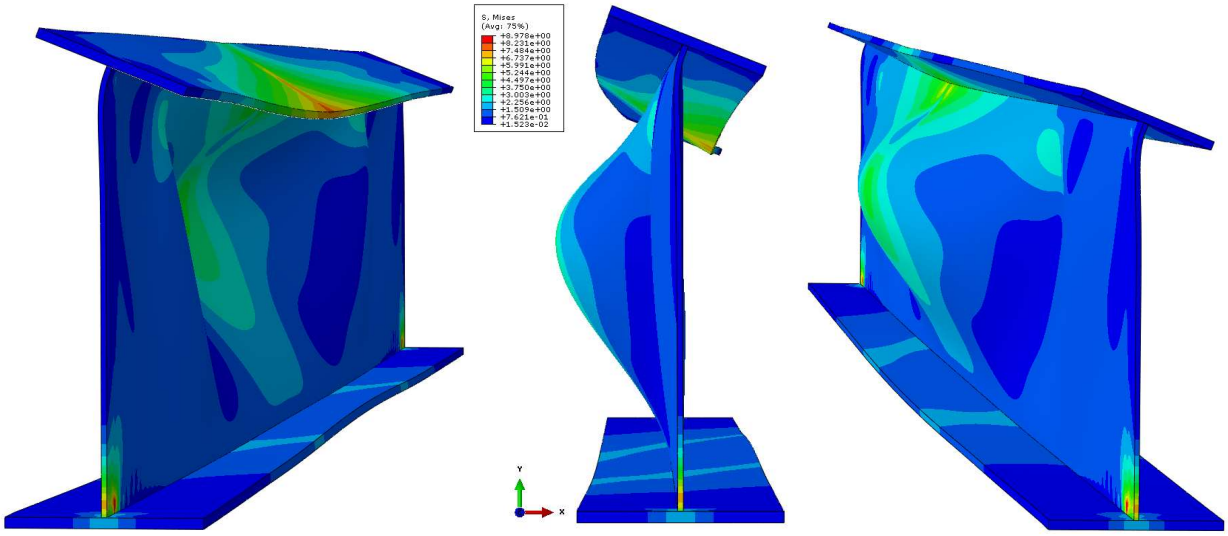

Figure C.47 Girder section view of the unskewed single span bridge model with 9.14 m [30 ft] cross-frame spacing, 80.1 kN [18 kips] center load, and 0.80 kN [0.18 kips] out-of-plane load – 3D solid elements

Error! Reference source not found. through **Error! Reference source not found.** shows the single span bridge model with solid elements used for all parts. A dynamic implicit analysis was used. Cross-frames were spaced at 9.14 m [30 ft]. An 80.1 kN [18 kips] vertical

load was applied to the center girder at midspan along with a 0.80 kN [0.18 kip] out-of-plane load along the top flange at the same location. The scale was set to 10 times and the Mises stress range was from 0 MPa [0 ksi] to 34.5 MPa [5 ksi]. The model achieved full run-time completion. While vertical deflections were small, lateral deflection of the top flange and buckling of the web can clearly be seen. Results were like that using static analysis.

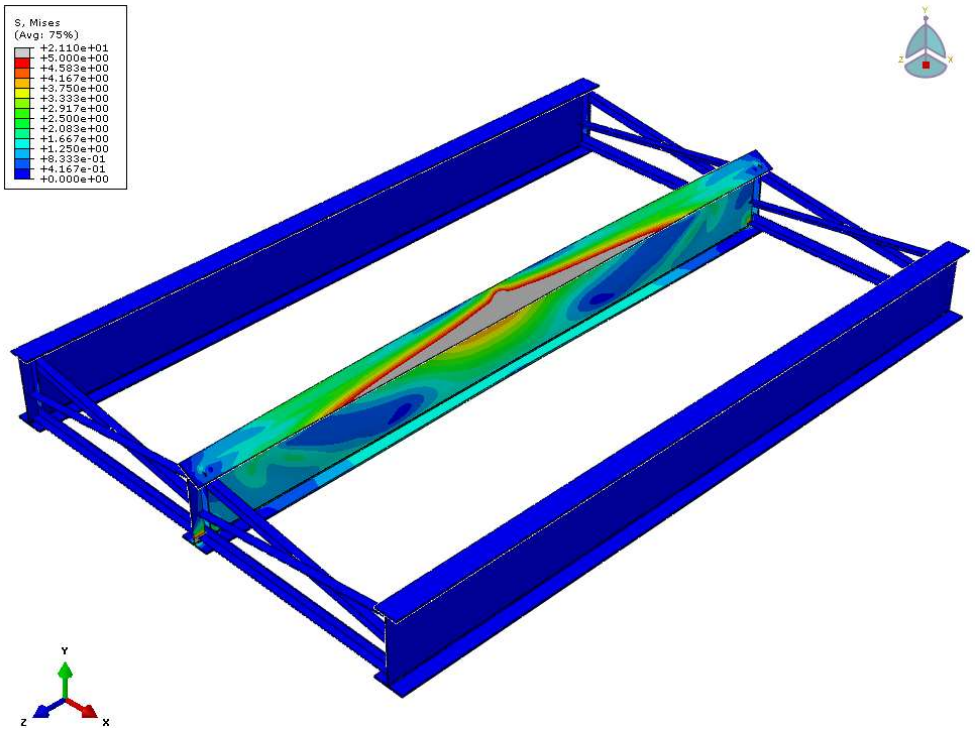

Figure C.48 Side view of the unskewed single span bridge model with 9.14 m [30 ft] cross-frame spacing, solid elements, 80.1 kN [18 kips] center load, and 0.80 kN [0.18 kips] out-of-plane load using dynamic implicit analysis

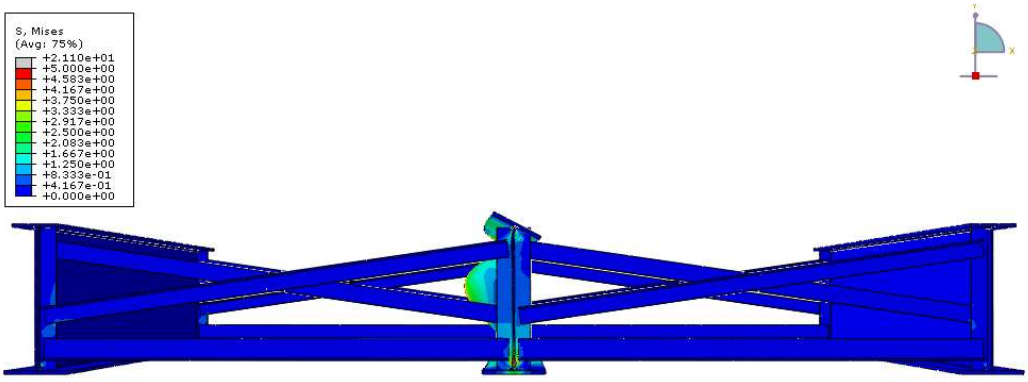

Figure C.49 Front elevation of the unskewed single span bridge model with 9.14 m [30 ft] cross-frame spacing, solid elements, 80.1 kN [18 kips] center load, and 0.80 kN [0.18 kips] out-of-plane load using dynamic implicit analysis

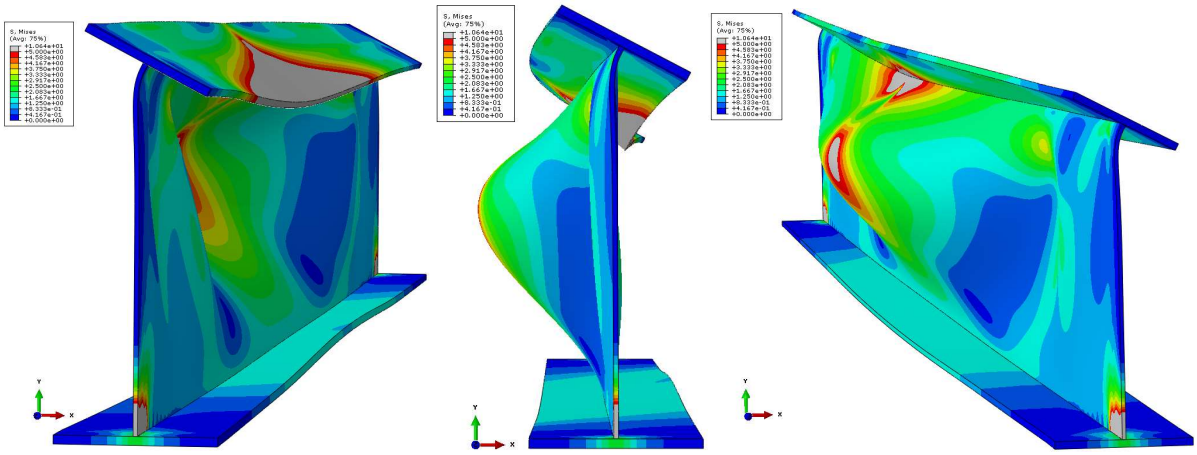

Figure C.50 Girder section view of the unskewed single span bridge model with 9.14 m [30 ft] cross-frame spacing, solid elements, 80.1 kN [18 kips] center load, and 0.80 kN [0.18 kips] out-of-plane load using dynamic implicit analysis

Error! Reference source not found. through **Error! Reference source not found.** shows the single span bridge model with solid elements used for all parts. Again, dynamic implicit analysis was used. Cross-frames were spaced at 9.14 m [30 ft]. An 801 kN [180 kips] vertical load was applied to the center girder at midspan along with a 0.80 kN [0.18 kip] out-of-plane load along the top flange at the same location. The scale was set to one and the Mises stress ranged from 0 MPa [0 ksi] to 689 MPa [100 ksi]. The model achieved full run-time completion. With the amplified vertical load, stresses and deflections increased significantly. The top flange and supporting web has completely collapsed at the area of applied load. While the dynamic implicit analysis could realize run-time completion where the static analysis was not, the same results was not achieved for a full-scale model. Convergence issues occurred before analysis completion and computational efficiency was worse than a static analysis. Therefore, dynamic implicit analysis was not considered for the full suite of bridge analysis used in the main study.

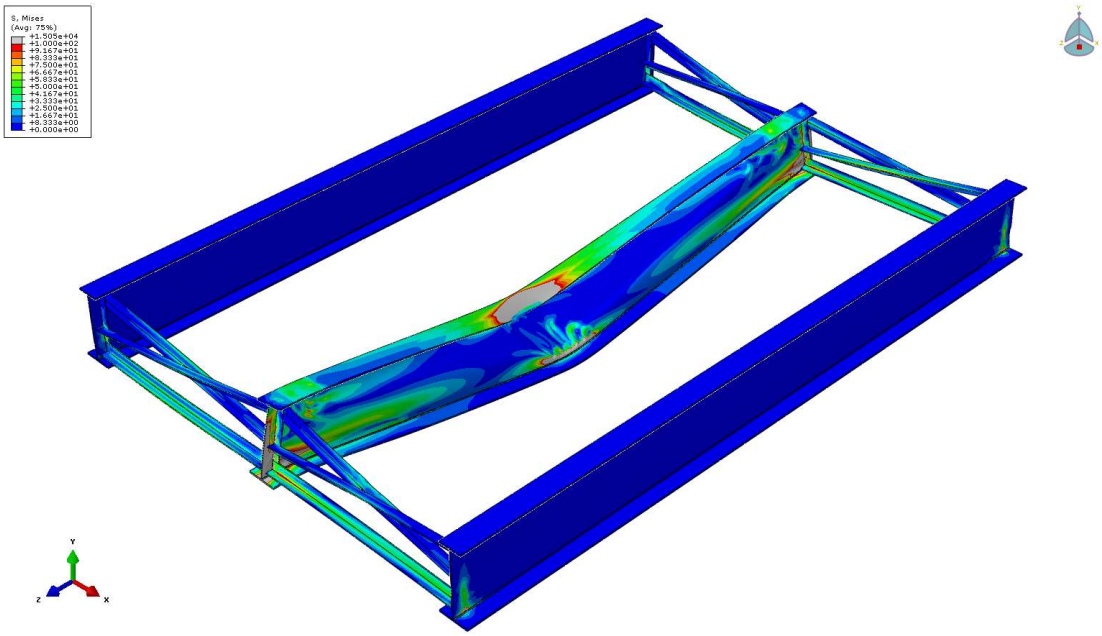

Figure C.51 Side view of the unskewed single span bridge model with 9.14 m [30 ft] cross-frame spacing, solid elements, 801 kN [180 kips] center load, and 0.80 kN [0.18 kips] out-of-plane load using dynamic implicit analysis

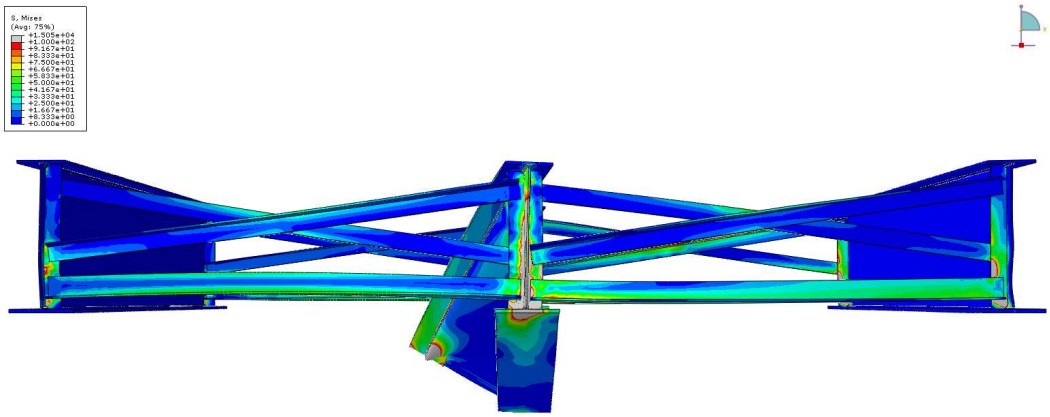

Figure C.52 Front elevation of the unskewed single span bridge model with 9.14 m [30 ft] cross-frame spacing, solid elements, 801 kN [180 kips] center load, and 0.80 kN [0.18 kips] out-of-plane load using dynamic implicit analysis

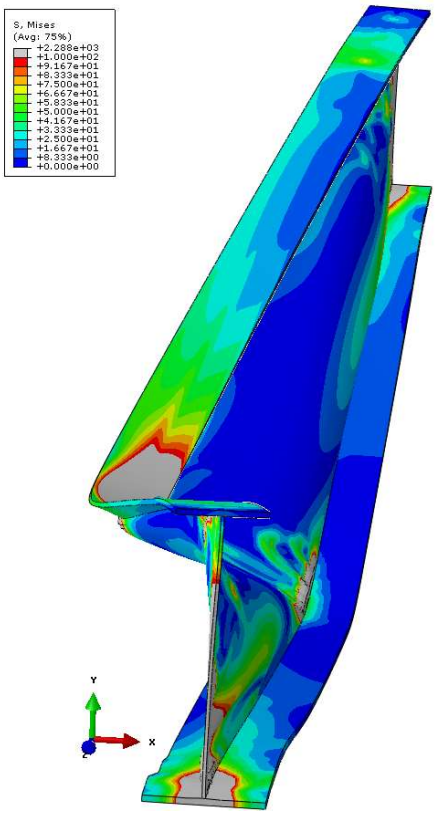

Figure C.53 Girder view of the unskewed single span bridge model with 9.14 m [30 ft] cross-frame spacing, solid elements, 801 kN [180 kips] center load, and 0.80 kN [0.18 kips] out-of-plane load using dynamic implicit analysis

Error! Reference source not found. through **Error! Reference source not found.** shows the single span bridge model with solid elements used for all parts. A dynamic explicit analysis was applied with a ten times mass scale. Cross-frames were spaced at 9.14 m [30 ft]. An 80.1 kN [18 kips] vertical load was applied to the center girder at midspan along with a 0.80 kN [0.18 kip] out-of-plane load along the top flange at the same location. The scale was set to 10 times and the Mises stress ranged widely from 0 MPa [0 ksi] to 6890 MPa [1000 ksi]. Surprisingly, the model achieved full run-time completion given the collapse of the center girder. It is interesting to note that only the center girder saw large deflections and stress. The side girders and cross-frames were relatively unaffected.

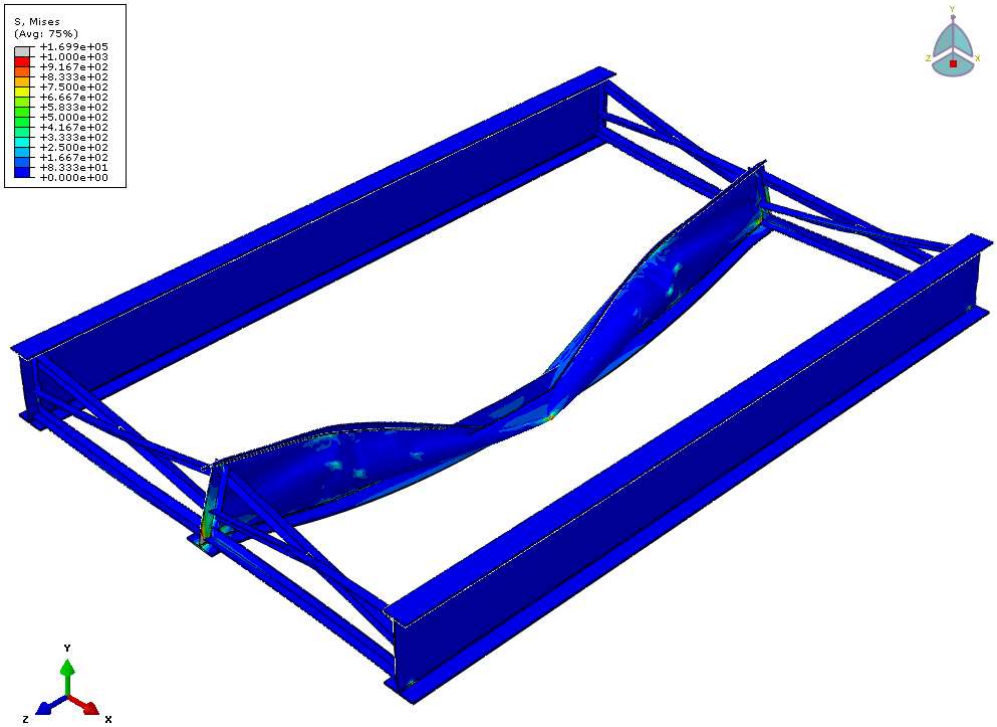

Figure C.54 Side view of the unskewed single span bridge model with 9.14 m [30 ft] cross-frame spacing, solid elements, 80.1 kN [18 kips] center load, and 0.80 kN [0.18 kips] out-of-plane load using dynamic explicit analysis with 10X mass scaling

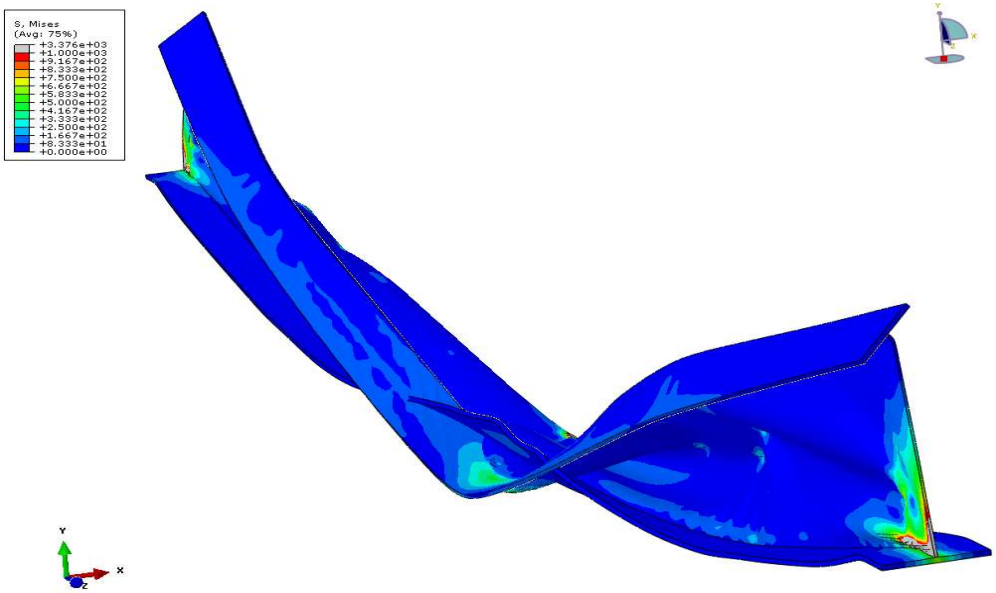

Figure C.55 Girder view of the unskewed single span bridge model with 9.14 m [30 ft] cross-frame spacing, solid elements, 80.1 kN [18 kips] center load, and 0.80 kN [0.18 kips] out-of-plane load using dynamic explicit analysis with 10X mass scaling

Error! Reference source not found. through **Error! Reference source not found.** shows the single span bridge model with solid elements used for all parts. A dynamic

explicit analysis was applied with a two times mass scale. Cross-frames were spaced at 9.14 m [30 ft]. An 80.1 kN [18 kips] vertical load was applied to the center girder at midspan along with a 0.80 kN [0.18 kip] out-of-plane load along the top flange at the same location. The scale was set to one and the Mises stress ranged from 0 MPa [0 ksi] to 6890 MPa [1000 ksi]. Even at a mass scale of two, collapse of the center occurred. The mass may be scaled at each step interval and therefore the load is amplified exponentially. By amplifying the mass and decreasing the step time, one could significantly reduce the total run-time of the model. However, it was found that knowledge of the correct mass and step time to be used was required to obtain accurate results.

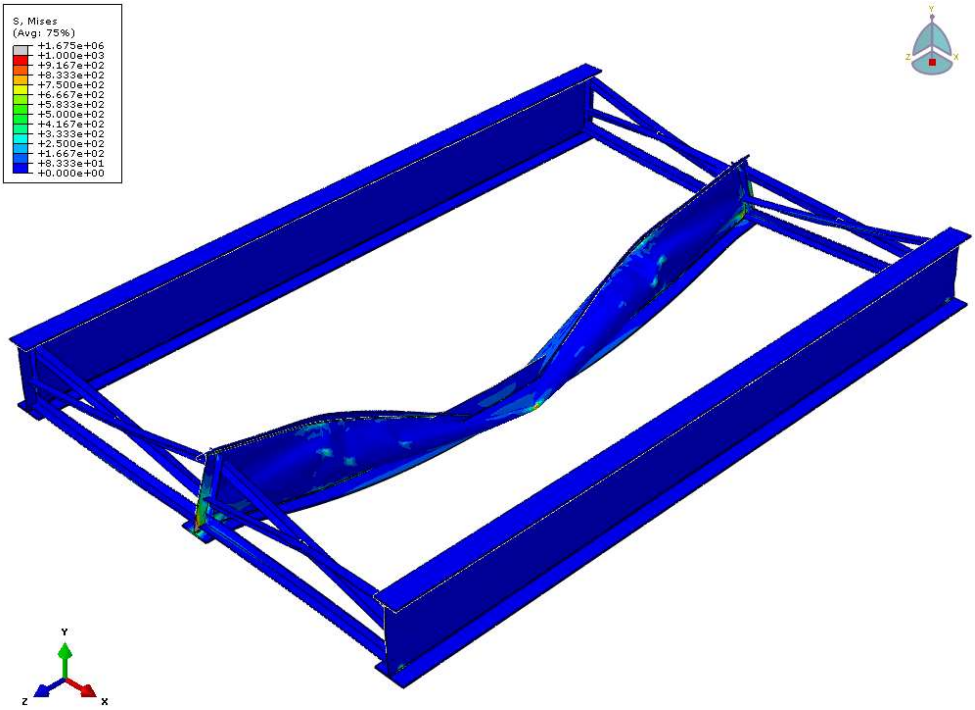

Figure C.56 Side view of the unskewed single span bridge model with 9.14 m [30 ft] cross-frame spacing, solid elements, 80.1 kN [18 kips] center load, and 0.80 kN [0.18 kips] out-of-plane load using dynamic explicit analysis with 2X mass scaling

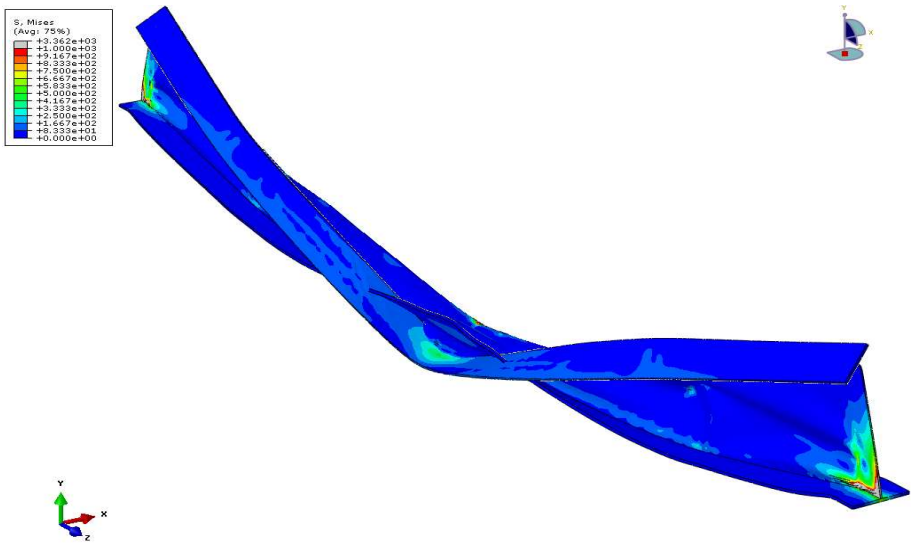

Figure C.57 Girder view of the unskewed single span bridge model with 9.14 m [30 ft] cross-frame spacing, solid elements, 80.1 kN [18 kips] center load, and 0.80 kN [0.18 kips] out-of-plane load using dynamic explicit analysis with 2x mass scaling

Error! Reference source not found. through **Error! Reference source not found.** shows the full-scale model of the 40° skewed-staggered bridge with 4.57 m [15 ft] cross-frame spacing at varying step times using a dynamic explicit analysis. The mass scale was set at 100 times. The bridge geometry, modeling methodology, and applied loads are described in the main body of the paper with the exception that the overhang brackets are modeled explicitly and the abutment cross-frames are composed of L152x152x25.4 mm [L6.0x6.0x1.0 in] angles with a 25.4 mm [1.0 in] thick stiffener. The deformation scale in the figures was set to 100 times and the Mises stress range was from a small 0 MPa [0 ksi] to 6.89 MPa [1 ksi]. Settings for the load amplitude is shown in Figure C.58 for a time period of one second. While the run-time was significantly faster than a static analysis, and it was found that one would be required to know the specific time period and step time to be used with any given mass scale to obtain accurate results. Therefore, dynamic explicit analysis was not considered for the main study of full-scale bridge models.

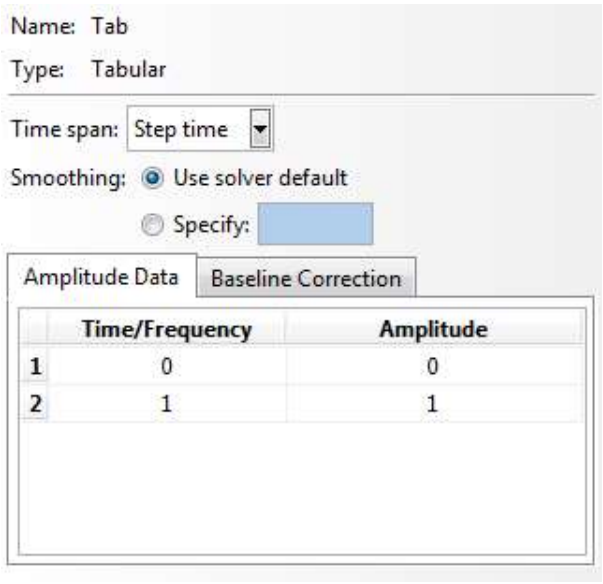

Figure C.58 Dynamic explicit load amplitude settings for the 40° skewed-staggered bridge model with 4.57 m [15 ft] cross-frame spacing

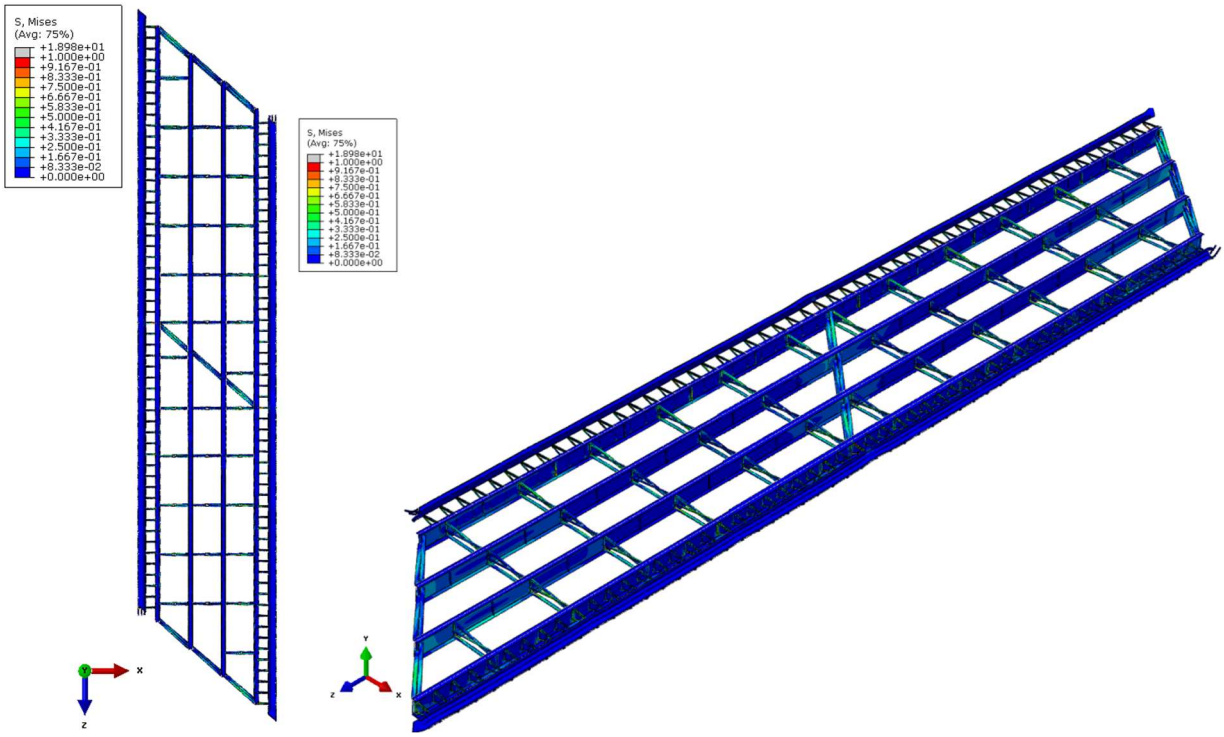

Figure C.59 40 deg. skewed-staggered bridge with 4.57 m [15 ft] cross-frame spacing using dynamic explicit analysis with 100X mass scaling

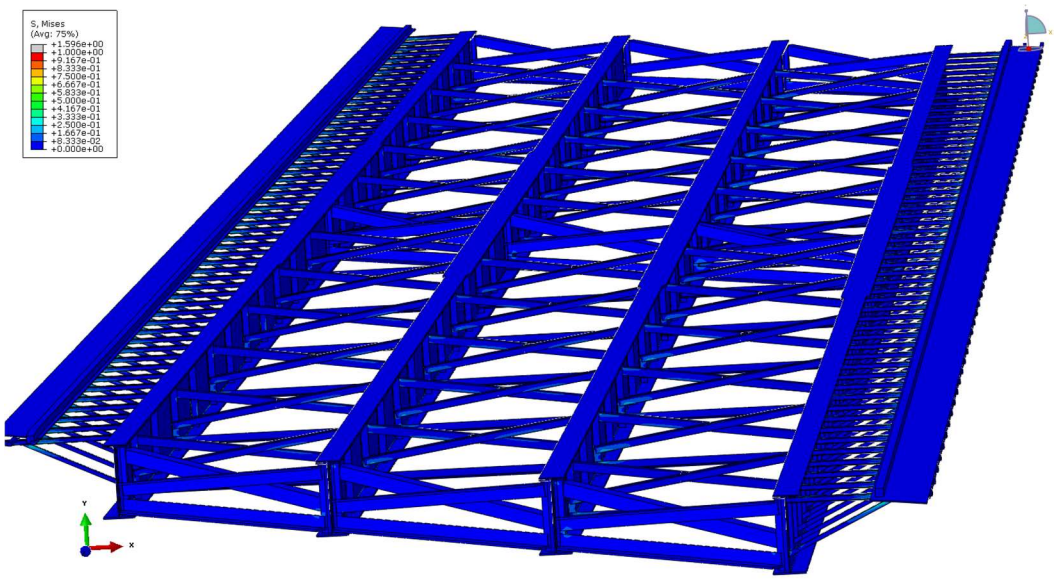

Figure C.60 40 deg. skewed-staggered bridge with 4.57 m [15 ft] cross-frame spacing using dynamic explicit analysis with 100X mass scaling at 0.05 step time

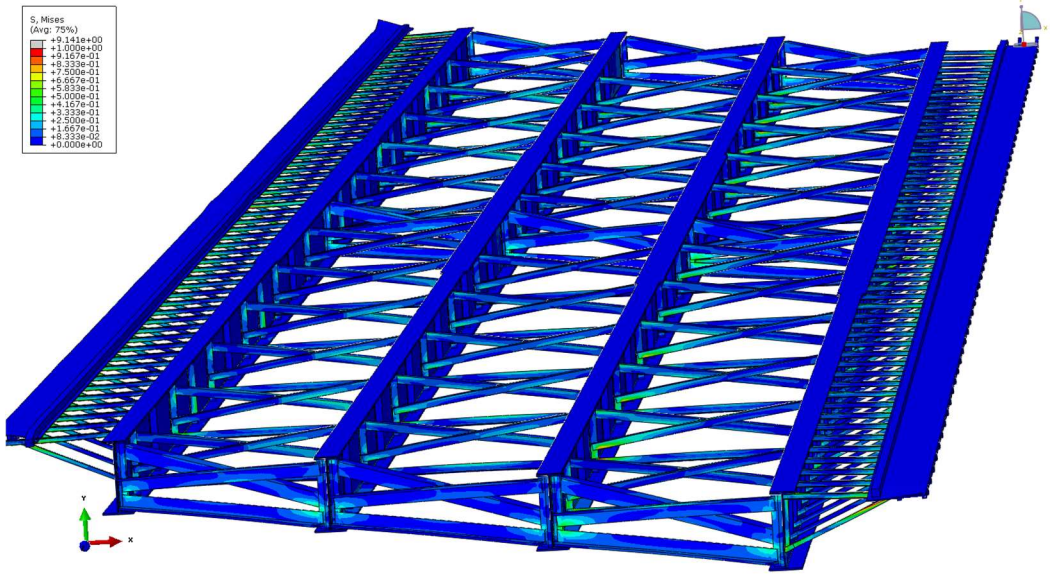

Figure C.61 40 deg. skewed-staggered bridge with 4.57 m [15 ft] cross-frame spacing using dynamic explicit analysis with 100X mass scaling at 0.10 step time

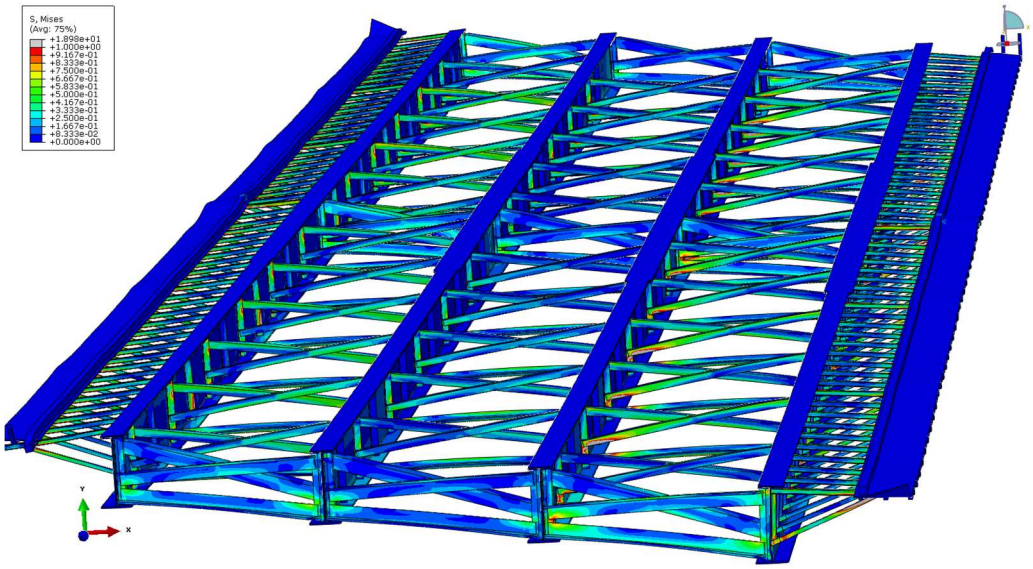

Figure C.62 40 deg. skewed-staggered bridge with 4.57 m [15 ft] cross-frame spacing using dynamic explicit analysis with 100X mass scaling at 0.15 step time

Figure C.63 shows energies as a function of time for the 40° skewed-staggered bridge with 4.57 m [15 ft] cross-frame spacing using dynamic explicit analysis with 100x mass scaling. ALLWK is defined as the work of external forces. ALLKE is kinetic energy. ALLWK, the work of external forces, and ALLKE, kinetic energy, increases exponentially with time. ALLIE is internal energy equal to the combination of ALLSE (stored strain energy), ALLPD (inelastic dissipated energy), ALLCD (energy dissipated by viscoelasticity), and ALLAE (artificial strain energy). Both ALLIE, internal energy, and ALLSE, stored strain energy, remain at a constant zero with time. ETOTAL is the energy balance equal to the addition of internal energy, viscous dissipated energy, frictional dissipated energy, and kinetic energy minus the work of the external forces. The energy balance decreases to a small negative value as time approaches one.

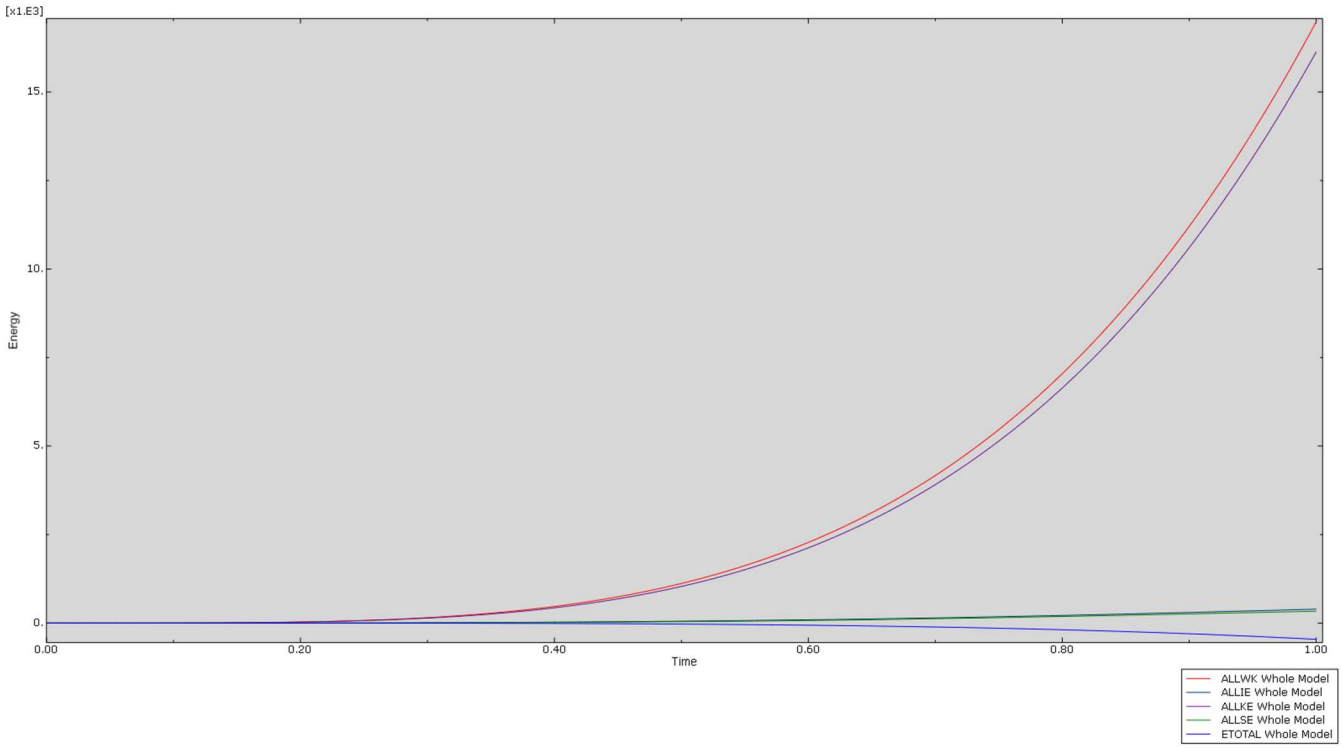

Figure C.63 Energy output for the 40° skewed-staggered bridge with 4.57 m [15 ft] cross-frame spacing using dynamic explicit analysis with 100X mass scaling

APPENDIX D: ABUTMENT FRAMING AND BEARING CONDITIONS

The objective of this study was to determine the effects of varying abutment and bearing fixities to create conditions representative of constructed bridges. Abutments or bearings that are very stiff draw load from connected girders and cross-frames, inaccurately reducing forces in these members. Conversely, bridges with abutments or bearings that are flexible will increase the forces and deflection of supported members. Selecting an accurate representation of abutment end conditions and bearing fixities is essential to gathering correct outputs from structural analysis models.

The bridge geometry, modeling methodology, and applied loads used are described in Part 3 of this paper. All models throughout this section are based on the 40 degree skewed-staggered bridge with 9.17 m [30 ft] cross-frame spacing, shown in Figure D.1 scaled to five times. An abutment diaphragm assembly utilizing a MC12x50 top chord was selected based on strength, stiffness, and ease of constructability relative to the other members studied. For bearings, the boundary condition would ideally only provide enough restraint to stabilize the bridge system but still have freedom of movement to not attract large loads at the supports. Among the bearing systems analyzed, a 406x12.7 mm [16x0.5 in] “knife edge” support surface was selected as the bearing condition used in the main part of this paper.

Several techniques were considered in modeling the bearings. To avoid placement of the boundary condition surface directly on the bottom flange, a 406x406x50.8 mm [16x16x2.0 in] square bearing pad was tied to the bottom flange at the center of the bridge to represent the pier support and at the girder ends where the abutments are located. The center bearings have pinned conditions while ends bearings have roller conditions in the longitudinal direction.

One bearing representation used the full bottom surface of the bearing pad as the boundary surface, called full bearing throughout this section. The full bearing condition is shown in Figure D.2 on the left A 12.7 mm [0.5 in] thick bearing pad was used as there was less concern with localized instabilities at the supports when the entire bottom surface is used as the fixity. Another bearing surface utilizes a 12.7 mm [0.5 in] or 50.8 mm [2.0 in] wide bearing surface at the center of the 406x406x50.8 mm [16x16x2.0 in] square bearing pad, shown in Figure D.2 on the right. This condition is referred to as a "knife edge" support and has a fixed translation surface in the vertical and out-of-plane directions.

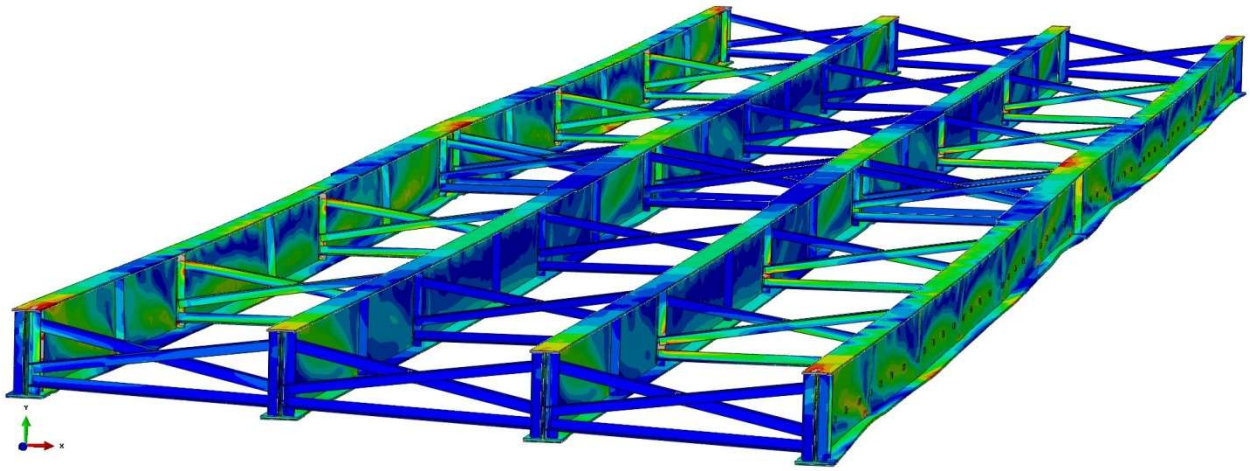

Figure D.1 40 degree skewed-staggered bridge with 9.14 m [30 ft] cross-frame spacing

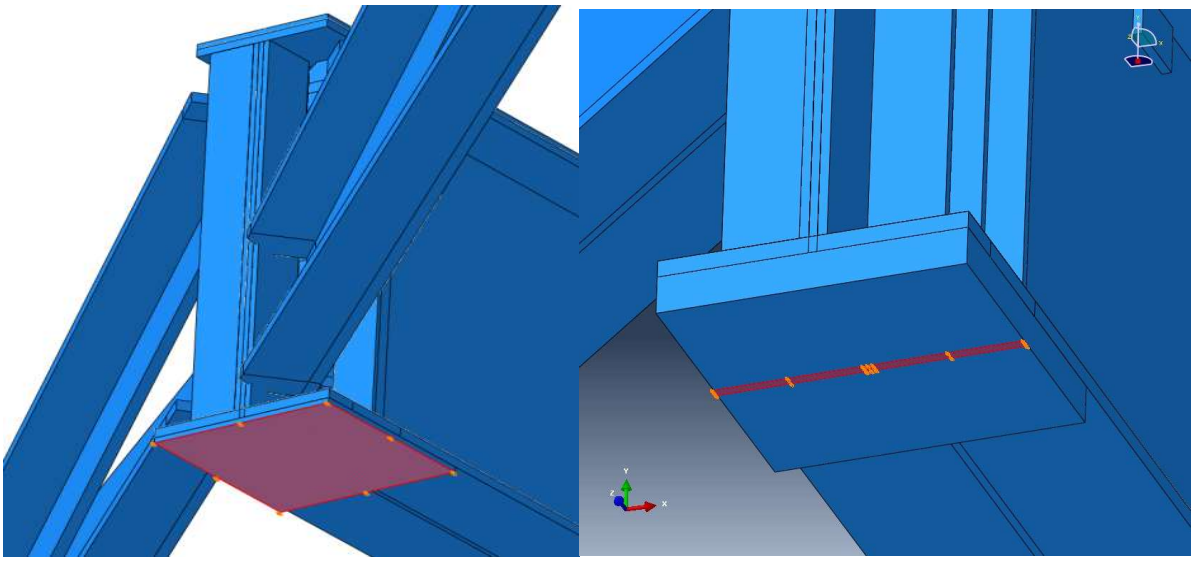

Figure D.2 Full bearing support (left) and knife edge support (right)

While many two span steel bridges have integral abutments, relatively heavy diaphragms are used to provide brace support to the ends prior to hardening of the concrete. Several different cross-frame members, placement, and conditions are used to evaluate the abutment end condition. The fixed end condition, shown in Figure D.3, fully fixes the girder ends against translation in all three directions. The deformed shape of the model with fixed ends is shown in Figure D.4 scaled to five times and with a color map showing Mises stress limits from 0 to 345 MPa [50 ksi].

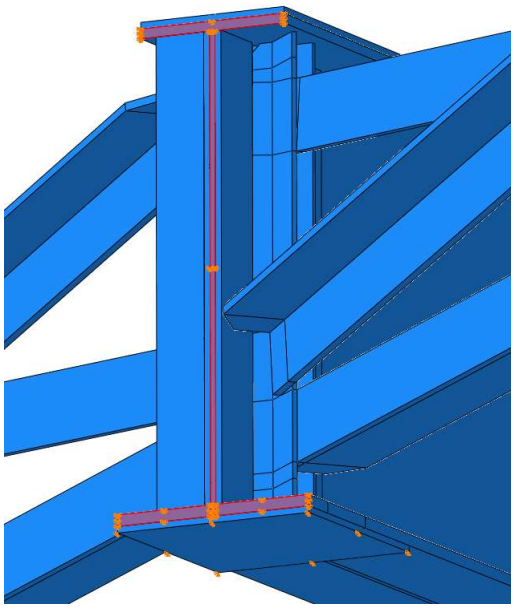

Figure D.3 Fixed Ends: Girder ends fully fixed against translation in 3 directions

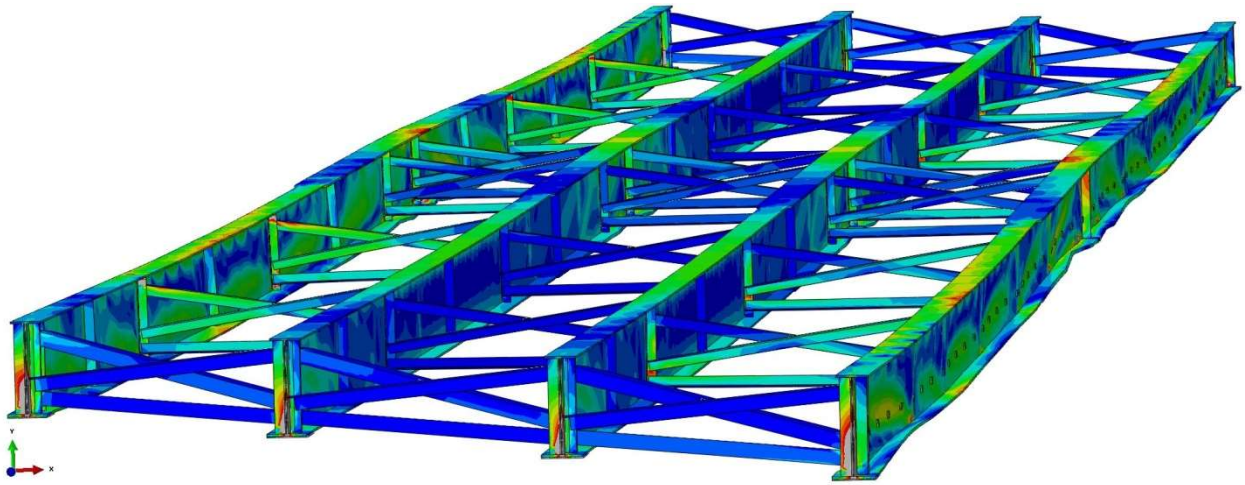

Figure D.4 40 degree skewed-staggered bridge with 9.14 m [30 ft] cross-frame spacing and fixed girder ends

L140x140x15.9 mm [L5.5x5.5x5/8 in] angles were used as diagonal and bottom chords in an X-brace for the abutment cross-frames. Angles with 1.5 and 2.0 times the modulus of elasticity of steel, 200 GPa [29,000 ksi], were also applied to increase the stiffness of the

abutment cross-frames. It should be noted that intermediate cross-frames have L108x108x12.7 mm [L4.25x4.25x1/2 in] angles.

Abutment cross-frames with L152x152x25.4 mm [L6.0x6.0x1.0 in] angles in an X-brace were also considered in the same vertical position as intermediate cross-frame as well as in a horizontally braced position along the top flange, shown in Figure D.5 and Figure D.6. The cross-frame is a K-brace and is labeled as a horizontal K-brace throughout this section. While this design is not traditionally used, it shows the effects of bracing the top flange along multiple points rather than at the girder ends.

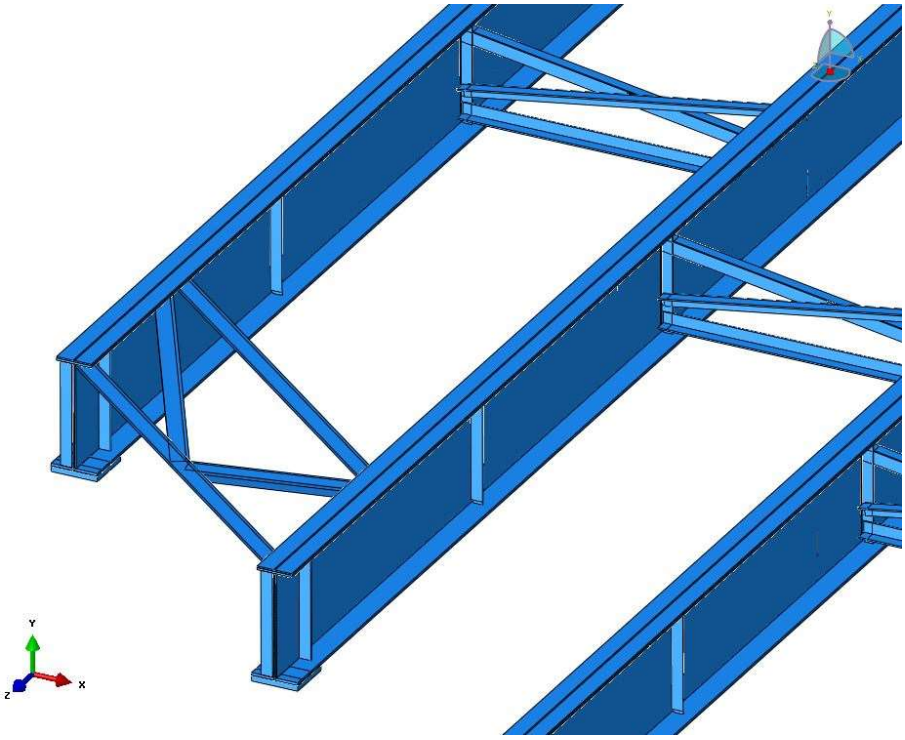

Figure D.5 Isotropic view of the abutment with L152x152x25.4 mm [L6.0x6.0x1.0 in] cross-frame angles in a horizontal K-brace

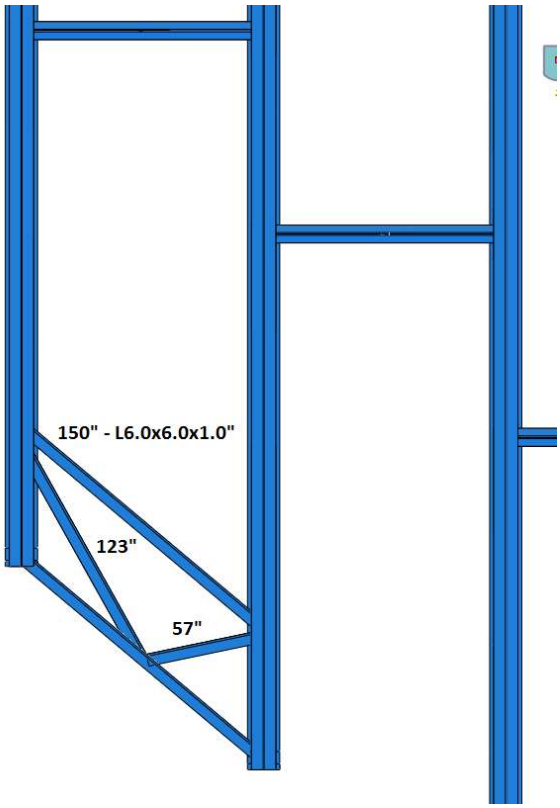

Figure D.6 Plan view of the abutment with L152x152x25.4 mm [L6.0x6.0x1.0 in] cross-frame angles in a horizontal K-brace

The flexural stiffness of L152x152x25.4 mm [L6.0x6.0x1.0 in] and L140x140x15.9 mm [L5.5x5.5x5/8 in] angles used in the abutment diaphragms and L108x108x12.7 mm [L4.25x4.25x1/2 in] used at intermediate cross-frames are shown below. Values are provided for strong axis and principle axis bending labeled in Figure D.7.

- EI_x/L of L152x152x25.4 mm [L6.0x6.0x1.0 in] = 7107 k*in
- EI_x/L of L140x140x15.9 mm [L5.5x5.5x5/8 in] = 3671 k*in
- EI_x/L of L108x108x12.7 mm [L4.25x4.25x1/2 in] = 1348 k*in

- EI_z/L of L152x152x25.4 mm [L6.0x6.0x1.0 in] = 3002 k*in
- EI_z/L of L140x140x15.9 mm [L5.5x5.5x5/8 in] = 1507 k*in
- EI_z/L of L108x108x12.7 mm [L4.25x4.25x1/2 in] = 554.2 k*in

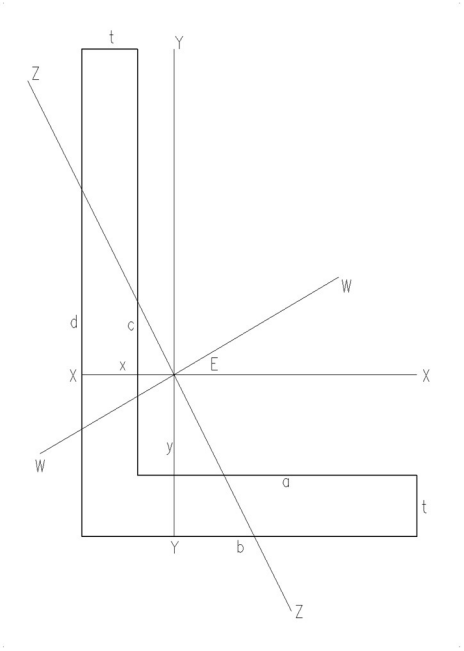

Figure D.7 L-shape angle axes label

Figure D.8 through Figure D.17 show the flange displacements and girder stresses of the 40 degree skewed-staggered bridge with 9.17 m [30 ft] cross-frame spacing for the interior and exterior girders. 1.0, 1.5, and 2.0 times the angle stiffness of an L140x140x15.9 mm [L5.5x5.5x5/8 in] was used along with an L152x152x25.4 mm [L6.0x6.0x1.0 in] angle for the abutment cross-frames. Cross-frames placed in a horizontal K-brace position and fixed abutment ends were also considered. Both knife edge supports and full surface bearings were used. Not all models were able to achieve a hundred percent analysis completion, but all models were able to run up to 90% of the applied load. Therefore, displacements and stresses are provided at 90% completion. While different abutment support and bearing conditions are given, one can compare the effects of varying bearing conditions, for example, by comparing models with the same abutment cross-frame angles. These graphs provide a starting point as to filter which conditions are unrealistic for bridges being built.

Figure D.8 shows the top flange lateral displacement in the exterior girder at 90% load. Models with fixed end abutments or horizontal bracing were stiffest and produced significantly smaller deflections relative to the other models. Since the largest deflections were found in the unbraced length between the abutment and first cross-frame, stiffer abutment bracing would result in smaller deflections at these locations. Models with knife edge supports produced the largest magnitude deflections while models with full bearing surface constraints produced slightly smaller deflections.

Figure D.9 shows the peak lateral displacement as a function of applied load in the exterior girder. While the models with L140x140x15.9 mm [L5.5x5.5x5/8 in], 1.5E L140x140x15.9 mm [L5.5x5.5x5/8 in], and L152x152x25.4 mm [L6.0x6.0x1.0 in] abutment angles had the largest displacements at 90% load, deflections at 80% load were almost the same as models with 2.0E L140x140x15.9 mm [L5.5x5.5x5/8 in] abutment angles and knife edge supports as well as the model with 50.8 mm [2.0 in] knife edge support. This shows that stiffer abutment diaphragms or larger bearing constraint areas do not affect top flange lateral displacements at smaller applied loads.

Figure D.10 through Figure D.13 show the interior girder top flange, bottom flange, and weak-axis section out-of-plane bending stresses along with the strong-axis sectional stress. Models with fixed abutment ends or diaphragms placed horizontally in the top flange tended to attract more stresses in the first unbraced length. The models with stiffer or more constrained abutments also produced stresses in the opposite direction near the abutment relative to other the models. Out-of-plane bending stresses were largest at mid-span in models with smaller abutment cross-frame angles and less bearing constraints. For vertical bending, stiffer abutments attracted

larger loads near the abutment diaphragms and thus reduced the overall stresses towards mid-span.

Figure D.14 through Figure D.17 show the exterior girder top flange, bottom flange, and weak-axis section out-of-plane bending stresses along with the strong-axis sectional stress. Models with stiffer bearings and abutment diaphragms produced smaller stress while models with smaller abutment angles and knife edge supports produced larger stress. However, this only occurred near the supports or mid-span; out-of-plane bending stresses were relatively similar throughout the bridge in the exterior girder. Stress magnitudes were much higher compared to the interior girder given the high overhang loads in the exterior girder. At larger loads, bearing and abutment end conditions had less effect on bending stresses.

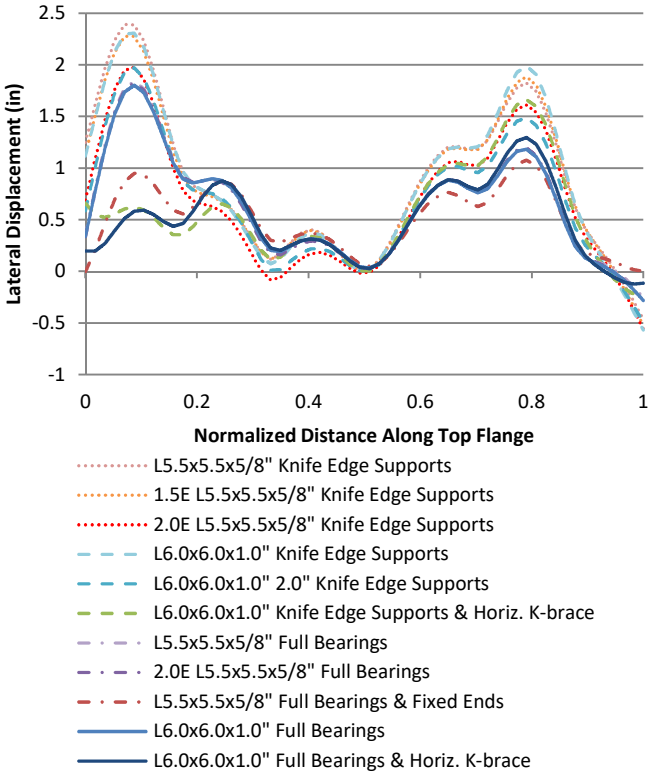

Figure D.8 G4 Top Flange Lateral Displacement vs. Normalized Distance at 90% Load

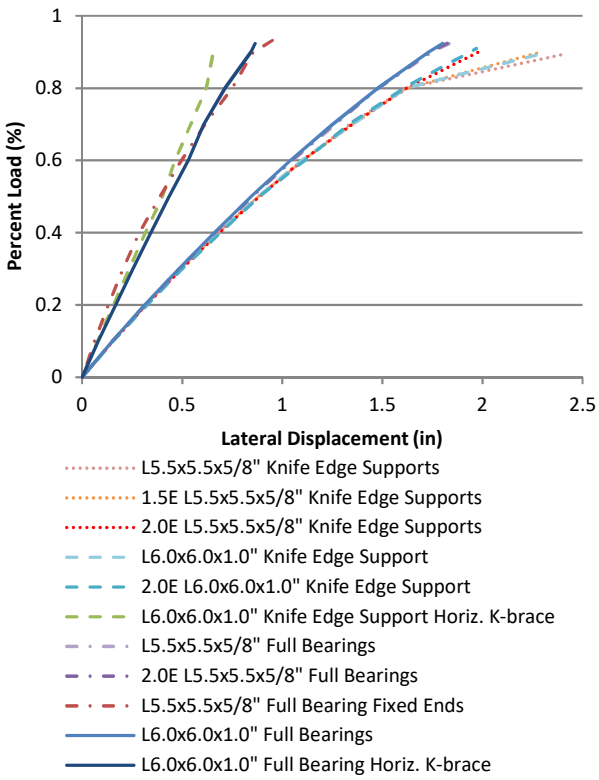

Figure D.9 Percent Load vs Peak Lateral Displacement in Span 1

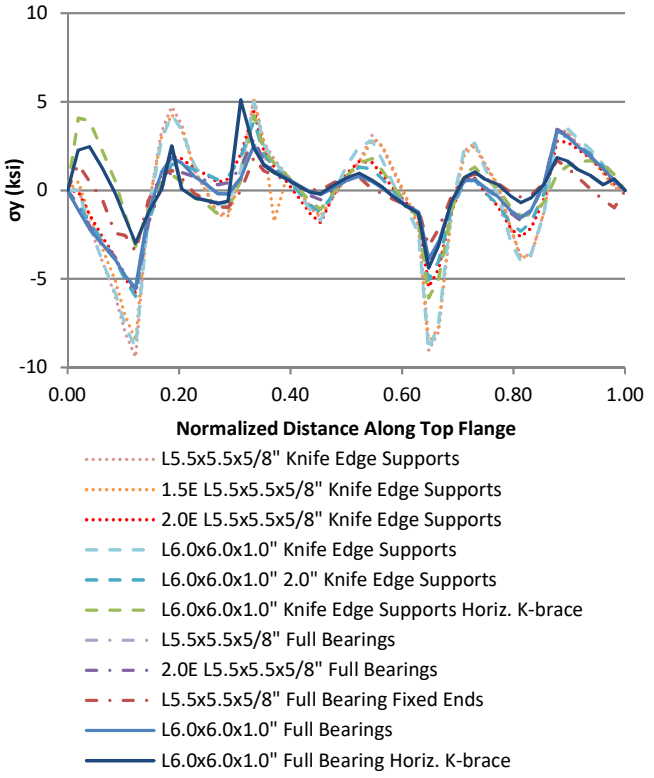

Figure D.10 G3 Top Flange Stress

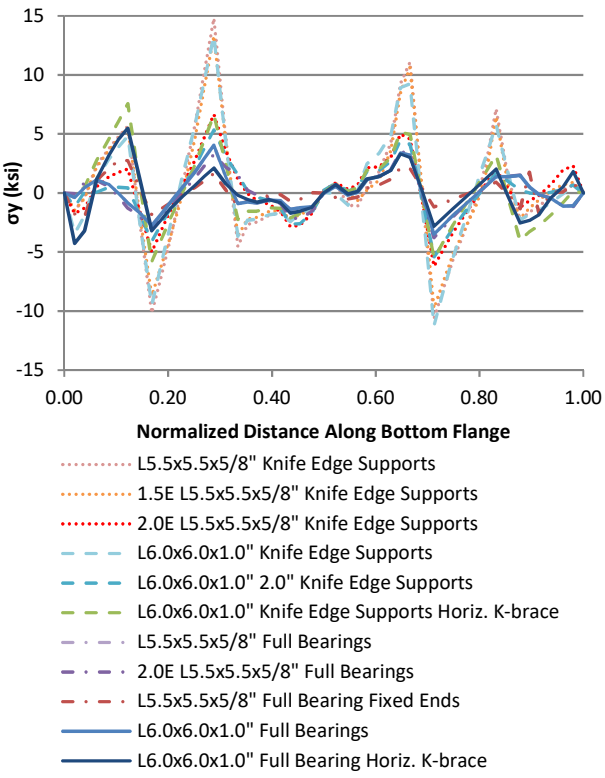

Figure D.11 G3 Bottom Flange Stress

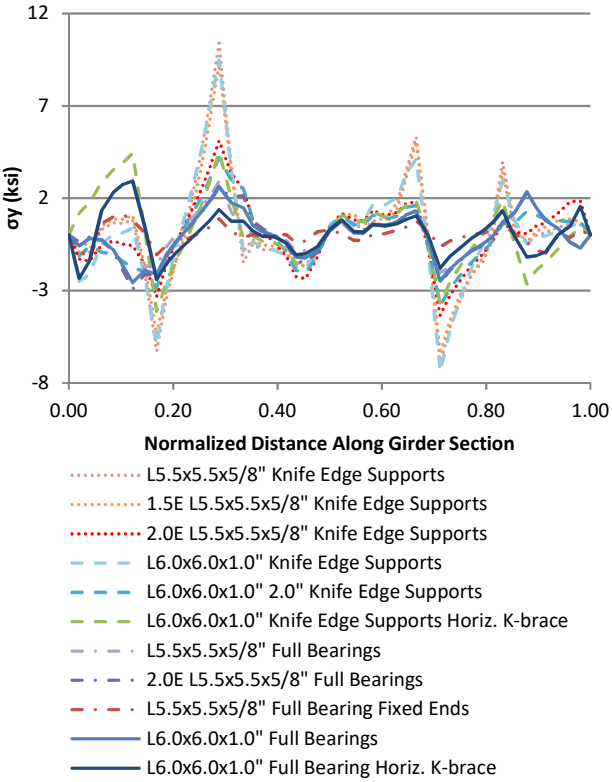

Figure D.12 G3 Weak Axis Sectional Stress

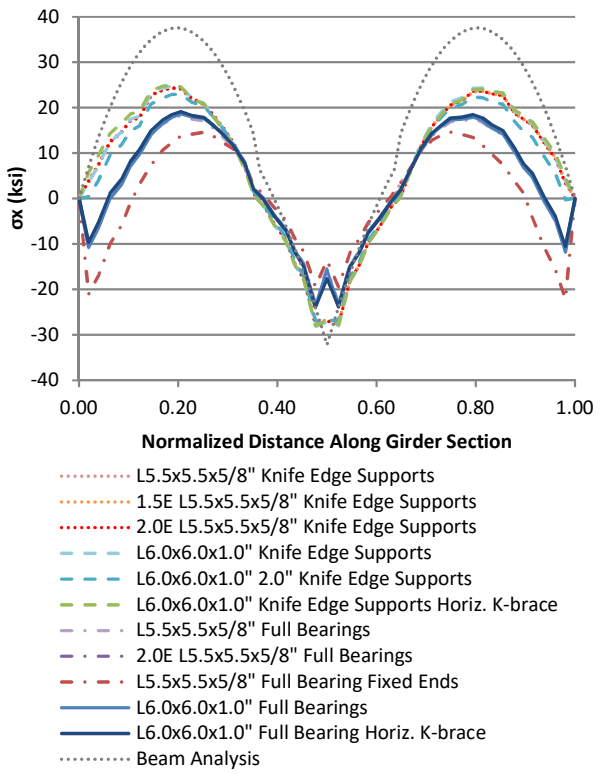

Figure D.13 G3 Strong Axis Sectional Stress

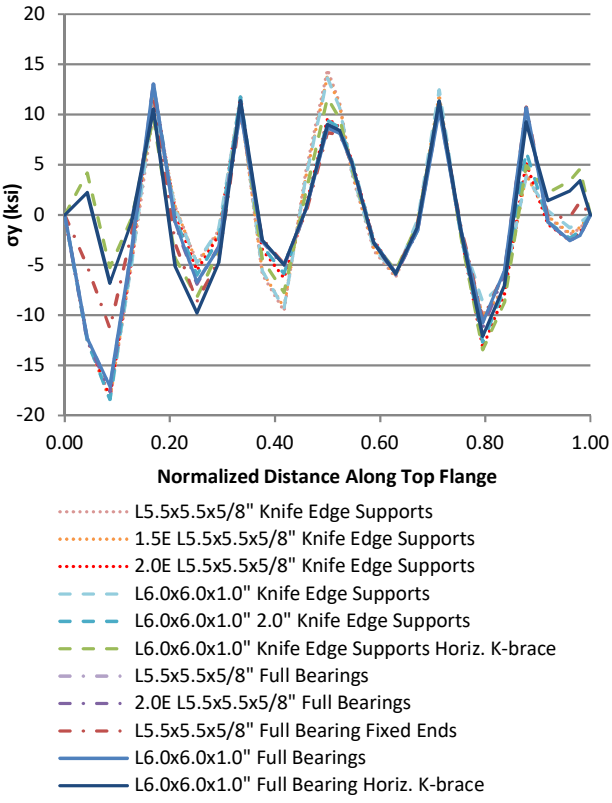

Figure D.14 G4 Top Flange Stress

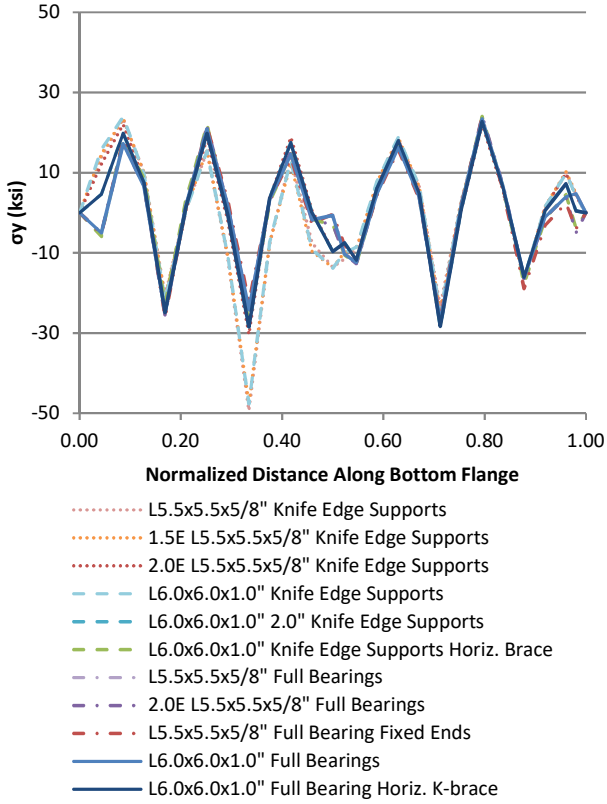

Figure D.15 G4 Bottom Flange Stress

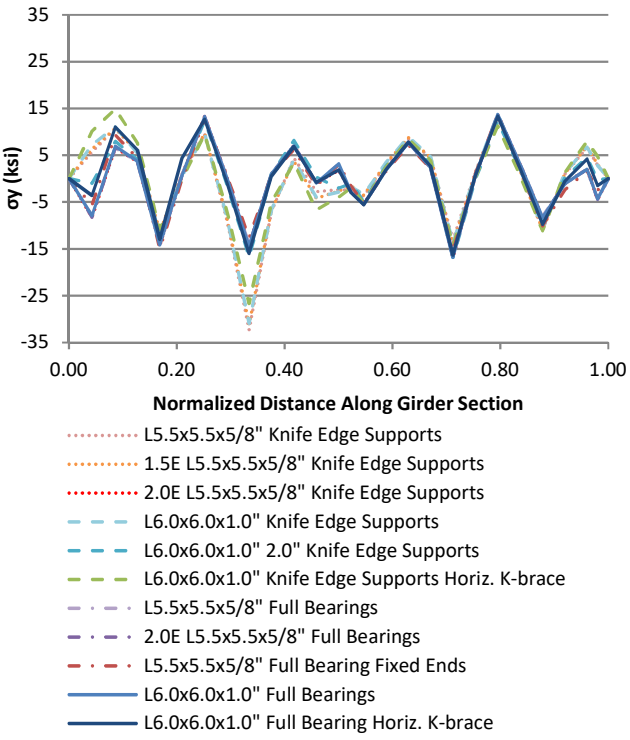

Figure D.16 G4 Weak Axis Sectional Stress

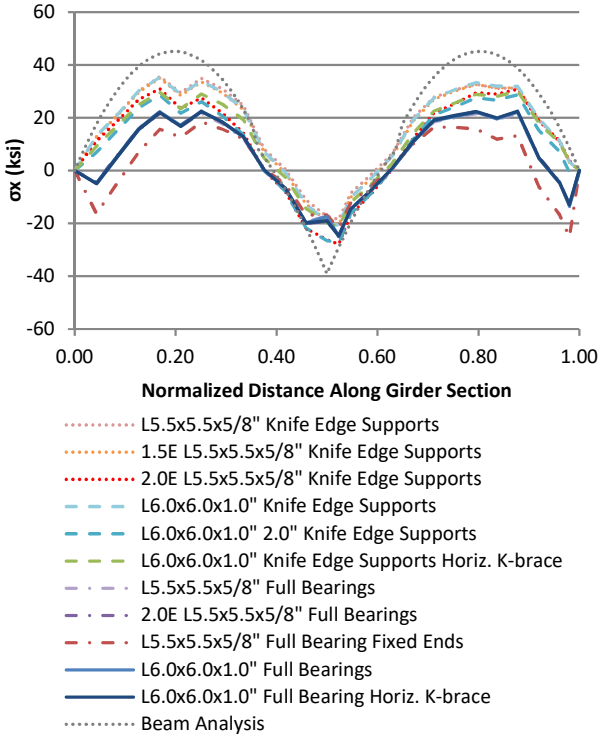

Figure D.17 G4 Strong Axis Sectional Stress

Figure D.18 through Figure D.27 show the flange displacement and girder stresses of the 40 degree skewed-staggered bridge with 9.17 m [30 ft] cross-frame spacing for the interior and exterior girders. 1.0, 1.5 and 2.0 times the modulus of elasticity used in the L140x140x15.9 mm [L5.5x5.5x5/8 in] abutment cross-frame angle is shown along with the L152x152x25.4 mm [L6.0x6.0x1.0 in] angle. L152x152x25.4 mm [L6.0x6.0x1.0 in] abutment cross-frames placed in a horizontal k-brace configuration is shown for comparison. The fully fixed condition at the girder ends is not displayed as it is difficult to achieve prior to the integral abutments hardening. Only the knife edge support condition was considered. While bearings may become frozen over time due to rust and deterioration, the full surface bearing condition is not typically designed for and thus was not considered. The knife edge support with a 50.8 mm [2.0 in] bearing strip produced deflections and stresses like that of the knife edge support with a 12.7 mm [0.5 in]

bearing strip and therefore is not shown. Again, as not all models were able to achieve run-time completion, displacements and stresses are given at 90% load.

Figure D.18 and Figure D.19 show the top flange lateral displacement and peak lateral displacement versus applied load for the exterior girder. The bridges with 1.0 and 1.5 times the stiffness of the L140x140x15.9 mm [L5.5x5.5x5/8 in] abutment angles and the abutment cross-frames with L152x152x25.4 mm [L6.0x6.0x1.0 in] angles produced the largest displacements, with stiffer angles producing slightly smaller deflections. The model with abutment cross-frames placed in a horizontal k-brace position produced the smallest deflections near the abutments. Away from the abutments, lateral deflections were very similar in magnitude. Angles with 2.0 times the stiffness of the L140x140x15.9 mm [L5.5x5.5x5/8 in] had a magnitude smaller but close to bridges with cross-frame in the normal vertical configuration. This shows that the effect of stiff abutment cross-frames diminish away from the braced location.

Figure D.20 through Figure D.23 show the interior girder top flange, bottom flange, and weak-axis section out-of-plane bending stresses along with the strong-axis sectional stress. For models with vertically positioned abutment cross-frames, more flexible angles produced higher stresses in out-of-plane bending, likely due greater bending of the girders. The cross-frame with angles configured horizontally in the top flange attracted larger stresses, usually in the opposite sign, as it braces the girder over a longer portion of the span. This effect was diminished away from the abutments, where models with stiffer abutment bracing attracted less stress.

Figure D.24 through Figure D.27 shows the exterior girder top flange, bottom flange, and weak-axis section out-of-plane bending stresses along with the strong-axis sectional stress. Similar to the interior girder out-of-plane bending stresses, the cross-frame with angles positioned horizontally caused lateral bending in the opposite direction to the rest of the span at

the brace location, especially in the top flange where the diaphragms are connected. This effect quickly diminished away from the abutments as large lateral loads forced the girders to bend toward the exterior of the bridge. Vertical bending stresses were slightly lower for stiffer abutment cross-frames.

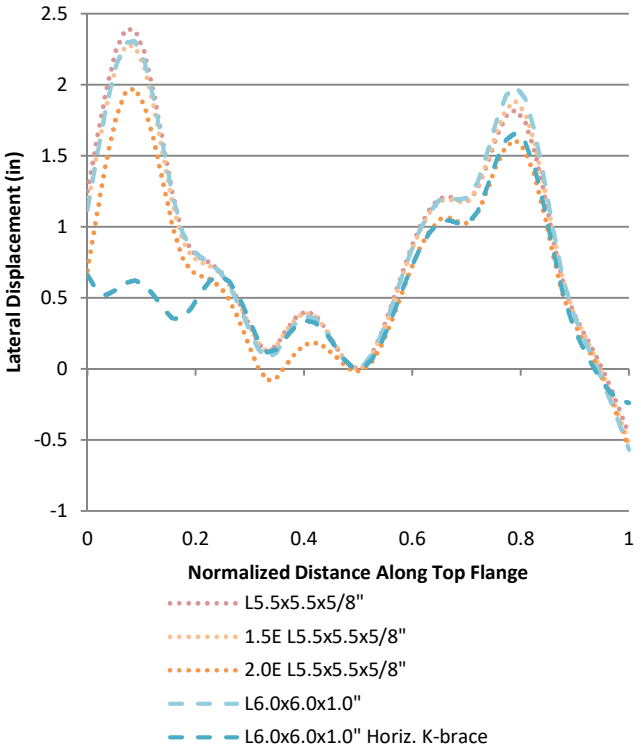

Figure D.18 G4 Top Flange Lateral Displacement vs. Normalized Distance at 90% Load

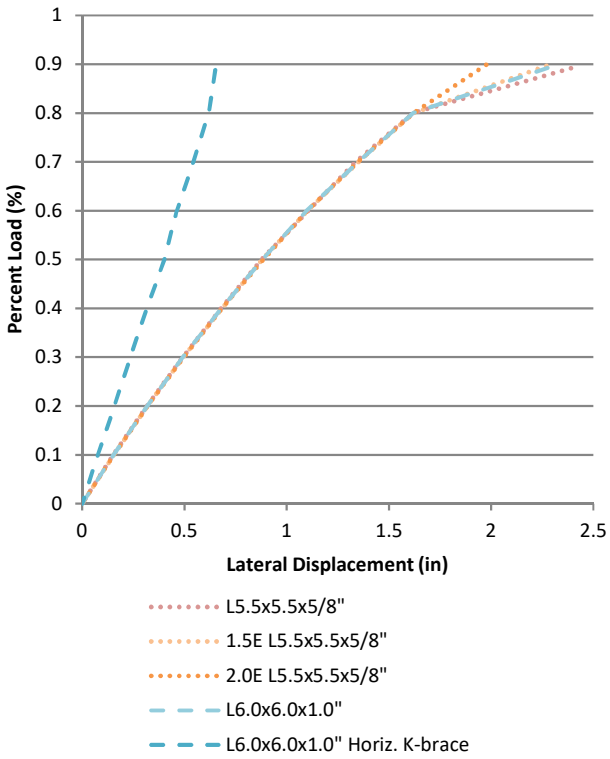

Figure D.19 Percent Load vs. Peak Lateral Displacement in Span 1

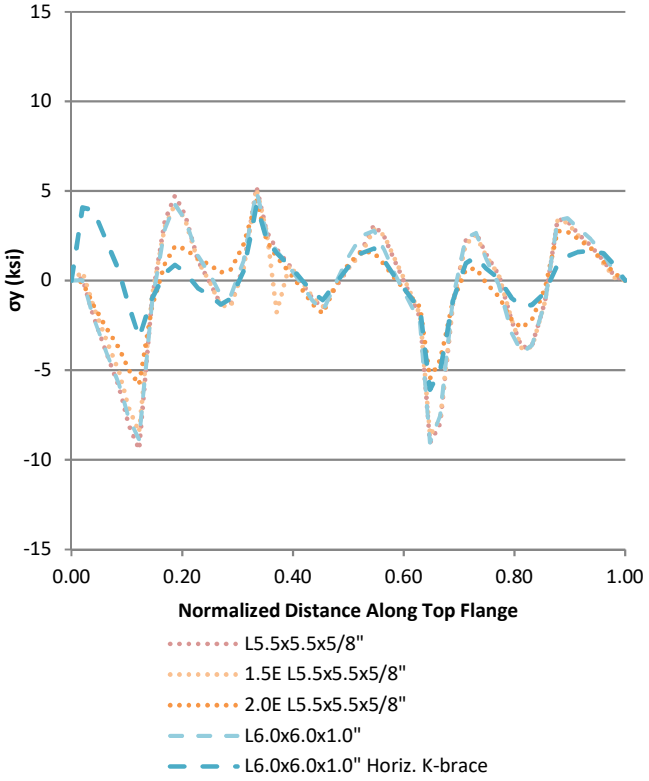

Figure D.20 G3 Top Flange Stress

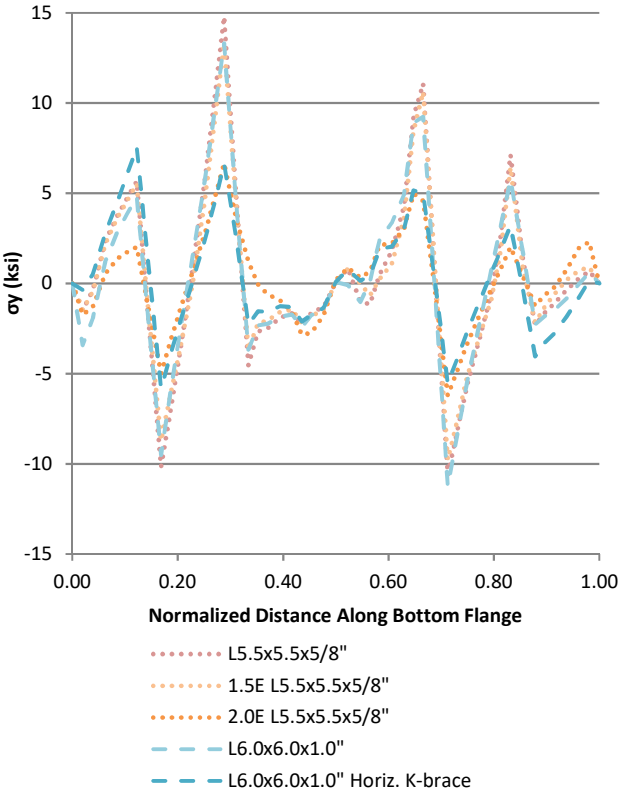

Figure D.21 G3 Bottom Flange Stress

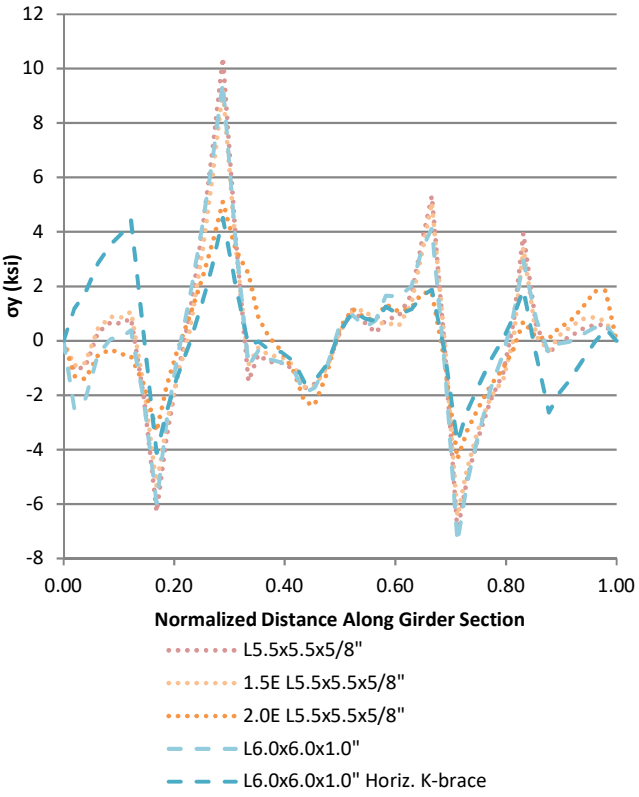

Figure D.22 G3 Weak Axis Sectional Stress

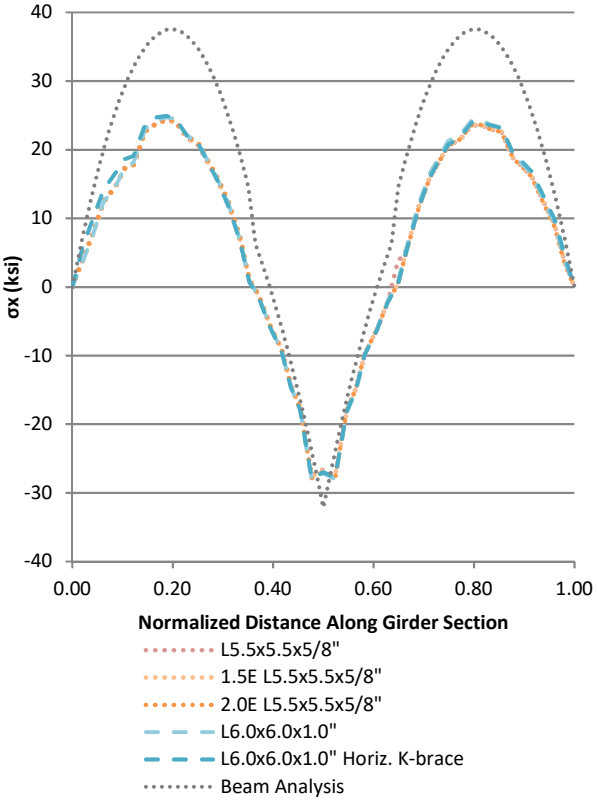

Figure D.23 G3 Strong Axis Sectional Stress

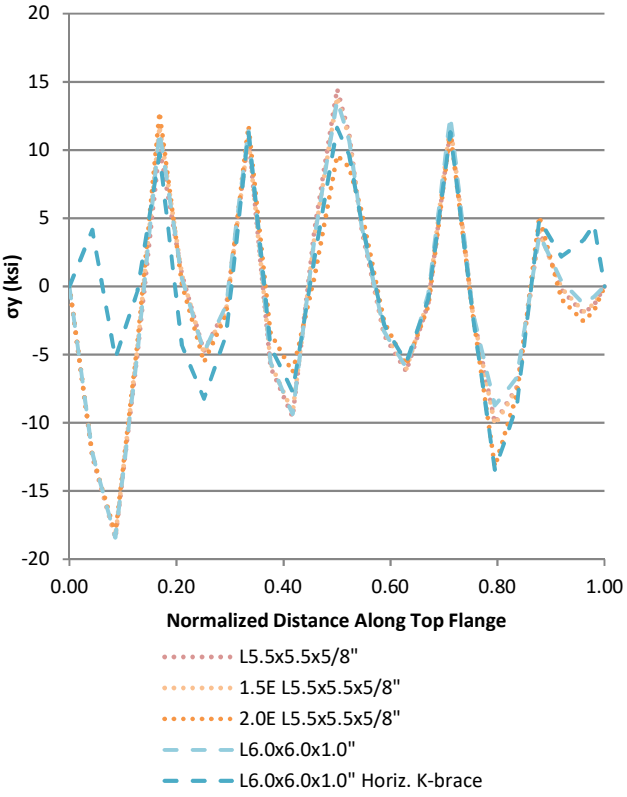

Figure D.24 G4 Top Flange Stress

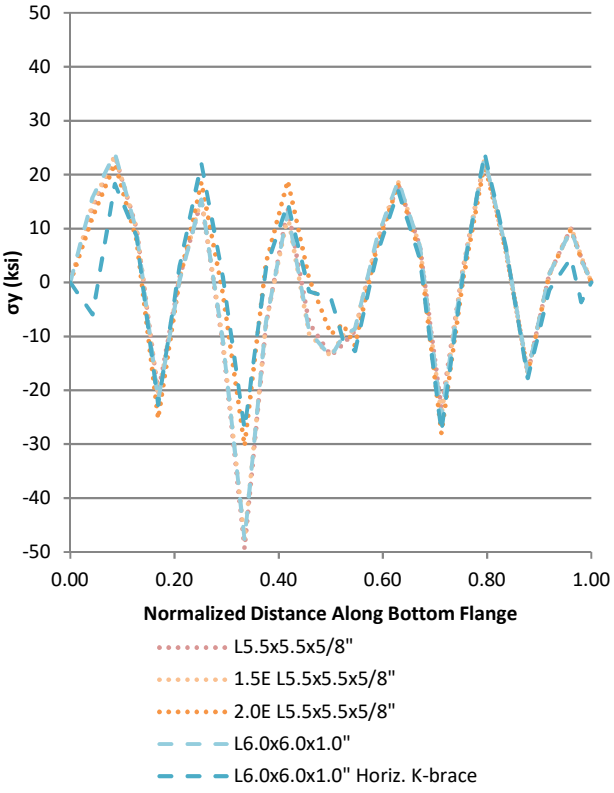

Figure D.25 G4 Bottom Flange Stress

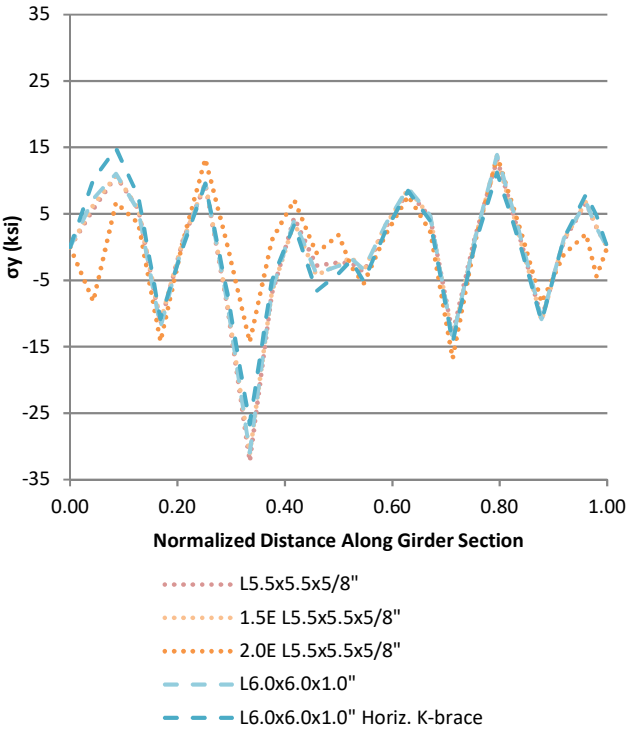

Figure D.26 G4 Weak Axis Sectional Stress

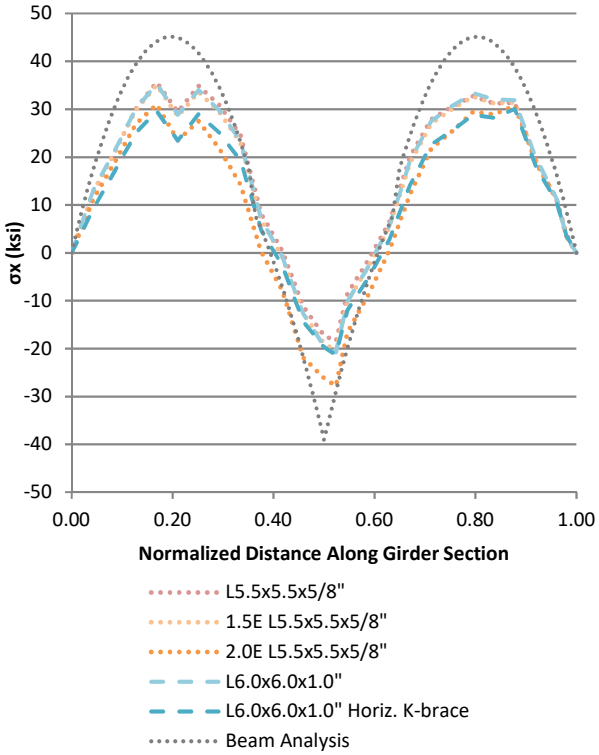

Figure D.27 G4 Strong Axis Sectional Stress

A W18x76 member connected to the web at the abutment was considered. Figure D.28 gives the dimensions for the W18x76 section. To provide connection to the webs, a 381x381x12.7 mm [15x15x0.5 in] connection plate ties the W18x76 to the 914x406x12.7 mm [36x16x0.5 in] abutment web plate, shown in Figure D.29, Figure D.30, and Figure D.31. The abutment web plate is tied to the web and provides stability against local buckling at the girder web ends along with the abutment stiffeners.

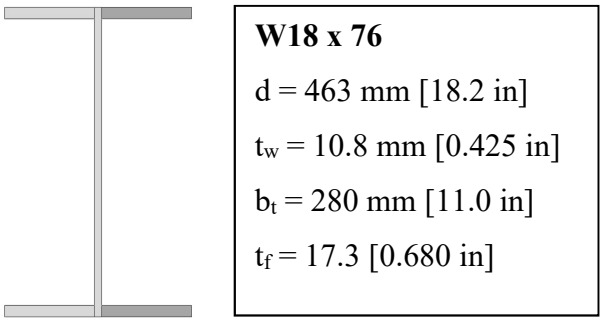

Figure D.28 W18x76 section properties

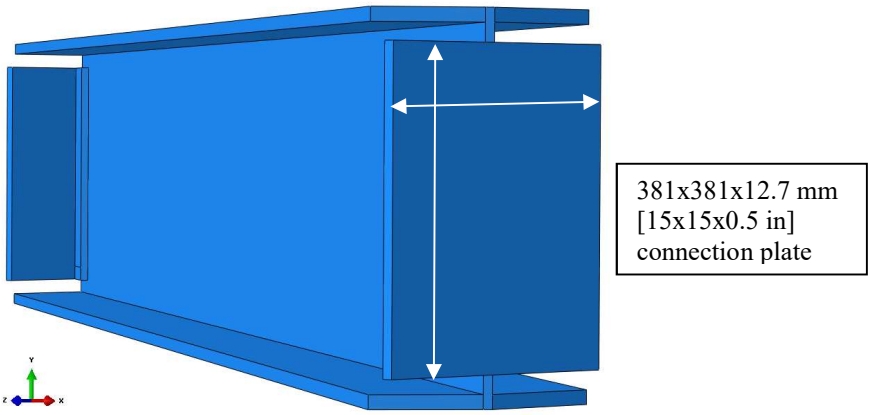

Figure D.29 W18x76 and connection plate dimensions

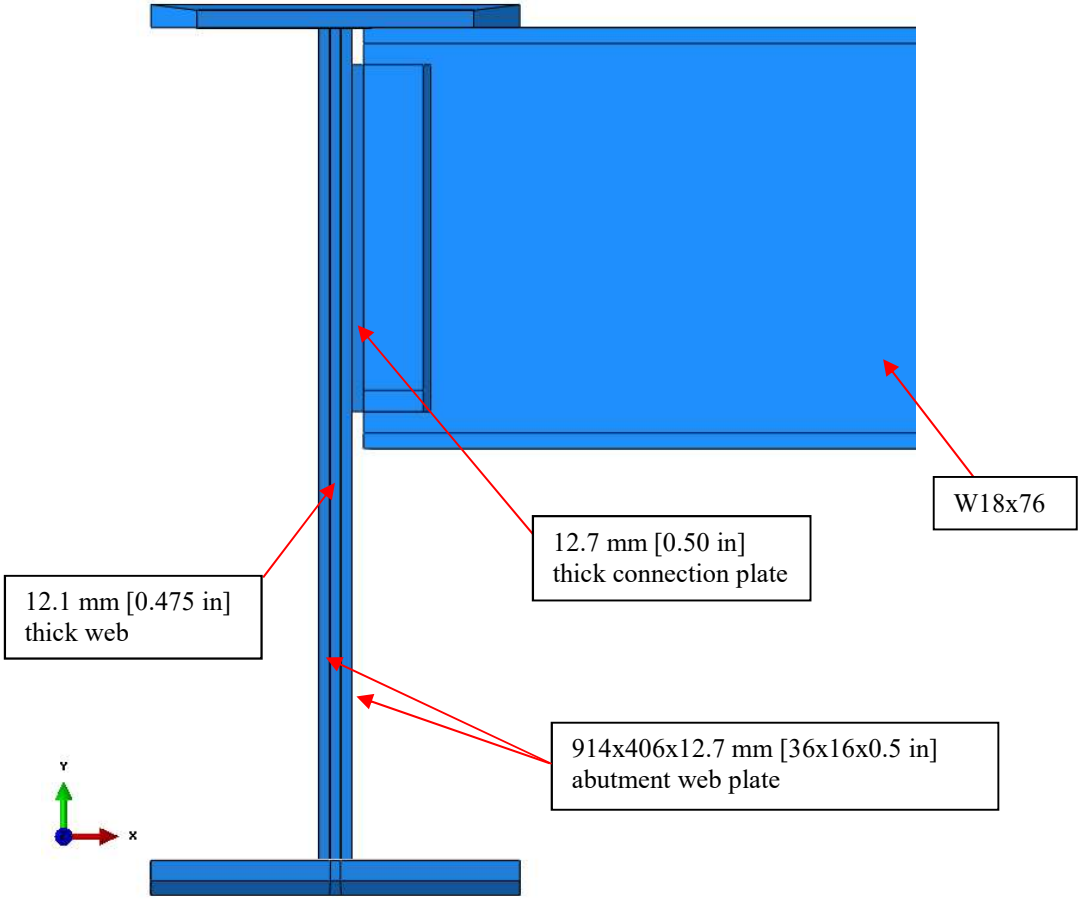

Figure D.30 Elevation view of exterior girder at the abutment showing girder and diaphragm connection plates

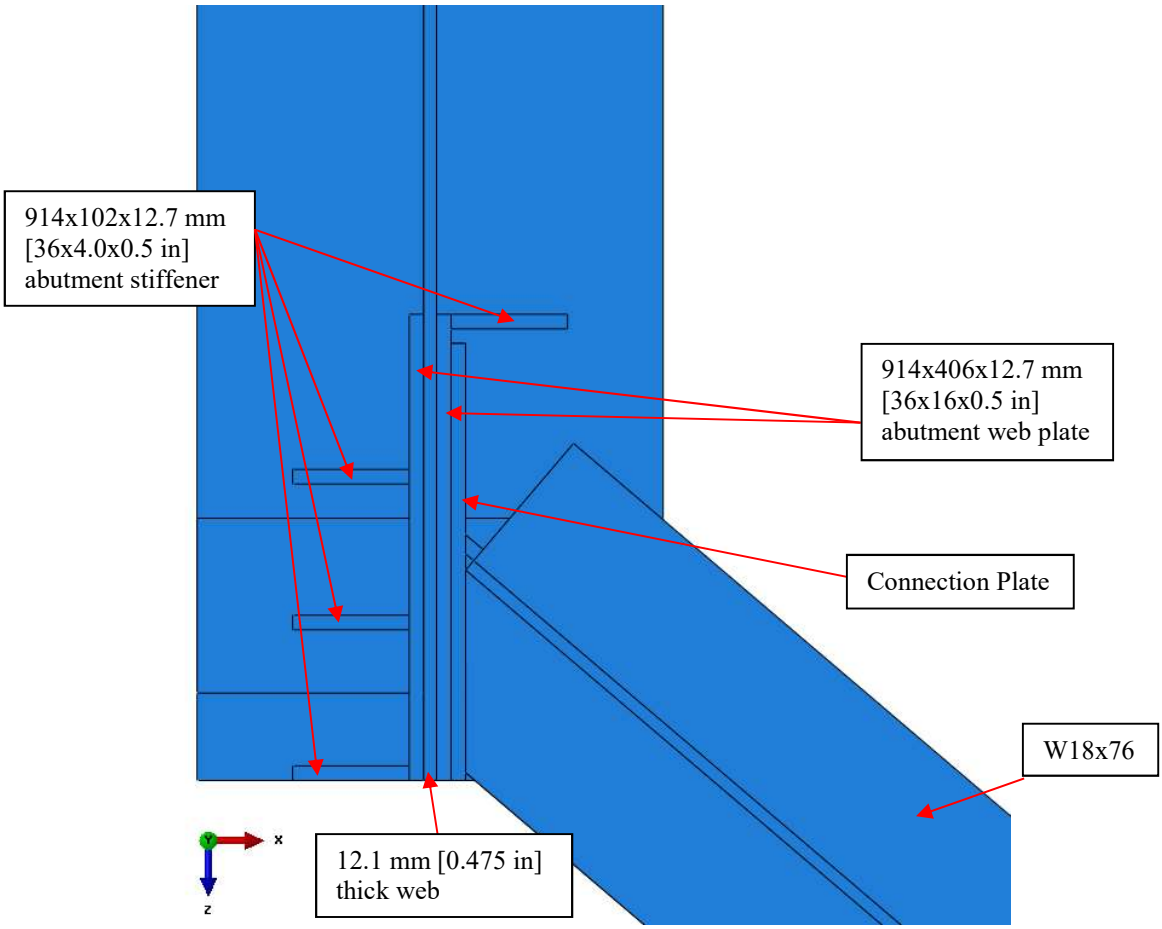

Figure D.31 Plan view of exterior girder at the abutment showing girder and diaphragm connection plates

A bearing utilizing a 406x50.8x12.7 mm [16x2.0x0.5 in] wide plate placed as shown in Figure D.32 was used to compare against the knife edge support. Both supports have a 12.7 mm [0.5 in] boundary surface against the 406x406x50.8 mm [16x16x2.0 in] square bearing pad and are fixed in vertical and out-of-plane translation. However, for the "rocker" bearing, as in the following figures, that surface is a hard contact with the square bearing pad. The edges of the surface in contact with the square bearing pad is also fixed to prevent the bearing pad from slipping. Figure D.33 and Figure D.34 shows the 40 degree skewed-staggered model with 9.14 m [30 ft] cross-frame spacing and W18x76 abutment diaphragms in which the rocker bearing is

used. The model is scaled to five times and the color map shows Mises stresses from 0 to 345 MPa [50 ksi].

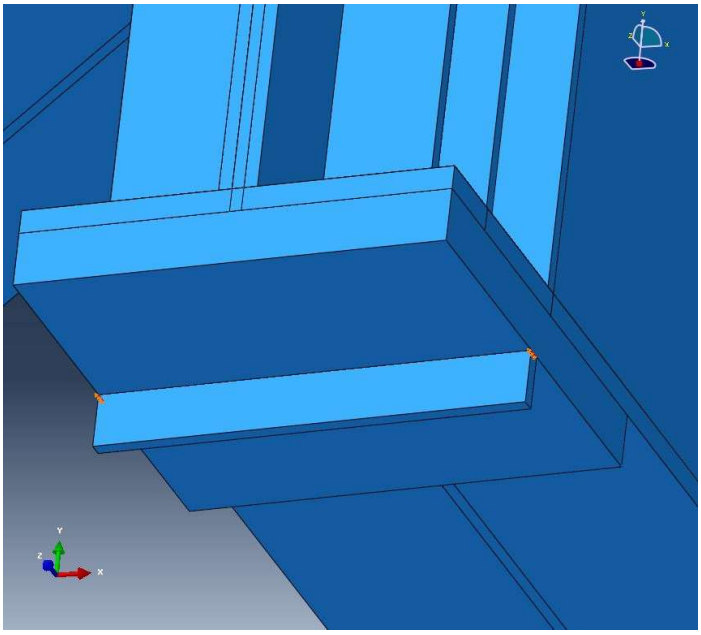

Figure D.32 Rocker bearing

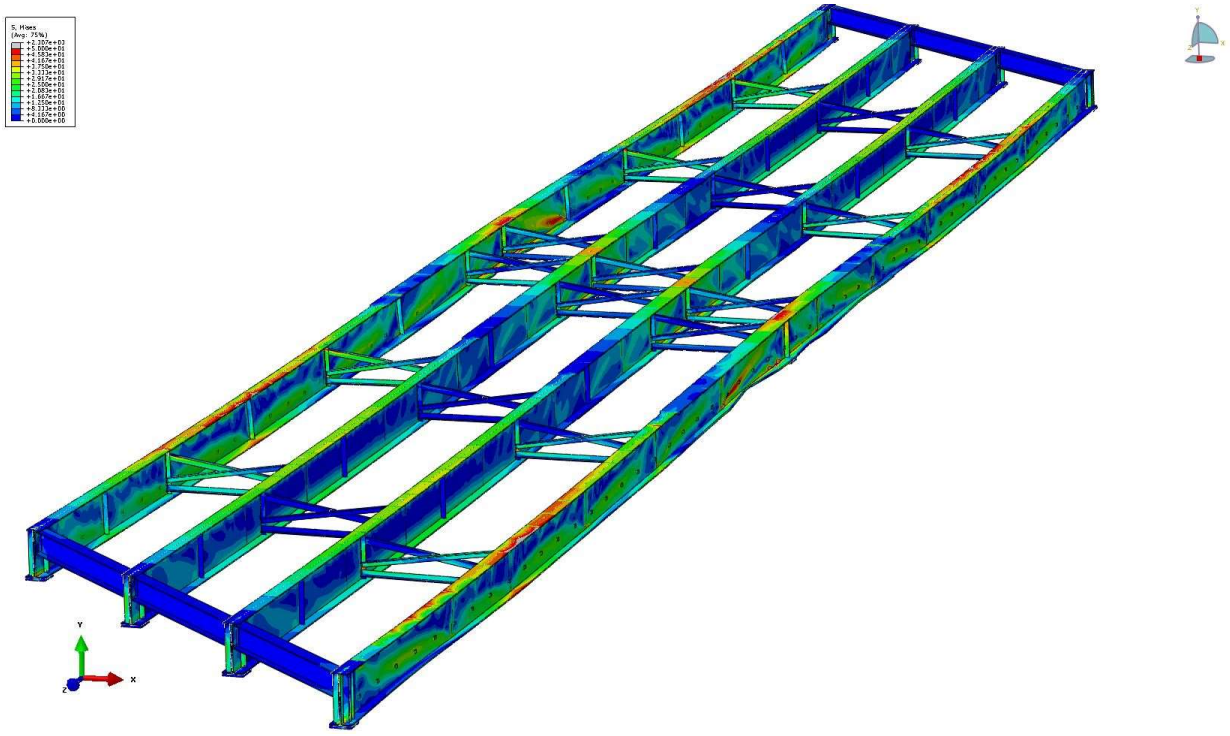

Figure D.33 Isotropic view of the 40 degree skewed-staggered bridge with 9.14 m [30 ft] cross-frame spacing, W18x76 abutment diaphragms, and rocker bearings

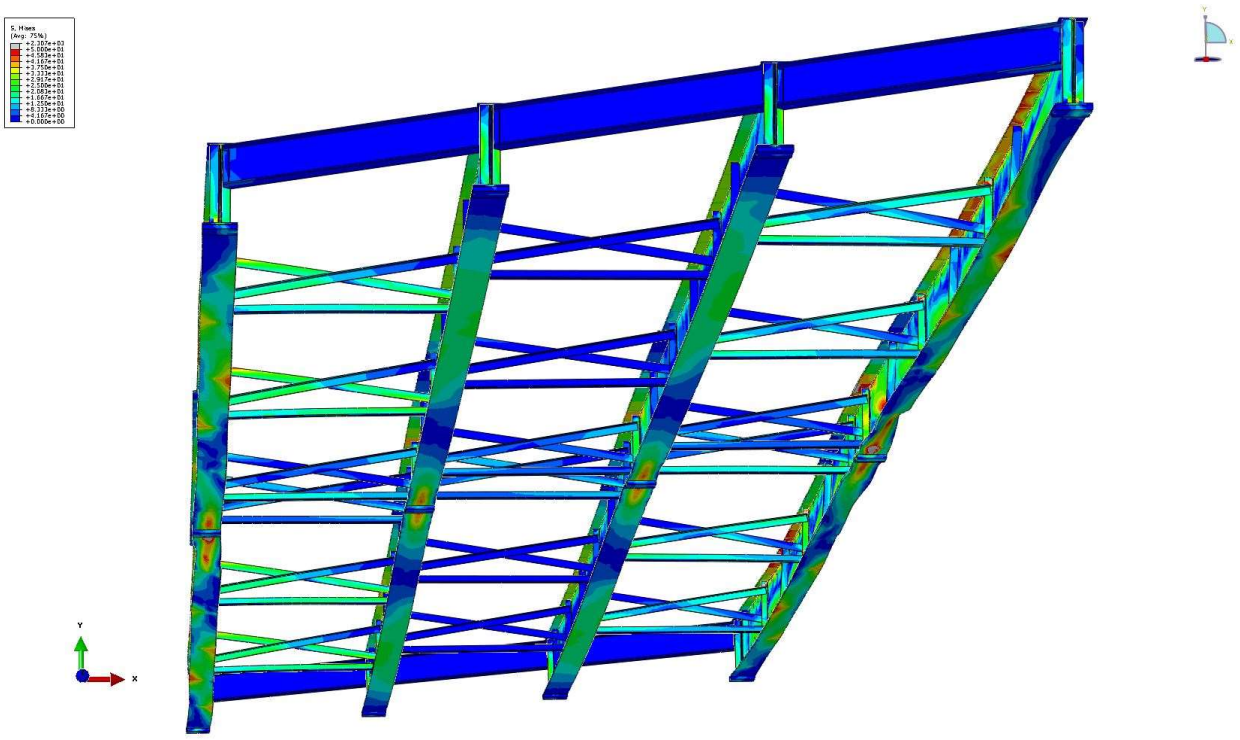

Figure D.34 40 degree skewed-staggered bridge with 9.14 m [30 ft] cross-frame spacing showing W18x76 abutment diaphragms and rocker bearings

Figure D.35 through Figure D.44 compare a model with L152x152x25.4 mm [L6.0x6.0x1.0 in] abutment cross-frames to models with W18x76 members for lateral deflection and bending stresses. The knife edge support and rocker bearings are compared for bridges with W18x76 members. Figure D.35 and Figure D.36 show the top flange lateral displacement and peak lateral displacement versus applied load for the exterior girder. As before, peak deflections and stresses are provided near 90% load. Deflections were higher throughout the bridge for abutments with cross-frames composed of angles and lower for abutments with W18x76 members. Top flange displacements for the model with W18x76 and knife edge supports was similar to the model with rocker bearings.

Figure D.37 through Figure D.40 show the top flange, bottom flange, and weak-axis section out-of-plane bending stresses along with the strong-axis sectional stress for the interior girder. The model with L152x152x25.4 mm [L6.0x6.0x1.0 in] abutment cross-frames typically

produced larger stresses along the girder for both in-plane and out-of-plane bending. While the horizontal K-brace configuration only constrained the top flange, the heavy W18x76 constrains a large section of the abutment ends. Preventing torsion and warping of the girder ends affect stresses throughout the span. Again, the knife edge supports produced almost the same stresses as the rocker bearings for bridges with W18x76 diaphragms.

Figure D.41 through Figure D.44 shows the exterior girder top flange, bottom flange, and weak-axis section out-of-plane bending stresses along with the strong-axis sectional stress. Exterior girder stresses followed a similar pattern as interior girder stresses. Abutment cross-frames with angle members generally produced larger peak stresses than abutment diaphragms with W18x76 members. The knife edge supports also produced the same stresses as the rocker bearings for bridges with W18x76 diaphragms. In the exterior girder, out-of-plane stresses were similar for a majority of the span due to higher lateral loads.

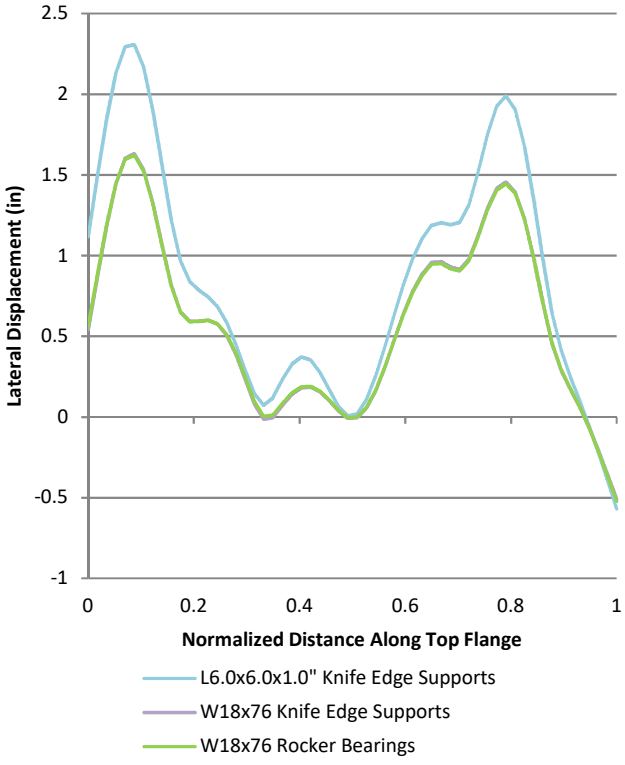

Figure D.35 G4 Lateral Displacement vs Normalized Distance ~90% Load

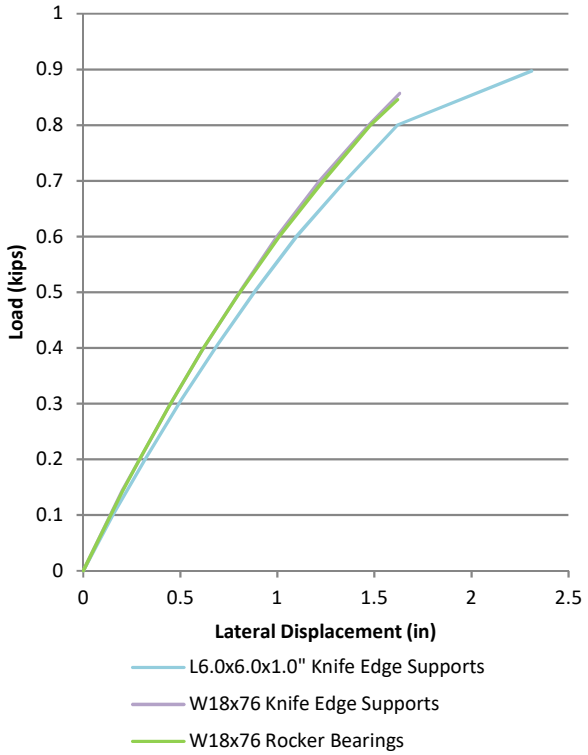

Figure D.36 Percent Load vs Peak Lateral Displacement in Span 1

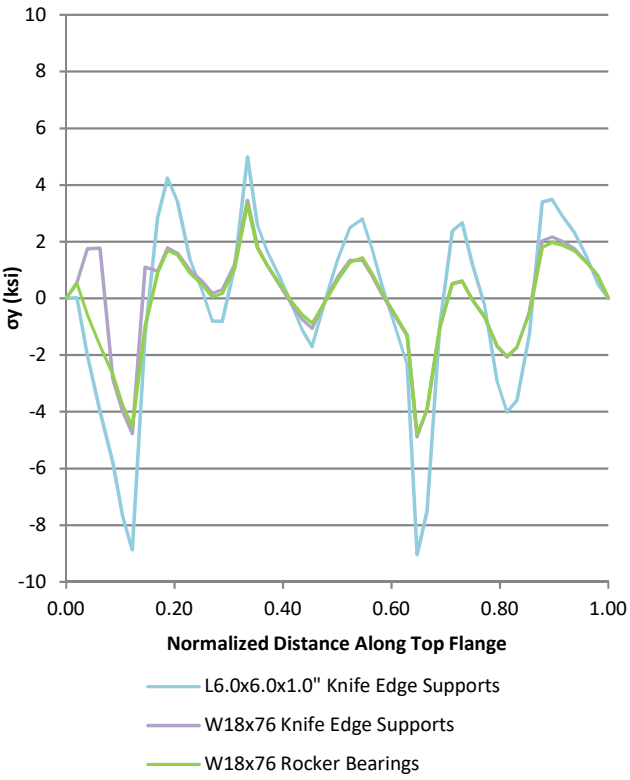

Figure D.37 G3 Top Flange Stress

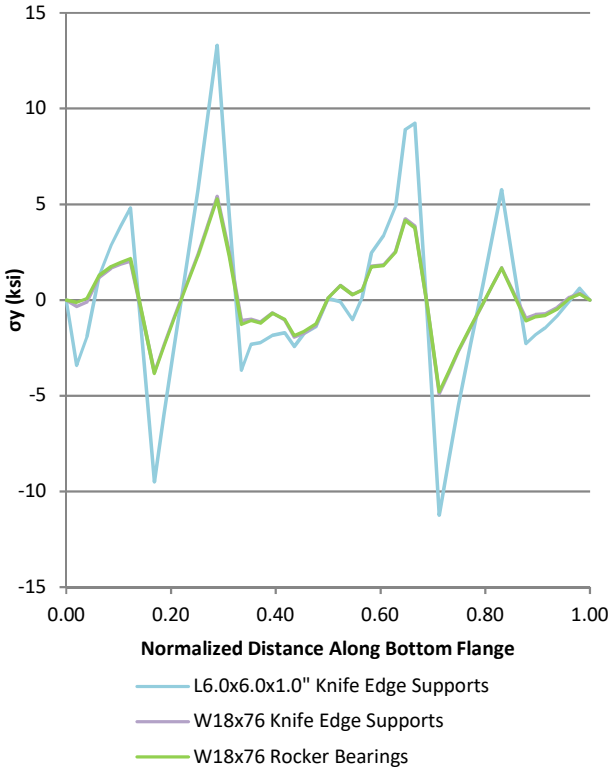

Figure D.38 G3 Bottom Flange Stress

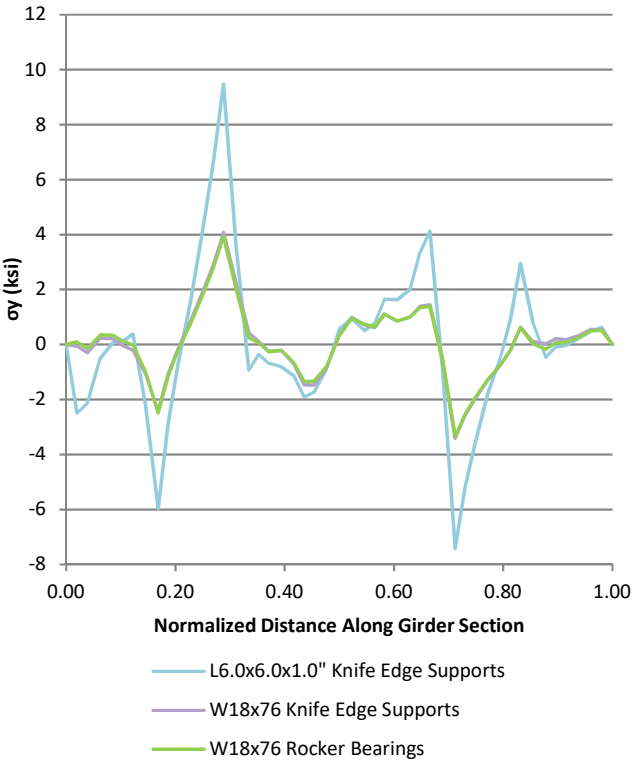

Figure D.39 G3 Weak Axis Sectional Stress

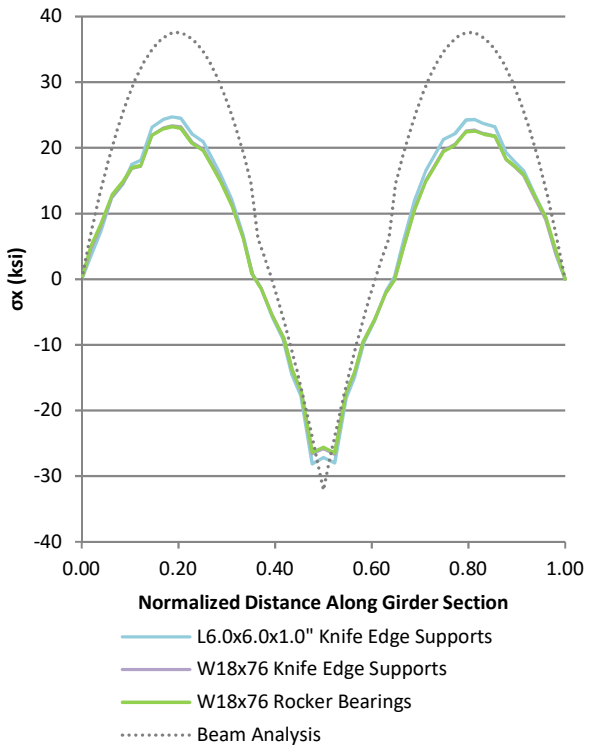

Figure D.40 G3 Strong Axis Sectional Stress

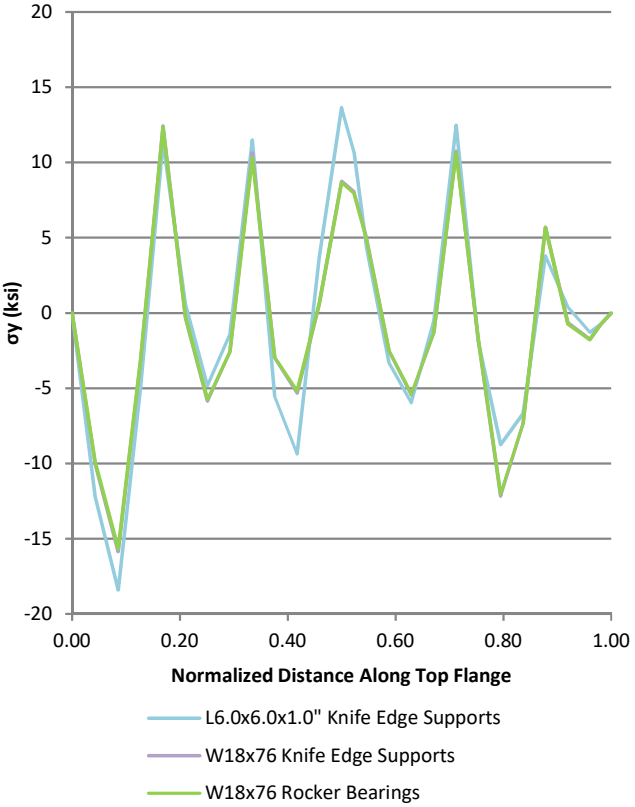

Figure D.41 G4 Top Flange Stress

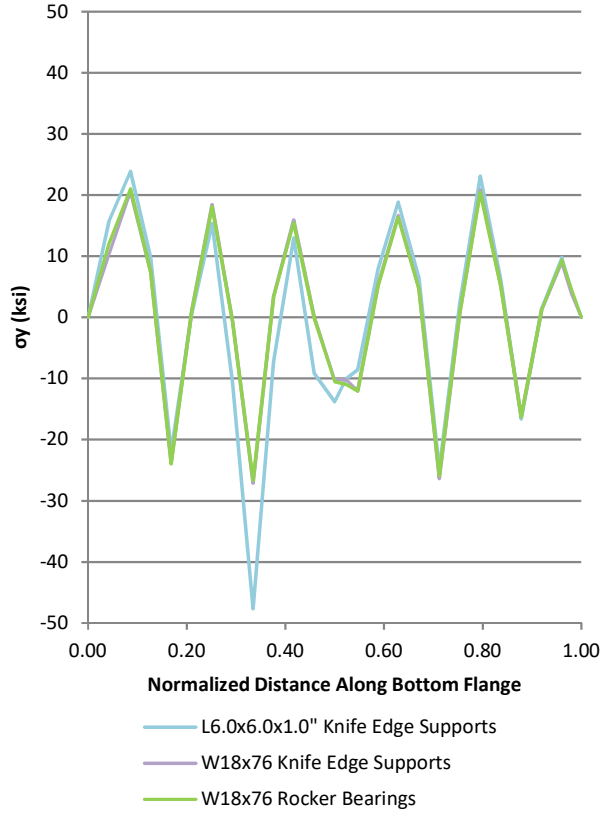

Figure D.42 G4 Bottom Flange Stress

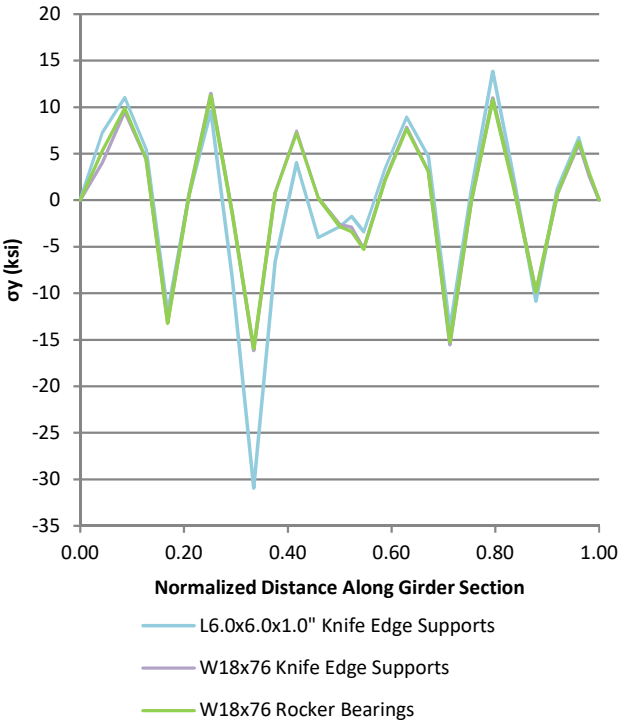

Figure D.43 G4 Weak Axis Sectional Stress

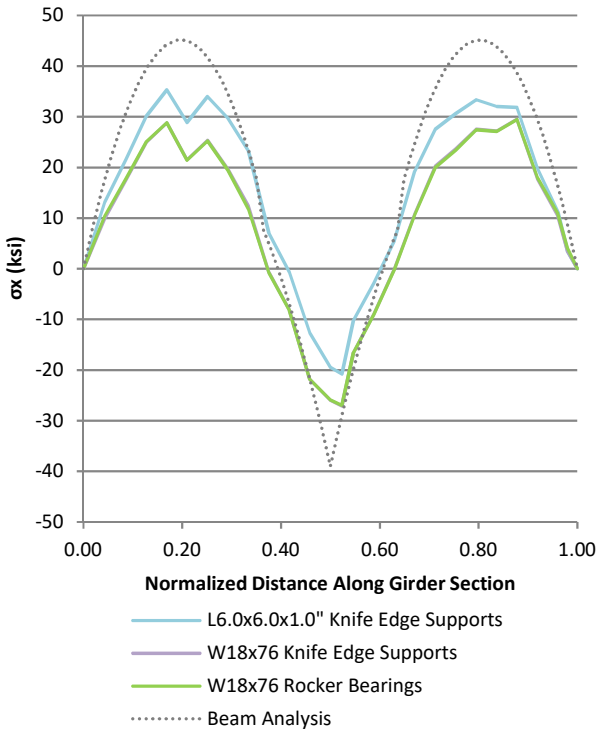

Figure D.44 G4 Strong Axis Sectional Stress

Cross-frames with MC12x50 top chords and L140x140x15.9 mm [L5.5x5.5x5/8 in] diagonals and bottom chords in a K-brace configuration were used at the abutments. Figure D.45 shows the two sides of the cross-frame configuration. Figure D.46 shows the bridge model with MC12x50 abutment cross-frame members scaled to five times and Mises stresses ranging from 0 to 345 MPa [50 ksi] in the color map.

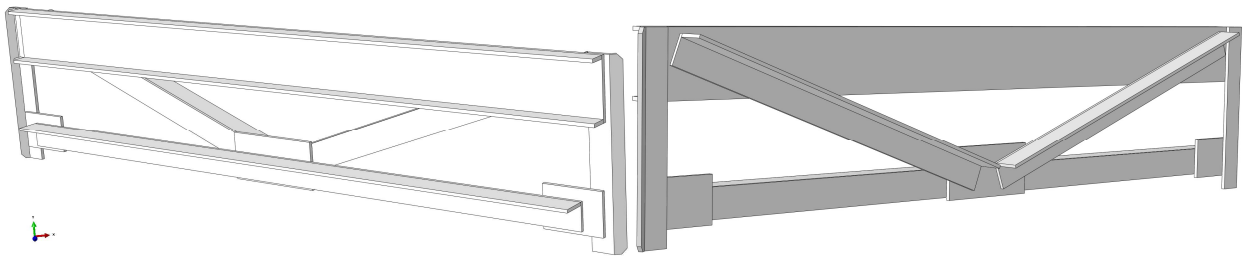

Figure D.45 MC12x50 abutment cross-frame

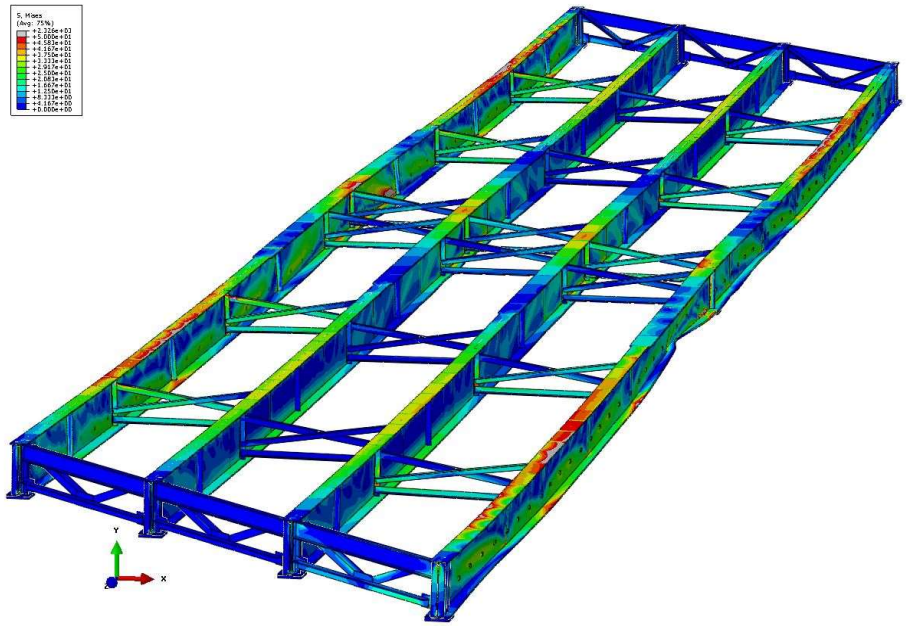

Figure D.46 40 degree skewed-staggered bridge with 9.14 m [30 ft] cross-frame spacing, MC12x50 abutment diaphragms, and knife edge bearing supports

Figure D.47 through Figure D.56 shows bridges with abutment diaphragm composed of L152x152x25.4 mm [L6.0x6.0x1.0 in] angles, MC12x50 members, and W18x76 members. As the rocker bearings produced almost the same results as the knife edge support, the knife edge support condition was used for all three models. Figure D.47 and Figure D.48 shows the top flange lateral displacement and peak lateral displacement versus applied load for the exterior girder. Peak deflections and stresses are given near 90% load. Abutment diaphragms with MC12x50 members produced the smallest deflections while abutment cross-frames with only L152x152x25.4 mm [L6.0x6.0x1.0 in] angles produced the largest deflection. While the W18x76 alone is heavier than the MC12x50 member, the cross-frame with MC12x50 has diagonals providing additional stiffness and bracing a longer length of the web.

Figure D.49 through Figure D.52 shows the interior girder top flange, bottom flange, and weak-axis section out-of-plane bending stresses along with the strong-axis sectional stress. Abutment cross-frames with L152x152x25.4 mm [L6.0x6.0x1.0 in] angles produced the largest

peak stresses. The models with MC12x50 and W18x76 members both produced relatively similar stresses. The model with MC12x50 members produced the highest strong axis bending stresses at mid-span while the other two models produced relatively similar but lower vertical bending stresses.

Figure D.53 through Figure D.56 shows the top flange, bottom flange, and weak-axis section out-of-plane bending stresses along with the strong-axis sectional stress for the exterior girder. While cross-frames composed only of angles produced higher peak out-of-plane stresses, stresses throughout the span were typically very similar for all three models due to the high overturning force from the overhangs. Again, abutment cross-frames with only of L152x152x25.4 mm [L6.0x6.0x1.0 in] angles had the highest peak strong-axis bending stresses. The models with MC12x50 and W18x76 members had similar vertical bending stresses.

While each newly constructed bridge requires its own design based on specific loads and conditions, the cross-frame with a MC12x50 member was chosen as the primary abutment diaphragm throughout Part 3 and Part 4. The W18x76 member is much stiffer relative to intermediate cross-frame angles, and W-shapes have flanges that must be cut to be bolted or welded to stiffeners or angles to form a brace connection. Using only L152x152x25.4 mm [L6.0x6.0x1.0 in] angles in the abutment diaphragm resulted in abutment cross-frame stiffnesses relatively similar to intermediate cross-frames. However, the abutment ends experience warping and torsion not found at intermediate span locations which must be braced effectively.

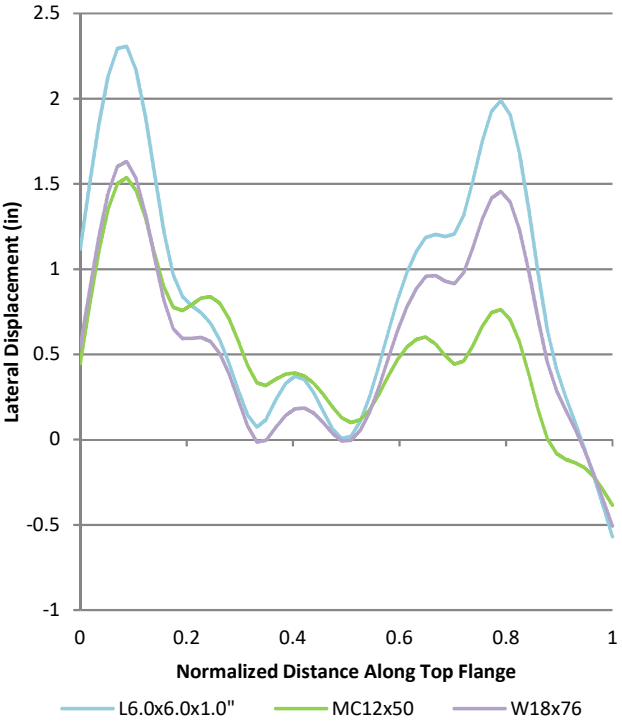

Figure D.47 G4 Lateral Displacement vs Normalized Distance ~90% Load

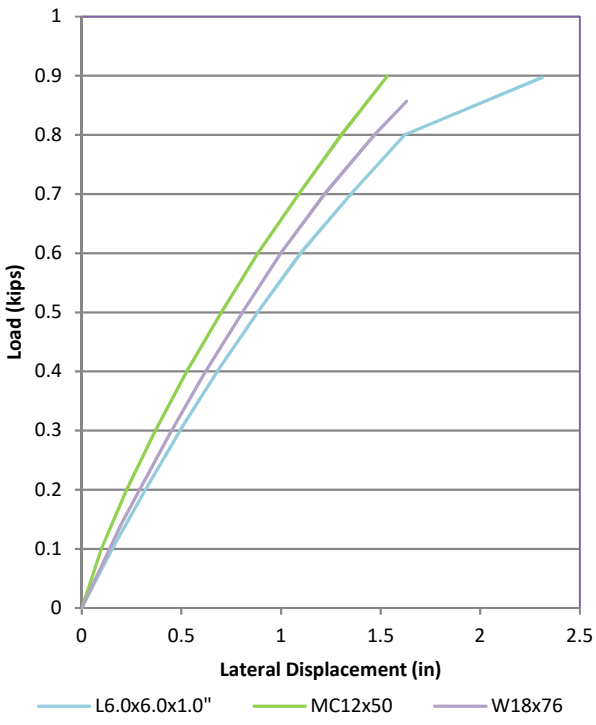

Figure D.48 Percent Load vs Peak Lateral Displacement in Span 1

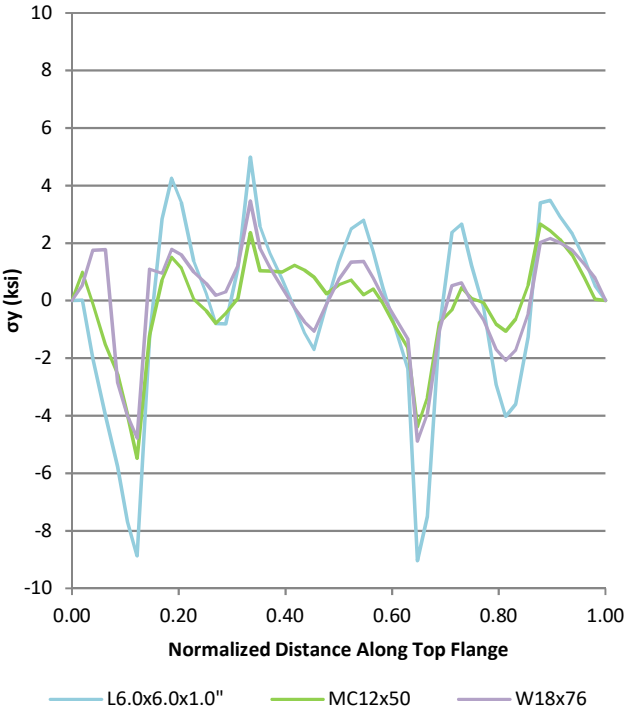

Figure D.49 G3 Top Flange Stress

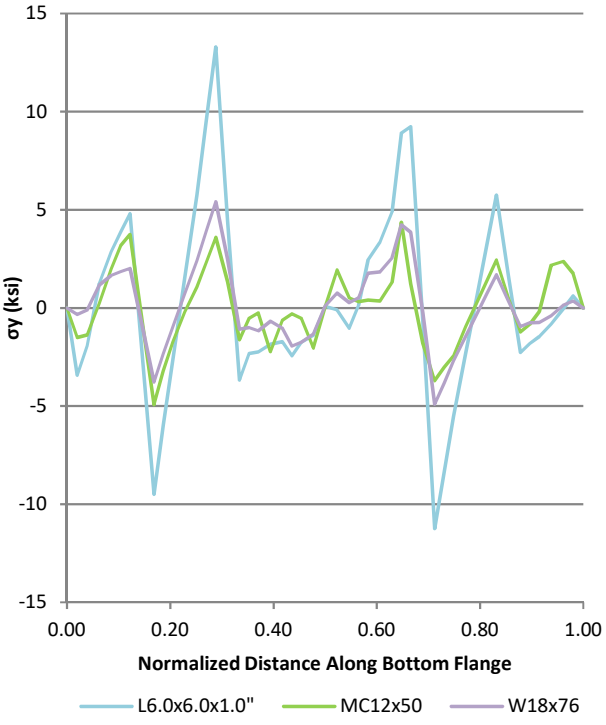

Figure D.50 G3 Bottom Flange Stress

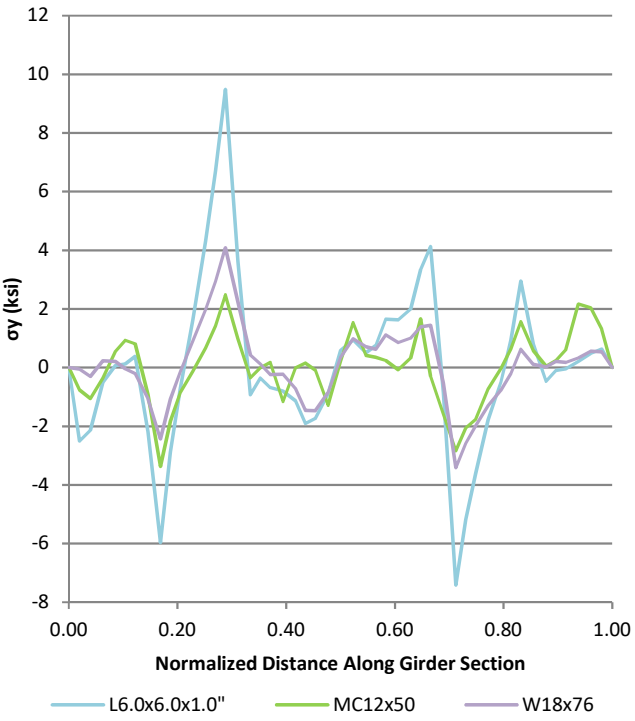

Figure D.51 G3 Weak Axis Sectional Stress

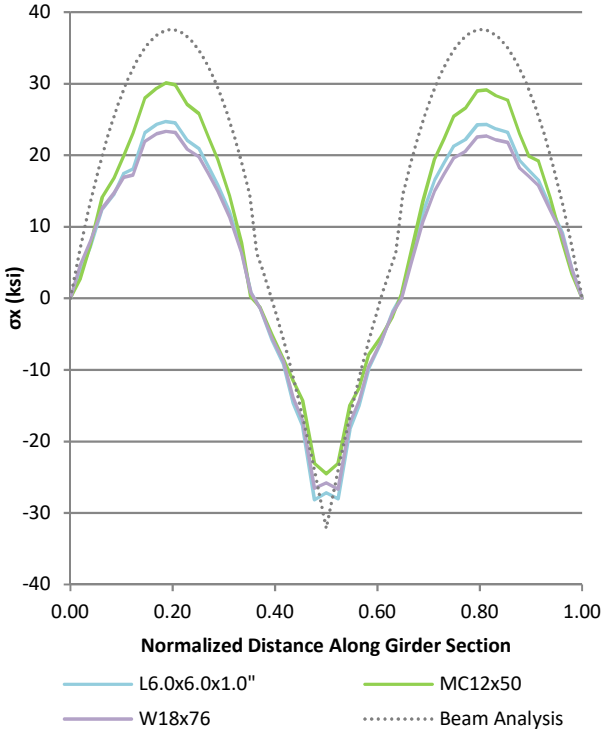

Figure D.52 G3 Strong Axis Sectional Stress

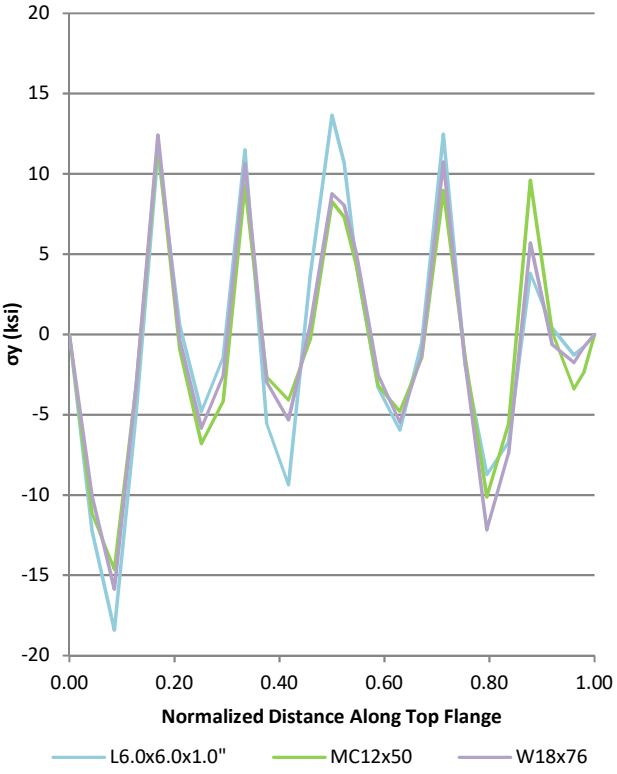

Figure D.53 G4 Top Flange Stress

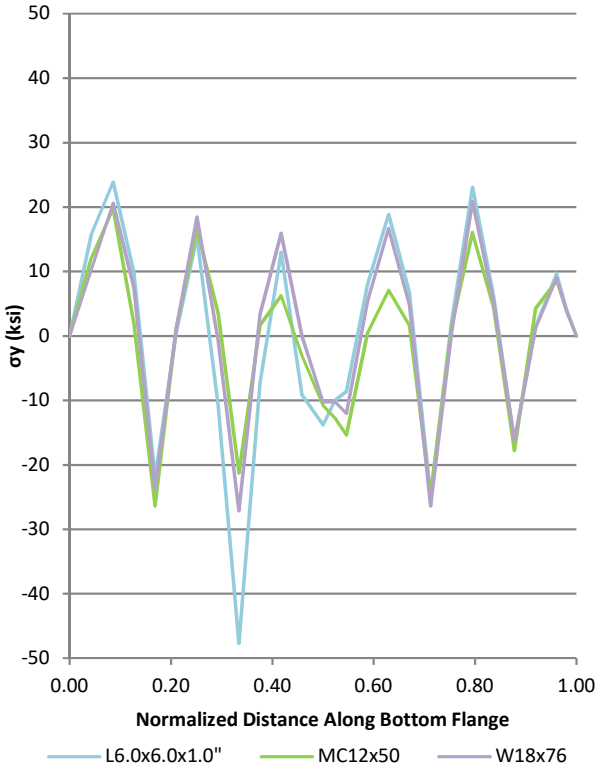

Figure D.54 G4 Bottom Flange Stress

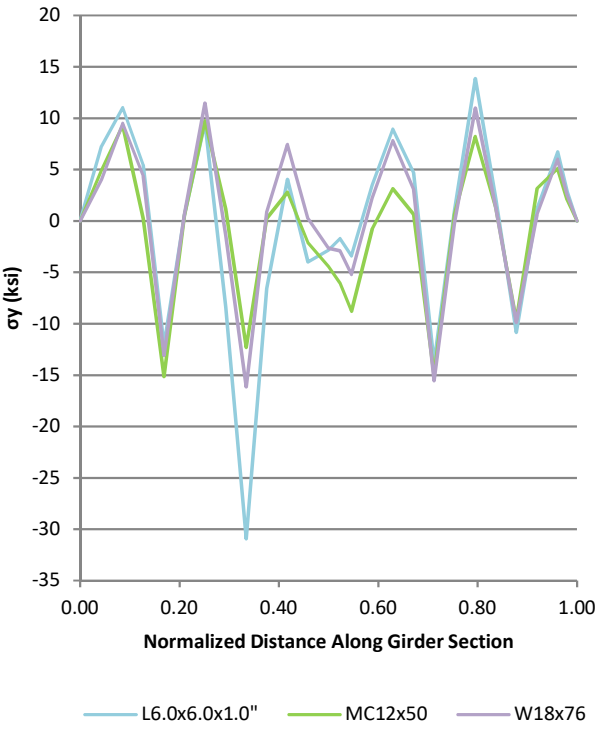

Figure D.55 G4 Weak Axis Sectional Stress

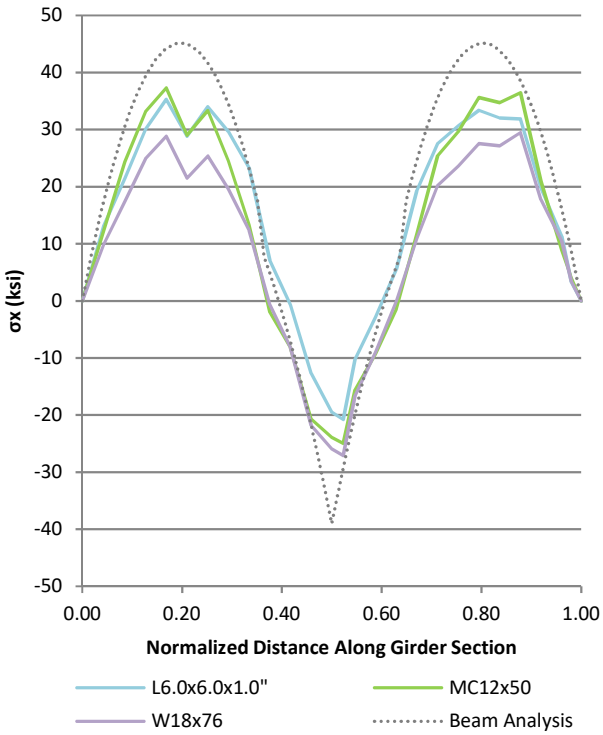

Figure D.56 G4 Strong Axis Sectional Stress

APPENDIX E: SINGLE GIRDER MODEL ANALYSIS

This study attempted to capture the girder behavior in a bridge system using a single girder connected to cross-frames with varying boundary condition fixities. These cross-frame boundary conditions model the cross-frame connection to the adjacent girder, allowing for a single girder model to capture the interaction with the adjacent girder as if in a girder system. Using a single girder reduces the complexity of the model and significantly lowers the computational run-time relative to a full scale model.

The bridge geometry and modeling methodology used are described in Part 3 of this paper along with the applied loads and bearing boundary conditions. Both the single girder model and girder system model have the same geometry, connections, meshing, applied loads, and bearing conditions for each respective girder. Cross-frames with fixed connections, vertical roller connections, and variable stiffness spring connections were used to mimic the cross-frame boundary condition. Overall, the single girder models did not effectively capture girder behavior found in the girder system models. As cross-frames transfer load laterally between girders, varying the boundary condition of the cross-frames alone was not enough to capture the girder-to-girder interaction and load distribution between girder systems.

Figure E.1 shows the boundary surface on the free end of the cross-frame for the single girder models. Settings for fixed translation in all three axes are also displayed. All models have fixed cross-frame boundary conditions at the piers and abutments. In Figure E.2, the boundary surface for the vertical roller fixity is shown, labeled as the unrestrained cross-frame condition in the rest of this section. Only translation parallel to the free end cross-frame surface is restrained.

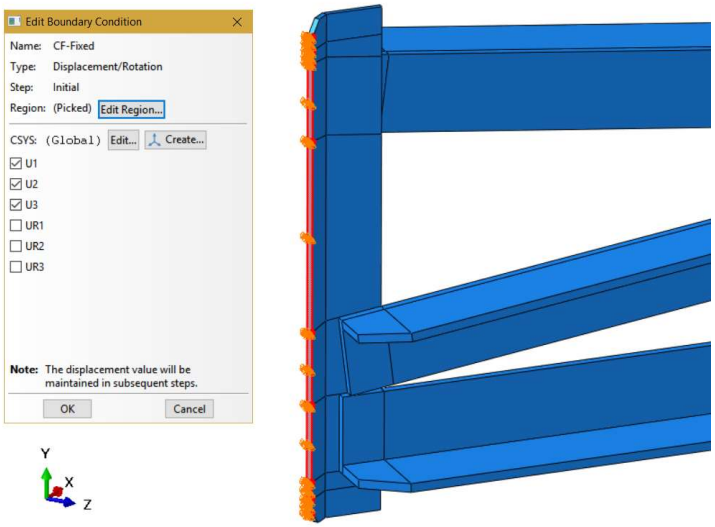

Figure E.1 Fixed cross-frame boundary condition

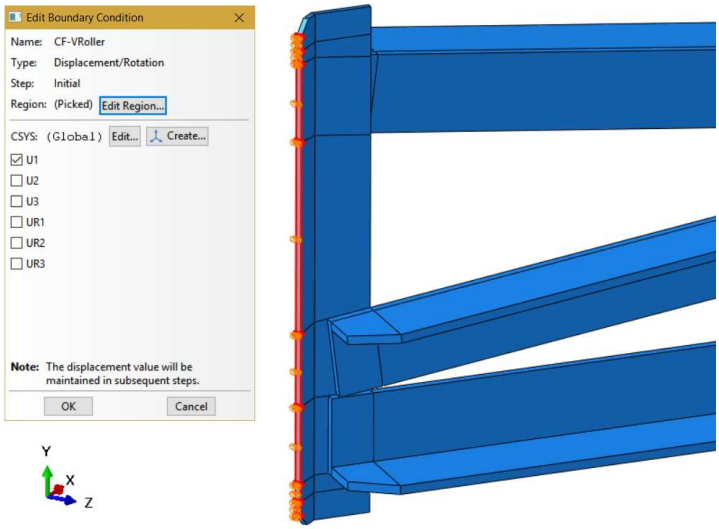

Figure E.2 Unrestrained (vertical rollers) cross-frame boundary condition

Figure E.3 shows the full bridge model of the 40 degree skewed-staggered bridge with 9.14 m [30 ft] cross-frame spacing. Figure E.4 and Figure E.5 shows the single girder versions of the interior and exterior girders, respectively, with fixed cross-frame boundary conditions. The color map represents Mises stress limits from 0 to 345 MPa [50 ksi]. In the fixed condition, cross-frame stresses appear to be larger for the single girder models compared to the full bridge

model. Conversely, girder stresses appear smaller, especially for the interior girder, in the single girder model than in the full bridge model. Stiffer members tend to attract greater loads.

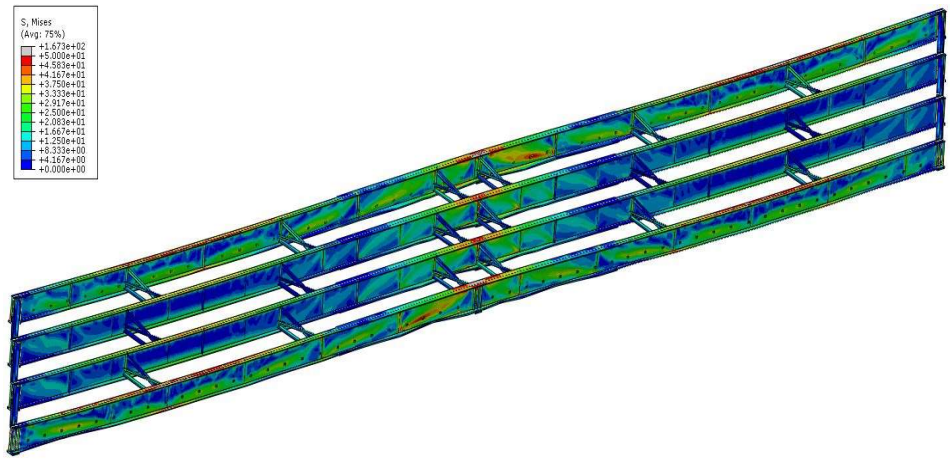

Figure E.3 40 degree skewed-staggered bridge with 9.14 m [30 ft] cross-frame spacing – full bridge model

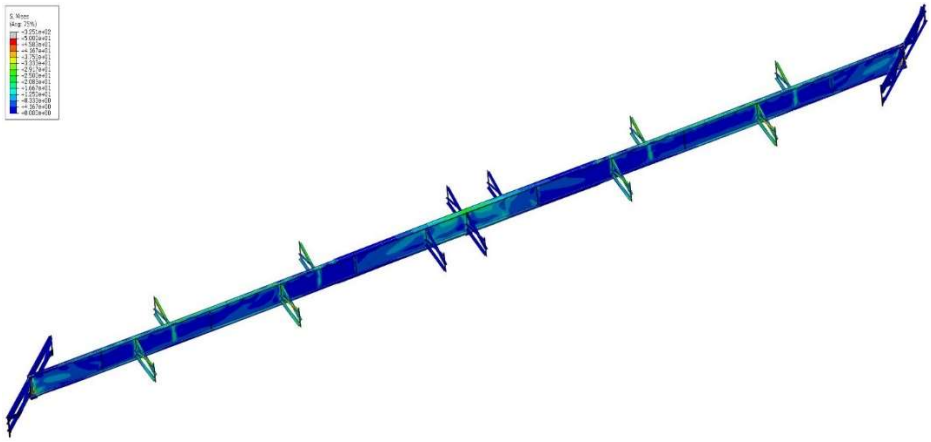

Figure E.4 40 degree skewed-staggered bridge with 9.14 m [30 ft] cross-frame spacing - interior girder with fixed cross-frame boundary condition

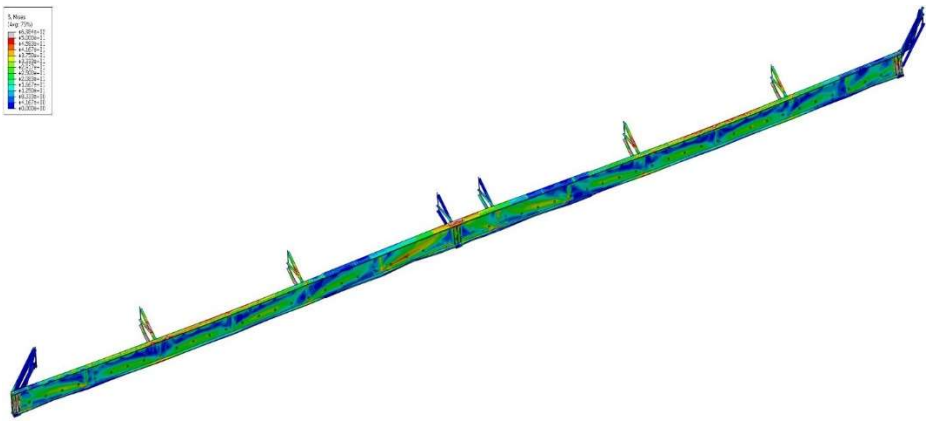

Figure E.5 40 degree skewed-staggered bridge with 9.14 m [30 ft] cross-frame spacing - exterior girder with fixed cross-frame boundary condition

Figure E.6 shows the full bridge model of the 40 degree skewed-parallel bridge with 9.14 m [30 ft] cross-frame spacing. Figure E.7 and Figure E.8 presents the single interior girder versions of the same configuration with fixed and vertical roller cross-frame boundary conditions, respectively. Figure E.9 and Figure E.10 shows the single exterior girder versions of the 40 degree skewed-parallel bridge with 9.14 m [30 ft] cross-frame spacing with fixed and vertical roller cross-frame boundary conditions, respectively. The color map represents Mises stress limits from 0 to 345 MPa [50 ksi]. Single girder cross-frame stresses in the fixed condition are larger than the full bridge model while single girder cross-frame stress in the unrestrained condition are similar compared the full bridge model. Girder stresses are smaller for cross-frames with fixed boundary condition relative to cross-frame with unrestrained boundary condition and the full bridge model.

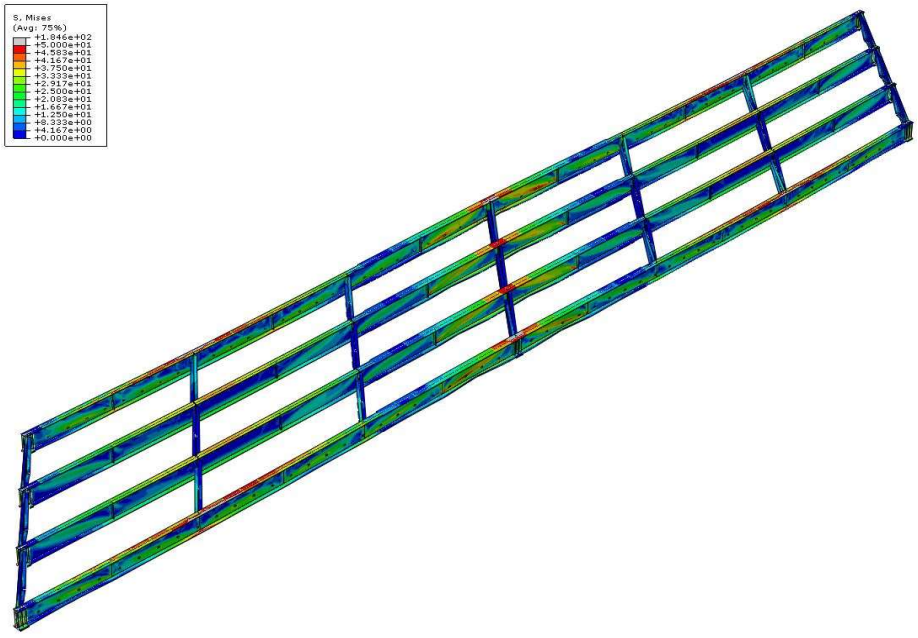

Figure E.6 40 degree skewed-parallel bridge with 9.14 m [30 ft] cross-frame spacing – full bridge model

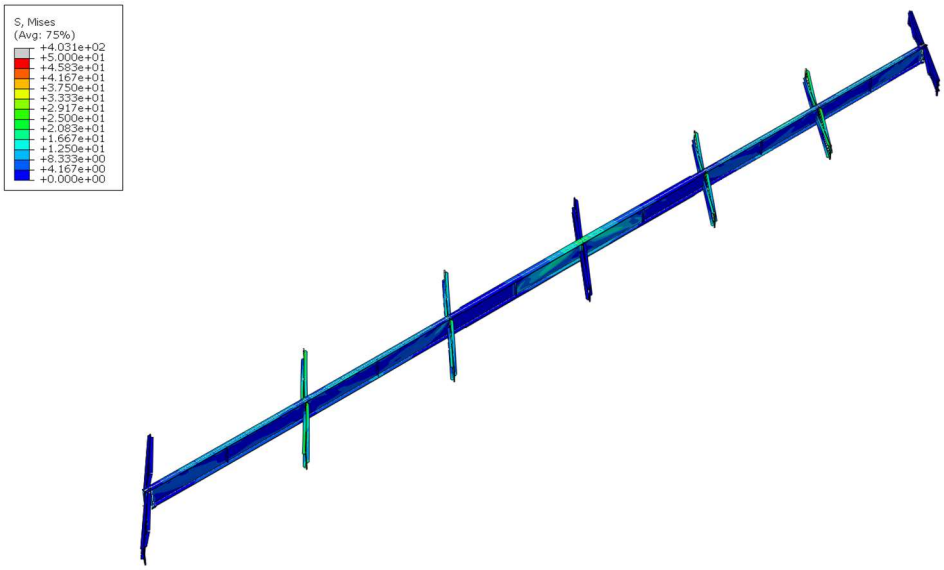

Figure E.7 40 degree skewed-parallel bridge with 9.14 m [30 ft] cross-frame spacing - interior girder with fixed cross-frame boundary condition

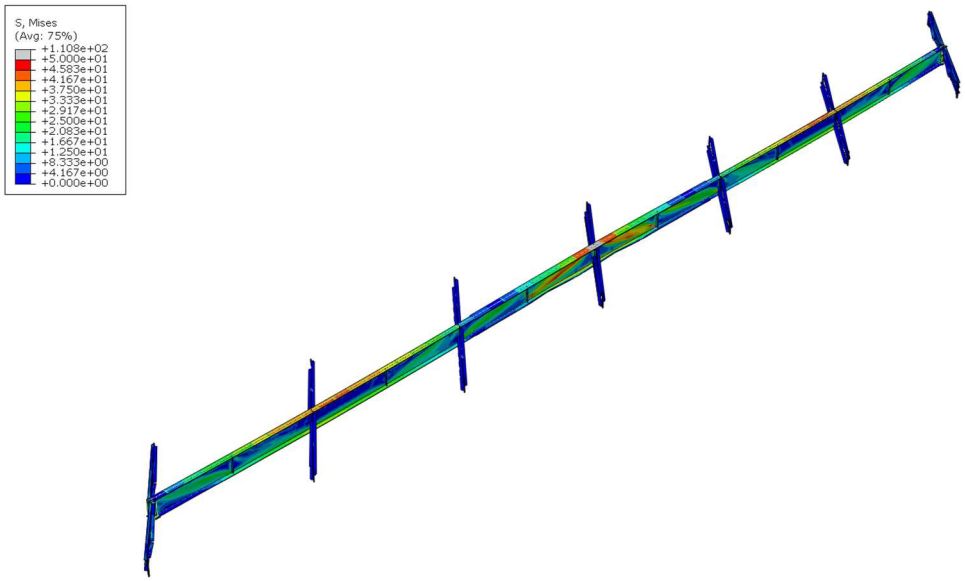

Figure E.8 40 degree skewed-parallel bridge with 9.14 m [30 ft] cross-frame spacing - interior girder with vertical roller cross-frame boundary condition

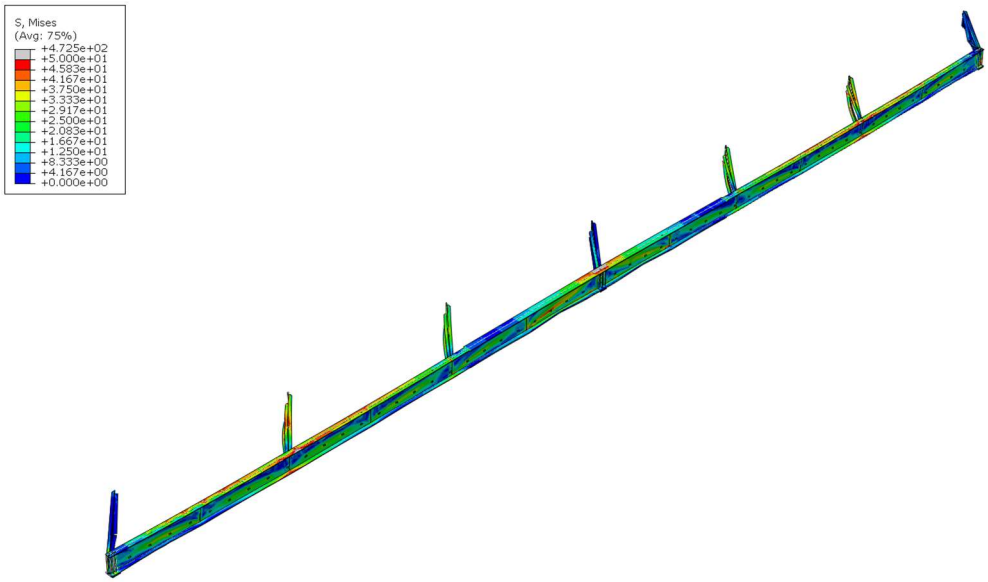

Figure E.9 40 degree skewed-parallel bridge with 9.14 m [30 ft] cross-frame spacing - exterior girder with fixed cross-frame boundary condition

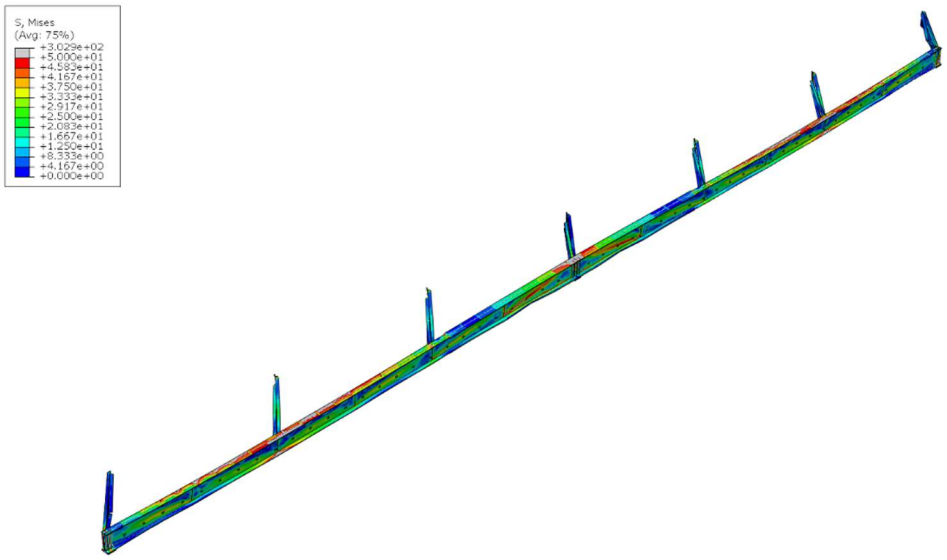

Figure E.10 40 degree skewed-parallel bridge with 9.14 m [30 ft] cross-frame spacing - exterior girder with vertical roller boundary condition

Figure E.11 and Figure E.12 shows the exterior girder top flange lateral displacement at full load along the entire bridge and the peak lateral displacement as a function of percent load in Span 1, respectively. Span 1 is labeled in Figure 3.12 of Part 3 and has similar brace locations for varying cross-frame orientations. The 40 degree skewed-staggered and skewed-parallel full bridge model along with single girder models with fixed cross-frames and unrestrained cross-frames are shown. Cross-frame are placed at 9.17 m [30 ft] for all models. The 40 degree skewed-parallel model with unrestrained cross-frames produced the largest lateral displacement while the 40 degree skewed-parallel full bridge model produced the smallest top flange lateral displacement. The 40 degree skewed-parallel model with fixed cross-frames produced the next largest lateral deflection values. One possibility for this behavior is that the unrestrained and fixed cross-frames single girder models were not stiff enough to brace the girder effectively relative to what is seen in the full scale model. Another reason for this behavior could be that the single girder cross-frame boundary conditions did not effectively capture the lateral load distributions in the girder and cross-frames.

Top flange lateral displacements of the skewed-staggered models were much more alike in Span 1 near the abutment but diverged towards center span, with the fixed cross-frame model producing larger displacements than the unrestrained cross-frame model. Similar to the skewed-parallel model, the full scale model of the skewed-staggered bridge produced the smallest top flange lateral displacements. Differences in peak lateral displacement of both the skewed-parallel and skewed-staggered models were greatest in Span 2.

Figure E.13 and Figure E.14 shows the bottom flange lateral displacement at full load and the percent load versus peak vertical displacement in the exterior girder of Span 1. The two full scale models had similar bottom flange lateral displacements in Span 1 and produced the

smallest values in the model set. Similar to the top flange lateral displacement, the single girder skewed-parallel model with unrestrained cross-frames produced the largest lateral displacements. The 40 degree skewed-staggered model with fixed cross-frames produced higher deflections than the skewed-staggered model with unrestrained cross-frames. For the skewed-staggered models, stiffer cross-frames resulted in more flexible flanges. One possibility for this occurrence is that since cross-frames are not aligned in the skewed-staggered orientation, lateral load must be transferred through bending of the flanges.

Figure E.15 and Figure E.16 shows the exterior girder top flange vertical displacement at full load and the percent load versus peak vertical displacement in Span 1, respectively. For vertical displacement, the unrestrained cross-frame models produced the largest displacements for both cross-frame orientations while the fixed cross-frame models produced the smallest displacements. The vertical stiffness of the cross-frames in the girder system model falls between the fully fixed and fully unrestrained condition. Overall, the graphs show that both the fixed cross-frame and the unrestrained cross-frame single girder models did not effectively capture girder behavior found in the girder system models.

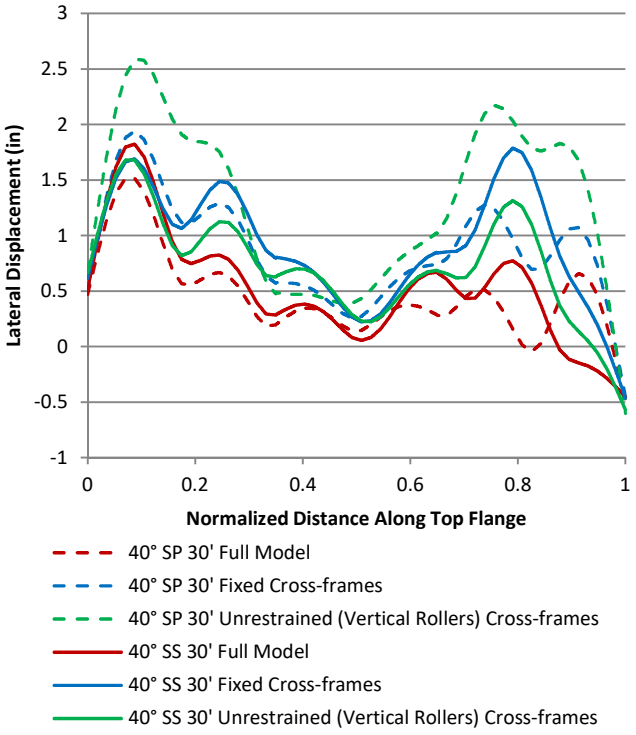

Figure E.11 Top flange lateral displacement along entire bridge – exterior girder (G4)

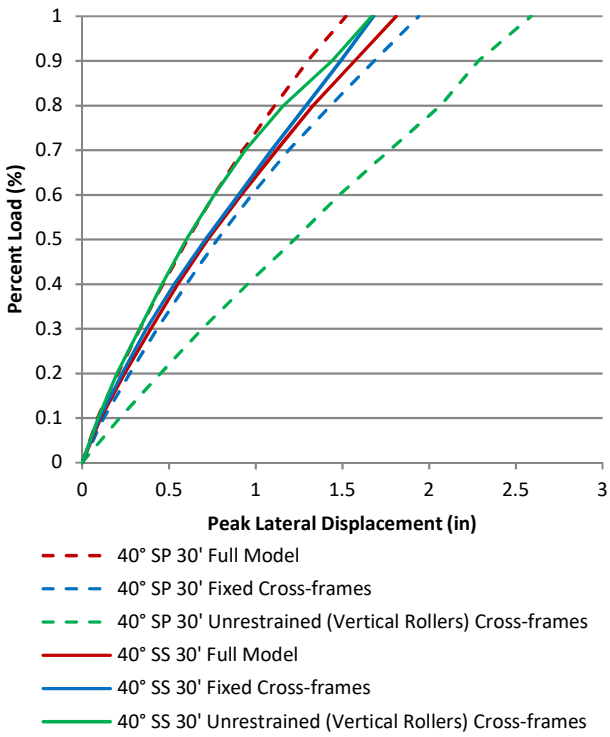

Figure E.12 Top flange percent load vs. peak lateral displacement in Span 1 – exterior girder (G4)

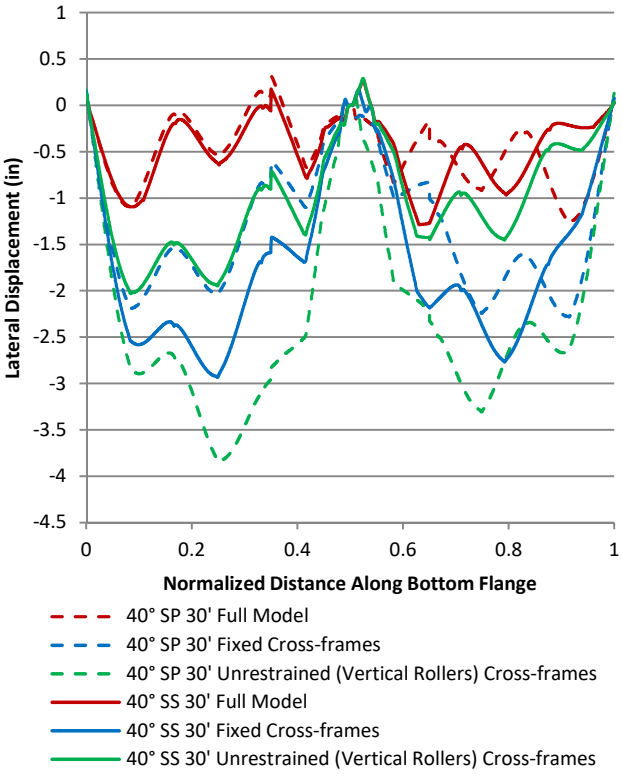

Figure E.13 Bottom flange lateral displacement along entire bridge – exterior girder (G4)

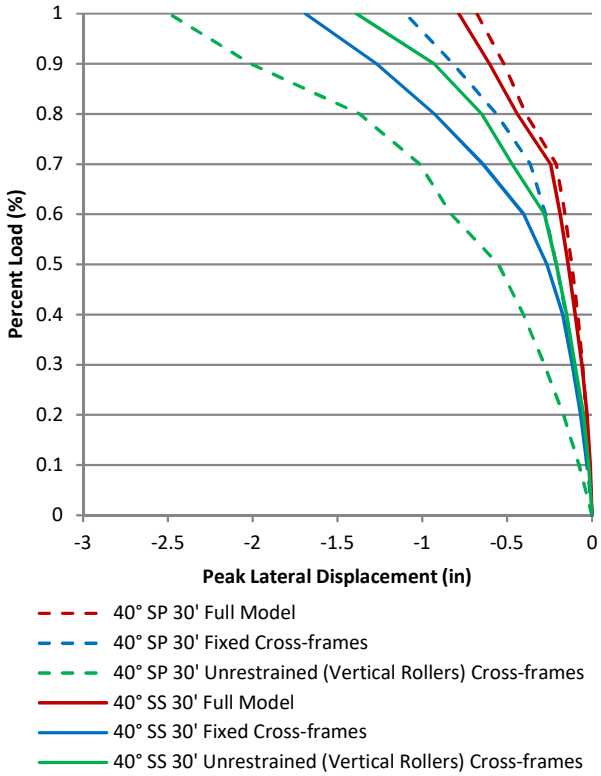

Figure E.14 Bottom flange percent load vs. peak lateral displacement in Span 1 – exterior girder (G4)

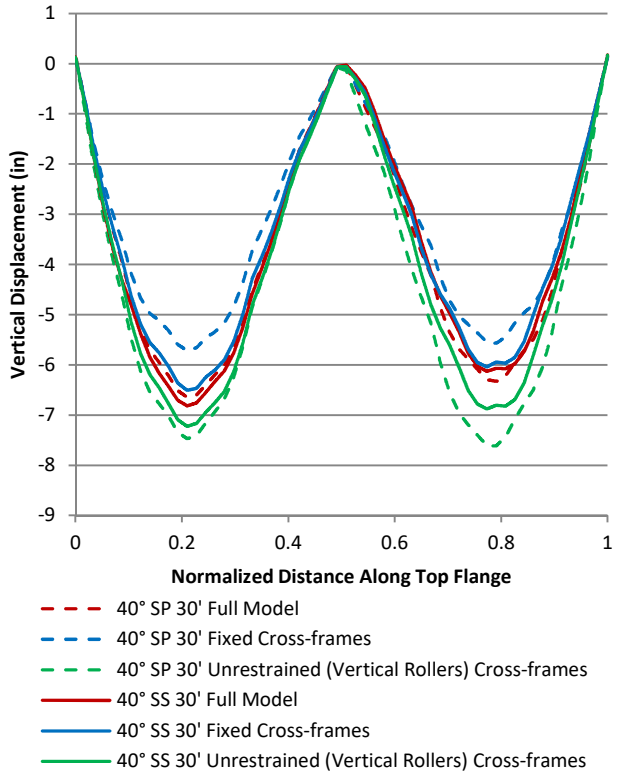

Figure E.15 Top flange vertical displacement along entire bridge – exterior girder (G4)

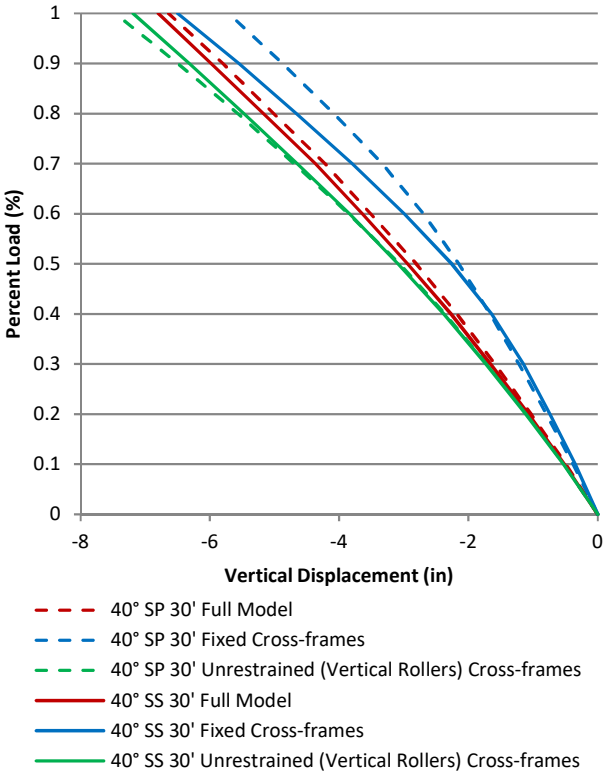

Figure E.16 Top flange load vs. peak vertical displacement in Span 1 – exterior girder (G4)

Figure E.17 and Figure E.18 shows the interior girder top flange lateral displacement at full load along the entire bridge and the percent load versus peak lateral displacement in Span 1, respectively. Again, Span 1, which has similar brace locations for varying cross-frame orientations, is labeled in Figure 3.12 of Part 3. The full bridge model and single girder models with fixed cross-frames and unrestrained cross-frames are shown for the 40 degree skewed-staggered and skewed-parallel bridges with 9.17 m [30 ft] cross-frame spacing. For the interior girder, the 40 degree skewed-staggered full bridge model produced the largest lateral displacement while the 40 degree skewed-parallel model with fixed cross-frames produced the smallest top flange lateral deflection. The skewed-staggered model with fixed cross-frames deflected in reverse to that of the full bridge system model. The unrestrained cross-frame single girder models produced large deflections at the abutments, which was not seen in the exterior girder. Conversely, the fixed cross-frame single girder models produced the smallest deflections at the abutments. While the magnitude of deflections were similar between the interior and exterior girders, the cross-frame boundary condition had a much greater effect on the interior girder at the abutments than the exterior girder.

Figure E.19 and Figure E.20 shows the interior girder bottom flange lateral displacement at full load and the percent load versus peak vertical displacement in Span 1. The full bridge model with cross-frames placed parallel to skewed produced the greatest bottom flange lateral displacements. As the cross-frames are aligned in the skewed-parallel model, lateral load from the exterior girder has a direct path to the interior girder through the cross-frames. Therefore, the large overhang loads from the exterior girder would also cause larger deflections in the interior

girder of the skewed-parallel model. As revealed previously, modeling the cross-frame boundary conditions alone is not enough to capture the force interactions between girder systems.

Figure E.21 and Figure E.22 shows the interior girder top flange vertical displacement at full load and the percent load versus peak vertical displacement in Span 1, respectively. Here, the fixed cross-frame single girder model produced significantly lower vertical displacements in the compared to the other models. Similar to the exterior girder, the unrestrained cross-frame model had the largest displacements. Overall, both the fixed cross-frame and the unrestrained cross-frame single girder models were unable to capture girder systems behavior.

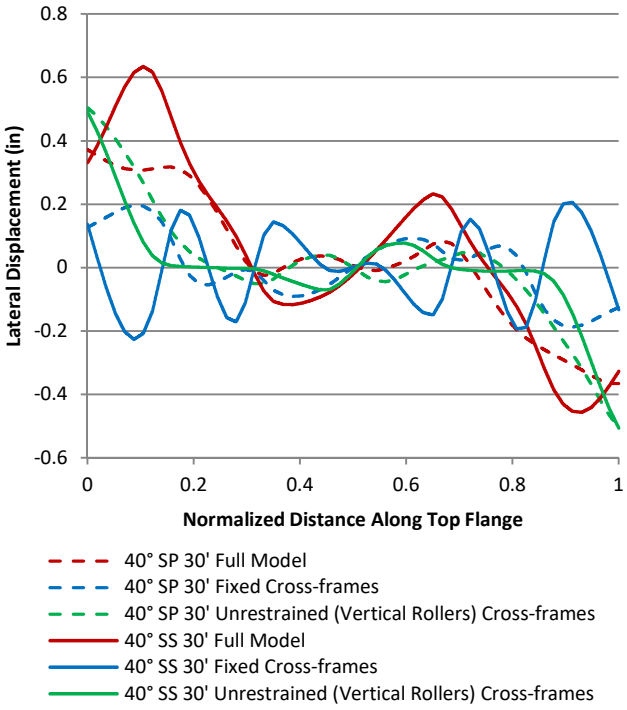

Figure E.17 Top flange lateral displacement along entire bridge – interior girder (G3)

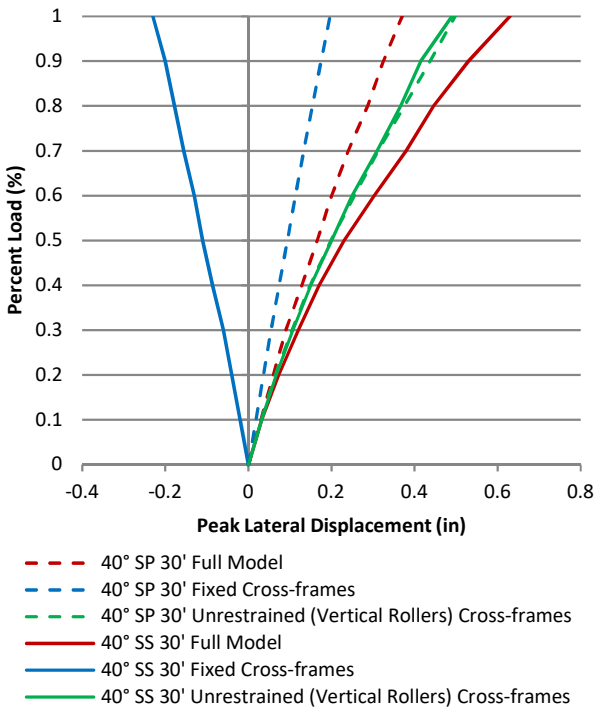

Figure E.18 Top flange percent load vs. peak lateral displacement in Span 1 – interior girder (G3)

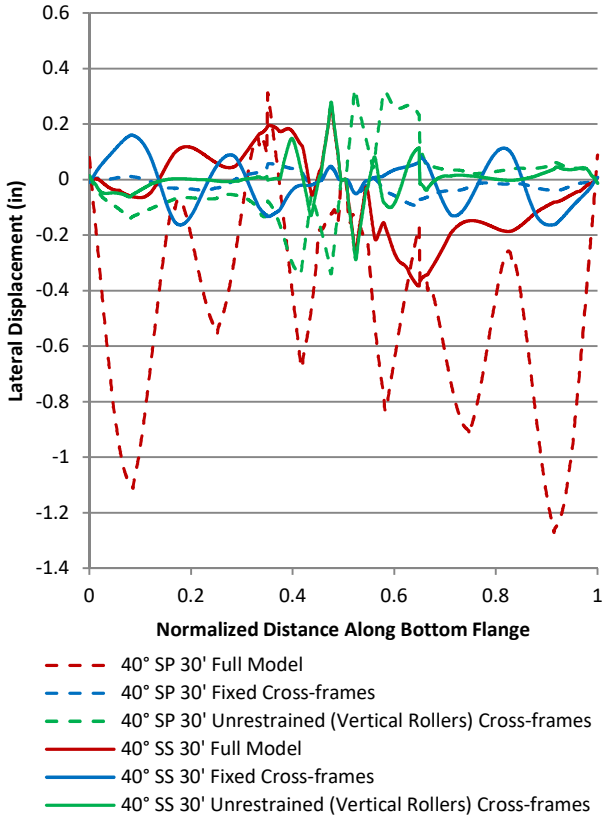

Figure E.19 Bottom flange lateral displacement along entire bridge – interior girder (G3)

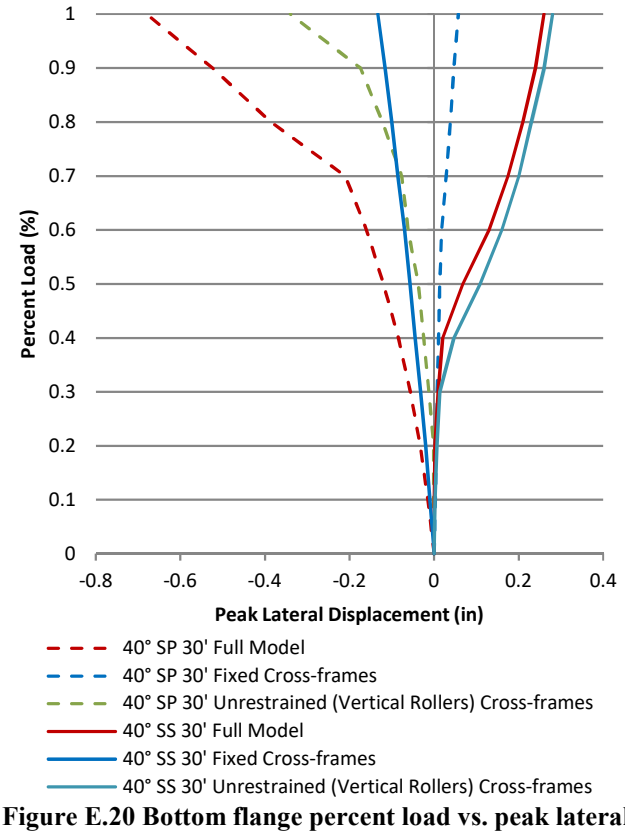

Figure E.20 Bottom flange percent load vs. peak lateral displacement in Span 1 – interior girder (G3)

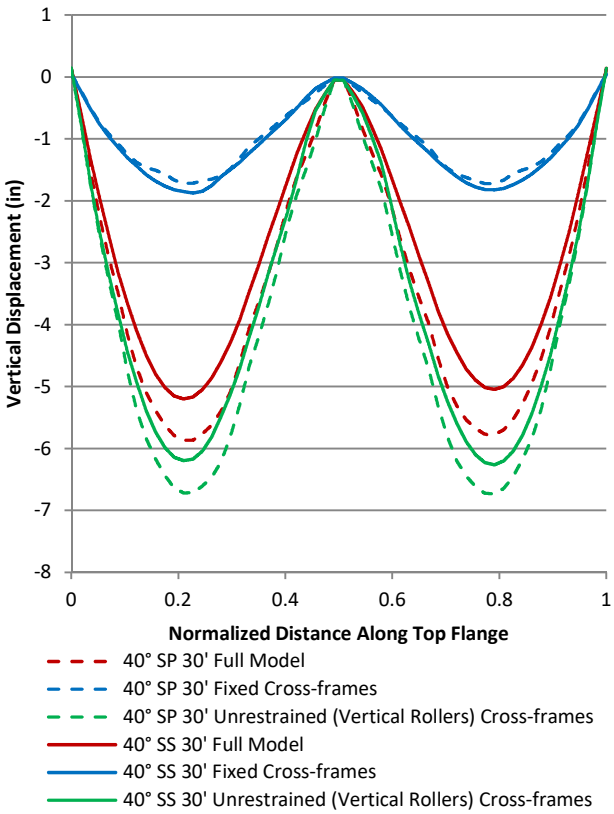

Figure E.21 Top flange vertical displacement along entire bridge – interior girder (G3)

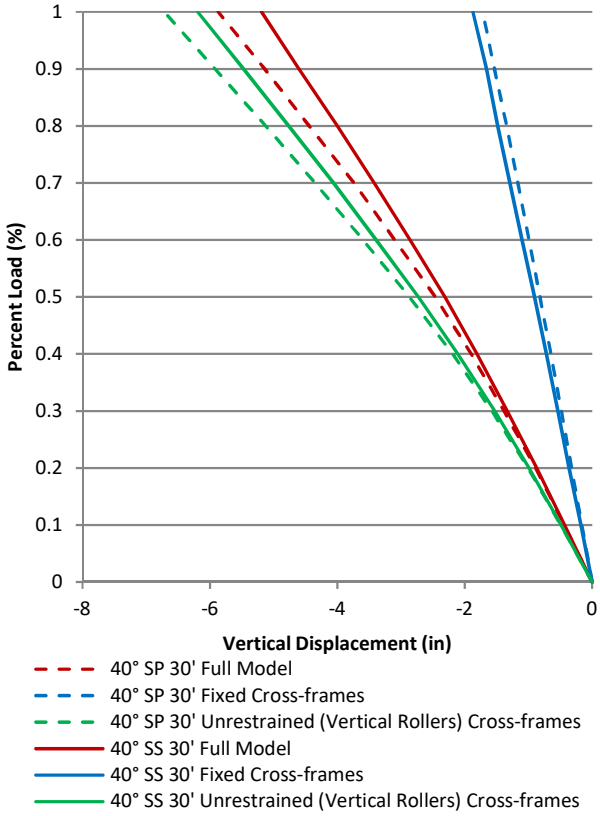

Figure E.22 Top flange load vs. peak vertical displacement in Span 1 – interior girder (G3)

Figure E.23 through Figure E.26 shows the top flange, bottom flange, and weak-axis out-of-plane bending stress along with the strong-axis bending stress in the exterior girder. The full bridge model and single girder models with fixed cross-frames and unrestrained cross-frames are shown. Stress differences between the varying models were small relative to peak stress levels in the exterior girder. The full bridge model typically produced smaller stresses compared to the single girder models. Due to the high magnitude of lateral load in the exterior girder from the overhangs, the cross-frame boundary condition had little effect on the stresses in the exterior girder.

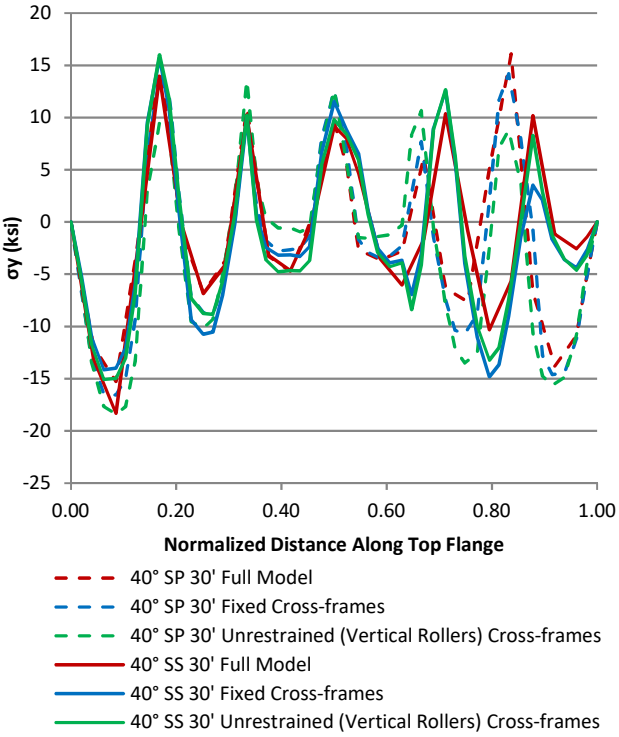

Figure E.23 Top flange out-of-plane stresses – exterior girder (G4)

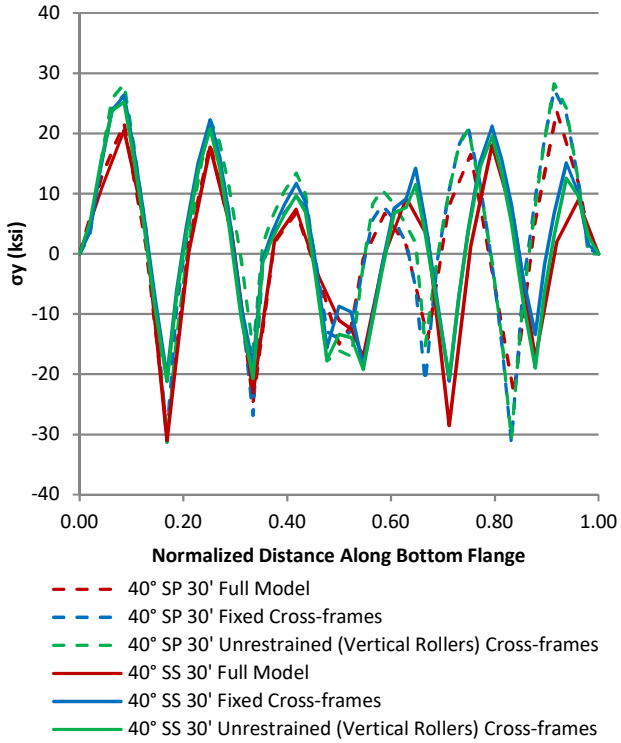

Figure E.24 Bottom flange out-of-plane stresses – exterior girder (G4)

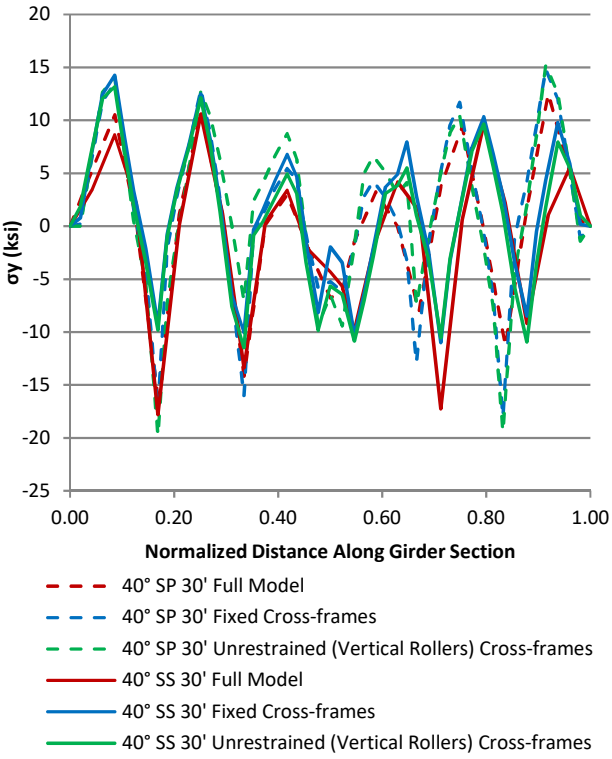

Figure E.25 Weak-axis out-of-plane stresses – exterior girder (G4)

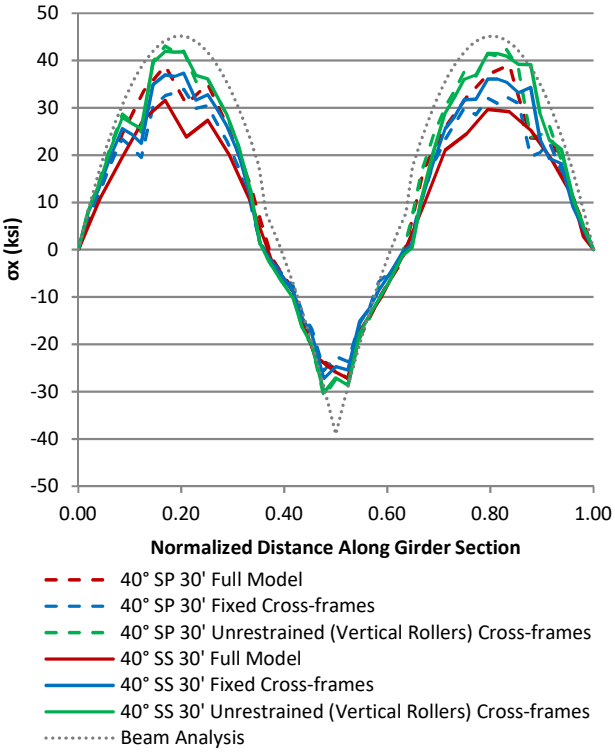

Figure E.26 Strong-axis in-plane stresses – exterior girder (G4)

Figure E.27 through Figure E.30 shows the top flange, bottom flange, and weak-axis out-of-plane bending stress along with the strong-axis bending stress in the interior girder. The full bridge model and single girder models with fixed cross-frames and unrestrained cross-frames are shown for the 40 degree skewed-staggered and skewed-parallel models with 9.17 m [30 ft] cross-frame spacings. The skewed-staggered single girder model with fixed cross-frames produced the largest out-of-plane bending stresses. As discussed previously, since the cross-frames are not aligned, lateral load is transferred through bending of flanges. Less flexible cross-frame connections transferred more load through bending of the flanges. The magnitude and direction of out-of-plane bending stresses are also different for varying cross-frame connection types. For vertical bending stress, the unrestrained cross-frame models produced the largest stresses and the fixed cross-frame models produced the smallest stresses, even at mid-span. Single girder model

stresses ranged widely and had little correlation with the full bridge model stresses for the interior girder.

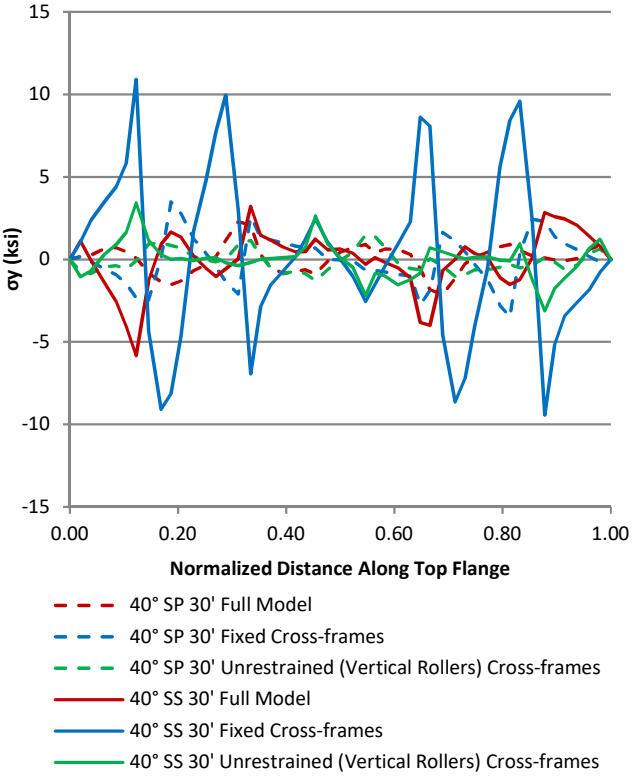

Figure E.27 Top flange out-of-plane stresses – interior girder (G3)

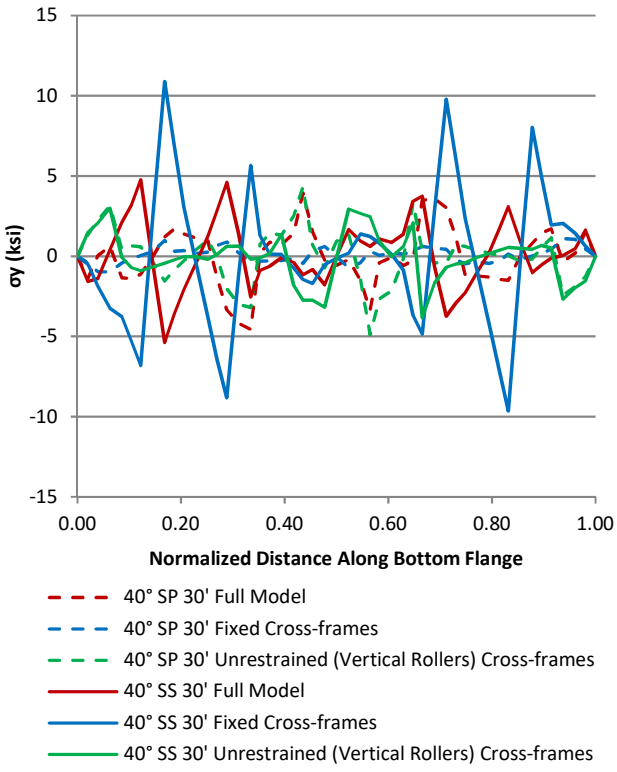

Figure E.28 Bottom flange out-of-plane stresses – interior girder (G3)

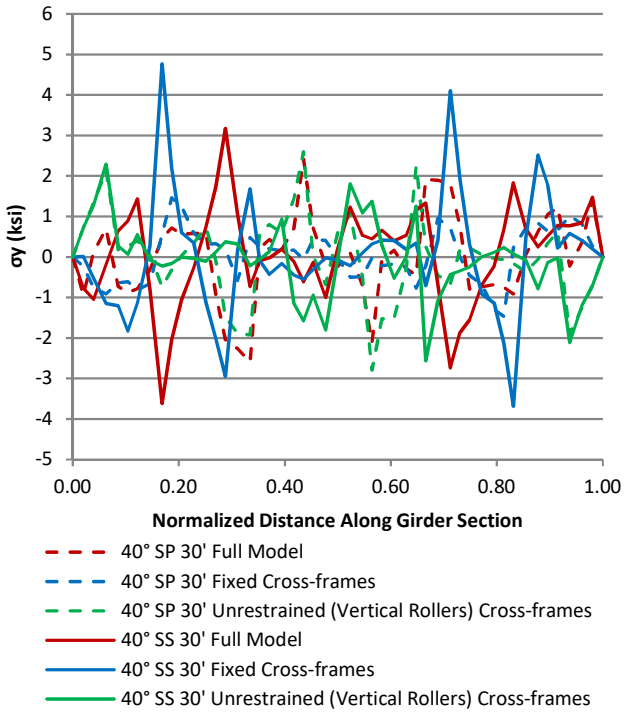

Figure E.29 Weak-axis out-of-plane stresses – interior girder (G3)

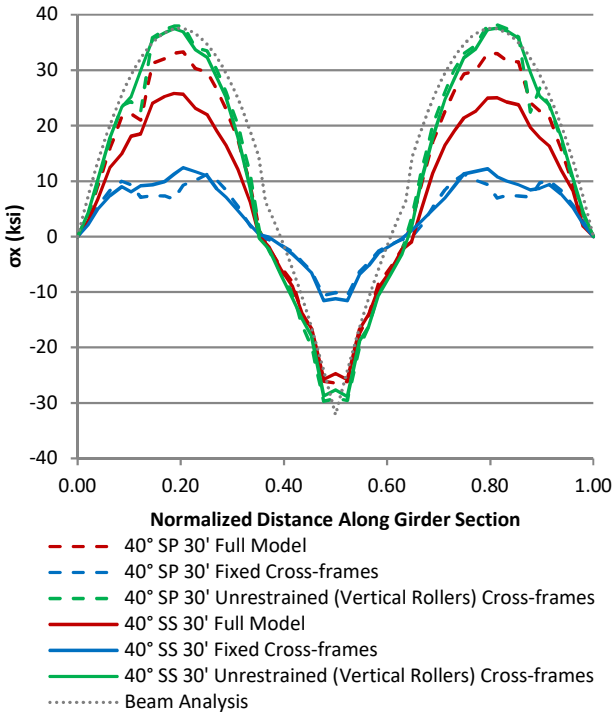

Figure E.30 Strong-axis in-plane stresses – interior girder (G3)

In order to capture cross-frame fixities with stiffnesses between that of the fully fixed and fully unrestrained conditions, springs were used as boundary conditions on the same surface as shown in Figure E.1 and Figure E.2. The exterior girder was selected to compare the effects of these connections as cross-frames are only on one side of the girder, reducing the number of different cross-frame boundary conditions. To determine the relative stiffness used at these boundary conditions, a model of the interior beam was created in Mastan2 (Ziemian and McGuire 2000). From the beam-line analysis, stiffness, k, was calculated from the following equations:

$$F = \sigma A = kx$$

$$\sigma = Mc/I$$

$$k = \sigma A/x$$

where:

F = force

σ = stress

A = cross-sectional area

k = stiffness

x = vertical displacement

M = sectional bending moment

c = distance from the extreme fiber to the neutral axis

I = moment of inertia of the section

Table E.1 shows the displacement, moment, calculated stress, force, and calculated stiffness at 4.57 m [15 ft] cross-frame spacings for the interior girder of the skewed-parallel bridge. Cross-frames in the skewed-parallel model are connected at constant spacings for all girders. For cross-frames spaced at 9.17 m [30 ft], the cross-frame connection nearest the abutment would have a stiffness of 51.3 MN/m [293 k/in] and the cross-frame connection nearest the center pier would have a stiffness of 13.8 MN/m [79 k/in]. Cross-frame boundary conditions with only spring fixies and fixed or unrestrained constraints removed are labeled as k=0.75, k=79, k=293, and k=variable in the graphs below. The value of k represents the cross-frame spring stiffness constrained in all three axes. Spring fixities in the vertical axis only were used in conjunction with vertical rollers that are fixed in the out-of-plane direction; these are labeled in the graphs below as unrestrained+ky= followed by the cross-frame spring stiffness. Cross-frame spring stiffnesses labelled as k=variable or ky=variable uses the stiffness shown in Table E.1 at each given cross-frame location.

Figure E.32 shows the full bridge model of the 40 degree skewed-parallel bridge with 13.7 m [45 ft] cross-frame spacing. Figure E.33 shows the exterior girder model of the 40 degree skewed-parallel bridge with 13.7 m [45 ft] cross-frame spacing. Vertical rollers and variable

stiffness springs in the vertical direction were used as the cross-frame boundary condition. The color map shows Mises stress limits from 0 to 345 MPa [50 ksi] and appear similar between the exterior girder of the full bridge model and the single girder model. The single girder model also captures the large lateral deflections in the first and last spans.

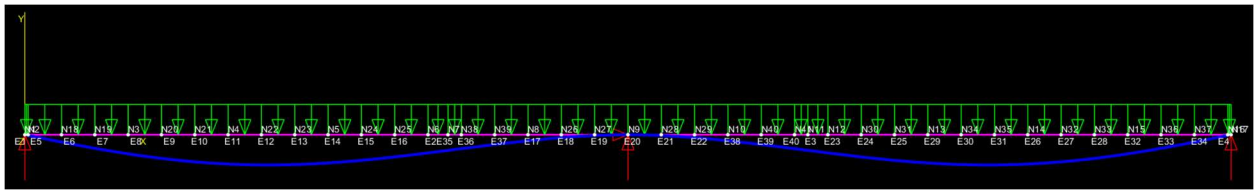

Figure E.31 Moment diagram for interior beam model

Table E.1 Calculated beam stiffness for the interior girder at cross-frame locations along the bridge

Position	Δ (in)	M (k-in)	σ (ksi)	F (k)	k (k/in)
0.09	-3.42	12892	29.39	1138.77	332.84
0.17	-5.25	17400	39.66	1536.97	292.85
0.25	-5.06	14071	32.08	1242.91	245.69
0.33	-3.25	2904	6.62	256.48	78.83
0.42	-1.08	-16293	-14.21	-937.83	-864.44
0.50	0.00	-43916	-38.30	-2527.81	Pier Fixed
0.58	-1.08	-16293	-14.21	-937.83	-864.44
0.67	-3.25	2904	6.62	256.48	78.83
0.71	-4.30	9467	21.58	836.22	194.64
0.75	-5.06	14071	32.08	1242.91	245.69
0.79	-5.40	16715	38.10	1476.46	273.28
0.83	-5.25	17400	39.66	1536.97	292.85
0.87	-4.58	16126	36.76	1424.43	311.34
0.91	-3.42	12892	29.39	1138.77	332.84

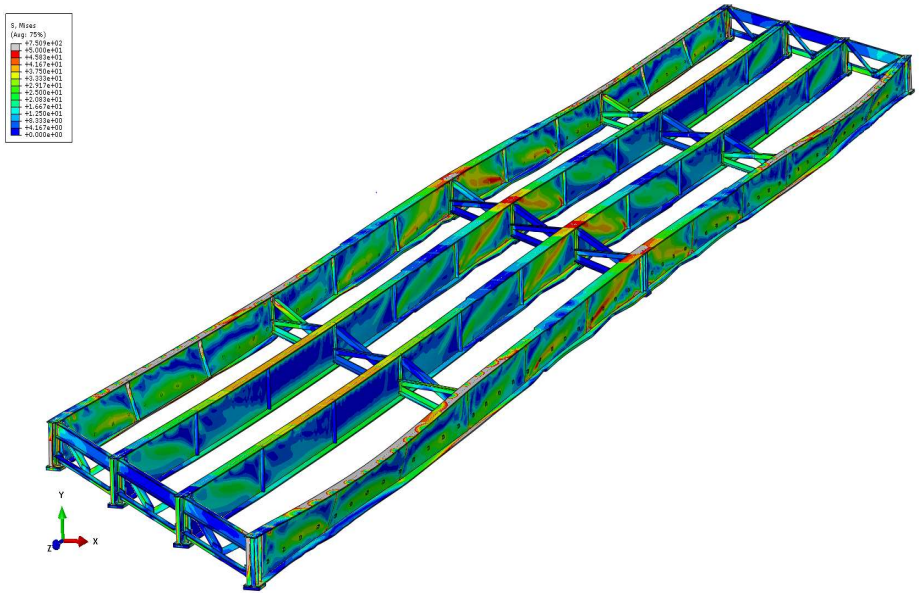

Figure E.32 40 degree skewed-parallel bridge with 13.7 m [45 ft] cross-frame spacing – full bridge model

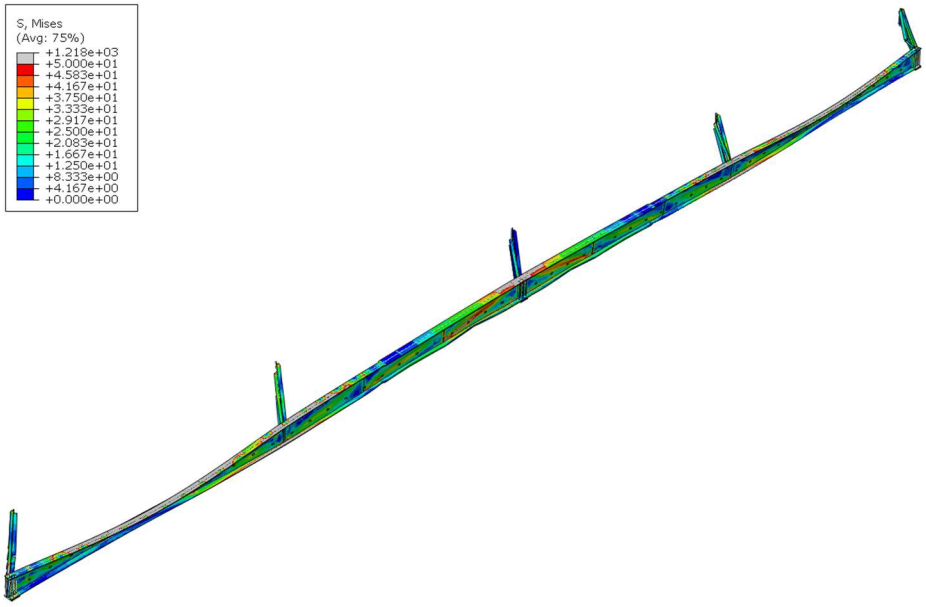

Figure E.33 40 degree skewed-parallel bridge with 13.7 m [45 ft] cross-frame spacing – exterior girder with vertical rollers and variable spring stiffness boundary conditions in the vertical axis.

Figure E.34 through Figure E.36 shows the exterior girder top and bottom flange lateral displacement and top flange vertical displacement at full load along the entire bridge. The full bridge model and single girder models with varying cross-frames boundary condition stiffnesses

are presented for the 40 degree skewed-parallel bridge. A single cross-frame configuration and spacing was selected in order to compare the different variations in cross-frame boundary conditions. Cross-frames with fixed, unrestrained, and varying spring stiffness fixities were analyzed. Variable stiffness springs were used to compare cross-frame fixities between that of the fully fixed or fully unrestrained condition.

Figure E.34 shows the top flange lateral displacement in the exterior girder. The full bridge model produced the smallest deflections. Cross-frames with fixed or spring fixities greater than 131 kN/m [0.75 k/in] produced the next largest peak deflections. Cross-frames with vertical rollers or a spring stiffness of 131 kN/m [0.75 k/in] produced the largest deflections. This shows that girders in the full bridge system will distribute load across the bridge and reduce total lateral deflection. Therefore, girder-to-girder interactions cannot be captured in single girder models through cross-frame fixities alone.

Figure E.35 shows the bottom flange lateral displacement in the exterior girder. Similar to the top flange, the full bridge model produced the smallest lateral deflections while the cross-frames with vertical rollers produced the largest deflections. The single girder model with fully fixed cross-frame boundary conditions produced deflections between that of the full bridge model and that of the unrestrained cross-frames model. Cross-frames with variable stiffness springs produced lateral deflections smaller than cross-frames fixed conditions but only by a little amount. Cross-frames with vertical rollers and springs in the vertical direction produced deflections closest to the full bridge model. This show that using a small vertical restraint with vertical rollers will reduce bottom flange lateral direction significantly, possibly through a change in load path compared to the vertical roller condition alone.

For vertical deflection in the top flange, shown in Figure E.36, the fixed cross-frames condition had the smallest deflections. The unrestrained cross-frame with or without vertical axis springs and the cross-frame with low 131 kN/m [0.75 k/in] spring stiffnesses had the largest displacements. The full bridge model and cross-frames with spring stiffnesses greater than 131 kN/m [0.75 k/in] produced deflections between that of the fixed and unrestrained cross-frame models.

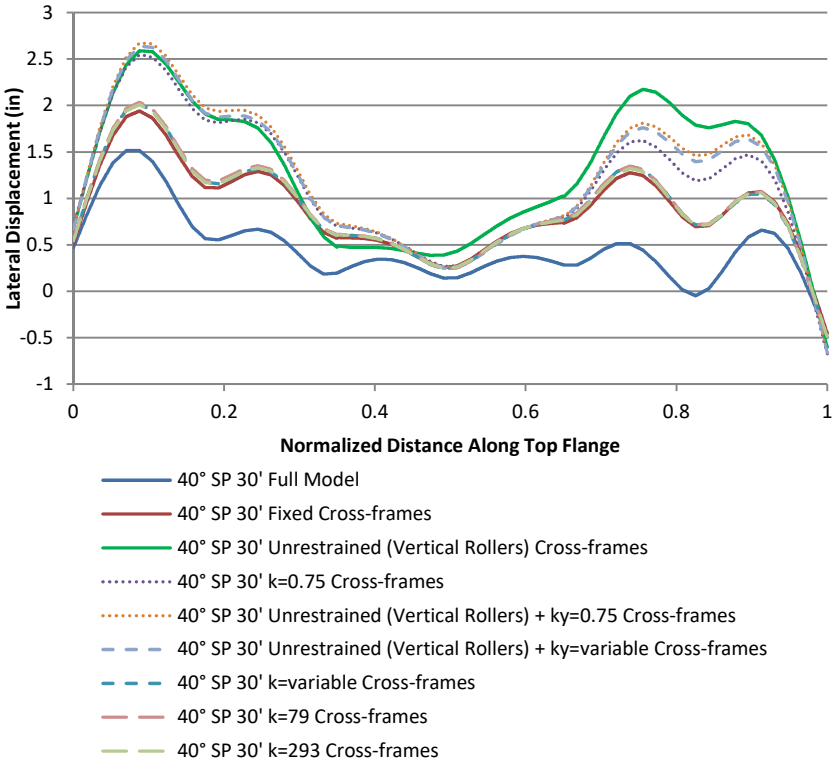

Figure E.34 Top flange lateral displacement along entire bridge - exterior girder (G4)

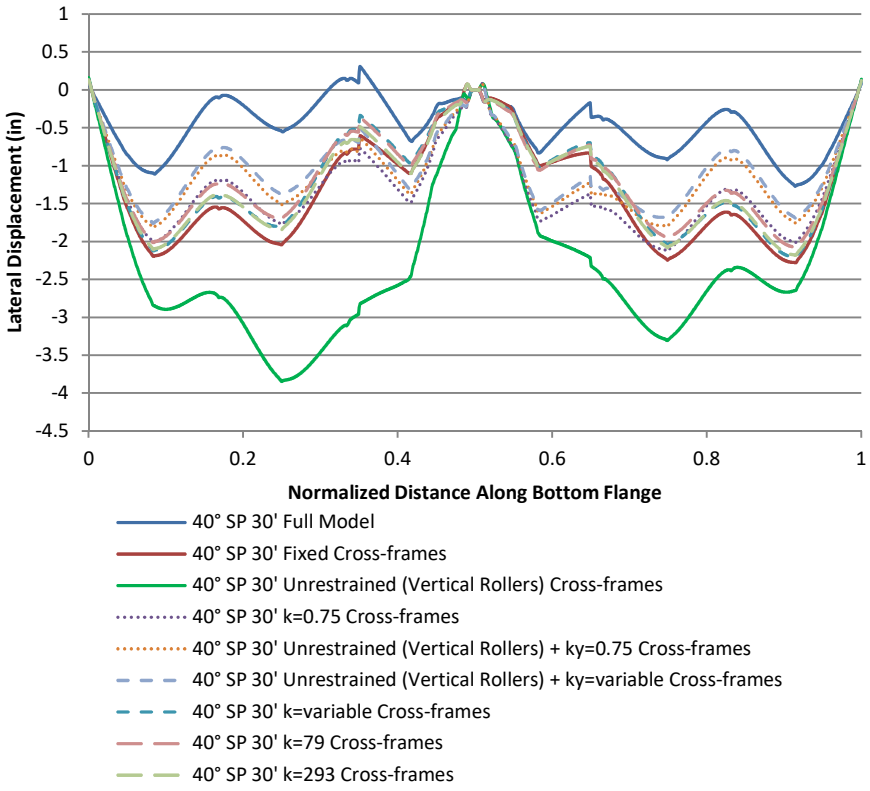

Figure E.35 Bottom flange lateral displacement along entire bridge - exterior girder (G4)

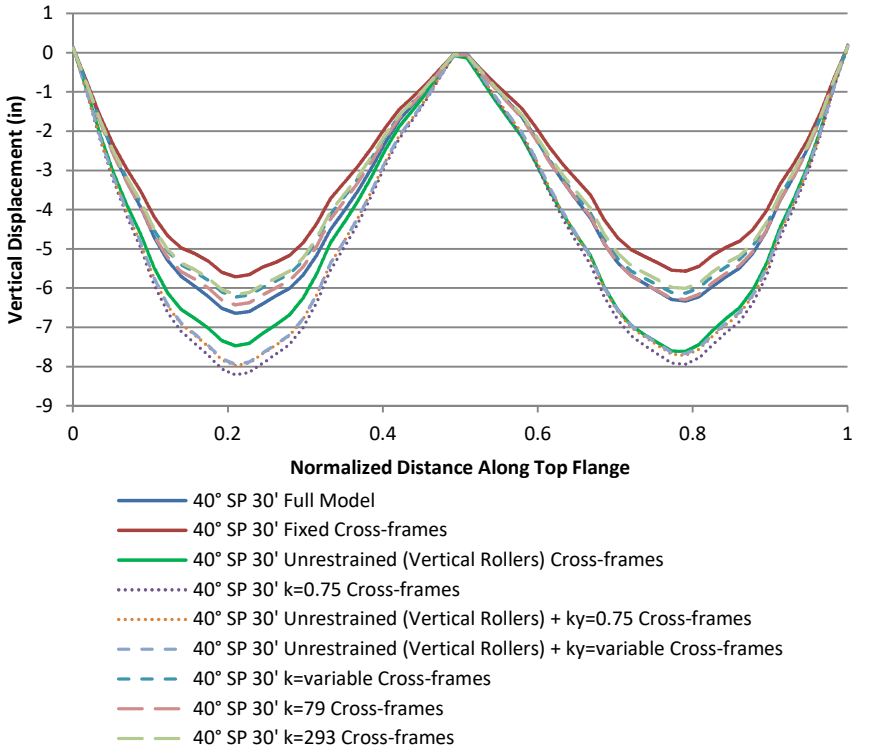

Figure E.36 Top flange vertical displacement along entire bridge - exterior girder (G4)

Figure E.37 through Figure E.39 shows the exterior girder top and bottom flange lateral displacement and top flange vertical displacement at full load along the entire bridge. The full bridge and single girder models are shown for the 20 and 40 degree skewed-parallel bridge with 9.17 m [30 ft] and 13.7 m [45 ft] cross-frame spacings. The unrestrained cross-frame fixities with variable stiffness springs in the vertical axis was selected as the representative condition to compare the effects of skew angle and cross-frame spacing on girder displacements.

Figure E.37 shows the top flange lateral displacement in the exterior girder. As expected, the 13.7m [45 ft] cross-frame spacing model produced larger deflections than the 9.17 m [30 ft] cross-frame spacing model. With the exception of the 20 degrees skewed-parallel bridge with cross-frames spaced at 13.7 m [45 ft], models with cross-frames skewed at 40 degrees produced higher lateral deflections than models with cross-frames skewed at 20 degrees. In addition, the single girder model with unrestrained cross-frame boundary condition had significantly larger deflections compared to its respective full bridge model.

Figure E.38 shows the bottom flange lateral displacement in the exterior girder. For the bottom flange, the full bridge models with 20 degree skew produced the same deflection as the full bridge models with 40 degree skew. For single girder models, cross-frames with 20 degree skews produced larger deflections than girders with 40 degree skewed cross-frames. Similar to the top flange, cross-frames spaced at 13.7m [45 ft] produced larger deflections than cross-frames spaced at 9.17 m [30 ft]. Again, the single girder model with unrestrained cross-frame boundary condition had significantly larger deflections than its respective full bridge model.

Figure E.39 shows the top flange vertical deflection in the exterior girder. Results showed a similar pattern to top flange lateral displacement. The 13.7m [45 ft] cross-frame spacing model produced larger deflections than the 9.17 m [30 ft] cross-frame spacing model. With the

exception of the full bridge model with cross-frames skewed at 20 degrees and spaced at 13.7 m [45 ft], models with cross-frames skewed at 40 degrees produced higher lateral deflections than models with cross-frames skewed at 20 degrees. The single girder model with unrestrained cross-frame boundary condition also had significantly larger deflections compared to its respective full bridge model.

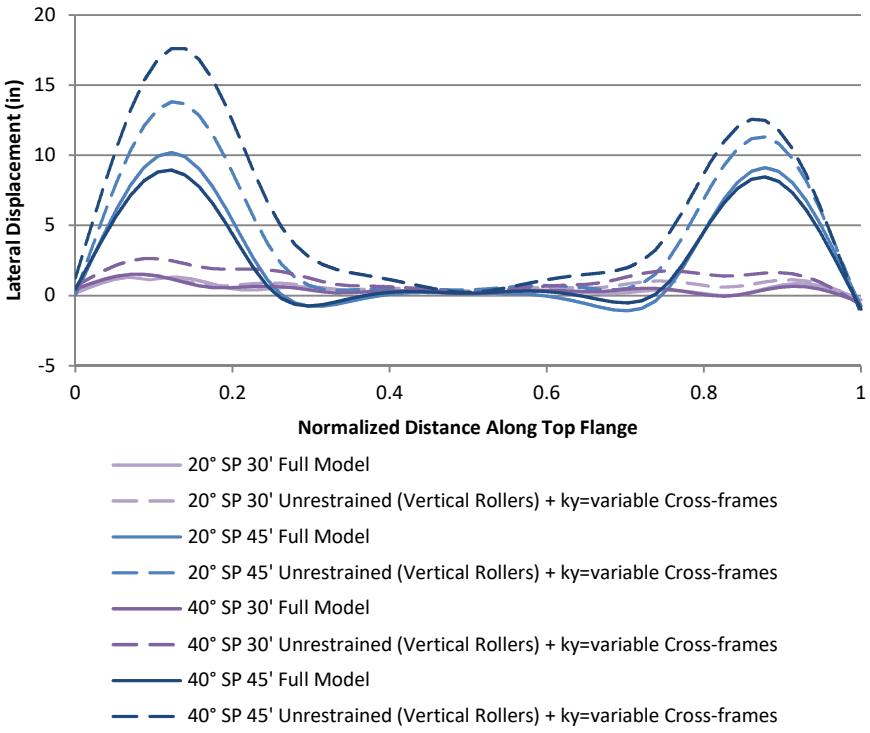

Figure E.37 Top flange lateral displacement along entire bridge - exterior girder (G4)

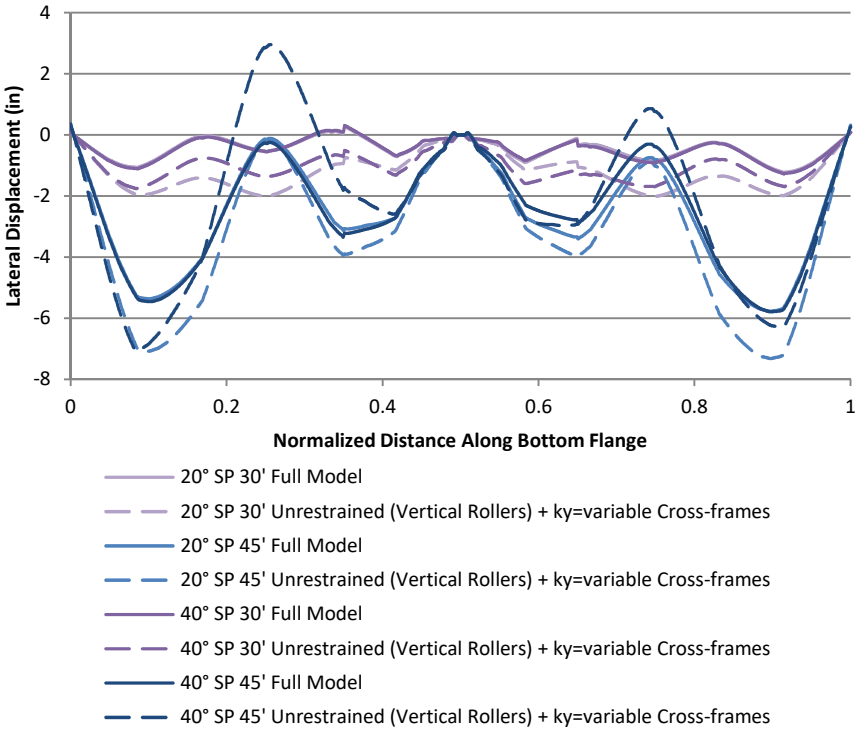

Figure E.38 Bottom flange lateral displacement along entire bridge - exterior girder (G4)

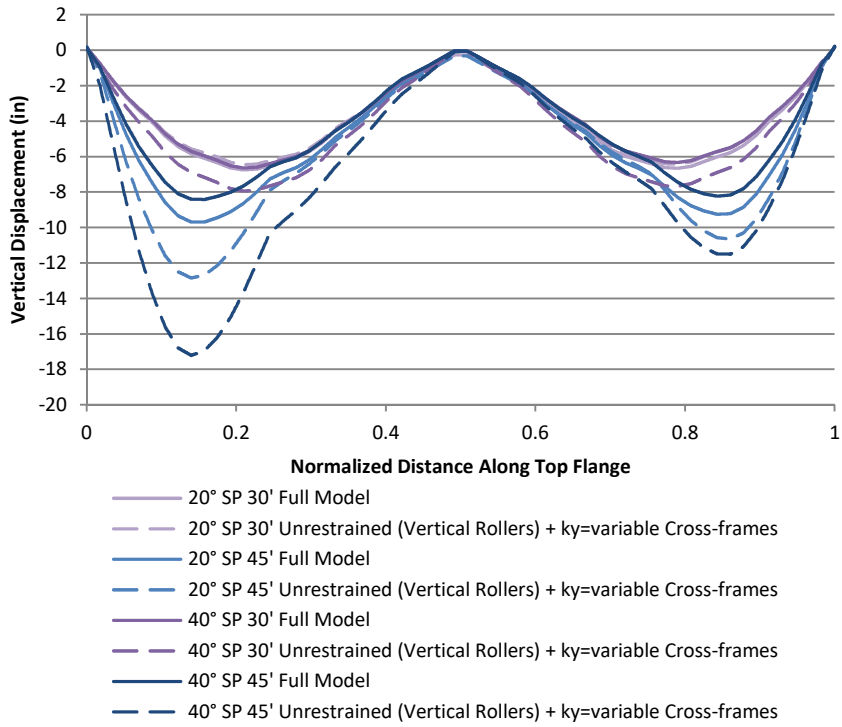

Figure E.39 Top flange vertical displacement along entire bridge - exterior girder (G4)

REFERENCES

Ziemian, R. D. and McGuire, W. (2000). Mastan2 Version 3.5. http://www.mastan2.com

APPENDIX F: CROSS-FRAME ANGLE WORK POINT FRAMING

This study was performed to provide insight into how the cross-frame/diaphragm framing detail and location of the work points affects girder behavior in a skewed bridge system. The work point is the intersection of the center of gravity lines of the members. When detailing cross-frames as a truss with equal or unequal angle members, the bolt gage line may be used rather than the center of gravity lines to simplifying the detailing process. These two lines are typically very close and so the eccentricity caused is usually negligible. For cross-frames bracing the girders, a work point of the angle members framing into the center of gravity lines of the web and flange will brace the flanges against lateral torsional buckling without causing eccentric forces through bending of the stiffeners or web. This will allow for more efficient force transfer and help reduce distortion induced fatigue due to the flexibility of the braces.

However, to accommodate the required positioning and provide a means of connection, gusset plates are typically used. While eccentricities in the main framing members may be removed, this may cause eccentricities in the bolts or welds that the gusset plates connect to. Avoiding the eccentricity on the gusset plate may result in eccentricities in other members and connections for which they may not have been designed. Accommodation for the ease of fabrication and erection will also apply. Member positioning and connections will depend on clearances for conduits, downspouts, catwalks, inspection railing, and other items that span along the girder.

The 40 degree skewed-staggered bridge model with 13.7 m [45 ft] cross-frame spacing was selected to study how variation in the cross-frame member framing and work point position affect top flange lateral deflection, girder bending stresses, and cross-frame member stresses. It

was found that lateral load transferred through the cross-frames were relatively small for cross-frames spaced at 4.57 m [15 ft] and 9.14 m [30 ft] and therefore the 13.7 m [45 ft] spacing was selected to amplify the force transferred through the cross-frame system. Cross-frames placed perpendicular to the girder line was selected because a larger component of the lateral load is transferred through the cross-frames compared to cross-frames placed parallel to skew.

The bridge geometry, modeling methodology, applied loads, and boundary conditions are described in Part 3. Figure F.1 and Figure F.2 shows the two sides of the cross-frame as described in Part 3 of this paper while Figure F.3 and Figure F.4 shows an alternate cross-frame used for the comparison. Gusset plates allow for the connection of the angle members to the stiffeners at a steeper angle of incline. The diagonals and bottom chord framing dimensions are provided at the center of the angle members from the top or bottom of the stiffener along the face of the web. An L108 x 108 x 12.7 mm [L4-1/4 x 4-1/4 x 1/2 in.] angle was selected for the skewed-staggered bridge with a stiffener thickness of 9.5 mm [3/8 in.]. Cross-frame partitioning and meshing techniques used are detailed in Part 3. Overall, it was found that the alternate cross-frame shown in Figure F.3 and Figure F.4 did not have a significant effect on top flange lateral deflection, girder bending stresses, and cross-frame member stresses compared to the typical cross-frame used throughout the paper.

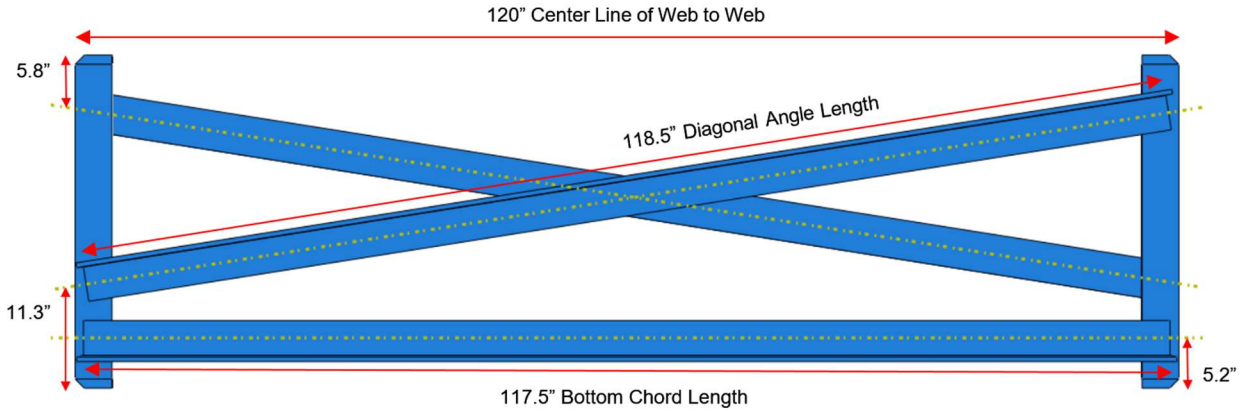

Figure F.1 Skewed-staggered cross-frame angle member framing dimensions as studied in Part 3

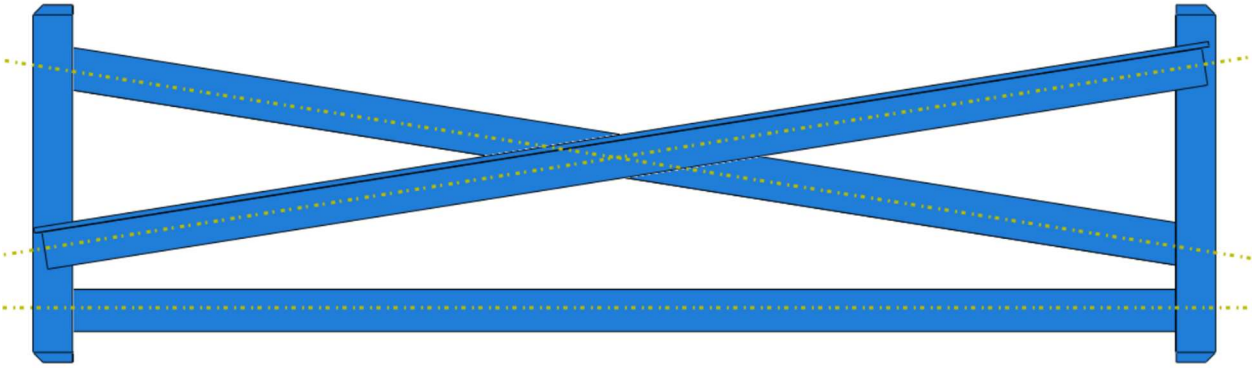

Figure F.2 Skewed-staggered cross-frame angle member framing dimensions as studied in Part 3 viewed from the other side

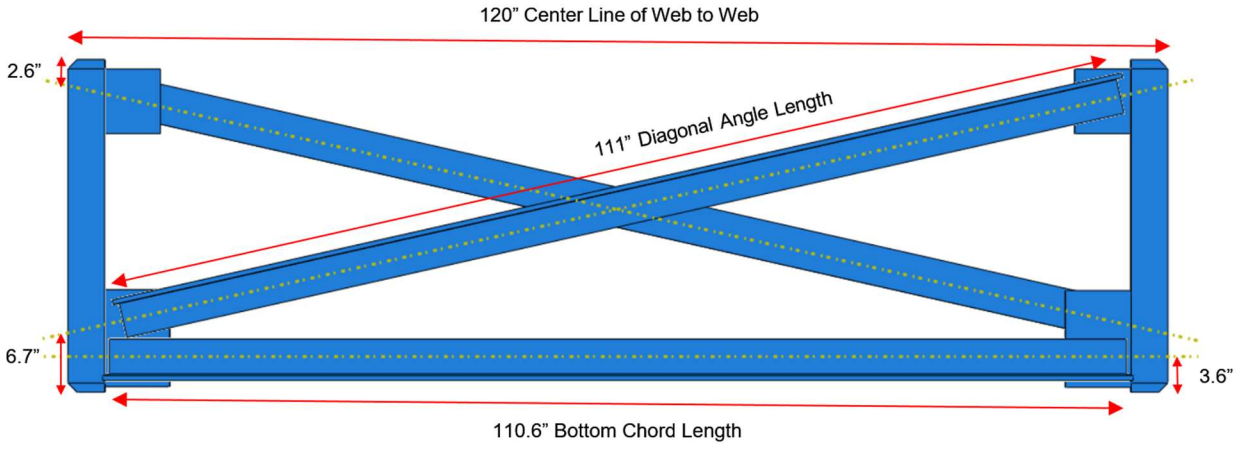

Figure F.3 Alternate cross-frame angle framing with dimensions

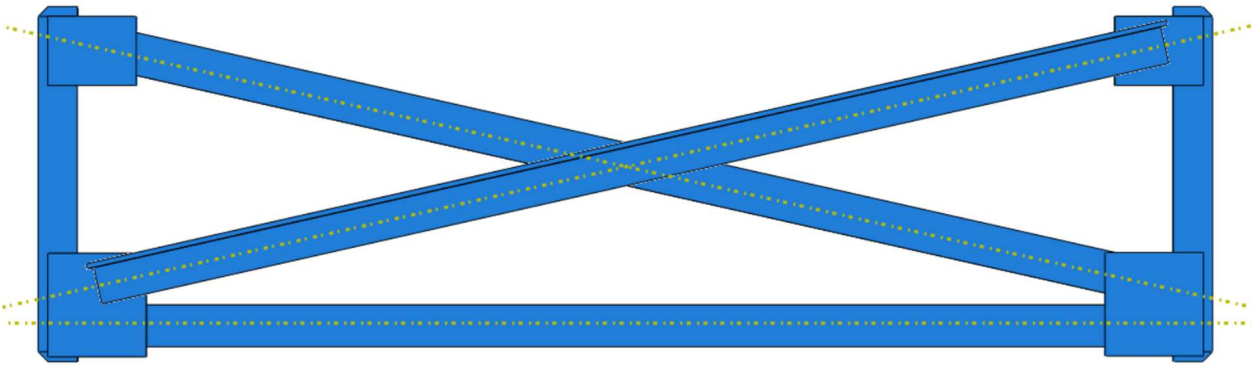

Figure F.4 Alternate cross-frame angle framing viewed from the other side

Figure F.6 shows the exterior girder top flange lateral displacement at full load along the entire length of the bridge. The typical cross-frame used throughout Part 3 is shown in blue-gray and the alternate cross-frame with gusset plates is shown in red. Top flange lateral displacements matched relatively closely throughout the girder length for both cross-frames selections. Figure F.7 shows the peak lateral displacement as a function of percent load in Span 1, labeled in Figure F.5. Figure F.8 shows the peak lateral displacement at full load, where the peak displacements occurred in Span 1. While the models with 13.7 m [45 ft] cross-frame spacings produced large magnitudes of displacement, the difference between the two models with varying cross-frames was only 11.7 mm [0.46 in].

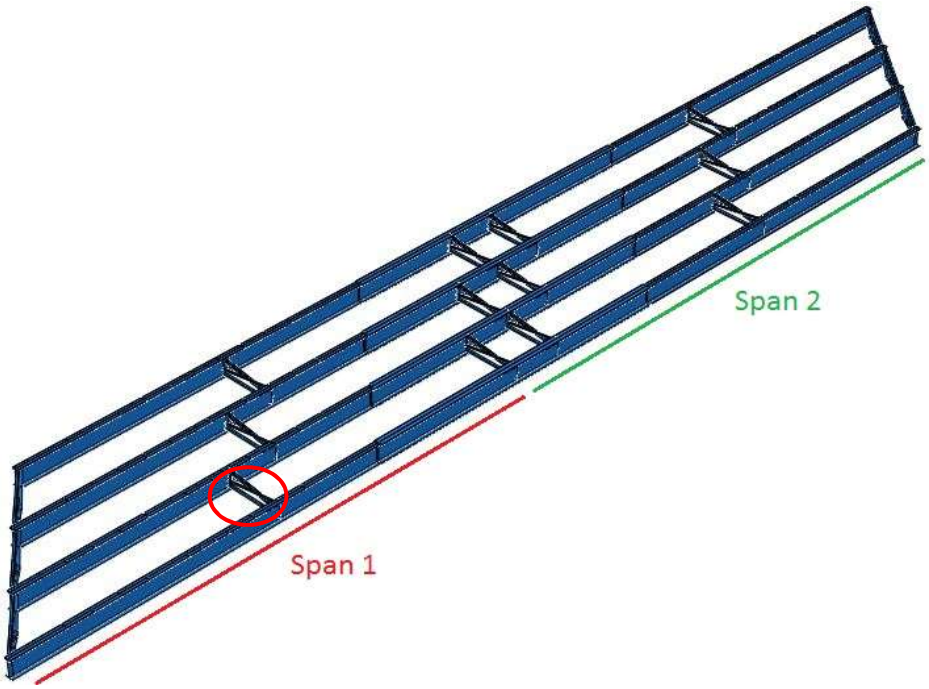

Figure F.5 Span label and cross-frame location corresponding to presented results for cross-frame stresses

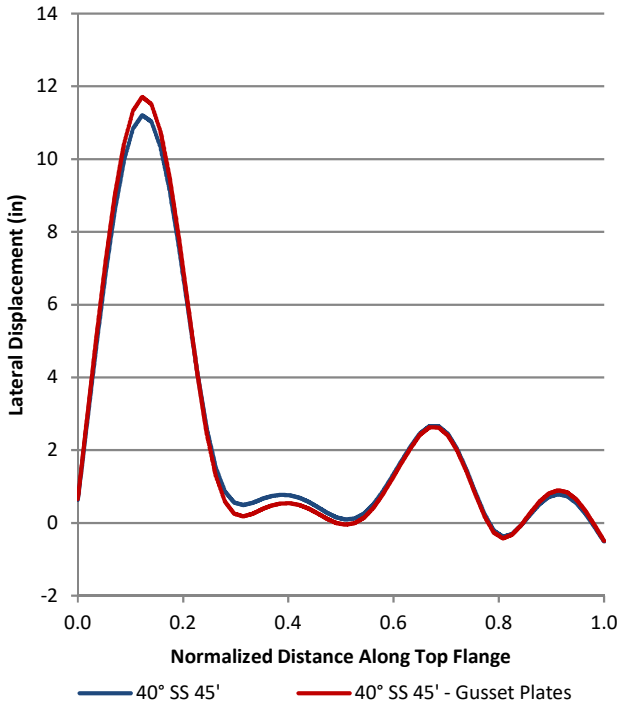

Figure F.6 Top flange lateral displacement along entire bridge – exterior girder (G4)

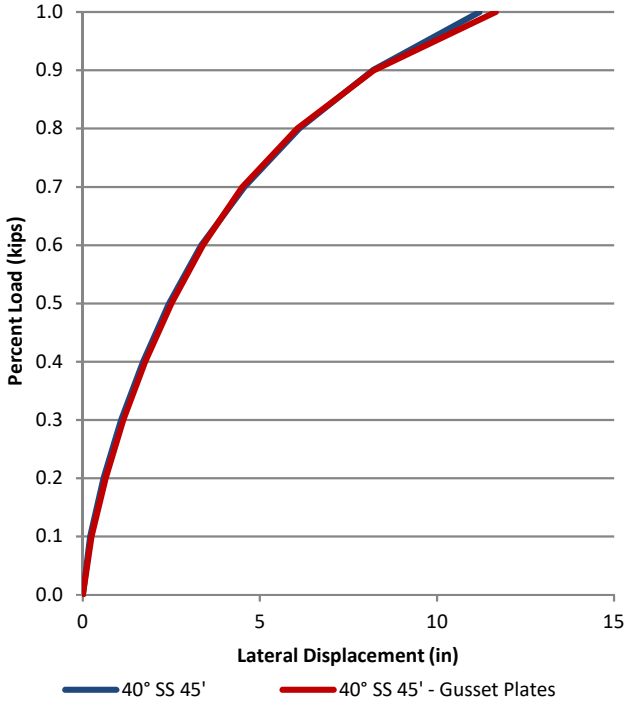

Figure F.7 Top flange percent load vs. peak lateral displacement in Span 1 – exterior girder (G4)

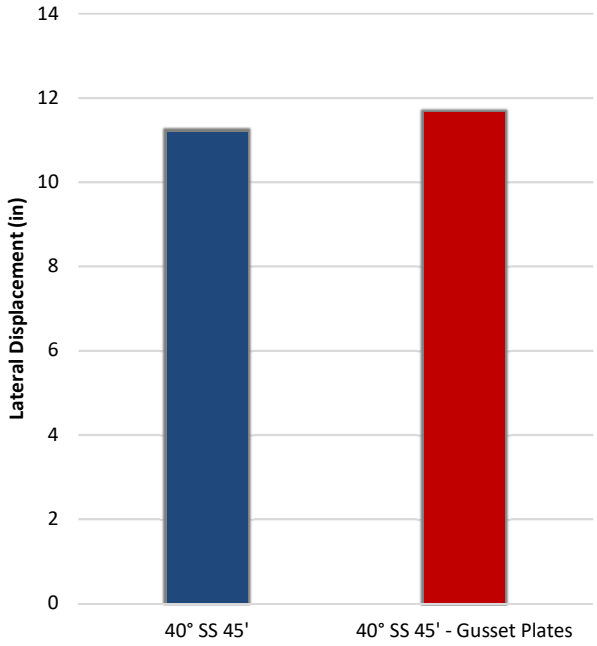

Figure F.8 Top flange peak lateral displacement at full load in Span 1 – exterior girder (G4)

Figure F.9 through Figure F.12 shows in-plane strong axis section and out-of-plane weak-axis section, top flange, and bottom flange bending stresses in the interior girder. Again, the typical cross-frame used throughout Part 3 is shown in blue-gray and the alternate cross-frame with gusset plates is shown in red. The strong axis bending stresses were almost identical between the two cross-frame selections. While the alternate cross-frame had a slightly greater effect on out-of-plane bending stresses of the interior girder, the overall magnitude of stress and pattern of behavior along the girder was relatively similar. The magnitude of stresses for out-of-plane bending was also very low.

Figure F.13 through Figure F.16 shows the exterior girder strong axis section and out-of-plane weak-axis section, top flange, and bottom flange bending stresses. Due to the large overturning load from the overhangs, both selection of cross-frames produced almost identical out-of-plane bending stresses in the exterior girder. As with the interior girder, strong axis bending stresses were almost identical between the two cross-frames.

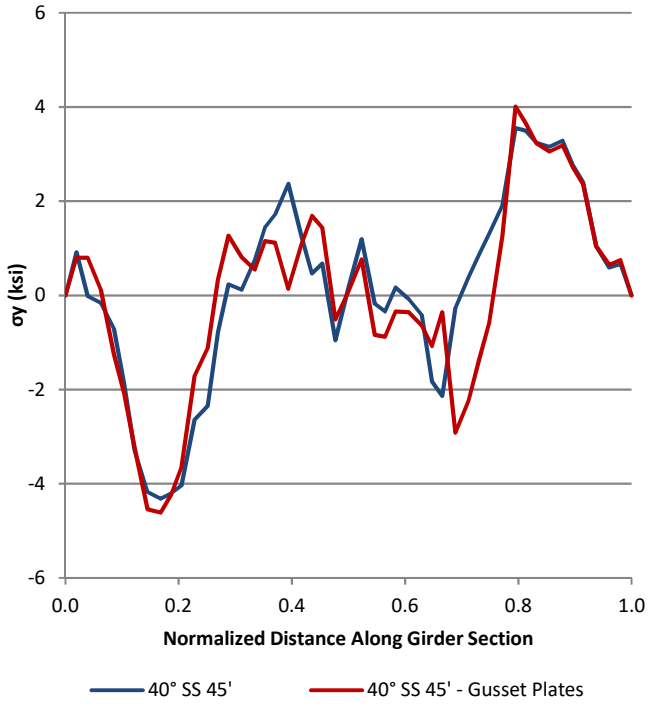

Figure F.9 Weak axis out-of-plane bending stress – interior girder (G3)

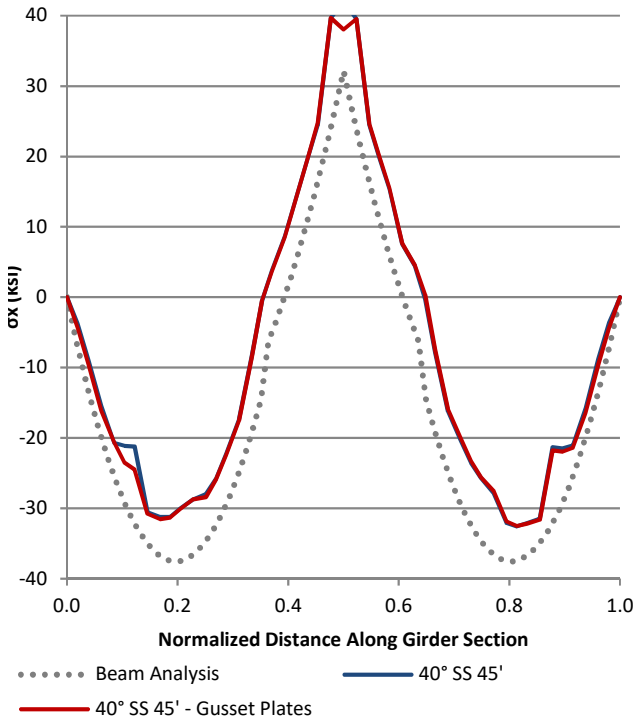

Figure F.10 Strong axis in-plane bending stress – interior girder (G3)

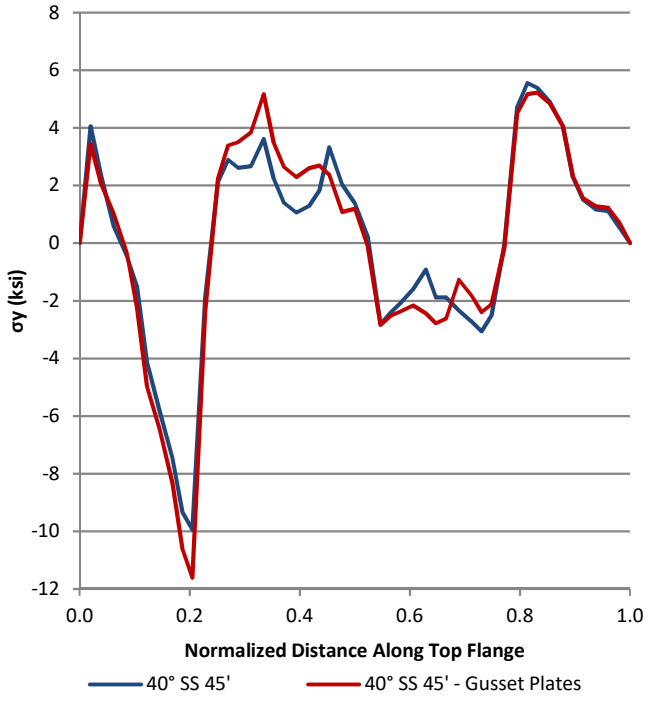

Figure F.11 Top flange out-of-plane bending stress – interior girder (G3)

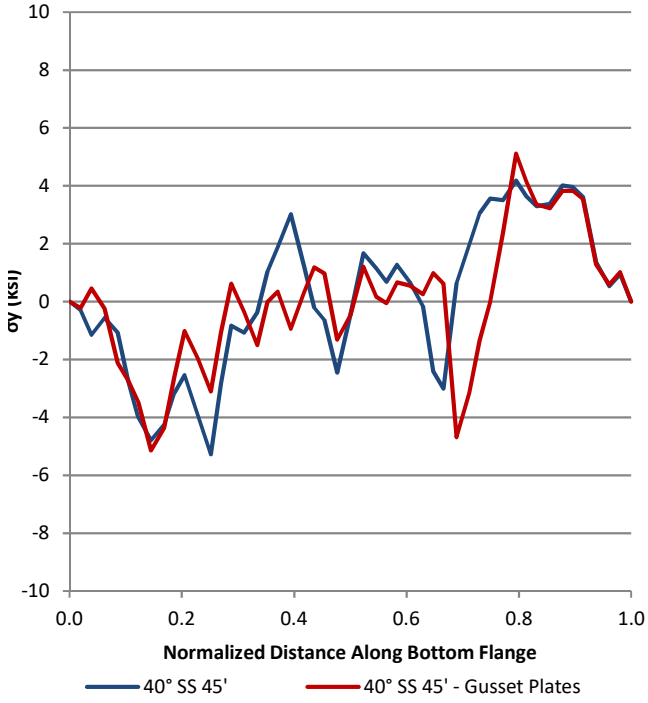

Figure F.12 Bottom flange out-of-plane bending stress – interior girder (G3)

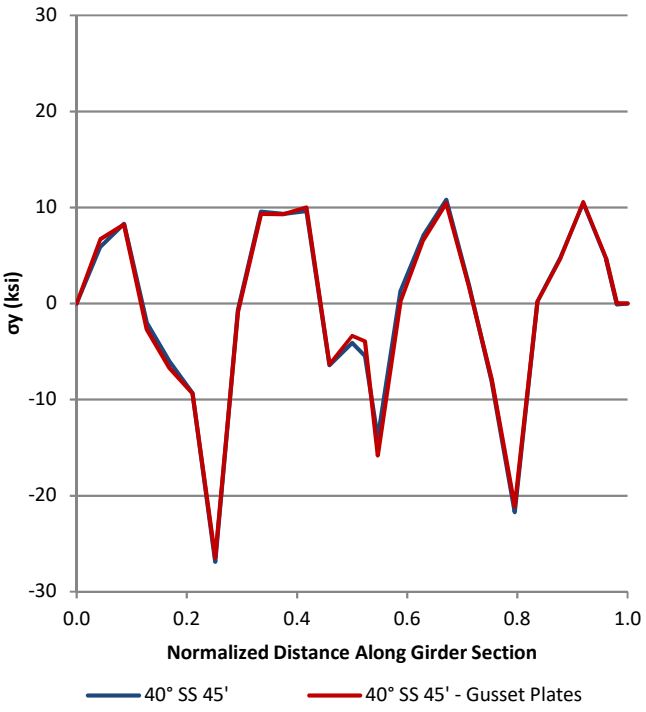

Figure F.13 Weak axis out-of-plane bending stress – exterior girder (G4)

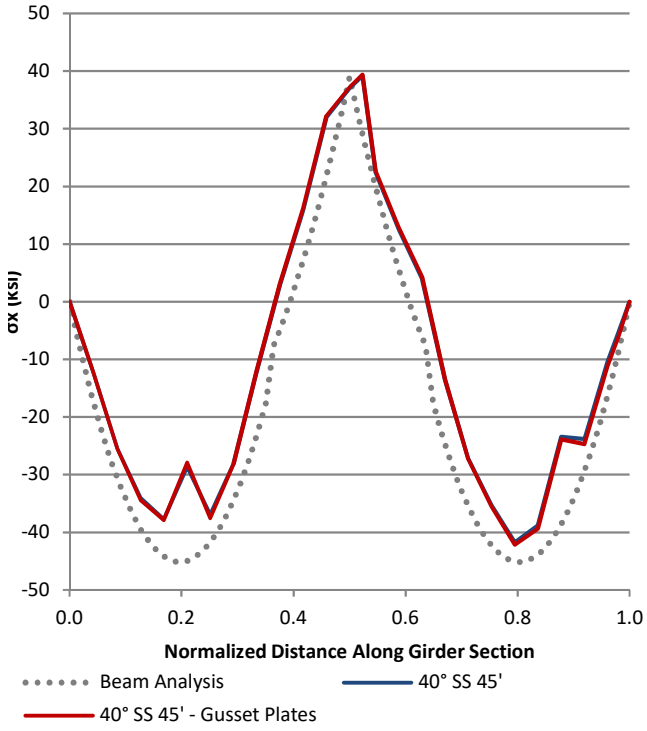

Figure F.14 Strong axis in-plane bending stress – exterior girder (G4)

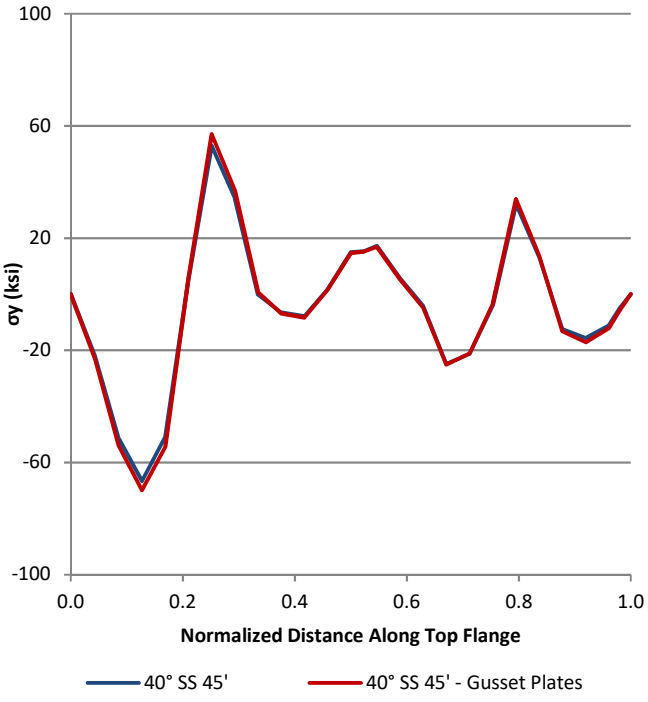

Figure F.15 Top flange out-of-plane bending stress – exterior girder (G4)

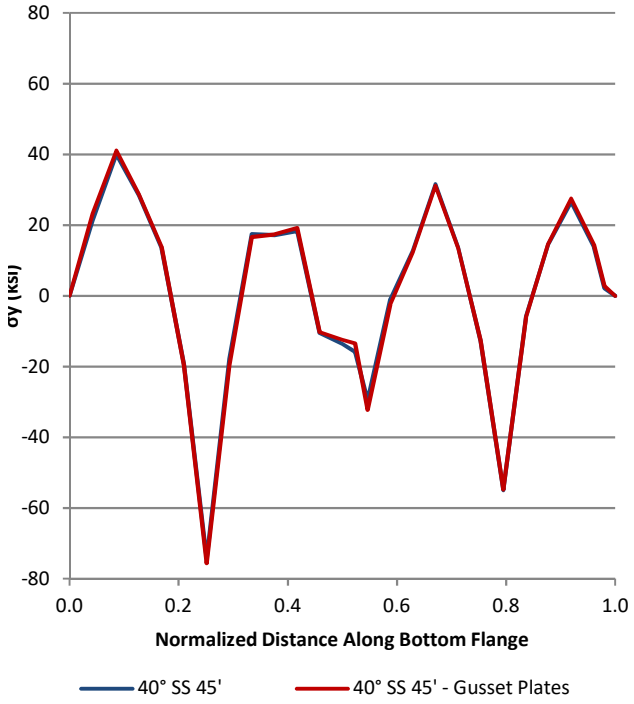

Figure F.16 Bottom flange out-of-plane bending stress – exterior girder (G4)

Figure F.18, Figure F.19, and Figure F.20 show cross-frame member stresses in the local longitudinal direction of Member A, Member B, and Member C, respectively. The cross-frame angle members are labeled in Figure F.17. The longitudinal stress direction of the cross-frame angle members, denoted as σ11, captures all stresses in the 11-direction, and includes both axial and bending stresses. Stresses were calculated as the average of the element stresses obtained by creating a cross-sectional cut through Member C for the cross-frame circled in Figure F.5.

While the stresses in the alternate cross-frame with gusset plates produced slightly lower stresses in Member A compared to the typical cross-frame presented in Figure F.1, the magnitude of stress in that member was low. Stresses found in Member B and Member C were much higher but the difference in magnitude of elements stresses between the two cross-frames were relatively the same. Member C shows a slightly different behavior of stresses across the bottom chord, likely due to the gusset plate connection used for the alternate cross-frame. However, as shown in Figure F.21, peak stresses found in Member C were almost identical.

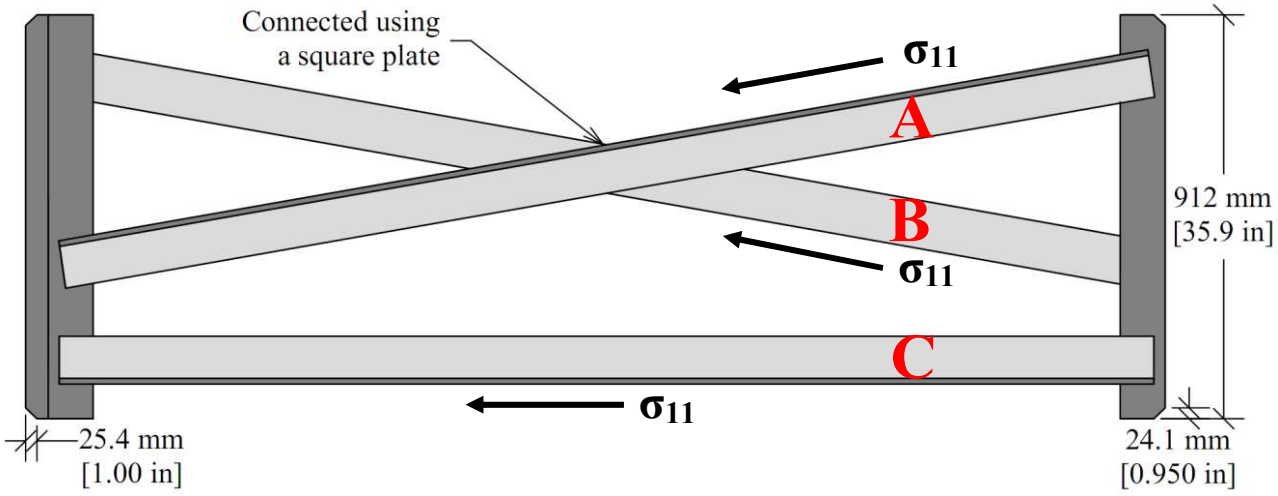

Figure F.17 Cross-frame angle member labels and stress direction

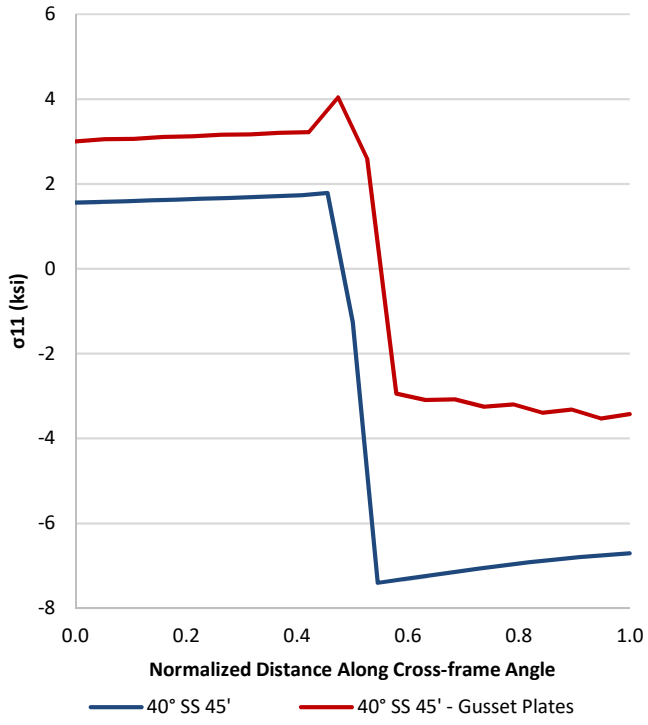

Figure F.18 Cross-frame Member A diagonal σ_{11}

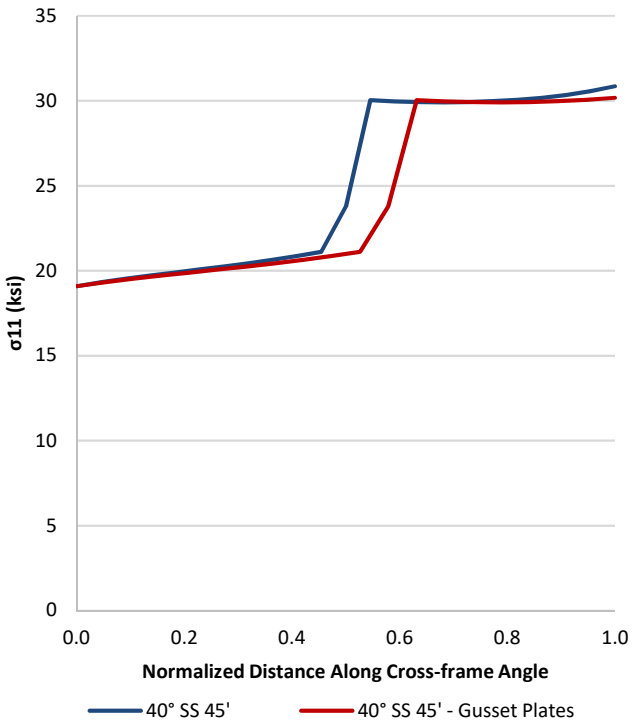

Figure F.19 Cross-frame Member B diagonal σ_{11}

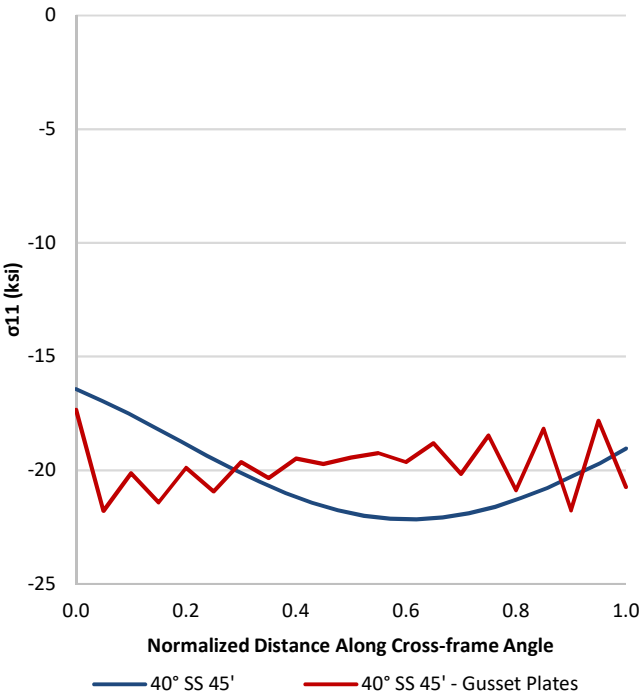

Figure F.20 Cross-frame Member C bottom chord σ_{11}

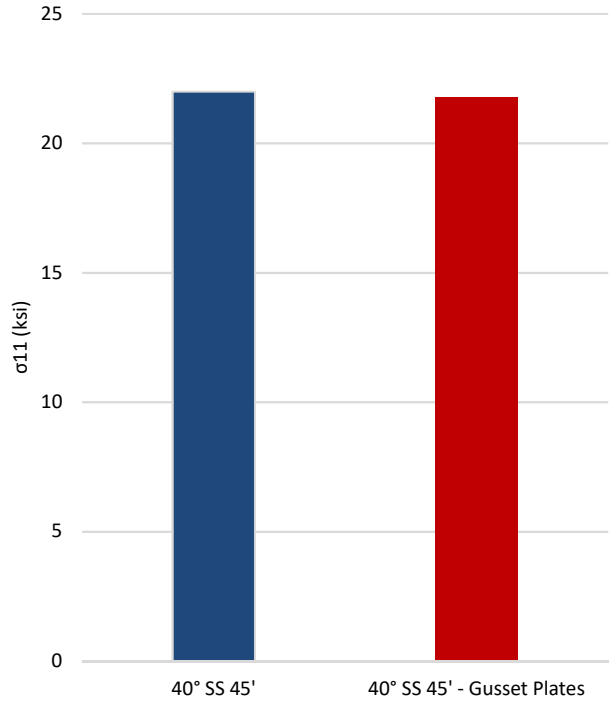

Figure F.21 Peak σ_{11} in cross-frame Member C

The alternate cross-frame angle framing and the addition of gusset plates had a minor effect on top flange lateral deflection in the exterior girder, girder bending stresses, and overall cross-frame member stresses. This shows that the lateral torsional buckling behavior of the girders as well as the brace capacity of the cross-frames were not significantly affected by the eccentricity found in the framing of the cross-frame members used through Part 2 and 3 of this paper. In the design of cross-frames, other considerations such as ease of construction, fatigue requirements, and fabrication costs may govern over the placement of the angle members.